

1A
DECLASSIFIED

CONFIDENTIAL

CLASSIFICATION CHANGED
UNCLASSIFIED


TO _____

By Authority of *Automatic* Date *12-20-65*
Downgrading Group

NACA CONFERENCE ON
AERODYNAMICS OF HIGH-SPEED AIRCRAFT
A Compilation of the Papers Presented

Ames Aeronautical Laboratory
Moffett Field, Calif.

July 8-10, 1953



DECLASSIFIED

CONFIDENTIAL

TABLE OF CONTENTS

INTRODUCTION

LIST OF CONFEREES

TECHNICAL PAPERS PRESENTED

PERFORMANCE AND GENERAL AERODYNAMICS

CHAIRMAN: John Stack

Chairman's Remarks

The Zero-Lift Drag Characteristics of Wing-Body Combinations at Transonic and Moderate Supersonic Speeds . . . by Richard T. Whitcomb

Theory of Wing-Body Drag at Supersonic Speeds . . . by Robert T. Jones

Drag of External Stores and Nacelles at Transonic and Supersonic Speeds . . . by Norman F. Smith, Ralph P. Bielat, and Lawrence D. Guy

Pressure Drag of Bodies at Mach Numbers Up to 2.0 . . . by Robert L. Nelson and William E. Stoney, Jr.

Drag Due to Lift at Mach Numbers Up to 2.0 . . . by Edward C. Polhamus

Longitudinal Characteristics of Wings . . . by Thomas A. Toll

Aerodynamic Characteristics of Low-Aspect-Ratio Wings at High Supersonic Mach Numbers . . . by Edward F. Ulmann and Mitchel H. Bertram

Boundary-Layer Control on Swept Wings . . . by Woodrow L. Cook

Inclined Bodies at High Supersonic Speeds . . . by Edward W. Perkins and David H. Dennis

Some Considerations Concerning Inlets and Ducted Bodies at Mach Numbers From 0.8 to 2.0 . . . by Richard I. Sears

The Performance of Conical Supersonic Scoop Inlets on Circular Fuselages . . . by Lowell E. Hasel

Recent Results on Inlet Instability . . . by Carl F. Schueller

0371281030

CONFIDENTIAL

- Inlet-Engine Matching Methods . . . by John L. Allen
- Recent Data on Diffuser Design . . . by John R. Henry
- Jet Effects on the Flow Over Afterbodies in a Supersonic Stream . . .
by Edgar M. Cortright, Jr., and Fred D. Kochendorfer
- Some Effects of a Jet on Surfaces Downstream of the Exit . . . by Maxime
A. Faget and Carlos A. de Moraes
- The Effects of Operating Propellers on Airplane Stability and Performance
. . . by Robert M. Crane
- Some Free-Flight Measurements of Turbulent Skin Friction and Heat Transfer
at High Supersonic Speeds . . . by Alvin Seiff, Simon C. Sommer, and
Barbara J. Short
- Factors Affecting Transition at Supersonic Speeds . . . by K. R. Czarnecki
and Archibald R. Sinclair
- Comments Pertaining to the Prediction of Shock-Induced Boundary-Layer
Separation . . . by Roy H. Lange
- A Study of the Motion and Aerodynamic Heating of Missiles Entering the
Earth's Atmosphere at High Supersonic Speeds . . . by H. Julian Allen
- Problems and Initial Experiments on Heat Transfer at Hypersonic Speeds
. . . by A. J. Eggers, Jr., and A. C. Charters, Jr.
- Exploratory Tests of the Alleviation of Aerodynamic Heating by Water
Transpiration Cooling at Mach Number 2 . . . by William J. O'Sullivan,
Jr., Leo T. Chauvin, and Charles B. Rumsey
- Model Experiments of Bomb Releases at Supersonic Speeds . . . by Robert
W. Rainey
- Considerations Affecting Hydro-Ski Airplane Design . . . by Kenneth L.
Wadlin
- Some Design Considerations Pertinent to the Rough-Air Behavior of
Airplanes at Low Altitude . . . by Philip Donely and Clarence L. Gillis

DECLASSIFIED
CONFIDENTIAL

STABILITY AND CONTROL

CHAIRMAN: Harry J. Goett

Additional Investigation of the Handling Qualities of Airplanes at High
Speeds . . . by A. Scott Crossfield, Hubert M. Drake, Jack Fischel,
and Joseph A. Walker

Relation Between Flight Behavior and Stall Progression on Swept Wings
. . . by Steven E. Belsley and Seth B. Anderson

Stall Progression on Swept Wings at Low and High Speeds . . . by Charles
W. Harper and Robert M. Crane

Recent Design Studies Directed Toward Elimination of Pitch-Up . . . by
Joseph Weil and W. H. Gray

Some Aerodynamic Considerations Governing the Static Stability of
Cruciform Missiles . . . by Donald D. Baals, M. Leroy Spearman, and
David G. Stone

Examination of Recent Stability Derivative Data . . . by Frank S.
Malvestuto, Jr., and Richard E. Kuhn

Design Trends in Relation to Airplane Lateral Stability . . . by John P.
Campbell

The Effect of Stability and Control Characteristics on the Tracking
Effectiveness of Airplanes . . . by George A. Rathert, Jr.

Data on Spoiler-Type Ailerons . . . by John G. Lowry

Recent Information on Flap and Tip Controls . . . by Douglas R. Lord
and K. R. Czarnecki

Several Factors Affecting Roll Control Systems of Interceptors . . . by
Leonard Sternfield

Application of Statistical Theory to the Reduction of Noise Effects in
Missile Guidance . . . Elwood C. Stewart

Investigations Toward Simplification of Missile Control Systems . . . by
Howard J. Curfman, Jr., H. Kurt Strass, and Harold L. Crane

Influence of Control-Surface Aerodynamics on Missile Simplification . . .
by Charles W. Frick, Henry C. Lessing, and Murray Tobak

A Combined Aerodynamic and Guidance Approach for a Simple Homing System
. . . by Robert A. Gardiner

DECLASSIFIED

CONFIDENTIAL

INTRODUCTION

This document contains unedited reproductions of technical papers on some of the most recent research results on the aerodynamics of high-speed aircraft from the NACA Laboratories. These papers were presented by members of the staff of the NACA Laboratories at the NACA Conference held at the Ames Aeronautical Laboratory July 8-10, 1953. The primary purpose of this conference was to convey to contractors of the military services and others concerned with the design of aircraft these recent research results and to provide those attending an opportunity to discuss the results.

A list of the conferees is included.

CONFIDENTIAL

The following were registered at the NACA Conference on Aerodynamics of High-Speed Aircraft at Ames Aeronautical Laboratory, Moffett Field, Calif., July 8-10, 1953.

ABBOTT, Ira H.
ALDRICH, Jerry F. L.
ALFORD, J. S.
ALGRANTI, Joseph S.
ALLEN, H. Julian
ALLEN, John L.
AMES, M. B., Jr.
ANDERSON, Harvey L.
ANDERSON, Major P. B., Jr.
ANDERSON, Seth B.
ANDREWS, E.
ANKENBRUCK, H. O.
ANTONATOS, P. P.
AMBROSE, Col. Elmer E.
ARMSTRONG, Donald P.
ARNOLD, Alison M.
ASHWORTH, Charles D.

BAALS, Donald D.
BAKER, T.
BARISH, Capt. D. T.
BATES, G. P.
BAYLESS, R. L.
BEKKEDAHL, James L.
BELL, Harold W.
BELLMAN, D. R.
BELSLEY, Steven E.
BELT, Robert H.
BENNETT, Theodore C.
BERGSTEDT, Lt. William C.
BERLER, Irving
BICKNELL, Joseph
BIOLETTI, Carlton
BIRCHILL, Joseph
BLAKE, C. L.
BLEAKNEY, William
BONNEY, Everard A.
BOTTENBERG, Cdr. William R., USN
BOUSHEY, Col. H. A.
BOYD, Maj. General Albert
BOYKIN, J. A.
BRATT, R. W.

NACA Headquarters
NAMTC - Pt. Mugu, Calif.
Subcommittee on Internal Flow
NACA - Lewis Laboratory
NACA - Ames Laboratory
NACA - Lewis Laboratory
NACA Headquarters
Subcommittee on High-Speed Aerodynamics
Wright Air Development Center
NACA - Ames Laboratory
Hughes Aircraft Company
NACA High-Speed Flight Research Station
Wright Air Development Center
Hdqrs. ARDC - Baltimore, Md.
Bureau of Aeronautics - Los Angeles
Stanley Aviation Corporation
David Taylor Model Basin

NACA - Langley Laboratory
NACA High-Speed Flight Research Station
Wright Air Development Center
NACA Headquarters
Subcommittee on High-Speed Aerodynamics
Douglas Aircraft Company
North American Aviation,
NACA High-Speed Flight Research Station
NACA - Ames Laboratory
McDonnell Aircraft Corporation
NADC - Johnsville, Pennsylvania
Bureau of Aeronautics - San Diego
Sperry Gyroscope Company
Project Meteor - M.I.T.
NACA - Ames Laboratory
Northrop Aircraft
Office of the Secretary of Defense
Hughes Aircraft Company
Applied Physics Laboratory, J.H.U.
David Taylor Model Basin
Wright Air Development Center
Wright Air Development Center
Wright Air Development Center
Douglas Aircraft Company

BRAUN, Dr. G. W.
BREUHAUS, W. O.
BROWN, Charles G.
BROWN, Clinton E.
BROWN, Robert Benton
BROWNE, Thomas P.
BURGESS, Neil

BURSTEIN, Adolph
BUSEMANN, Adolph
BUTTERWORTH, W. T.

CAMPBELL, John P.
CAMPBELL, Kenneth
CARR, Cdr. Donald E., Jr.
CASH, George M.
CATHAWAY, R.
CAWTHON, J. A.
CESARO, Richard S.
CHAMPINE, Robert A.
CHAPMAN, Dean R.
CHASE, Thomas W.
CHRISTIENSEN, W. N.
CLARK, Edward E.
CLOUSING, Lawrence A.
COATES, Wendell M.

COLE, Rossa W.
COLEMAN, T. F.
COLMAN, P. A.
CONNORS, J. F.
COOK, W. H.
COOK, Woodrow L.
COOPER, George E.
COOPER, Lewis G.
CORTRIGHT, Edgar M., Jr.
COWGILL, L. C.
CRANE, Robert M.
CRITES, Sherman E.
CROOK, N. L.
CROSSFIELD, A. Scott

CROTSLEY, Harmon
CROWLEY, J. W.
CULBERTSON, P. E.
CURFMAN, Howard J., Jr.
CZARNECKI, K. R.

Wright Air Development Center
Cornell Aeronautical Laboratory
Douglas Aircraft Company
NACA - Langley Laboratory
Boeing Airplane Company
Douglas Aircraft Company
Subcommittee on Power Plants for
Aircraft
Consolidated Vultee Aircraft Corp.
NACA - Langley Laboratory
North American Aviation

NACA - Langley Laboratory
Curtiss-Wright Corporation
U.S. Naval Air Sta., Moffett Field, Calif.
Cornell Aeronautical Laboratory
Lockheed Aircraft Corporation
Consolidated Vultee Aircraft Corp.
NACA Headquarters
NACA - Langley Laboratory
NACA - Ames Laboratory
Minneapolis-Honeywell Regulator Co.
Douglas Aircraft Company
Glenn L. Martin Company
NACA - Ames Laboratory
U. S. Naval Post Graduate School,
Monterey, California
Curtiss-Wright Corporation
Hughes Aircraft Company
Subcommittee on Internal Flow
NACA - Lewis Laboratory
Boeing Airplane Company
NACA - Ames Laboratory
NACA - Ames Laboratory
Glenn L. Martin Company
NACA - Lewis Laboratory
Lockheed Aircraft Corporation
NACA - Ames Laboratory
General Electric Company
TEMCO Aircraft Corporation
NACA High-Speed Flight Research
Station
North American Aviation
NACA Headquarters
Consolidated Vultee Aircraft Corp.
NACA - Langley Laboratory
NACA - Langley Laboratory

DECLASSIFIED
CONFIDENTIAL

DAILEY, Vance C.
DALE, Lt. Col. James R.
DALLOW, Thomas P.
DAVIS, Frank W.

DAVIS, Robert A.
DAVIS, Wallace F.
DEEP, Raymond A.
DeFRANCE, Dr. Smith J.
DENNEN, Major Richard L.
DENNIS, David H.
DEYARMOND, Albert B.
DIEHL, Capt. W. S., USN(Ret.)
DISHER, J. H.
DOMMASCH, D. O.
DONLY, Philip
DONLAN, Charles J.
DRAKE, Hubert M.
DRYDEN, Dr. Hugh L.
DUKE, Will
DUNHOLTER, Howard F.
DWINNELL, J. H.

EBER, Gerhard R.
EGGERS, A. J., Jr.
EISELSTEIN, Lt. William E.
ELLIOTT, John M.
ELLIS, J. A.
EMMONS, Paul
ENGLERT, G. W.
ENSINGER, Willis B.
EPES, Cdr. H. H., Jr.
EPSTEIN, Albert
ERICKSON, Albert L.
ERICKSON, Myles D.
EVANS, A. J.
EVVARD, John C.

FAGET, Maxime A.
FALLIS, Dr. W. B.
FARKAS, A. S.
FEDZIUK, Henry A.
FELDMEIER, Lt. Col. A. L.
FINCH, T.
FINCH, Volney C.
FISCHEL, Jack
FISHER, Robert E.

NADC - Johnsville, Pennsylvania
SAC - Offutt AFB
Wright Air Development Center
Subcommittee on Power Plants for
Aircraft
Sperry Gyroscope Company
NACA - Ames Laboratory
Redstone Arsenal
NACA - Ames Laboratory
AF Flight Test Center - Edwards AFB
NACA - Ames Laboratory
Ryan Aeronautical Company
Committee on Aerodynamics
NACA - Lewis Laboratory
NATC - Patuxent River
NACA - Langley Laboratory
NACA - Langley Laboratory
NACA High-Speed Flight Research Station
NACA Headquarters
Subcommittee on Aircraft Structures
Consolidated Vultee Aircraft Corporation
Boeing Airplane Company

Holloman Air Development Center
NACA - Ames Laboratory
Air Technical Intell. Center - WPAFB
NACA - Langley Laboratory
Wright Air Development Center
Bell Aircraft Corporation
NACA - Lewis Laboratory
Bureau of Ordnance
Air Squadron 5, Moffett Field, Calif.
Republic Aviation Corporation
NACA - Ames Laboratory
NACA - Ames Laboratory
NACA Headquarters
NACA - Lewis Laboratory

NACA - Langley Laboratory
Consolidated Vultee Aircraft Corp.
Bureau of Aeronautics - Washington, D.C.
NACA - Langley Laboratory
Office of Naval Operations
NACA High-Speed Flight Research Station
Consultant, ONR
NACA High-Speed Flight Research Station
Marquardt Aircraft Company

FISHOW, Morris
 FLANAGAN, Lindley E.
 FLEISIG, Ross
 FLEMING, W. A.
 FORRY, John E.
 FOX, J. L.
 FREDETTE, Raymond O.
 FRICK, Charles W., Jr.
 FRIEND, C. F.
 FRITZ, Raymond
 FUHRMAN, Robert A.

GARDINER, Robert A.
 GARDNER, Capt. A. J.
 GATEWOOD, Dr. B. E.
 GAZLEY, Dr. Carl
 GLOECKLER, Frederick M.
 GODDARD, Frank E.
 GOETT, Harry J.
 GORANSON, R. F.
 GORE, Marvin R.
 GRAETZER, Dr. Gunther R.
 GRAHAM, Donald J.
 GRANDFIELD, J.
 GREENE, Lawrence P.

GROGAN, G. C., Jr.
 GUMBEL, Harold
 GUSTAFSON, Robert L.
 GUTHRIE, John M.

HARGIS, C. B.
 HARPER, Charles W.
 HARRIS, Fred
 HART, John A.
 HARTLEY, Lt. Cdr. G. E.
 HARTMAN, Edwin P.
 HASEL, Lowell E.
 HEALD, Ervin R.
 HEASLET, Max. A.
 HEATON, Col. Donald H.
 HEGE, Jeremiah C.
 HEIMER, H. J.
 HELFMAN, Sidney
 HENDERSON, Lt. Col. David L.
 HENRY, Lt. Col. H. C.
 HENRY, John R.

NBS - Corona Laboratories
 North American Aviation
 Sperry Gyroscope Company
 NACA - Lewis Laboratory
 Bureau of Aeronautics
 NACA - Lewis Laboratory
 Bureau of Ordnance
 NACA - Ames Laboratory
 Lockheed Aircraft Corporation
 Marquardt Aircraft Company
 Ryan Aeronautical Company

NACA - Langley Laboratory
 Wright Air Development Center
 USAF Institute of Technology
 The RAND Corporation
 NADC - Johnsville, Pennsylvania
 Jet Propulsion Laboratory - C.I.T.
 NACA - Ames Laboratory
 NACA Headquarters
 Aerojet Engineering Cop.
 USAF - Institute of Technology
 NACA - Ames Laboratory
 United Aircraft Corporation
 Subcommittee on High-Speed
 Aerodynamics
 Consolidated Vultee Aircraft Corp.
 Naval Air Missile Test Center
 Grumman Aircraft Engineering Corp.
 North American Aviation

Wright Air Development Center
 NACA - Ames Laboratory
 Wright Air Development Center
 NBS - Corona Laboratories
 Bureau of Ordnance
 NACA - Western Coordinator Office
 NACA - Langley Laboratory
 Douglas Aircraft Company
 NACA - Ames Laboratory
 Air Research and Development Command
 Applied Physics Laboratory, J.H.U.
 Hughes Aircraft Company
 Republic Aviation Corporation
 Hdqrs. USAF
 Wright Air Development Center
 NACA - Langley Laboratory

DECLASSIFIED
CONFIDENTIAL

HEPPE, R.
HERALD, John M.
HESSELL, Cdr. E. W.
HIGGINS, George J.

HIGGINS, Harry
HILL, Dr. Freeman
HOEL, Robert A.
HOLLAND, E. P.
HOLLEMAN, E. C.

HOLTBY, Kenneth
HONG, Jim
HOOD, Manley J.
HORNER, Richard E.

HUNTER, Maxwell W.
HUNTSBERGER, Ralph F., Jr.
HURTT, W. W.
HYATT, Abraham

JAEGER, B. F.
JAGIELLO, L. T.
JANSEN, George R.
JARRETT, A. L.
JEFFS, George W.
JENNY, R. B.
JERGER, Joseph
JOHNSON, Bernard T.
JOHNSON, Cdr. E. B.
JOHNSON, R. P.
JOHNSTONE, C. A.
JONES, Alun R.
JONES, Robert T.
JORDAN, G.

JUDIN, Jas. P.

KAHR, Charles H., Jr.

KARPOV, Dr. B. G.
KASLEY, Jack H.
KAUFFMAN, William M.
KEENER, Earl

KELLY, Joseph A.

Lockheed Aircraft Corporation
Subcommittee on Seaplanes
Office of Naval Operations
U. S. Naval Post Graduate School,
Monterey, California
Boeing Airplane Company
Applied Physics Laboratory, J.H.U.
Minneapolis-Honeywell Regulator Co.
Boeing Airplane Company
NACA High-Speed Flight Research
Station
Boeing Airplane Company
Lockheed Aircraft Corporation
NACA - Ames Laboratory
Air Force Flight Test Center,
Edwards AFB
Douglas Aircraft Company
NACA - Ames Laboratory
TEMCO Aircraft Corporation
Bureau of Aeronautics

NOTS - Inyokern
NOTS - Inyokern
Douglas Aircraft Company
Chance Vought Aircraft
North American Aviation
Douglas Aircraft Company
Raytheon Manufacturing Company
Boeing Airplane Company
Office of the Secretary of Defense
The RAND Corporation
NOP - Indianapolis
NACA - Ames Laboratory
NACA - Ames Laboratory
NACA High-Speed Flight Research
Station
NOTS - Inyokern

U. S. Naval Post Graduate School,
Monterey, California
Ballistic Research Lab.
Curtiss-Wright Corporation
NACA - Ames Laboratory
NACA High-Speed Flight Research
Station
NBS - Corona Laboratories

KIRKWOOD, Thomas F.
KLEPINGER, R. H.
KNEMEYER, F.
KOCH, Charles J.
KOETSCH, Major Julius F.
KOTONIAS, T. J.
KURZWEG, Dr. Herman H.

LAMBERT, A. A.
LANGE, Adolf H.
LANGE, Roy H.
LATHAM, Major D. R., USAF
LAU, C. A.
LAWRENCE, Herbert R.
LESSING, Henry C.
LIESKE, Hans
LIGON, William M.
LINDEN, Jack E.
LIVINGSTON, Lt. Cdr. W. H.
LOBB, Rodmond K.
LOBRECHT, D., Jr.
LOMAX, Harvard
LONGFELDER, H. J.
LORD, Douglas R.
LOUDEN, F. A.
LOVE, Eugene S.
LOW, G. M.
LOWELL, A. L.
LOWRY, John G.
LU, H. R.
LUECK, Capt. David W., USAF
LUKE, Major Ernest P.
LUSKIN, Harold

MABRY, George C.
MACK, Charles E.
MAHOFF, Andrew A.
MALVESTUTO, Frank S., Jr.
MARTIN, Harry E.
MASTROCOLA, N.
MATTHEWS, Howard F.
MAY, R. W.
MAY, T. J.

MAYDEW, Randall C.
MERSMAN, Dr. William A.
MIELZINER, Walter
MILLER, R. T.

The RAND Corporation
Wright Air Development Center
NOTS - Inyokern
Glenn L. Martin Company
David Taylor Model Basin
NAMTC - Pt. Mugu, Calif.
Subcommittee on High-Speed
Aerodynamics
McDonnell Aircraft Corporation
Naval Ordnance Laboratory
NACA - Langley Laboratory
AFDFO - Moffett Field, Calif.
Chance Vought Aircraft
Cornell Aeronautical Laboratory
NACA - Ames Laboratory
The RAND Corporation
Bureau of Aeronautics
Bureau of Aeronautics
NATC - Patuxent
Naval Ordnance Laboratory
Consolidated Vultee Aircraft Corp.
NACA - Ames Laboratory
Boeing Airplane Company
NACA - Langley Laboratory
Committee on Aerodynamics
NACA - Langley Laboratory
NACA - Lewis Laboratory
McDonnell Aircraft Corporation
NACA - Langley Laboratory
Republic Aviation Corporation
Subcommittee on Aircraft Loads
Holloman Air Development Center
Douglas Aircraft Company

Douglas Aircraft Company
Grumman Aircraft Engineering Corp.
Douglas Aircraft Company
NACA - Langley Laboratory
Douglas Aircraft Company
NAMTC - Pt. Mugu, Calif.
NACA - Ames Laboratory
NACA Headquarters
AF Development Field Office -
Los Angeles
Sandia Corporation - Albuquerque
NACA - Ames Laboratory
Stanley Aviation Corporation
Subcommittee on Internal Flow



DECLASSIFIED

CONFIDENTIAL

MILLIKAN, Dr. Clark B.
MITCHELL, Lt. R. E., Jr.
MOSES, Jason J.
MOSES, Kurt
MOSKOVITZ, Abraham I.

MULHOLLAND, Frank
MULTHOPP, Hans
MURRAY, Peter R.
MUSE, T. C.
MYERS, B. C.
MYERS, Dale De Haven

McCABE, Arthur P.
McCOURT, A. W.
McGOWAN, Wayne A.
McKEE, Col. D. B.
McKEE, Paul D.

NAY, Col. P. F.

NELSON, Lt. Col. Conrad N.
NELSON, Norman E.

NELSON, Robert L.
NEWTON, F. C.
NICHOL, Capt. B. B.

NORTH, Warren J.

O'DONNELL, Dr. William J.
O'KEEFE, Charles
OLNEY, Adm. Alfred E. (Ret.)
O'MALLEY, J. A.
O'MARA, Col. John A.

ORBAN, Lt. Col. Henry A.
OSBORN, Earl P.
OSTRACH, S.
O'SULLIVAN, William J., Jr.
OSWALD, Dr. W. Bailey
OUTMAN, V.

PADGETT, Joseph E., Jr.
PAPPAS, C. E.

Committee on Aerodynamics
Wright Air Development Center
Ryan Aeronautical Company
Bendix Aviation Corporation
Subcommittee on Stability and
Control
Republic Aviation Corporation
Glenn L. Martin Company
Wright Air Development Center
Office of the Secretary of Defense
NACA Headquarters
Subcommittee on Stability and
Control
Project Meteor - M.I.T.
Westinghouse Electric Corporation
Bureau of Aeronautics - Inglewood
Wright Air Development Center
Wright Air Development Center

Committee on Power Plants for
Aircraft
Hq. USAF
AF Development Field Office -
Los Angeles
NACA - Langley Laboratory
Douglas Aircraft Company
U. S. Naval Air Station, Moffett
Field, Calif.
NACA - Lewis Laboratory

Subcommittee on Internal Flow
Raytheon Mfg. Company
TEMCO Aircraft Corporation
Bell Aircraft Corporation
ATIC - Wright-Patterson Air
Force Base
AFDFO - Washington, D. C.
Subcommittee on Aircraft Loads
NACA - Lewis Laboratory
NACA - Langley Laboratory
Committee on Aerodynamics
McDonnell Aircraft Corporation

Westinghouse Electric Corporation
Subcommittee on High-Speed
Aerodynamics

PARCHEM, John A.
PARKE, D. B.
PARSONS, John F.
PARSONS, Thomas R.
PASSMAN, Richard
PATTERSON, Raymond T.
PAVELKA, J.
PEARSON, E. O.
PEELE, J. R.
PEIRCE, Chester
PELLEGRINO, Frank J.
PERKINS, Edward W.
PETERSEN, Norman
PETTINGALL, Charles E.
PHILLIPS, William H.
PIERCE, Ernest W.
PIERCE, Erol F.

PLATOU, Anders S.
POLHAMUS, Edward C.
POOR, C. L.
POTTER, J. Leith
PRACHAR, O. P.
PUCKETT, Dr. Allen E.
PULA, T. J.
PURSER, Paul E.

RAINEY, Robert W.
RANDELS, Dr. W. C.
RATHERT, George A., Jr.
RAYMOND, Dr. Arthur E.
RECAAT, I. G.
REED, T. G.
REID, Elliott G.
RETHORST, Scott
RHODE, R. V.
RICHARDS, Capt. John E.
RIDLEY, Lt. Col. Jackie L.
RITTER, Dr. Alfred
RITTER, Eugene Kerfoot
ROBBINS, Major Harold W., USAF
ROBINSON, Major James B., USAF
ROBINSON, Prof. R. F.
ROBINSON, Russell G.
ROLFE, Rial
ROSE, Major Eugene S., USAF

SATIN, Alexander
SCHINDEL, Leon H.

Bendix Aviation Corporation
McDonnell Aircraft Corporation
NACA - Ames Laboratory
Transonic Control Project - M.I.T.
Bell Aircraft Corporation
David Taylor Model Basin
Republic Aviation Corporation
NACA Headquarters
NACA High-Speed Flight Research Station
ARDC - Hollywood, Calif.
Bureau of Aeronautics
NACA - Ames Laboratory
Sperry Gyroscope Company
Douglas Aircraft Company
NACA - Langley Laboratory
Douglas Aircraft Co.
Subcommittee on Engine Performance
and Operation
Ballistics Research Laboratory
NACA - Langley Laboratory
Subcommittee on High-Speed Aerodynamics
Redstone Arsenal
Allison Division
Committee on Aerodynamics
Westinghouse Electric Corporation
NACA - Langley Laboratory

NACA - Langley Laboratory
NOTS - Inyokern
NACA - Ames Laboratory
Member NACA
NACA - Langley Laboratory
Redstone Arsenal
Tracerlab, Stanford University
USAF Hdqrs.
NACA Headquarters
Holloman Air Force Base
AF Flight Test Center - Edwards AFB
Subcommittee on Internal Flow
Naval Proving Ground - Dahlgren
AFDPR - Cleveland, Ohio
AFDFO - Washington, D. C.
USAF Institute of Technology
NACA - Ames Laboratory
McDonnell Aircraft Corporation
AFSWP - Albuquerque

Subcommittee on Seaplanes
Project Meteor - M.I.T.

DECLASSIFIED
CONFIDENTIAL

SCHNEYER, Ray I.

SCHUELLER, Carl F.
SCHURMEIER, Harris M.
SCHWEIGER, M.
SEA, A. L.
SEARS, Richard I.
SEIDMAN, Oscar
SEIFF, Alvin
SELNA, J.
SHARP, Dr. E. R.
SHEVELL, Richard S.
SHICK, R. H.
SHORT, Barbara J.
SIBILA, A. I.
SISK, T. R.
SKAVDAHL, Howard
SMELT, Ronald

SMITH, Apollo Milton O.
SMITH, Howard W.
SMITH, Norman F.
SMITH, Robert B.
SMULL, T. L. K.
SNODGRASS, Richard B.
SOMMER, Simon C.
SORGEN, Carl C.

SPANGENBERG, G. A.
SPRINGER, Burdell L.
STACK, John
STALDER, Jackson R.
STEELE, Paul
STEINHOFF, Dr. Ernst A.
STERNFIELD, Leonard
STEVENS, Victor I.
STEVENS, William P.
STEWART, Clyde R.
STOLP, Philip C.
STOOLMAN, Leo
STRANG, Charles R.
SULKIN, Maurice
SWANSON, Robert S.

TAYLOR, Richard W.
THAW, Russell W.
THOMPSON, Floyd L.

Sverdrup - Parcel, Inc., Arnold Engr.
Dev. Center
NACA - Lewis Laboratory
Jet Propulsion Laboratory - C.I.T.
United Aircraft Corporation
Wright Air Development Center
NACA - Langley Laboratory
Bureau of Aeronautics
NACA - Ames Laboratory
Northrop Aircraft
NACA - Lewis Laboratory
Douglas Aircraft Company
Subcommittee on Stability and Control
NACA - Ames Laboratory
Subcommittee on Aircraft Loads
NACA High-Speed Flight Research Station
Sperry Gyroscope Company
Sverdrup - Parcel, Inc., Arnold Engr.
Dev. Center
Douglas Aircraft Company, Inc.
Subcommittee on Aircraft Loads
NACA - Langley Laboratory
Subcommittee on Propellers for Aircraft
NACA Headquarters
SAC - Offutt Air Force Base
NACA - Ames Laboratory
Subcommittee on Engine Performance
and Operation
Bureau of Aeronautics
Subcommittee on Aircraft Loads
NACA - Langley Laboratory
NACA - Ames Laboratory
North American Aviation
Holloman Air Development Center
NACA - Langley Laboratory
NACA - Ames Laboratory
Northrop Aircraft
NACA - Ames Laboratory
Allison Division
Hughes Aircraft Company
Douglas Aircraft Company
North American Aviation
NAMIC - Pt. Mugu, Calif.

Boeing Airplane Company
Douglas Aircraft Company
NACA - Langley Laboratory

TILGNER, Charles, Jr.	Subcommittee on Stability and Control
TITUS, Paul V.	North American Aviation
TOBAK, Murray	NACA - Ames Laboratory
TOLL, Thomas A.	NACA - Langley Laboratory
TRACZ, S. C.	Bell Aircraft Corporation
TURNER, W.	Hughes Aircraft Company
ULMANN, Edward F.	NACA - Langley Laboratory
UNDERWOOD, William J.	NACA Liaison Office at WADC
VAN EVERY, K. E.	Subcommittee on High-Speed Aerodynamics
VAN METER, James T.	Transonic Control Project - M.I.T.
VAUGHN, Harold R.	Sandia Corp. - Albuquerque
VINCENTI, Walter G.	NACA - Ames Laboratory
VOLLUZ, R. J.	Consolidated Vultee Aircraft Corp.
WADLIN, Kenneth L.	NACA - Langley Laboratory
WALDO, Robert D.	Aerojet Engineering Corp.
WALKER, Dr. Chapman C. J.	General Electric Company
WALKER, James H.	Applied Physics Laboratory, J.H.U.
WALKER, Joseph A.	NACA High-Speed Flight Research Station
WALTERS, Donald E.	Lockheed Aircraft Corporation
WARD, Emmett	Bureau of Aeronautics
WATSON, Jack O.	Bureau of Ordnance
WEIL, Joseph	NACA - Langley Laboratory
WESTERBACK, Ivar	Sperry Gyroscope Co.
WHITAKER, Henry P.	Project Lincoln - M.I.T.
WHITCOMB, Richard T.	NACA - Langley Laboratory
WILLIAMS, Walter C.	NACA High-Speed Flight Research Station
WITHINGTON, H. W.	Boeing Airplane Company
WITTE, N.	NOTS - Inyokern
WOERSCHING, Thomas B.	Goodyear Aircraft Corporation
WOLANSKY, John	Air Technical Intell. Center - WPAFB
WOOD, Donald H.	NACA - Ames Laboratory
WOODALL, R. F.	Wright Air Development Center
WOODS, R. J.	Committee on Aerodynamics
WOODWORTH, Lee R.	Subcommittee on Engine Performance and Operation
WRIGHT, Cdr. Kenneth E., USN	Office of Naval Research (Air Branch)
WRIGHT, Dr. T. P.	Committee on Aerodynamics

DECLASSIFIED

**PERFORMANCE AND
GENERAL AERODYNAMICS**


DECLASSIFIED
CONFIDENTIAL

CHAIRMAN'S REMARKS

Nearly a year ago in an experimental investigation of wing-body interference at transonic speeds Richard T. Whitcomb showed that for zero lift a wing-body combination had the same drag rise as a body of revolution having the same axial distribution of cross-sectional area as the wing-body combination. This, in fact, constituted the experimental proof of what we call the area rule. Once the area rule had been clearly stated and proven experimentally it occurred to many that the essence of this idea may have existed in the body of linear theory. This, in fact, has proved to be the case but these parts of the theory and their significance had been overlooked by everyone.

Since the first work establishing the area rule for the transonic range, a very considerable study of the problem has been made to attain: first, maximum benefit from its application; second, establishment of its limitations; and third, extension from the transonic to the supersonic range. As of the date of this conference there has been insufficient time to accumulate the necessary information to answer every question that might be raised.

The first four papers, however, are presented to review, to extend, and to summarize the area-rule question theoretically, experimentally, and in applications.



DECLASSIFIED

CONFIDENTIAL

THE ZERO-LIFT DRAG CHARACTERISTICS OF WING-BODY

COMBINATIONS AT TRANSONIC AND

MODERATE SUPERSONIC SPEEDS

By Richard T. Whitcomb


Langley Aeronautical Laboratory

WHITCOMB

This paper is concerned primarily with the application of the "area rule" to the interpretation and improvement of the drag-rise characteristics of wing-body combinations at transonic and moderate supersonic speeds.

Consideration of the general physical nature of the flow at transonic speeds, together with comparisons of the flow fields and drag-rise characteristics for wing-body combinations and bodies of revolution has led to the conclusion that near the speed of sound the drag rise for a thin low-aspect-ratio wing-body combination is primarily dependent on the axial distribution of cross-sectional area normal to the airstream (ref 1). (The drag rise, sometimes referred to as pressure drag, is the difference between the drag level near the speed of sound and the drag level at subsonic speeds where the drag is due primarily to skin friction.) In order to illustrate the concept, figure 1 shows a wing-body combination and a body of revolution. A typical cross-section normal to the airstream for the wing-body combination is shown at AA. The cross-sectional area of the wing is wrapped around the body of revolution so that the body has the same cross-sectional area at BB. All the other cross-sectional areas of the body of revolution are the same as those for the wing-body combination at the same axial stations. On the basis of the conclusion just stated, the drag rise for this body of revolution should be similar to that for the wing-body combination.


This relationship of the drag-rise increments for the wing-body combination and the comparable body of revolution is due primarily to the general similarities of the major portions of the extensive flow fields of the configurations. These similarities are illustrated in figures 2 and 3 which present schlieren photographs of the flow fields for unswept- and sweptback-wing-body combinations, together with those for equivalent bodies of revolution. The combinations have been rolled to three positions so that side, plan, and intermediate views are seen. Near the edges of the pictures, the observed shocks for the combinations in each view are generally similar to those for the equivalent bodies. These comparisons



are indicative of the similarities of the extensive fields beyond the view of the schlieren. Near the configurations there are differences of the flow fields for the wing-body combinations and equivalent bodies of revolution. However, the major portion of the energy losses associated with the shocks is produced in the extensive regions at appreciable distance from the configuration. Therefore, from a drag standpoint, it may be assumed that these differences near the configuration are of secondary importance. The general similarities of the extensive flow fields at distances from the configuration may be attributed to several aerodynamic phenomena characteristics of flow near the speed of sound. First, the field of any given displacement is concentrated in a plane nearly normal to the airstream. Because of this fact, the streamwise locations of the effects of the displacements of the wing are essentially the same as those for the corresponding effects produced by the comparable body of revolution. Secondly, at these considerable lateral distances from the configuration, the field is primarily dependent on the general displacement of the configuration rather than on the details of the shape. The generally close similarities of the effective fields for the wing-body combination and the comparable body of revolution in the regions producing the main portion of the shock losses suggests that the energy losses associated with the shocks for the two configurations should be similar. Since the drag rise for thin low-aspect-ratio wings is due primarily to shock losses, the drag rise for the combination should be approximately the same as that for the equivalent body of revolution.

In figure 4, the measured drag-rise increments for various swept-, delta-, and unswept-wing-body combinations and complete airplanes at a Mach number of 1.03 are compared with the increments for equivalent bodies of revolution. The aspect ratios of the wings are 4 or less and the thickness ratios are 7 percent or less. Except for one configuration, there is a general qualitative agreement between these drag-rise increments. Deviations from exact agreement are due to second-order effects, such as differences of the flow fields as shown in figures 2 and 3. The single case of marked disagreement is for a swept-wing airplane configuration. This disagreement cannot be fully explained at present. As would be expected, the correlation between the drag-rise increments of the wing-body combinations and the equivalent body of revolution generally becomes less close as the Mach number is increased beyond 1.0. The severity of this divergence varies markedly depending on the configuration.

It would be expected on the basis of this concept that, near the speed of sound, the minimum drag rise would be obtained by designing a wing-body combination with an area distribution similar to that for a smooth body of revolution with the highest possible fineness ratio. The fineness ratio that should be used is probably considerably less than that required for minimum total drag because of such problems as airplane



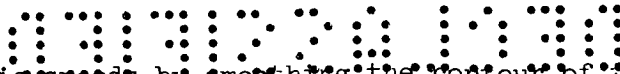
DELETED

stability and structural weight. One method of obtaining this favorable area distribution is to reshape the body. A number of experiments have been made to determine the effectiveness of such reshaping. Representative results, obtained in the Langley 8-foot transonic tunnel, are presented in figure 5.

On the left-hand side of this figure are shown the effects of such a body modification on the zero-lift drag-rise characteristics of a 6-percent-thick, aspect-ratio-4, 45° swept-wing-body combination. The solid line shows the variation of drag for the wing in combination with a body of revolution of fineness ratio of 11. The wing is placed on the body in such a manner that the leading edge of the wing is at the maximum diameter of the body. With this arrangement, the indentation used did not change the maximum cross-sectional area of the body. The dashed lines are the results obtained for the wing in combination with a body of revolution indented circularly to obtain the same area distribution as for the original body alone. For comparison, the results for the body alone are also shown. Indentation eliminated approximately 90 percent of the drag rise associated with the wing at Mach numbers from 1.00 to 1.05. When the Mach number is increased beyond 1.05, the drag rise for the indented wing-body combination approaches that for the original wing-body combination.

On the right-hand side of figure 5 are presented the effects of body indentation on the zero-lift drag-rise characteristics for a 4-percent-thick, 60° delta-wing-body combination. The solid curve shows the drag characteristics for the wing in combination with a body of revolution having a fineness ratio of 7.5. The dashed line indicates the drag variation after the body has been indented circularly to produce an area distribution for the combination the same as that for the original body alone. In this case the indentation reduced the maximum cross-sectional area of the body somewhat. It may be noted that again a significant reduction in the drag rise was obtained by such an indentation at transonic speeds. However, in this case, the drag rise for the indented wing-body combination is significantly greater than that for the body alone. This deviation from the result which might be expected on the basis of the area-distribution concept is probably due to the fact that the body required to obtain the smooth area distribution of the combination had a rather abrupt change in shape near the trailing edge of the wing. This shape probably led to severe local velocity gradients. Since the proper functioning of the body fields in offsetting the drag of the wing depends to a great extent on the velocity gradients being small, it might be expected that these severe gradients would lead to an incomplete reduction in drag. Also, near the speed of sound, a shock was present over this corner and may have caused some separation at this point, which would not be expected on the original body alone. It is probable that a further reduction in drag could have been obtained

[REDACTED]




at transonic speeds by smoothing the contour of the body slightly. Similar reductions in drag near the speed of sound have been obtained by body indentation for other delta and unswept wings.

Results obtained with smooth-surfaced configurations have indicated a marked reduction in drag at subsonic speeds associated with the use of indentation with swept and delta wings. However, with fixed transition this difference is not present. The influence of surface conditions on the effects of indentation apparently decreases with increase in the Mach number to supersonic speeds. The effect of body indentation on the drag characteristics at lifting conditions is discussed in the paper by Edward C. Polhamus. Obviously, the volume of the indented wing-body combination is not as great as that for the original wing-body combination. However, increasing the size of the body to recover the volume lost in indentation would increase the drag for the indented combination by a small fraction of this reduction in drag obtained.

The question now might arise as to whether it would be possible to obtain drag reductions at transonic speeds by adding to an existing wing-body combination to obtain a more favorable area distribution. Recently, investigations have been made of such additions on a 60° delta-wing airplane. Results are presented in figure 6. First, the fuselage was extended approximately 8 percent to obtain a more favorable area distribution of the rearward portion of the airplane. This addition resulted in significant reductions in the drag rise. Further reduction was obtained by adding side fairings to the extended configuration to fill the dip in the area distribution as shown. The body lines with these additions were still relatively smooth. Additions which lead to severely irregular body lines would not be recommended.

The effects of the changes in body shape on the total drag coefficients at Mach numbers up to 2.0 are shown in figure 7. The configurations are the same as those shown in figure 5. The results for Mach number above 1.15 were obtained in the Langley 4- by 4-foot supersonic pressure tunnel. For the swept-wing-body combination, body indentation had little effect on the drag at Mach numbers from 1.4 to 2.0. For the delta-wing-body combination, body indentation reduced the drag at all Mach numbers up to 2.0 but by a progressively smaller amount. The fact that reductions were obtained at these supersonic speeds indicates that to a certain extent the factors affecting drag at moderate supersonic speeds may be similar to those for transonic speeds for low-aspect-ratio thin wings such as this one. However, since the waves are conical rather than plane in nature when the Mach number is increased to supersonic values, it would be expected that the use of the transonic concept would not give the maximum reductions in drag possible at supersonic speeds.

Considering the conical nature of the flow at moderate supersonic speeds, a method has been developed which interrelates the wave drag of



SECRET

wing-body combinations at these speeds with axial distributions of cross-sectional area. With this method a number of area distributions are used to determine the drag at a given supersonic Mach number. These distributions are obtained by cutting the configuration with planes inclined to the airstream at the Mach angle. This method is basically the same as one developed by Jones considering the linear theory of Hayes. A description of the method, together with a discussion of its applications, is presented in the next paper by Robert T. Jones. However, some preliminary results obtained at Langley are presented in figure 8 which show how the drag may be reduced at supersonic speeds by reshaping the fuselage on the basis of this method. The results are for a delta-wing-body combination. The first three configurations shown are the same as those shown in figure 7. The body of the fourth configuration was indented circularly so that the various area distributions determined by this supersonic method for a Mach number of 1.4 were relatively smooth. It may be seen that this indentation reduced the total drag coefficients at supersonic speeds by significantly greater amounts than did the indentation designed for a Mach number of 1.0 (dashed line). At a Mach number of 1.4, the further reduction is roughly half the remaining pressure drag of the wing.

In conclusion, the results presented have shown that, near the speed of sound, the drag rise for a low-aspect-ratio thin wing-body configuration is generally a function of the axial distribution of cross-sectional area normal to the airstream. By using this relationship, it is possible to reduce greatly the drag rise of the conventional wing-body combinations by redesigning the fuselage to produce a smooth axial distribution of area for the combination. The resulting reshaped fuselage of the combination should not have abrupt changes in contour. Of course, to obtain the lowest possible drag coefficients, the fineness ratio of the equivalent body should be sufficiently high.

REFERENCE

1. Whitcomb, Richard T.: A Study of the Zero-Lift Drag-Rise Characteristics of Wing-Body Combinations Near the Speed of Sound. NACA RM L52H08, 1952.
- [REDACTED]
- [REDACTED]

0371229 1030

WING-BODY COMBINATION AND EQUIVALENT BODY OF REVOLUTION

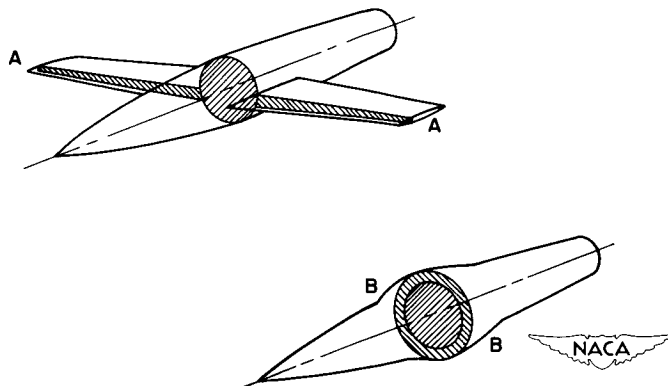


Figure 1

TRANSONIC FLOW PAST BODY WITH STRAIGHT WING

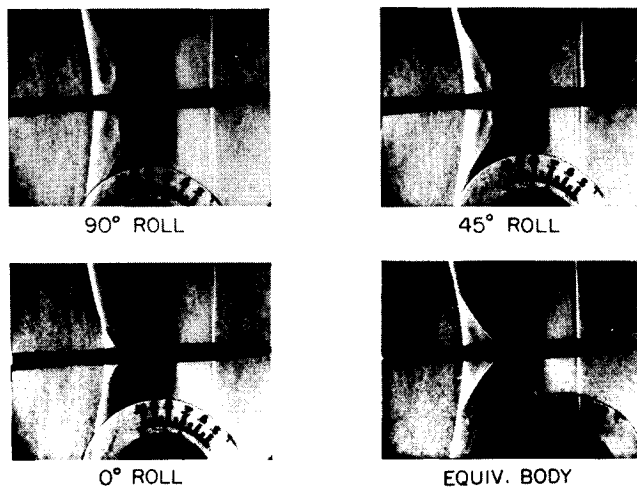


Figure 2

DECLASSIFIED

TRANSONIC FLOW PAST BODY WITH 45° SWEPT WING

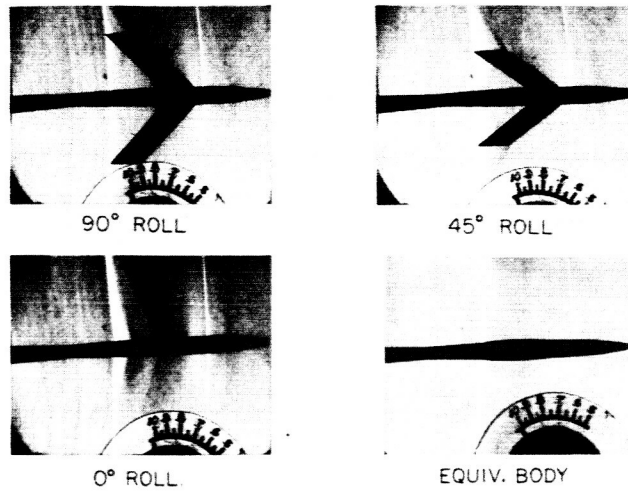


Figure 3



COMPARISON OF DRAG-RISE INCREMENTS AT $M=1.03$

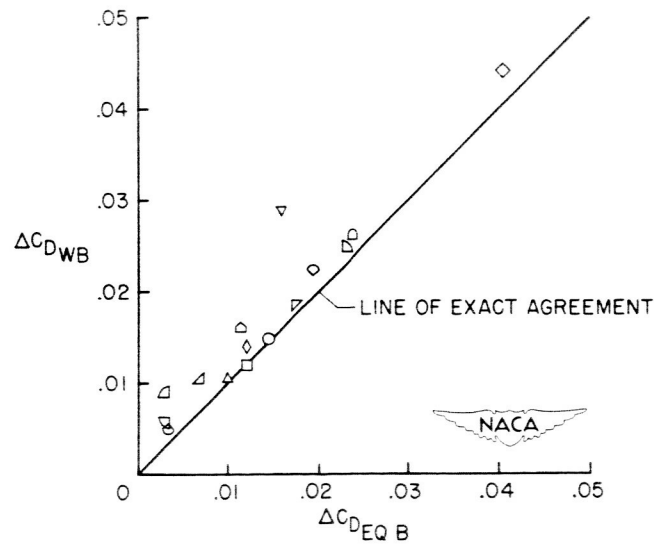





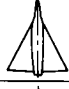
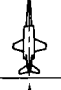
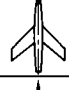
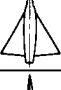
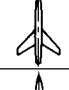


Figure 4(a)



CONFIDENTIAL

03712501030


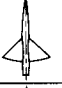
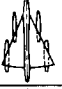


DETAILS OF CONVENTIONAL CONFIGURATIONS

PLAN FORM	Δ	A	t/c	λ	SYMBOL	PLAN FORM	Δ	A	t/c	λ	SYMBOL
	11° L.E.	2.6	.04	.2	○		52° L.E.	2	.06	.33	◻
	34° L.E.	4	.04	0	◻		60° L.E.	2.2	.04	0	◊
	23° L.E.	3	.045	.4	◊		45° C/4	4	.06	.6	◊
	60° L.E.	2.2	.03	0	◻		45° C/4	4	.06	.3	◻
	65° L.E.	1.87	.04	0	◻		45° C/4	3.5	.07	.3	◻

NACA

Figure 4(b)

DETAILS OF INDENTED CONFIGURATIONS

PLAN FORM	Δ	A	t/c	λ	SYMBOL
	11° L.E.	2.6	.04	.2	◻
	34° L.E.	4	.04	0	◻
	60° L.E.	2.3	.03	0	◻
	60° L.E.	2.2	.04	0	◻
	45° C/4	4	.06	.3	◊

NACA

Figure 4(c)

DECLASSIFIED

EFFECT OF BODY INDENTATION ON TRANSONIC DRAG RISE

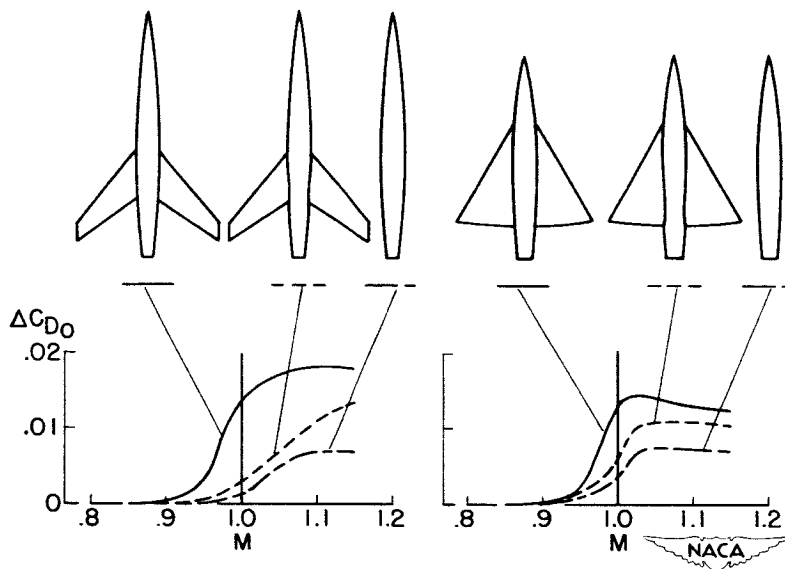


Figure 5

EFFECT OF ADDITIONS TO BODY

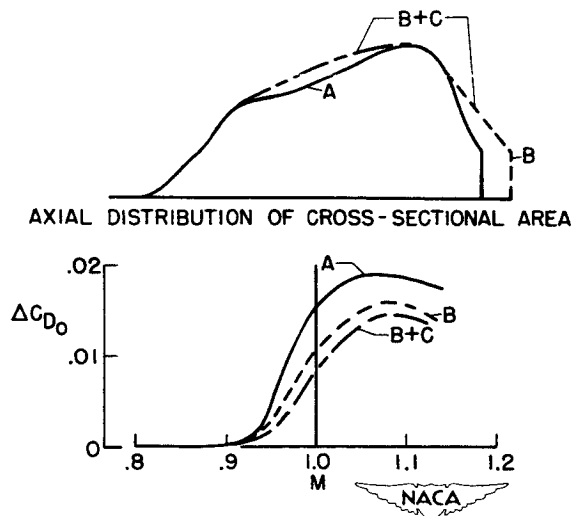


Figure 6

CONFIDENTIAL

03712301030

EFFECT OF BODY INDENTATION ON SUPERSONIC ZERO-LIFT DRAG

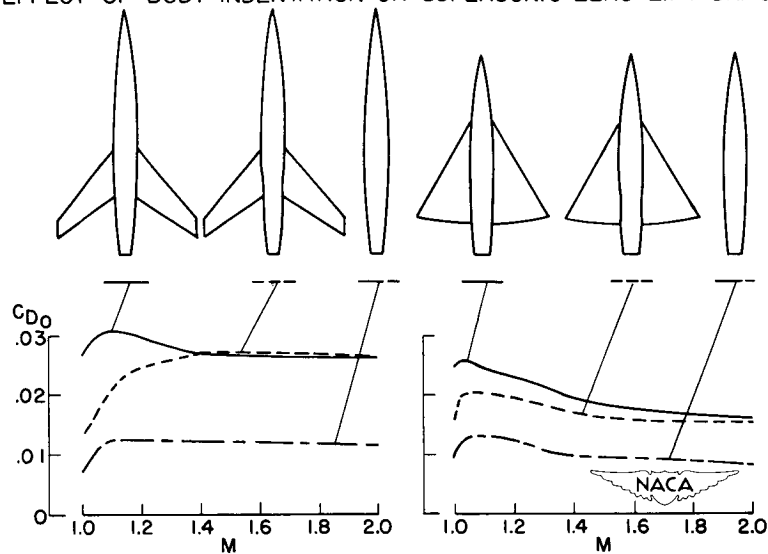


Figure 7

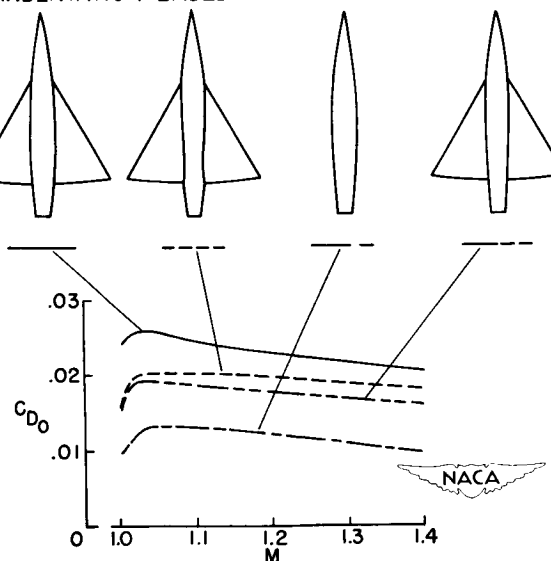
EFFECT OF INDENTATION BASED ON OBLIQUE AREA CUTS FOR $M=1.4$ 

Figure 8

CONFIDENTIAL

THEORY OF WING-BODY DRAG AT SUPERSONIC SPEEDS

By Robert T. Jones

Ames Aeronautical Laboratory

At subsonic speeds the pressure drag arising from the thickness of the body or wings is negligible as long as the shapes are sufficiently well streamlined to avoid flow separation. In that range there exists no possibility of either favorable or adverse interference on the pressure distributions themselves. If one body is so placed as to receive a drag from the pressure field of another, then the second body is sure to receive a corresponding increment of thrust from the first.

At supersonic speeds this tolerance, which was permitted the designer, disappears, and the drag becomes sensitive to the shape and arrangement of the bodies. The primary factor certainly is the thickness ratio; nevertheless, there exist arrangements in which a large cancellation of drag occurs. Examples of the latter are the sweptback wing and the Busemann biplane.

In the preceding paper Richard T. Whitcomb has shown how the drag at transonic speeds may be reduced to a surprising extent by simply cutting out a portion of the fuselage to compensate for the area blocked by the wing. The purpose of the present paper is to discuss some of the theoretical aspects of this method of drag reduction and to show how the basic idea may be extended to higher speeds in the supersonic range.

The deduction by Richard T. Whitcomb of the "area rule" was based on considerations of stream-tube area and the phenomenon of "choking," which follow from one-dimensional-flow theory. Each individual stream tube of a three-dimensional flow field must obey the laws of one-dimensional flow. Although the three-dimensional field cannot actually be determined on this basis alone, nevertheless it provides a good starting point for our thinking. The results demonstrate again the effectiveness of basic and simple considerations.

Although one-dimensional-flow theory thus provides a clue to the area rule, the necessary principle appears more specifically in the three-dimensional-flow theory. Thus, the formulas for wave drag given by linear theory, if followed toward the limit as M approaches 1.0 (from above), show that the wave drag of a system of wings and bodies depends solely on the longitudinal area distribution of the system as a whole. This phenomenon was first noted by W. D. Hayes in his 1946 thesis (ref. 1). For a more complete derivation of Hayes' formula the reader may consult reference 2. However, because of the limitations of the theory at transonic speeds, this result was not thought to be of

JONES



practical significance. Later G. N. Ward (ref. 3), E. W. Graham (ref. 4) and others, restricting themselves to very narrow shapes, expressed the wave drag in terms of the longitudinal area distribution for Mach numbers above 1.0, where the linear theory has a better justification.

It should be noted, however, that both of the problems cited are limiting cases of the more general problem of supersonic drag and it should be borne in mind that only in certain cases has it been possible to reduce the general theoretical formulas to the form of an area rule. It can be shown that the flow field about any system of bodies may be created by a certain distribution of sources and sinks over the surfaces of the bodies. Hayes' formula relates the drag of such a system to the distribution of these singularities. In order to obtain a formula for the wave drag in terms of area distributions, a simplified relation between the source strength and the geometry of the bodies, namely, that the source strength is proportional to the normal component of the stream velocity at the body surface, has been adopted.

There are examples (e.g., Busemann biplanes) for which this assumption is not valid. If, on the other hand, we limit ourselves to thin symmetrical wings mounted on vertically symmetrical fuselages, there are indications that a good estimate of the wave drag at supersonic speeds can be obtained on the basis of the simplified relation assumed.

If Hayes' method of calculation is followed, at $M = 1.0$ the expression for the wave drag of a system of wings and bodies reduces to Von Kármán's well-known formula for the wave drag of a slender body of revolution, that is,

$$D_{(M \rightarrow 1.0)} = \frac{\rho V^2}{4\pi} \int_{-l/2}^{l/2} \int_{-l/2}^{l/2} S''(x) S''(x_1) \log |x - x_1| dx dx_1$$

Here $S(x)$ represents the total cross-sectional area intercepted by a plane perpendicular to the stream at the station x (see fig. 1) and $S''(x)$ is the second derivative of S with respect to x . If Sears method (ref. 5) is followed, $S'(x)$ may be expanded in a Fourier's series and, in this way, a formula for the drag which is completely analogous (ref. 6) to the well-known formula for the induced drag of a wing in terms of its spanwise load distribution may be obtained. Thus, if

$$x = \frac{l}{2} \cos \theta$$

DECLASSIFIED

and

$$S'(x) = \sum A_n \sin n\theta$$

(see fig. 2), the wave resistance is

$$D = \frac{\pi \rho V^2}{8} \sum n A_n^2$$

Of all the terms of the series, each contributes to the drag but only A_1 and A_2 contribute to the volume or the base area of the system. Thus, in order to achieve a small drag with a given base area or with a given over-all volume within the given length, the higher harmonics in the curve $S'(x)$ should be suppressed. This formula enables us to classify a given shape as "rough" or "smooth" in a quantitative fashion.

In order to extend these considerations to supersonic speeds a series of cross sections of the system made, not by planes perpendicular to the stream but by planes inclined at the Mach angle or "Mach planes" must be considered. By means of a set of parallel Mach planes (fig. 3), an "equivalent body of revolution" using the intercepted areas was constructed and the drag was computed by Von Kármán's formula. The theoretical basis of this step is the fact that the complete three-dimensional disturbance field may be constructed by the superposition of elementary one-dimensional disturbances in the form of plane waves. (See ref. 7.) It is evident that the set of parallel Mach planes may be placed at various angles around the x-axis (fig. 3). When the flow field is constructed, it is necessary to superimpose disturbances at all these angles and, when the drag is completed, to consider the drag of all the equivalent bodies of revolution. The final value of the drag is simply the average of the values obtained through a complete rotation of the Mach planes.

In order to make these statements more specific, the equation of one such Mach plane may be written as follows:

$$X = x - y' \cos \psi - z' \sin \psi$$

where $y' = \sqrt{M^2 - 1} y$ and $z' = \sqrt{M^2 - 1} z$. By assigning different values to X while keeping ψ constant, a series of parallel planes at the same angle ψ around the x-axis is obtained. By assigning different values to ψ while keeping X constant, a set of planes enveloping that Mach cone whose apex lies at the point $X = x$ can be obtained.

CONFIDENTIAL



After a value of ψ is selected, the wing-body system is cut through with a series of planes corresponding to different values of X . The total intercepted area in each plane is then equated to the area intercepted by this plane passing through the equivalent body of revolution. If we denote the area intercepted obliquely by $s(X, \psi)$, then the area $S(X, \psi)$ is defined by:

$$S(X, \psi) = s(X, \psi) \sin \mu$$

where μ is the Mach angle (i.e., $\sin \mu = \frac{1}{M}$). The term $S(X, \psi)$ is thus the area intercepted by normal planes passing through the equivalent body of revolution on the assumption that this body is slender. Therefore,

$$S'(X, \psi) = \frac{\partial}{\partial X} S(X, \psi) = \sum A_n \sin n\theta$$

with

$$\cos \theta = \frac{X}{X_0}$$

Here, however, both the length $2X_0$ and the shape of the equivalent body vary with the angle ψ . The drag of each equivalent body of revolution, which is denoted by $D'(\psi)$, is then determined by applying Sears' formula:

$$D'(\psi) = \frac{\pi \rho V^2}{8} \sum n A_n^2$$

The total drag of the wing-body system is the average of all these values between $\psi = 0$ and $\psi = 2\pi$; that is,

$$D = \frac{1}{2\pi} \int_0^{2\pi} D'(\psi) d\psi$$

In general, the coefficients A_n are functions of the angle of projection ψ . However, the calculation shows that the first two coefficients A_1 and A_2 are again related in a simple way to the base area and the volume V . Thus,



DECLASSIFIED

$$A_1 = \frac{2}{\pi} \frac{S(X_0)}{X_0}$$

$$A_2 = 2A_1 - \frac{4}{\pi} \frac{V}{X_0^2}$$

None of the higher coefficients contribute to the base area or volume, but they invariably contribute to the drag.

The rules for obtaining a low wave drag now reduce to the rule that each of the equivalent bodies obtained by the oblique projections should be as smooth and slender as possible, the "smoothness" again being associated with an absence of higher harmonics in the series expression for $S'(X)$.

In order to check the agreement between these theoretical formulas for the wave drag and experimental values, comparisons of the calculations with the results of tests made on falling models at Ames Aeronautical Laboratory have been made. This comparison was made by George H. Holdaway who supplied the accompanying illustration (fig. 4). In some of these cases it was found necessary to retain more than 20 terms of the Fourier's series in order to obtain a convergent expression for the drag.

If the variety of the shapes represented here are considered, the agreement is certainly as good as can be expected from the linear simplifications. The agreement is naturally better in those interesting cases in which the drag is small.

Figure 5 shows an analysis of one of the experiments of Richard T. Whitcomb. The linear theory, of course, shows the transonic drag rise simply as a step at $M = 1.0$. Such a variation may be expected to be approached more closely as the thickness vanishes. In order to represent actual values here, a nonlinear theory would be needed. For many purposes, it will be sufficient to estimate roughly the width of the transonic zone by considerations such as those given in reference 8. In the present case it will be noted that agreement with the linear theory is reached at Mach numbers above about 1.06 and the linear theory clearly shows the effect of the modification.

For further theoretical studies of wing-body drag, shapes have been selected that are especially simple analytically, namely, the Sears-Haack body and the biconvex wing of elliptic plan form. Figure 6 shows the effect of wing proportions on the variation of wave drag with Mach number, both with and without the Whitcomb modification. In each case, the modification has the effect of reducing the wave drag to that of the body



alone at $M = 1.0$. In the case of the low-aspect-ratio wing, this drag reduction remains effective over a considerable range of higher Mach numbers. With the higher aspect ratio, however, the drag increases sharply at higher speeds so that, at $M = 1.6$, the modification nearly doubles the wave drag.

The rapid increase of drag in the case of the high-aspect-ratio wing is, of course, the result of the relatively abrupt curvatures introduced into the fuselage lines by the cutout. Such abrupt cutouts are necessarily associated with wings having small fore-and-aft dimensions, that is, unswept wings of high aspect ratio.

These considerations led us to the problem of determining a fuselage shape for such wings that is better adapted to the higher Mach numbers. The first step in this direction is obviously simply to lengthen the region of the cutout; thus, the rapid increase of drag with Mach number is avoided. The problem of actually determining the best shape for the fuselage cutout at any specified Mach number has been undertaken by Harvard Lomax and Max. A. Heaslet at Ames Laboratory. Their solution of this problem provides a definite method for determining the distribution of sources and sinks along the fuselage axis that will achieve a minimum value of the drag for a given wing shape at any specified Mach number. Furthermore, by admitting singularities of higher order, quadrupoles, and so forth, which would distort the rotational symmetry of the fuselage, they have been able to show that the wave drag of a wing-body system can be reduced, in principle at least, to a minimum value associated with the given over-all length and volume of the system, that is, to the value for a simple Sears-Haack body containing the whole volume of the system.

By adopting the simplified relation between the source strength and the body shape, the result of this theory may be described by a relatively simple concept, which is illustrated by figure 7. If modifications of the first type only are considered, the problem is to determine the area ΔS_f to be removed from the fuselage to make the best compensation for a given wing. (See fig. 7.) If a station along the fuselage axis and a Mach plane passing through this station are selected, this plane can be revolved around the axis, and at each angle ψ the normal projection, or frontal projection, of the area intercepted where the plane cuts through the wing can be measured. After these areas are plotted against ψ and integrated between 0 and 2π , the term $-\Delta S_f$ is obtained as the average of the values of S_w . At any Mach number the total volume to be subtracted from the fuselage is equal to the wing volume. At higher Mach numbers, since the modification extends over a greater length, the area subtracted at individual cross sections becomes less.

Figure 8 shows the calculated result of designing the fuselage cutout for a specific Mach number, $M = 1.2$ in this case. The lower curve



DECLASSIFIED

is an envelope showing the minimum values that can be achieved by such a radially symmetric cutout.

Figure 9 shows the magnitude of the gains that are possible by higher-order modifications of the fuselage shape. There are three lower bounds here and the symbols a_0 , a_2 , . . . attached to them refer to a representation of the fuselage shape by singularities of increasingly higher order. The curve labeled a_0 is that given in figure 8 and shows the maximum effect of radially symmetric modifications. Although the fuselage shapes for the other curves have not actually been determined, the curve labeled $a_0 + a_2$ may be thought of as referring to a cutout with an additional elliptic modification. It will be interesting to pursue this investigation further and ascertain just how the fuselage must be distorted to cancel the wave drag of the wing completely, as indicated by the lowest envelope curve. Of course, it will be necessary to start with a certain minimum diameter in order to preserve a real shape.


In order to test this theory of determining optimum body shapes we have started a program, using models similar to those investigated theoretically. Several of these models have already been tested in the Ames 2- by 2-foot wind tunnel and the results agree fairly well with calculations made on the assumptions given earlier. Figures 10 and 11 show the theoretical and the experimental curves. The aspect ratio of the wing in these preliminary cases is not sufficiently high ($A = 2$) to enable really striking gains to be shown. However, it is evident that the calculated differences are all reproduced in the experimental values. The experimental series include models having higher aspect ratios and more significant gains are expected to appear.

There are, of course, examples of wing-body systems which would hardly benefit by any change in shape of the fuselage. It is easy to decide whether a gain is possible or worthwhile by comparing the actual wave drag of the system with that of a Sears-Haack body containing the over-all volume of the system. In the case of a 63° wing-body combination (ref. 9), this comparison yields 0.0045 as a lower bound for the wave drag coefficient and 0.005 for the actual value. In such cases, for which the wave drag is initially very low, further reduction by reshaping the fuselage is not worthwhile. Appreciable savings in drag, however, can be made in many cases by a calculated shaping of the fuselage. Unswept wings of high aspect ratio are benefited most and require the most careful consideration of the fuselage shape.

These new developments illustrate again the fact that the disturbance fields at transonic and supersonic speeds are essentially three-dimensional phenomena. It was not long ago that our ideas concerning the wing section, which had their origin in the older incompressible flow theory, had to be relinquished because of the predominating effects of wing plan form. Now the wing and the fuselage must be designed together.

[REDACTED]

03713001300
REFERENCES

1. Hayes, Wallace D.: Linearized Supersonic Flow. Rep. No. AL 222, North American Aviation, Inc., June 18, 1947, pp. 94-95.
 2. Heaslet, Max. A., Lomax, Harvard, and Spreiter, John R.: Linearized Compressible-Flow Theory for Sonic Flight Speeds. NACA Rep. 956, 1950. (Supersedes NACA TN 1824.)
 3. Ward, G. N.: Supersonic Flow Past Slender Pointed Bodies. Quarterly Jour. Mech. and Appl. Math., vol. II, pt. 1, Mar. 1949, pp. 75-97.
 4. Graham, Ernest W.: Pressure and Drag on Smooth Slender Bodies in Linearized Flow. Rep. No. SM-13417, Douglas Aircraft Co., Inc., Apr. 20, 1949.
 5. Sears, William R.: On Projectiles of Minimum Wave Drag. Quarterly Appl. Math., vol. IV, no. 4, Jan. 1947, pp. 361-366.
 6. Busemann, A.: Heutiger Stand der Geschosstheorie. Bericht 139 der Lilienthal-Gesellschaft für Luftfahrtforschung, 1941, pp. 5-13.
 7. Jones, Robert T.: Theoretical Determination of the Minimum Drag of Airfoils at Supersonic Speeds. Jour. Aero. Sci., vol. 19, no. 12, Dec. 1952, pp. 813-822.
 8. Busemann, Adolf: Application of Transonic Similarity. NACA TN 2687, 1952.
 9. Jones, Robert T.: Estimated Lift-Drag Ratios at Supersonic Speed. NACA TN 1350, 1947.
- 

DECLASSIFIED

CALCULATION OF WAVE DRAG FOR $M \rightarrow 1.0$

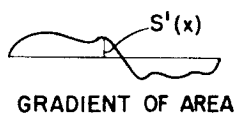
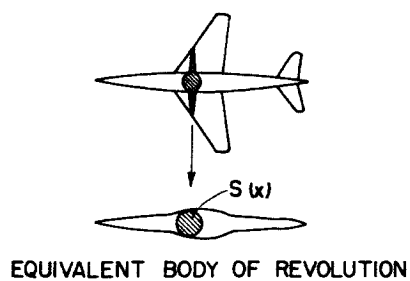
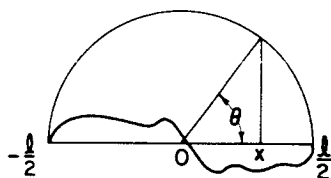


Figure 1

CALCULATION OF WAVE DRAG FOR $M \rightarrow 1.0$



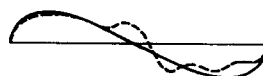
FOURIER'S SERIES;

$$S'(x) = \sum A_n \sin n\theta$$

$$x = \frac{1}{2} \cos \theta$$

WAVE DRAG: ($M \rightarrow 1.0$)

$$D = \frac{\pi \rho V^2}{8} \sum_n A_n^2$$



OPTIMUM SHAPE;

$$S'(x) = A_2 \sin 2\theta$$

(SEARS-HAACK BODY)



Figure 2

CONFIDENTIAL

03712201030

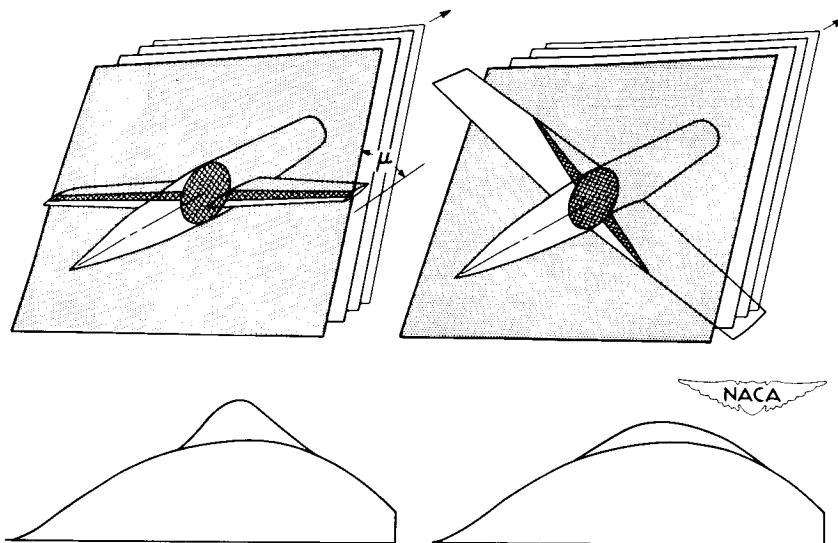
AREA DIST. GIVEN BY INTERSECTIONS OF
MACH PLANES

Figure 3

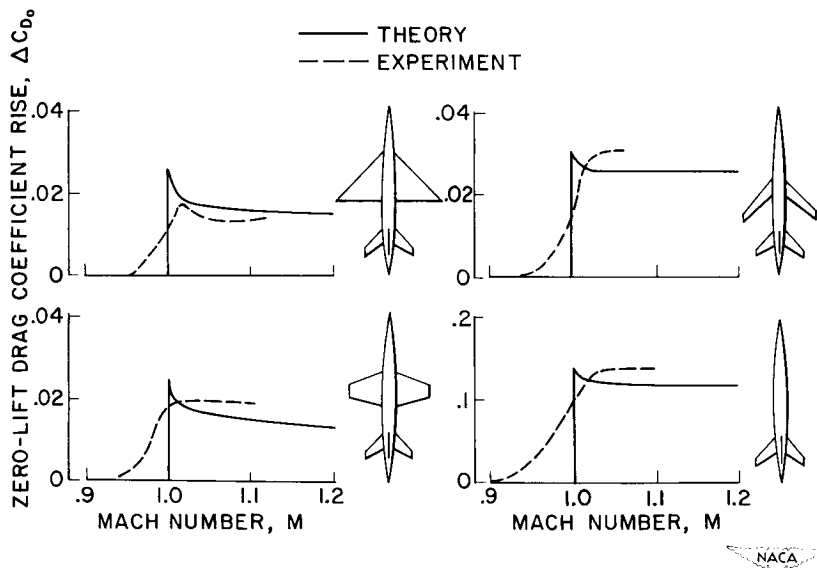
COMPARISON OF THEORY WITH RESULTS OF
AMES LAB. DROP TESTS

Figure 4

DECLASSIFIED COMPARISON OF WHITCOMB'S EXPERIMENTS WITH THEORY

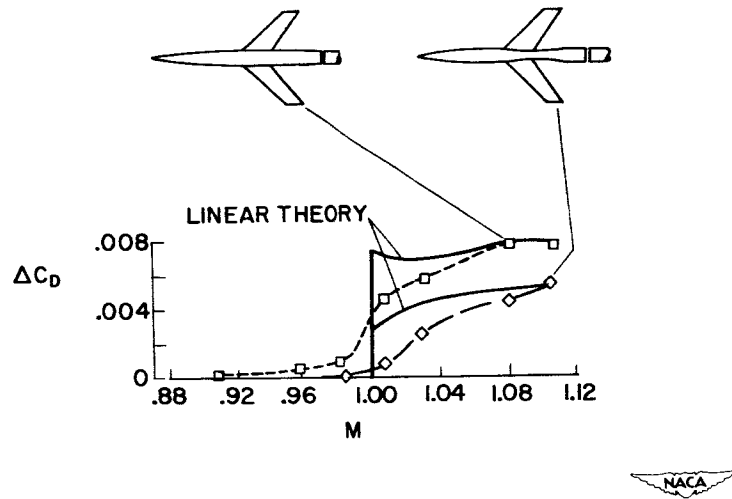


Figure 5

EFFECT OF WHITCOMB MODIF. ON CALCULATED WAVE DRAG

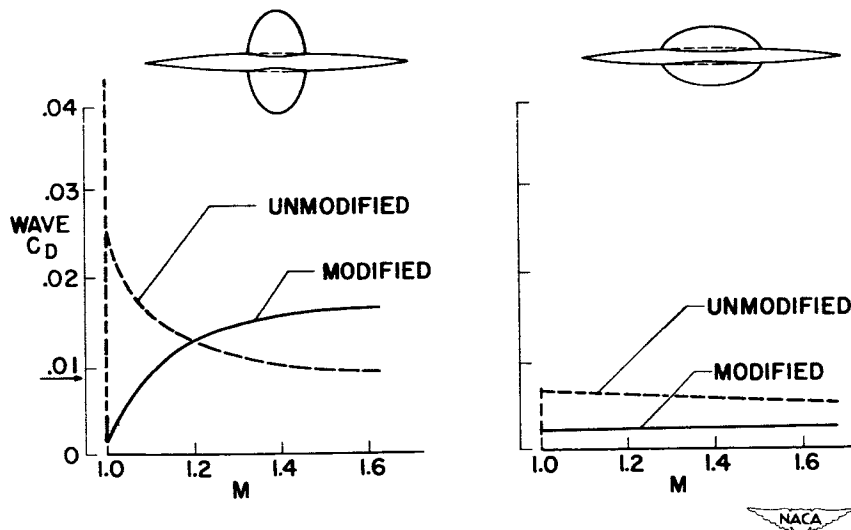
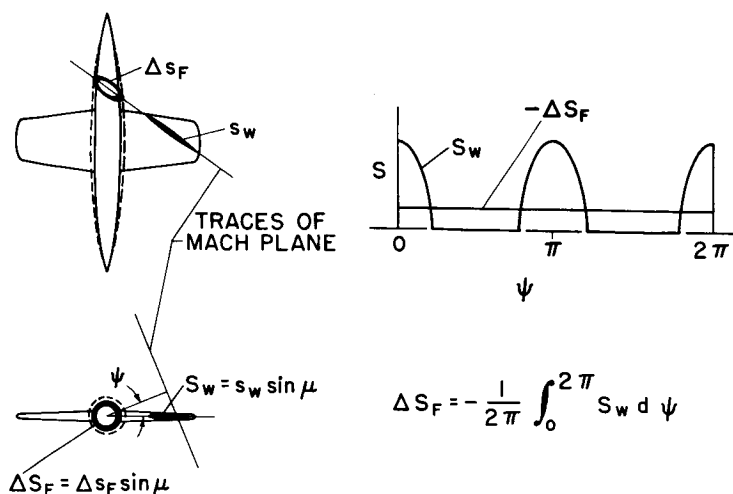


Figure 6

CONFIDENTIAL

03772501030

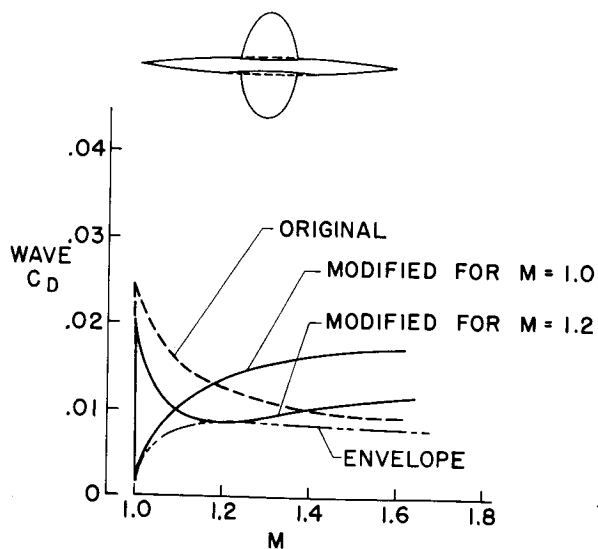
DESIGN OF FUSELAGE MODIFICATION FOR SPECIFIED MACH NUMBER



NACA

Figure 7

EFFECT OF MODIF. DESIGNED FOR A SPECIF. MACH NUMBER



NACA

Figure 8

ENVELOPES FOR DRAG AT DESIGN MACH NUMBER

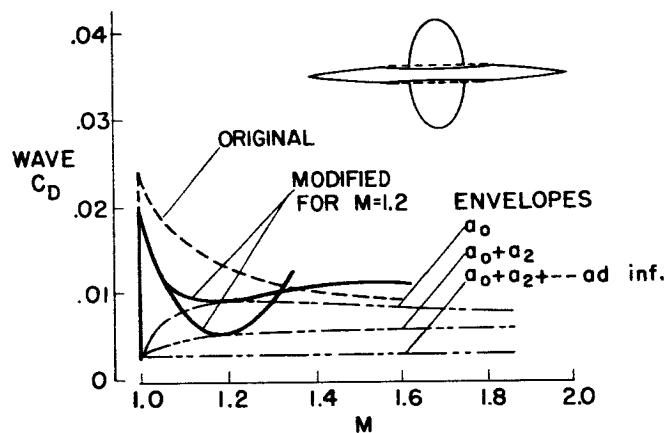


Figure 9

EXPERIMENTS ON BODIES WITH ELLIPTIC WINGS

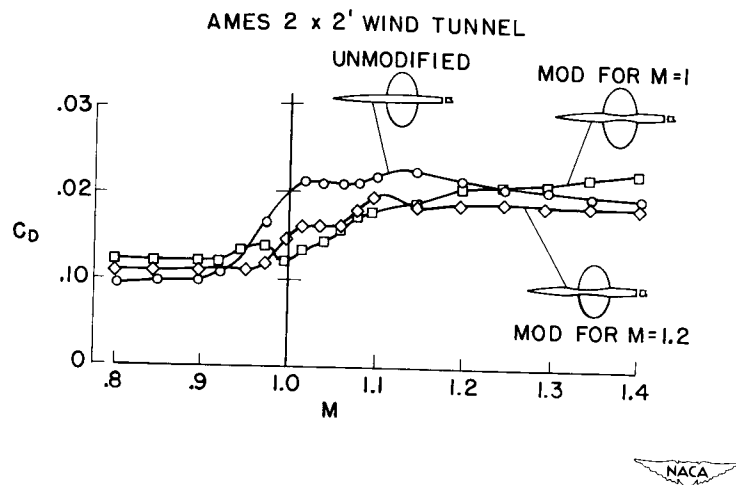


Figure 10

CALCULATED VALUES FOR BODIES WITH ELLIPTIC WINGS

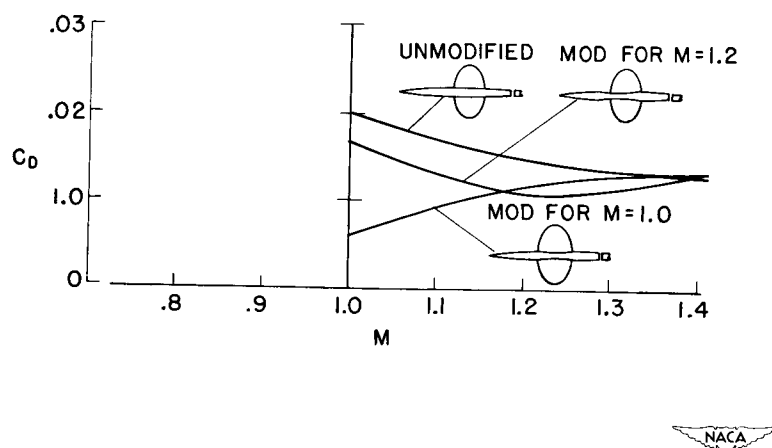


Figure 11

DECLASSIFIED

CONFIDENTIAL

DRAG OF EXTERNAL STORES AND NACELLES AT TRANSONIC

AND SUPERSONIC SPEEDS

By Norman F. Smith, Ralph P. Bielat, and Lawrence D. Guy


Langley Aeronautical Laboratory

INTRODUCTION

The problem of designing nacelles and stores is one of providing the desired volume in an acceptable shape or position at the lowest possible cost in airplane performance. There is considerable evidence that such volume can often be more efficiently carried within the basic wing-body combination, especially at supersonic flight speeds. Discussion of submerged or integral arrangements, however, involves complex design studies which are beyond the scope of this paper. This paper deals entirely with external stores and nacelles, primarily wing-mounted on airplane-type configurations. The status of the problem is reviewed and the research which has been done on the subject examined in the light of recent developments.

DISCUSSION

Figure 1 shows a plot of drag coefficient based upon individual frontal area against Mach number. The shaded areas show the Mach numbers and drag-coefficient values corresponding to nacelles and stores which have been investigated to date. All of these data have been published. A list of the ones which are used in detail in this paper is given in the references. The values of drag coefficient which have been obtained in the transonic range vary from above 0.8 to near zero. At the three higher supersonic Mach numbers, the values vary from nearly 0.8 to around 0.23. The lower shaded band shows the range of drag values covered by isolated-body drags for satisfactory supersonic bodies of fineness ratio 6 to 9, approximately (refs. 1, 2, and others). This figure shows that zero interference and even greatly beneficial interference have been obtained on configurations in the transonic range up to $M = 1.2$ (refs. 3 to 5, for example). Apparently, however, no beneficial interference has yet been encountered with airplane-type configurations at the three higher supersonic Mach numbers shown, and only in a few cases has interference near zero been attained. It should be noted here that nacelle drags near zero have in some cases been obtained for large ram-jet nacelles mounted on missile configurations (ref. 6). This large favorable interference was obtained in extreme aft positions wherein half the nacelle length



SMITH, BIELAT
& GUY

extended beyond the fuselage base, positions very different from those used for airplane nacelles. (Further evidence of large favorable interference for nacelles in this region has been found in the theoretical work of ref. 7.)


The store and nacelle data which make up these shaded areas in figure 1 have been examined in detail to determine some of the factors which govern the drag of these installations.

Transonic Speeds

The drag level for nacelles or stores at subsonic Mach numbers is important, of course, as is the Mach number at which drag rise begins. The principles governing these items are relatively well known and are not discussed herein.

In the transonic region, the type of flow which follows the onset of shocks - with shock interactions and interference, local choking, separation, and so forth - is very complex. The interference problem is therefore a very difficult one for theoretical treatment. Also, the nature of the flow plus the large number of configuration variables involved makes experimental investigation difficult in that results tend to be rather specific in nature. It is therefore of interest to apply a simplifying principle, when one is available, such as the transonic area rule discussed in a previous paper by Richard T. Whitcomb. Consequently, the bulk of the transonic data which have been obtained on stores and nacelles, most of which have been published and analyzed with respect to spanwise and chordwise position, has been re-examined in the light of the area rule.

Figure 2 shows the transonic drag-rise data for the series of spanwise symmetrically mounted nacelles tested in flight by the Langley Pilotless Aircraft Research Division on a 45° swept wing of aspect ratio 6, $t/c = 0.09$ (ref. 5). On the right-hand side of the figure is a sketch which shows the location of the nacelle and a diagram of the cross-sectional area variation of each configuration. In this figure and in figures 3 and 4, the data are plotted as drag increments above the level for $M = 0.8$ in order to eliminate the skin-friction drag. Figure 2 shows that the highest drag rise is obtained with the nacelle position giving the highest peak on the area diagram and the highest slopes forward and aft. The lowest drag is obtained with the nacelle position which affects the wing-body area diagram least. In looking at the transonic drag rises in terms of spanwise variation of nacelle position, it is noted that the drag is least at the tip, rises to a peak value at $0.4b/2$, and decreases again as the nacelle is moved still farther inward to $0.18b/2$. This phenomenon had thus far gone unexplained. The area rule provides, in this case and others to be mentioned subsequently,



a simple explanation. It will be noted that the differences between the drag curves are small. This is a result of the fact that these nacelles are small, corresponding roughly to single-engine units.

Figures 3 and 4 show similar results obtained from wind-tunnel tests conducted in the Langley 8-foot transonic tunnel and 4- by 4-foot supersonic pressure tunnel (refs. 8 to 10 and some unpublished data) of a sting-mounted configuration involving a series of nacelles of twin-engine size on a swept wing of aspect ratio 3.5 with 47° sweep and a thickness ratio of 6 percent. The series shown in figure 3 is a family of pylon-mounted nacelles which involves a forward and downward movement at one spanwise station, and the series in figure 4 consists of different types of nacelles. Again correlation with the area diagram is clear, with the top configurations having the least favorable area diagrams and the highest transonic drag rises.

The equivalent stream-tube area corresponding to the internal flow has been subtracted from the areas shown in figure 4. Note the particularly low drag rise for the installation buried in the wing root with provisions for air intake at the leading edge. This installation is actually more a submerged installation than an external one but is shown here because of its excellent drag characteristics and because it was a part of the test series. Plots of drag-rise data for the configurations shown in these two figures at lift coefficients up to 0.5 have been made and show that the curves maintain the same relationship to each other as do the curves shown here for $C_L = 0$.

Examination of the nacelle and store information from the Langley Pilotless Aircraft Research Division, 7- by 10-foot tunnels, and 8-foot transonic tunnel shows area-diagram correlations consistent with those shown in these three examples.

The dashed lines in figures 3 and 4 connect the limited number of supersonic points which are available for some of these configurations. The supersonic points in figure 3 show that the high drag levels obtained transonically do not necessarily persist into the supersonic speed range. The indication is thus that the requirements for low wave drag in the transonic range may be different from those in the supersonic speed range. The supersonic range will be treated in more detail subsequently.

Because interpretation of area diagrams tends to become somewhat indefinite in some cases, a very simple parameter concerning the area diagram has been devised. In figure 5 the data from the series of different nacelles and the series of pylon-mounted nacelles, most of which were shown in figures 3 and 4, have been plotted as incremental drag coefficients against x/l , where x is the distance from the area peak of the wing-fuselage combination to the area peak of the complete-model configuration, the areas having been obtained by sectioning the models

CONFIDENTIAL

in planes perpendicular to the longitudinal axis. Data for $M = 1.0$ are shown at the left; data for $M = 1.1$, at the right. The $M = 1.1$ condition corresponds to the completion of the drag rise, while at $M = 1.0$ the drag values are still rising rapidly. The correlation at both Mach numbers is very good. A number of different nacelle configurations and different types of area diagrams are involved, as will be remembered from figures 3 and 4. The correlation shows that the highest drags are obtained when the area peaks coincide, with the drag decreasing rapidly as the area peaks are displaced. Note that the parameter used does not show effects of area coincidence alone. As the peaks are moved, slope changes forward and aft also occur. This parameter is therefore only one small step removed from visual interpretation of the area diagram.

Thus, by reanalysis of a large amount of nacelle and store data, it was found that correlation with the area rule is found for many types of nacelles or stores in positions from wing root to wing tip, and that explanation of phenomena not heretofore explained is afforded. Because the configurations considered were all designed without regard for the area rule, it is very difficult to extract quantitative data from this work. Changes in area-diagram characteristics from one configuration to another involve random simultaneous changes in peak height, local slopes, and over-all shapes. Controlled experiments are needed to provide valid quantitative data.

Proof of the importance of the area rule is strengthened by demonstration of its use in the design of configurations complete with nacelles. Figures 6 and 7 show unpublished results for two delta-wing configurations from wind-tunnel and flight tests by the Pilotless Aircraft Research Division. The configuration shown in the left side of figure 6 has an area diagram which shows a very high peak and high slopes forward and aft, due largely to the nacelles. The drag for this configuration is very high, as is the drag (plus interference) for the nacelles, obtained by subtraction. Data obtained in the Langley 16-foot transonic tunnel for the same configuration, but with air flow through the nacelles, show somewhat lower drag. The area diagram for this case, which is reduced by allowance for the equivalent stream-tube area through the nacelles, is shown by the long dashed lines.

A sketch of a second version of this configuration is shown in the right side of this figure. The wing ~~was~~ enlarged and thinned somewhat and the nacelles were split into forward and aft pairs. The fuselage was lengthened and was undercut slightly in order to make the area diagram for the complete configuration correspond closely to a parabolic distribution of higher fineness ratio than the previous model. The drag curve shows a drag reduction for this configuration of nearly 50 percent, or 40 percent of the configuration at left with air flow. The nacelle contribution in this case is not known, but it is clear that a similar reduction in nacelle drag and interference has occurred.




Figure 7 shows that in both of these cases, the drag characteristics of the complete configuration are closely simulated by drag characteristics of the body of revolution having an equivalent longitudinal area development. The measured drags for the equivalent bodies have been corrected to the skin-friction level of the complete configuration in each case. The configuration at the left is one of the configurations discussed by Richard T. Whitcomb in a previous paper wherein the item of equivalent bodies was treated in some detail.

Supersonic Speeds

In the supersonic speed range, the bulk of the experimental data, which have been obtained in addition to the data from the Langley 4- by 4-foot supersonic pressure tunnel shown in figures 3 and 4, is that obtained in the Langley 9- by 12-inch supersonic blowdown tunnel (refs. 11 to 13). Figure 8 shows the configurations tested: a half-model fuselage with a semispan unswept, a 45° swept, and a 60° delta wing. The store is of the Douglas store shape and was tested with the store center of gravity in the locations shown on the sketches. The store and wing surfaces were tangent for those chordwise positions where the maximum thicknesses coincided and were separated by a very short pylon for other positions. The store size may be considered to correspond roughly to a single-engine nacelle on a large bomber airplane.

The data presented in figure 9 are plotted in the form of store-plus-interference drag C_{D_N} against spanwise position for $M = 1.41$ and 1.96 .

Data for $M = 1.62$ are also available and agree well with the other two Mach numbers but are omitted here for simplicity. The data show that, in general, for all three wing configurations, moving the store outward decreases the store drag. A similar plot of chordwise positions (fig. 10) shows that moving the store forward decreases the drag. Exceptions to these generalizations are evident, however, in the solid symbols connected by dashed lines for the swept and delta wings, for which positions the drag is a great deal lower than would be expected or predicted by a straight line drawn through the remaining symbols.

Attempts to correlate these and some unpublished data on the basis of nacelle position with respect to the wing leading edge, fuselage nose Mach line, wing local maximum thickness, to mention a few, all failed - if any correlation was obtained it contained exceptions which could not be explained. This difficulty of correlating or generalizing is, of course, similar to that mentioned previously for nacelle and store studies at transonic speeds.

An extension of the transonic area rule was utilized in an attempt to correlate these data. The more complete supersonic theory, which



involves sectioning the configuration by a series of planes tangent to Mach cones, has been described in a previous paper by Robert T. Jones.


The method used here, as an exploratory approach, involves only one set of the planes indicated by the theory; that is, parallel vertical planes which intersect the configuration plan form along Mach lines. It will be noted that the fuselage in this case employed a cylindrical afterbody. The fuselage nose, therefore, can affect the pressure drag of the nacelle and wing, but the nacelle and wing cannot appreciably affect the pressure drag of the fuselage afterbody. It therefore appeared that the principal lines of influence or interference were Mach lines originating at the fuselage center line and that sectioning or viewing the model along these particular Mach lines might correlate the principal variations. Figure 11 shows the results of the correlation. The drag data for all the configurations shown in figure 8 have been plotted against x/l , which is the area-peak displacement parameter defined in the sketch (top part of fig. 11). (x is the distance between the peak of the area diagram of the store and the peak of the area diagram of the wing-fuselage combination, the area diagrams being obtained by sectioning the semispan configuration along Mach lines in the lateral plane and plotting the cross-sectional area given by each slice at the intercept on the fuselage center line.)

Clearly, the data show a strong trend similar to the one shown in figure 5 for the transonic case. If located in a region where its area peak adds to the wing-fuselage peak (viewed along the Mach line), the store produces higher drag than if located a short distance forward or aft of the $X = 0$ point. It will be noted that data from three different wing configurations, a straight, a swept, and a delta wing, and data at three supersonic Mach numbers, 1.41, 1.62, and 1.96, are all included in this plot.

This correlation plot explains the low drag points which appeared to contradict the spanwise and chordwise trends shown in figures 9 and 10. The solid symbols to the right of $x/l = 0$ are for these configurations. These drag values are in proper positions as located by the area diagram parameter x/l , and the low drag is explained by area-peak displacement.

It will be noted that at neither end of the curve of figure 11 has a minimum drag been reached. This means that minimum drag values will be attained at more extreme forward or aft nacelle positions than those tested. Practical difficulties may appear, however, in using such positions for airplane configurations.

There is considerable scatter of points from the trend line which has been drawn through the data. Only a part of this scatter can be explained by the data-accuracy spread shown by the width of the trend line. Some scatter in any correlation of this kind is to be expected, inasmuch as it is not reasonable to expect a perfect explanation of a complicated




flow condition in terms of this very simple parameter. There are a large number of details which can greatly affect the drag. These details are wing-fuselage and wing-nacelle junctures, the detail design of each component, the effects of localized shock patterns, and so forth. Such details would influence the pressure drags to some extent and would particularly influence the friction drag which is not included in the area rule.


It should be mentioned that attenuation of interference effects as bodies are separated is also involved in the supersonic case. This factor causes the pressure interference between store and fuselage to diminish as the store is moved tipward on the wing. This item is included in the complete treatment mentioned previously which considers all the planes. The interference problem in the case of the tipward store is reduced to one of local interference of a more familiar nature between wing and store.


CONCLUSIONS

The following conclusions are indicated:

1. The transonic area rule can be applied to configurations involving many kinds of stores or nacelles in locations from wing root to wing tip.
 2. The area rule is shown to function at supersonic Mach numbers in a similar fashion, utilizing in this first analysis, sectioning vertically along Mach lines originating at the fuselage center line.
 3. The appreciable scatter which is present in the area-rule correlations may be reduced in later refinements but will always be present because of detail conditions or differences. It is emphasized, therefore, that good detail design of components, junctures, and so forth, must be adhered to. The area rule then offers a useful means by which the designer may arrange or integrate these components into the complete configuration having the best possible area and drag characteristics.
 4. Quantitative data are lacking in all correlations because this analysis was based upon previous investigations which were not planned for obtaining such data. Further research is needed, using the area rule and other theory as a guide, to obtain quantitative design data on the interference and optimum location of stores and nacelles.
- 

REFERENCES

1. Jackson, H. Herbert, Rumsey, Charles B., and Chauvin, Leo T.: Flight Measurements of Drag and Base Pressure of a Fin-Stabilized Parabolic Body of Revolution (NACA RM-10) at Different Reynolds Numbers and at Mach Numbers From 0.9 to 3.3. NACA RM L50G24, 1950.
 2. Hart, Roger G., and Katz, Ellis R.: Flight Investigations at High-Subsonic, Transonic, and Supersonic Speeds To Determine Zero-Lift Drag of Fin-Stabilized Bodies of Revolution Having Fineness Ratios of 12.5, 8.91, and 6.04 and Varying Positions of Maximum Diameter. NACA RM L9I30, 1949.
 3. Welsh, Clement J., and Morrow, John D.: Effect of Wing-Tank Location on the Drag and Trim of a Swept-Wing Model As Measured in Flight at Transonic Speeds. NACA RM L50A19, 1950.
 4. Silvers, H. Norman, and King, Thomas J., Jr.: A Small-Scale Investigation of the Effect of Spanwise and Chordwise Positioning of an Ogive-Cylinder Underwing Nacelle on the High-Speed Aerodynamic Characteristics of a 45° Sweptback Tapered-in-Thickness Wing of Aspect Ratio 6. NACA RM L52J22, 1952.
 5. Pepper, William B., Jr., and Hoffman, Sherwood: Comparison of Zero-Lift Drags Determined by Flight Tests at Transonic Speeds of Symmetrically Mounted Nacelles in Various Spanwise Positions on a 45° Sweptback Wing and Body Combination. NACA RM L51D06, 1951.
 6. Kremzier, Emil J., and Dryer, Murray: Aerodynamic Interference Effects on Normal and Axial Force Coefficients of Several Engine-Strut-Body Configurations at Mach Numbers of 1.8 and 2.0. NACA RM E52B21, 1952.
 7. Friedman, Morris D.: Arrangement of Bodies of Revolution in Supersonic Flow To Reduce Wave Drag. NACA RM A51I20, 1951.
 8. Driver, Cornelius: Aerodynamic Characteristics at Supersonic Speeds of a Series of Wing-Body Combinations Having Cambered Wings With an Aspect Ratio of 3.5 and a Taper Ratio of 0.2. Effect at $M = 2.01$ of Nacelle Shape and Position on the Aerodynamic Characteristics in Pitch of Two Wing-Body Combinations With 47° Sweptback Wings. NACA RM L52F03, 1952.
- 

9. Hasel, Lowell E., and Sevier, John R., Jr.: Aerodynamic Characteristics at Supersonic Speeds of a Series of Wing-Body Combinations Having Cambered Wings With an Aspect Ratio of 3.5 and a Taper Ratio of 0.2. Effect at $M = 1.60$ of Nacelle Shape and Position on the Aerodynamic Characteristics in Pitch of Two Wing-Body Combinations With 47° Sweptback Wings. NACA RM L51K14a, 1952.
 10. Bielat, Ralph P., and Harrison, Daniel E.: A Transonic Wind-Tunnel Investigation of the Effects of Nacelle Shape and Position on the Aerodynamic Characteristics of Two 47° Sweptback Wing-Body Configurations. NACA RM L52G02, 1952.
 11. Jacobsen, Carl R.: Effects of Systematically Varying the Spanwise and Vertical Location of an External Store on the Aerodynamic Characteristics of an Unswept Tapered Wing of Aspect Ratio 4 at Mach Numbers of 1.41, 1.62, and 1.96. NACA RM L52F13, 1952.
 12. Jacobsen, Carl R.: Effects of the Spanwise, Chordwise, and Vertical Location of an External Store on the Aerodynamic Characteristics of a 45° Sweptback Tapered Wing of Aspect Ratio 4 at Mach Numbers of 1.41, 1.62, and 1.96. NACA RM L52J27, 1953.
 13. Jacobsen, Carl R.: Effects of the Spanwise, Chordwise, and Vertical Location of an External Store on the Aerodynamic Characteristics of a 60° Delta Wing at Mach Numbers of 1.41, 1.62, and 1.96. NACA RM L52H29, 1952.
- 

EXPERIMENTAL EXTERNAL-STORE AND NACELLE DRAGS

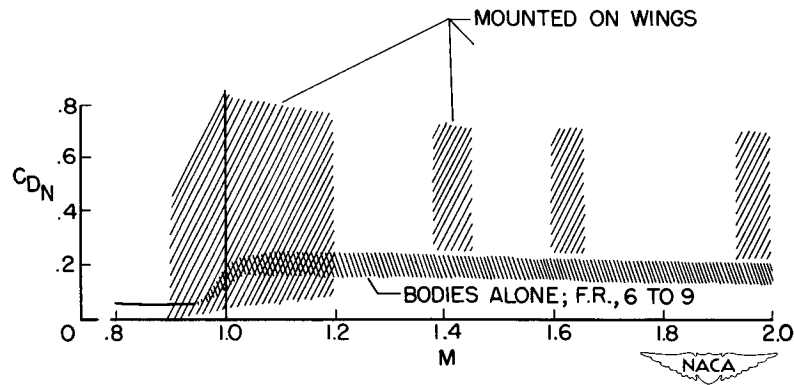


Figure 1

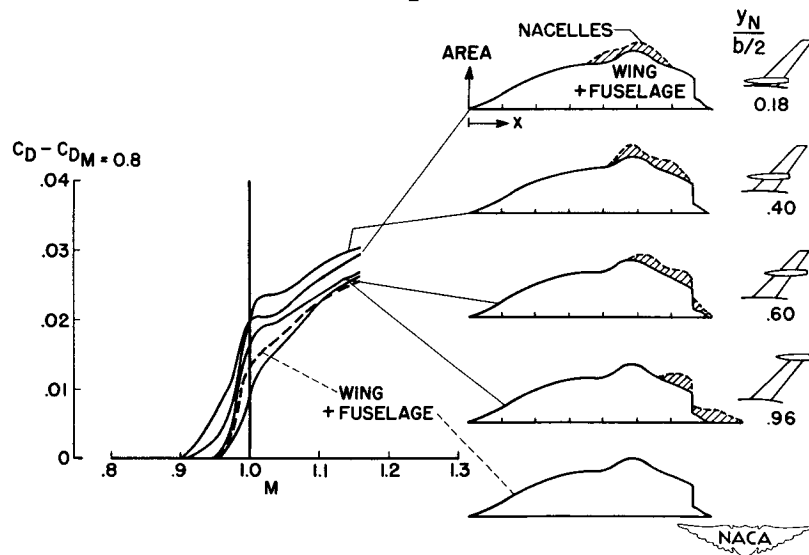
DRAG OF SPANWISE SERIES OF SYMMETRICALLY MOUNTED NACELLES
 $C_L = 0$ 

Figure 2

DRAG OF PYLON-MOUNTED NACELLES
NACELLES AT 40% SEMISPAN; $C_L = 0$

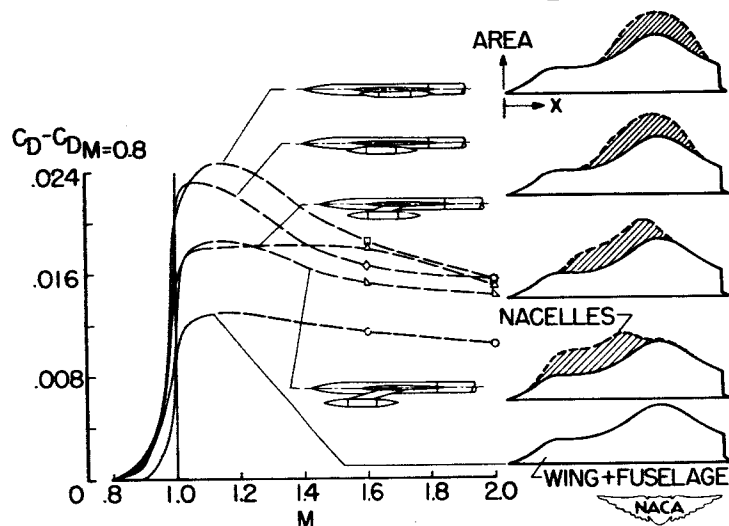


Figure 3

DRAG OF DIFFERENT TYPES OF NACELLES

$C_L = 0$

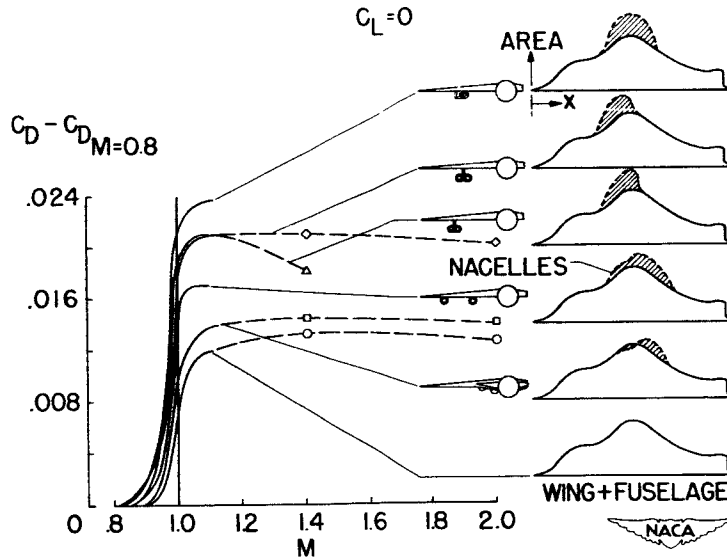


Figure 4

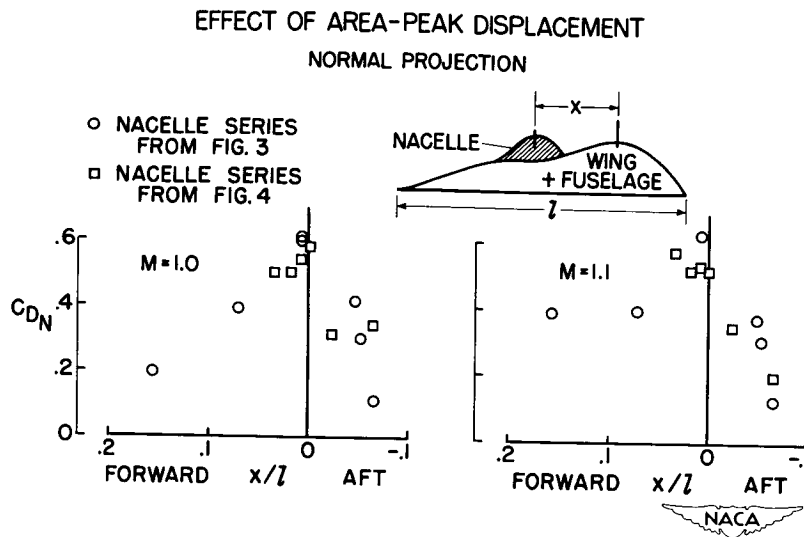


Figure 5

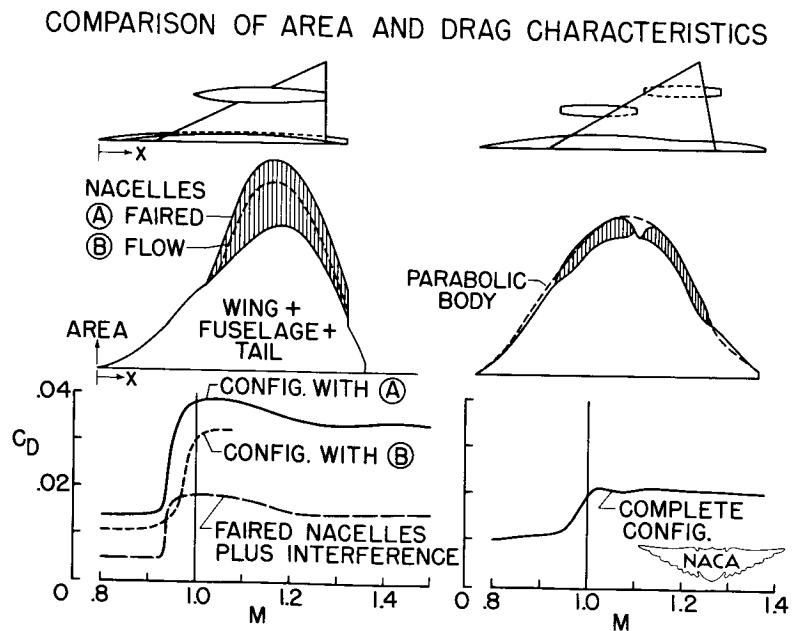


Figure 6

DRAW OF COMPLETE CONFIGURATIONS AND EQUIVALENT BODIES

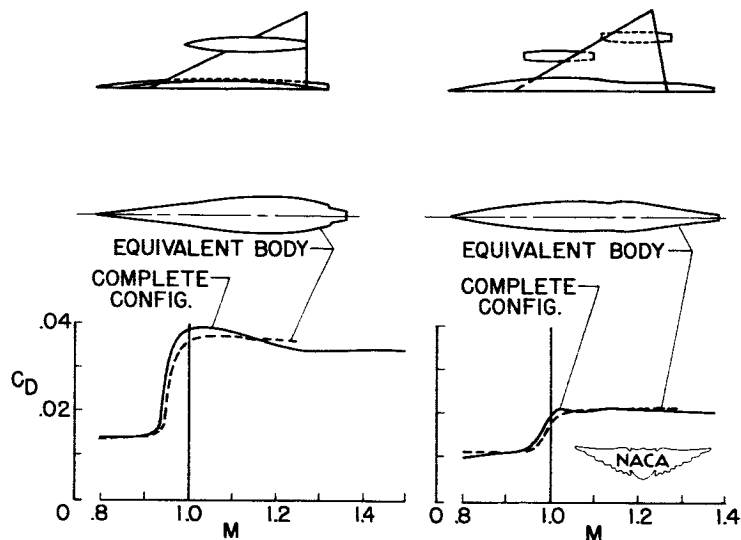


Figure 7

WING FUSELAGE, AND STORE GEOMETRY

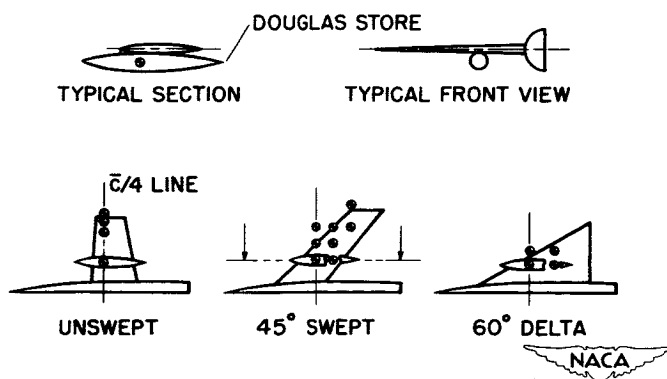
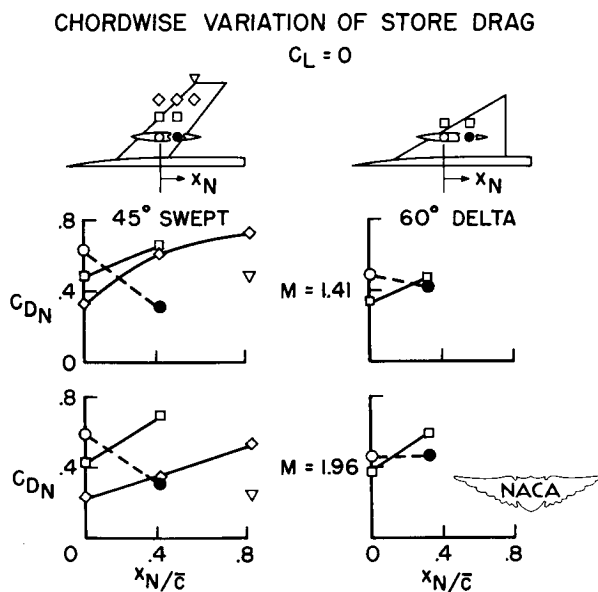
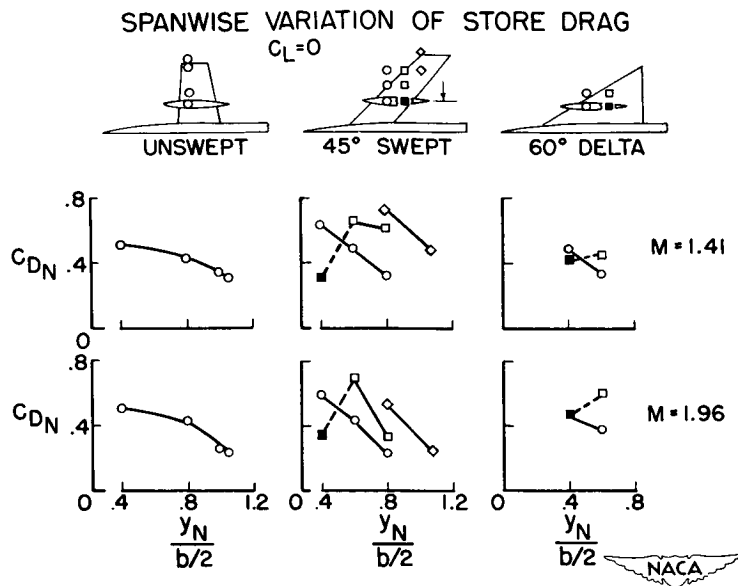


Figure 8



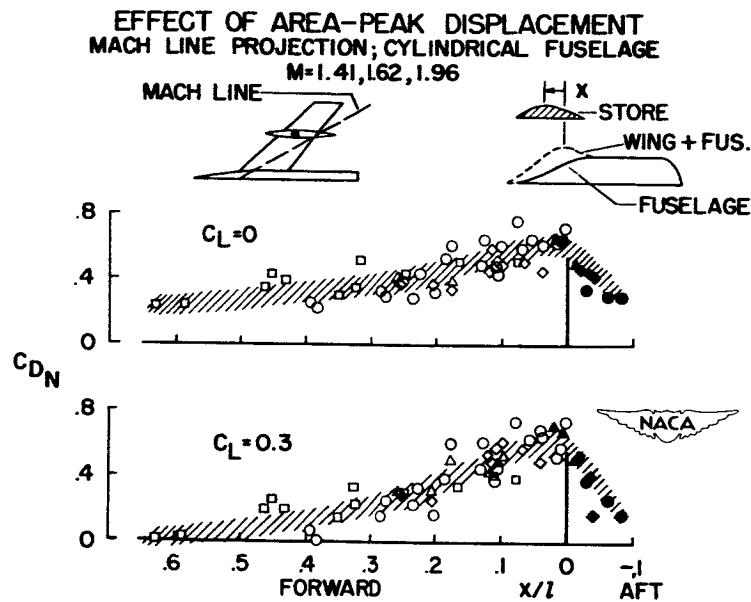


Figure 11

DECLASSIFIED
CONFIDENTIAL

PRESSURE DRAG OF BODIES AT MACH NUMBERS UP TO 2.0


By Robert L. Nelson and William E. Stoney, Jr.

Langley Aeronautical Laboratory

The drag of bodies has now assumed greater importance because, as shown in the previous papers by Richard T. Whitcomb and Robert T. Jones, the transonic drag rise of an airplane can be the same as its equivalent body. Obviously, the airplane designer would like his airplane to have a low-drag equivalent body. This paper shows some of the factors which minimize the drag of bodies at transonic and supersonic speeds and shows some of the penalties caused by deviating from low-drag body shapes.

Drag reductions can be obtained in two ways, first, through increasing the body fineness ratio, and secondly, through better shaping the body profile at a given fineness ratio. The effects of fineness ratio are discussed first and then, more completely, detail shape effects.

Largest reductions in body drag result from increases in body fineness ratio as is shown in figure 1. In figure 1 the variation of airplane drag with equivalent body fineness ratio at $M = 1.05$ is plotted. In order to do this the pressure drag of an airplane is assumed to be the same as that of its equivalent body and C_D is based on wing area in order to get the results in more familiar terms. For the calculations, airplane volume and wing area are assumed to be constant. The values used are representative of a bomber-type airplane. The data points are from free-flight model tests of parabolic bodies having different maximum-diameter positions and base sizes (refs. 1 and 2). The curve simply connects the lower drag points. The difference between the total-drag curve and the friction-drag curve represents the minimum pressure drag for a given volume and fineness ratio for these body shapes. The minimum total-drag curve shows the large reduction in airplane drag obtained with an increase in equivalent body fineness ratio. Largest reductions in drag occur at fineness ratios below 12, whereas the minimum drag occurs at about a fineness ratio of 24. This value will change somewhat for other Mach numbers and Reynolds numbers. Careful attention must be given to the nose and afterbody components which make up the body as indicated by the spread of test points at a given fineness ratio. Although not shown in figure 1, two wing-body configurations from the previous paper by Norman F. Smith, Ralph P. Bielat, and Lawrence D. Guy had approximately the same ratio of volume-to-wing area as for this plot. One configuration, of fineness ratio 6.5, had a C_D of 0.036 while the other, having an equivalent body fineness ratio of 9 and a better shape, had a C_D of 0.022. This effect of fineness ratio and the level of drag therefore is verified by the actual wing-body tests. The prime importance of fineness ratio on drag has been shown and the problem will now be analyzed in more detail.



NELSON & STONEY

In figure 2 the breakdown of a typical curve of drag coefficient against Mach number for a body neglecting base drag is shown. For bodies with bases, the base drag can be calculated by using the results of Love, Chapman, Cortright and Shroeder, and others (refs. 3 to 5). The friction drag can be calculated by the usual methods. The supersonic pressure drag for good bodies can be calculated at Mach numbers above that for shock attachment M_S by the second-order theory of Van Dyke (ref. 6). This paper considers mainly the range of Mach number below M_S where the problem is difficult to analyze theoretically. This range is defined by the Mach number for peak drag M_p and the drag rise Mach number M_{DR} .

Figure 3 shows correlations of drag rise and peak drag Mach numbers for a number of parabolic bodies (refs. 1 and 2). For the upper series of test points the Mach number for peak drag is plotted against nose fineness ratio. The curve shown is the Mach number for shock attachment to parabolic noses. The curve and the test points show the same general trends and indicate the dependence of the Mach number for peak drag on the Mach number for shock attachment.

For the lower series of test points, the drag rise Mach number is plotted against the nose or afterbody fineness ratio, whichever is the least. The nose and afterbody test points fall within the same band and indicate that the drag rise Mach number may be determined by either the nose or afterbody and is dependent mainly on fineness ratio.

Before discussing the peak drag of bodies, an examination is made of some of the effects of nose shape on drag at various Mach numbers. Figure 4 shows the drags of a number of fineness-ratio-3 noses. Although drags at this fineness ratio are relatively high, this fineness ratio was chosen so that the drag increments between the different shapes were more easily measurable. The results are presented in bar-graph form at $M = 1.05$, 1.24 , and 2.0 . The nose shapes include the cone, the parabolic nose having its vertex at maximum diameter, the L-V Haack nose (designed for minimum drag for a given volume and length), the hypersonic optimum or $x^{3/4}$ nose, the Von Kármán nose (designed for minimum drag for a given length and diameter), and the $x^{1/2}$ nose (which is a parabolic nose having its vertex at the tip). At $M = 1.05$, the results are from free-flight model tests from the Langley helium gun (at the testing station at Wallops Island, Va.); at $M = 1.24$ and 2.0 , the results are from the Ames 1- by 3-foot supersonic tunnel (ref. 7) except for the parabolic nose. For the parabolic nose, the results are from second-order theory. At $M = 1.05$, the $x^{1/2}$ nose, which has a relatively blunt tip, has the least drag and is followed by the Von Kármán nose. At $M = 1.24$, the same result holds true. At $M = 2$, the hypersonic optimum nose has the least drag. This result also holds true at Mach numbers greater than 2. The $x^{1/2}$ nose at $M = 2$ has higher drag as a result of its blunt tip.

DECLASSIFIED

CONFIDENTIAL

3

Although the Von Kármán nose has good drag characteristics over the Mach number range tested, it must be remembered that this nose was derived for vanishing thickness. For finite thickness, this slender-body-theory result does not apply. Recent work at the Langley Laboratory has solved the minimum problem for finite thickness by using linearized theory. The resulting nose shapes have finite slopes at their maximum diameters.

Another indication that noses with finite slope at maximum diameter can have lower drag than noses with zero slope at maximum diameter is shown by some results for a family of noses generated by parabolic arcs. In figure 5 the nose pressure drag coefficient is plotted against the shape parameter K which is related to the slope of the nose at maximum diameter. For $K = 1$, the parabolic nose has zero slope at maximum diameter. Reducing K gives slope at maximum diameter and for $K = 0$, the result is a cone. Both helium-gun tests at $M = 1.2$ and second-order theory at $M = 1.4$ show the same trend; therefore, minimum drag in the vicinity of $K = 0.7$ is indicated. This result indicates that, for parabolic noses, removing the restriction of zero slope at maximum diameter has resulted in a reduction in nose drag. For complete bodies, the reduction of nose drag by the use of such shapes may be offset by a greater interference drag of the nose on the afterbody.

In order to obtain an explanation of this drag reduction, the geometrical changes in the noses with a change in the shape parameter K have been examined. Examination of the nose profile shapes and the nose area distributions yielded no significant clues. However, the slopes of the nose-area distribution curves give an important result as is shown in figure 6.

The nondimensional slope of the nose area distribution is plotted against nose station x/l for a number of values of K . Note that in going from $K = 1.0$ to 0.75 , the peak slope of the area distribution curve is reduced, whereas a further decrease of K to 0.5 and to 0 causes an increase in the peak slope; therefore, the lowest drag nose has the lowest peak slope. In figure 5 is also shown the drag value at $M = 1.2$ for the $x^{1/2}$ nose, which had the lowest drag at low supersonic speeds of all the noses presented earlier. The slope of the area distribution curve for the $x^{1/2}$ nose is the lowest value possible and is constant as is shown in figure 6. Thus, from this experimental and theoretical study of the effect of nose shape on drag, the peak slope of the area distribution curve is seen to be an important parameter which influences the drag at low supersonic speeds. This parameter has less importance at higher Mach numbers since the $x^{3/4}$ nose with a relatively high peak slope had the least drag at $M = 2$.

A correlation of the peak drag of bodies using as part of the correlation parameter a function which is proportional to the slope of total body area distribution curve has been made.

0371200000
CONFIDENTIAL

Figure 7 shows 39 body shapes included in the drag correlation for smooth bodies. The bodies have different fineness ratios, maximum-diameter locations, base sizes, and profile shapes. In figure 8 the peak pressure drag coefficient is plotted against a shape parameter which includes the function f which is related to the slope of the body area distribution curve, the base diameter ratio, and an effective body fineness ratio, which neglects any parallel portion of the body. The neglect of this cylindrical section presupposes small interference effects between the nose and afterbody. The drags of all the bodies are from free-flight model tests at high Reynolds numbers so that the flow is turbulent at both subsonic and supersonic speeds. The peak pressure drag was obtained by taking the difference between the peak total drag and the subsonic drag. For bodies having base areas greater than 20 percent of the maximum area, the drags were corrected for base pressure. Fin drag was subtracted for all models. The peak pressure drag correlates well by using this correlation parameter and indicates that for these body shapes the interference drag is small. The one body for which the correlation is poor has a low-fineness-ratio, highly convergent afterbody. This correlation is similar to a transonic drag correlation made by the Fort Worth Division of Convair in that the slopes of the area distributions are weighted in the same manner.

Since the correlation appears good, one would obviously seek low drag, for a given fineness ratio, by minimizing the quantity

$$f - 2 \left(1 - \frac{db}{dm} \right).$$

However, this minimization cannot be done directly since base drag must be included and the proper combination of base size and afterbody length must be found for low drag.

Figure 9 shows the results of some tests (ref. 2) in which the afterbody drag included both afterbody pressure drag and base drag. The tests were made with free-flight models flown from the helium gun. The noses on all the models were of high fineness ratio to minimize the interference of the nose on the afterbody. The stabilizing fins were thin and swept back to reduce the interference drag between the fins and the afterbody and to minimize the effect of the fins on the base pressure. At $M = 1.05$, the test Reynolds numbers for all models were over 8×10^6 ; at these Reynolds numbers and with the presence of the fins, the flow at the base is turbulent and thus the results are representative of full-scale values. Twelve bodies had parabolic afterbodies of three fineness ratios and four base sizes, whereas four additional models had conical afterbodies. In the left-hand plot of figure 9 at $M = 1.05$, the pressure plus base drag coefficient of the afterbody is plotted against the base radius ratio r_b/r_{max} for the three afterbody fineness ratios. The plot shows that, as the afterbody fineness ratio increases, the base size for minimum drag approaches zero. The right-hand plot shows the base size for low drag against afterbody fineness ratio. It can be seen that the three points fall on a straight line through $r_b/r_{max} = 1$, which corresponds to a

conical boattail angle which is constant and equals 4.5° . This angle of 4.5° corresponds with previous ballistic experience. Since the afterbodies have bases at fineness ratios below 6, any jet flow through the base must not cause higher base drag. This effect of the jet on base pressure is discussed in the paper by Edgar M. Cortright, Jr., and Fred D. Kochendorfer.

By using this plot of base size for low drag against afterbody l/d in conjunction with the peak-drag correlation parameter, a series of bodies have been designed which should have low drag based on body frontal area at $M = 1.05$. The bodies had profiles of the $x^{1/2}$ shape with maximum diameters located so as to minimize the correlation factor f for a given base size.

However, drags of these supposedly reduced drag bodies were no lower than those of the lowest drag parabolic bodies presented in figure 1. The drag reduction indicated by the correlation parameter therefore was not realized. A comparison of the peak pressure drags of two of these bodies with the drags predicted by the correlation is presented in figure 10. As indicated by the vertical distance between the mean line from the correlation and the data points, the predicted drags are 40 to 60 percent below the actual values. It is felt that this difference is due to interference between the nose and afterbody components. The 39 bodies for which the data correlated well had either zero slope of the nose at maximum diameter or had finite slope followed by a long parallel portion; as a result, the interference drag was small. However, for these two models, the nose with finite slope at maximum diameter was followed by the afterbody which also had finite slope at maximum diameter. In any event the correlation should be used with caution in designing low-drag bodies for body shapes for which the interference drag can be high. A qualitative estimate of the interference drag between the nose and afterbody is given in a recent paper by Fraenkel (ref. 8).

Up to this point only smooth bodies have been discussed. Designing an airplane to a good area distribution, however, is difficult and bumps may occur in the area distribution curve. Figure 11 shows the area distributions of twelve bumpy bodies which were equivalent bodies of airplane configurations. In order to get a rough indication of the effects of the bumps on the drag, a comparison of the drag for each model with that for a parabolic body having the same length, maximum diameter, maximum-diameter location, and base size was made. Figure 12 shows a plot of the measured peak pressure drags of the twelve bumpy bodies against the peak pressure drags of the corresponding parabolic bodies, calculated by using the correlation shown earlier. The vertical distance from the dashed line to the data point represents the drag increment due to the bump. Except for one case, the drags of the bumpy bodies are from about 20 to 60 percent greater than for the parabolic bodies. The one case for which the drag of the bumpy body appears lower probably results from the

0371220 030
CONFIDENTIAL


drag of the bumpy body being low as a result of separation of flow over the afterbody, and, of course, the calculation of the parabolic-body drag does not account for this effect.

Since the effects of the bumps can be large, it is of interest to see whether the peak-drag correlation for smooth bodies will hold for bumpy bodies.

Figure 13 shows the peak drag correlation for the twelve bumpy bodies. The peak pressure drag was obtained in the same manner as for the smooth bodies except that an additional correction was made for bodies with forward facing steps in the area distribution curves. It was assumed that the pressure over the step area corresponded to the pressure rise through an oblique shock ahead of a two-dimensional forward facing step as given in a recent paper by Love (ref. 3). The peak drags for the bumpy bodies show the same trends as for smooth bodies; however, the scatter about the mean curve is much greater. Again, two bodies with highly convergent low-fineness-ratio afterbodies do not agree with the correlation.

The drag rise Mach numbers for these twelve bodies followed the same trend as for the parabolic bodies shown earlier. The Mach numbers for peak drag were more complex, being more a function of detail nose geometry, than for the smooth bodies.

In conclusion, first, largest reductions in drag are possible through increases in both total body fineness ratio and the fineness ratio of the component parts. Second, the drag rise Mach number is dependent mainly on the shortest body component fineness ratio, whereas the Mach number for peak drag is a function of nose fineness ratio and shape. Third, the peak drags of smooth bodies and bumpy bodies can be correlated by using a simple parameter which depends only on body shape if the interference drag is small.



REFERENCES

1. Hart, Roger G., and Katz, Ellis R.: Flight Investigations at High-Subsonic, Transonic, and Supersonic Speeds To Determine Zero-Lift Drag of Fin-Stabilized Bodies of Revolution Having Fineness Ratios of 12.5, 8.91, and 6.04 and Varying Positions of Maximum Diameter, NACA RM L9I30, 1949.
2. Stoney, William E., Jr.: Some Experimental Effects of Afterbody Shape on the Zero Lift Drag of Bodies for Mach Numbers Between 0.8 and 1.3. (Prospective NACA paper.)
3. Love, Eugene S.: The Base Pressure at Supersonic Speeds on Two-Dimensional Airfoils and Bodies of Revolution (With and Without Fins) Having Turbulent Boundary Layers. NACA RM L53C02, 1953.
4. Chapman, Dean R.: An Analysis of Base Pressure at Supersonic Velocities and Comparison With Experiment. NACA Rep. 1051, 1951. (Supersedes NACA TN 2137.)
5. Cortright, Edgar M., Jr., and Schroeder, Albert H.: Investigation at Mach Number 1.91 of Side and Base Pressure Distributions Over Conical Boattails Without and With Jet Flow Issuing From Base. NACA RM E51F26, 1951.
6. Van Dyke, Milton Denaan: Practical Calculation of Second-Order Supersonic Flow Past Nonlifting Bodies of Revolution. NACA TN 2744, 1952.
7. Perkins, Edward W., and Jorgensen, Leland H.: Investigation of the Drag of Various Axially Symmetric Nose Shapes of Fineness Ratio 3 for Mach Numbers From 1.24 to 3.67. NACA RM A52H28, 1952.
8. Fraenkel, L. E.: The Theoretical Wave Drag of Some Bodies of Revolution. Rep. No. Aero. 2420, British R.A.E., May 1951.



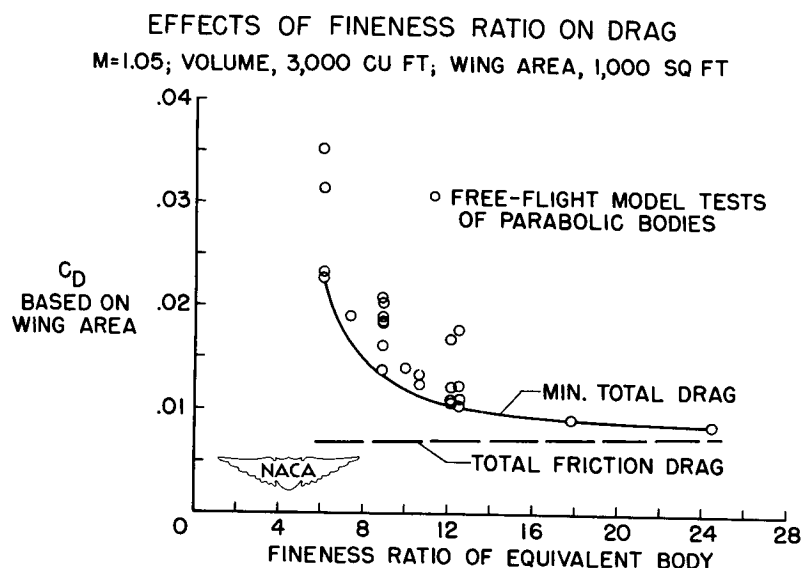


Figure 1

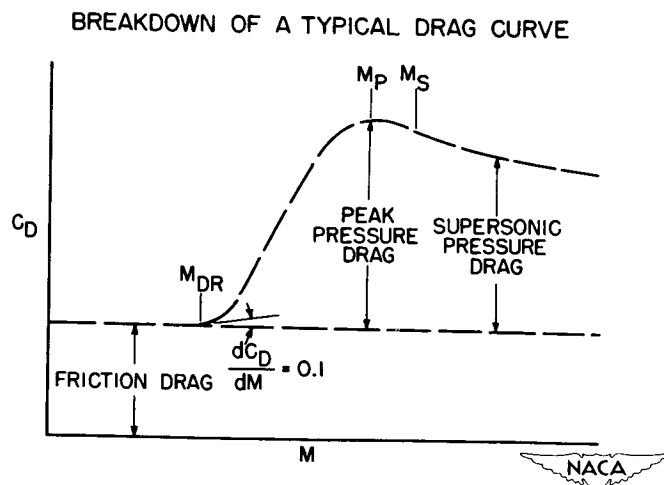


Figure 2

DRAG RISE AND PEAK DRAG MACH NUMBERS PARABOLIC BODIES

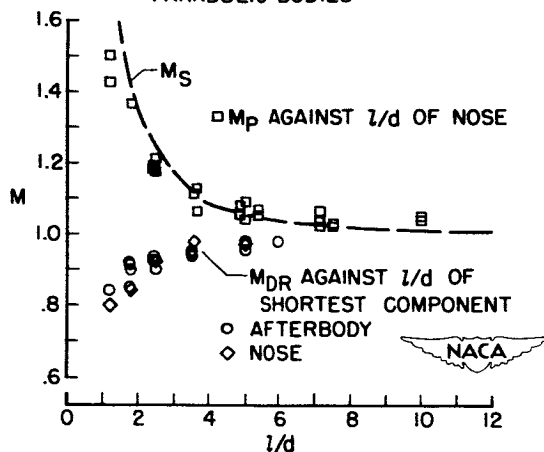


Figure 3

EFFECT OF NOSE SHAPE ON DRAG $l/d = 3$

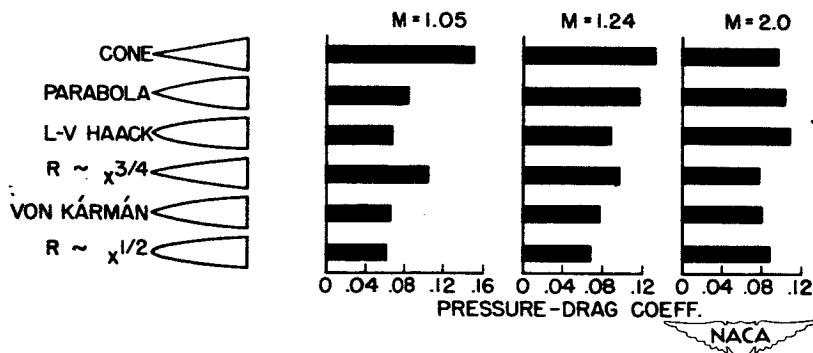


Figure 4

03112201030

CONFIDENTIAL

PRESSURE DRAG FOR A FAMILY OF PARABOLIC NOSES

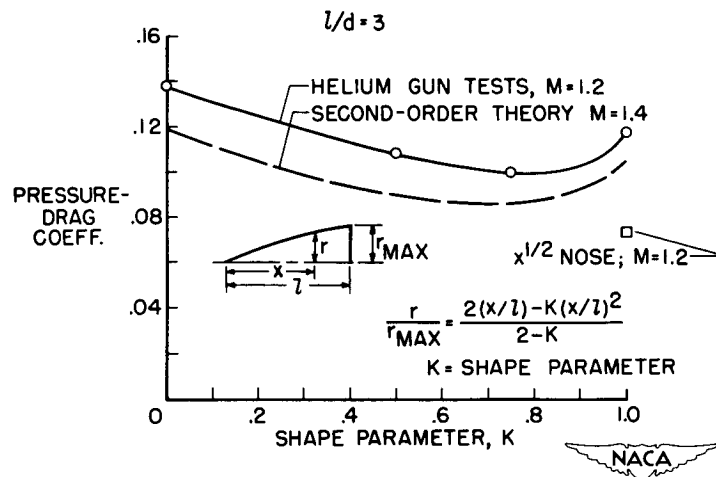


Figure 5

SLOPE OF AREA-DISTRIBUTION CURVE

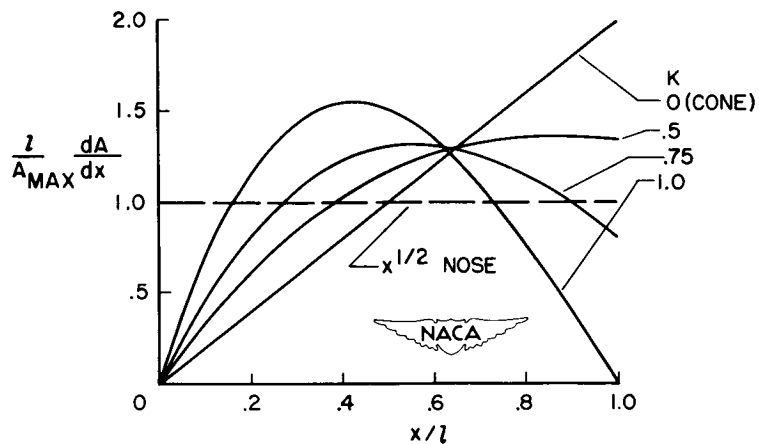


Figure 6

SMOOTH BODIES IN PEAK-PRESSURE-DRAG CORRELATION

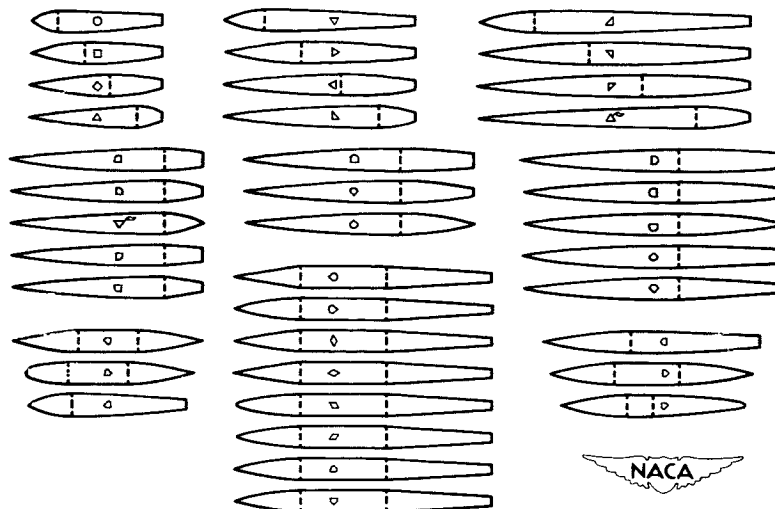


Figure 7

PEAK PRESSURE DRAG FOR SMOOTH BODIES

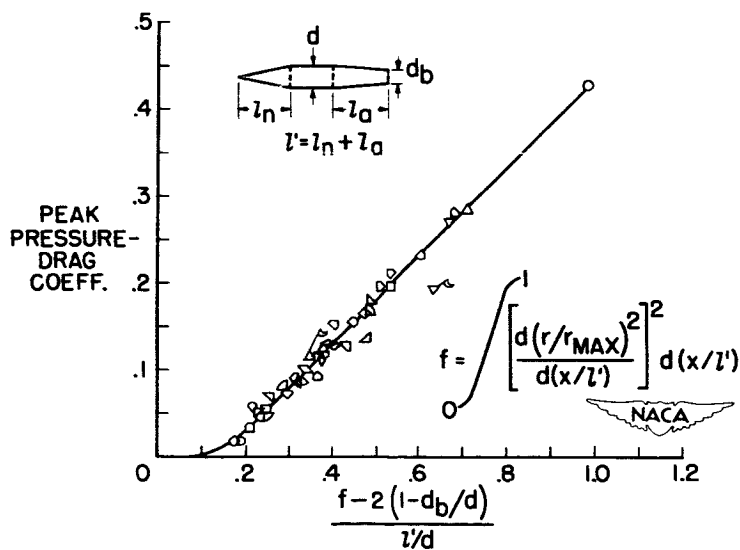


Figure 8

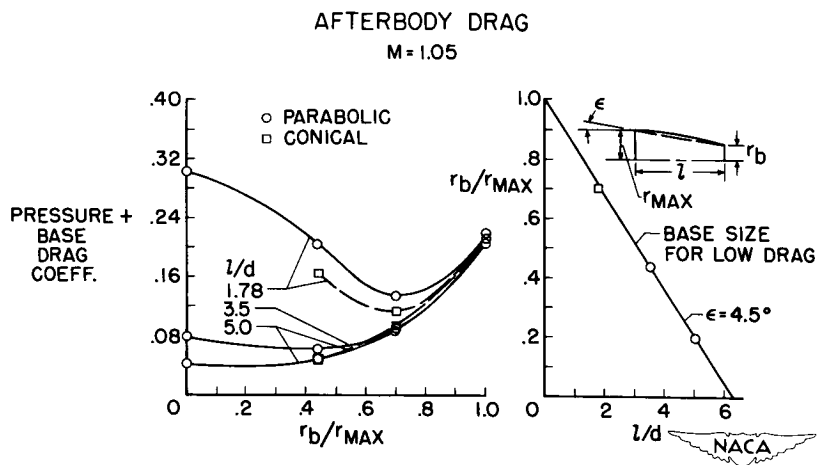


Figure 9

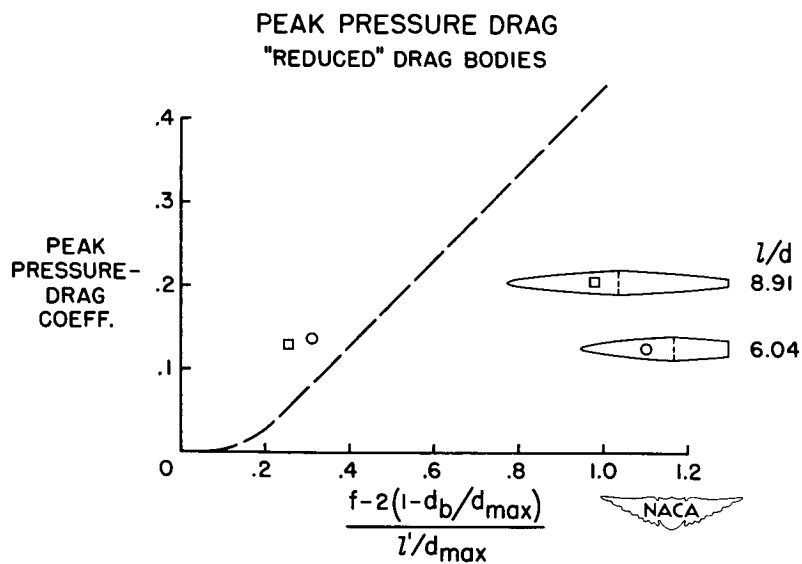


Figure 10

AREA DISTRIBUTIONS FOR BUMPY BODIES

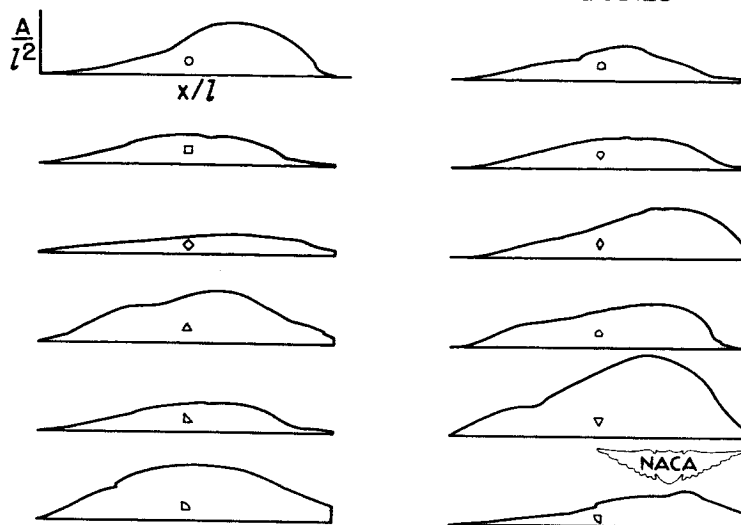


Figure 11

EFFECT OF BUMPS IN AREA DISTRIBUTION ON DRAG

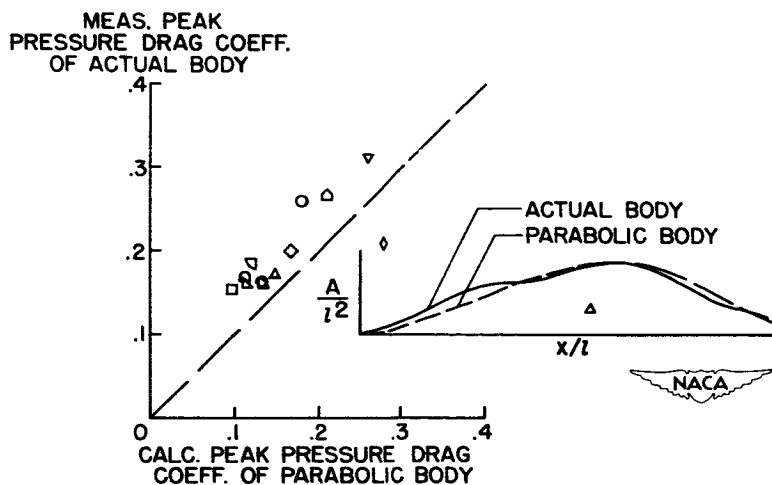


Figure 12

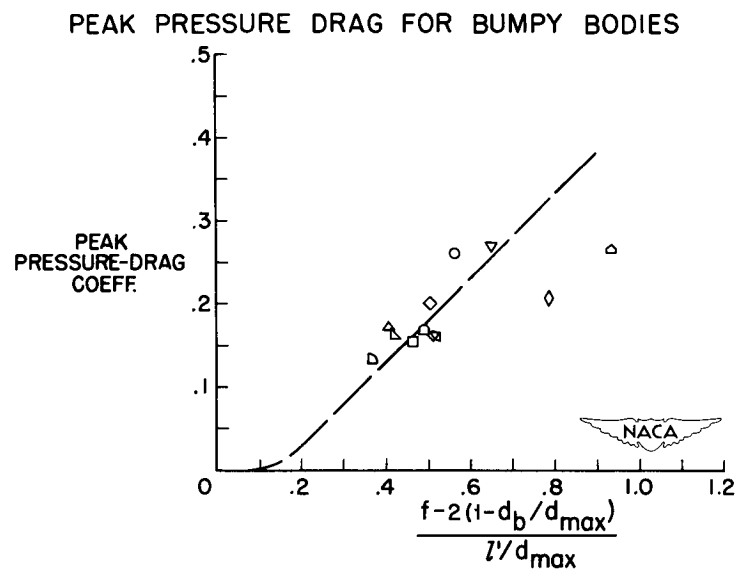


Figure 13

CONFIDENTIAL

DRAG DUE TO LIFT AT MACH NUMBERS UP TO 2.0

By Edward C. Polhamus


Langley Aeronautical Laboratory

INTRODUCTION

The previous papers have shown that, if the "area rule" is utilized properly, it is possible to obtain values of zero-lift drag which, for a wide variety of wing-fuselage configurations, approach that for the basic fuselage alone. This fact makes the selection of a wing somewhat less dependent on its zero-lift drag and therefore allows a wider range of wings to be considered with regard to other problems. The purpose of this paper therefore is to discuss the effect of wing geometry on the drag due to lift and methods of reducing the drag at lifting conditions.

In figure 1 a typical variation of the drag with lift coefficient for a plane, or flat, wing is shown by the solid line on the left-hand side of the figure. For a plane wing the minimum drag occurs at zero lift and theoretically has a parabolic shape with the increment due to lift ΔC_D equal to a constant times the lift coefficient squared. In general, the data for the wings presented in this paper were fairly linear plotted against C_L^2 up to lift coefficients of about 0.3 and therefore the slope $\Delta C_D / C_L^2$ will be used to describe the drag-due-to-lift characteristics of plane wings in this lift range. For a cambered or cambered and twisted wing the drag curve, as shown by the dashed line, does not have its minimum at zero lift and therefore the drag polars will be used to describe the characteristics of this type of wing.

Now, if viscous forces are neglected, the drag due to the lift can be divided into two components - a thrust component of the suction force caused by the flow about the nose of the airfoil, and a drag component of the normal force. For a two-dimensional wing these two components exactly balance each other; however, for a three-dimensional wing the drag component of the normal force is greater than the thrust component of the suction force, since a higher angle of attack is required to develop the same lift, and an induced drag results. At subsonic speeds the rate of change of the induced drag with lift squared can be approximated by $1/\pi A$ as illustrated in the bottom part of the right-hand side of figure 1. Additional drag also occurs if the suction force is not fully developed at the leading edge. For the extreme case of zero suction the drag due to lift is equal to the component of the normal force, and the rate of change is therefore equal to the reciprocal of the




lift-curve slope as illustrated in the top part of the figure. The drag curve of a wing usually lies somewhere between these two extremes and its relative position between these two limits is dependent to a large extent on the amount of suction developed at the leading edge and is therefore a function of such parameters as Reynolds number, Mach number, thickness, and leading-edge radius. The two limits, of course, are primarily a function of plan form and Mach number.

EFFECT OF REYNOLDS NUMBER

Figure 2 shows the effect of Reynolds number on the drag due to lift of an aspect-ratio-2 delta wing having an NACA 0005-63 airfoil section (ref. 1 and unpublished data). The results are presented in the form of the drag-rise parameter $\Delta C_D / C_L^2$ against Reynolds number for several Mach numbers. Also shown are the subsonic and the $M = 1.7$ theories for full leading-edge suction and the values for zero suction given by $1/C_{L\alpha}$.

The results indicate that at a Mach number of 0.25 there is a rather large increase in drag due to lift with decreasing Reynolds number but that as the Mach number increases the effect of Reynolds number diminishes and is relatively unimportant at a Mach number of 1.7. The increase with decreasing Reynolds number is probably due in part to the fact that the combination of low Reynolds number and a relatively sharp leading edge is conducive to leading-edge separation resulting in a loss of leading-edge suction. In addition, a part of this variation is probably due to the fact that at low Reynolds numbers the transition point moves forward with increasing lift resulting in an increase in viscous forces with lift. The decreasing effect of Reynolds number with increasing Mach number is due to the fact that the difference between the theory and the zero-suction case decreases with increasing Mach number and the fact that the flow about the leading edge is affected by compressibility. It should be pointed out that, while the Reynolds number based on the mean aerodynamic chord was used here to define more clearly the variation with Reynolds number for a given wing, it appears that the drag due to lift at a given Mach number is more dependent upon the Reynolds number based on leading-edge radius. A recent correlation (ref. 2) based on this parameter succeeded in bringing the drag-due-to-lift parameter into fair agreement for a large number of aspect-ratio-2 delta wings having various airfoil sections. It should also be pointed out, however, that, for plan forms where compressibility effects are a function of thickness ratio or leading-edge radius, correlations based on the leading-edge Reynolds number would not be expected to bring the data into agreement at all Mach numbers.



EFFECT OF THICKNESS

Figure 3 illustrates the effect of wing thickness ratio on the drag-due-to-lift factor for unswept wings of aspect ratio 4 at Reynolds numbers of approximately 4×10^6 (refs. 3, 4, and unpublished data from the Langley 16-foot transonic tunnel). In addition to the experimental data, the theory for full suction is also shown. It will be noted that at subsonic speeds a decrease in thickness ratio from 8 percent to 4 percent increased the drag-due-to-lift factor; for example, at a Mach number of 0.6 it was increased by approximately 60 percent. This increase with decreasing thickness ratio is probably due to the fact that the 4-percent-thick airfoil section has a considerably smaller leading-edge radius and therefore develops less leading-edge suction. However, it will be noted that as the Mach number is increased the curves tend to converge and at a Mach number of about 0.88 there is little effect of thickness. This is due to the fact that, although the thick wing develops more suction at low speeds, the effect of compressibility on the flow about the leading edge is greater than for the thin wing. Above a Mach number of 0.88, the 4-percent-thick wing has considerably less drag due to lift than the 6-percent- and 8-percent-thick wings due to the fact that in this Mach number range the resultant force is normal to the wing chord, and since the thin wing has the higher lift-curve slope it has the lower drag due to lift. This is illustrated by the two dashed curves representing the reciprocal of the lift-curve slope for the 4-percent- and 6-percent-thick wings.

Figure 4 shows the effect of thickness on the drag due to lift of a delta wing of aspect ratio 2 at a Reynolds number of 3×10^6 (ref. 1). At subsonic Mach numbers it will be noted that the results are similar to those for the unswept wings (fig. 3) with the thin wing having the highest value of drag due to lift. However, at the higher Mach numbers the effect of thickness did not reverse for the delta wing as it did for the unswept wing and the thin wing still had the highest drag due to lift. It will also be noted that even at the highest Mach number tested the drag is lower than the reciprocal of the lift-curve slope, an indication of some suction being developed. This is due to the fact that the Mach number normal to the leading edge of this wing never exceeded a value of about 0.80. The vertical dashed line represents the free-stream Mach number for which the Mach number normal to the leading edge is equal to 0.9 which is approximately equal to the Mach number of the unswept wings for the case of zero suction. In order to indicate the variation with Mach number in the transonic range, the results of a rocket-propelled model of similar plan form having a thickness of $6\frac{1}{2}$ percent (ref. 5) is shown by the long and short dashed curve.

EFFECT OF LEADING-EDGE RADIUS

The effect of leading-edge radius on the drag due to lift of an unswept wing (ref. 1) is illustrated in figure 5. The wing had an aspect ratio of 3, a taper ratio of 0.39, and a thickness of 3 percent and was tested with a biconvex section and with a biconvex section modified with an elliptical nose having a radius of 0.045 percent of the chord. It will be noted that the results are similar to those obtained in the thickness investigation, with improvements with increasing leading-edge radius occurring only at subsonic speeds. It should be pointed out that the two curves are coincident at supersonic speeds.


Figure 6 presents the results obtained on a 45° swept wing of aspect ratio 4 which was tested with several modifications to the basic NACA 65A006 airfoil section in the Langley high-speed 7- by 10-foot tunnel. The three configurations tested were a sharp edge having zero radius, the normal radius of 0.24 percent chord, and a radius of 0.72 percent chord. Inasmuch as only a limited Mach number range was covered in these tests, the results are presented as ΔC_D plotted against C_L at a Mach number of 0.90. The results indicate that no improvement occurred with increase in the leading-edge radius at this Mach number.

EFFECT OF ASPECT RATIO

Figure 7 illustrates the effect of aspect ratio on the drag due to lift through the Mach number range. The wings were of delta plan form and 3 percent thick and had aspect ratios of 2 and 4 (ref. 1). The results indicate, as would be expected, that the higher aspect ratio has the lower drag due to lift throughout the Mach number range. However, it will be noted that the difference between the two aspect ratios is considerably greater than that indicated by the theory. It will be noted, however, that the effect of aspect ratio on the reciprocal of the lift-curve slope, which represents the zero-suction case, is approximately twice that for the full-suction theory at subsonic speeds. The larger effect of aspect ratio obtained in the experiments is therefore not surprising since these thin wings lose a good portion of suction.

EFFECT OF SURFACE SHAPE

The previous figures have illustrated the effect of various parameters on the drag due to lift of planar wings, and have shown that, in general,



the drag due to lift is considerably higher than the theoretical values due largely to separation at the nose and the accompanying loss of thrust. However, a theoretical study by Jones (ref. 6) has shown that an effective leading-edge thrust can be obtained by cambering and twisting the wing.

Figure 8 presents the results of cambering and twisting a 45° swept wing of aspect ratio 4 (ref. 7 and unpublished data from the Langley 8-foot transonic tunnel and the low-turbulence pressure tunnel). On the left-hand side of the figure the results are presented for the case of the cambered and twisted wing having 4.5° incidence at the fuselage which results in low fuselage angles at moderate lift coefficients. The results are presented as a plot of C_D against C_L at a Mach number of 0.9 for the plane wing at zero incidence, for the wing cambered and twisted for a uniform load distribution at a C_L of 0.4 and $M = 1.2$ ($\epsilon = 4.5^\circ$), and for the wing cambered and twisted for a triangular span load and a rectangular chord load at a C_L of 0.4 and $M = 0.9$ ($\epsilon = 13^\circ$). The triangular span load of the latter case was used in an attempt to improve the pitching-moment characteristics. The results indicate large increases in drag for both the camber and twist distributions. However, on the right-hand side of the figure, results are presented for the wing cambered and twisted for a uniform load tested on a slightly different fuselage but having approximately zero incidence at the fuselage. These results indicate substantial reductions in drag above a lift coefficient of about 0.15 for the cambered and twisted wing. For the case of zero incidence the fuselage is developing lift at the design condition and therefore the wing-fuselage combination represents the wing alone for which the camber and twist were designed considerably better than the configuration having 4.5° incidence which results in low fuselage angles in the moderate lift range.

Figure 9 presents the results of an aspect-ratio-2 delta wing tested with three different surface shapes (ref. 1): a planar surface, a surface cambered and twisted for a trapezoidal spanwise load distribution, and a surface which was planar over the inboard 80 percent of the local semispans. This third surface was a modification of the surface required for an elliptical span loading and was used in order to simplify construction. It should be mentioned that the wing incidence was zero at the plane of symmetry for all three cases. At a Mach number of 0.91, it will be noted that both types of surface modification resulted in improvements in the drag characteristics but that the simple nose camber was superior below a lift coefficient of about 0.3. As the Mach number increased the improvements diminished for both surfaces and at a Mach number of 1.53 no improvement was obtained; however, less penalty occurred for the simple nose camber.




Figure 10 shows the results obtained from tests in the Langley 8-foot transonic tunnel of a similar wing in which the extent of the nose camber was varied. The wing had an aspect ratio of 2.2 and a modified NACA 0004-65 airfoil section. Two nose cambers were tested and both were of constant chord, one being 4 percent (modification A) and the other 8 percent (modification B) of the mean aerodynamic chord. The camber covering 4 percent of the mean aerodynamic chord was obtained by shearing the ordinates so that the bottom surface was parallel to the chord line. The camber covering 8 percent of the mean aerodynamic chord was obtained by extending the chord and displacing the leading edge an amount equal to 1.3 percent of the longitudinal distance X from the wing apex. This was a modification of the surface shape required for an elliptical loading at a lift coefficient of 0.15 and was similar to that presented in figure 9 except that it was of constant chord. On the left-hand side of the figure drag polars are shown for the basic wing and the two modifications at a Mach number of 1.0. The results indicate that modification A (4 percent) had no effect on the drag while modification B (8 percent) resulted in a substantial reduction in drag except for an extremely small increase at zero lift. Although the coefficients are based on the actual areas, it should be pointed out that even the actual drag for a given lift is less for modification B than for the basic wing. The effect of Mach number on the variation of drag at a lift coefficient of 0.3 for the three configurations is shown on the right-hand side of the figure. It will be noted that both modifications resulted in improvements at the lower Mach number but that modification A had no effect above a Mach number of about 0.90; however, modification B resulted in improvements throughout the Mach number range investigated.

EFFECT OF TRIMMING

In order to reduce the weight and zero-lift drag of an aircraft, tailless configurations are sometimes used. However, since a tailless design, in general, obtains its trim from a surface on the wing, large deflections of this surface are required because of the short moment arm. These large deflections, of course, result in additional drag which could have an important effect on the performance. This is especially true at supersonic speeds because of the increased stability caused by the rearward movement of the wing aerodynamic center in going from subsonic to supersonic speeds and the higher drag due to flap deflection. Figure 11 illustrates this effect of trimming on the variation of the drag with lift. The model was an aspect-ratio-2 delta wing having an NACA 0005-63 airfoil and a constant-chord flap equal to 10 percent of the wing mean aerodynamic chord (ref. 8). At a Mach number of 0.90, it will be noted that a positive flap deflection of 4° resulted in a reduction in the drag due to lift. However, for a stable tailless

[REDACTED]

configuration negative deflections are required to trim the airplane through the positive lift range which results in an increase in the drag due to lift. At a Mach number of 1.90, the increase due to trimming the airplane is considerably greater than at 0.90 because of the aforementioned increase in stability and drag due to flap deflection at supersonic speeds.

EFFECT OF APPLICATION OF THE AREA RULE

In the previous papers it was shown that indentations of the fuselage according to the Mach number of 1.0 area rule resulted in large decreases in the zero-lift drag of wing-fuselage combinations at transonic speeds. The question now arises as to whether these benefits are maintained under lifting conditions. Figure 12 shows the effect of a Mach number of 1.0 body indentation on the drag of a wing-fuselage combination. The wing had an aspect ratio of 4, 45° of sweep, a taper ratio of 0.3, and an NACA 65A006 airfoil section and was tested in the Langley 8-foot transonic tunnel. The results are presented as total drag coefficient against Mach number for lift coefficients of 0 and 0.3 and indicate that the large reductions in drag at transonic speeds due to body indentation were to a large extent maintained in the lifting condition. At supersonic speeds the Mach number 1.0 indentation had negligible effect at either lift coefficients of 0 or 0.3.

Figure 13 shows the improvement in the maximum lift-to-drag ratio associated with this application of the area-rule concept. The results for both the basic configuration and the configuration with the indented body are plotted against Mach number and it will be noted that, below a Mach number of about 1.4, the lift-to-drag ratios were improved and at a Mach number of 1.0 (the design condition) the increase amounted to approximately 37 percent.

At the present time little has been done in attempting to develop area distributions which might actually reduce the drag increment due to lift. However, figure 14 presents the results of one such investigation conducted on a wing of aspect ratio 4 having 45° of sweep (ref. 9). The basic body was cylindrical rearward of the wing leading edge and was modified by several types of indentations. The first indentation, designated by the letter (B) in the figure, was symmetrical around the fuselage and was determined by the Mach number 1.0 area rule. The other two indentations tested were more abrupt indentations superimposed first on the upper half (C) and then on the lower half (D) of the symmetrical indentation. On the left-hand side of the figure the drag at zero lift is presented against Mach number and it will be noted that all the modifications gave about the same reduction in drag. On the right-hand part

of the figure the same comparison is made for a lift coefficient of 0.3. The results indicate that the symmetrical area-rule indentation resulted in about the same reduction in drag as at zero lift which is consistent with figure 12. However, when the more abrupt indentations were added, additional reductions in drag resulted with the lowest occurring for the indentation below the wing.


COMBINED EFFECTS

At transonic speeds it has been shown that application of the area rule and the use of camber and twist results in significant reductions in drag. Figure 15 shows the effect of combining these two methods at transonic speeds. The tests were conducted in the Langley 8-foot transonic tunnel on a model having 45° of sweep, an aspect ratio of 4, a taper ratio of 0.6, and an NACA 65A006 airfoil section. The model was tested (1) with the basic wing and body, (2) with the basic wing and the body indented according to the area rule, and (3) with the wing cambered and twisted for a uniform load at $C_L = 0.4$ and $M = 1.2$ in combination with the indented body. On the left-hand side of the figure drag polars are presented for the three configurations at a Mach number of 1.0. It will be noted that indenting the fuselage resulted in large reductions in drag throughout the lift range. Camber and twist resulted in a rather large increase in minimum drag but resulted in improvements above a lift coefficient of about 0.2. On the right-hand side of the figure the maximum lift-to-drag ratios are plotted as a function of Mach number. At a Mach number of 0.8 the improvement is due mainly to the camber and twist and resulted in an increase from 13 to 17. At a Mach number of 1.0, the improvement is due mainly to the body indentation and resulted in an increase from about 7.5 to 11.5.

CONCLUDING REMARKS

In conclusion, it appears that Reynolds number has a rather large effect on the drag due to lift of thin wings at low speeds but that this effect decreases considerably with increasing Mach number.

Comparisons of wings of various thicknesses indicate that at subsonic speeds an increase in thickness is beneficial, whereas, in general, at transonic and supersonic speeds no gains and possible losses occur unless the wing leading edge is highly swept which results in relatively low subsonic speeds normal to the leading edge. Similar results are indicated with regard to leading-edge radius.



DECLASSIFIED


CONFIDENTIAL

9

Although camber and twist are effective in reducing the drag due to lift at the design condition, providing the correct wing incidence is used, it appears that simple nose camber will result in similar gains with less penalty near zero lift.

The reductions in minimum drag associated with application of the area rule by means of fuselage indentations are maintained in the lifting condition and significant improvements in the lift-to-drag ratios result. In addition, from preliminary tests, it appears that local modifications to the fuselage indentations may result in additional reductions in drag at lifting conditions.

REFERENCES

1. Hall, Charles F.: Lift, Drag, and Pitching Moment of Low-Aspect-Ratio Wings at Subsonic and Supersonic Speeds. NACA RM A53A30, 1953.
 2. Osborne, Robert S., and Kelly, Thomas C.: A Note on the Drag Due to Lift of Delta Wings at Mach Numbers Up to 2.0. NACA RM L53A16a, 1953.
 3. Allen, Edwin C.: Experimental Investigation of the Effects of Plan-Form Taper on the Aerodynamic Characteristics of Symmetrical Unswept Wings of Varying Aspect Ratio. NACA RM A53C19, 1953.
 4. Wiggins, James W., and Kuhn, Richard E.: Wind-Tunnel Investigation of the Aerodynamic Characteristics in Pitch of Wing-Fuselage Combinations at High-Subsonic Speeds. Sweep Series. NACA RM L52D18, 1952.
 5. Mitcham, Grady L., Crabill, Norman L., and Stevens, Joseph E.: Flight Determination of the Drag and Longitudinal Stability and Control Characteristics of a Rocket-Powered Model of a 60° Delta-Wing Airplane From Mach Numbers of 0.75 to 1.70. NACA RM L51IO4, 1951.
 6. Jones, Robert T.: Estimated Lift-Drag Ratios at Supersonic Speeds. NACA TN 1350, 1947.
 7. Harrison, Daniel E.: A Transonic Wind-Tunnel Investigation of the Characteristics of a Twisted and Cambered 45° Sweptback Wing-Fuselage Configuration. NACA RM L52K18, 1952.
 8. Boyd, John W., and Pfyl, Frank A.: Experimental Investigation of Aerodynamically Balanced Trailing-Edge Control Surfaces on an Aspect Ratio 2 Triangular Wing at Subsonic and Supersonic Speeds. NACA RM A52LO4, 1953.
 9. Loving, Donald L.: A Transonic Wind-Tunnel Investigation of the Effect of Modifications to an Indented Body in Combination With a 45° Sweptback Wing. NACA RM L53F02, 1953.
- 

FUNDAMENTAL CONCEPTS

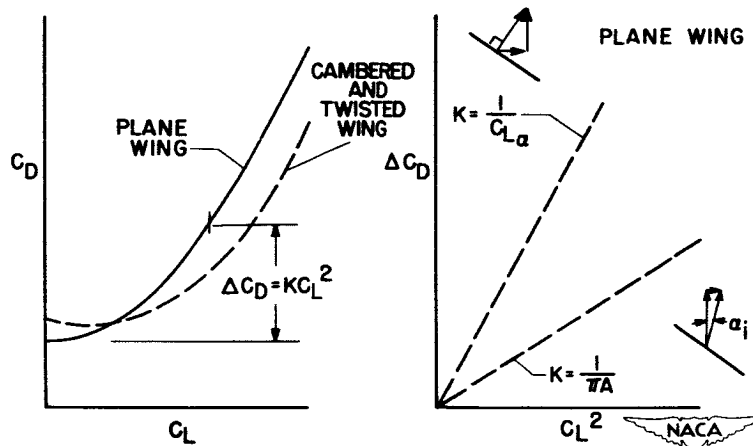


Figure 1

EFFECT OF REYNOLDS NUMBER

A=2; NACA 0005-63

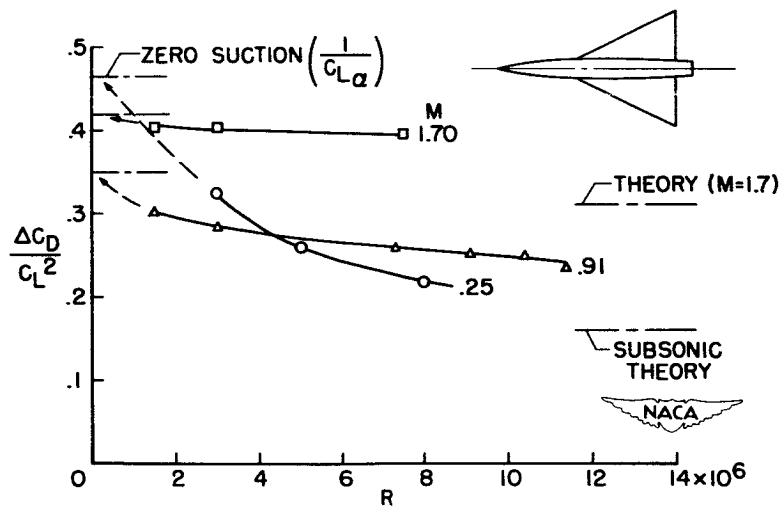


Figure 2

03712001030
CONFIDENTIAL

EFFECT OF WING THICKNESS

$A=4; \Delta \approx 0^\circ; \lambda \approx 0.5$

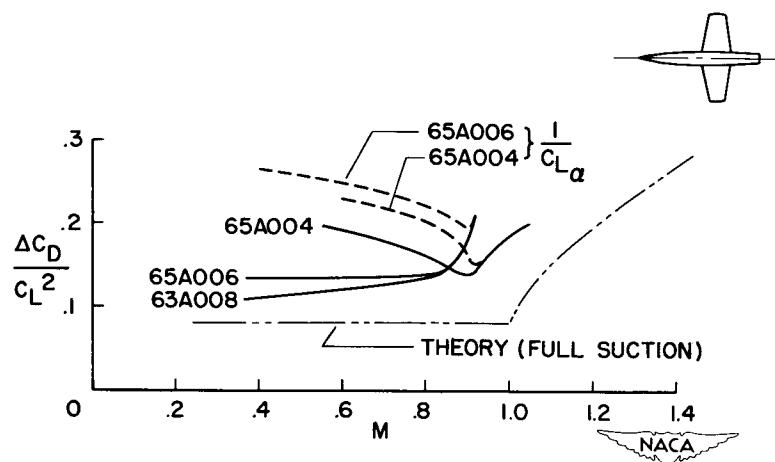


Figure 3

EFFECT OF WING THICKNESS

$A=2; \text{NACA00XX-63}$

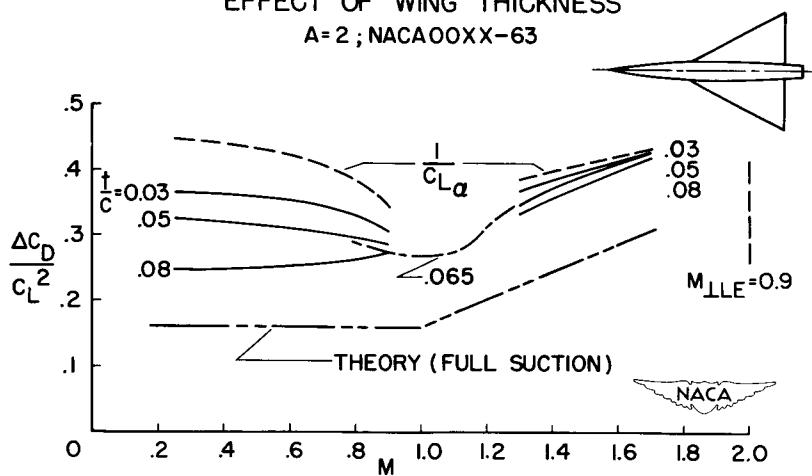


Figure 4

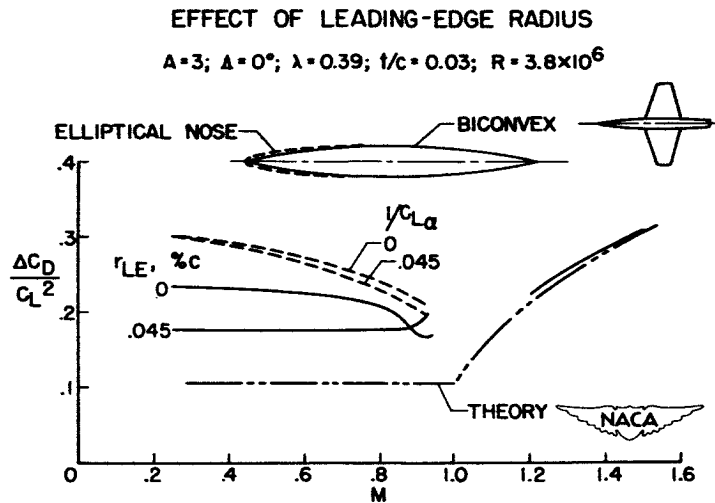


Figure 5

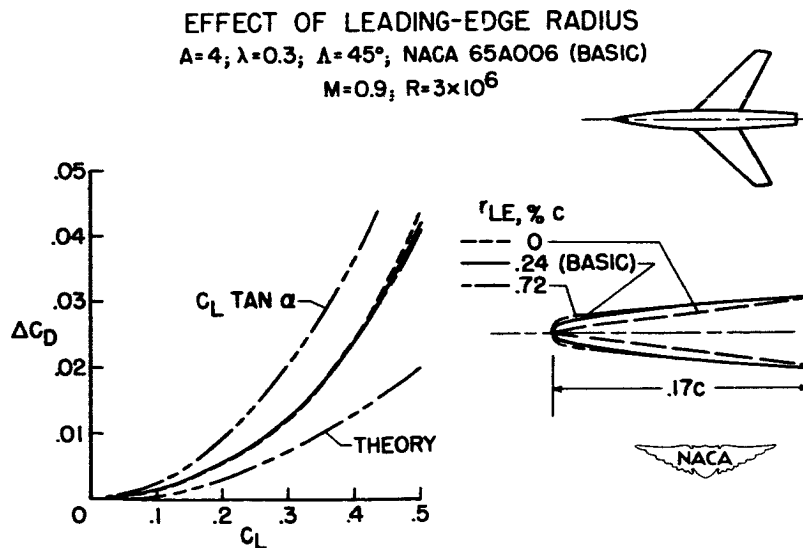


Figure 6

EFFECT OF ASPECT RATIO

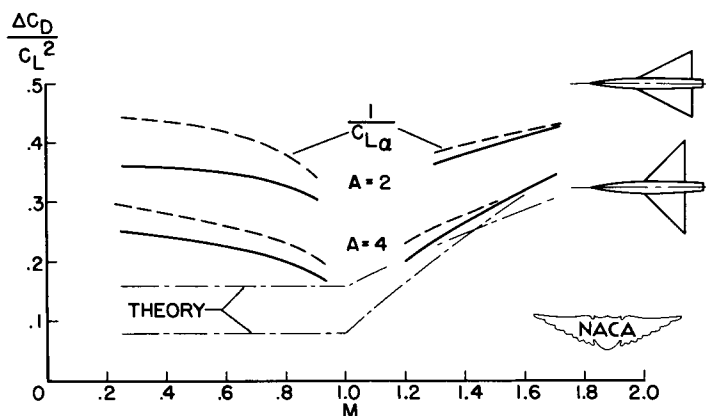
 $t/c = 0.03; R = 3 \times 10^6$


Figure 7

EFFECT OF INCIDENCE ON CAMBER AND TWIST

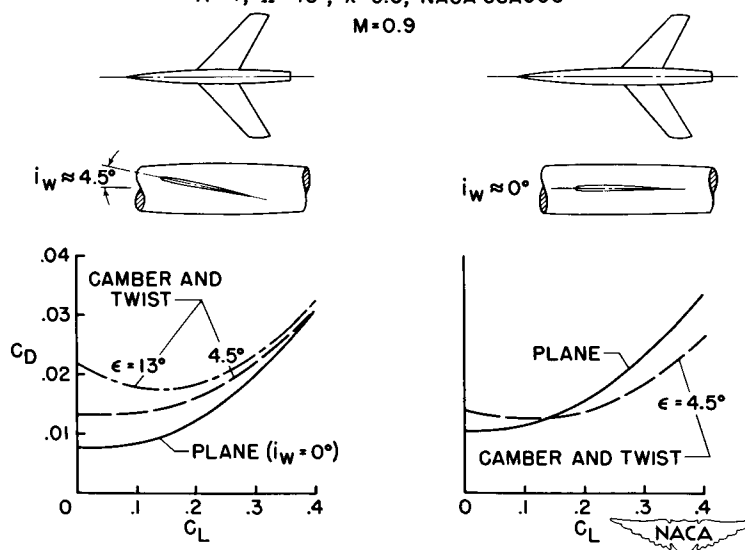
 $A=4; \Lambda=45^\circ; \lambda=0.6; \text{NACA } 65A006$
 $M=0.9$


Figure 8

EFFECT OF SURFACE SHAPE

A=2; NACA 0005-63; $R = 7.5 \times 10^6$

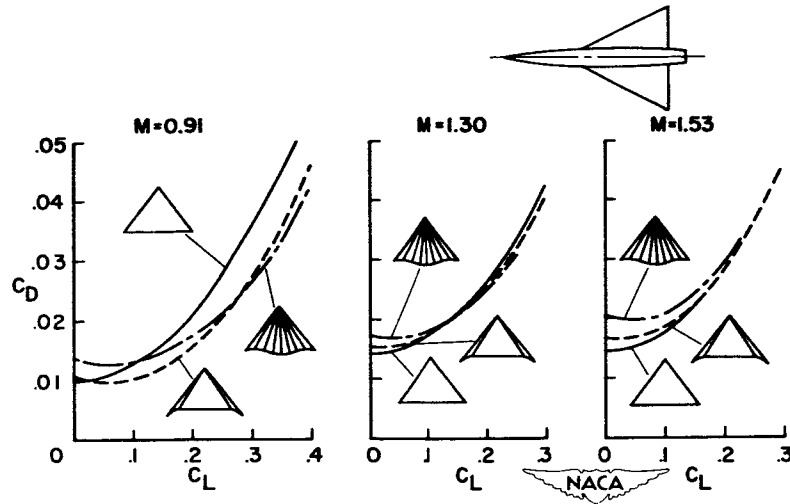


Figure 9

EFFECT OF EXTENT OF NOSE CAMBER

A=2.2; NACA 0004-65 (MOD.), $R = 4 \times 10^6$

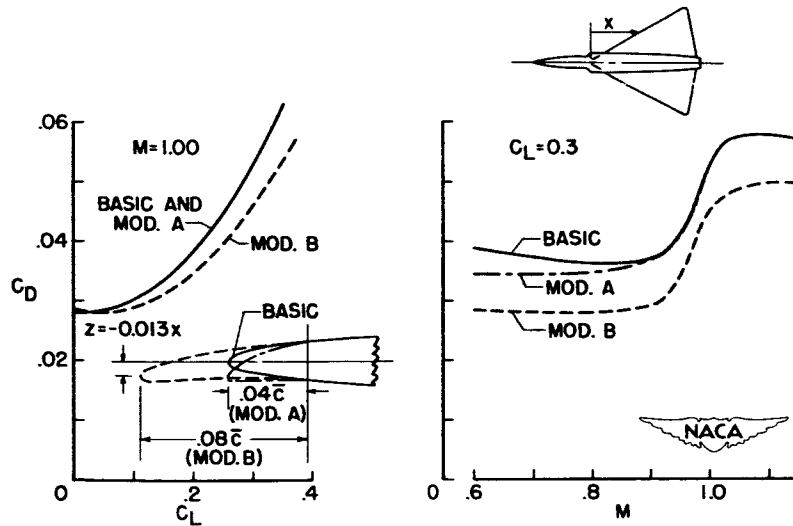


Figure 10

03742240000
CONFIDENTIAL

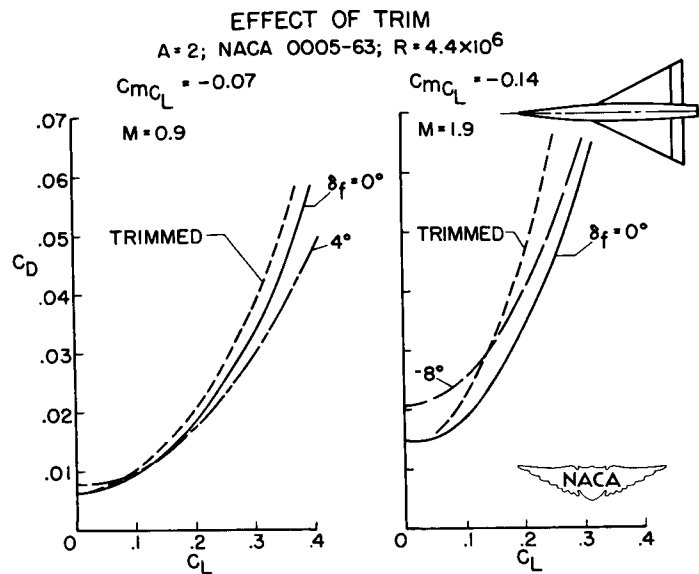


Figure 11

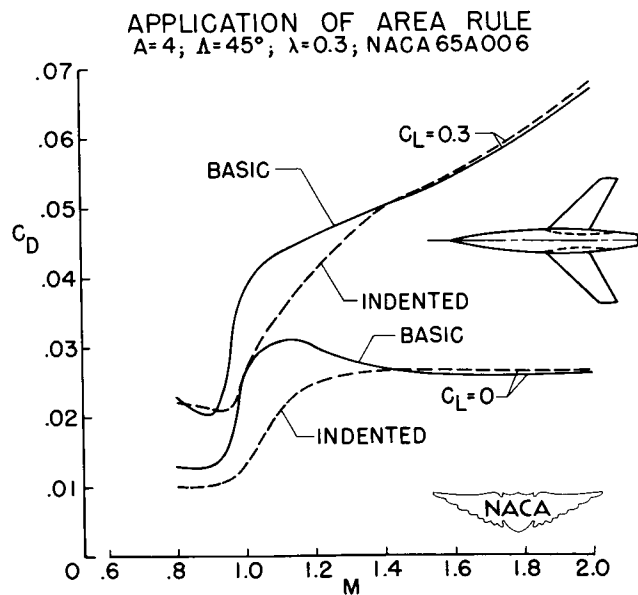


Figure 12

APPLICATION OF AREA RULE
 $A=4$; $\Lambda=45^\circ$; $\lambda=0.3$; NACA 65A006

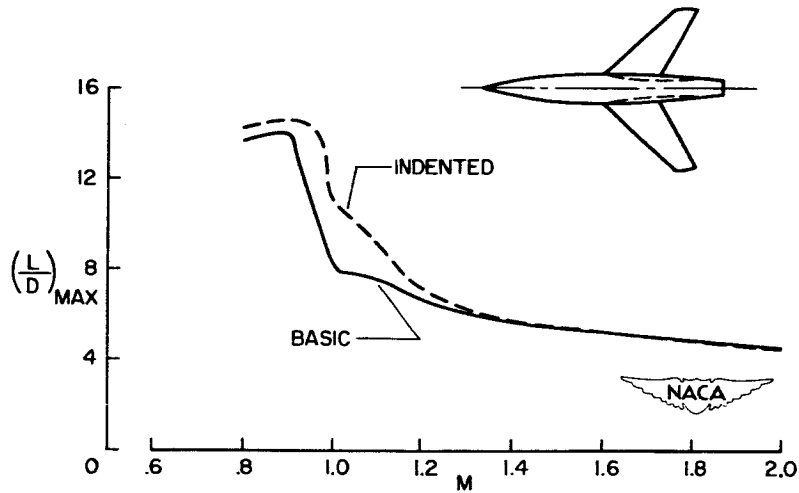


Figure 13

EFFECT OF LOCAL BODY INDENTATIONS
 $A=4$; $\lambda=0.6$; NACA 65A006

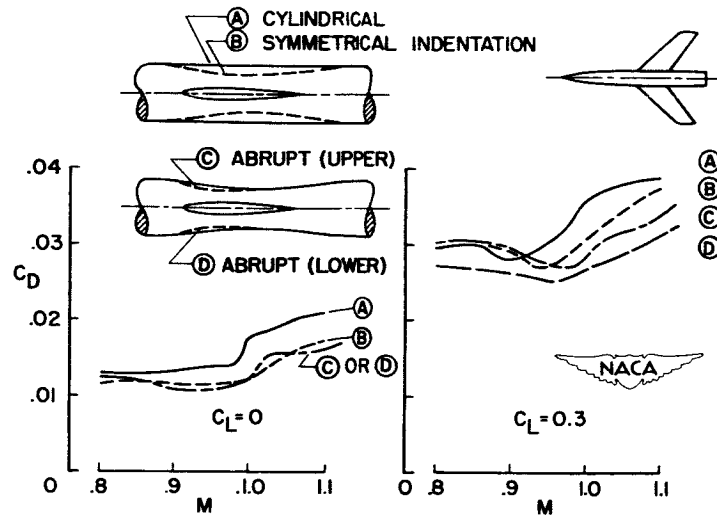


Figure 14

APPLICATION OF AREA RULE AND CAMBER AND TWIST

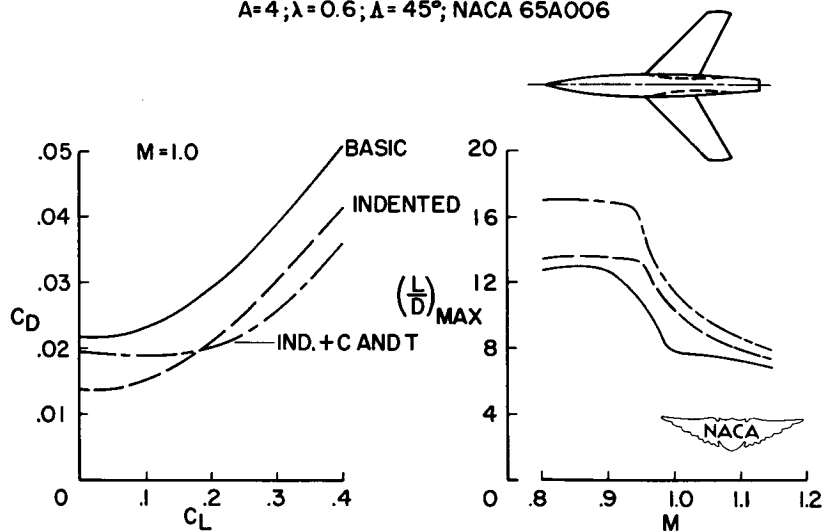
 $A=4; \lambda=0.6; \Delta=45^\circ$; NACA 65A006

Figure 15

CONFIDENTIAL

LONGITUDINAL CHARACTERISTICS OF WINGS

By Thomas A. Toll

Langley Aeronautical Laboratory

INTRODUCTION

The previous papers have summarized recent information relative to the drag at zero lift and the variation of drag within the lower range of lift coefficients. In considering the complete range of lift coefficients for normal flight operations, the performance characteristics and longitudinal stability are perhaps equally important factors in the selection of the wing configuration. One objective of the designer can be regarded as the achievement of the best possible compromise between performance and stability over the ranges of Mach number and lift coefficient that are likely to be encountered. This paper deals with various approaches toward realization of this objective in so far as the wing or wing-fuselage characteristics are concerned. Consideration is given only to wings of 6-percent thickness or less.

SYMBOLS

A	wing aspect ratio
C_L	lift coefficient
C_m	pitching-moment coefficient
L/D	lift-drag ratio
M	Mach number
R	Reynolds number
b	wing span
c	local wing chord
\bar{c}	mean aerodynamic chord
r	wing section leading-edge radius

TOLL

t	maximum thickness of wing section
x_{ac}	distance measured rearward from leading edge of wing mean aerodynamic chord to wing aerodynamic center
Δx_{ac}	shift in longitudinal position of wing aerodynamic center at low lift
Δx_{cp}	change in longitudinal position of wing center of pressure
Δy_{cp}	change in lateral position of wing center of pressure
λ	wing taper ratio; ratio of tip chord to root chord
$\Lambda_{c/4}$	wing sweep angle measured with respect to quarter-chord line
Λ_{LE}	wing sweep angle measured with respect to leading edge
δ_n	deflection of leading-edge flap, measured in plane parallel to plane of symmetry, positive when leading edge is down


RESULTS AND DISCUSSION

Wing Plan Forms

Wing plan forms which are representative of those in which interest has been centered are shown in figure 1. The three wings at the left have attracted considerable interest because of their attractive performance capabilities. In general, these wings require some modification or "fix" if satisfactory high-lift stability is to be attained. The three composite wings shown at the center represent an approach toward achieving good stability while maintaining the benefits of a moderately high aspect ratio and at least a part of the benefits resulting from large sweep. The wings at the right represent plan forms that might be expected to avoid high-lift stability problems through use of small sweep angles.

Wings of Large Sweep

Basic characteristics.— The nature of the stability problem that exists for wings of the type shown at the left of figure 1 is illustrated in figure 2. Results for several such wings are published in references 1 to 8. The wing geometry and Reynolds numbers are given at the right of




the figure. Each of these wings shows some pitching-moment instability within the normal operating lift range. Although the magnitude of the instability and the lift coefficient at which the instability begins vary somewhat for the different wings, the most severe condition exists at a Mach number of about 0.9 for each of these wings. At a Mach number of 1.0 the stability problem is essentially eliminated for two of the wings and is alleviated somewhat for the third. At supersonic speeds higher than those considered in figure 2, the wing-fuselage normally does not present a major stability problem. Of the plan forms shown in this figure, wings having about the aspect ratio and sweep angle of the wing at the top have received the greatest amount of attention with regard to means for improving their behavior. The objective in the studies that have been made is not necessarily the achievement of linear pitching-moment characteristics of the wing-fuselage combination, since, when a tail is used, the additional contribution of a tail generally is not linear. It is desirable however to avoid abrupt changes in slope such as those shown in figure 2.

Before considering the effects of variations in the geometry of the wing shown at the top of figure 2, it is appropriate to study the manner in which aerodynamic characteristics are altered through application of the area-rule concept in the design of the fuselage. The pitching moments and lift-drag ratios obtained at Mach numbers of 0.9 and 1.0 for the wing mounted on a cylindrical fuselage and on the fuselage modified by an indentation in accordance with the area-rule concept are presented in figure 3. (For additional details, see refs. 2 and 9). The results at $M = 0.9$ are representative of conditions in the subsonic speed range where the indentation has little effect on the lift-drag ratio. The results at a Mach number of 1.0 represent a transonic condition for which the indentation provides an appreciable gain in lift-drag ratios. At either Mach number, the effect of the indentation on pitching moments is small and amounts primarily to a slight extension of the lift range before instability begins. Indentations applied to some other wing-fuselage configurations have provided considerably larger performance gains than that indicated here; however, the effect on stability still was small.

It should be pointed out that the lift-drag ratios presented in the various figures contained herein should be interpreted only with respect to the variables considered on a given figure, since the investigations to be summarized employed different fuselage shapes and also differed in certain other details.

In considering wings of the aspect ratio and sweep angle shown in figure 3, the question arises as to whether benefits can be derived by selecting some taper ratio different from the value of 0.6 used. Figure 4 presents results from reference 8 at Mach numbers of 0.8 and 0.91 for wings having taper ratios varying from 0.3 to 1.0. The assumed centers of gravity for these wings have been adjusted to give the same slope of the moment curves for all wings near zero lift and at low Mach numbers.




The moment curves show that high-lift instability occurs for all wings, but that there is a progressive increase in the lift coefficient at which instability begins as the taper ratio is increased from 0.3 to 1.0. Essentially no change in the lift-drag ratios is indicated for these wings over the range of taper ratios considered. These wings, however, all were of 6-percent thickness. Since the taper-ratio-0.3 wing would seem to be the most efficient structure, its thickness probably could be reduced somewhat and some performance advantage thereby achieved at transonic and supersonic speeds. This wing was selected as the basic plan form for an extensive study of various modifications.

Modifications to swept wings.- The effect of a variation in leading-edge radius is compared in figure 5 with the effect of 6° droop of a 20-percent-chord leading-edge flap. The point symbols give results for a sharp nose, for the normal nose of the basic 65A006 airfoil, and for a nose having three times the radius of the nose of the basic airfoil. The solid-line curves were obtained from reference 10 and represent results obtained with the nose flap deflected 6° on the basic wing. At the selected Mach numbers of 0.8 and 0.9 the variation in leading-edge radius had no significant effect on either the stability or the lift-drag ratios of this wing. Deflection of the leading-edge flap improved the lift-drag ratios and extended the linear range of the pitching-moment curves. The advantage of droop was smaller at the higher Mach number. Some limited tests at transonic speeds (refs. 11 to 13) and at supersonic speeds have indicated that only a very small advantage can be expected by deflecting a leading-edge flap on a wing of the type used here.

The effects of leading-edge droop indicated in figure 5 also are representative of effects resulting from camber, camber and twist (refs. 14 and 15), and large-span slats. In general, such modifications improve the drag characteristics and extend the linear range of the pitching-moment curves but do not alleviate the instability at high lift.

More significant effects on stability at high lift have been obtained by such devices as fences, leading-edge chord-extensions, and notches in the wing leading edge. (See refs. 4, 5, and 10.) About the same effect has been indicated (ref. 16) for external stores if they are carefully positioned along the wing span. Each of these devices appears to depend largely on an ability to upset the stability of the leading-edge vortex that frequently exists on thin swept wings at moderately high angles of attack. Any change in flow phenomena that destroys the vortex will greatly decrease the effectiveness of these devices. The effects of these devices on pitching moments result largely from controlling the location at which stalling is initiated and not through any appreciable reduction in the amount of separation. As would be expected, therefore, such devices have little effect on drag characteristics.



It has been shown in references 10 and 11 that combining a leading-edge chord extension with a full-span drooped nose flap permits both the performance benefit of the nose flap and the stability advantage of the chord extension to be obtained simultaneously. The effects of this combination and of some additional modifications are shown in figure 6. The results for the basic wing are given by the solid curves. Results for the chord-extension combined with the deflected nose flap are given by the short-dashed curves. Note the rather large gains in both stability and lift-drag ratios that are obtained. The additional modifications consisted of a wing cutout with refairing of the wing contour near the fuselage intersection and a trailing-edge extension. These additional modifications provided some additional control over the pitching-moments at high lift but did not provide completely satisfactory stability at the selected Mach numbers of 0.8 and 0.9. It is a point of interest that a modification opposite to the wing cutout shown here - that is, a forward extension of the wing chord near the fuselage - has been found to aggravate the high-lift stability problem (ref. 17, for example). A comparison of the lift-drag ratios of the latter two modifications with those obtained with only the nose flap and chord-extension shows that the trailing-edge extension sometimes gave some improvement, but the leading-edge cutout had an adverse effect. All three modifications provided improvements over results obtained with the basic wing.


Composite wings. - A more extreme method of handling the stability problem involves use of composite wing plan forms. In figure 7 results for an M-wing, a W-wing, and a plan form sometimes referred to as a "cranked wing" are compared with results for the basic 45° swept wing from which the composite plan forms were derived. In order to facilitate the comparison, the pitching-moment curves for all wings were adjusted to the same slope near zero lift at Mach number 0.8. The results indicate that the M-wing at least offers an effective means for controlling high-lift stability in the critical Mach number range near 0.9. Selection of different juncture locations or different sweep angles of the inboard and outboard panels should make it possible to achieve additional improvements in the shapes of the pitching-moment curves. It must be emphasized, however, that the more favorable stability characteristics obtained with these plan forms again result from controlling the locations at which flow separation is initiated and not from any material decrease in the amount of separation. Tuft surveys indicate separation at the root and tips of the M-wing and at the panel junctures for the W and cranked wings. At the selected Mach numbers of 0.8 and 0.9 the lift-drag ratios for the M-wing compare favorably with those of the basic swept wing. It is not known, however, to what extent the characteristics of the composite wings might be improved by such devices as nose flaps or camber. Some minimum drag penalty has been indicated for M- and W-wings at transonic speeds; however, no penalty has been noted above a Mach number of about 1.25. (See ref. 18.)

Modifications to triangular wings.- Experience in applying modifications to triangular wings so far has been quite limited. The effects of one modification - a leading-edge chord-extension - are shown in figure 8. The characteristics of the basic model without chord-extensions are given at Mach numbers of 0.85 and 0.95 by the solid-line curves. The instability which covered only a small lift-coefficient range was essentially eliminated by the chord-extensions (dashed curves). The results shown here are representative of the entire Mach number range for which instability of the basic model existed. In this case the effect of the fix might be regarded as being complete; however for some other triangular-wing models having different fuselage configurations, this type of fix did not completely eliminate the instability. The effect of the modification on lift-drag ratios generally has been found to be insignificant, as is indicated in this figure. It has not yet been clearly established whether the stability advantages of modifications such as the chord-extension and the performance advantage of a cambered leading edge can be obtained simultaneously by combining the two devices.

Wings of Small Sweep

Considerations regarding use of small sweep.- In considering the possible use of straight wings or wings of reduced sweep as a means of avoiding stability difficulties, the possibility of a penalty in performance is of course of paramount interest. Whether such a penalty exists can be determined only as a result of detailed design studies with consideration given to aerodynamic data of the type discussed in the preceding papers and in references 19 to 24.

Another factor that needs careful consideration is the magnitude of the shift in aerodynamic center of these wings while passing from subsonic to supersonic speeds. An attempt to correlate this shift for thin wings in the region of zero lift is indicated in figure 9. The incremental change in aerodynamic-center position (defined as the difference between maximum forward and maximum rearward aerodynamic-center positions below a Mach number of 1.15) is plotted against sweep angle. Results are considered for aspect ratios of 2, 3, 3.5, and 4. Wings having values of the taper ratio parameter λ less than 0.4 are indicated by open symbols and wings with λ greater than 0.4 are indicated by solid symbols. For the range of plan forms considered, there appeared to be very little correlation with aspect ratio and, in general, little correlation with taper ratio; although for small sweep angles there is an indication of a larger aerodynamic-center shift for the larger taper ratios. A fairly definite trend with sweep angle results and indicates an increase in the aerodynamic-center shift by about 6 percent of the chord as the sweep angle is reduced from 45° to 0° .



Straight wings.- The stability characteristics of two straight wings are shown in figure 10. The results for the aspect-ratio-4 wing shown at the top were obtained in the Langley 16-foot transonic tunnel at a Reynolds number of 6×10^6 . Results given in the bottom plot are for an aspect-ratio-3 wing tested in the Ames 2- by 2-foot transonic tunnel at a Reynolds number of 1.5 million. The characteristics of these wings are generally similar. Nonlinearities again appear in the pitching-moment curves, particularly at Mach number 0.9. In these cases, however, difficulties may result from excessive stability, rather than from a loss in stability, at high lift. As was indicated for the other wings, a final evaluation depends on the stability characteristics that are obtainable with the horizontal tail installed.

Selection of Sweep Angle.- With regard to the wing contribution to stability, it would be desirable to indicate some quantitative relation between pitching-moment nonlinearities - whether they are stabilizing or destabilizing - and the wing geometry. Results of an attempt to form such a relation are indicated on figures 11 and 12. The analysis has been made in terms of the center-of-pressure change with increasing lift. Evaluations of this change were made by subtracting center-of-pressure locations at low lift from the center-of-pressure locations at a lift coefficient of 0.6 and at the maximum lift coefficient. Results from a systematic series of wings tested on a transonic bump through maximum lift and to Mach numbers of about 1.2 at a Reynolds number of 1.0×10^6 were used in the analysis. The six wings considered on figure 11 had a taper ratio of 0, an aspect ratio of 4.0, and sweep angles varying from -14° to 45° . Figure 12 gives results obtained with the same wings, but with the tips clipped to give an aspect ratio of 3 and a taper ratio of 0.14.


Since the wings were tested as reflection-plane models, both the longitudinal change $\left(\frac{\Delta x_{cp}}{c}\right)$ and the lateral change $\left(\frac{\Delta y_{cp}}{b/2}\right)$ in center of pressure could be determined. The results show that, in general, the longitudinal center-of-pressure changes at a Mach number of 1.1 were considerably smaller than the changes at a Mach number of 0.9. Fairly large lateral changes occurred at both Mach numbers, however. Whether a rearward or a forward change in wing center of pressure is desired for a particular design will depend on factors not dealt with in this paper; however, for purposes of illustration, it is of interest to consider the case for which a minimum change in longitudinal position of the center of pressure is desired. For the pointed wings of aspect ratio 4, a sweep angle in the vicinity of 20° or 30° would be selected to meet this requirement. For the clipped wings of aspect ratio 3, a sweep angle between 30° and 40° is indicated. It is important to note that for either wing series, the wings that would be expected to give the smallest longitudinal changes in center of pressure would experience appreciable inward changes in center of pressure at a Mach number of 0.9,

even at the relatively low lift coefficient of 0.6. Such inward displacements are associated with tip stalling and a reduction in the effective span of the trailing vortex sheet. This may cause erratic changes in downwash as well as buffeting and erratic changes in the lateral stability derivatives.

Wings of intermediate sweep.- The charts of figures 11 and 12 are of limited use for general design purposes in that they deal with only two specific series of wings; also, the test Reynolds number was only 1.0×10^6 . It should be of interest to inspect the stability characteristics of two wings tested at higher Reynolds number but having aspect ratios and sweep angles such that small changes in center of pressure would be expected. The results are given in figure 13. Both wings are of aspect ratio 3. One wing, having 37° sweep and a taper ratio of 0.2, conforms closely to the conditions for minimum change in center of pressure indicated by figure 12. The other wing, because of its smaller sweep angle, would be expected to experience some increase in stability at high lift. Results for both wings show some jogs in the pitching-moment curves, particularly at Mach numbers near 0.9. In general, however, the nonlinearities are smaller than those indicated for most of the wings discussed previously, and the major trends are about as would be expected from the preceding charts.

CONCLUDING REMARKS

In summary, this paper has treated three approaches to the problem of wing selection. The first involves use of modifications or "fixes" to correct the basic instability of wings with relatively large sweep angles. Such modifications, if carefully tailored to the wing being considered, may provide marked improvements in both stability and performance at the lower subsonic Mach numbers; however, in general, there is no assurance that the modifications will be sufficiently effective, particularly at Mach numbers near 0.9. The other two approaches involve use of composite wings - particularly the M-type plan form - or wings of intermediate sweep. These latter methods provide a more positive means of dealing with the stability problem. The methods considered do not necessarily provide alleviation of flow separation at high lift, and therefore problems involving buffeting, erratic downwash, and erratic lateral-stability derivatives may exist even though the static longitudinal stability of the wing-fuselage combination is apparently good.



REFERENCES

1. Osborne, Robert S., and Mugler, John P., Jr.: Aerodynamic Characteristics of a 45° Sweptback Wing-Fuselage Combination and the Fuselage Alone Obtained in the Langley 8-Foot Transonic Tunnel. NACA RM L52E14, 1952.
2. Carmel, Melvin M.: Transonic Wind-Tunnel Investigation of the Effects of Aspect Ratio, Spanwise Variations in Section Thickness Ratio, and a Body Indentation on the Aerodynamic Characteristics of a 45° Sweptback Wing-Body Combination. NACA RM L52L26b, 1953.
3. Hallissy, Joseph M., and Bowman, Donald R.: Transonic Characteristics of a 45° Sweptback Wing-Fuselage Combination - Effect of Longitudinal Wing Position and Division of Wing and Fuselage Forces and Moments. NACA RM L52K04, 1953.
4. Hieser, Gerald: An Investigation at Transonic Speeds of the Effects of Fences, Drooped Nose, and Vortex Generators on the Aerodynamic Characteristics of a Wing-Fuselage Combination Having a 6-Percent-Thick, 45° Sweptback Wing. NACA RM L53B04, 1953.
5. West, F. E., Jr., Liner, George, and Martz, Gladys S.: Effect of Leading-Edge Chord Extensions on the Aerodynamic Characteristics of a 45° Sweptback Wing-Fuselage Combination at Mach Numbers of 0.40 to 1.03. NACA RM L53B02, 1953.
6. Kuhn, Richard E., and Wiggins, James W.: Wind-Tunnel Investigation of the Aerodynamic Characteristics in Pitch of Wing-Fuselage Combinations at High Subsonic Speeds - Aspect-Ratio Series. NACA RM L52A29, 1952.
7. Wiggins, James W., and Kuhn, Richard E.: Wind-Tunnel Investigation of the Aerodynamic Characteristics in Pitch of Wing-Fuselage Combinations at High Subsonic Speeds - Sweep Series. NACA RM L52D18, 1952.
8. King, Thomas J., Jr., and Pasteur, Thomas B., Jr.: Wind-Tunnel Investigation of the Aerodynamic Characteristics in Pitch of Wing-Fuselage Combinations at High Subsonic Speeds - Taper-Ratio Series. NACA RM L53E20, 1953.
9. Robinson, Harold L.: A Transonic Wind-Tunnel Investigation of the Effects of Body Indentation As Specified by the Transonic Drag-Rise Rule on the Aerodynamic Characteristics and Flow Phenomena of a 45° Sweptback-Wing-Body Combination. NACA RM L52L12, 1953.

[REDACTED]

10. Spreeman, Kenneth P., and Alford, William J., Jr.: Investigation of the Effects of Leading-Edge Chord-Extension and Fences in Combination With Leading-Edge Flaps on the Aerodynamic Characteristics at Mach Numbers From 0.4 to 0.93 of a 45° Sweptback Wing of Aspect Ratio 4. NACA RM L53A09a, 1953.
11. Donlan, Charles J., and Weil, Joseph: Characteristics of Swept Wings at High Speeds. NACA RM L52A15, 1952.
12. Alford, William J., Jr., and Spreeman, Kenneth P.: Small-Scale Transonic Investigation of a 45° Sweptback Wing of Aspect Ratio 4 With Combinations of Nose-Flap Deflections and Wing Twist. NACA RM L52K13, 1953.
13. Spreeman, Kenneth P., and Alford, William J., Jr.: Small-Scale Transonic Investigation of the Effects of Full-Span and Partial-Span Leading-Edge Flaps on the Aerodynamic Characteristics of a 50° 38° Sweptback Wing of Aspect Ratio 2.98. NACA RM L52E12, 1952.
14. Harrison, Daniel E.: A Transonic Wind-Tunnel Investigation of the Characteristics of a Twisted and Cambered 45° Sweptback Wing-Fuselage Configuration. NACA RM L52K18, 1952.
15. Harrison, Daniel E.: The Influence of a Change in Body Shape on the Effects of Twist and Camber as Determined by a Transonic Wind-Tunnel Investigation of a 45° Sweptback Wing-Fuselage Configuration. NACA RM L53B03, 1953.
16. Silvers, H. Norman, and O'Bryan, Thomas C.: Some Notes on the Aerodynamic Loads Associated With External-Store Installations. NACA RM L53E06a, 1953.
17. Weil, Joseph, Sleeman, William C., Jr., and Byrnes, Andrew L., Jr.: Investigation of the Effects of Wing and Tail Modifications on the Low-Speed Stability Characteristics of a Model Having a Thin 40° Swept Wing of Aspect Ratio 3.5. NACA RM L53C09, 1953.
18. Katz, Ellis, Marley, Edward T., and Pepper, William B.: Flight Investigation at Mach Numbers From 0.8 to 1.4 to Determine the Zero-Lift Drag of Wings With "M" and "W" Plan Forms. NACA RM L50G31, 1950.
19. Hall, Charles F.: Lift, Drag, and Pitching Moment of Low-Aspect-Ratio Wings at Subsonic and Supersonic Speeds. NACA RM A53A30, 1953.

20. Polhamus, Edward E.: Summary of Results Obtained by Transonic-Bump Method on Effects of Plan Form and Thickness on Lift and Drag Characteristics of Wings at Transonic Speeds. NACA RM L51H30, 1951.
21. Bielat, Ralph P.: A Transonic Wind-Tunnel Investigation of the Aerodynamic Characteristics of Three 4-Percent-Thick Wings of Sweepback Angles 10.8° , 35° , and 47° , Aspect Ratio 3.5, and Taper Ratio 0.2 in Combination With a Body. NACA RM L52B08, 1952.
22. Bielat, Ralph P., Harrison, Daniel E., and Coppolino, Domenic A.: An Investigation at Transonic Speeds of the Effects of Thickness Ratio and of Thickened Root Sections on the Aerodynamic Characteristics of Wings With 47° Sweepback, Aspect Ratio 3.5, and Taper Ratio 0.2 in the Slotted Test Section of the Langley 8-Foot High-Speed Tunnel. NACA RM L51I04a, 1951.
23. Robinson, Ross B.: Aerodynamic Characteristics at Supersonic Speeds of a Series of Wing-Body Combinations Having Cambered Wings With an Aspect Ratio of 3.5 and a Taper Ratio of 0.2 - Effects of Sweep Angle and Thickness Ratio on the Aerodynamic Characteristics in Pitch at $M = 2.01$. NACA RM L52E09, 1952.
24. Robinson, Ross B., and Driver, Cornelius: Aerodynamic Characteristics at Supersonic Speeds of a Series of Wing-Body Combinations Having Cambered Wings With an Aspect Ratio of 3.5 and a Taper Ratio of 0.2 - Effects of Sweep Angle and Thickness Ratio on the Aerodynamic Characteristics in Pitch at $M = 1.60$. NACA RM L51K16a, 1952.

WING PLAN FORMS

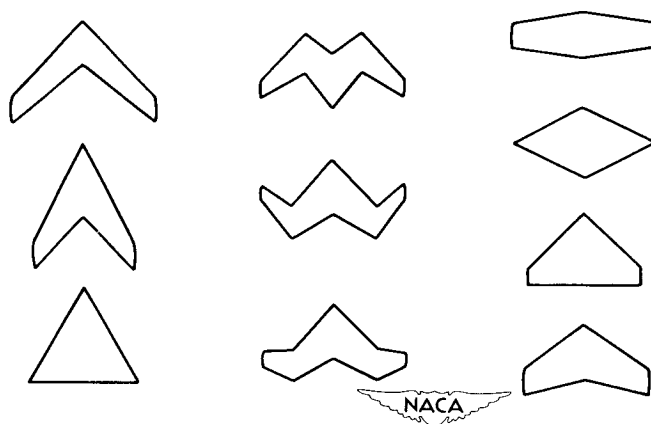


Figure 1

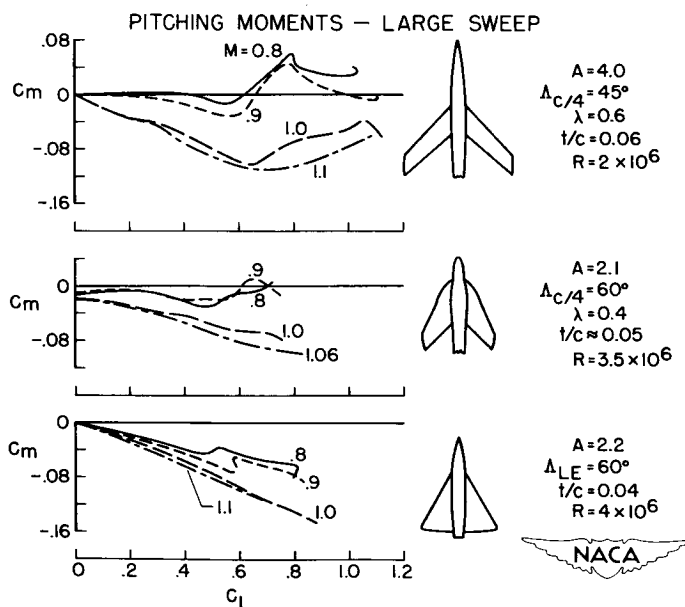


Figure 2

EFFECT OF APPLICATION OF AREA-RULE CONCEPT

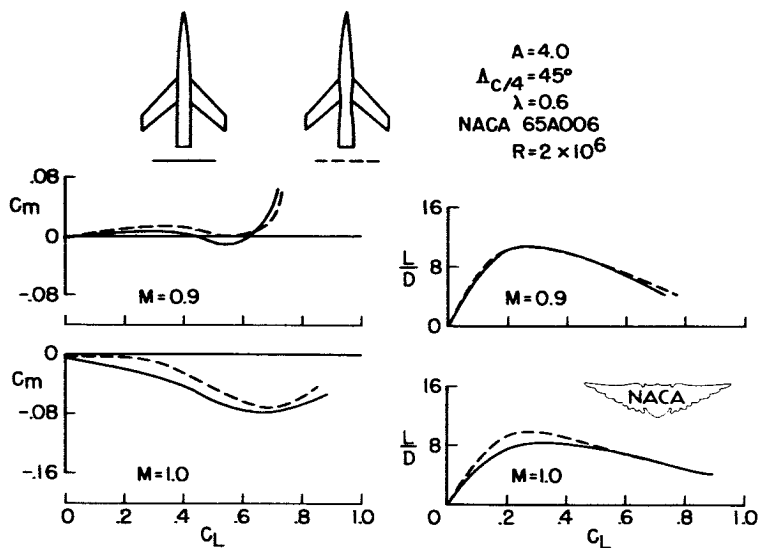


Figure 3

EFFECT OF TAPER RATIO

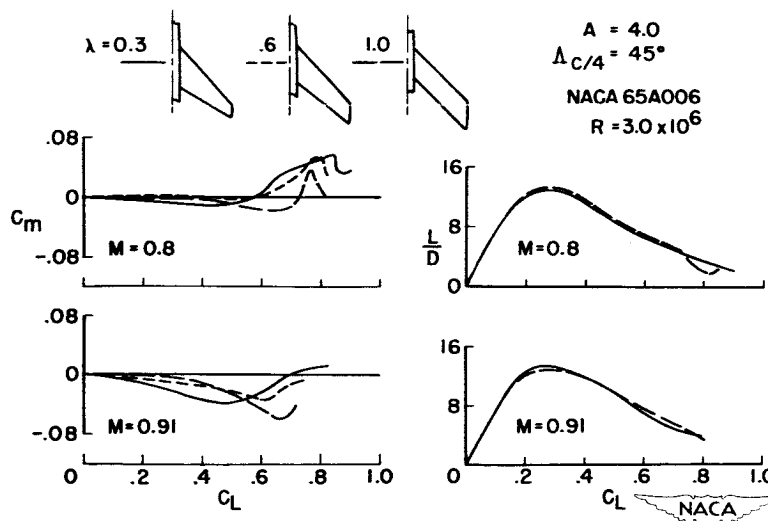


Figure 4

EFFECT OF NOSE RADIUS AND DROOP

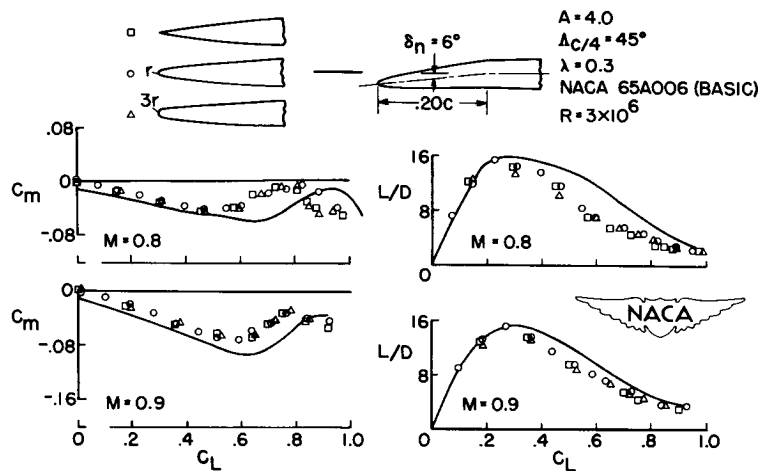


Figure 5

EFFECT OF MODIFICATIONS IN COMBINATION

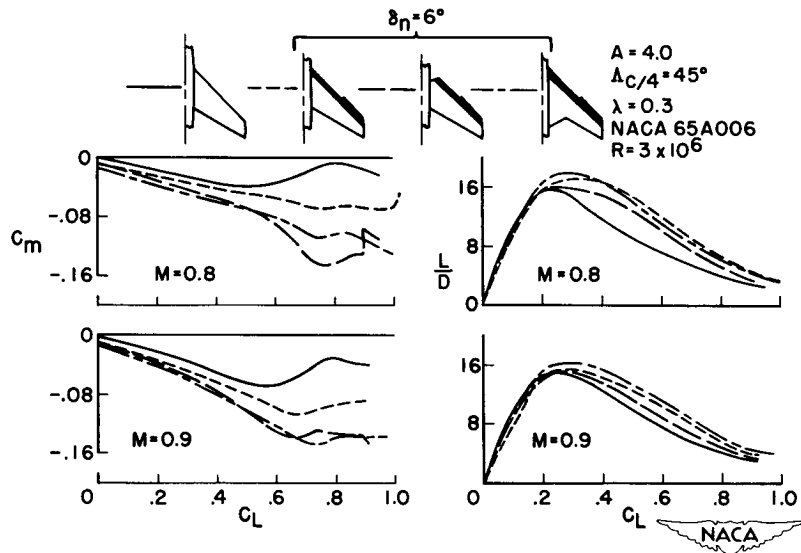


Figure 6

COMPOSITE WINGS

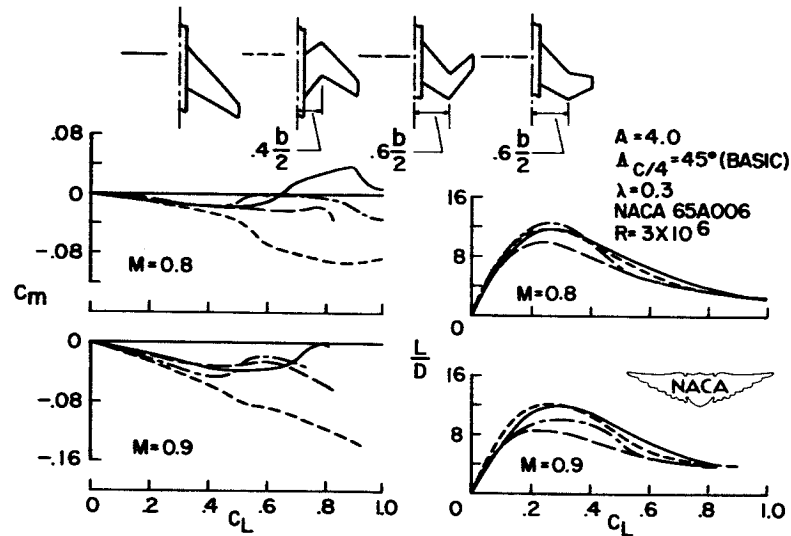


Figure 7

TRIANGULAR WINGS — EFFECT OF CHORD-EXTENSIONS

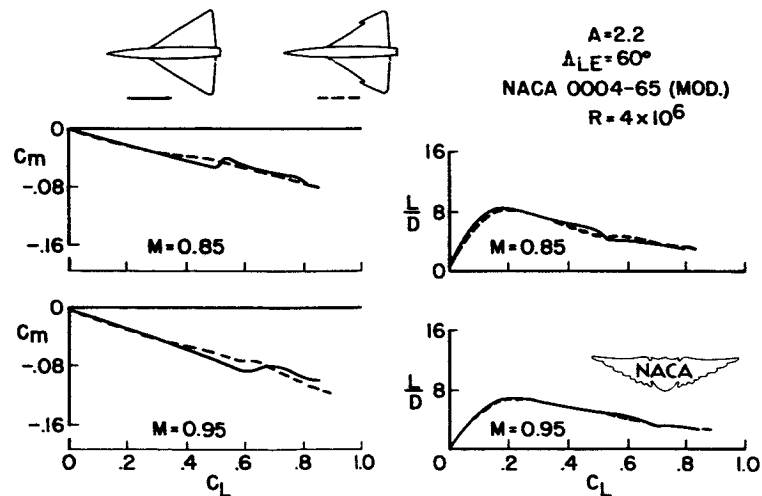


Figure 8

TRANSONIC AERODYNAMIC-CENTER SHIFT

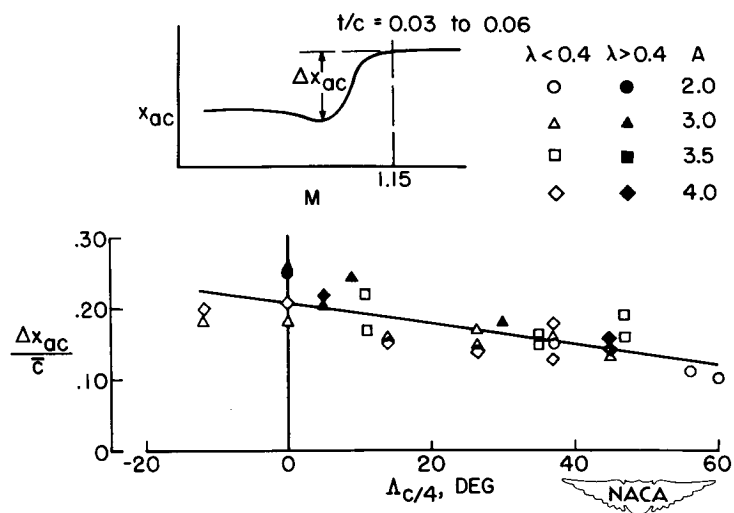


Figure 9

PITCHING MOMENTS—STRAIGHT WINGS

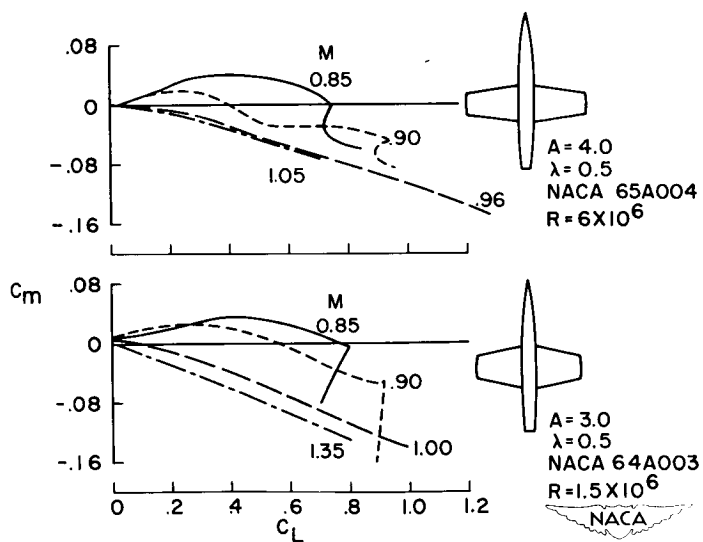


Figure 10

CENTER OF PRESSURE CHANGE WITH INCREASING LIFT

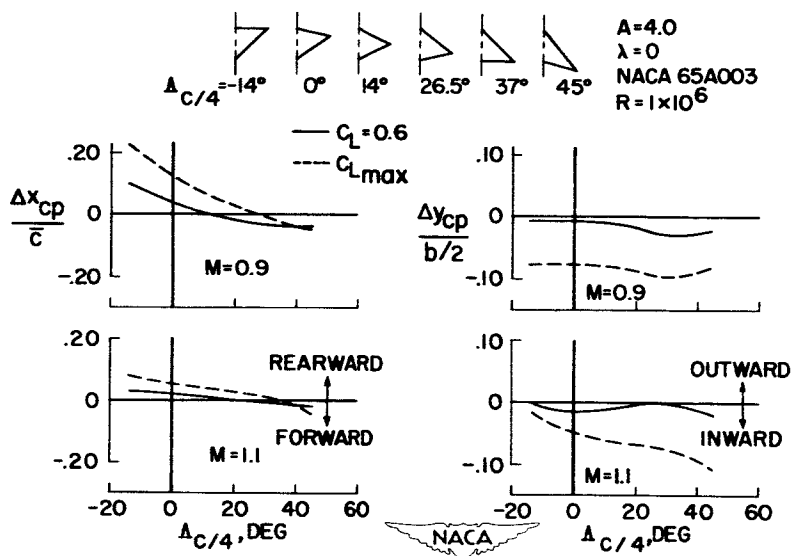


Figure 11

CENTER OF PRESSURE CHANGE WITH INCREASING LIFT

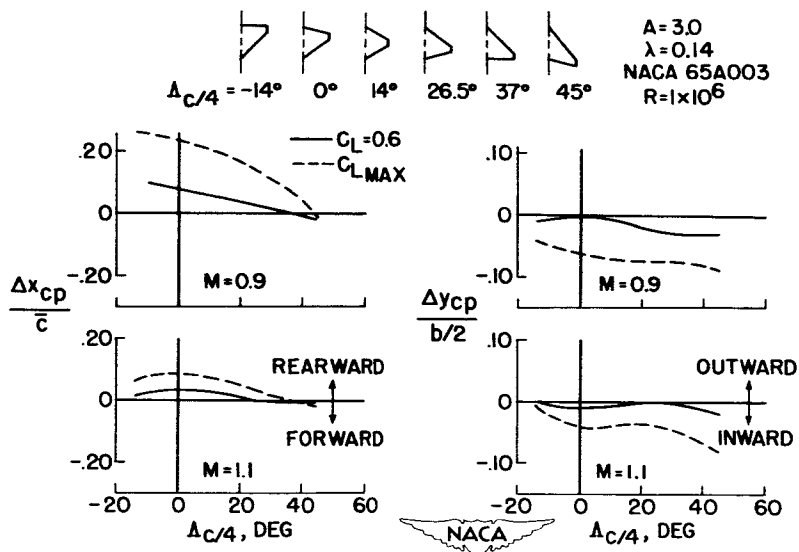


Figure 12

CONFIDENTIAL

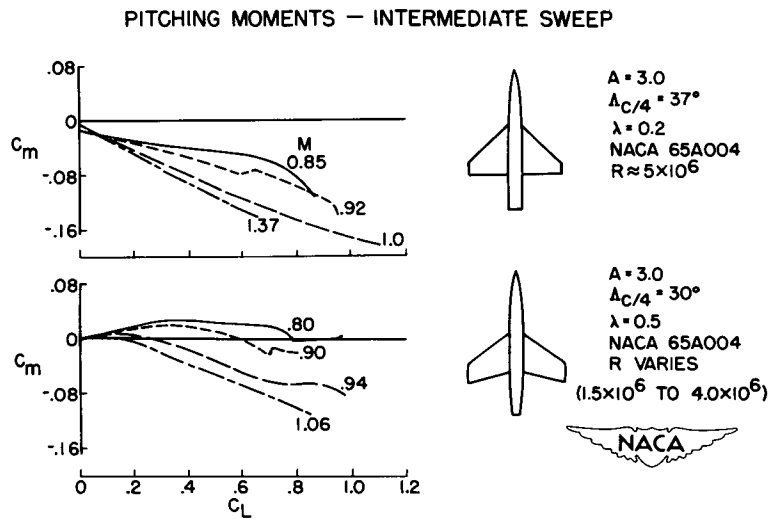


Figure 13

CONFIDENTIAL

CONFIDENTIAL

AERODYNAMIC CHARACTERISTICS OF LOW-ASPECT-RATIO WINGS

AT HIGH SUPERSONIC MACH NUMBERS

By Edward F. Ulmann and Mitchel H. Bertram

Langley Aeronautical Laboratory


This paper presents some recently obtained data on the aerodynamic characteristics of low-aspect-ratio wings at supersonic Mach numbers of 4.04 and 6.9 and discusses some new methods of predicting the lift and drag of such wings. Data on lifting wings in the Mach number range above 2.5 are not plentiful and most of the available data may be found in references 1 to 8.

The plan forms, airfoil section, and thickness ratios of the wings tested are given in figures 1 and 2. The wings shown in figure 1 all have double-wedge airfoil sections, with constant thickness ratios over the wing span. The wings of figure 2 are all of the same family, having hexagonal airfoil sections with constant thickness outboard to the 56-percent-semispan station and double-wedge sections with maximum thickness at the 69.2-percent-chord station from there to the wing tips. Exceptions to this are the two delta wings which have rounded leading edges and the clipped delta wings. The wings were selected to extend the Mach number range of data on wings previously tested and to investigate the effects of changes in the aspect ratio of delta wings, changes in wing plan form, and changes in airfoil section and thickness. The models tested at Mach number 6.9 in the Langley 11-inch hypersonic tunnel were sting-mounted, and lift and drag data were obtained. The models tested at Mach number 4.04 in the Langley 9- by 9-inch Mach number 4 blow-down jet were tested as semispan models extending out into the stream from a boundary-layer bypass plate; lift, drag, pitching moment, and wing-root bending moment were measured.

The aerodynamic characteristics of the double-wedge section delta wings will be considered first. A summary of the lift-curve slopes at zero angle of attack for the double-wedge section wings of this investigation is presented in figure 3, together with some data on delta wings of the same section from the Langley 9-inch supersonic tunnel at Mach numbers 1.62, 1.93, and 2.40. The ordinate in figure 3, the ratio of the delta-wing lift-curve slope to the linear-theory two-dimensional lift-curve slope, and abscissa, the ratio of the tangent of the semi-apex angle of the wing to the tangent of the free-stream Mach angle, are basic parameters obtained from the linear theory of delta wings (refs. 9 and 10). Tangent ratios less than 1 represent wings with subsonic leading edges, whereas at tangent ratios greater than 1 the wing leading edges are nominally supersonic, but may be actually

subsonic because of shock detachment due to wing thickness. The shaded region in figure 3 includes points obtained in various other facilities throughout the country from tests of delta wings with thickness ratios equal to or less than 3 percent at Mach numbers from 1.2 to 2.4 (refs. 11 to 16). In the past, the analysis of delta-wing data for Mach numbers below 2.5, plotted to the variables of figure 3, has led to several conclusions: first, that delta wings having the same section and the same tangent ratio have lift ratios which are relatively independent of Mach number; and, second, that the linear theory gives a fairly accurate prediction of the lift of thin delta wings at low values of the tangent ratio, but overestimates the lift at tangent ratios from about 0.7 to 1.5. As wing thickness ratios increased, the lift-curve slopes were found to become increasingly less than the linear-theory values. The only theoretical methods which take leading-edge shock detachment into account, and thus might be expected to give better predictions for the lift of delta wings in the shock-detached region, are methods using conical characteristics solutions, such as that of Maslen (ref. 17). These nonlinear methods are very laborious and simpler methods are desirable. The data from the tests of double-wedge section delta wings at Mach numbers 4.04 and 6.9 (fig. 3) indicate that these linear-theory parameters are not adequate for correlating higher Mach number data, since the high Mach number tests generally gave higher lift ratios than the low Mach number tests. In the region of attached leading-edge shocks, it was found that the lift-curve slopes were very close to the shock-expansion two-dimensional values for the wing airfoil sections. Accordingly, the data were plotted (fig. 4) as the ratio of the experimental lift-curve slope to the two-dimensional shock-expansion lift-curve slope for the streamwise airfoil section of the wing. In general, lift ratios close to 1 were obtained at high values of the tangent ratio, indicating that the two-dimensional shock-expansion theory gives good predictions of lift-curve slopes of delta wings when the leading-edge shock is attached.


At values of the tangent ratio close to those for shock detachment, the experimental lift ratios dropped abruptly below 1, as was noted at the lower Mach numbers by Love (ref. 18). Some simple method of predicting the variation of lift ratio in this region is desirable. Since the predictions of the linear theory are the same as those of the characteristics theory for wings of zero thickness, it was assumed that the lift of these finite-thickness wings in the shock-detached region varies in a manner similar to linear-theory prediction for the zero-thickness wing. The similarity constant was determined by the shock-detachment value of the tangent ratio for each wing. Using these constants, curves were drawn from the shock-detachment points to predict the wing lifts, as shown in figure 4. This modification to the linear theory predicts the experimental results with a maximum error of 5 percent for the five Mach numbers shown in figure 4. When extended to the prediction of lift-curve slopes of arrow- and diamond-plan-form wings tested at Mach



number 4.04 by modifying the results of Puckett and Stewart's theory (ref. 19), given in chart form in reference 20, the method gave predictions within 7 percent of the experimental values for one arrow wing with a single-wedge section and one diamond-plan-form wing with a hexagonal section.

The previous figures have presented data on lift-curve slopes at zero angle of attack. Figures 5 and 6 present typical lift curves for double-wedge-section delta wings at Mach numbers 4.04 and 6.9. At both Mach numbers the curves are essentially linear at low angles of attack. Nonlinearities are evident at angles of attack above approximately 6° , especially at Mach number 6.9. An estimate of the lift of the wing having a 30° semiapex angle at Mach number 6.9 at 10° angle of attack would be 20 percent low if based on the lift-curve slope at 0° angle of attack. The experimental data for the wings of figures 5 and 6 follow very closely the predictions of the shock-expansion two-dimensional theory for the streamwise airfoil sections of the wings at both Mach numbers, as long as the leading-edge shock is attached. When the angle of attack becomes so large that the leading-edge shock detaches, the experimental values begin to fall below the shock-expansion theory. This is especially noticeable at Mach number 6.9, where an abrupt change in the slope of the lift curves occurs at the angles of attack at which leading-edge shock detachment is predicted theoretically. At Mach number 4.04, the data for the 5-percent-thick wing, which has an attached leading-edge shock, agree very well with the shock-expansion theory, whereas the experimental lift coefficients for the much blunter 8-percent-thick wing, which has a detached shock at zero angle of attack, fall below the theoretical values. The shock-expansion theory gives predictions of the lifts of the double-wedge wings tested within about 2 percent of the experimental value at Mach number 4.04 and within 5 percent at Mach number 6.9, as long as the angle of attack is below that for leading-edge shock detachment.

The next section of this paper discusses methods of predicting and correlating the drag of low-aspect-ratio delta wings. The prediction of drag results involves, of course, three factors: predictions of friction drag, minimum pressure drag, and drag due to lift. In order to make a theoretical prediction of friction drag, predictions of the type of boundary layer and the location of boundary-layer transition must be made. Satisfactory theoretical methods of predicting boundary-layer transition on wings are not available at present, but the transition point, the nature of the boundary layer, and the value of the friction-drag coefficient can often be determined by experimental means in wind tunnels or in free flight. For example, an experimental value of the friction-drag coefficient at Mach number 4.04 was obtained by plotting the drag coefficients of wings having the same plan form and section against the square of the wing-thickness ratio and making a straight-line extrapolation through the experimental points to the zero-thickness



ordinate. A value of 0.0036 was obtained. Furthermore, the boundary-layer-transition lines on these same wings were determined by fluorescent-lacquer tests and, by using this information and by assuming no variation of C_{Df} with wing thickness ratio, estimates of the friction-drag coefficients of the wings were made using Van Driest's value of laminar skin-friction-drag coefficient (ref. 21), corrected for differences in stream static temperature (ref. 22), and the Frankl and Voishel extended value of the turbulent skin-friction-drag coefficient (ref. 23). An estimated value of 0.0033 was obtained by this method, which compares favorably with the experimental value of 0.0036. The experimentally determined value of the skin-friction drag coefficient was used to obtain the minimum pressure-drag coefficients at Mach number 4.04 used in the following discussion. Theoretically determined friction-drag coefficients were used at Mach number 6.9.

The next component of wing drag which will be considered is the minimum pressure drag. The linear theory for delta wings as derived by Puckett (ref. 24) indicates that all delta wings with double-wedge airfoil sections having a given maximum-thickness location and the same

value of the tangent ratio will have the same value of
$$\frac{C_{DP_{min}} \sqrt{M^2 - 1}}{(t/c)^2},$$

the ordinate of figures 7 and 8, for all thickness ratios and Mach numbers. Thus, the linear theory for each family of delta wings investigated appears as single curves in figures 7 and 8. The predictions of linear theory are rather poor for the wings shown in figure 7; however, all the experimental data for the wings with maximum thickness at 50 percent chord, wings $2\frac{1}{2}$, 5, and 8 percent thick, tested at Mach numbers from 1.62 to 6.9, fall very nearly on one curve, showing that these parameters successfully correlate experimental data for this family of wings. This result is found only for wings with sections that are symmetrical about the midchord point, since the higher order effects are small for such wings. For other wing sections with maximum thicknesses ahead of or behind the 50-percent-chord point, the higher order terms become important and the theory indicates Mach number effects in the shock-attached region which cannot be correlated by these parameters.

This point is illustrated by the results obtained from the wings with maximum thickness at 18 percent chord presented in figure 8. The predictions of the linear theory are poor for these blunt wings at low values of the tangent ratio due to the transonic nature of the flow over the wings; however, the lower Mach number data correlate well, since the second-order effects for this wing section are small at these Mach numbers. The data at the higher Mach numbers, the three experimental points obtained at Mach number 6.9 and the experimental value

obtained at Mach number 4.04, indicate that the high Mach number data do not correlate with the lower Mach number data at tangent ratios close to and beyond the shock-attachment value. The trend of the data at each Mach number indicates that the pressure drags become constant at values close to those predicted by shock-expansion theory for the wing section at each test Mach number. This same trend was clearly evident in figure 7 for the symmetrical double-wedge wings. Thus, it can be seen that, with the aid of shock-expansion two-dimensional theory, satisfactory predictions of the pressure drags of double-wedge delta wings can probably be made throughout the supersonic Mach number range up to 6.9. (Some of the data of figures 7 and 8 were presented in figure 11 of reference 5. The discussion of the pressure-drag data in reference 5 and the second conclusion of that reference are correct with reference to the wings with maximum thickness at 50 percent chord but apply only for Mach numbers from 1.62 to 2.4 for the wings with maximum thickness at 18 percent chord.)

If the skin-friction drag and the minimum pressure drag of a wing have been determined, the variation of the drag due to lift must be known if any estimates of lift-drag ratios are to be made. For all the wings of this investigation it was found that the drag due to lift was equal to the normal force times the sine of the angle of attack. This has also been found to be the case for a large number of low-aspect-ratio wings tested at lower supersonic Mach numbers in the Ames 6- by 6-foot supersonic tunnel (ref. 16).

Some characteristics of the family of wings shown in figure 2, which have hexagonal sections and were tested at Mach number 4.04, are now considered and the experimental results will be compared with the predictions of the modified theory. The delta and the diamond-plan-form wings have constant-thickness sections out to 56 percent of the semispan and double-wedge sections from there to the wing tip. The tapered wing was made by cutting the tip from the delta wing at 56 percent of the semispan. Two of the wings were tested with both wedge leading edges and NACA 0003-63 leading-edge sections.

Wings with rounded leading edges are of interest at high Mach numbers, since rounded leading edges have better heat-conducting properties than sharp leading edges and thus will be more likely to keep their strength at the high temperatures which will be encountered at high supersonic Mach numbers. Figure 9 shows the effects on the lift and drag of two delta wings at Mach number 4.04 of replacing the wedge-leading-edge sections by NACA 0003-63 leading-edge sections. The shock was attached to the wedge leading edge of the wing having the 30° semiapex angle and was detached from the wedge leading edge of the wing having the 10° semiapex angle. The change from sharp to rounded leading edge resulted in a 50 percent increase in the minimum drag of the 30° wing, which is about a 90-percent increase in the pressure drag. This result has also


been found at lower supersonic Mach numbers. The maximum lift-drag ratio was decreased 20 percent from 6 to 4.9 by rounding the leading edge of the wing.

The data for the lower-aspect-ratio wing, which has a subsonic leading edge, indicate that rounding the leading edge of this wing may have also caused an increase in drag. This is contrary to lower Mach number experience (for example, see ref. 25) and must be investigated further.

The methods discussed previously gave predictions of the lift of the sharp-leading-edge wings within $3\frac{1}{2}$ percent of the experimental values and predictions of pressure drag of the same wings within about 10 percent of the experimental values. The methods of predicting delta wing lift and pressure drag which have been proposed here are, of course, not applicable to wings with rounded nose sections. Therefore, pressure distributions over the two wings having NACA 0003-63 nose sections were estimated by the hypersonic approximation or Newtonian method (ref. 26), combined with a Prandtl-Meyer expansion over the lee surfaces of the wings and empirical values of base pressure. Drag coefficients were obtained by this method that were within 5 percent of the estimated experimental pressure drags. Using the modified method and the Newtonian method, the drag increments for these wings due to rounding the leading edges were predicted within 25 percent. It should be pointed out that the friction drag of the wings with the rounded leading edge is not known with the same accuracy as that of the sharp-leading-edge wings, so that the estimates of total drag may not be as accurate as the calculations indicate. The drag due to lift of these wings was found to be equal to the normal force times the sine of the angle of attack, as was the case for the double-wedge-section wings.


At Mach number 4.04 the locations of the wing-panel centers of pressure were determined experimentally. The chordwise location of the centers of pressure ranged from about 1.5 percent of the root chord downstream to 5 percent of the root chord upstream of the center of area of the wing panel. The spanwise location of the centers of pressure of the semispan models ranged from 2.5 to 5 percent of the semispan outboard of the center of area of the wing panel.

These methods of predicting wing lift and drag should give improved predictions of wing-body characteristics when used with wing-body-interaction methods such as the method of Nielsen and Kaattari (ref. 27). Figure 10 presents an example of some improvements in wing-body predictions obtained by the use of the more accurate values of wing lift obtained from the modified theory. The data are for four delta wing-body combinations for which the Mach lines, starting from the wing-body juncture, lie inside the wing leading edge, but which are actually




operating with detached shocks due to wing thickness. Three of the configurations were tested at Mach number 1.93 (ref. 28) and one at a Mach number 4.04 (ref. 4). The ordinate of figure 10 is the experimental value of the lift produced by the wing when in combination with the body. The abscissa is the theoretical value of the same quantity. The open points show the relatively poor predictions obtained by the use of the simple-linear-theory lift coefficients. The solid points show the improved predictions obtained by the use of the modified-theory wing-lift coefficients. The good prediction by the linear theory at Mach number 4.04 is fortuitous, since it is the result of the compensating effects, and such agreement should not be expected for other configurations at high Mach numbers.

To summarize, some simple methods of predicting lifts and pressure drags of thin delta wings at supersonic Mach numbers up to 6.9 have been presented. These methods are mainly modifications to the linear theory based on the physical realities of the flow, including shock detachment. Tests of a considerable number of low-aspect-ratio wings at Mach numbers 1.6 to 6.9 have indicated that these methods accurately predict the wing lift and pressure drags. The effects of rounding the leading edge of two delta wings at Mach number 4.04 were predicted satisfactorily by the use of the modified theory and the hypersonic approximation.





REFERENCES

1. McLellan, Charles H.: Exploratory Wind-Tunnel Investigation of Wings and Bodies at $M = 6.9$. Jour. Aero. Sci., vol. 18, no. 10, Oct. 1951, pp. 641-648.
 2. McLellan, Charles H., Bertram, Mitchel H., and Moore, John A.: An Investigation of Four Wings of Square Plan Form at a Mach Number of 6.86 in the Langley 11-Inch Hypersonic Tunnel. NACA RM L51D17, 1951.
 3. Ulmann, Edward F., and Lord, Douglas R.: An Investigation of Flow Characteristics at Mach Number 4.04 Over 6- and 9-Percent-Thick Symmetrical Circular-Arc Airfoils Having 30-Percent-Chord Trailing-Edge Flaps. NACA RM L51D30, 1951.
 4. Ulmann, Edward F., and Dunning, Robert W.: Some Effects of Fin Plan Form on the Static Stability of Fin-Body Combinations at Mach Number 4.06. NACA RM L52D15a, 1952.
 5. Ulmann, Edward F., and Dunning, Robert W.: Aerodynamic Characteristics of Two Delta Wings at Mach Number 4.04 and Correlations of Lift and Minimum-Drag Data for Delta Wings at Mach Numbers From 1.62 to 6.9. NACA RM L52K19, 1952.
 6. Dunning, Robert W., and Ulmann, Edward F.: Aerodynamic Characteristics at Mach Number 4.04 of a Rectangular Wing of Aspect Ratio 1.33 Having a 6-Percent-Thick Circular-Arc Profile and a 30-Percent-Chord Full-Span Trailing-Edge Flap. NACA RM L53D03, 1953.
 7. Dunning, Robert W., and Smith, Fred M.: Aerodynamic Characteristics of Two Delta Wings and Two Trapezoidal Wings at Mach Number 4.04. NACA RM L53D30a, 1953.
 8. Flake, H. M.: Supersonic Wind Tunnel Tests of a 0.020-Scale Model of the NA-705 Missile at Mach Number 2.87 To Determine Effect of Aspect Ratio and Planform of Wings on the Aerodynamic Characteristics of Wing Plus Body. Rep. No. AL-1156, North American Aviation, Inc., Oct. 25, 1950 (Rev. Dec. 1, 1950).
 9. Stewart, H. J.: The Lift of a Delta Wing at Supersonic Speeds. Quarterly Appl. Math., vol. IV, no. 3, Oct. 1946, pp. 246-254.
 10. Robinson, A.: Lift and Drag of a Flat Delta Wing at Supersonic Speeds. Tech. Note No. Aero. 1791, British R.A.E., June 1946.
- 

DECLASSIFIED

CONFIDENTIAL

11. Delameter, H. D.: Model XAAM-N-2 - Preliminary Analysis of Wind Tunnel Test Data - Second Daingerfield Wind Tunnel Test Period - Mach Number = 2.00. Rep. No. SM-13428, Douglas Aircraft Co., Inc., Dec. 21, 1948.
 12. Clark, J. M., Jr.: Wind Tunnel Tests of a Forty-Five Percent Scale Semispan XAAM-N-2 Model at $M = 2.00$ and $M = 1.50$. OAL Reps. 185 and 185-1, Ordnance Aerophysics Lab., Sept. 9, 1949.
 13. Delameter, H. D., Stamper, J. C., and Solvason, J. C.: Model XAAM-N-2. Preliminary Analysis of Force and Moment Characteristics From Supersonic Wind Tunnel Tests of a 45% Scale Semi-Span Model. Mach No. = 1.72. Rep. No. SM-13469, Douglas Aircraft Co., Inc., Aug. 10, 1949.
 14. Beal, R. R., and Goldbaum, G. C.: Analysis of Force and Moment Characteristics From Supersonic Wind-Tunnel Tests of a 13.5-Percent-Scale Model of the Sparrow 13-D at Mach Number = 1.50. Rep. No. SM-13735, Douglas Aircraft Co., Inc., Oct. 19, 1950.
 15. Shevell, R. S.: Project Nike - Second Aberdeen Wind Tunnel Test - Mach Number = 1.28. Rep. No. SM-11900, Douglas Aircraft Co., Inc., July 8, 1946.
 16. Hall, Charles F.: Lift, Drag, and Pitching Moment of Low-Aspect-Ratio Wings at Subsonic and Supersonic Speeds. NACA RM A53A30, 1953.
 17. Maslen, Stephen H.: Supersonic Conical Flow. NACA TN 2651, 1952.
 18. Love, Eugene S.: Investigations at Supersonic Speeds of 22 Triangular Wings Representing Two Airfoil Sections for Each of 11 Apex Angles. NACA RM L9D07, 1949.
 19. Puckett, A. E., and Stewart, H. J.: Aerodynamic Performance of Delta Wings at Supersonic Speeds. Jour. Aero. Sci., vol. 14, no. 10, Oct. 1947, pp. 567-578.
 20. Lapin, Ellis: Charts for the Computation of Lift and Drag of Finite Wings at Supersonic Speeds. Rep. No. SM-13480, Douglas Aircraft Co., Inc., Oct. 14, 1949.
 21. Van Driest, E. R.: Investigation of Laminar Boundary Layer in Compressible Fluids Using the Crocco Method. NACA TN 2597, 1952.
 22. Bertram, Mitchel H.: An Approximate Method for Determining the Displacement Effects and Viscous Drag of Laminar Boundary Layers in Two-Dimensional Hypersonic Flow. NACA TN 2773, 1952.
- 

23. Rubesin, Morris W., Maydew, Randall C., and Verga, Steven A.: An Analytical and Experimental Investigation of the Skin Friction of the Turbulent Boundary Layer on a Flat Plate at Supersonic Speeds. NACA TN 2305, 1951.
 24. Puckett, Allen E.: Supersonic Wave Drag of Thin Airfoils. Jour. Aero. Sci., vol. 13, no. 9, Sept. 1946, pp. 475-484.
 25. Hightower, Ronald C.: Lift, Drag, and Pitching Moments of Low-Aspect-Ratio Wings at Subsonic and Supersonic Speeds - Comparison of Three Wings of Aspect Ratio 2 of Rectangular, Swept-Back, and Triangular Plan Form, Including Effects of Thickness Distribution. NACA RM A52L02, 1953.
 26. Grimmering, G., Williams, E. P., and Young, G. B. W.: Lift on Inclined Bodies of Revolution in Hypersonic Flow. Jour. Aero. Sci., vol. 17, no. 11, Nov. 1950, pp. 675-690.
 27. Nielsen, Jack N., and Kaattari, George E.: Method for Estimating Lift Interference of Wing-Body Combinations at Supersonic Speeds. NACA RM A51J04, 1951.
 28. Rainey, Robert W.: An Investigation of Several Supersonic Missile Configurations Directed Toward Minimizing Center-of-Pressure Travel. NACA RM L52G01, 1952.
- 

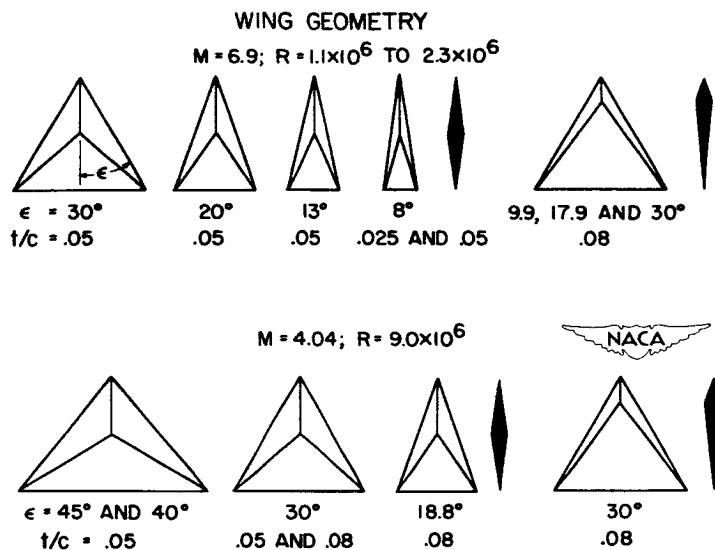


Figure 1

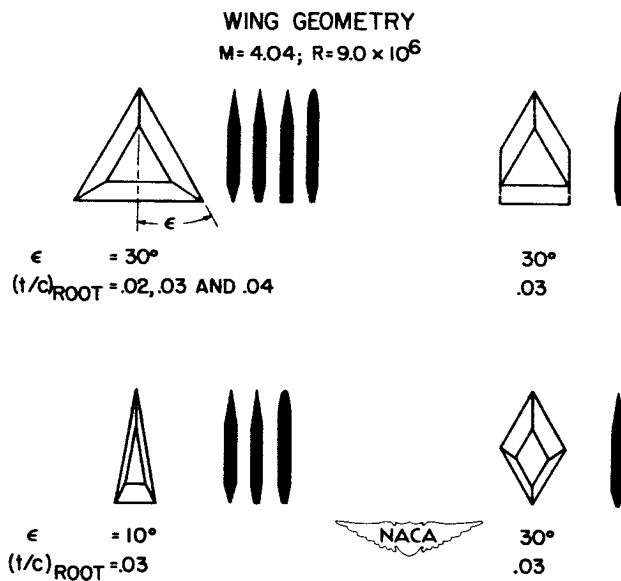


Figure 2

LIFT OF DOUBLE-WEDGE SECTION DELTA WINGS

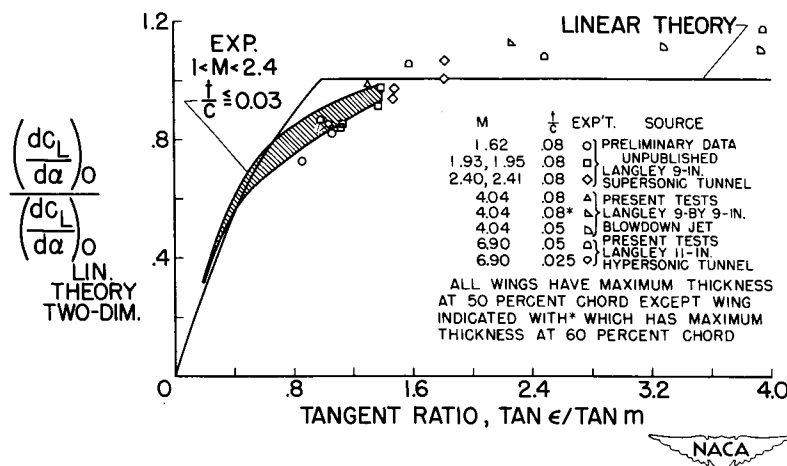


Figure 3

LIFT PREDICTIONS FOR DOUBLE-WEDGE DELTA WINGS

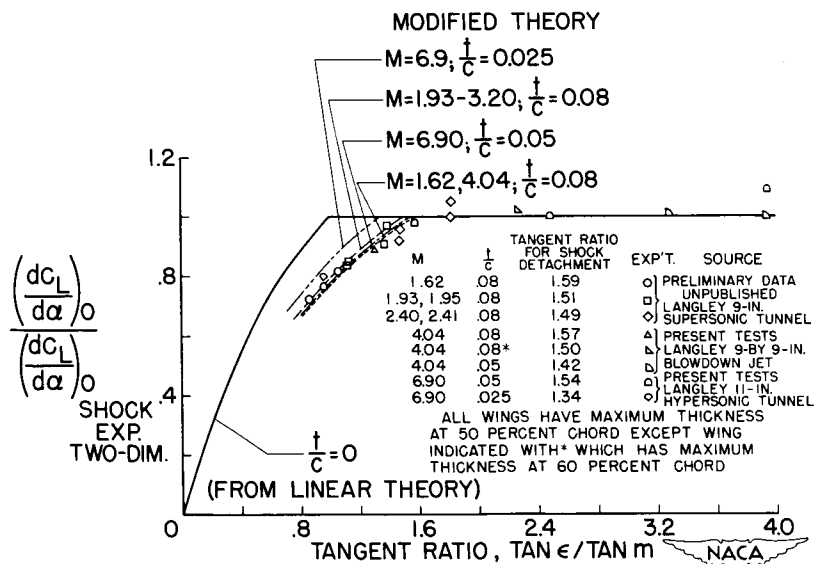


Figure 4

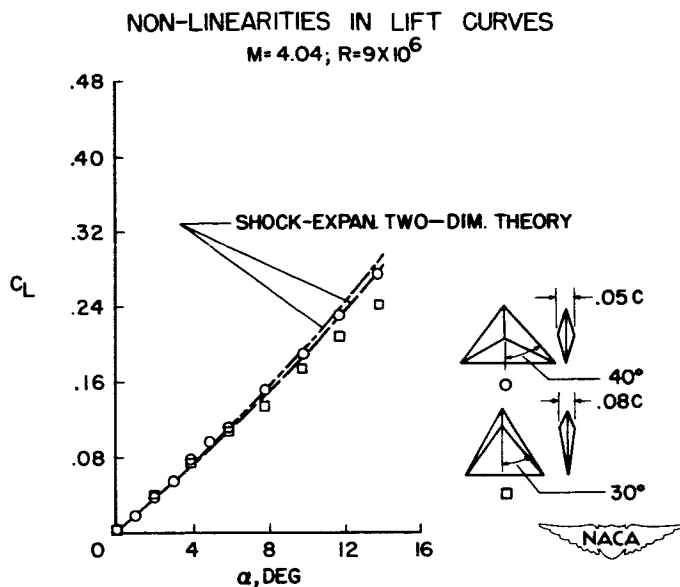


Figure 5

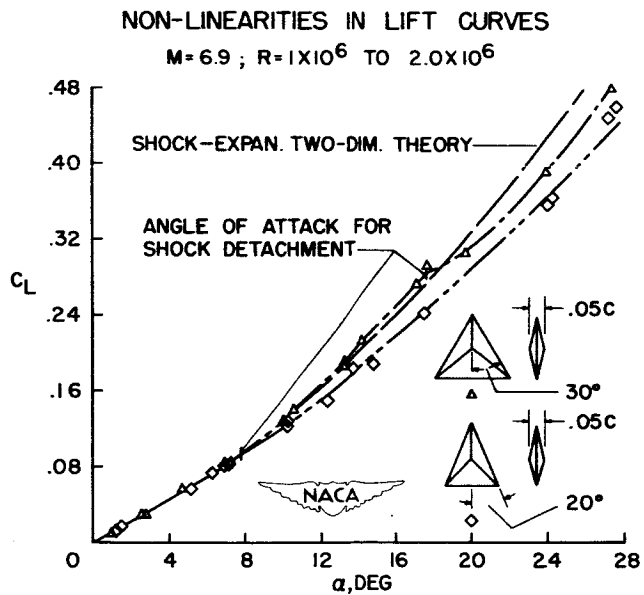


Figure 6

MINIMUM DRAG OF DOUBLE-WEDGE DELTA WINGS t/c_{MAX} AT $0.5c$

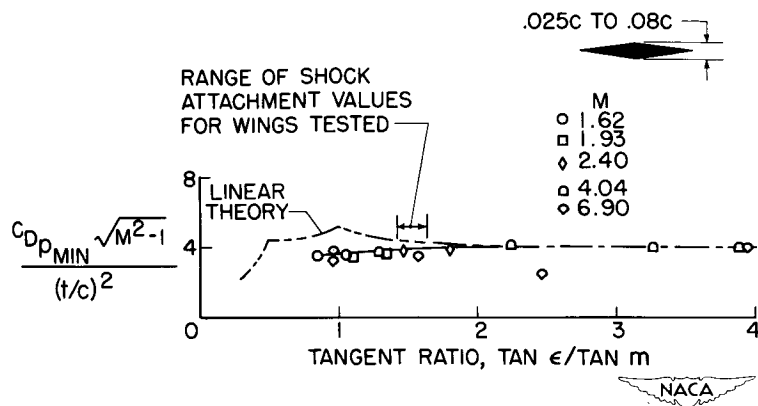


Figure 7

MINIMUM DRAG OF DOUBLE-WEDGE DELTA WINGS t/c_{MAX} AT $0.18c$

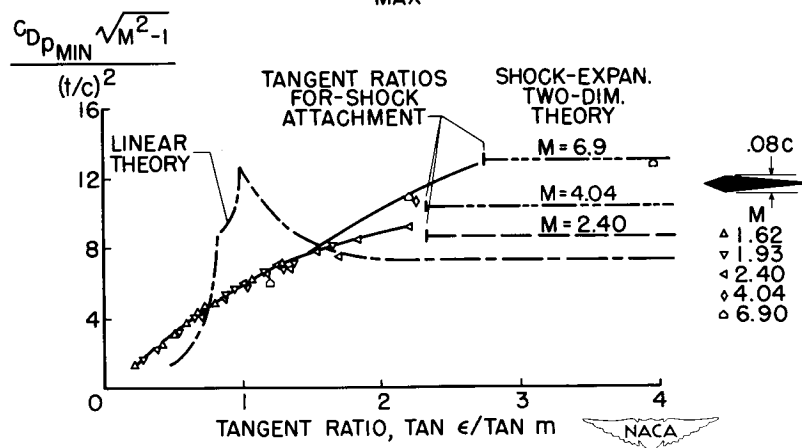


Figure 8

EFFECT OF LEADING-EDGE SHAPE

$M=4.04$; $R=9 \times 10^6$

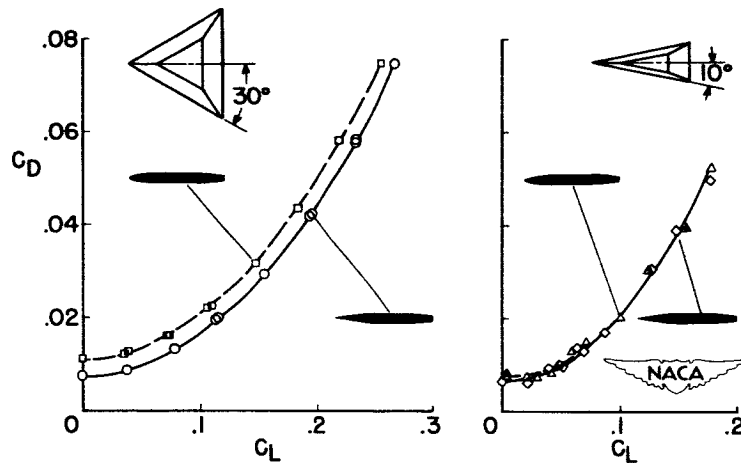


Figure 9

WING-BODY PREDICTIONS AFTER NIELSEN AND KAATTARI

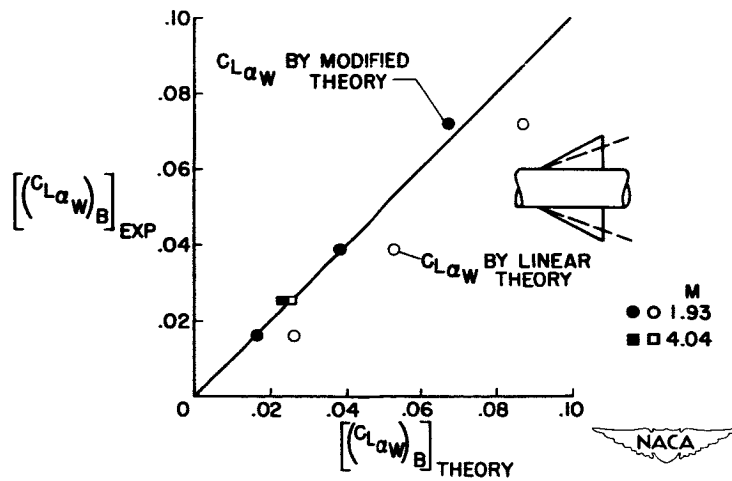


Figure 10

DECLASSIFIED
CONFIDENTIAL

17A

BOUNDARY-LAYER CONTROL ON SWEEP WINGS

By Woodrow L. Cook

Ames Aeronautical Laboratory

This paper presents a discussion of recent results that have been obtained on the use of area-suction type of boundary-layer control for the purpose of increasing lift on wings during low-speed flight. The lift increments obtainable and the air-flow and power requirements for this type of boundary-layer control are compared with those associated with boundary-layer control applied by the blowing or sucking of air through slots.

The maximum lift of an airfoil section is normally limited by the occurrence of air-flow separation due to a pressure rise too great for the boundary-layer air to penetrate without the aid of some form of boundary-layer control. In figure 1 the upper part illustrates the usual location on an airfoil section of these pressure peaks and the consequent pressure rises. In all three cases, boundary-layer control applied in the region shown by the dots permits, as indicated by the dashed curves, the attainment of greater pressure peaks without air-flow separation. The curves in the lower part of the figure illustrate the type of lift gains attainable with boundary-layer control applied at the three positions. For the left-hand and center cases an increase in angle of attack is required to realize the lift gains; whereas, for the third case, only an increase in flap deflection is necessary.

Comparison of two-dimensional section data (refs. 1 to 3) obtained with boundary-layer control applied through slots and through a porous area at the leading edge indicates that area-suction boundary-layer control requires much less power than boundary-layer control applied through slots. Therefore, for swept wings efforts have been concentrated on studies of area-suction type of boundary-layer control. The main portion of the results to date have been obtained from tests in the Ames 40- by 80-foot tunnel (refs. 4 to 7). Some work on suction through a porous leading edge has also been done at the Langley Laboratory (ref. 8). Tests have been made of North American F-86 wing panels with area suction applied to the wing leading edge, to the nose flap, and to the trailing-edge flaps. As a result, the major part of this discussion deals with the use of area suction as a means of boundary-layer control although some comparisons of power requirements of various methods is made subsequently.

The primary analytical work on area suction for high lift was due to Thwaites of England (ref. 9). He made a study of the problem of controlling separation of air flow from the wing leading edge. The method of applying Thwaites' analysis to determine the required extent

[REDACTED]

COOK

CONFIDENTIAL

of area suction is illustrated in figure 2. Shown here are two pressure distributions, one, the solid curve, on a section with no boundary-layer control at an angle of attack just prior to air-flow separation on the section and the other, shown by the dashed curve, the pressure distribution at the desired lift coefficient. The shaded area at the leading edge which is shown to an enlarged scale in the inset indicates the chordwise extent of the section over which area suction must be applied. This chordwise extent of suction is determined analytically by assuming that no suction is required to the rear of the point where the pressure rise is equal to that on the section with no boundary-layer control. Thus, area suction need only be applied over the chord length between the desired peak pressure of -30 and the point where the pressure recovery is equal to the maximum value attainable on the section without boundary-layer control. This reasoning has been verified in several cases by experiment and, although three-dimensional effects modify the results to some degree, the method appears to be sound. Application of area suction to the leading-edge flap or trailing-edge flap is accomplished by using the same method. In each case, the position of application is in the region of pressure rise directly following the pressure peak.

Experimental studies of each of these applications of boundary-layer control have been made. However, because of the limited landing attitudes of current and proposed airplanes, and because boundary-layer control applied to the flap increases lift without increasing landing attitude, the discussion in this paper is restricted to this application.

Shown in figure 3 are lift curves obtained on the F-86 (ref. 7) for three flap conditions. The lowest curve is for the standard F-86 slotted flap deflected 38° ; the next highest is for a plain flap deflected 65° ; and the highest is for the 65° flap with area suction applied. The increase in lift shown means that at an assumed landing attitude of 12° an increase in wing loading from 50 pounds per square foot to 65 pounds per square foot could be accepted with no increase in landing speed. Further, it is evident that, on this design, little would be gained by achieving large increases in maximum lift because the maximum ground angle of the F-86 is about 14° . For many of the airplane designs now under consideration, the landing speeds will be established by maximum ground angle rather than maximum lift.

Figure 4 shows the variation of flap lift increment with flap deflection angle with and without boundary-layer control and also the variation of flap lift increment with flow coefficients for three flap deflections. The values of lift increment are compared with theoretical values, computed by the method of DeYoung as presented in NACA Technical Note 2278 (ref. 10) and shown by the dashed curve in the left-hand plot and the horizontal lines in the right-hand plot. It is apparent from these curves that area suction succeeds in its purpose of eliminating air-flow separation and attaining near-theoretical values of lift. The general

DECLASSIFIED

CONFIDENTIAL


3

shape of the curves on the right indicate that the flow separation is eliminated very abruptly as a particular value of flow coefficient is reached. The curves also indicate that the value of flow coefficient required increases with flap deflection and that higher values of flow coefficient produce little increase in lift. Not capable of being shown here, but an important fact to note, is that no measurable hysteresis was found; regardless of whether suction was being increased or decreased, a nearly unique value of lift increment was measured for each value of flow coefficient.

Such lift gains have been known to be obtainable from several types of boundary-layer control for some time. One reason they have not been used is that the air-flow-quantity and pumping requirements were large. The use of the area-suction type of boundary-layer control considerably reduces both of these quantities. Figure 5 illustrates this point. The comparison of flow-quantity requirements is presented in figure 5(a) and the comparison of horsepower requirements is shown in figure 5(b) for three types of boundary-layer control applied for a particular level-flight condition for the F-86 airplane at 125 mph. The curves for the flaps with suction and blowing of air through slots were obtained by applying German two-dimensional results (refs. 11 and 12) to the F-86 partial-span flap. It is obvious that area-suction boundary-layer control shown by the curves at the left of each figure has greatly reduced the power and flow requirements.

In order to study flight characteristics of an airplane with this type of boundary-layer control, an installation in the F-86 airplane for flight test is now in progress. Figure 6 shows a schematic diagram of the installation. The duct for removing the air shown by the shaded area in the upper figure is placed in the flap itself and has an area of approximately 20 square inches. The suction pump shown in true relative size to the components of the airplane in the lower figure has a diameter of 8 inches and is 10 inches in length. For these tests the turbine-driven pump will require less than one-half of 1 percent of the main-engine-compressor air for operation, which means a thrust loss of less than 1 percent. This thrust loss is relatively unimportant during landing and is sufficiently small to enable the suction flap to be used for normal or catapult take-offs.

All discussion to this point has been based on experimental data obtained on the F-86 wing panels tested in the Ames 40- by 80-foot tunnel. The question arises as to how these data can be generalized to wings of other plan forms. In establishing a method, the basic concepts of simple sweep theory have been used. The three main steps of the approximate procedure are illustrated in figure 7. The first step involves estimation of the maximum flap lifts attainable. For this purpose, it can be assumed that the maximum flap deflection for which linear effectiveness can be maintained by boundary-layer control is 65°. Based on this




assumption, the flap lift increment can be calculated for any wing-flap arrangement by DeYoung's method of NACA Technical Note 2278 (ref. 10). The second step, to determine the flow quantity of air that must be removed, can be accomplished by estimation from values of the flow coefficients required for the F-86 wing panels. In the previous figures the flow coefficient C_Q was based on the total wing area and the free-stream velocity. For the purpose of application to other wing plan forms and flap spans, the reference area used is that illustrated by the shaded area in the center figure and the reference velocity is the component of the free-stream velocity normal to the flap hinge line as shown. The values of flow coefficient C_Q' for the F-86 based on these references are shown in the figure. These values of flow coefficients can be converted to flow quantities for any wing plan form and flap span by the relationship shown in the figure. The third step requires estimation of the pumping pressure. The pressure-coefficient distribution over the wing and flap are computed by two-dimensional theory and corrected for the effect of sweep of the flap hinge line by simple sweep theory. Adding the pressure losses due to flow through the porous surface and the ducts, which were negligible for the F-86 wing panels, to the maximum pressure over the flap will give the total pumping pressure. Combining this pressure with the flow quantity will give an approximation of the required power. A fuller discussion of the procedure outlined in this figure is given in the report on the area-suction flap (ref. 7).

The acceptability of this method can be indicated to a certain degree by recent results obtained with area suction applied to the flap on a delta wing of aspect ratio 2. The suction requirements and the increment of flap lift obtained for this wing which is of greatly different plan form than the F-86 wings were within 10 percent of the estimated values.

Although the main emphasis in this paper has been on the use of area suction for boundary-layer control, some additional information on the use of suction and blowing slots is available in references 13 to 15.

In summary, first, it has been demonstrated that area-suction type of boundary-layer control will enable realization of the maximum theoretical values of lift for flap deflections up to 65° . Second, it has been demonstrated that application of boundary-layer control by means of area suction will result in lowering the flow requirements and power requirements to values far below those necessary for any other form of boundary-layer control. Third, a method has been outlined which enables use of the data obtained on the F-86 wing panels with wings of different plan form and flap span.




DECLASSIFIED

CONFIDENTIAL


5

REFERENCES

1. McCullough, George B., and Gault, Donald E.: An Experimental Investigation of an NACA 63₁-012 Airfoil Section With Leading-Edge Suction Slots. NACA TN 1683, 1948.
 2. Dannenberg, Robert E., and Weilberg, James A.: Section Characteristics of a 10.5-Percent-Thick Airfoil With Area Suction as Affected by Chordwise Distribution of Permeability. NACA TN 2847, 1952.
 3. Nuber, Robert J., and Needham, James R., Jr.: Exploratory Wind-Tunnel Investigation of the Effectiveness of Area Suction in Eliminating Leading-Edge Separation Over an NACA 64₁A212 Airfoil. NACA TN 1741, 1948.
 4. Cook, Woodrow L., Griffin, Roy N., Jr., and McCormack, Gerald M.: The Use of Area Suction for the Purpose of Delaying Separation of Air Flow at the Leading Edge of a 63° Swept-Back Wing. NACA RM A50H09, 1950.
 5. Cook, Woodrow L., and Kelly, Mark W.: The Use of Area Suction for the Purpose of Delaying Separation of Air Flow at the Leading Edge of a 63° Swept-Back Wing - Effects of Controlling the Chordwise Distribution of Suction-Air Velocities. NACA RM A51J24, 1952.
 6. Holzhauser, Curt A., and Martin, Robert K.: The Use of Leading-Edge Area Suction To Increase the Maximum Lift Coefficient of a 35° Swept-Back Wing. NACA RM A52G17, 1952.
 7. Cook, Woodrow L., Holzhauser, Curt A., and Kelly, Mark W.: The Use of Area Suction for the Purpose of Improving Trailing-Edge Flap Effectiveness on a 35° Swept-Back Wing. NACA RM A53E06. (Prospective NACA paper.)
 8. Graham, Robert R., and Jacques, William A.: Wind-Tunnel Investigation of Stall Control by Suction Through a Porous Leading Edge on a 37° Sweptback Wing of Aspect Ratio 6 at Reynolds Numbers From 2.50×10^6 to 8.10×10^6 . NACA RM L52L05, 1953.
 9. Thwaites, B.: On the Flow Past a Flat Plate With Uniform Suction. R. & M. No. 2481, British A.R.C., 1952.
 10. DeYoung, John: Theoretical Symmetric Span Loading Due to Flap Deflection for Wings of Arbitrary Plan Form at Subsonic Speeds. NACA TN 2278, 1951.
- 

0371320 1030

CONFIDENTIAL

11. Schwier, W.: Lift Increase Produced by Blowing a Wing of a Profile Thickness of 9%, Equipped With a Slat and a Slotted Flap. Translation No. F-TS-645-RE, Air Materiel Command, U. S. Army Air Forces, Sept. 1946.
 12. Regenscheit, B.: Suction Flap Wing No. 23012 Interim Report on a Systematic Thickness Series. British Ministry of Supply, TPA.3/TIB Translation No. GDC 10/1302 T, Jan. 25, 1942.
 13. Nunemaker, John J., and Fisher, Jack W.: Two-Dimensional Wind Tunnel Investigation of Boundary-Layer Control by Blowing on an NACA 23015 Airfoil. Eng. Rep. No. 023 (Contract N8ONR-75600), Municipal Univ. of Wichita, Apr. 1950.
 14. Rebuffet, P., and Poisson-Quinton, Ph.: Investigations of the Boundary-Layer Control on a Full Scale Swept Wing With Air Bled Off From the Turbojet. NACA TM 1331, 1952.
 15. Schwier, W.: Lift Increase by Blowing Out Air, Tests on Airfoil of 12 Percent Thickness, Using Various Types of Flaps. NACA TM 1148, 1947.
- 

LIFT INCREASES OBTAINED WITH BOUNDARY-LAYER CONTROL

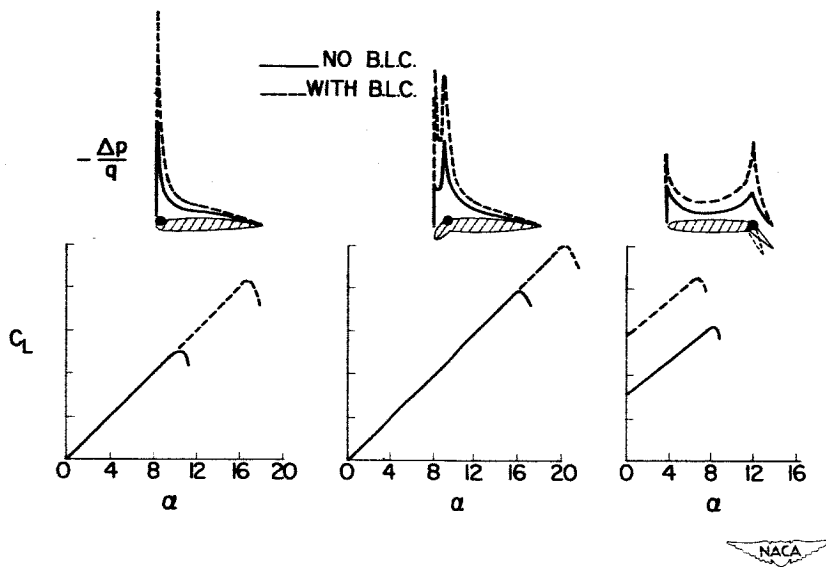


Figure 1

PRINCIPLE OF AREA SUCTION

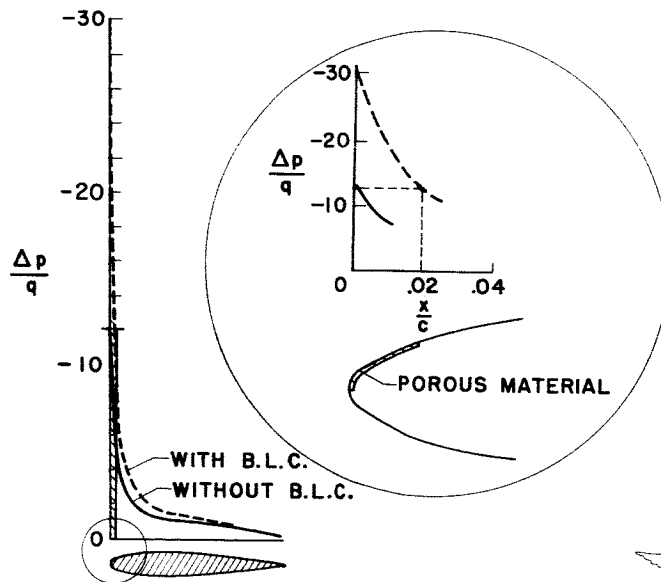


Figure 2

EFFECT OF B.L.C. ON LIFT, F-86 AIRPLANE

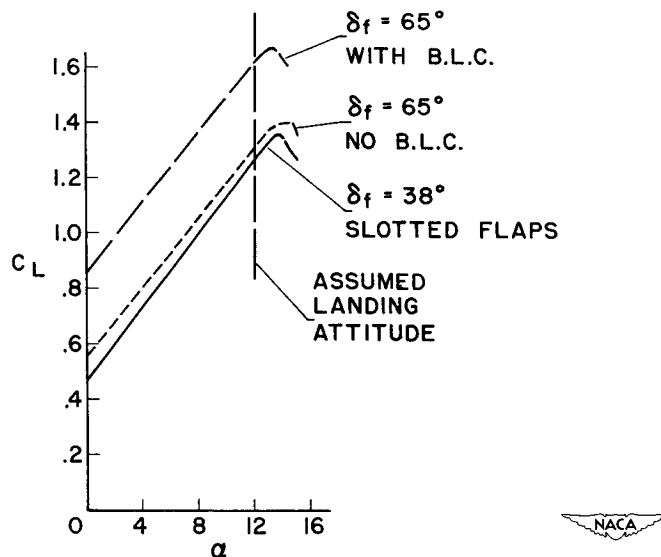


Figure 3

EFFECT OF B.L.C. ON FLAP LIFT INCREMENT

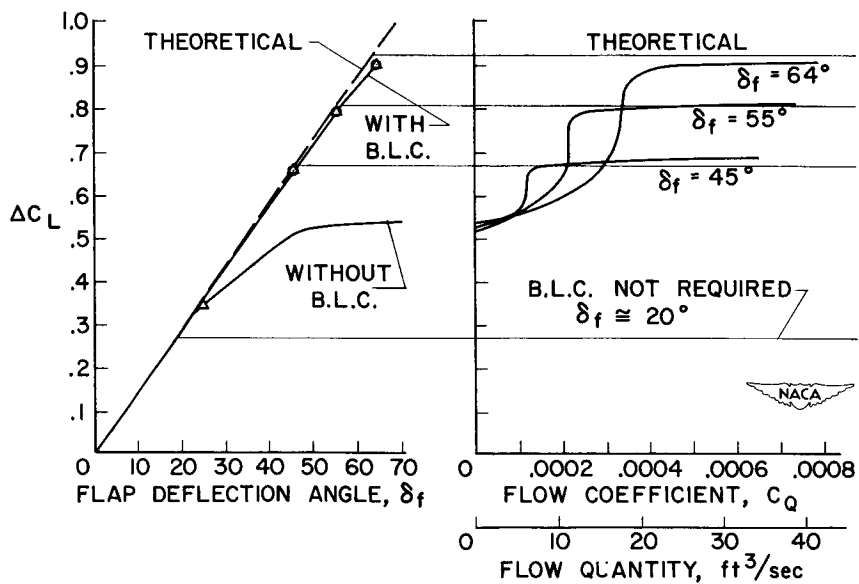


Figure 4

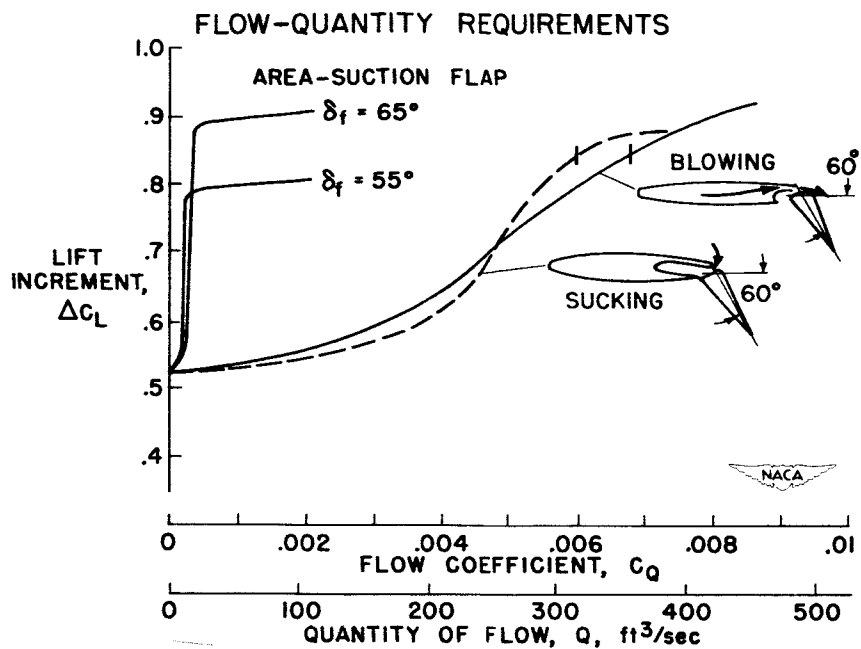


Figure 5(a)

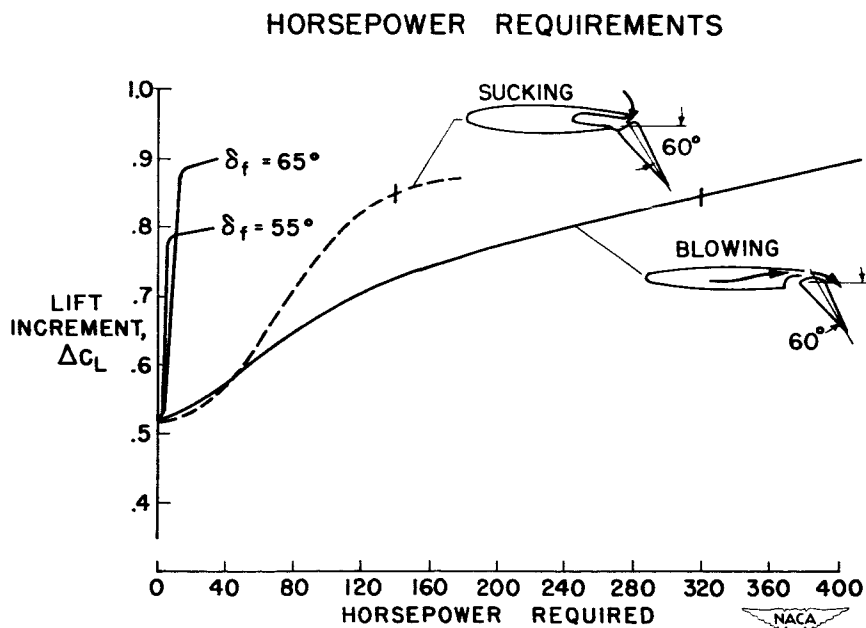


Figure 5(b)

B.L.C. INSTALLATION ON F-86

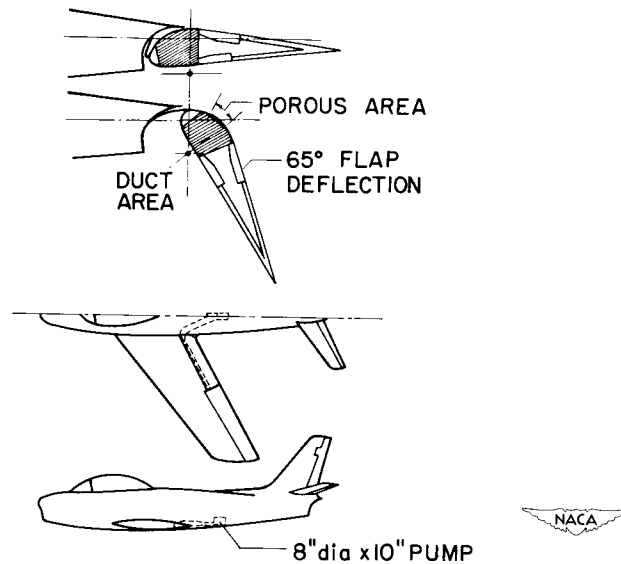


Figure 6

STEPS IN DESIGN PROCEDURE

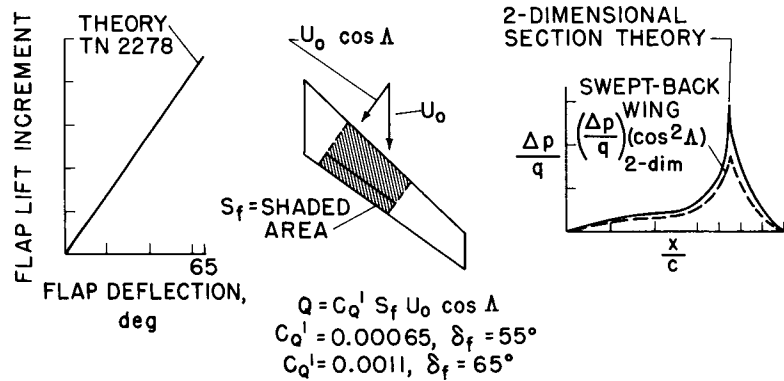
1. CALCULATION OF
LIFT INCREMENT2. DETERMINATION
OF FLOW QUANTITY3. CALCULATION OF
PUMPING PRESSURE

Figure 7

INCLINED BODIES AT HIGH SUPERSONIC SPEEDS

By Edward W. Perkins and David H. Dennis


Ames Aeronautical Laboratory

INTRODUCTION

The purpose of this paper is to review the results of recent research on the aerodynamic characteristics of inclined bodies. For the most part current work includes investigation of the details of the cross-force distribution on bodies of revolution at high angles of attack, measurement of the forces and moments for a wide variety of body shapes at hypersonic speeds, and determination of the applicability of presently available theoretical methods for predicting these characteristics. Experimental data used in the following discussion have been obtained from various facilities of the three NACA laboratories.


CROSS-FORCE DISTRIBUTION

It has long been evident that viscosity plays an important role in determining the characteristics of the flow about inclined bodies. In particular, the nonlinearities of the force characteristics of inclined bodies are attributed principally to viscous effects. A practical method of estimating the effects of viscosity on the force characteristics was suggested by Allen (ref. 1). Comparisons of the measured forces and moments for a large number of inclined bodies with those predicted by this method show that the lift and the drag due to lift are adequately predicted but that the center of pressure is, in general, approximately 1 body diameter downstream of the predicted position (ref. 2). A tentative explanation of this discrepancy has been proposed, in which it was indicated that, although it was assumed that the viscous effects acted uniformly along the length of the body, in reality the development of the cross flow with distance along the body should be much the same as the development with time of the two-dimensional flow about a circular cylinder impulsively set in motion from rest. Hence, the longitudinal distribution of cross-flow drag coefficient would not be constant, as assumed, but should resemble the variation with time of the drag of the impulsively started circular cylinder. In order to test this hypothesis the normal-force distributions for the body shown in figure 1 have been determined. The data are for a model consisting of a fineness-ratio-3 ogival nose tangent to a cylindrical afterbody 6 diameters long and have been plotted as longitudinal distributions of the local normal-force coefficient per radian for easy comparison with the distribution



calculated with Tsien's linearized theory (ref. 3). It is apparent that, even at as low an angle of attack as 5° , the experimental distribution differs appreciably from that predicted by linearized theory. Assuming that the differences between the theoretical and experimental values of the local normal-force coefficients may be attributed to the effects of viscosity, these differences may be used to evaluate the longitudinal distributions of the cross-flow drag coefficient. Examination of the data in the region near the apex of the model shows that, although the local normal-force coefficient is greater than the value given by potential theory, it is a linear function of the angle of attack for an appreciable angle range indicating, therefore, that the lack of agreement results primarily from failure of the potential theory in this region and that viscous effects are negligible. A comparison may then be made, as in figure 2, between the distribution of cross-flow drag coefficient along the inclined body and the variation with time (or as plotted with distance traveled in diameters) of the drag coefficient of a circular cylinder impulsively set in motion from rest. For the impulsively started cylinder, the cross force starts at zero, rises to a value almost twice the steady-state value, and then, at some time later, dependent on the test conditions, drops to the steady-state value. Similarly, for the inclined body, the cross-force coefficient starts near zero at the apex, rises with distance along the body to a peak value on the cylindrical afterbody, and then decreases, approaching a constant value far downstream on the cylindrical afterbody. Thus, as anticipated, the distribution of additional loading attributable to viscous effects differs from that assumed by Allen for calculation of the over-all forces and moments. In spite of this, the total additional cross force predicted by the approximate method is very nearly equal to the measured values. However, because of the differences between the assumed distribution and the true distribution, the actual center of pressure is downstream of the calculated position.

It may be noted (fig. 2) that the cross-flow drag coefficient for 10° angle of attack does not rise to as large a maximum value as that for the higher angles of attack and appears to approach a lower value near the base of the body. This lower value of the cross-flow drag coefficient results from the effects of boundary-layer transition. Although the cross-flow Reynolds number was less than the critical value for a cylinder in two-dimensional flow (approx. 250,000) the length Reynolds number was sufficiently high, so that, within the particular wind tunnel in which these measurements were made, boundary-layer transition occurred near the point of tangency of the nose with the afterbody even at zero angle of attack. It is evident, therefore, that in this instance the principle of cross-flow and axial-flow independence is not applicable, and the cross-flow characteristics are not those associated with the cross-flow Reynolds number.



DECLASSIFIED

CONFIDENTIAL


3

UNSTEADY WAKE FLOW

The formation of vortices in the wake of inclined bodies and the subsequent asymmetry and unsteadiness at large angles of attack have been shown by Mead and Gowen (refs. 4 and 5) to result in undesirable body-tail interference effects. For missiles which must operate at large angles of attack, the asymmetric and unsteady nature of this flow will promote unexpected and erratic rolling, as well as undesirable forces and moments in yaw. It has been found that the angle of attack at which the vortex flow becomes asymmetric and that at which it becomes unsteady are largely dependent upon the nose fineness ratio. The results of the tests of a series of cones of various apex angles to determine the angles of attack at which the vortex flow first becomes unsteady are shown in figure 3. The boundary curve for the conical noses represents the lowest angles of attack at which unsteadiness in the wake was observed for the various fineness ratio cones. From the results for the cones alone it is apparent that the lowest angle of attack at which unsteady flow was observed increases with decreasing nose fineness ratio. Body shapes other than conical were also tested to determine the effect of nose profile. For nose shapes which are relatively blunter than cones it was found that the angle of attack at which the vortex wake became unsteady was greater than that of the cone of the same fineness ratio. This is shown in figure 3 by the typical results plotted for the parabolic-arc nose and the ogival nose. For nose shapes which are less blunt than cones (for example, a cusped nose which has a smaller apex angle than the cone of the same fineness ratio) the angle of attack at which the vortex flow became unsteady was approximately the same as that of the cone. It is apparent, therefore, that insofar as it may be desirable to avoid the unsteady flow at large angles of attack the lower fineness ratio or blunter nose shapes appear desirable.

COMPARISON OF THEORY AND EXPERIMENT


Up to this point detailed flow characteristics resulting from viscous effects at relatively low supersonic Mach numbers have been considered. Although similar studies of the flow about bodies at high Mach numbers have not been made, there are now available sufficient experimental data for the over-all forces and moments to permit an assessment of the applicability of the available methods for predicting these characteristics. The two simple methods which can be used by the designer are the Newtonian or impact theory (ref. 6) and the method proposed by Allen (ref. 1). Because of the nature of the simplifying assumptions involved in the derivation of the methods, each would be expected to be most applicable for a certain range of flow conditions - Newtonian theory for very high velocity flow ($M \rightarrow \infty$), and Allen's method for



CONFIDENTIAL

aerodynamically slender bodies at large angles of attack. For the potential contribution to the cross force, the use of slender-body theory in conjunction with Allen's method of estimating the viscous effects has proved adequate for high-fineness-ratio bodies at low Mach numbers. However, for such combinations of Mach number and fineness ratio that the body under consideration cannot be considered aerodynamically slender, it is known that the potential contribution to the cross force must be calculated by a more accurate method. One such method is the so-called "hybrid theory" suggested by Van Dyke (ref. 7). A typical example of the improvement in the prediction of lift and drag characteristics resulting from the use of Van Dyke's theory is shown by the data of figure 4. The experimental lift and the drag characteristics at $M = 3.0$ of a fineness-ratio-5 cone in combination with a cylindrical afterbody 5 diameters in length are compared with the theoretical characteristics calculated with Allen's method. The difference in the two theoretical curves results from the different values used for the potential-flow contribution. It is evident that the use of Van Dyke's theory rather than slender-body theory for the potential-flow contribution results in considerable improvement in the prediction of both the lift and the drag. It should be noted that the difference between the drag curves is due in part to the fact that the two theories predict different directions for the resultant force due to potential flow. As shown by Ward (ref. 8), the slender-body theory requires that the resultant force be directed midway between the normals to the free-stream direction and to the body axis, whereas the force calculated with Van Dyke's theory is assumed to act in a direction normal to the body axis. Within the assumptions of Allen's method of estimating the forces (e.g., $\cos \alpha = 1$), this difference does not affect the theoretical lift curves.

Although the use of Van Dyke's theory extends the Mach number range for which valid predictions of the forces can be made, the theory would not be expected to provide accurate results for arbitrarily high Mach numbers. A study of Van Dyke's second-order axial-flow solution (ref. 9) which, combined with the first-order cross-flow solution, constitutes the hybrid theory, has shown that, if the combination of Mach number and nose fineness ratio is such that the hypersonic similarity parameter is in excess of unity, the error resulting from the use of the second-order solution is large. Similarly, comparisons of the experimental initial lift-curve slopes with those predicted with Van Dyke's hybrid theory for a large number of cone-cylinder combinations at Mach numbers between 3 and 7 show that, for values of the similarity parameter of unity and greater, the errors in the theoretical initial lift-curve slopes become very large. This is illustrated by the data in figure 5 where typical comparisons of the theoretical and experimental initial lift-curve slopes for a series of cone-cylinder combinations are made. Sketches of the models and the Mach numbers of the tests are shown in the first two columns. A measure of the relative aerodynamic slenderness of the bodies is indicated by the values of the similarity parameter in the third column.



The larger the value of the parameter the less the aerodynamic slenderness. The results are divided into three groups, cones alone, cone-cylinder combinations of constant over-all fineness ratio but varying nose fineness ratios, and cone-cylinders with relatively short cylindrical afterbodies. These data are typical of results obtained for a large number of tests and serve to illustrate several points of interest. For the cones alone, Van Dyke's theory yields reasonably accurate values of the initial lift-curve slopes even for the least slender configuration. For the second series of models, those of constant over-all fineness ratio, the theory tends to overestimate the initial lift-curve slope by increasingly larger amounts as the relative aerodynamic slenderness of the noses decreases. Consideration of the results for these two series of bodies, that is, the good agreement of the theory with experiment for the conical noses alone and the poor agreement at the higher Mach numbers for the same cones with cylindrical afterbodies, shows that the theory overestimates the lift carry-over onto the cylindrical afterbody for the nonslender bodies. The overestimation is particularly serious for the models with short cylindrical afterbodies as shown by comparison of the theoretical values with the experimental results for the last two bodies. For these cases the theory overestimates the initial lift-curve slopes by approximately 18 percent. It is evident then that, for values of the slenderness parameter of less than 1, Van Dyke's theory yields reasonably accurate results for the initial lift-curve slopes, whereas, for bodies with aerodynamically nonslender noses, the values predicted by the theory are too large. Hence, for a value of the slenderness parameter of 1, the combination of Van Dyke's theory for the potential-flow contribution with Allen's estimate of the viscous effects yields values of lift and drag due to lift which are too large throughout the angle-of-attack range. This typical result is illustrated in figure 6 by comparison of the experimental results for a cone-cylinder body of revolution with the predicted characteristics. Also shown for comparison are the lift and the drag predicted with impact theory. For this high Mach number the impact theory predicts the drag very well and is only slightly low for the lift.

The variations of lift and drag due to lift are very close to those predicted by impact theory as shown by the data presented in figure 7 for a Mach number of 6.86. (All data at this Mach number were obtained from unpublished experiments in the Langley 11-inch hypersonic tunnel by Herbert W. Ridyard.) Also shown for comparison are the lift and the drag due to lift predicted with Allen's method in which the slender-body value of 2 has been used for the potential-flow contribution. The fact that such excellent agreement with the experimental lift characteristics is obtained appears fortuitous, since at this high Mach number the body cannot be considered aerodynamically slender. However, additional experimental data at $M = 6.86$ for this same conical nose in combination with various lengths of cylindrical afterbody are essentially in as good agreement with this theory as shown here.

From the foregoing observations it is apparent that for the intermediate range of aerodynamic slenderness, that is, for values of the similarity parameter near 1, neither of the simple theories is adequate. At present, the shock-expansion method as developed by Eggers and Savin (ref. 10) for nonlifting bodies is being extended to inclined bodies to provide a relatively simple means of predicting aerodynamic characteristics in this intermediate range.


MAXIMUM LIFT-DRAG RATIOS

In addition to the aerodynamic characteristics so far discussed, the lifting efficiency of bodies may often be of importance. The efficiency, or lift-drag ratio, of bodies at high supersonic speeds is being investigated experimentally with particular regard to the effects of variations of body geometry on maximum lift-drag ratios.

In analyzing the effects on lift-drag ratio of changing body geometry, consideration must be given to factors other than simply the aerodynamic forces. For example, considerations such as that of the usable volume and that of aerodynamic heating may rule out the use of a body shape which is aerodynamically the most efficient. According to the Newtonian concept, a flat plate of zero thickness has the highest lift-drag ratio. However, from the standpoint of usable volume and aerodynamic heating the flat plate is perhaps the least desirable body shape.

These two considerations, usable volume and aerodynamic heating, suggest a parameter which may be used in conjunction with lift-drag ratio for assessing the relative desirability of various body shapes. Accordingly, the ratio of the volume of a body to the product of its surface area and its length has been selected. Surface area is used simply as an indication of the aerodynamic heating since the heat absorbed will be approximately proportional to the body surface area. This measure of heat input does not, of course, account for localized heating, the magnitude of which is determined, in general, by the details of a particular body shape. Body length has been included to make the parameter dimensionless and therefore restricts the comparisons to bodies of the same length. This ratio might also be termed a measure of the structural efficiency of a body shape since a high ratio of volume to surface area corresponds roughly to a high ratio of carrying capacity to structural weight. It is evident then that large values of the parameter, as well as high lift-drag ratios, are desirable for lifting bodies.

The effects on maximum forebody lift-drag ratios of four systematic variations of body shape are shown in figure 8. The values of the lift-drag ratios are based upon the forebody drag only and hence do not include any base drag. The test Mach number range in which these data were



DECLASSIFIED

CONFIDENTIAL

7

obtained was from 3 to 5. It has been found experimentally that, for approximately constant Reynolds numbers, Mach number variations in this range have relatively little effect on maximum forebody lift-drag ratios. Large Reynolds number variations, on the other hand, would alter $(L/D)_{\max}$ because of the corresponding large changes in skin-friction drag. Plotted in the upper left-hand side of figure 8 are the results for conical bodies of varying fineness ratio. It is apparent that increases in the nose fineness ratio result in increases in the maximum lift-drag ratios. This is accompanied, however, by decreases in the volume-to-surface-area ratios. Similarly, the addition of various-length cylindrical afterbodies to a fineness-ratio-3 conical nose as shown at the bottom left-hand side also results in an increase in maximum forebody lift-drag ratio with a loss in the volume-to-area ratio.

At the upper right of the figure is shown the effect of varying the nose profile shape of a body. It is evident that there is little effect on the maximum lift-drag ratio. It is interesting to note, however, that the body having the nose shape for minimum drag at zero lift at high supersonic speeds retains its low drag advantage at angle of attack and has the highest maximum lift-drag ratio of this group.


The results presented in the plot in the lower right of the figure show that the maximum forebody lift-drag ratio is increased with a relatively small decrease in volume-to-surface-area ratio by increasing the nose fineness ratio of cone-cylinder bodies of given over-all length and diameter. For bodies of revolution this latter method of increasing the $(L/D)_{\max}$ may be said to be the most effective.

It has been suggested that body shapes other than bodies of revolution might be employed advantageously as lifting bodies at high supersonic speeds. Accordingly, experimental investigations of the aerodynamic characteristics of various body shapes at high Mach numbers have recently been conducted at both the Langley and Ames Laboratories. Figure 9 shows the maximum forebody lift-drag ratios obtained at $M = 6.86$ for various flat-bottom body shapes of constant length. Because base-pressure-drag data were unavailable for three of the bodies shown, it was necessary to estimate the magnitude of the base pressure drag. A reasonable estimate of the base drag was found to be approximately 7 percent of the total drag at $(L/D)_{\max}$. The data points for which this estimate was made are indicated by the flagged symbols. The cone-cylinder body of revolution is included for comparative purposes. These data show again that, in general, as body shapes are altered to obtain higher forebody lift-drag ratios, the ratio of volume to surface area for the shapes decreases. An exception to this trend is noted in the result for body C of this group. This wide body is related to body E in that it was obtained by simply slicing model E along the vertical plane of symmetry and inserting a rectangular center section. This particular alteration in body shape results in increases in both the maximum forebody lift-drag ratio and the volume parameter. The

extent to which further such alteration of shape might continue to be advantageous is unknown at present.

Figure 10 shows, in summary, the results just presented, as well as additional data from various other sources (refs. 11, 12, 13, and 14). These data points represent maximum forebody lift-drag ratios at Mach numbers from approximately 2.5 to 7 for a relatively wide range of Reynolds numbers. The abscissa of this figure is the ratio of the volume parameter of the particular bodies to that of a sphere which has the maximum possible value of V/S . At 1 on the horizontal scale is the sphere which has zero lift-drag ratio. At the other extreme, 0 on the horizontal scale, is the maximum lift-drag ratio of a flat plate. For the conditions imposed the theoretical $(L/D)_{\max}$ of the flat plate is 6. These data show the general trend of the variation of maximum forebody lift-drag ratio with the volume-to-surface-area ratio for a wide range of Mach numbers and Reynolds numbers. The data points repeated from figures 8 and 9 are indicated by closed symbols and show the effectiveness of the systematic changes in body shape that have been considered relative to the general trend indicated by the curve. It should be noted that, in general, over-all body fineness ratios decrease as the volume parameter increases; that is, bodies represented by points on the left-hand side of the figure are of relatively large fineness ratio (10 or greater) and those farthest to the right are of small fineness ratio (3).

As stated previously, it is desired that efficient lifting bodies have both a large maximum forebody lift-drag ratio and a large value of the volume-to-area ratio. It is apparent, however, that at high supersonic Mach numbers for a wide range of body shapes the two requirements are, in general, not compatible and therefore compromises are necessary.



REFERENCES

1. Allen, H. Julian: Estimation of the Forces and Moments Acting on Inclined Bodies of Revolution of High Fineness Ratio. NACA RM A9I26, 1949.
 2. Allen, H. Julian, and Perkins, Edward W.: Characteristics of the Flow Over Inclined Bodies of Revolution. NACA RM A50L07, 1951.
 3. Tsien, Hsue-Shen: Supersonic Flow Over an Inclined Body of Revolution. Jour. Aero. Sci., vol. 5, no. 12, Oct. 1938, pp. 480-483.
 4. Mead, Merrill H.: Observations of Unsteady Flow Phenomena for an Inclined Body Fitted With Stabilizing Fins. NACA RM A51K05, 1952.
 5. Gowen, Forrest E.: Buffeting of a Vertical Tail on an Inclined Body at Supersonic Mach Numbers. NACA RM A53A09, 1953.
 6. Grimminger, G., Williams, E. P., and Young, G. B. W.: Lift on Inclined Bodies of Revolution in Hypersonic Flow. Jour. Aero. Sci., vol. 17, no. 11, Nov. 1950, pp. 675-690.
 7. Van Dyke, Milton D.: First- and Second-Order Theory of Supersonic Flow Past Bodies of Revolution. Jour. Aero. Sci., vol. 18, no. 3, Mar. 1951, pp. 161-178.
 8. Ward, G. N.: Supersonic Flow Past Slender Pointed Bodies. Quarterly Jour. Mech. and Appl. Math., vol. II, pt. 1, Mar. 1949, pp. 75-97.
 9. Ehret, Dorris M.: Accuracy of Approximate Methods for Predicting Pressures on Pointed Nonlifting Bodies of Revolution in Supersonic Flow. NACA TN 2764, 1952.
 10. Eggers, A. J., Jr., and Savin, Raymond C.: Approximate Methods for Calculating the Flow About Nonlifting Bodies of Revolution at High Supersonic Airspeeds. NACA TN 2579, 1951.
 11. Cooper, Ralph D., and Robinson, Raymond A.: An Investigation of the Aerodynamic Characteristics of a Series of Cone-Cylinder Configurations at a Mach Number of 6.86. NACA RM L51J09, 1951.
 12. Jack, John R.: Aerodynamic Characteristics of a Slender Cone-Cylinder Body of Revolution at a Mach Number of 3.85. NACA RM E51H17, 1951.
 13. Rainey, Robert W.: Langley 9-Inch Supersonic Tunnel Tests of Several Modifications of a Supersonic Missile Having Tandem Cruciform Lifting Surfaces. Three-Component Data Results of Models Having Ratios of Wing Span to Tail Span Equal to 1. NACA RM L9L30, 1951.
-



- [REDACTED]
- [REDACTED]

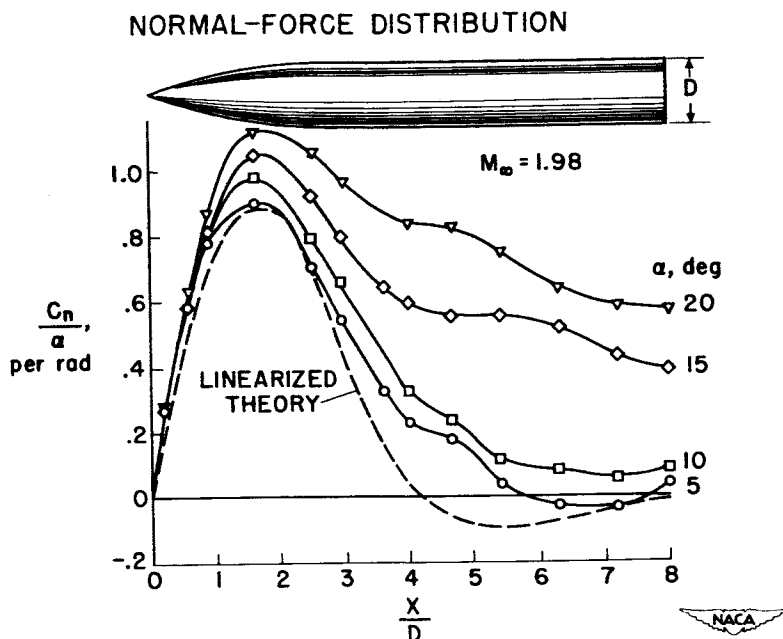


Figure 1

CROSS FORCE DUE TO VISCOSITY

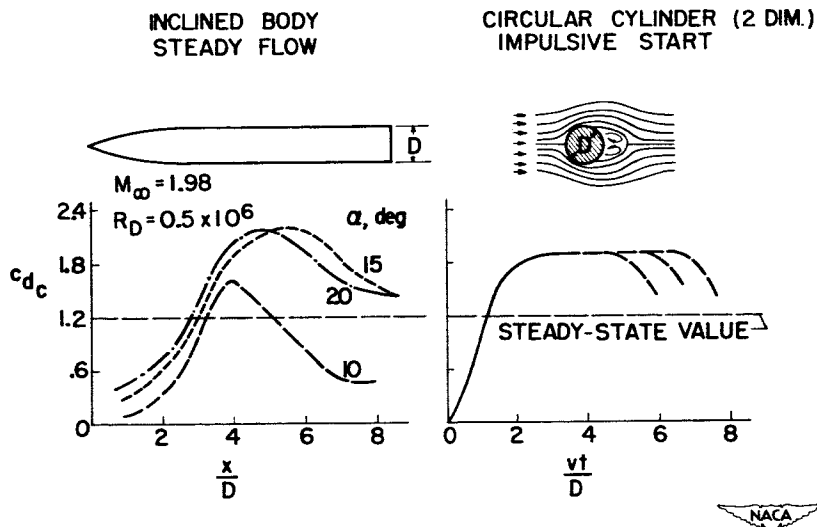
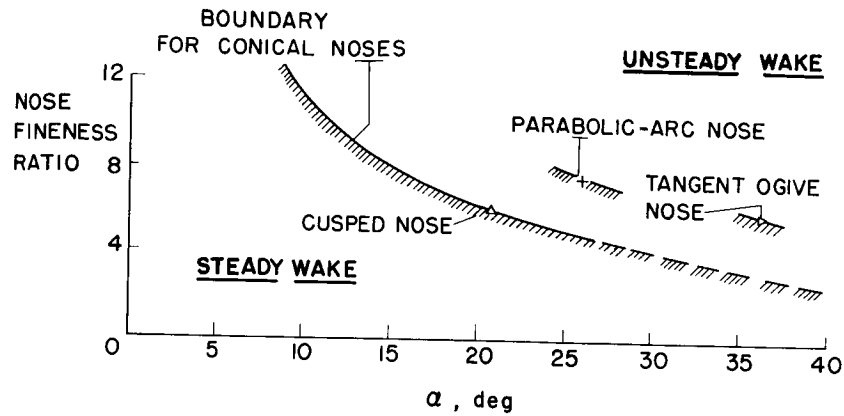


Figure 2

EFFECT OF NOSE SHAPE ON α FOR UNSTEADY FLOW

$$M_\infty = 1.98$$

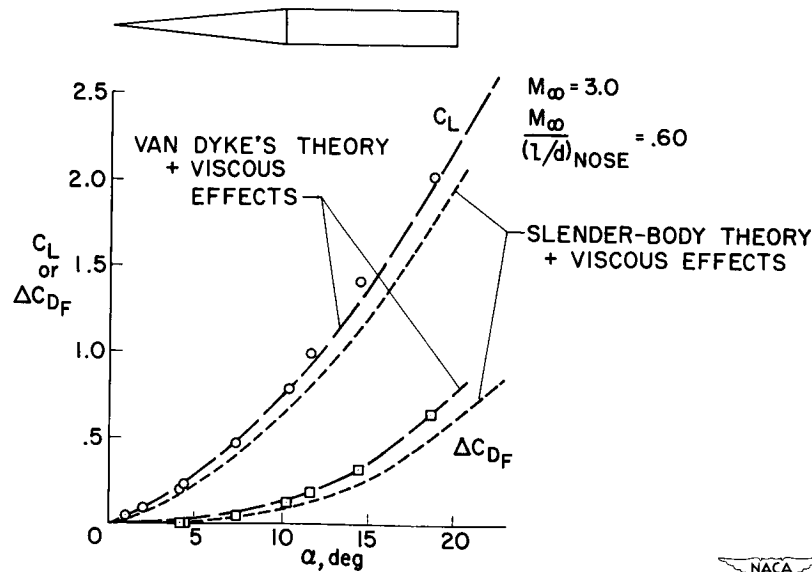
$$R_D = 0.4 \times 10^6$$



NACA

Figure 3

COMPARISON OF THEORY & EXPERIMENT



NACA

Figure 4

COMPARISON OF INITIAL LIFT-CURVE SLOPES

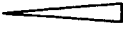
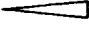


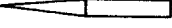
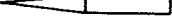
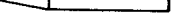
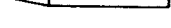
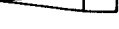
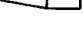
MODEL	M_∞	$K = \frac{M_\infty}{(l/d)_{NOSE}}$	THEORY (VAN DYKE)	EXPERIMENT
	3	0.43	1.98	1.95
	5	1.00	1.96	2.01
	5	1.67	2.04	1.90
	3	0.43	2.36	2.46
	3	0.60	2.66	2.66
	5	1.00	3.16	2.87
	3	1.00	2.97	2.92
	5	1.67	3.66	3.24
	5	1.00	2.69	2.29
	5	1.67	3.06	2.56

Figure 5

COMPARISON OF THEORY AND EXPERIMENT

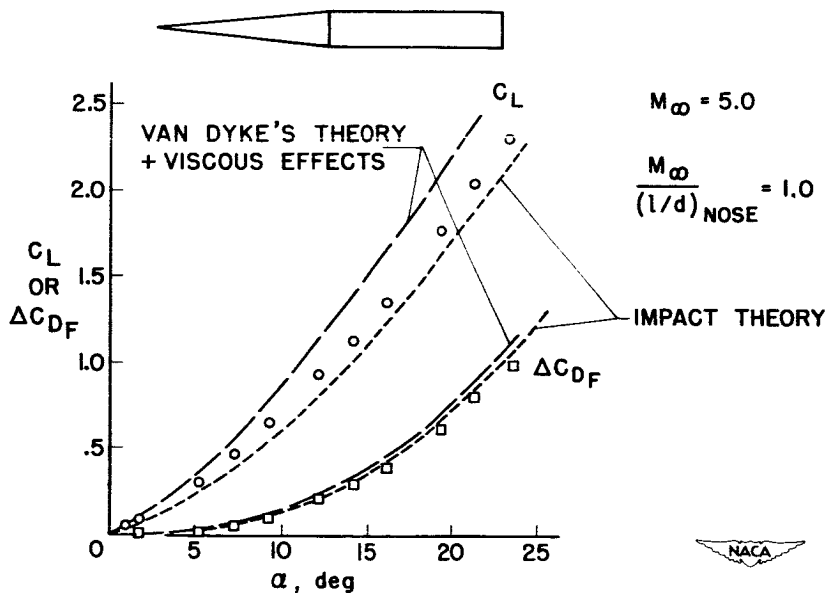


Figure 6

COMPARISON OF THEORY AND EXPERIMENT

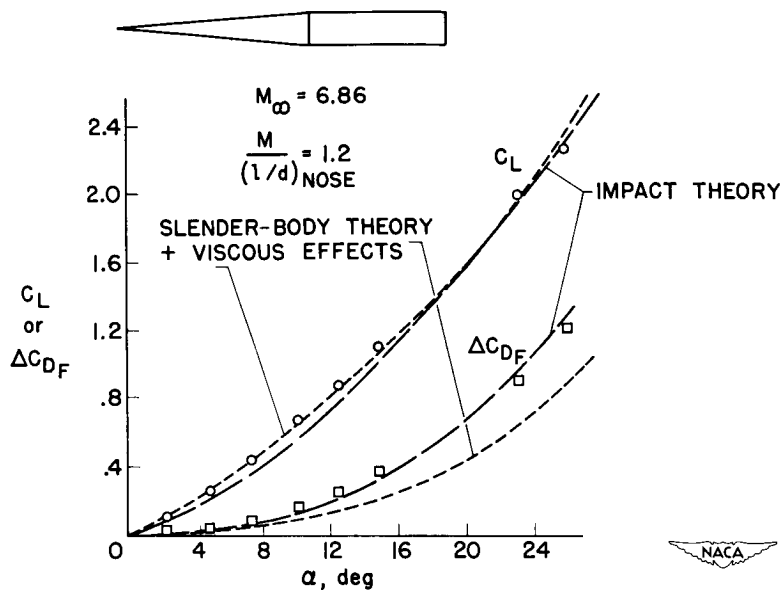


Figure 7

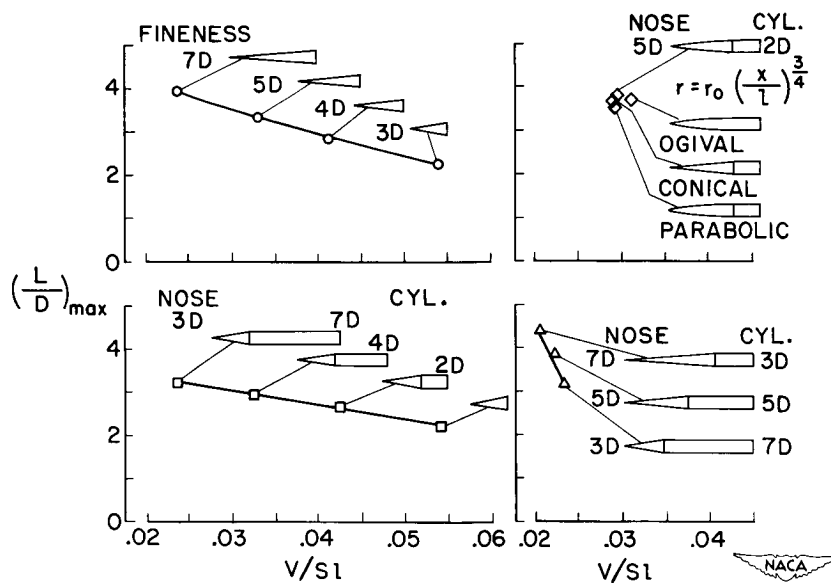
FOREBODY $(L/D)_{MAX}$, BODIES OF REVOLUTION

Figure 8

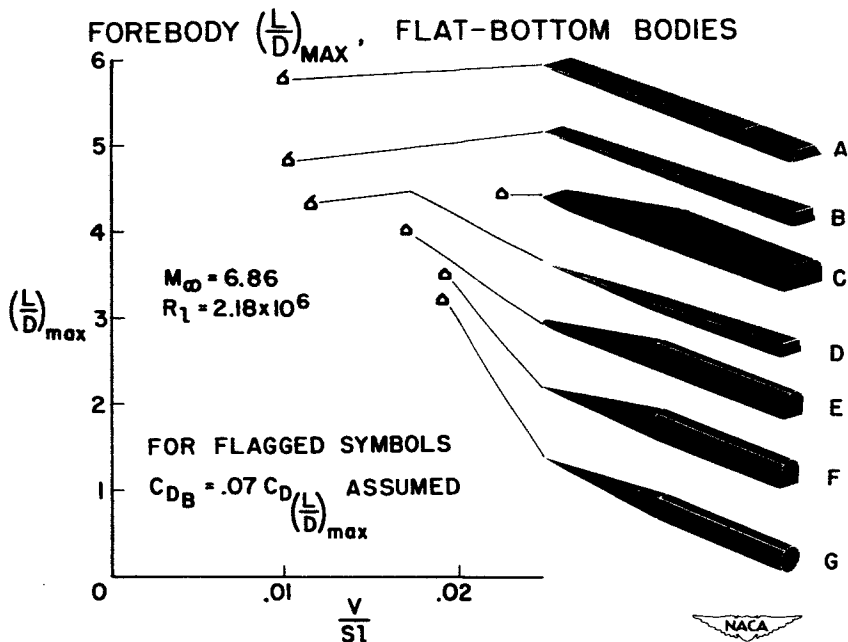


Figure 9

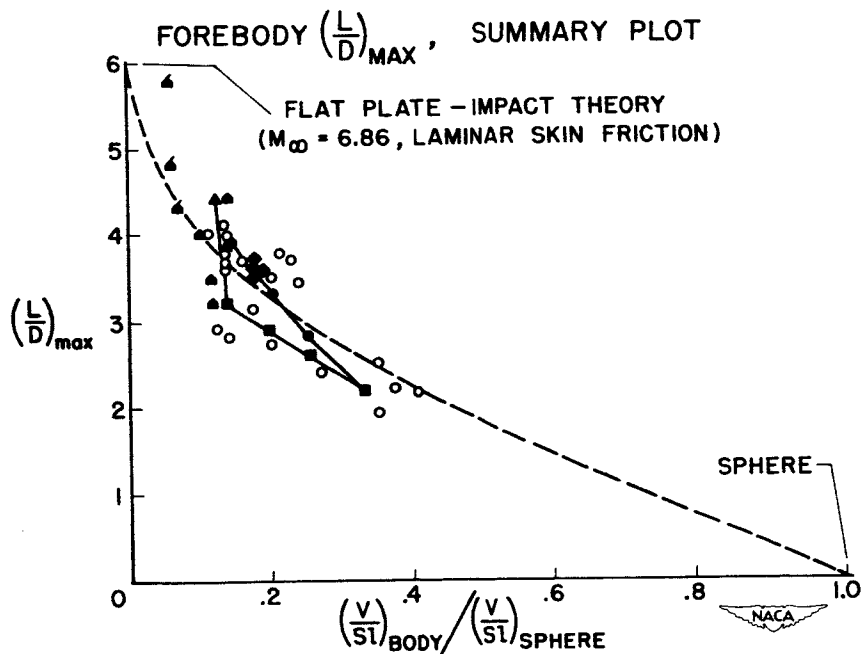


Figure 10

REF ID: A53110
CONFIDENTIAL

SOME CONSIDERATIONS CONCERNING INLETS AND DUCTED BODIES

AT MACH NUMBERS FROM 0.8 TO 2.0

By Richard I. Sears

Langley Aeronautical Laboratory

The study of air-inlet design is essentially a study of thrust and drag. With an adequately sized inlet, the thrust available is proportional to the total pressure the inlet can provide. Many data have been presented in the past concerning the pressure recoveries attainable at supersonic Mach numbers with various types of inlets. Some information on this subject is presented in this and the following paper.


Much less data relative to the drag of bodies having air inlets and internal-flow systems are available. The drag characteristics of non-ducted bodies of revolution as affected by various shape parameters have been fairly well established and a considerable amount of experimental data is published. Incorporation in a body of a turbojet engine and its associated inlets and ducting can cause a major departure in geometry from the more idealized body of revolution.

This paper presents some drag information from systematic tests of nose inlets and from isolated tests of scoop and wing root inlets.

Figure 1 shows configurations tested by means of rocket techniques to evaluate effects of cowl profile on the drag of normal-shock nose inlets. Five different cowl shapes were tested, each with identical afterbody shape, and are shown in figure 1. All cowls were of fineness ratio 3 and the inlet area was 24 percent of the body frontal area. Over-all model fineness ratio was 8. The top cowl is of the NACA 1-series family; the second is defined by a parabolic arc with its vertex at the maximum diameter. The next three are conical with beveled, blunt, and sharp lips, respectively.

Figure 2 shows the measured external drag coefficient C_D (based on body frontal area) of the complete models, at the left as a function of M for $\frac{m}{m_0} = 1$ and at the right as a function of m/m_0 for $M = 1.3$.

For maximum flow rate at Mach numbers up to about 1.1, all cowl shapes have about the same C_D , but the curves spread apart at higher M , the 1-series cowl having the greatest C_D and the cone with sharp lips the least. The other cowls fell in between and in the same order as shown in figure 1. The solid line gives the drag of the nonducted, pointed



body, derived by extending the lines of the parabolic cowling as shown at the top of figure 1. The drag of the models with conical cowls are significantly lower than that of the pointed body because of the air admitted.


At $M > 1.35$, the value of C_D for the body with blunt-lip conical cowl is about 0.04 less than that for the l-series cowl. Since both the l-series cowl and the blunt-lip conical cowl had identical profiles in the region of the inlet lip, it is apparent that the lower drag of this conical cowl is associated with its lesser fullness of profile farther back than the region of the lips.

The curves of figure 2 show that at $M = 1.3$ all cowls except the l-series have about the same value of C_D at $\frac{m}{m_0} \approx 0.8$. Thus, whereas the sharp lip configuration had least drag at maximum flow rate, the beveled and blunt-lip conical cowls gave less increase in C_D as air was spilled. Actually, the increase in C_D for the sharp-lip conical cowl is just about equal to the additive drag calculated from momentum considerations. The other inlets all benefit to some extent from leading-edge suction, the increment in C_D associated with spilling air being less than the computed additive drag. The fact that blunt lips can be tolerated on conical cowls without large drag penalties is encouraging because they may be necessary structurally and for operation at take-off and at angles of attack.

The effect of cowl shape on the drag of conical-shock nose-inlet models in the transonic and supersonic range has been recently obtained from rocket tests. The configurations tested are shown in figure 3. The models had afterbodies and fins similar to those of figure 1. The cowls were of fineness ratio 3 and the inlet area was 24 percent of the body frontal area. The cowls had external lip angles of 12° and 17° faired into conical and parabolic cowl shapes as shown. The cone position was varied as indicated by the values of θ_1 at the right of figure 3.

The data obtained for these models are given in figure 4. The internal flow for each model was the maximum that the inlet would pass and is given by the upper curves, one for each cone position. The designation for each drag curve specifies first, the cowl shape, parabolic or conical; second, the external lip angle of the cowl; and lastly, the cone position angle.

Inspection of the drag curves shows that changes in lip angle and cone position result in small changes in the drag in the direction to be



expected. However, that shown for changes in cone position borders on the accuracy of the tests. The effects of cowl shape are more pronounced. The conical-cowl models had lower drag than did the parabolic-cowl models; this result is consistent with the results shown in figure 2 for the normal-shock nose-inlet models.

Let us now examine some aspects of the pressure-recovery problem. The total pressure recovery at supersonic Mach numbers of nose inlets, with and without external compression, are fairly well known for operation at an angle of attack of 0° . Tests have indicated that at higher angles of attack the pressure recovery decreases rapidly.


Figure 5 shows some results from exploratory tests of a swept inlet expected to have better recovery at high angles of attack than a normal-shock inlet. The latter is also shown for comparison. The swept inlet was made from a circular pipe by cutting it obliquely at 45° to the axis and beveling the lips on the outside. Total-pressure recoveries were measured at $M = 1.42$ without any diffusion and at $M = 1.84$ with some diffusion. The portion of the inlet and duct ahead of the rake station is shown in the sketches. Positive angles of attack are taken as indicated by the arrows. The normal-shock inlet, tested only at $M = 1.42$, had rounded inner lips and some diffusion.

The models were tested with a choking nozzle at the duct exit, which simulates constant-engine-inlet Mach number operation. The mass-flow ratio therefore varied with angle of attack, it being proportional to the pressure recovery. The upper set of curves show the values of mass-flow ratio obtained, and the corresponding pressure recoveries are shown in the lower set of curves.

It appears, from these data, that use of a swept nose inlet provides reasonably good recoveries at positive angles of attack as high as 20° to 30° at the expense of low flow rates and poor recoveries at negative angles of attack. Other published data (ref. 1) show that a swept nose inlet with a vertical-wedge compression surface maintains a nearly constant recovery of about 0.85 for angles of attack from 0° to 10° at $M = 1.9$. The drag characteristics of the swept inlet have not been measured.

Fairly extensive data are available on the pressure recoveries attainable with nose inlets, and these will not be discussed further here. However, in many cases it is not practical to use nose inlets. Many different types of scoop inlets have been tested with widely differing results dependent, to a large extent, on the treatment of the boundary layer ahead of the inlet.

Figure 6 is intended to give a brief perspective of the relative standing of various types of scoops with regard to total pressure recovery.




The data presented are the maximum average total pressure after diffusion at about an angle of attack of 0° and for mass-flow ratios above 0.75. It is assumed that for a scoop to be considered for use it must have good recovery, at least for these operating conditions. The symbols without flags represent wind-tunnel-data test points and the symbols with flags represent the end points of curves defined by rocket data. The open symbols represent scoops with some type of boundary-layer removal system, whereas the solid points indicate scoops with no boundary-layer removal system. Detailed results for many of these scoops are reported in references 2 to 11. Scoop inlets are of several types as indicated in the lower left corner of figure 6 and by the sketches shown.

The data presented are sample data for each type of scoop, but the maximum recoveries shown are believed quite representative of those that have been obtained for each type. Problems of matching are treated in a subsequent paper by John L. Allen and are not considered here.

Inspection of these data indicates that the recoveries obtained at supersonic speeds can be either good or bad depending on the scoop configuration used and on the treatment of the boundary layer. Best recoveries have been obtained with scoops located just under the nose of the body and with external-compression-type scoops having complete boundary-layer removal. At $M < 1.4$ and $m/m_0 > 0.75$, the nose scoop apparently needs no boundary-layer removal and has good recovery at positive angles of attack (refs. 4, 5, and 9). The following paper treats the external compression scoop in more detail. Annular or semiannular scoops which enclose an appreciable part of the body circumference give low recoveries and pulsations at reduced flow rates (refs. 2, 3, and 7). The submerged inlet suffers also from boundary-layer shock interaction aggravated by superstream Mach numbers ahead of the inlet, caused by the curving ramp floor inherent in the design (ref. 8).

Whereas the pressure recovery of scoop inlets can be rather easily compared, the drag characteristics cannot be except in special cases where several scoop arrangements are tested for a particular airplane. Such systematic tests are rare. The installation of the power plant, ducting, and scoop inlet largely determine the fuselage lines which, of course, govern the drag. Although drag data for scoop configurations are very meager, it is possible to report the results from several isolated investigations.

Figure 7 shows about all the fuselage models having scoop inlets for which drag data are available. Above the sketch of each configuration, the curve of area distribution normal to the longitudinal axis is shown in order to define the geometry better. The solid line represents areas corresponding to the physical outline of the model and the dashed line represents deduction of the entering free-stream tube area, a procedure



which recent tests have shown to result in an equivalent nonducted body having the same drag. All the diagrams are shown to the same scale.

For the upper three models, only the forward portion of the fuselage was tested. Models B, C, and G and the forward half of model E are models of actual aircraft. The models on the left are research configurations.


Drag curves as a function of Mach number are given for some of these configurations in figures 8 and 9 and a comparison of the drag results is given in figure 10. Because these configurations are not related in any manner except that all models had scoop inlets, it is convenient to plot their drag as a function of effective body fineness ratio. This value is taken as the length divided by the diameter of a circle of area equal to the maximum frontal area.

The data are shown at the top of figure 10 for the fuselage nose configurations, A, B, and C, and at the bottom of figure 10, for the complete fuselage models. The two solid lines, shown for reference purposes, give the drag of parabolic bodies of revolution without internal air flow. The solid line on the top of figure 10 was computed for parabolic-nose shapes from second-order theory with an allowance for skin friction included. The curve on the bottom of figure 10 was obtained from rocket tests of parabolic bodies of revolution. If the drag shown by these curves at high fineness ratio is taken as that for a good parabolic body of revolution, then the scale at the right gives the ratio of drag to that of a good body.

Many of the models have nearly twice the drag of good bodies and almost all have appreciably more drag than parabolic bodies of the same fineness ratio.

For model E (ref. 7), the area curve shows a forward location for the maximum area station which results in a low nose fineness ratio. Data presented in the paper by Robert L. Nelson and William E. Stoney, Jr., indicated that the increase in drag for model E over that shown in figure 10 by the solid line for a parabolic body of the same over-all fineness ratio and in figure 8 can be just about accounted for on the basis of difference in nose fineness ratio. Thus, although, as will be shown in a subsequent paper by Lowell E. Hasel, forwardly located scoops are favorable from boundary-layer considerations, they can cause high drag if they result in a low effective nose fineness ratio.

The forwardly located underslung scoop of model D was added to a parabolic body of revolution without increasing or changing the location of the maximum frontal area. Thus, the nose fineness ratio was not changed and, as indicated by point D on the lower part of figure 10 and by figure 8, the drag of the ducted model was, within the experimental accuracy, the same as that of the body without scoop. Although the scoop of model D had



an area only 8 percent of the body frontal area, tests in the Langley 8-foot transonic tunnel (ref. 9) of a similar scoop of area twice as large relative to the fuselage also indicated negligible drag increment, at least to $M = 1.1$, the limit of the test. The underslung nose scoop, therefore, looks good from drag as well as pressure-recovery considerations.


Although the effective fineness ratio (as defined) is fairly large for model C, dragwise it acted like a nose of much lower fineness ratio (ref. 11). The distribution of area in this case was important.

Fuselage drag usually accounts for the greater portion of airplane zero lift drag. Therefore, it is obviously important to make the drag of fuselages, with scoop inlets and associated bumps for ducting and engine housing, approach the drag of good bodies of revolution. It is recognized that greater research effort is needed to indicate ways of achieving this effect.

Another important class of inlets is the wing root inlet. Data published in reference 12 show that a wing-root inlet could be added to an 8-percent-thick swept wing with very little increase in drag at Mach numbers less than 1.4, the limit of the tests. Figure 11 presents data to $M = 2$ which lead to similar conclusions for a somewhat different wing-root-inlet arrangement.

The basic wing was swept 47° on the quarter-chord line and was 5.5 percent thick. Inboard of the one-third semispan station the wing was split and the lower portion dropped to form the root inlet as shown in the sketch. The modified wing root housed two semiburied turbojet engines on each side as well as the inlet. The upper curve gives the mass-flow ratios at which the inlet was operated. The lower two curves give the measured external drag coefficients of the wing. These values are based on exposed-wing plan-form area. The solid points indicate data for the wing with inlet and engine installation and the open symbols are for the unaltered basic wing. These drag coefficients were obtained from tests of the configuration with and without the wing. Wing-fuselage interference drag is thus included in values given in figure 11. The data are given for the zero-lift condition only.

Comparison of the two drag curves indicates that addition of this root inlet increased the wing drag coefficient by about 10 percent at supersonic speeds. Inasmuch as the wing frontal area was increased 20 percent by the inlet, this result means that the drag per unit frontal area of the wing with inlet and engine installation was only 92 percent of that of the basic wing. This effect is, of course, caused by the fact that the wing was admitting air. However, the reduction in drag per unit frontal area for this wing root inlet and engine configuration is in marked contrast to the increases in drag per unit frontal area shown previously for fuselage configurations having scoop inlets.



Although adequate pressure-recovery data are not available for this inlet configuration, figure 12 shows recoveries measured in the Langley transonic blowdown tunnel for another wing root inlet. Adding this elliptically shaped root inlet to the basic swept wing-fuselage configuration caused increments of drag coefficient of about the same magnitude as those shown in figure 11.


The inlet lips were round and staggered as shown in the sketch. Tests were made with and without a boundary-layer bleed. The basic fuselage lines just ahead of the inlet were altered to permit installation of the boundary-layer bleed scoop. The boundary-layer duct exited normal to the wing on the lower surface just back of the inlet.


The three sets of curves show the effects of Mach number, angle of attack, and mass-flow ratio on the average pressure recovery measured after diffusion, for operation with and without the boundary-layer bleed.

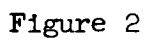
Analysis of the data shown in figure 12 and in figure 11 shows swept-wing root inlets to be potentially low drag configurations and, without external-compression devices, to be potentially capable of giving normal-shock recoveries over a fairly large angle-of-attack range. The need for further development to provide a workable boundary-layer bleed system is indicated.

In conclusion, this paper has attempted to point out some of the large differences that can exist at supersonic speeds in the pressure recovery and drag of good and not-so-good inlet and engine installation arrangements. Best pressure-recovery results have been obtained with scoop inlets located close under the nose and, for farther rearward locations, with external compression inlets having complete boundary-layer removal. Best drag results have been obtained with conical nose inlets, with scoop inlets located close to the nose and causing little or no increase in frontal area, and with a wing-root-inlet buried-engine configuration. More work is needed to define the minimum drag arrangements of scoop configurations wherein the engine installation causes large increases in frontal area of a basically good fuselage. At present, available tests have shown such configurations to be of high drag relative to those previously mentioned.

REFERENCES

1. Leissler, L. Abbott, and Hearth, Donald P.: Preliminary Investigation of Effect of Angle of Attack on Pressure Recovery and Stability Characteristics for a Vertical-Wedge-Nose Inlet at Mach Number of 1.90. NACA RM E52E14, 1952.
 2. Pendley, Robert E., Milillo, Joseph R., Fleming, Frank F., and Bryan, Carroll R.: An Experimental Study of Five Annular-Air-Inlet Configurations at Subsonic and Transonic Speeds. (Prospective NACA paper.)
 3. Davis, Wallace F., Brajinikoff, George B., Goldstein, David L., and Spiegel, Joseph M.: An Experimental Investigation at Supersonic Speeds of Annular Duct Inlets Situated in a Region of Appreciable Boundary Layer. NACA RM A7G15, 1947.
 4. Merlet, Charles F., and Carter, Howard S.: Total-Pressure Recovery of a Circular Underslung Inlet With Three Different Nose Shapes at a Mach Number of 1.42. NACA RM L51K05, 1952.
 5. Boswinkle, Robert W., Jr., and Mitchell, Meade H., Jr.: Experimental Investigation of Internal-Flow Characteristics of Forward Underslung Fuselage Scoops With Unswept and Sweptback Entrances at Mach Numbers of 1.41 to 1.96. NACA RM L52A24, 1952.
 6. Dryer, Murray, and Beke, Andrew: Performance Characteristics of a Normal-Shock Side Inlet Located Downstream of a Canard Control Surface at Mach Numbers of 1.5 and 1.8. NACA RM E52F09, 1952.
 7. Carter, Howard S., and Merlet, Charles F.: Flight Determination of the Pressure Recovery and Drag Characteristics of a Twin Side-Inlet Model at Transonic Speeds. NACA RM L53E05, 1953.
 8. Braden, John A. and Pierpont, P. Kenneth: Pressure and Force Characteristics at Transonic Speeds of a Submerged Divergent-Walled Air Inlet on a Body of Revolution. NACA RM L53C13, 1953.
 9. Pierpont, P. Kenneth, and Braden, John A.: Investigation at Transonic Speeds of a Forward-Located Underslung Air Inlet on a Body of Revolution. NACA RM L52K17, 1953.
 10. Wittliff, Charles E., and Byrne, Robert W.: Preliminary Investigation of a Supersonic Scoop Inlet Derived From a Conical-Spike Nose Inlet. NACA RM L51G11, 1951.
- 

11. Valerino, Alfred S.: Performance Characteristics at Mach Numbers to 2.0 of Various Types of Side Inlets Mounted on Fuselage of Proposed Supersonic Airplane. I - Two-Dimensional Compression-Ramp Inlets With Semicircular Cowls. NACA RM E52E02, 1952.
 12. Howell, Robert R., and Keith, Arvid L., Jr.: An Investigation at Transonic Speeds of the Aerodynamic Characteristics of an Air Inlet Installed in the Root of a 45° Sweptback Wing. NACA RM L52H08a, 1952.
- 

$$\frac{A_i}{A_f} = 0.24$$
$$\alpha=0^\circ; R \approx 42 \times 10^6 \text{ AT } M=1.4$$


CONICAL-SHOCK INLET MODELS

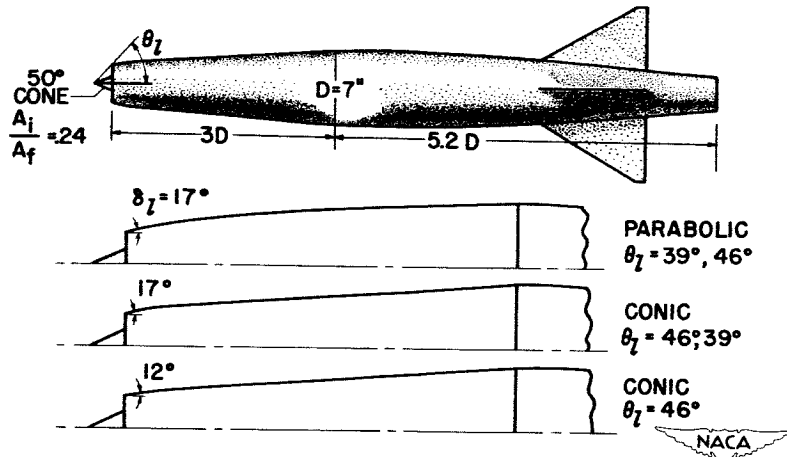


Figure 3

EXTERNAL DRAG OF CONICAL-SHOCK NOSE-INLET MODELS

$\alpha = 0^\circ$; $R \approx 42 \times 10^6$ AT $M = 1.4$

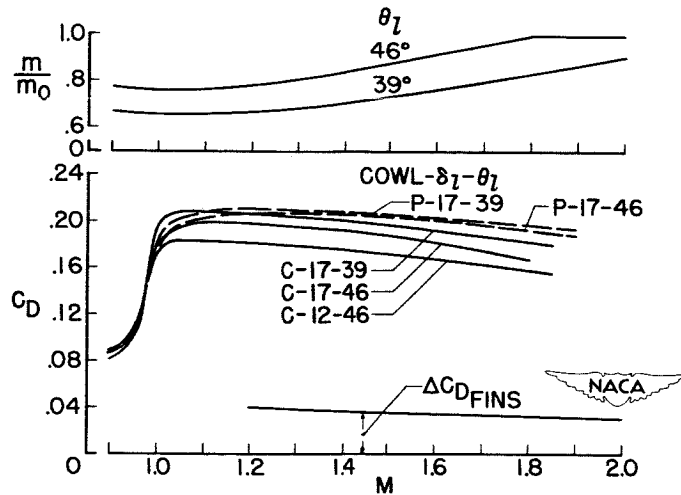


Figure 4

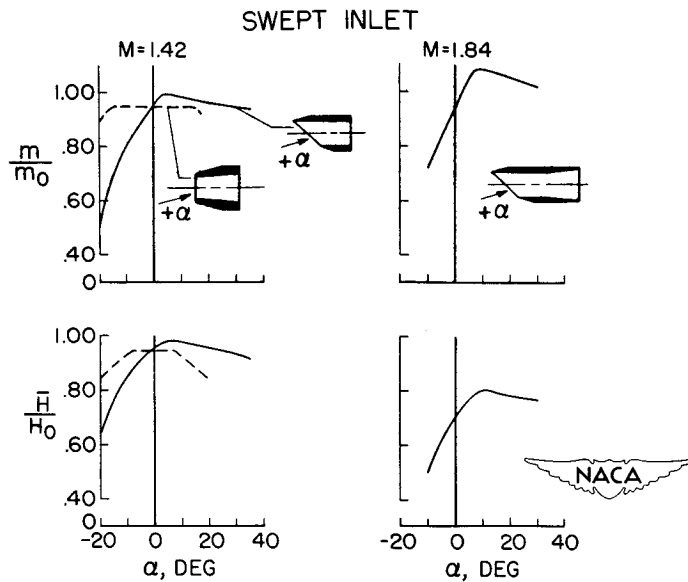


Figure 5

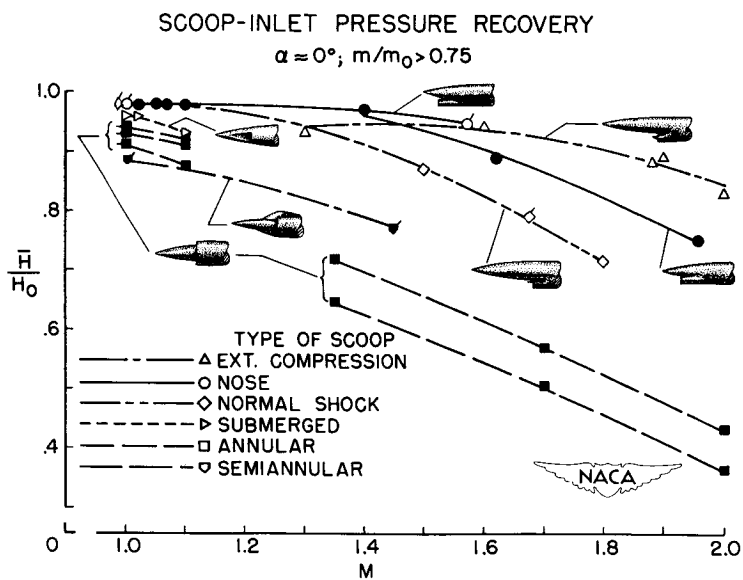


Figure 6

SCOOP-INLET MODELS

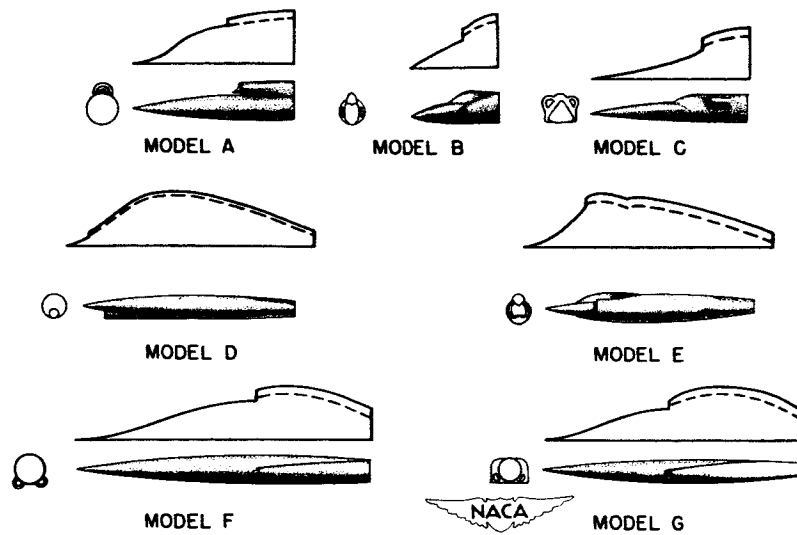


Figure 7

EXTERNAL DRAG OF SCOOP-INLET ROCKET MODELS

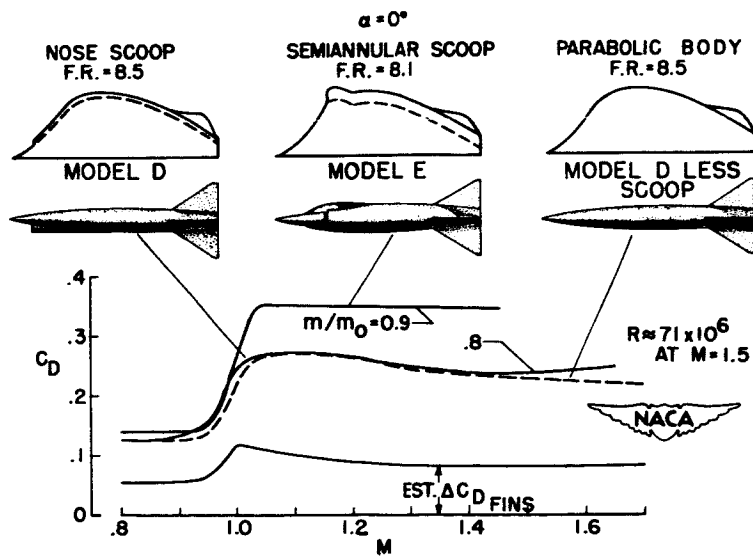


Figure 8

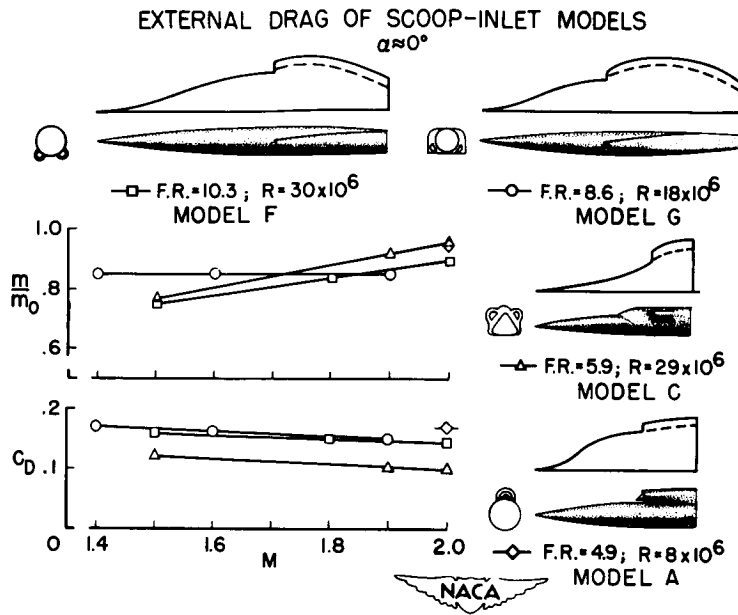


Figure 9

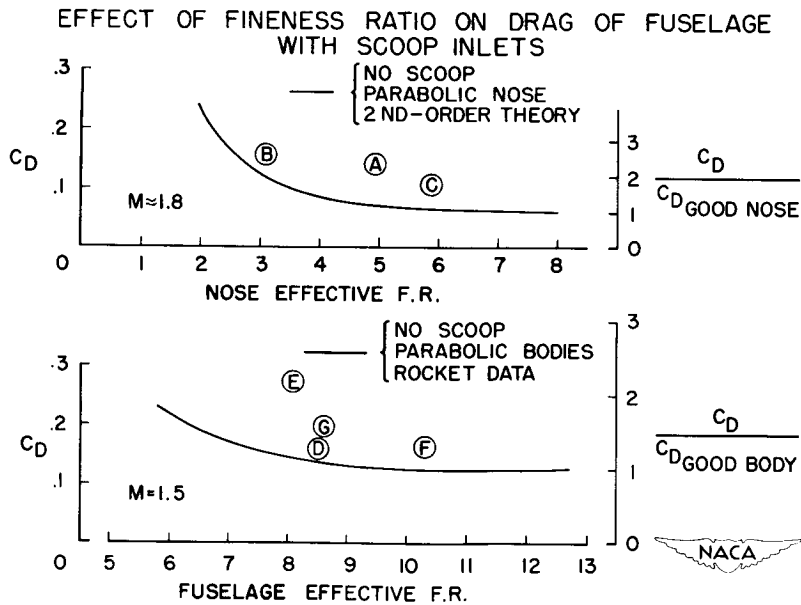


Figure 10

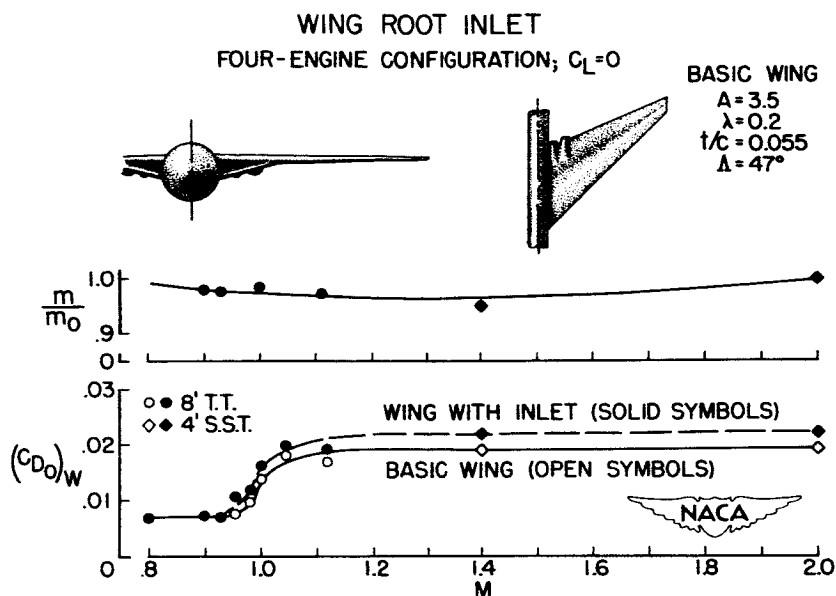


Figure 11

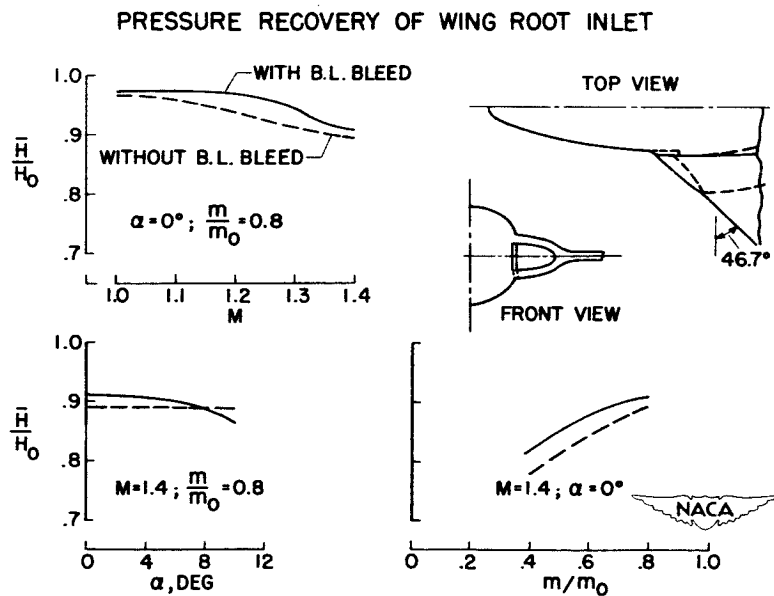


Figure 12

THE PERFORMANCE OF CONICAL SUPERSONIC SCOOP INLETS

ON CIRCULAR FUSELAGES

By Lowell E. Hasel

Langley Aeronautical Laboratory

Supersonic-scoop-inlet research has, for the most part, been conducted either with the inlet on a flat plate at 0° angle of attack (refs. 1 and 2, e.g.) or with the inlet at a fixed position on a fuselage (ref. 3, e.g.). Such angle-of-attack data as are available (refs. 3, 4, and unpublished data) are not complete enough to enable a detailed evaluation to be made of scoop-inlet characteristics at angles of attack.

The Langley Aeronautical Laboratory and the Lewis Flight Propulsion Laboratory are concurrently investigating the angle-of-attack characteristics of scoop inlets (refs. 5, 6, and unpublished data obtained at the Langley Laboratory) using the models shown in figures 1 and 2. Throughout the remainder of the discussion these configurations will be designated as models A and B, respectively. The inlets on both models are of the conical type, having 25° half-angle cones, and are designed for a Mach number of approximately 2. The inlet on model A has a capture area of about 25 percent of the fuselage frontal area. Model B utilizes two completely independent inlet and diffuser systems. Each inlet is similar to the one illustrated in figure 2. The total capture area of the twin inlet installation is about 22 percent of the fuselage frontal area. On both models the splitter plate separating the inlet from the boundary-layer bleed is swept back from the tip of the central body to the lip of the inlet. The boundary layer is removed by means of a suction bleed on model A; whereas on model B a 16° included-angle wedge diverter is used to displace the boundary layer around the sides of the inlet. The tip of the wedge is located at the same axial position as the tip of the central body. Provisions are incorporated in both configurations for varying the bleed height. On model A the maximum bleed height is twice that illustrated in figure 1. The fuselage forebody fineness ratios of model A are 4.0 and 6.5. The nose section is an ogive of fineness ratio 3.5. The forebody of configuration B has a fineness ratio of 7.5 and corresponds to the RM-10 forebody shape.

Before discussing the test results, a brief review will be given of those features of the flow about bodies of revolution (ref. 7) at angles of attack which influence scoop performance.


At angles of attack the boundary layer flows from the windward to the leeward side of the fuselage, figure 3, thus reducing the thickness on the bottom and increasing the thickness on top. As the angle of attack

increases the boundary layer separates and creates a stable vortex pattern similar to that known to exist under certain conditions behind circular cylinders. The angle of attack at which the vortices are first evident at the inlet varies with axial position of the inlet on the fuselage and the Reynolds number. A typical effect of the vortex formation is to thin the boundary layer over a small portion of the top of the fuselage. It is probable that on fuselages which are bodies of revolution a portion of these vortices will enter an inlet located on the top section of the fuselage. If the angle of attack becomes very large, the vortex flow will become unstable. The latter condition may be expected to produce very unsatisfactory engine operation.

The forebody also has a significant effect, especially at angles of attack, on the local Mach number distribution at the inlet. High local Mach numbers and large cross-flow angles are created near the side of the fuselage; while on the bottom the local Mach number decreases.

The boundary-layer conditions which existed a short distance ahead of the inlets of models A and B at $M = 2.0$ are illustrated in figure 4. The boundary-layer thickness expressed in terms of the boundary-layer thickness at 0° angle of attack is presented as a function of fuselage position. These data were obtained without the inlet installed on the fuselage. Transition wires were used on the two shorter forebodies to insure a turbulent boundary layer at the inlet, since this is the condition most likely to occur in flight. On the long forebody natural transition occurred upstream of the inlet. On the top section of the fuselages the increase of boundary-layer thickness at both angles of attack is smallest on the short forebody. (For reasons of clarity the boundary-layer data obtained on the long body at 10° have been omitted from fig. 4. The boundary-layer growth on this forebody at an angle of attack of 10° was greater than on the short forebody at 12° .) At 6° the vortex formation is evident only on the long forebody. At 12° a vortex has formed on the medium-length forebody but none is evident on the short forebody. On the bottom of the fuselages the boundary-layer thickness decreases considerably at angles of attack. It is interesting to note that the vortex thins the boundary layer over only a relatively small portion of the top of the fuselage, and that this region of thin boundary layer appears to be too narrow to be utilized by typical inlets such as the one on configuration A.

Figure 5 presents a typical set of data obtained at $M = 2.0$ from the configuration having the short forebody, showing the effect on pressure recovery of circumferential location of the inlet. Maximum pressure recoveries are presented as a function of fuselage position and angle of attack. The bleed-height ratio, $h/\delta_{\alpha=0^\circ}$ of 1.25, chosen for this figure represents the ratio of the boundary-layer bleed height to the boundary-layer thickness at 0° angle of attack. Preliminary examination of the data has indicated that the bleed system was removing all of the air



which could enter its capture area. The maximum pressure recovery is adversely affected by angle of attack if the inlet is located anywhere in the region extending from the top to the side of the fuselage. These losses are caused either by the thickening of the boundary layer, high local Mach number and accompanying large cross-flow angles, or a combination of the two effects. On the bottom of the fuselage the pressure recovery increases with angle of attack because of the decrease in local Mach number ahead of the inlet.

The effect of bleed height on scoop performance is illustrated in figure 6 which presents the maximum pressure recoveries as a function of bleed-height ratio for three angles of attack and for three inlet positions. At 0° the pressure recovery continues to increase when the bleed-height ratio exceeds 1. This is possibly due to the fact that, as the bleed height increases, the average Mach number of the air entering the inlet decreases slightly. When the inlet is on top of the fuselage, the pressure recovery at 6° continues to increase until the bleed-height ratio is about equal to the maximum boundary-layer thickness ratio. At 12° the pressure recovery appears to become constant at a bleed-height ratio near 2 although the maximum boundary-layer thickness ratio is about 3.7. At the side position, increasing the bleed-height ratio has less beneficial effect on the pressure recoveries at angles of attack since the losses are primarily caused by high local Mach numbers and large cross-flow angles. At the bottom position the bleed height has only a small effect on the pressure recovery of the inlet.

These pressure-recovery characteristics (figs. 5 and 6) at angles of attack may be expected to change to some extent with forebody length. The variations will be greatest at the top inlet position because of the differences in the rate of boundary-layer thickening (fig. 4) and because of the vortex formation which may exist at an inlet mounted farther to the rear on a fuselage.


The effect of forebody length on pressure recovery is illustrated in figure 7. The pressure recoveries, expressed in terms of the 0° recovery, are presented as a function of angle of attack for the top and bottom inlet positions. The bleed-height ratio is 1.25. The effect of the more rapid thickening of the boundary layer on the top of the two longer forebodies is most evident at moderate angles where the decrease in pressure recovery of these configurations is appreciably more than for the short body configuration. At the higher angles of attack an abrupt and favorable change in the scoop characteristics on the longer forebody occurs, probably because of the effect of the vortices generated on this forebody. On the bottom of the fuselages, the effect of the forebody length is smaller. The reasons for the consistent variation of pressure recovery with forebody length have been investigated to some extent but no conclusions have as yet been reached.

If the forebody is long enough to produce a vortex flow ahead of the inlet, the variation of the pressure-recovery characteristics with bleed-height ratio will be somewhat different from those previously discussed. These differences may be noted in figure 8 which presents the recovery characteristics of an inlet mounted on top of the long forebody. On the left side of the figure the pressure recovery is presented as a function of the bleed-height ratio for several angles of attack. On the right side the distribution of the ratio of pitot pressure to free-stream-total pressure on the fuselage just ahead of the inlet is shown for 0° and 10° . The free-stream value of this ratio is 0.72 at $M = 2.0$. The boundary-layer surveys indicated that the vortex formed on this forebody at the inlet station at about 4° . The action of the vortices is most evident when none of the boundary layer is removed from the inlet. At this condition the pressure recovery decreases as the angle of attack increases to 3° . Further increases of the angle of attack to 6° and 10° result in large increases in the pressure recovery. The pitot-pressure contours indicate that at 10° a relatively large amount of the vortex enters the inlet. It is thought that the primary effect of the vortex is to prevent separation of the boundary layer inside the inlet and thus increase the pressure recovery. As the bleed height increases, the pressure recoveries at the lower angles increase and the effect of the vortex becomes much less apparent.

Model B, which is the long forebody configuration (fig. 2), has also been tested at Mach numbers of 1.5 and 1.8. In general, the Mach number had little effect on the over-all pressure-recovery characteristics of the inlets. As the Mach number decreased the changes in pressure recovery with angle of attack also decreased.

It is obvious that the pressure-recovery characteristics of inlets operating on top of a fuselage can be improved if the boundary-layer thickness can be decreased. Several possible solutions to this problem exist in addition to methods such as minimizing fuselage angle of attack and keeping the inlet as far forward as is consistent with low-drag considerations. The use of fuselages having noncircular cross-sectional shapes should be investigated. On fuselages of circular cross section, methods of producing a larger region of thin boundary layer should also be studied. If the transverse distance between the vortices can be increased and the vortices induced to form at smaller angles of attack, some benefit may result. This latter scheme has been briefly tried on configuration A by the use of axial and diagonal vortex-generator strips. To date, the desired increase in pressure recovery has not been obtained.

Figure 9 illustrates the drag characteristics of the top and bottom inlet positions. The external drag at a mass-flow ratio of about 0.9 is presented on the left side of the figure as a function of bleed-height ratio for angles of attack of 0° and 6° . At 6° the drag of the bottom inlet is higher than the drag of the top inlet. Since this difference



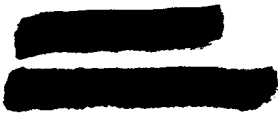
in drag tends to counteract the pressure-recovery advantage of the bottom position the optimum location of the inlet should be determined on the basis of net thrust so that the effect of drag, as well as pressure recovery, may be considered. The maximum values of net thrust for a typical turbojet engine, expressed in terms of the net thrust at 0° are presented on the right side of the figure as a function of bleed-height ratio. In calculating the net thrust the assumption was made that the drag associated with the removal of the boundary-layer air was equal to one-half its kinetic energy. This assumption concerning the drag of the boundary-layer removal system is not critical to the net-thrust comparison because the bleed mass-flow ratios were about the same for the two inlet positions. It appears on the basis of net-thrust ratio that the top and bottom inlet positions are comparable for this particular configuration and angle of attack. It should be mentioned that this figure is based on preliminary data and may be subject to some changes after analysis of the data is complete. Nevertheless, it is important to note the compensating effects of drag and pressure-recovery characteristics which may exist for the top and bottom inlet positions.

The pressure recoveries of scoop inlets at a given bleed-height ratio may be affected by the characteristics of the boundary-layer removal system. A series of practical removal systems have been investigated at the Lewis Laboratory by mounting half-inlets on flat plates. These configurations and the results (refs. 2 and 8) are presented in figures 10 and 11. On the suction-bleed configurations the boundary-layer air was removed by means of an internal duct system while on the three diverter systems the boundary-layer air was displaced around the sides of the inlet. The suction-bleed configurations differ only in the leading-edge shape of the splitter plate separating the inlet from the boundary-layer removal system. The diverter configurations employ a blunt edge, a 68° included-angle wedge, and the central body to displace the boundary-layer air. The effect of bleed-height ratio on the pressure-recovery characteristics of these configurations is illustrated in figure 11 for a Mach number of 1.88 and 0° angle of attack. The characteristics of the two suction-bleed configurations are comparable and are slightly superior to the blunt diverter. Both the 68° wedge and central-body diverter systems require a considerably larger bleed-height ratio than the other systems to obtain a corresponding inlet pressure recovery. It should be mentioned that a normal shock must exist ahead of the 68° wedge diverter. Since the tip of the wedge is at the same location as the tip of the central body this normal shock can affect the inlet flow. On another configuration the wedge was moved rearward 20 percent of the distance between the tip of the central body and the cowl lip. The pressure-recovery characteristics of this configuration were comparable with those of the suction bleed. Configuration B utilized a 16° wedge diverter with the tip of the wedge located at the tip of the central body. No adverse effects on inlet pressure recovery were noted. At a Mach number of 2.93 the characteristics of these systems, relative to each other, are not different.


The pressure drag of the wedge-diverter systems, neglecting the wedge base drag, has been investigated by Piercy and Johnson and is illustrated in figure 12. These data were obtained from a simplified configuration which consisted of a wedge diverter mounted between two flat plates to simulate the fuselage and inlet floor surfaces. Static pressures were measured on the wedge leading edges to determine the wedge pressure drag as a function of bleed-height ratio, wedge apex angle, Mach number, and axial location of wedge with respect to the top flat plate. The typical set of data presented in figure 12 was obtained at a bleed-height ratio of 1.0, and is based on the wedge frontal area. The pressure drag increases as the wedge apex angle θ increases and is highest for the curved diverter. The maximum value of the drag for these configurations is relatively small, however, when referenced to the frontal area of a typical inlet-fuselage configuration. The exact effect of Mach number is not known since data are available for only two Mach numbers. This effect, however, appears to be small. It should be mentioned that a consideration of the skin friction of the wedges will decrease the drag differences between the various configurations. The effects of the boundary-layer flow over the rear portion of an actual configuration may also alter the comparison to some extent.

The flat-plate inlets (fig. 10) which have efficient boundary-layer removal systems are essentially operating at free-stream conditions when the bleed-height ratio exceeds 1.0. Therefore, a comparison of the recoveries of these inlets and of practical scoop installations on a fuselage, such as A and B represent, is of interest to evaluate the recovery penalties which are associated with the fuselage installations. Such a comparison is made in figure 13 which presents, for an angle of attack of 0° , the maximum pressure recoveries of the flat-plate- and fuselage-mounted inlets as a function of the bleed-height ratio. Since the flat-plate data were obtained at $M = 1.88$ an estimate of the recovery of this inlet at $M = 2$ has been made. The best recovery obtained from the fuselage configurations is about 4 percent less than the recovery of the flat-plate inlet. Between one-fourth and one-half of this loss is due to the fuselage nose shock and the fact that the local inlet Mach number is higher than the free-stream Mach number. The cause of the remainder of the loss is not fully understood at present. There are some indications that the nonuniform velocity distribution at the inlet may be causing some of the additional loss. The difference which exists between the recoveries of the two shorter body configurations is considered to be due to slightly different local Mach numbers existing ahead of the inlet.


In conclusion, it appears that on circular fuselages the best pressure recoveries at angles of attack are obtained when a scoop inlet is located on the bottom of the fuselage. If the inlet must be placed on top, it should, in general, be located as far forward as is consistent with low-drag considerations. Location of a top inlet farther to the



rear on a fuselage where it may be affected by the vortex flow will have a beneficial effect on the pressure recovery only if the boundary-layer bleed-height ratio is small and the angle of attack is large. The net thrust characteristics of top and bottom inlet installations may be comparable because of the compensating effects of the drag and pressure-recovery characteristics. Finally, it appears possible to design relatively simple and efficient boundary-layer removal systems which remove the low-energy air by diverting it around the sides of the inlet.



REFERENCES

1. Wittliff, Charles E., and Byrne, Robert W.: Preliminary Investigation of a Supersonic Scoop Inlet Derived From a Conical-Spike Nose Inlet. NACA RM L51G11, 1951.
 2. Goelzer, H. Fred, and Cortright, Edgar M., Jr.: Investigation at Mach Number 1.88 of Half of a Conical-Spike Diffuser Mounted As a Side Inlet With Boundary-Layer Control. NACA RM E51G06, 1951.
 3. Simon, Paul C.: Performance Characteristics at Mach Numbers to 2.0 of Various Types of Side Inlets Mounted on Fuselage of Proposed Supersonic Airplane. IV - Rectangular-Cowl Inlets With Two-Dimensional Compression Ramps. NACA RM E52H29, 1952.
 4. Schaefer, Raymond F.: Some Design Configurations for Half-Round Side Inlets. Wright Aero Rep. No. 1692, Supersonic Inlet Symposium, Curtiss-Wright Corp. (Wood-Ridge, N. J.) Jan. 23, 1953.
 5. Hasel, Lowell E., Lankford, John L., and Robins, A. W.: Investigation of a Half-Conical Scoop Inlet Mounted at Five Alternate Circumferential Locations Around a Circular Fuselage - Pressure-Recovery Results at a Mach Number of 2.01. NACA RM L53D30b, 1953.
 6. Valerino, A. S., Pennington, D. B., and Vargo, D. J.: Effect of Circumferential Location on the Angle of Attack Performance of Twin Scoop Half Conical Type Inlets Mounted Symmetrically on the RM-10 Body of Revolution. (Prospective NACA paper.)
 7. Allen, H. Julian, and Perkins, Edward W.: Characteristics of Flow Over Inclined Bodies of Revolution. NACA RM A50L07, 1951.
 8. Piercy, Thomas G., and Johnson, Harry W.: A Comparison of Several Systems of Boundary Layer Removal Ahead of a Typical Conical External Compression Side Inlet at Mach Numbers 1.88 and 2.93. (Prospective NACA paper.)
- 

LANGLEY SCOOP-INLET CONFIGURATION
MODEL A

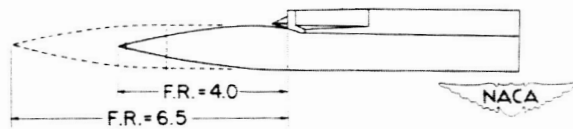
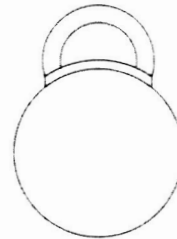
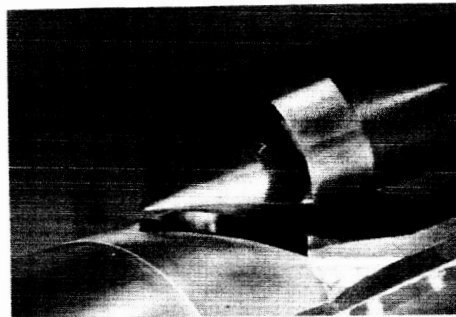


Figure 1

LEWIS SCOOP-INLET CONFIGURATION
MODEL B

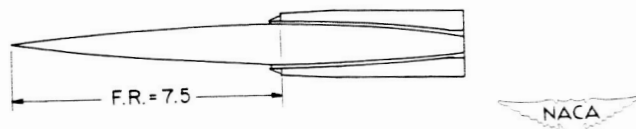
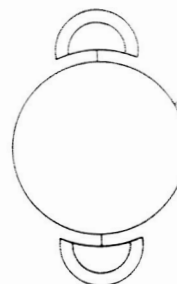
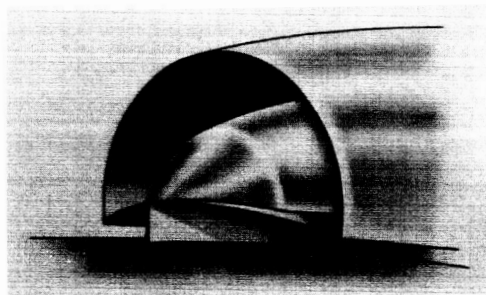


Figure 2



BOUNDARY-LAYER DISTRIBUTION ON A CYLINDRICAL FUSELAGE AT ANGLE OF ATTACK

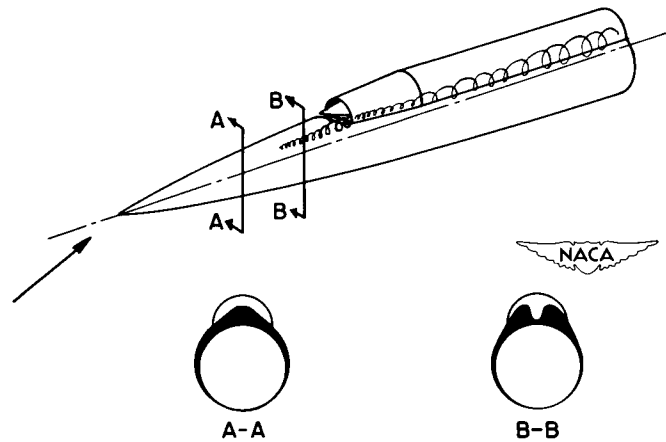


Figure 3

EFFECT OF FOREBODY LENGTH ON BOUNDARY-LAYER THICKNESS AT ANGLES OF ATTACK M=2.0

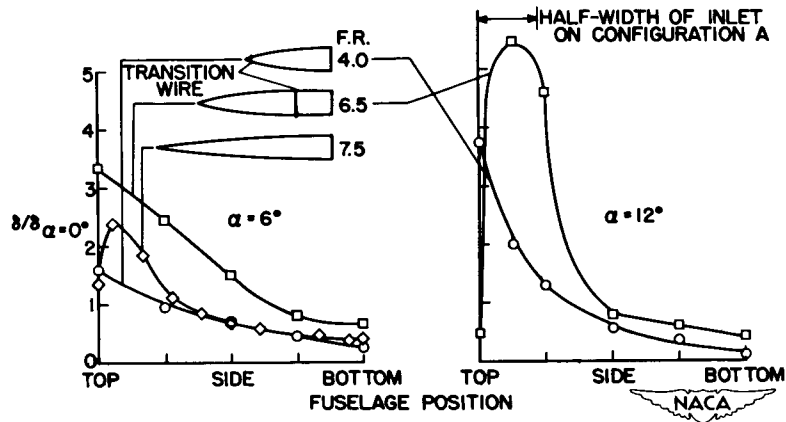


Figure 4

EFFECT OF INLET POSITION ON PRESSURE RECOVERY
AT $h/\delta_{\alpha=0^\circ} = 1.25$
 $M = 2.0$

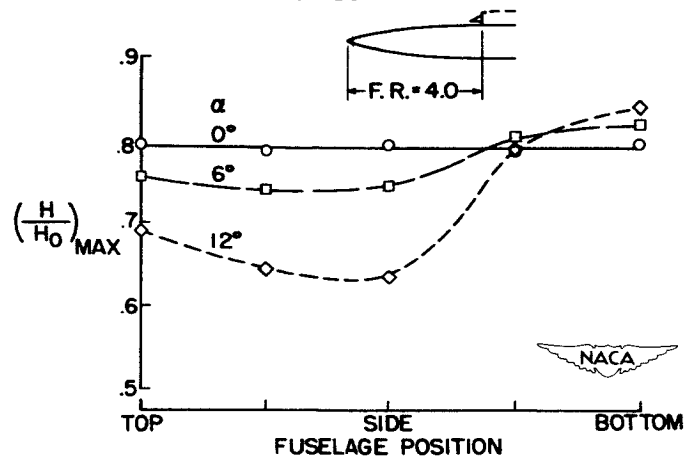


Figure 5

EFFECT OF BLEED HEIGHT ON PRESSURE RECOVERY
 $M = 2.0$

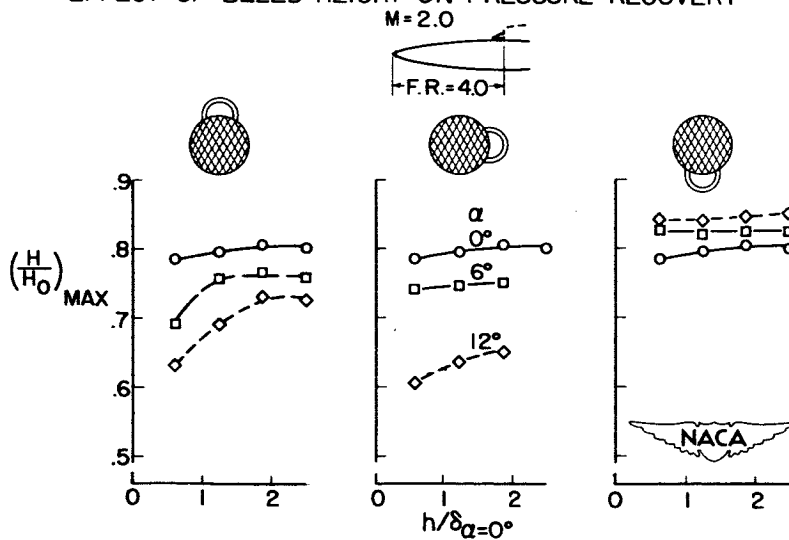


Figure 6

EFFECT OF FOREBODY LENGTH ON PRESSURE RECOVERY
AT ANGLES OF ATTACK
 $M=2.0$; $h/\delta_{\alpha=0^\circ}=1.25$

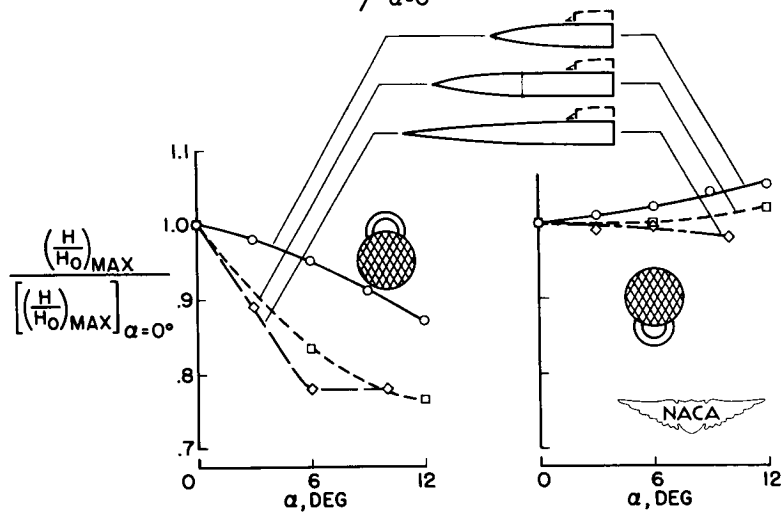


Figure 7

EFFECT OF FUSELAGE VORTEX ON PRESSURE RECOVERY
 $M=2.0$

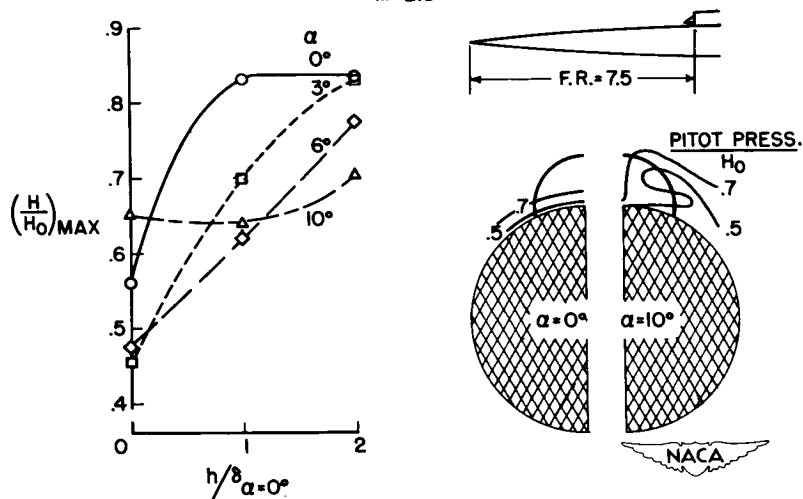


Figure 8

EFFECT OF INLET POSITION ON NET THRUST

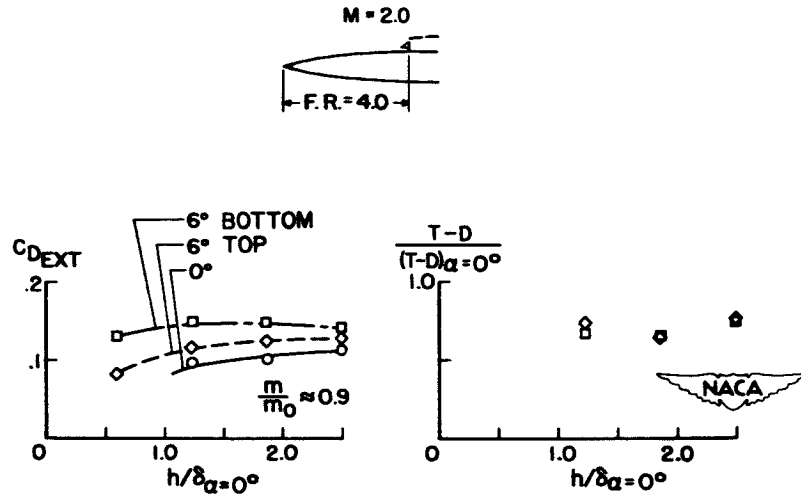


Figure 9

BOUNDARY-LAYER CONTROL SYSTEMS

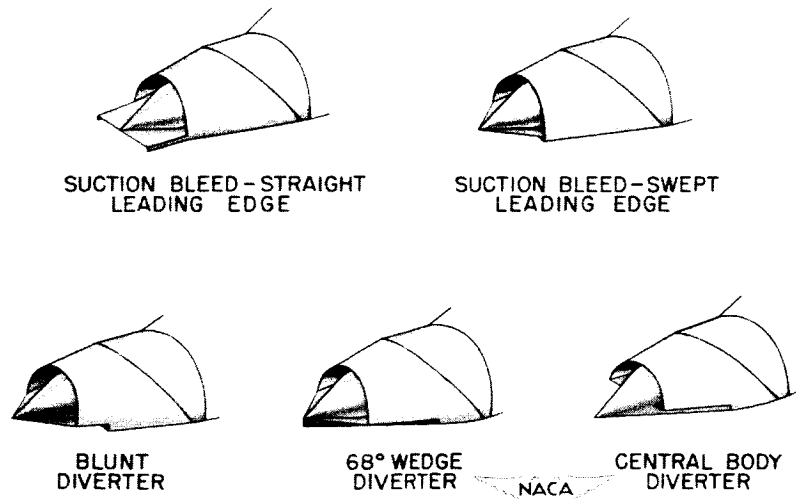


Figure 10

CHARACTERISTICS OF BOUNDARY-LAYER CONTROL SYSTEMS $M=1.88; \alpha=0^\circ$

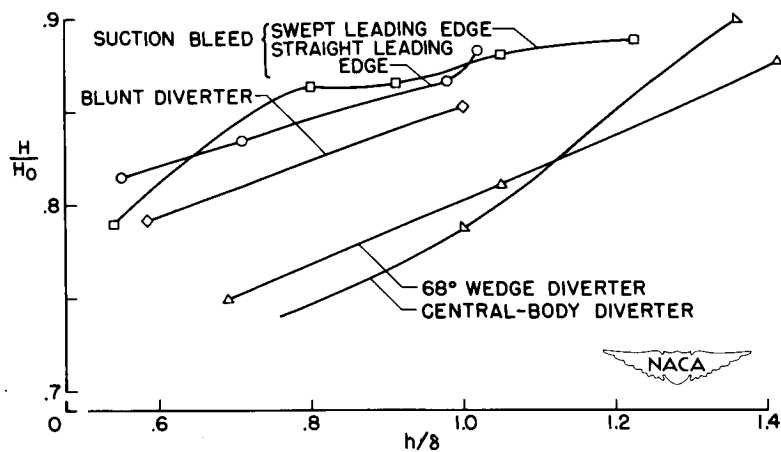


Figure 11

PRESSURE DRAG OF BOUNDARY-LAYER DIVERTERS $h/8=1.0$

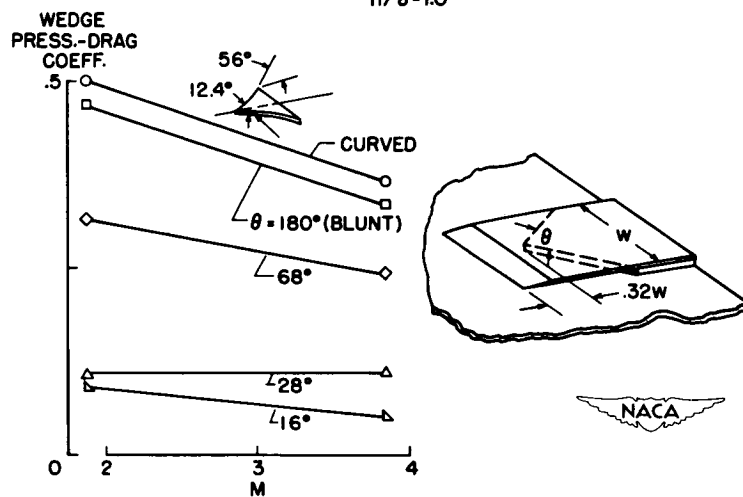
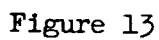


Figure 12



DECLASSIFIED
CONFIDENTIAL

RECENT RESULTS ON INLET INSTABILITY


By Carl F. Schueller

Lewis Flight Propulsion Laboratory

Supersonic diffusers generally exhibit steady pressure-recovery air-flow characteristics in the supercritical or constant air-flow region. However, rapid flow pulsations accompanied by inlet shock oscillations are often encountered as the mass flow of air is decreased below its maximum value, that is, into the region commonly referred to as subcritical operation. These large fluctuations in pressure and air flow result in numerous adverse and often catastrophic consequences.

This phenomenon of buzz was first recognized but not explained by Oswatish. In the intervening years many inlets having various amounts of stability have been reported and a few of them are indicated in figure 1. The minimum stable mass-flow ratio corresponding to any one of these points represents the lowest air flow obtained just prior to buzz on fixed-geometry conical center-body inlets operating without burning. Of the inlets surveyed those incorporating excessive drag or pressure-recovery penalties in order to obtain stability have been deleted. Admittedly not all the existing literature has been examined and, therefore, isolated investigations having greater stable subcritical ranges than indicated here may exist. In general, however, this figure is believed to be representative of the current status and shows that the stable range decreases significantly with increasing Mach number. This decrease is due not only to the lack of experimental data but also to the presence of more adverse pressure gradients and curvatures in the high Mach number inlet designs. Even at the lower Mach numbers the minimum stable mass-flow ratios reported by different investigators vary from no subcritical operation, that is, a mass-flow ratio of 1.0, to fairly respectable values at the lower Mach numbers. Such a wide variation in stable range emphasized that which most inlet investigators will readily admit, namely that inlet buzz is a very complex problem. This complexity results from the many sources of buzz exciting force available in a supersonic diffuser. As a result this paper will concentrate on a discussion of the known buzz exciting forces and the techniques utilized to counteract them. Before proceeding further, however, the existing theories which have been proposed to explain the mechanism of buzz will be reviewed briefly in order to provide a better insight into the buzz problem.

It has been recognized for many years that a compressor discharging into a relatively large volume having a fixed orifice will surge during that portion of its operation when the pressure increases with increasing air flow, that is, when the slope is positive. The supersonic diffuser was considered to be analogous to a compressor system in reference 1 and



SCHUELLER


it was concluded that a diffuser which had a positive-slope characteristic would buzz. A slightly different approach which led to the same conclusion was used in reference 2.

Since a complete cycle of buzz will result in the diffuser air being alternately accelerated and decelerated, the authors of reference 3 visualized a portion of the diffuser air column to be a plug resonating against the diffuser discharge volume in a manner crudely analogous to a Helmholtz resonator. The resulting calculations indicated that, if the positive-slope characteristic were of a sufficient magnitude, the diffuser would buzz with a frequency which depended on its geometry. At least qualitative agreement with experiment was obtained for the models considered.

Still another viewpoint on the mechanism of buzz was presented in reference 4. By means of detailed measurements and calculations it has been established that longitudinally traveling expansion and compression waves are present in the diffuser during the buzz cycle. The traveling-wave argument leads to an accurate prediction by theory of the experimentally determined variation of pressure with time in the diffuser.

The complex nature of the mechanism of buzz is apparent even in this simplified discussion. However, since an exciting force is required to initiate the buzz cycle for any of these theories, the known buzz exciting forces are discussed next.

It was shown in reference 5 that buzz may result from the slip line crossing the inlet lip. This slip line (see fig. 2) separates two filaments of air which have the same static pressure but different velocities and total pressures. If no other exciting force is assumed to be present, the inlet will be stable when the slip line is outside the cowl such as in figure 1(a). As the air flow is reduced by decreasing the exit area the slip line crosses the inlet (see fig. 1(b)) and two filaments of air having different velocities enter. If it is assumed that there is no mixing and the static pressure remains constant across the slip line, then the simultaneous diffusion of the two streams of different total pressure will require that the outer filament occupy an undue proportion of the passage. This causes the main flow portion near the center body to accelerate from a design Mach number of 0.2 to 0.6. As a result, compression waves travel forward and expansion waves rearward (fig. 2(b)). Based on the work of reference 4, an hypothesis may be that these traveling waves promote the pulsing as follows: the forward traveling compression wave forces the inlet shock to the position shown in figure 2(c). In the meantime the expansion waves reflect from the exit as expansion waves and travel forward decreasing the pressure. Finally the shock is sucked inside to the supercritical condition shown in figure 2(d). This causes the inlet to operate at increased mass flow. The exit area cannot pass all of this air, however, because of the reduced total pressure



behind the normal shock. The ensuing accumulation of air flow generates compression waves which increase the diffuser discharge pressure and drives the shock towards the inlet to the condition shown in figure 2(a). Since the exit area cannot pass all the air flow corresponding to this shock configuration, the terminal shock continues forward to the position shown in figure 2(b) and the exciting force is repeated to start another buzzing cycle.


Another triggering mechanism which acts like the slip line just discussed is flow separation. This can occur on the inside of the cowl lip, in the subsonic diffuser, or on the center body as shown in figure 3. In this case, separation occurs because of shock-wave—boundary-layer interaction. Again, if we assume no mixing, the low-energy air in the separated region occupies most of the passage, causing the outer filament to accelerate. Because of the inertia effects traveling waves are again generated and the shock is moved forward. As it moves forward the cone-surface-friction shearing stress increases and the tendency to separate decreases. The disappearance or reattachment of the separated flow permits the air flow to increase and the normal shock, as shown in figure 3(b), moves to the position shown in figure 3(a) and the separation reappears, starting another buzz cycle. From this, the conclusion can be drawn that there are at least two potential exciting forces, namely entrance of the slip line or boundary-layer separation.

The discussion is now restricted to the known techniques for avoiding or absorbing these exciting forces before they trigger buzz. One technique available to the designer is the addition of a constant-area section in the diffuser throat. This technique was proposed in reference 6 and applied by reference 7 to stabilize the normal shock in convergent-divergent diffusers. It has been applied to center-body type diffusers with varying degrees of success in references 5, 8, and 9. Such a technique could provide a mixing length to damp out the exciting force due to either the slip line or boundary-layer separation.

The model investigated in reference 5 had an extremely long section of very low divergence which increased the minimum stable mass-flow ratio approximately 16 percent at $M = 1.9$ but at the expense of a significant decrease in pressure recovery. References 8 and 9, on the other hand, indicated both adverse and beneficial effects of constant-area sections. Therefore, to define better the effect of diffuser area variation on stability in the presence of either the slip-line or boundary-layer exciting force, and to define better the length of stabilizing section required, a limited but systematic study of the effect of diffuser area variation on inlet stability has been conducted in the Lewis 8- by 6-foot supersonic tunnel and is reported in reference 10. Figure 4 presents some pertinent dimensions of the model used in this study. The variation of the ratio of local diffuser flow area to diffuser discharge area with axial distance per hydraulic diameter is also

included. Hydraulic diameter is defined in the usual manner, that is, four times the inlet annular area divided by the wetted perimeter, and for spike-type inlets this reduces to the cowl diameter minus the center-body diameter at the cowl lip station. The solid line represents the inlet having the longest stabilizing length and it has a nearly constant-area section for 3.5 hydraulic diameters after which it gradually expands. Although not apparent in this figure an area increase of 1 percent per hydraulic diameter was included in the first 3.5 diameters of length to approximately compensate for the boundary-layer growth. The dashed-line curve represents the other extreme, that is, no stabilizing section, but a continuous increase in area corresponding to a 6° conical diffuser. Intermediate stabilizing sections of 1 and 2 hydraulic diameters were also investigated. It should be noted that all of the diffusers were faired to a common area in approximately 9 hydraulic diameters of length.

The effect of these diffuser-area variations on the inlet stability is shown in figure 5 where the variation of minimum stable mass-flow ratio with diffuser stabilizing length is presented. The 6° diffuser, zero stabilizing length, has practically no stable range; however, modification of this inlet to incorporate stabilizing sections having a length greater than 2 hydraulic diameters increases the stable range to a mass-flow ratio of 0.55 for the diffuser having a stabilizing section 3.5 hydraulic diameters in length even though the slip-line criterion is violated. This did not decrease the critical pressure recovery from the value of 0.85 obtained with the 6° diffuser. Recent results on a model about one-half the size of this one and operating at about one-third the Reynolds number showed even larger gains in stable range due to a stabilizing section of 3.1 hydraulic diameters. It would thus appear that adequate stable ranges can be attained up to a Mach number of 2.0. A word of caution is necessary, however, since the difference between an unsuccessful and a successful stabilizing section appears to be associated with slight differences in design detail as shown in figure 6. The solid line represents the area variation of the 3.5 hydraulic diffuser on an enlarged scale. The dashed line represents a local area change of 4 percent occurring in the first 3 hydraulic diameters or $1\frac{1}{2}$ cowl diameters in length. The lowest curve represents a 10-percent change in area which corresponds to 0.1 inch in a cowl radius of 2.7 inches. Unfortunately, these area changes also involve a slight change in the shoulder radius of the center body and a shift in axial location of the center-body shoulder, either of which may be affecting the results. In any case, these local changes adversely affect the stable range as may be noted by the change in minimum stable mass-flow ratio from 0.55 to 0.84. From the diffuser-area variations investigated, it may be concluded that a properly designed stabilizing section of 3.5 hydraulic diameters in length will provide stable air-flow regulation at a Mach number of 2.0 and an angle of attack of 0° .




The effect on inlet stability characteristics of operating at angles of attack other than 0° is shown in figure 7 for the 6° and the 3.5-hydraulic-diameter diffusers. The 6° diffuser has practically no stable subcritical operation for the range of angles of attack investigated. The 3.5 hydraulic diameter diffuser on the other hand maintains good stability up to about 3° after which it rapidly deteriorates. This abrupt decrease in stable range probably indicates that the mixing length provided becomes inadequate for the increased separation on the leeward side of the center body.

Since the models discussed so far could be subjected to the exciting force due to separation or the exciting force due to the slip line or both, it was decided to vary the cowl position parameter θ_L over a wide enough range to avoid the slip-line criterion for some conditions. Reference 5 has shown that the triggering force due to the slip line can be avoided by positioning the oblique shock ahead of the inlet. The resulting calculated minimum stable mass-flow ratios are as indicated by the dashed line in figure 8. Another way to avoid the triggering force due to the slip line, at the expense of pressure recovery, is to move the oblique shock inside the inlet. This had no beneficial effect on the 6° diffuser for the range investigated. Since the slip line is too far inside the cowl to trigger the buzz, particularly for cowl position parameters greater than 44° , another exciting force such as separation must be present. For the 3.5-hydraulic-diameter diffuser the stable range is progressively increased as the oblique shock is moved inside, and in all cases the instability, when it finally occurred, was due to center-body separation without a slip line. This indicates that flow separation may be the more predominant of the two exciting forces considered here. Therefore, the various techniques which have been proposed to alleviate center-body separation will be briefly reviewed.

First of all, scoops can be installed on the center body to remove the separated flow before it enters the inlet. Also, the boundary layer can be removed ahead of the terminal shock, which results in a new boundary layer of higher friction shearing stress that is capable of withstanding a higher pressure rise without separation. Such systems are of practical application for relatively small decreases in air flow. It is also often proposed that the boundary-layer separation be avoided by increasing the cone angle in order to decrease the cone-surface Mach number. This increase in cone angle decreases the pressure rise across the terminal shock and alleviates the tendency to separate. Unfortunately, the recommended limiting cone-surface Mach numbers vary from 1.15 to 1.55. The reason for such a wide variation is believed to be associated with feedback in the boundary layer and is indicated qualitatively in figure 9. Both of these models have 50° cones and are operating at a Mach number of 2.0 and the same Reynolds number. The region of separated flow is much more extensive on model a than model b. Also model a is just out of pulsing. Apparently, the significant difference is that model a has a

rather abrupt but small change in area in the first 2 hydraulic diameters of length as measured from the cowl lip, whereas model b is the 3.5-hydraulic-diameter diffuser. It is believed that the resulting adverse pressure gradient causes pressure feedback in the boundary layer and increases the separation for model a. Thus although a separation criterion may be used to predict the occurrence of separation in the absence of an adverse pressure gradient, application of this criterion to the prediction of whether the separation will increase or reattach in diffusers will require a modification which includes any local adverse pressure gradients.

The previous discussion has shown that the stable range of spike-type inlets is very sensitive to diffuser-area variation. For example, at a Mach number of 2.0 the stable range was increased from a mass-flow ratio of 0.92 for a 6° diffuser to 0.55 for a diffuser incorporating a stabilizing section of 3.5 hydraulic diameters in length. Furthermore, the stability characteristics appear to be very sensitive, in the cases investigated, to relatively small but rapid area changes at the diffuser entrance.



REFERENCES

1. Pearce, R. B.: Causes and Control of Powerplant Surge. Aviation Week, vol. 52, no. 3, Jan. 16, 1950, pp. 21-25.
 2. Orlin, W. J., and Dunsworth, L. C.: A Criterion for Flow Instability in Supersonic Diffuser Inlets. Rep. No. 5144 (Contracts NOa(s) 9403 and AF 33(038)-11231), Marquardt Aircraft Co., Apr. 2, 1951.
 3. Sterbentz, William H., and Evvard, John C.: Criteria for Prediction and Control of Ram-Jet Flow Pulsations. NACA RM E51C27, 1951.
 4. Trimpi, Robert L.: An Analysis of Buzzing in Supersonic Ram Jets by a Modified One-Dimensional Nonstationary Wave Theory. NACA RM L52A18, 1952.
 5. Ferri, Antonio, and Nucci, Louis M.: The Origin of Aerodynamic Instability of Supersonic Inlets at Subcritical Conditions. NACA RM L50K30, 1951.
 6. Kantrowitz, Arthur: The Formation and Stability of Normal Shock Waves in Channel Flows. NACA TN 1225, 1947,
 7. Wyatt, DeMarquis D., and Hunczak, Henry R.: An Investigation of Convergent-Divergent Diffusers at Mach Number 1.85. NACA RM E50K07, 1951.
 8. Dailey, C. L., and McFarland, H. W.: Development of Ramjet Components. Item 1: Investigation of Supersonic Diffusers. Progress Rep. 9961-9 (Contract NOa(s) 9961), Univ. Southern Calif. Aero. Lab., Apr. 7, 1950.
 9. Dailey, C. L.: Diffuser Instability in Subcritical Operation. Univ. of Southern Calif., Sept. 26, 1950.
 10. Nettles, J. C.: The Effect of Initial Rate of Subsonic Diffusion on the Stable Subcritical Mass-Flow Range of a Conical Shock Diffuser. NACA RM E53E26, 1953.
-

CURRENT STABILITY RANGE

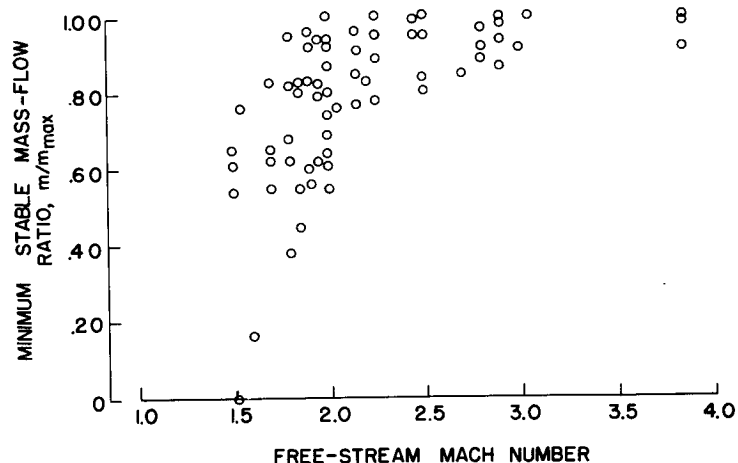


Figure 1

SLIP LINE

$M_0 = 2.0$

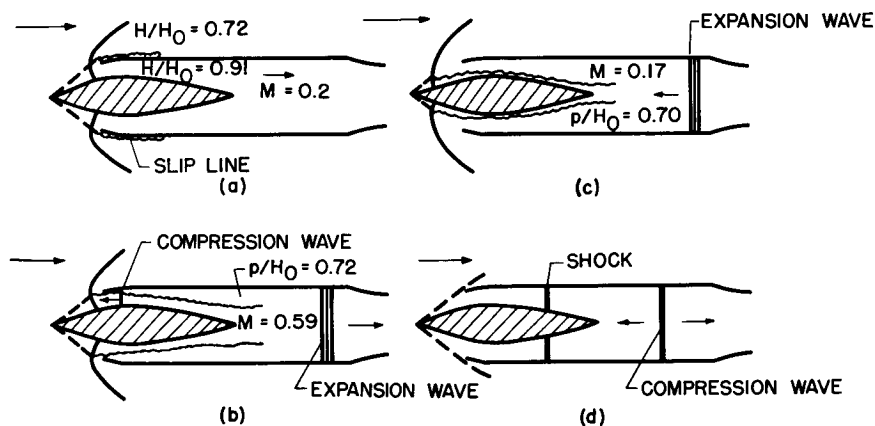
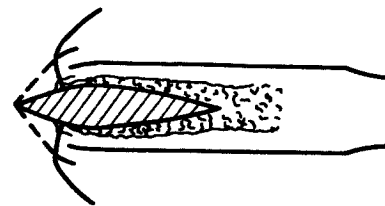
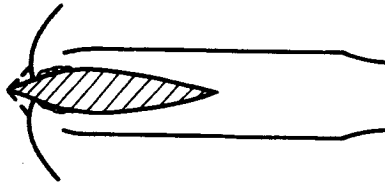


Figure 2

CENTERBODY SEPARATION



(a)



(b)



Figure 3

MODEL AND DIFFUSER DETAILS

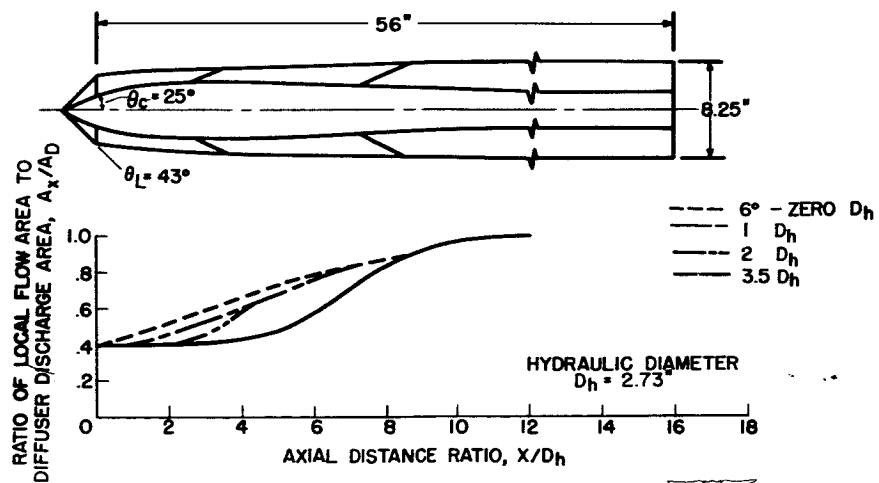


Figure 4

EFFECT OF STABILIZING LENGTH ON STABILITY

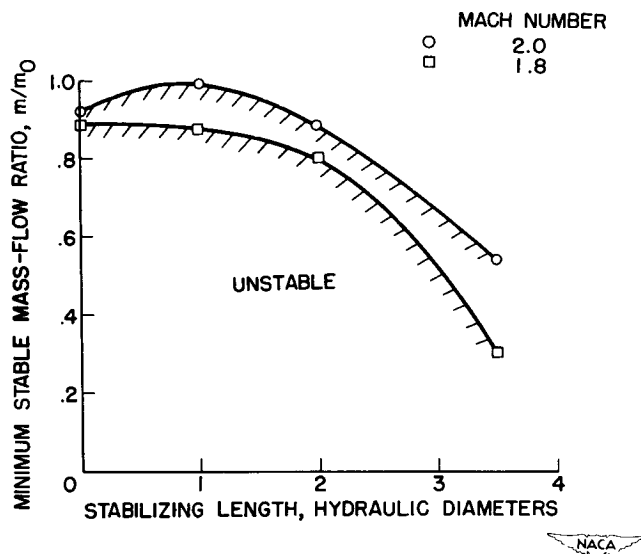


Figure 5

EFFECT OF LOCAL CHANGES IN DIFFUSER ON STABILITY

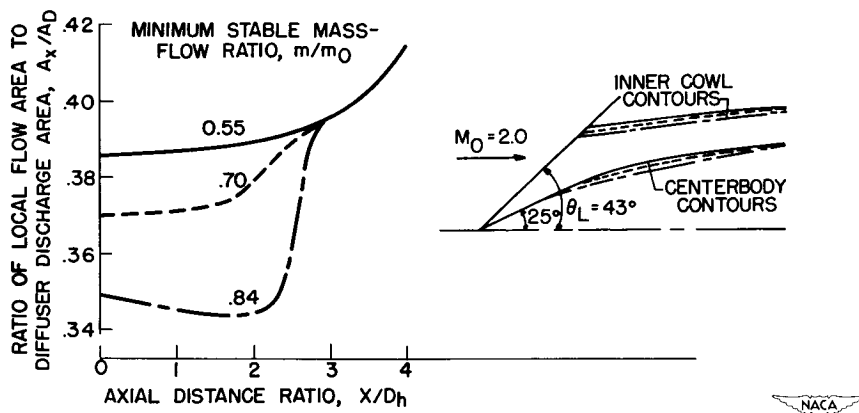


Figure 6

STABILITY AT ANGLE OF ATTACK

$M_0 = 2.0$

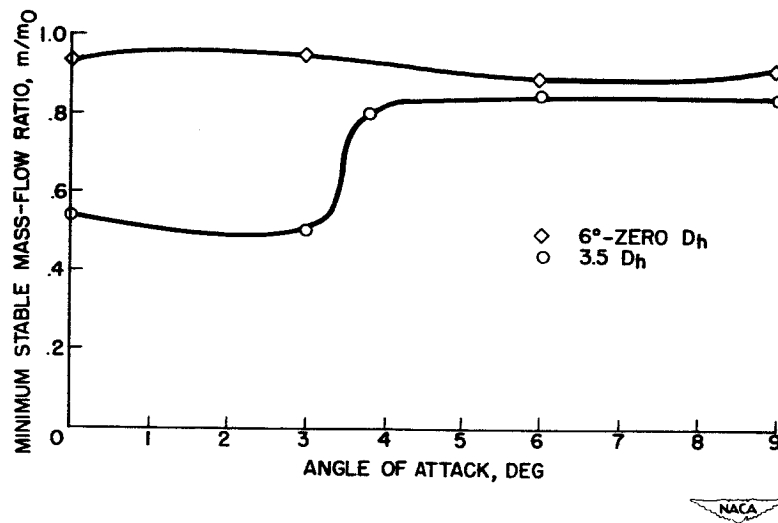


Figure 7

EFFECT OF OBLIQUE SHOCK POSITION

AT $M = 2.0$

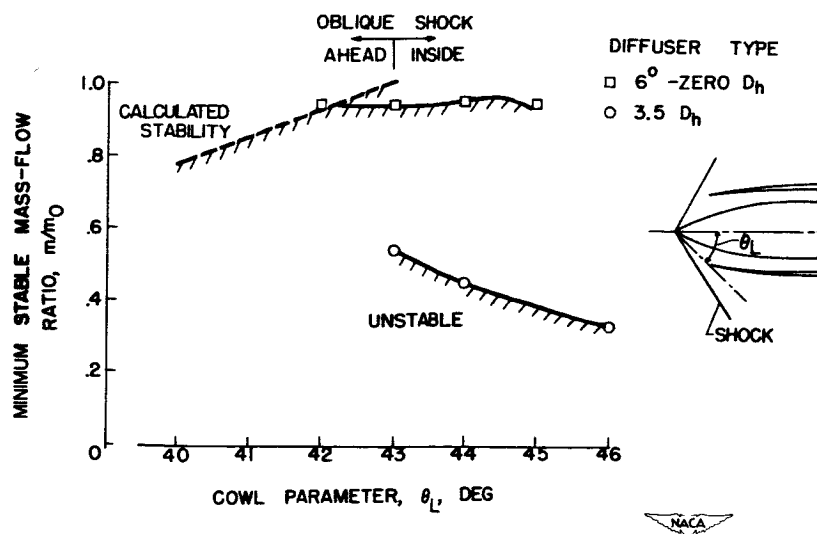
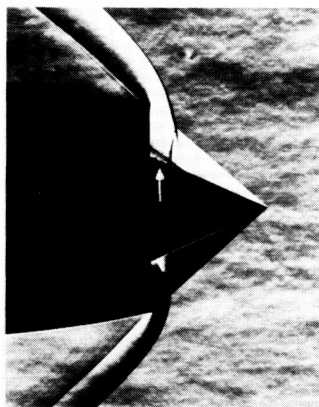


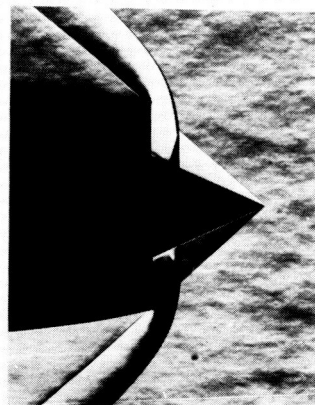
Figure 8

SHOCK-BOUNDARY-LAYER INTERACTION
MACH NUMBER, 2.0; 50° CONE



(a) $m/m_0 = 0.79$

MINIMUM STABLE = 0.79



(b) $m/m_0 = 0.76$

MINIMUM STABLE = 0.55

NACA

Figure 9

INLET-ENGINE MATCHING METHODS

By John L. Allen

Lewis Flight Propulsion Laboratory

Inlet-engine matching is essentially a problem of relating the inlet air-flow characteristics to those of the engine so that the net propulsive thrust of the inlet-engine combination can be evaluated. A brief review of the matching problem is presented in figure 1 for constant engine rotational speed at an altitude of 35,000 feet and for a range of flight Mach numbers. Both inlet and engine characteristics are presented in terms of corrected rate of weight flow of air evaluated at the diffuser exit or compressor inlet. Since the engine regulates the air entering the inlet, the inlet will operate along the engine line. When a fixed-geometry inlet is just large enough for efficient operation at the high-speed condition, as shown by the intersection of the curves at $M_0 = 2.0$, the engine requires more weight flow than the inlet can efficiently provide as flight speed is reduced; this condition is indicated by the spread between the solid line and lower dashed line. Consequently, the engine will force the inlet to operate in the supercritical region. Throughout the flight region below design Mach number this condition results in total-pressure losses, although the drag remains at a minimum. Accordingly, the net propulsive thrust is reduced.

A fixed-geometry inlet which is large enough to provide efficiently the weight flow demanded by the engine at a subsonic Mach number, as shown by the curve intersection at $M_0 = 0.85$, has an efficient inlet capacity at higher Mach numbers much greater than that required by the engine. The distance between the solid line and the upper dashed line represents an excess of inlet capacity that must be spilled behind a bow shock with the attendant high additive drag at supersonic speeds; however, the pressure recovery remains reasonably high. Again, the net propulsive thrust of the unit is reduced.

Previous conferences and analytical and experimental studies in several reports have shown that the efficient inlet-performance line can be shifted to approach the engine curve by varying the geometry of the inlet. These methods primarily consist of varying the angle or projection of the compression surface. More complete discussions of the matching problem can be found in references 1 and 2.

In order to provide the designer with a greater degree of freedom in solving inlet-engine matching problems, two additional methods have recently been investigated by the National Advisory Committee for Aeronautics. These methods, which literally amount to putting holes

in the diffuser to let in needed weight flow or to let out excess weight flow, are shown schematically in figure 2. The inlet geometry is fixed in each case and the auxiliary inlet or outlet can be located to the rear of the inlet entrance.

Normal-shock-type inlets are shown in figure 2(a) since present auxiliary-inlet data are confined to flight Mach numbers of 1.5 and below. The function of the auxiliary inlet is to supplement the critical weight flow furnished by the undersized main inlet at below-design speeds, as was indicated in figure 1. Thus, at the high-speed point, the auxiliary inlet would be closed and, as flight speed is reduced, the auxiliary inlet would be opened so that the normal shock would remain at the lip and supercritical pressure losses would be avoided.


The purpose of the internal auxiliary flap is to equalize the static pressure where the two flows merge so that the mixing of the main and auxiliary flows will not result in large total-pressure losses. Furthermore, if the propulsive thrust is to be increased, the drag added by the auxiliary inlet must not be too large.

The function of the auxiliary outlet or bypass (see fig. 2(b)) is to discharge weight flow in excess of engine requirements and thus avoid bow-shock additive drag penalties. The bypass is simply a scoop or nozzle located in the diffuser forward of the engine. The size of the bypass would be increased as flight speed is increased so that the normal shock remains at the cowl lip. Again, improvements in net propulsive thrust will depend on the drag due to bypassing as compared with bow-shock drag as well as pressure-recovery losses.

The remainder of this paper is concerned with an evaluation of experimental results of these auxiliary systems.

Small-scale investigations of the auxiliary inlet are presented in references 3 and 4. Recent preliminary data obtained in the Ames 6- by 6-foot supersonic tunnel for a nose inlet with and without a fixed-area auxiliary inlet are presented in figure 3. The auxiliary-inlet area was 11.7 percent of the main inlet area and the external-drag coefficient is based on maximum fuselage cross-sectional area.

Total-pressure-recovery losses were on the order of 1 to 3 percent because of mixing losses and boundary layer admitted by the auxiliary inlet. This loss was highest at supersonic speeds, probably because of shock-boundary-layer interaction. The external drag was increased, because of the auxiliary inlet, throughout the Mach number range. In order to illustrate the application of these data to the problem of inlet-engine matching, the data have been replotted and are presented in figure 4 for flight Mach numbers of 0.70 and 1.5.



The fixed-geometry data, indicated by the solid line, are for subcritical and supercritical flow. The circular symbol corresponds to critical flow for the main inlet and the triangular symbol represents the main inlet plus the 11.7-percent auxiliary inlet at critical flow. A linear interpolation corresponding to variable auxiliary inlet area has been assumed as shown by the dashed line. Incremental drag is the drag increase from the critical value because of bow-shock spillage for subcritical flow and because of the auxiliary inlet for weight flows greater than critical.


In the subcritical region, the pressure recoveries are higher than those at critical flow and the incremental drag curve has a low slope indicating appreciable cowl recovery for the cowl profile represented by these data. This effect was discussed in a previous paper by Richard I. Sears.

At a flight Mach number of 1.5, the highest thrust minus drag was obtained in the subcritical region where pressure recovery could be traded for incremental drag up to the point indicated by the engine match line. Accordingly, the inlet size was selected at this condition of peak thrust minus drag where the inlet area is about 6 percent greater than that needed for matching at critical flow.

At a subsonic Mach number of 0.7, this optimum high-speed design is too small and supercritical pressure losses occur as shown by the engine match line; however, the drag remains at a minimum. Using the auxiliary inlet increases the pressure recovery from about 0.89 to 0.94 for a drag increase of about 0.02.

Evaluation of these results is presented in figure 5 in the form of effective thrust ratio which is defined as the thrust at the operating pressure recovery minus the spillage drag or auxiliary-inlet drag, as the case may be, divided by the ideal thrust at 100-percent pressure recovery. A fixed-geometry inlet sized for a subsonic Mach number is shown in addition to the high-speed design with and without an auxiliary inlet.

The fixed-geometry inlet, sized for optimum thrust minus drag at a flight Mach number of 1.5, operated in the subcritical region down to a Mach number of about 1.2, and, at lower speeds, supercritical operation occurred and resulted in low effective thrust ratios. Using the variable-area auxiliary inlet to avoid supercritical operation resulted in higher effective thrust ratios at below-design speed as indicated by the dashed line. At a flight Mach number of 0.70, the effective thrust ratio of the fixed-geometry inlet was increased 8 percent by means of the auxiliary inlet. However, if the size of the inlet is increased to provide optimum thrust minus drag at a subsonic Mach number of 0.8, slightly higher effective thrust ratios are obtained up to a flight




Mach number of 1.2; at higher Mach numbers, the effective thrust ratios are only slightly less. The inlet area for this case is about 17 percent larger than that for the high-speed design; the effect of this area increase on incremental drag is included in the thrust parameter; however, any increase in basic body drag is not included.

Thus, for the particular engine characteristic and constant-altitude flight plan considered herein at Mach numbers up to 1.5, the auxiliary inlet does not appear necessary. At flight Mach numbers higher than 1.5 or for other engine characteristics and flight plans such as a tactical mission requiring high Mach number operation over a range of altitudes, the auxiliary inlet may offer higher performance. The auxiliary inlet would also be useful for improving existing hardware, for instance, an inlet that is too small or for growth situations where an engine having a larger weight-flow capacity is to be installed in an existing airframe.

At flight Mach numbers higher than 1.5, the spillage required for a subsonic inlet sizing increases as discussed previously. Also, at these higher speeds, sharp cowl lips are generally necessary to avoid drag penalties. Thus, auxiliary-inlet performance for higher Mach number designs may be more competitive, although this effect has not been experimentally demonstrated up to the present time. The auxiliary inlet may well require a compression surface and control or removal of the boundary layer so that its performance will approximate more nearly that of the main inlet.

The bypass system can be used for the oversized inlet that required large spillage at the high-speed point in order to attain efficient subsonic operation. Data, which were obtained from references 5, 6, and 7 with an axially symmetric spike-type inlet with and without a bypass system, are presented in figure 6 for flight Mach numbers of 1.6, 1.8, and 2.0. The inlet had a relatively sharp cowl and the compression surface tip projection was selected so that the conical shock would meet the lip at $M_0 = 2.0$. The bypass-data points were obtained by using one and then two fixed-area bypasses having a nearly axial discharge angle. The dashed line through the symbols represents a variable-area bypass system that maintains critical inlet flow as diffuser-exit weight flow is reduced. Spillage-drag coefficient is the increase in drag as weight flow is decreased. For the fixed-geometry inlet, the spillage drag increases appreciably as weight flow is reduced. However, spillage-drag coefficients for the bypass inlet were only one-fifth to one-fourth of those for equivalent bow-shock spillage for the fixed-geometry inlet, and diffuser total-pressure recoveries were not significantly changed. The engine match lines indicate progressively greater spillage requirements as flight Mach number is increased. Interpretation of these data in terms of effective thrust ratio is shown in figure 7 for an altitude of 35,000 feet and an inlet sized at a flight Mach number of 0.85. A reference curve corresponding to an inlet of variable size or area operating at critical pressure recovery without drag is also shown and,




as such, represents the best performance attainable with this particular fixed-angle compression surface and diffuser. Over the range of flight Mach numbers, the effective thrust ratios for the bypass inlet were consistently higher than those for the fixed-geometry inlet. If the performance at a flight Mach number of 2.0 where the excess weight flow is about 20 percent of that captured by the inlet is considered, the effective thrust of the bypass is 10 percent greater than that of the fixed-geometry inlet and 98 percent of that attainable with critical pressure recovery and zero drag. At a flight Mach number of 1.6, the required spillage is smaller and, hence, the effective thrust ratios attained for both the bypass and fixed-geometry inlets are comparable.

For this reason the bypass would probably not be needed at Mach numbers where the required spillage is small and the drag due to bypassing or bow-shock spillage becomes small compared to net thrust.

In conclusion, it has been shown experimentally that it is possible to mix the auxiliary and main inlet flows with rather small pressure-recovery losses at flight Mach numbers up to 1.5. Thus, the performance of an undersized fixed-geometry inlet that experiences supercritical operation at below-design speeds can be improved by means of an auxiliary inlet. However, for the engine characteristics and flight plan considered herein, a fixed-geometry inlet sized at a subsonic Mach number had effective thrust ratios comparable to those obtainable by using an auxiliary inlet in conjunction with an inlet sized at a high Mach number. Other flight plans and engine characteristics may indicate beneficial application of the auxiliary inlet. Application of the auxiliary inlet at flight Mach numbers greater than 1.5 in conjunction with inlets having efficient compression surfaces remains to be demonstrated.

For the oversized inlet, it was shown that discharging weight flow in excess of engine requirements by means of a bypass resulted in effective thrust ratios as much as 10 percent greater than those of a fixed-geometry inlet since the drag due to bypassing was only one-fifth to one-fourth of bow-shock spillage drag. Thus, two additional methods have been demonstrated that aid in solving inlet-engine matching problems.



APPENDIX

For the unpublished auxiliary-inlet data, the following pertinent area ratios are given:

$$\frac{\text{Maximum fuselage cross-sectional area}}{\text{Minimum inlet area}} = 6.0$$

$$\frac{\text{Minimum inlet area}}{\text{Diffuser-exit area}} = 0.685$$

The engine characteristics given in figure 1 are used throughout the paper. However, the relation of absolute values of engine corrected weight flow to those of subsequent figures is

$$\frac{w\sqrt{\theta}/\delta}{(w\sqrt{\theta}/\delta)_{\text{fig. 1}}} = 1.116$$

REFERENCES

1. Schueller, Carl F., and Esenwine, Fred T.: Analytical and Experimental Investigation of Inlet-Engine Matching for Turbojet-Powered Aircraft at Mach Numbers Up to 2.0. NACA RM E51K20, 1952.
2. Brajnikoff, George B.: Method and Graphs for the Evaluation of Air-Induction Systems. NACA TN 2697, 1952.
3. Scherrer, Richard, Stroud, John F., and Swift, John T.: Preliminary Investigation of a Variable-Area Auxiliary Air-Intake System at Mach Numbers From 0 to 1.3. NACA RM A53A13, 1953.
4. Brajnikoff, George B., and Stroud, John F.: Experimental Investigation of the Effect of Entrance Width-to-Height Ratio on the Performance of an Auxiliary Scoop-Type Inlet at Mach Numbers From 0 to 1.3. NACA RM A53E28, 1953.
5. Beke, Andrew, and Allen, J. L.: Force and Pressure-Recovery Characteristics of a Conical-Type Nose Inlet Operating at Mach Numbers of 1.6 to 2.0 and at Angles of Attack to 90° . NACA RM E52I30, 1952.
6. Allen, J. L., and Beke, Andrew: Force and Pressure Recovery Characteristics at Supersonic Speeds of a Conical Spike Inlet With Bypasses Discharging in an Axial Direction. NACA RM E52K14, 1953.
7. Allen, J. L., and Beke, Andrew: Force and Pressure Recovery Characteristics at Supersonic Speeds of a Conical Spike Inlet With a Bypass Discharging From the Top or Bottom of the Diffuser in an Axial Direction. NACA RM E53A29, 1953.

TYPICAL TURBOJET AND INLET AIRFLOW CHARACTERISTICS CONSTANT ROTATIONAL SPEED

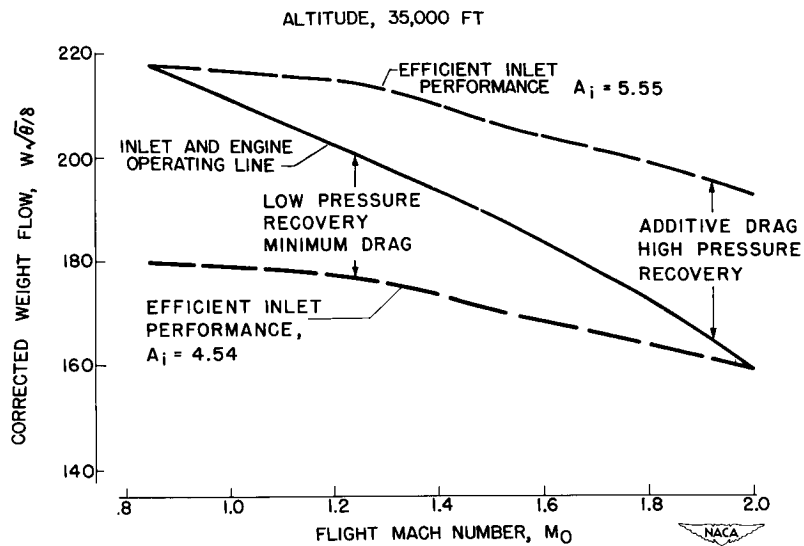


Figure 1

MATCHING METHODS USING AUXILIARY SYSTEMS

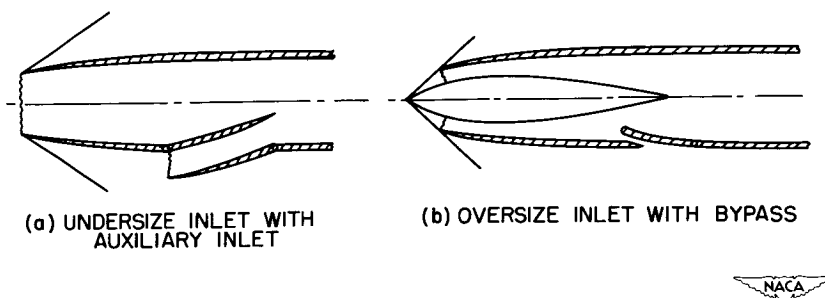


Figure 2

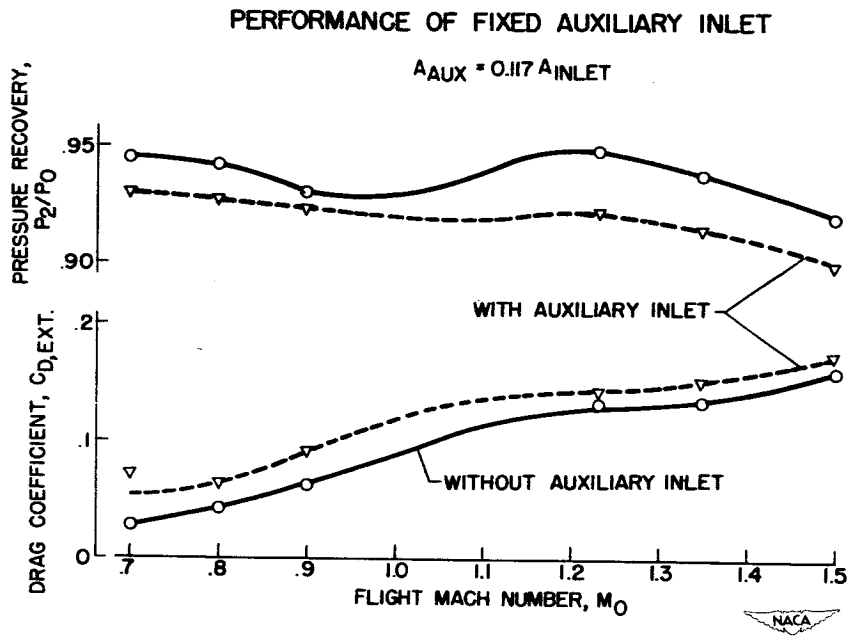


Figure 3

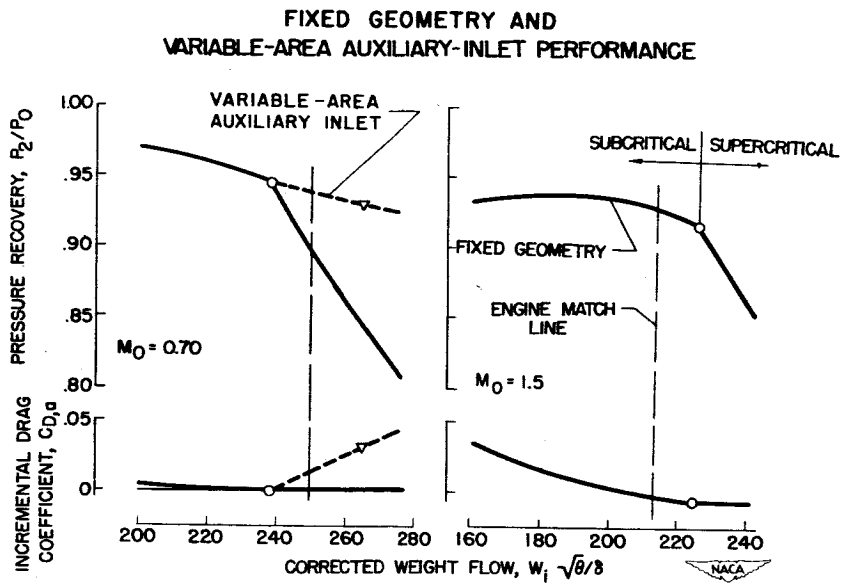


Figure 4

EFFECTIVE THRUST RATIO ALTITUDE, 35,000 FT

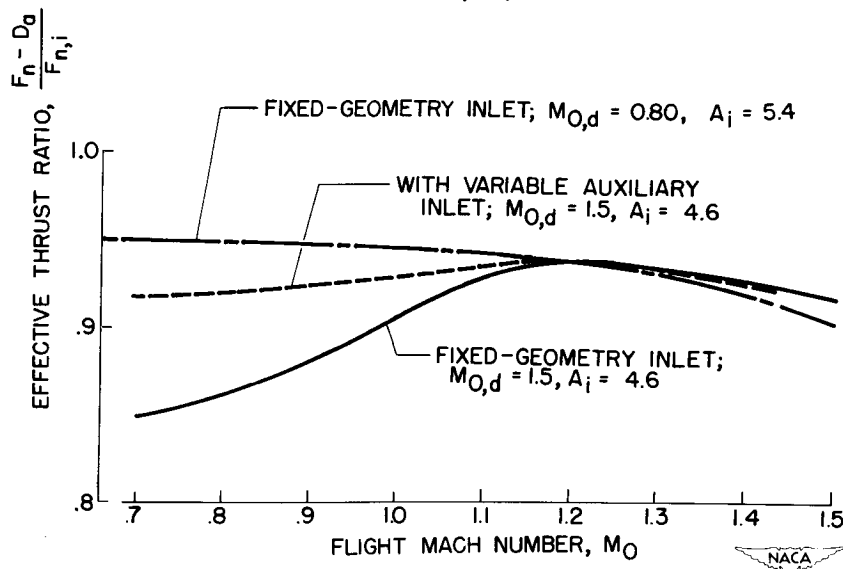


Figure 5

PERFORMANCE OF BYPASS INLET

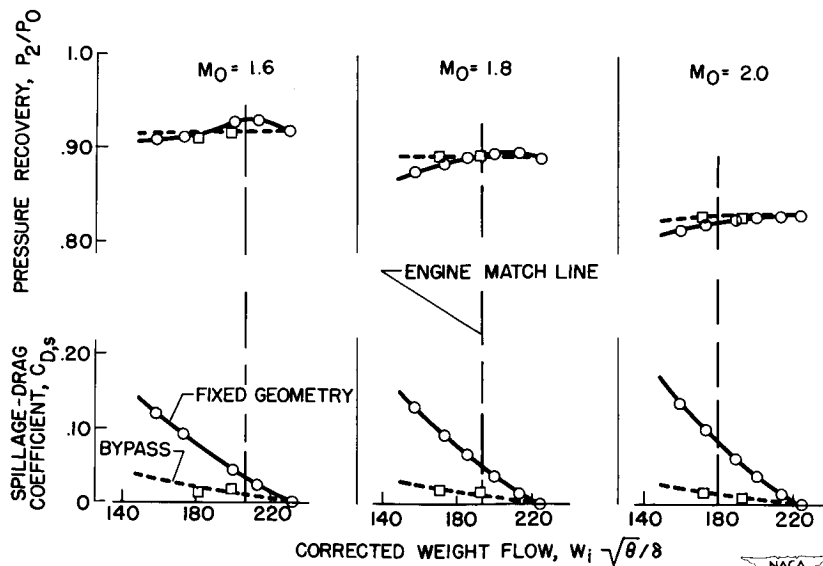


Figure 6

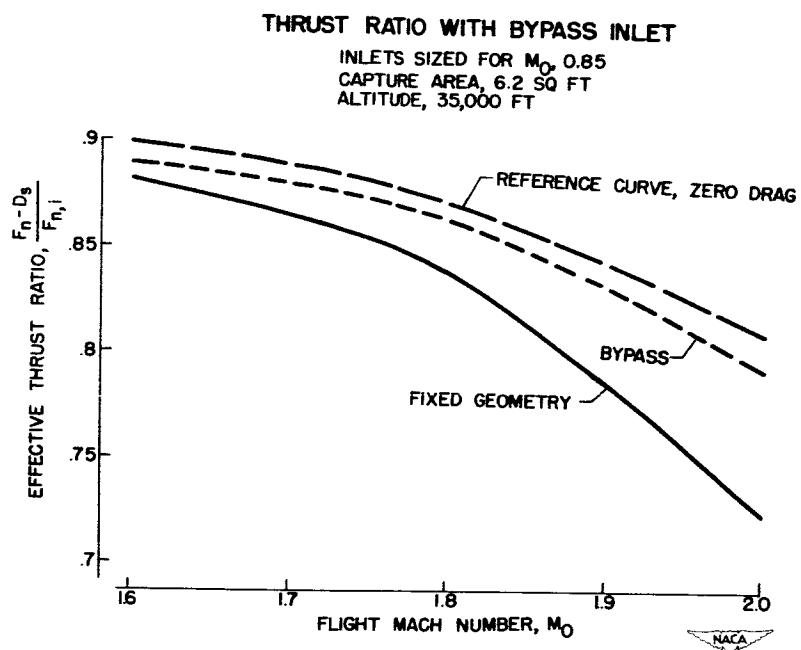


Figure 7

RECENT DATA ON DIFFUSER DESIGN

By John R. Henry

Langley Aeronautical Laboratory

INTRODUCTION

In the past a number of successful correlations of performance data and comprehensive collections of design data for subsonic diffusers have been accomplished for the general case of favorable boundary-layer velocity distribution or shape factor at the diffuser inlet (see refs. 1 and 2). One of the more critical subsonic diffuser problems existing in the aircraft industry today, however, is the design and performance of subsonic diffusers preceded by supersonic diffusers or inlets. For these cases the boundary layer at the start of subsonic diffusion has been subjected to considerable pressure rise through shocks and no longer has a favorable velocity distribution or shape factor. Design and performance information corresponding to these conditions has not reached a satisfactory state of development.

In the first section of this paper the problem of subsonic diffusion downstream from supersonic inlets will be investigated briefly by examining a breakdown of the measured over-all pressure losses to determine the losses attributable to the subsonic diffuser.

SUBSONIC DIFFUSION AFTER SHOCK

Supersonic Inlet Pressure Recovery

In order to obtain an idea of the order of magnitude of the problem of subsonic diffusion downstream from a supersonic inlet the literature was surveyed and a number of representative total-pressure-recovery data from references 3 to 11 were selected for study. These data are illustrated in figure 1 for the spike-type inlet. For simplicity the selections were limited to the case of a single angle spike with no internal contraction and with the normal shock approximately at the minimum area section. The plotted points represent, for a number of different geometries, the measured total-pressure recovery to the exit of the subsonic diffuser expressed as a function of free-stream Mach number. The curves represent the calculated total-pressure recovery through the shock system for several values of spike half-angle. The difference in pressure recovery between any point and the appropriate shock curve represents approximately the loss chargeable to the subsonic diffusion. It is apparent that in many cases

the subsonic loss is of the same order as the shock loss, which emphasizes the importance of the subsonic diffusion problem.


The data shown in figure 1 cause one to speculate as to how such high losses can be generated in subsonic flow. A reasonable explanation appears to be that the boundary layer, in negotiating the pressure rise through the normal shock, is drained of dynamic energy to the extent that a state of flow separation or incipient separation exists at the start of subsonic diffusion. These phenomena in the past have been referred to as shock-boundary-layer interaction effects. In order to study these effects in more detail, one must reduce the measured over-all subsonic loss values to a loss chargeable entirely to the interaction effect. A necessary step is to predict what the subsonic loss would have been if the flow had been free from shock effects.

Basic Data Loss Estimate

Subsonic diffuser M of 0.2 loss correlation.- The first step in obtaining the basic data loss estimate, a value which does not include shock effects on the boundary layer, was to obtain the loss coefficient which each diffuser geometry would have had at an inlet Mach number of 0.2. The loss correlation curves of figure 2, which are based on data from references 12 to 18, were used for this purpose. The loss factor K, which is the ratio of the conventional total-pressure-loss coefficient to the calculated loss coefficient for a sudden expansion of the same area ratio, is presented as a function of the diffuser expansion angle 2θ . The use of the factor K eliminates the need for a separate curve for each area ratio in the angle range of 9° or higher. Older correlations of this type ignored the effect of inlet boundary layer but recent investigations have indicated that a curve exists for each value of the ratio of inlet-boundary-layer displacement thickness to inlet radius. Note that increasing the relative boundary-layer thickness up to a value of 0.040 produces significant increases in the loss factor and that further increases in thickness have little effect on K.

For expansion angles of 9° or less friction losses become appreciable and the K factor is no longer independent of area ratio. For this reason, calculated values of friction K have been plotted for angles from 1° to 9° .

The plotted points represent an annular diffuser correlation which is based on the observation that the annular diffuser loss is greater than an equivalent conical diffuser by the amount of the extra friction loss of the annular diffuser. The points as plotted are measured values reduced by the amount of the extra calculated friction loss and good agreement with the conical correlation is obtained.



Effect of inlet Mach number on loss.- In order to obtain a fair estimate of the loss that each diffuser geometry would have had if the flow had not been influenced by shock effects, it was necessary to correct the loss from the low Mach number correlation of figure 2 to values corresponding to the test Mach number at the start of subsonic diffusion. Increasing the diffuser inlet Mach number is known to have a detrimental effect on performance for subsonic diffusers which do not have appreciable friction loss. Most of this depreciation is believed due to increased values of Reynolds number based on boundary-layer thickness; however, the increased values of nondimensional pressure gradient must also be responsible for some decreases in performance. A number of investigations described in references 13 to 17 have furnished data evaluating this effect for both conical and annular diffusers over a range of inlet-boundary-layer thicknesses. The results of these investigations are given in figure 3 which presents the ratio of the loss coefficient at a particular inlet Mach number to that for a Mach number of 0.2 as a function of diffuser expansion angle. Each curve corresponds to a particular Mach number. Results are given for a thin and a thicker inlet boundary layer. It is evident that the loss coefficient may be approximately doubled in some cases through increases in the inlet Mach number. Annular diffuser data up to an expansion angle of 12° have shown little or no effect due to inlet Mach number. By the use of these inlet Mach number correction data in conjunction with the low-speed loss data of figure 2 accurate loss estimates can be made for diffusers where shock effects are absent.

Subsonic Loss Due to Shock Effect

Returning to the analysis of the performance of subsonic diffusers operating downstream from supersonic inlets, three inlet designs were investigated: the spike type, the converging-diverging type, and the normal-shock type. With the shock pattern known it was possible to calculate the Mach number just downstream from the normal shock. The Mach number in conjunction with the subsonic diffuser geometry provided enough information to predict, in the manner just described, the loss which the diffuser would have had in the absence of shock interaction effects. This basic data loss was then subtracted from the measured over-all subsonic loss to obtain the shock-boundary-layer interaction loss coefficients shown in figure 4. The total-pressure loss due to shock-boundary-layer interaction divided by the total pressure at station 1 is expressed as a function of Mach number at station 1.

It was reasoned that station 1, which is located at a position just upstream from the normal shock, should be used as a reference station for the total pressure and Mach number because these variables determine the strength of the normal shock which in turn should determine the effect of the shock on the boundary layer. This reasoning is supported by the

manner in which the data for several relatively high angle subsonic diffusers, the circle points, with various supersonic inlet designs fall on a single curve.


At a given pre-shock Mach number the losses for the three inlet configurations for comparable subsonic diffusers should vary according to the differences in the boundary-layer development upstream from the normal shock. This view is supported by the data because the spike inlet, which had the largest amount of wetted surface exposed to the supersonic flow and therefore the greatest opportunity for boundary-layer thickness development prior to the normal shock, had the highest interaction losses.

For the curve shown for the spike inlets the losses reach values on the order of 10 times the "basic" subsonic diffusion loss. One would expect extensive separation under these conditions. This view is supported by the fact that the maximum losses are on the order of one dynamic pressure at the start of subsonic diffusion.

The square symbols in each case identify subsonic diffusers of expansion angles of 5° or less, which produced relatively low losses. This result suggests that an expansion angle as low as 5° has a favorable effect on the poor boundary-layer velocity distribution or shape factor delivered by the normal shock, or in the case of shock-induced separation, the low angle permits early reattachment.

The effect of a 5° expansion angle on boundary-layer development downstream from a shock is illustrated by figure 5. The model used to obtain these data was a converging-diverging inlet; surveys of the flow were made at several cross sections of the 5° diffuser for several locations of the normal shock. The data are presented here in terms of boundary-layer shape factor, defined as the ratio of boundary-layer displacement to momentum thickness. Increasing values of shape factor indicate increasing distortion of the boundary-layer velocity distribution and high values of shape factor correspond to separated flow. It has been observed that flow separation does not occur for shape factors below a value of 1.8 whereas separation almost always exists at values above 2.6.

Shape factor is presented as a function of the ratio of the distance x , measured from the normal-shock location, to the diffuser diameter at the shock location. Three curves, which correspond to three different positions of the normal shock, are given with the Mach number just upstream from the shock indicated in each case. The value of the shape factor delivered to the normal shock differed in each of the three cases due to changes, with normal-shock position, of the flow characteristics between the throat and the normal shock. The normal shock caused a large increase in the shape factor in the Mach number of 1.52 case indicating local separation; then the 5° expansion angle reduced these high shape factors to favorable values within the range below 1.8



resulting in attached flow and reasonable velocity distributions. A number of investigations of boundary-layer development in higher expansion angle diffusers have indicated progressively increasing values of shape factor in the x direction, a characteristic which would have produced extensive separation in the Mach number of 1.35 and 1.52 cases. These results all support the conclusions relative to the 5° diffuser performance indicated in figure 4.


Much additional research work is necessary to obtain a complete understanding of subsonic diffusion preceded by supersonic flow; however, on the basis of the preliminary analysis presented, certain limited conclusions can be formed. To avoid subsonic diffuser losses on the same order as the shock losses, at least the initial section of the subsonic diffuser should have an expansion angle no greater than 5° . This indicates a long diffuser or else the use of boundary-layer control. Many of the usual boundary-layer control types do not appear attractive for this application, especially if any degree of stream blockage is involved. If post-shock separation is present, any form of control downstream from the shock will be inefficient. Pending the development of new control concepts, the most obvious solution appears to be to eliminate all boundary layer in the region just upstream from the normal shock by scoops, bleeds, or wall suction.

DIFFUSERS WITH FLOW CONTROL

The second part of the paper will be devoted to another problem, that of obtaining satisfactory performance from short diffusers for use where space requirements are severe. The designs required fall in the range of expansion angles from 15° to 45° ; stable operation and uniform exit distributions are paramount requirements. It is obvious that such operating conditions cannot be met without flow control.

Forms of flow control under investigation are removal of low-energy boundary-layer air by suction, energization of the boundary layer by injection, accelerated boundary-layer momentum transfer by use of vortex generators, and flow control through use of turning vanes and splitters.

An investigation pertaining to the effectiveness of various types of flow controls as applied to annular diffusers suitable for turbojet afterburners is now in progress at the National Advisory Committee for Aeronautics. These data have been reported in part in references 19 to 22. The more important configurations tested are sketched in figure 6. The same cylindrical outer body was used in all cases while the design of the inner body was modified. With vortex generators mounted near the inlet station, three different lengths of inner body were tested producing equivalent cone angles of 15° , 24° , and 31° . A suction-control



configuration consisting of two rows of drilled holes on the inner body has been evaluated. Boundary-layer control consisting of injecting high-energy air parallel and adjacent to the wall through a circular slot between the cowl and center plug was also investigated. It was found that the injection air could not prevent separated flow over a large portion of the cowl surface, necessitating the installation of the cylindrical turning vane as illustrated on the sketch. Injection model performance referred to hereafter will refer to the complete model including the vane.


Note that two downstream measuring stations, stations 2 and 3, are indicated on each sketch. Station 2 always corresponds approximately to the end of the inner body and permits performance comparisons for several over-all diffuser lengths or equivalent expansion angles. Station 3 is a common tailpipe station for all the models and is located at a position corresponding to the end of the 15° diffuser inner body. Measurements at this station permit performance comparisons for several inner-body lengths with the same over-all diffuser length.

The inlet conditions correspond to fully developed boundary layer filling the annulus, inlet Mach numbers up to 0.5, and angles of flow rotation from 0° to 21° . These conditions appeared for a general investigation to be as representative as possible from a study of surveys of typical turbine discharge conditions.

Static-Pressure-Coefficient Performance

Static-pressure-rise performance on these two bases with the various types of control is presented in figure 7. The static pressure rise, of course, is an indication of the reduction in mean velocity between the inlet station and a particular downstream station. It is presented here in terms of the mean inlet dynamic pressure. For the diffuser exit or station 2 measurements, the independent variable is expansion angle. For the station 3 measurements, for which the over-all length or expansion angle is constant, the independent variable of center-body length in terms of the outer-body diameter was chosen. The curves apply to vortex-generator control, and a no-control curve is given for reference purposes. The circle symbols represent the suction model performance, and the square symbol represents the injection model.

The vortex-generator control provided substantial increases in performance for all cases. The station 2 measurements indicate, however, that as the expansion angle increased, or the diffuser was shortened, the performance fell off appreciably. If the over-all length of the diffuser was held constant, station 3 measurements, shortening of the center body produced little change in performance. This result is presumably due to the rapid adjustment of the radial velocity distribution



DECLASSIFIED

in the free mixing region between stations 2 and 3 for the shorter center body cases. The conclusion is reached that the added weight and structure of the longer center bodies may be saved with little sacrifice to performance.

The circle points indicate that suction control is much more effective than vortex generators. Suction control has the disadvantage of requiring more auxiliary equipment and some thrust penalties if the suction air is wasted.


The injection control, as indicated by the square symbol, provides equivalent performance to the vortex generators. The injection would also require auxiliary equipment. It has an advantage over the suction in that there is no waste of air involved; however, it is unlikely that the injection air would have been subjected to the combustion process.

Exit-Velocity Distributions

Uniform velocity distribution at the afterburner inlet and flow stability are considered prime requisites for this application. A general statement concerning the somewhat intangible quality of flow stability can be made as follows: Manometer and tuft surveys indicated that control measures which provided significant improvements in the performance also produced more stable flow. Typical radial velocity distributions with and without control for all the control systems are given in figure 8 for both stations 2 and 3. At station 2 vortex generators produced improvements in the distributions but did not eliminate separation for the 24° and 31° diffusers. The suction model, which produced superior static-pressure coefficients, also produced superior velocity distributions by maintaining attached flow for the full length.

At the tailpipe station, station 3, with vortex-generator control the velocity distribution improves appreciably with shortening of the center body, which also is consistent with the observed static-pressure-rise performance. Possible flow instabilities associated with flow separation in the 24° and 31° diffusers could probably be eliminated by cutting off the end of the center body just upstream from the separation point. This type of design is sometimes employed when pilot flame devices are located on the end of the center body.


The suction and injection data at station 3 indicate good distribution, as would be expected. It is believed that appreciably better injection performance is to be had with a model conforming to the contour of the 31° center-body design, which permits attached flow on the center body for an appreciable axial distance. Also better injection performance could have been obtained by realining the injection direction to eliminate the peak velocities near the center line as indicated at station 3.



The investigations to date have resulted in obtaining good performance from a diffuser which has a length over maximum diameter ratio of about $1/2$, as compared to a previously accepted value of more than 1.0. This result has been accomplished under the unfavorable conditions of a maximum thickness of boundary layer at the inlet and all the area expansion taken on the inner wall. The investigation is not complete; however, tests of still shorter diffusers indicate that the length-diameter ratio of $1/2$ cannot be significantly reduced without excessive penalties to performance.

CONFIDENTIAL

REFERENCES

1. Patterson, G. N.: Modern Diffuser Design. Aircraft Engineering, vol. X, no. 115, Sept. 1938, pp. 267-273.
 2. Henry, John R.: Design of Power-Plant Installations. Pressure-Loss Characteristics of Duct Components. NACA WR L-208, 1944. (Formerly NACA ARR L4F26.)
 3. Reid, J., and Fuller, L.: Cold Flow Tests on a Pitot Diffuser at $M = 1.34$. Tech. Note No. G.W. 186, British R.A.E., Apr. 1952.
 4. Weinstein, Maynard I.: Investigation of Perforated Convergent-Divergent Diffusers With Initial Boundary Layer. NACA RM E50F12, 1950.
 5. Wyatt, DeMarquis D., and Hunczak, Henry R.: An Investigation of Convergent-Divergent Diffusers at Mach Number 1.85. NACA RM E50K07, 1951.
 6. Kantrowitz, Arthur, and Donaldson, Coleman duP.: Preliminary Investigation of Supersonic Diffusers. NACA WR L-713, 1945. (Formerly NACA ACR L5D20.)
 7. Baughman, L. Eugene, and Gould, Lawrence I.: Investigation of Three Types of Supersonic Diffuser Over a Range of Mach Numbers From 1.75 to 2.74. NACA RM E50L08, 1951.
 8. Leissler, L. Abbott, and Hearsh, Donald P.: Preliminary Investigation of Effect of Angle of Attack on Pressure Recovery and Stability Characteristics for a Vertical-Wedge-Nose Inlet at Mach Number of 1.90. NACA RM E52E14, 1952.
 9. Nussdorfer, Theodore J., Obery, Leonard J., and Englert, Gerald W.: Pressure Recovery, Drag, and Subcritical Stability Characteristics of Three Conical Supersonic Diffusers at Stream Mach Numbers from 1.7 to 2.0. NACA RM E51H27, 1952.
 10. Esenwein, Fred T., and Valerino, Alfred S.: Force and Pressure Characteristics for a Series of Nose Inlets at Mach Numbers from 1.59 to 1.99. I - Conical Spike All-External Compression Inlet With Subsonic Cowl Lip. NACA RM E50J26, 1951.
 11. Goldsmith, E. L., and Griggs, C. F.: The Estimation of Pressure Recovery and Drag of Conical Centre Body Intakes at Supersonic Speeds. Rep. No. Aero. 2463, British R.A.E., May 1952.
- 

12. Peters, H.: Conversion of Energy in Cross-Sectional Divergences Under Different Conditions of Inflow. NACA TM 737, 1934.
13. Persh, Jerome: The Effect of the Inlet Mach Number and Inlet-Boundary-Layer Thickness on the Performance of a 23° Conical-Diffuser - Tail-Pipe Combination. NACA RM L9K10, 1950.
14. Little, B. H., Jr., and Wilbur, Stafford W.: High-Subsonic Performance Characteristics and Boundary-Layer Investigations of a 12° 10-Inch-Inlet-Diameter Conical Diffuser. NACA RM L50C02a, 1950.
15. Copp, Martin R., and Klevatt, Paul L.: Investigation of High-Subsonic Performance Characteristics of a 12° 21-Inch Conical Diffuser, Including the Effects of Change in Inlet-Boundary-Layer Thickness. NACA RM L9H10, 1950.
16. Copp, Martin R.: Effects of Inlet Wall Contour on the Pressure Recovery of a 10° 10-Inch-Inlet-Diameter Conical Diffuser. NACA RM L51E11a, 1951.
17. Nelson, William J., and Popp, Eileen G.: Performance Characteristics of Two 6° and Two 12° Diffusers at High Flow Rates. NACA RM L9H09, 1949.
18. Squire, H. B.: Experiments on Conical Diffusers. Rep. No. Aero. 2216, British R.A.E., Aug. 1947.
19. Wood, Charles C.: Preliminary Investigation of the Effects of Rectangular Vortex Generators on the Performance of a Short 1.9:1 Straight-Wall Annular Diffuser. NACA RM L51G09, 1951.
20. Wood, Charles C., and Higginbotham, James T.: The Influence of Vortex Generators on the Performance of a Short 1.9:1 Straight-Wall Annular Diffuser With a Whirling Inlet Flow. NACA RM L52L01a, 1953.
21. Wood, Charles C., and Higginbotham, James T.: Flow Diffusion in a Constant Diameter Duct Downstream of an Abruptly Terminated Center Body. NACA RM L53D23, 1953.
22. Wood, Charles C., and Higginbotham, James T.: Performance Characteristics of a 24° Straight-Outer-Wall Annular-Diffuser-Tailpipe Combination Utilizing Rectangular Vortex Generators for Flow Control. (Prospective NACA paper.)

TOTAL-PRESSURE RECOVERY FOR SPIKE INLETS

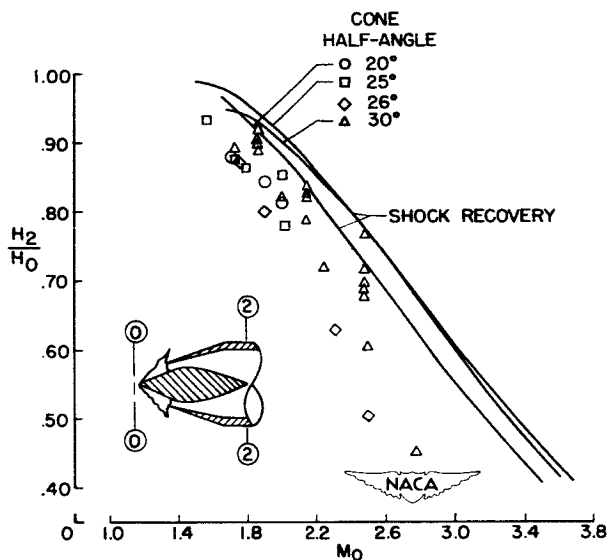


Figure 1

LOSS-COEFFICIENT CORRELATION

$M_1 \leq 0.2$

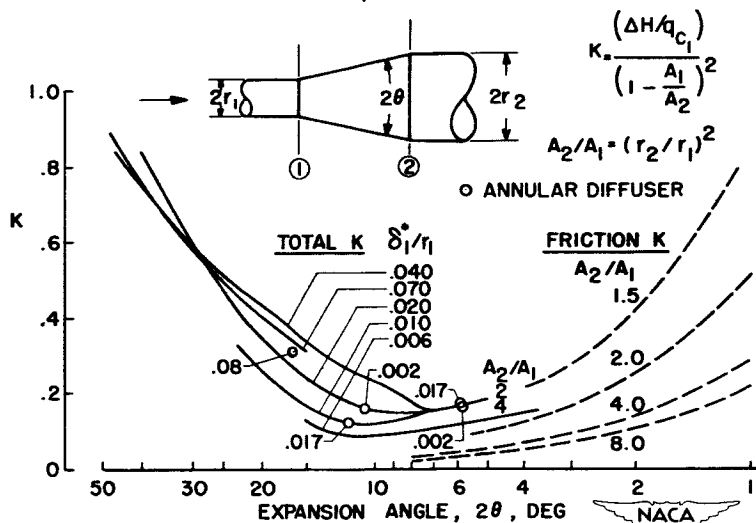


Figure 2

EFFECT OF INLET MACH NUMBER ON LOSS COEFFICIENT

$$A_2/A_1 = (R_2/R_1)^2 = 2$$

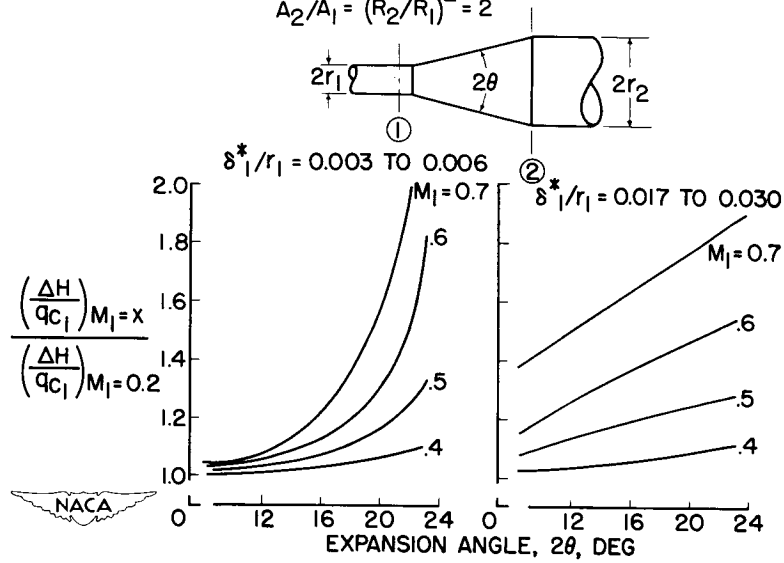


Figure 3

SHOCK - BOUNDARY-LAYER INTERACTION LOSS

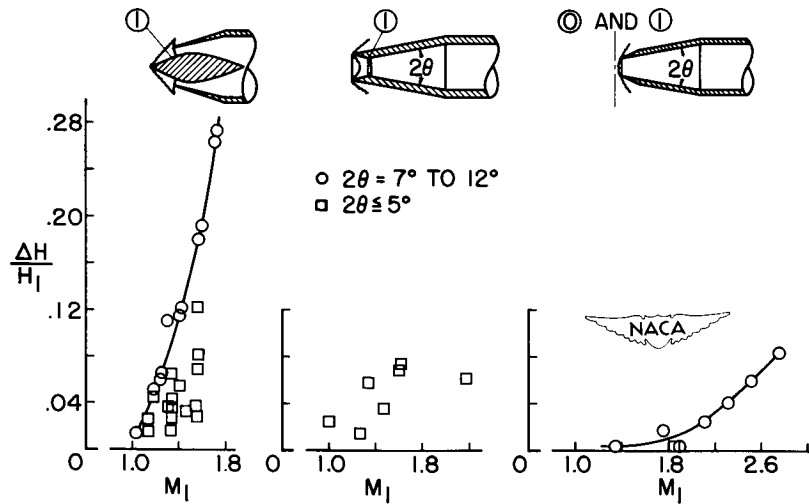


Figure 4

EFFECT OF A 5° EXPANSION ANGLE ON BOUNDARY-LAYER SHAPE-FACTOR DEVELOPMENT

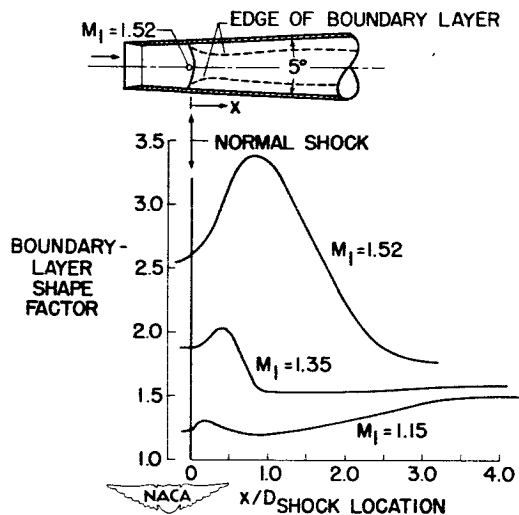


Figure 5

CONTROL MODELS TESTED FOR AFTERBURNER APPLICATION $A_2/A_1 = 1.91$

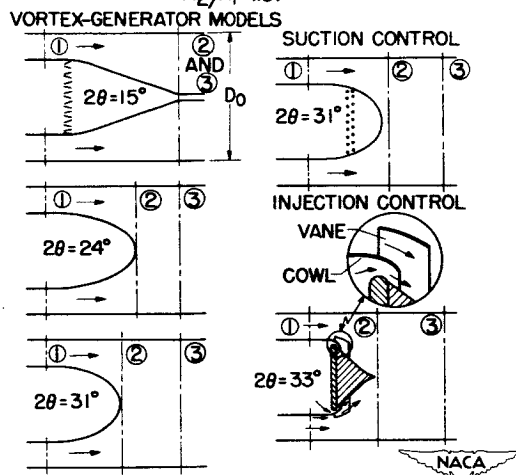


Figure 6

AFTERBURNER DIFFUSER PERFORMANCE WITH CONTROL

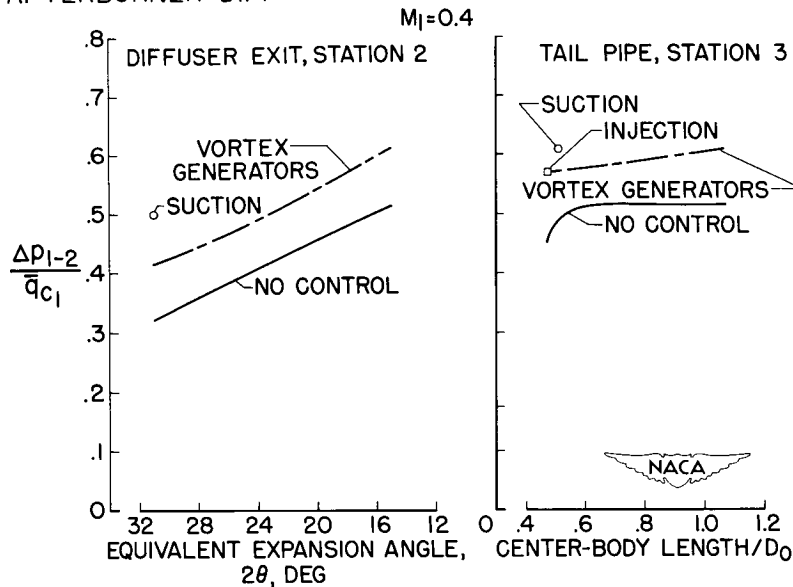


Figure 7

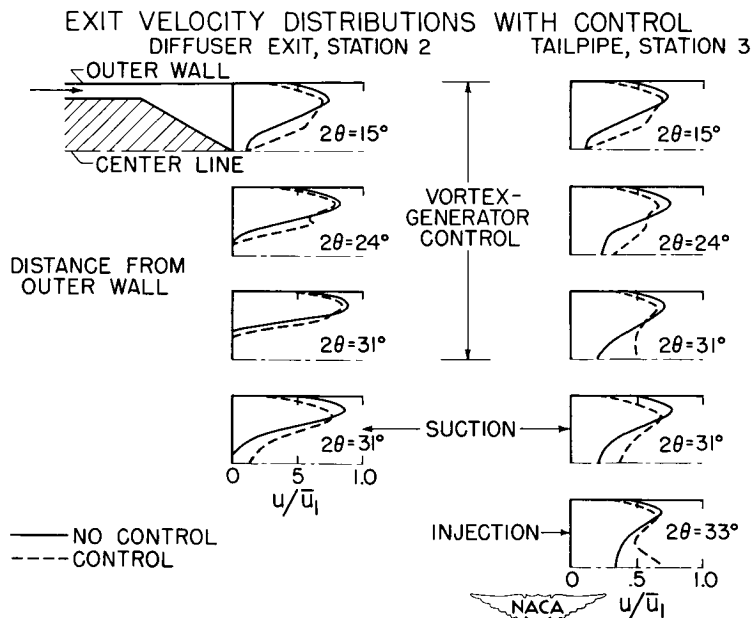


Figure 8

SECRET

JET EFFECTS ON THE FLOW OVER AFTERBODIES

IN A SUPERSONIC STREAM

By Edgar M. Cortright, Jr., and Fred D. Kochendorfer

Lewis Flight Propulsion Laboratory

INTRODUCTION

Increased attention is currently being directed to the problem of afterbody aerodynamics. This is a logical result of the fact that afterbody drag frequently represents an appreciable portion of the total body drag of aircraft and missiles. In the case of engine-in-fuselage and nacelle configurations, the problem of predicting the flow field over afterbodies or boattails is complicated by interference effects from the propulsive jet which issues from the base of the body. This jet disturbs a flow which is already contaminated by heavy boundary layer and which is subject to wing and tail interference effects. In addition, the flow is attempting to negotiate the adverse pressure gradient usually present over at least the rearmost portions of the boattail. Clearly, the problem is a complex one.

In the present paper an attempt will be made to summarize some of the results of current research on the problem of jet effects. Emphasis will be placed on providing a clear definition of the various phases of the problem, as well as on presenting some of the important concepts and parameters which contribute to their understanding. Previous research on the subject of jet effects on external aerodynamics may be found in references 1 to 7.

SYMBOLS

 A_A area of annular blunt base A_M maximum cross-sectional area of body C_p boattail pressure coefficient, $\frac{p - p_0}{q_0}$ C_{p_A} pressure coefficient at rearmost boattail station, $\frac{p_A - p_0}{q_0}$

C_{P_B}	base pressure coefficient, $\frac{P_B - P_O}{q_O}$
C'_{P_B}	base pressure coefficient referenced to rearmost boattail station, $\frac{P_B - P_A}{q_A}$
C_D	drag coefficient, $\frac{D}{q_O A_M}$
C_{D_A}	annular base drag coefficient for case of base bleed, $\frac{D_A}{q_O A_A}$
D	drag force
D_A	annular base drag force
D_B	diameter of base
D_M	maximum body diameter
D_N	diameter of nozzle exit
D_T	diameter of throat of convergent-divergent nozzle
H	total pressure
H_B	total pressure of base-bleed air
M	Mach number
m_B	mass flow of base-bleed air
m_j	mass flow of jet
m_s	mass flow of secondary ejector air
N_R	Reynolds number based on body length
p	static pressure

[REDACTED]

P_R	critical pressure-rise coefficient
$\overline{P_R}$	mean critical pressure-rise coefficient
q	dynamic pressure, $\gamma p M^2/2$
R	gas constant
T_B	total temperature of base-bleed air
T_j	total temperature of jet air
T_s	total temperature of secondary ejector air
V_B	velocity of base-bleed air at exit
V_O	velocity of free-stream air
x	axial distance upstream of base
β	angle at rearmost station on boattail, deg
δ	thickness of boundary layer at point where the velocity equals 0.99 times the local stream velocity
ϵ	angle of nozzle at the exit station
γ	ratio of specific heats
ν	angle that edge of jet stream makes with body axis immediately after leaving nozzle
ψ	angle that external stream makes with body axis immediately after separating from end of boattail

Subscripts:

O	measured in free stream
A	measured at rearmost boattail station with no jet flow
B	measured in semidead air region of blunt base
J	jet conditions measured in plane of nozzle exit




APPARATUS

Consider first some of the experimental techniques which have been used to gather the data for this paper; in figure 1 are shown four of the models used to measure jet effects on the flow over afterbodies. The first model (upper left) utilized a half-sting with splitter-plate arrangement wherein the unheated jet air was reversed in direction within the body and discharged through half an afterbody. The two small strut-mounted models (lower), which provide most of the data presented herein, differed from each other in that one utilized an oxygen-alcohol rocket engine for a gas supply while the other utilized unheated air. Support interference effects are larger for this system. The most recently utilized is the large-scale strut-mounted model for the Lewis 8- by 6-foot supersonic tunnel (upper right). This model has a gasoline combustor which makes possible jet temperatures from atmospheric to 2,500° R. Forces and pressures on the nozzle and body may be independently measured.

DISCUSSION

Parameters and nomenclature.- Before the results of this research are considered, it is necessary to define some of the geometric and flow parameters inherent in the problem. A typical conical afterbody is depicted in the upper portion of figure 2. Both the jet and external flow are from left to right. Important geometric parameters are the boattail angle or contour and the diameters of the body, the base, and the nozzle exit. The most frequent parameter involving diameters is the ratio of the base diameter to the nozzle exit diameter D_B/D_N , which indicates the size of the blunt annulus. The pressures of interest include the free-stream pressure p_0 , the boattail pressures p , the pressure just ahead of the base p_A , the base pressure p_B , and the jet static pressure p_J . In addition, the jet total pressure H_J and total temperature T_J are of importance.


Now consider some of the nozzle configurations which may be installed within the afterbody shell and which discharge various types of jet streams through the exit opening in the base. The simplest of these is the convergent nozzle, which will be retained in the analysis for reference purposes even at the higher Mach numbers where convergent-divergent or ejector nozzles would be required to yield maximum thrust potential. The convergent-divergent nozzle will have an increasing ratio of exit diameter to throat diameter D_N/D_T as the design pressure



ratio increases. The nozzle exit angle ϵ is not necessarily zero for this nozzle or for the other nozzles. With the ejector nozzle the ratio of exit diameter to throat diameter D_S/D_P also increases as the design pressure ratio increases. In addition, however, a supply of secondary air is provided to cushion the expansion of the primary stream and thus provide more nearly isentropic flow. Lastly, the case in which air is discharged into the blunt annular base in order to realize the drag reducing effects of base bleed is considered briefly.

Jet effects on boattail pressures.- Consider first the question of jet effects on boattail pressures shown qualitatively in figure 3 for the case of supersonic flight. The basic physical phenomena are illustrated in the lower portion of the figure, which depicts the effects of the jet from a convergent nozzle on the flow over a 5.6° conical boattail. The jet, which is at a higher-than-ambient static pressure at the exit, expands on leaving the nozzle and thus deflects the external stream. If the flow were inviscid, a shock wave would originate precisely at the point of meeting of the internal and external streams and a pressure discontinuity would exist. The presence of the body boundary layer with its low-energy subsonic region precludes the possibility of a discontinuous rise in pressure with the result that the required pressure rise begins ahead of the shock wave, where the boundary layer thickens and originates compression waves. If the deflection is sufficiently great and the shock wave sufficiently strong for the particular state of the boundary layer, the flow will be separated from the boattail inasmuch as the low-energy regions of the boundary layer will be unable to negotiate the required pressure rise. Translation of these simple concepts into quantitative form is most difficult with the result that there is no current method to predict the magnitude of jet effects on boattail pressures. It may be possible, however, to predict approximately the onset of separation by use of the critical-pressure-rise-coefficient concept of Donaldson and Lange (ref. 8) about which more will be said subsequently. Plotted above the sketch of the boattail in figure 3 are the experimental pressure distributions for various values of the jet static-pressure ratio p_J/p_0 . For large amounts of overpressure, appreciable thrust is seen to exist over the rearmost portions of the boattail.

Modifying factors.- Many factors influence the exact nature of jet effects on boattail pressures. Some of these factors are illustrated in figure 4. The jet effect will be decreased by reducing the overpressure at the exit either by reducing the jet total pressure or by adding an expansion section to the nozzle. Also, the presence of an annular base can partially or entirely shield the boattail from jet interference, depending on the size of the annulus. This occurs inasmuch as the internal and external streams separate from the body and meet downstream of the base. The jet then influences the base pressure




and will usually not influence the boattail pressure until the base pressure has risen sufficiently far above the rearmost pressure on the boattail. The jet effect may be increased by the use of a large boattail angle which both increases the strength of the trailing shock wave and increases the adverse pressure gradient over the boattail, thus making it more susceptible to flow separation. Lastly, the use of large nozzle exit angles may result in a relative increase in the trailing-shock strength and, hence, an increased jet effect.

With angle of attack or yaw at supersonic speeds, the jet effect is asymmetrical and causes a destabilizing shift in the body center of pressure, in addition to influencing nearby control surfaces. Angle-of-attack effects are beyond the scope of this paper, however.

Jet effects on boattail drag. - Some jet effects on boattail pressure drags at a free-stream Mach number near 2 are presented in figure 5 to illustrate the qualitative considerations just discussed. Consider the variation with boattail shape of the drag-reducing effect of a jet from a convergent nozzle. In the case of the three conical boattails of base-to-body-diameter ratio of 0.5 (broken lines), the drag with no jet increases considerably as the boattail angle increases. The jet interference also increases, however, so that all three experience a pressure-drag reduction approaching 25 percent at a jet total-pressure ratio of 14. The highly sloping ($\beta = 16^\circ$ at rearmost station) parabolic afterbody experiences a much greater jet interference so that at the higher pressure ratios the drag is reduced to 40 percent and is the same as that of a more gently sloping boattail. Drag data for the parabolic body were obtained from force measurements in the 8- by 6-foot tunnel, whereas the conical boattail drags were obtained from the integration of pressure distributions on small-scale models (ref. 5). Certain irregularities in the force data have been faired out that may actually have occurred because of the possibility of abrupt separation on the boattail.

It may be noted that the larger drag reductions in the case of the parabolic afterbody were obtained despite the presence of a slightly larger annulus than was present on the sharp-edged conical boattails, although annular pressure forces are not included in these drag data. Actually, a small annulus corresponding to this base-to-nozzle-diameter ratio of 1.11 appears to afford little shielding of the boattail even in the case of the low-angle boattails. However, with a larger annulus of $\frac{D_B}{D_N} = 1.41$, the boattail drag for the three conical boattails was virtually invariant with jet pressure ratio.

The second portion of this figure illustrates the fact that an increased nozzle exit angle increases the favorable jet interference



effects both for the convergent and the convergent-divergent nozzle. The nozzle exit angle was increased 12° in the case of the convergent nozzle, resulting in the indicated downward displacement of the drag curve. In the case of the convergent-divergent nozzle ϵ was increased 18° with the same effect. It may be noted that no appreciable drag reductions result from the convergent-divergent nozzles until the nozzle design total-pressure ratio is exceeded.

Critical pressure-rise coefficient. - Attention is now directed to the pressures which act on annular blunt bases. Before looking at the details of the problem, it is instructive to consider in figure 6 the concept of critical pressure rise, which was mentioned briefly in regard to the trailing shock wave separating the flow on a boattail. Consider the case of a forward-facing step in the presence of a boundary layer. The detached bow wave which would normally exist ahead of the step in supersonic inviscid flow creates a pressure rise which is too great for the boundary layer and causes it to separate. Donaldson and Lange (ref. 8) originally proposed that a critical pressure-rise coefficient

$$P_R = \frac{P_2 - P_1}{q_1} \text{ is proportional to } (\text{Reynolds number})^{\frac{1}{5}} \text{ for turbulent}$$

boundary layers for any given Mach number. Additional experimental evidence reported by Love (ref. 9) indicates that the effect of Reynolds number for turbulent boundary layers is negligible. Love has also shown that the experimentally determined critical pressure rise for a blunt step is in approximate agreement with that of a two-dimensional airfoil, if defined as indicated under the sketch, and that this pressure-rise coefficient varies with Mach number. If the blunt step is rearward facing, data derived from Beastall and Eggink (ref. 10) indicate P_R to be invariant with Mach number at a value of approximately 0.36. Thus, certain differences exist which require investigation.

If a section of a blunt annulus is considered, it is immediately apparent that the flow is similar but more complex. In this case the two streams which separate from the surface of the nozzle and body are generally inclined at different angles and are at different levels of pressure, temperature, and Mach number. In addition, the state of the boundary layers is markedly different in the two streams. As a first step, however, it is possible to define a mean pressure-rise coefficient $\overline{P_R}$ which is the average of pressure-rise coefficients based on the internal and external streams. Unfortunately, the reduction of base, body, and nozzle pressures to yield a value of $\overline{P_R}$ requires a knowledge of the external and internal stream curvatures after separation since a two-dimensional solution of this flow field is markedly inadequate. Most of the values of $\overline{P_R}$ presented herein were obtained with the use of schlieren photographs to determine jet curvature as well as with the


use of a few existent characteristic solutions for the external flow. As a result, they must be considered as only a crude first effort pending more accurate theoretical treatment. This will require the determination by characteristics of a great many overpressure jet shapes and, although they are less significant, the free streamlines of some separated external flows.

The important fact to observe in figure 6 is not the somewhat irregular behavior of the individual variations, which may be largely scatter, but rather that most of the values for the convergent nozzles at both Mach numbers fall between a \overline{P}_R of 0.3 and 0.4. This is in the range to be expected from the experiments with steps and wings. Although the data are presented only for conical boattails of 5.6° , values of β from 0° to 11° also yield values of \overline{P}_R in this range.

In the case of the convergent-divergent nozzles designed for a pressure ratio of 10.5, only the case of the small annulus is presented. This is done since sufficient information to correct the data for three-dimensional effects was not available; a two-dimensional solution, which may not be far in error for a small annulus, was thus utilized. Again, the critical pressure-rise coefficient varies only slightly over a wide range of pressure ratios, but the values are below those obtained with a convergent nozzle; a satisfactory explanation for the discrepancy in values is not known at this time. Attempted correlation of \overline{P}_R and the two terms of \overline{P}_R with the basic variation of P_R with Mach number for a step as presented by Love (ref. 9) has been inconclusive. In general, it can be concluded that the concept of mean critical pressure-rise coefficient is a unifying one but one which requires additional study.

Jet effects on base pressure.- Consider now in figure 7 the actual behavior of annular base pressure for a variety of nozzle and boattail geometries and for a wide range of operating pressures¹. Base pressure coefficient is plotted as a function of jet static-pressure ratio for 5.6° conical boattails at a Mach number of 1.9. Initial base pressure coefficients for no jet flow are indicated on the ordinate. The clarity of this figure is enhanced if the jet effect with single base-to-nozzle-diameter ratio is first studied. For the case of a convergent nozzle with D_B/D_N of 1.11, a slight amount of jet flow produces an appreciable increase in base pressure; further increases in jet pressure and thus jet flow result in the jet stream tending to aspirate the annulus to a lower pressure. However, as the jet pressure is increased still

¹These data, as well as a considerable portion of the data to follow, were obtained in unpublished experiments at the Lewis laboratory by E. Baughman, F. Kochendorfer, and M. Rouso.



REF ID: A66515
CONFIDENTIAL


further, the jet expands more and increases the strength of the trailing shock wave at its juncture with the external stream. The wake pressure thus increases and the existence of a critical pressure-rise coefficient forces the base pressure to increase also, as indicated by the data. As the base diameter becomes larger relative to nozzle exit diameter, the expanding jet flow curves increasingly toward the axis before meeting the external flow. Thus, in order to maintain a nearly constant value of \overline{P}_R , a larger initial expansion angle corresponding to a lower base pressure coefficient must exist for the given jet pressure ratio; this is seen to be the case. The portions of these curves corresponding to a very low jet total pressures are not included except in the single illustrative case.

Compressed into the lower end of the pressure-ratio range are the variations of base pressure coefficient with a convergent-divergent nozzle having an expansion ratio corresponding to a design total-pressure ratio of 10.5. A nozzle of this type has a design static-pressure ratio of 1 and requires a total-pressure ratio of 21 to operate at a static-pressure ratio of 2. It can be seen that the variations are essentially parallel to the corresponding variations with convergent nozzles (if the portions of the convergent-nozzle curves which turn in the positive direction at low pressure ratios are neglected) but are displaced slightly in the positive direction. A single variation obtained with an ejector nozzle designed for the same pressure ratio is included and is seen to fall somewhat higher than might be expected from the other data. It is believed that there is a logical reason for this, however. The secondary weight flow, which was 4 percent of the primary

$\left(\frac{m_S}{m_J \sqrt{T_S/T_J}} = 0.04 \right)$, created a layer of relatively low-energy air around

the primary jet stream which would be expected to lower the critical pressure-rise coefficient and thus increase the base pressure.

For a practical comparison of the effects of jets from a convergent and convergent-divergent nozzle, consider the case of a jet total-pressure ratio of 10.5 corresponding to a turbojet engine at a Mach number of 1.9. The convergent nozzle with its static-pressure ratio near 5.5 generally increases the base pressure over its no-flow value except for extremely large annuli and may generate appreciably positive base pressures. The convergent-divergent nozzle ($\epsilon = 0$), however, with its jet static-pressure ratio of 1 decreases the base pressures below the no-flow values with the resulting tendency to create relatively large base drags. An additional point of interest in this figure is the fact that replacing the idealized blunt base with a 45° bevel, such as might occur with an iris or clamshell nozzle, did not greatly alter the basic variation of base pressure with jet pressure. The same result was found true with a convergent-divergent nozzle.



This entire family of pressure variations for the convergent nozzle could be crudely reproduced theoretically starting with only a value of $\overline{P}_R = 0.35$, with the possible exception of the $\frac{D_B}{D_N} = 1.11$ variation. An indication of the approximate order of accuracy is given by the fact that for the case of $\frac{D_B}{D_N} = 1.4$ and $\frac{P_j}{P_0} = 4$ a variation of 0.04 in \overline{P}_R results in a variation of 0.04 in base pressure coefficient. It should again be cautioned, however, that a more accurate analysis of this approach is required.

Effect of stream Mach number. - The effect of stream Mach number on these characteristic curves is shown in figure 8, in which the data at a Mach number of 1.9 are reproduced, in part, for reference. At the left are shown data obtained at a Mach number of 0.9 and at the right are shown data obtained at a Mach number of 3.1; the same boattails and nozzles were used throughout.


In order to obtain the data at a Mach number of 0.9, the afterbodies were mounted on the end of a pipe which extended through the tunnel bellmouth into the cylindrical test section (unpublished research by R. Salmi of the Lewis laboratory). With no jet flow the base pressure was found to vary considerably with boattail shape. As the extent of boattailing increased, corresponding to lower values of D_B/D_N and smaller bases, the external stream was diffused further prior to separation at the base; hence, the base pressure increased. Boattail angle also had an appreciable effect, but treatment of this parameter at subsonic speeds is beyond the scope of this paper. The action of the jet bears a certain similarity to that observed at supersonic speeds. With a small annulus the expanding jet tends to impede the flow near the annulus with a resultant increase in pressure. Since subsonic flow will tolerate no abrupt changes, these increases in base pressure are also indicative of increases in pressures on the boattail. For large base annuli, the jet turns axially before meeting the external flow in this pressure-ratio range and, rather than decelerating the flow, pumps the base and boattail pressures to lower values; higher jet pressure ratios, however, reverse the direction of the curves as at supersonic speeds. Comparison of the curves with those obtained at a Mach number of 1.9 in the same pressure-ratio range shows the general resemblance at the two Mach numbers as well as the larger spread in base pressure coefficients existing at the high subsonic speeds.

At a Mach number of 3.1, the effect of increased Mach number in reducing the total spread of this family of curves is again seen; the jet effect on base pressure coefficient is appreciably reduced. The correlation of the effect of convergent and convergent-divergent nozzles

is even more striking at this Mach number where, for the same jet static-pressure ratio, the base pressure is nearly the same with either nozzle type (if the very low pressure-ratio range of the convergent nozzle is again neglected). In addition, for the case of a diameter ratio D_B/D_N of 1.4, convergent-divergent nozzles designed for pressure ratios from 10.5 to 50 yielded essentially the same base-pressure variation. Again, the no-flow values of base pressure are indicated on the ordinate but are unlabeled since they follow the same order as the curves with flow. It can again be seen that, with the range of annulus size likely to be encountered ($D_B/D_N \leq 1.4$), the convergent nozzle usually produces base thrusts at values of jet static-pressure ratio corresponding to the various flight Mach numbers. With the same annulus sizes the convergent-divergent nozzles generally produce base drag at supersonic speeds.

Effect of boattail geometry. - The base pressure coefficients which have been presented so far have been obtained with a specific family of afterbodies. Changes in afterbody geometry do not alter the basic trends, provided the flow remains unseparated over the boattail, but they do change somewhat the pressure level of the family of characteristic curves. For two convergent nozzles the effect of changing conical boattail angles is shown in figure 9. The data were obtained with a jet total-pressure ratio of 8, but the analysis applies to other pressure ratios as well. Two forms of base pressure coefficient, the conventional C_{PB} and also C'_{PB} are utilized. The base pressure coefficient C'_{PB} , originally used by Chapman (ref. 11) for bodies of revolution, essentially references the base pressure to conditions just ahead of the base and is thus a measure of the change in pressure from the end of the boattail to the base. Adding C'_{PB} to the pressure coefficient just upstream of the base yields C_{PB} approximately.

As the boattail angle increases, the expansive turning at the base decreases and may even turn to compression; the value of C'_{PB} thus increases in the positive direction. However, with a fixed base diameter the pressure ahead of the base generally decreases, resulting in only a moderate variation in the conventional base pressure coefficient with boattail angle in this case. The solid lines are predicted variations which were obtained from the data for $\beta = 5.6^\circ$ and from assumptions similar to those of reference 5 which have had limited success in estimating the effects of boattail shape on base pressure with no jet at supersonic speeds. The flow separation angle ψ is calculated from the initial data and is then assumed to remain invariant with boattail shape for the particular jet pressure ratio and value of D_B/D_N . Combining the resulting values of C'_{PB} with values of C_{PA} predicted for inviscid



flow by reference 12 yielded the indicated variation of C_{PB} ; agreement with experiment is not always this good, however, and the method breaks down if the flow separates ahead of the base. In order to illustrate this assumption further, if the boattail angle is held constant and the nozzle scaled up to yield a shorter boattail while maintaining the fixed value of D_B/D_N , the following condition would be predicted to result: The pressure ahead of the base would decrease without a change in the value of C'_{PB} and would thus lower the base pressure coefficient C_{PB} below the value obtained with the longer boattail. The successful application of this simple estimate in some cases may fortuitously result from the possibility that a fixed value of ψ is not greatly at variance with a fixed value of mean critical pressure-rise coefficient \overline{P}_R . The following table presents values of C_{PA} for the afterbodies considered herein to permit conversion of C_{PB} to C'_{PB} for use with other afterbody shapes:

β	Values of C_{PA} for -				
	$\frac{D_B}{D_N} = 2.67$	$\frac{D_B}{D_N} = 2.0$	$\frac{D_B}{D_N} = 1.67$	$\frac{D_B}{D_N} = 1.4$	$\frac{D_B}{D_N} = 1.11$
$M_0 = 1.9$					
3 5.6 7 11	0.018	0 -0.035	-0.01	0 -0.005 -0.049	0.03
$M_0 = 3.1$					
5.6	-0.016	-0.04		-0.027	-0.022

Effect of nozzle exit angle. - It was shown in the case of jet effects on boattail pressure that increasing the nozzle exit angle increases the strength of the trailing shock and, hence, the interference effect. From a consideration of \overline{P}_R the same result with an annular base may be expected. In figure 10 the effect of nozzle exit angle on base pressure is shown for the case of three nozzle angles in two afterbodies at $M_0 = 1.6$. Pertinent geometric parameters are indicated. The data, which were obtained by Carlos A. deMoraes at the




Langley laboratory with solid propellant rocket gases, clearly indicate that increased nozzle exit angles increase the annular base pressure.

Effect of jet temperature.- The consideration of rocket gases gives rise to the problem of the applicability of data obtained with unheated jet fluids. This problem is considered in figure 11. In the left-hand portion of the figure, data were obtained with a fixed model geometry with unheated air, unheated CO_2 , and the products of combustion of an oxygen-alcohol rocket used for jet fluids. The use of CO_2 with a γ (ratio of specific heats) of 1.3 produced a moderate upward shift in the curve. The rocket gases produced a much larger increase in the base pressures. In the right-hand portion of the figure, data are presented which were obtained with the large-scale model in the 8- by 6-foot tunnel with unheated and heated air. The effect of heating the air to $2,500^\circ \text{R}$ was to raise the curve slightly. Thus, it can be seen that the use of data obtained with unheated air is conservative in that the values of base pressure are too low.

Analysis of the temperature effect is complicated by variations in γ , T_j , and R , which affect the jet shape and mixing and, hence, the value of pressure-rise coefficient \overline{P}_R expected across the trailing shock. The results of a simple empirically derived calculation to estimate the temperature effects by consideration of the γ of the jet are presented, however. The assumption was made that the jet total pressures which will produce the same base pressure for various values of γ and any given nozzle-afterbody combination are those which yield the same value of jet exit angle ν . With this assumption it is possible to correct the data at $\gamma = 1.4$ to other values of γ as indicated by the dashed lines. As can be seen, this correction appears adequate for correlating the air and CO_2 data from the small-scale experiments, as well as the hot- and cold-air data from the 8- by 6-foot tunnel; in addition, the correction correlates boattail pressure drags for the latter model. The good agreement is perhaps fortuitous since the data obtained with a rocket are not predicted with even the lowest possible value of γ . Several considerations in the rocket tests, such as the unknown temperature and velocity distributions at the nozzle exit, the possibility of burning downstream of the nozzle exit, and the appearance of an unburned layer of liquid alcohol flowing over portions of the internal nozzle surface make conclusions difficult, however. Additional research is obviously required.

Effect of Reynolds number.- Another question which arises in considering the validity of small-scale unheated jet effects is the influence of Reynolds number, which has been investigated briefly as indicated in figure 12. The effective Reynolds number of a turbulent boundary layer was varied in three ways and the influence on jet effects



determined. In the first case, Reynolds number N_R was varied by running similar models in the Lewis 18- by 18-inch supersonic tunnel ($M = 1.9$) and in the 8- by 6-foot supersonic tunnel ($M = 2$) at values of N_R of 5.5×10^6 and 35×10^6 , respectively. The jet effects on base pressure were nearly the same. Also, at a Mach number of 1.9 and a low Reynolds number, the thickness of the boundary layer ahead of the base was increased $3\frac{1}{2}$ times by artificial transition (ref. 5) with only a small increase in base pressure. Lastly, at a Mach number of 3.1, the Reynolds number was appreciably increased by a change in tunnel pressure with only a slight decrease in base pressure. It might thus be concluded that, as in the case of plain bodies of revolution, Reynolds number has only a small effect on base pressure provided the boundary layer is turbulent ahead of the base. This result is compatible with the fact that critical pressure-rise coefficient is relatively independent of Reynolds number for turbulent boundary layers.


Annular base bleed.- It is now of interest to consider in figure 13 the case in which a blunt annulus is present and it is desired to reduce the drag by discharging air from the annulus as proposed in reference 12 (also see ref. 14). Since blunt bases with convergent-divergent nozzles exhibit the most drag, it would be desirable to study such a case; however, because of model limitations it was necessary to simulate this case with a convergent nozzle at low pressure ratio. The base drag coefficient (based on annular base area) with bleed flow may be expressed as the sum of three terms: (1) that due to base pressure, (2) that due to exit velocity, and (3) that due to inlet momentum (considered herein as free-stream momentum with $m_0 = m_B$). The sum of terms (1) and (2) is the exit total momentum. This quantity drops rapidly from a positive to a negative drag (thrust) as the bleed total pressure increases. As shown in the right-hand portion of the figure, the bleed weight flow also increases. If the bleed air is charged with the full free-stream momentum ((1) + (2) + (3)), there is only an initially small reduction in drag and then an increase which levels out with large weight flows. Thus, as in the case of plain bodies of revolution, if air is to be taken aboard for the express purpose of reducing base drag, it should not come from a free-stream inlet but rather from a low-energy source. For example, the data indicate that a bleed flow parameter of 1.7 percent of the jet flow could be obtained by venting the annulus to ambient static pressure. If the induced flow came primarily from the low-energy region of the boundary layer with negligible momentum charge, the base drag would be eliminated. In cases in which the air must be taken aboard for air conditioning or tail-pipe cooling, the inlet momentum charge to the aircraft cannot be avoided and it appears that a blunt annulus, if present, is a good place to discharge the air.

Base-burning schemes such as those suggested in references 15 and 16 may be very effective in reducing base drag but are more difficult to apply to aircraft.

Total afterbody drag.- Many of the important parameters influencing jet effects on base pressure have now been considered. Figure 14 is presented to illustrate both the utility of the data and the fact that annular base pressure may influence the choice of afterbody designs. Afterbody drag coefficient including jet interference effects is presented as a function of the ratio of base diameter to nozzle exit diameter for both convergent and convergent-divergent nozzles with the same throat areas and with axial exit flow. The curves are predicted with the aid of the data contained herein as well as from the results of references 5 and 12. Only the case of a small boattail angle is considered at a Mach number of 1.9 with a jet total-pressure ratio of 10. In the case of the convergent nozzle, the total afterbody drag decreases slightly as the base diameter is increased because of positive pressures (thrust) on the annulus. Furthermore, a relatively large base annulus may be utilized without incurring any drag penalty at this Mach number. In the case of the convergent-divergent nozzle designed for a pressure ratio of 10, however, the drag is indicated to increase immediately as an annulus is added. It is thus desirable to keep the size of the base annulus to a minimum in order to avoid costly drag penalties.


CONCLUDING REMARKS

In conclusion, it may be said that sufficient investigations of the problem of jet effects on boattail and base pressures have been conducted to clarify many of the important parameters. With the use of existing data and some of the concepts presented herein, it appears possible to estimate to a crude order of accuracy the drags of many afterbody-nozzle combinations. Thus, although the results may not serve to provide precise drag calculations, they can serve as a guide to good-afterbody-design practice. Finally, while answering some questions, these studies have served to point out additional problems which are in need of investigation.



CONFIDENTIAL

REFERENCES

1. Erdmann: Widerstandsbeiwerte für das A4VLP mit Berücksichtigung des Strahl- und Reibungseinflusses für Unter- und Überschallgeschwindigkeiten - Untersuchung der Strahlexpansion. Archiv Nr. 66/105 g.Kdos, Aerodynamisches Institut, Heeres Versuchsstelle, Peenemünde, Mar. 24, 1943.
 2. Purser, Paul E., Thibodaux, Joseph G., and Jackson, H. Herbert: Note on Some Observed Effects of Rocket-Motor Operation on the Base Pressures of Bodies in Free Flight. NACA RM L50I18, 1950.
 3. Stoney, William E., Jr., and Katz, Ellis: Pressure Measurements on a Sharply Converging Fuselage Afterbody With Jet On and Off at Mach Numbers From 0.8 to 1.6. NACA RM L50F06, 1950.
 4. Love, Eugene S.: Aerodynamic Investigation of a Parabolic Body of Revolution at Mach Number of 1.92 and Some Effects of an Annular Jet Exhausting From the Base. NACA RM L9K09, 1950.
 5. Cortright, Edgar M., Jr., and Schroeder, Albert H.: Investigation at Mach Number 1.91 of Side and Base Pressure Distributions Over Conical Boattails Without and With Jet Flow Issuing From Base. NACA RM E51F26, 1951.
 6. Gillespie, Warren, Jr.: Jet Effects on Pressures and Drags of Bodies. NACA RM L51J29, 1951.
 7. Cantrell, H. N., and Gazley, Carl, Jr.: Base Pressure on Bodies of Revolution at Subsonic and Supersonic Velocities With and Without Jet Exhausts. PROJECT HERMES Aero. Fundamentals Memo. #18, Gen. Elec. Co., Apr. 11, 1952.
 8. Donaldson, Coleman duP., and Lange, Roy H.: Study of the Pressure Rise Across Shock Waves Required to Separate Laminar and Turbulent Boundary Layers. NACA TN 2770, 1952. (Supersedes NACA RM L52C21.)
 9. Love, Eugene S.: The Base Pressure at Supersonic Speeds on Two-Dimensional Airfoils and Bodies of Revolution (With and Without Fins) Having Turbulent Boundary Layers. NACA RM L53C02, 1953.
 10. Beastall, D., and Eggink, H.: Some Experiments on Breakaway in Supersonic Flow (Part II). TN No. Aero. 2061, British R.A.E., June 1950.
 11. Chapman, Dean R.: An Analysis of Base Pressure at Supersonic Velocities and Comparison With Experiment. NACA Rep. 1051, 1951. (Supersedes NACA TN 2137.)
- 

Declassified

12. Jack, John R.: Theoretical Pressure Distributions and Wave Drags for Conical Boattails. NACA TN 2972, 1953.
13. Cortright, Edgar M., Jr., and Schroeder, Albert H.: Preliminary Investigation of Effectiveness of Base Bleed in Reducing Drag of Blunt-Base Bodies in Supersonic Stream. NACA RM E51A26, 1951.
14. Hebrank, W. H., Scanland, T. S., Platou, A. S., and Hicks, B. L.: The Effects on Base Pressure of Air Ejection From the Base of a Model Projectile at $Ma = 1.7$ - Partial Evaluation of the External Ram Jet Principle. Memo. Rep. No. 539, Ballistic Res. Lab., Aberdeen Proving Ground, Aug. 1951.
15. Scanland, T. S., and Hebrank, W. H.: Drag Reduction Through Heat Addition to the Wake of Supersonic Missiles. Memo. Rep. No. 596, Ballistic Res. Lab., Aberdeen Proving Ground, June 1952.
16. Baker, W. T., Davis, T., and Matthews, S. E.: Reduction of Drag of a Projectile in a Supersonic Stream by the Combustion of Hydrogen in the Turbulent Wake. CM-673 (Contract NOrd 7386), The Johns Hopkins Univ., Appl. Phys. Lab., June 4, 1951.



0371229 1038

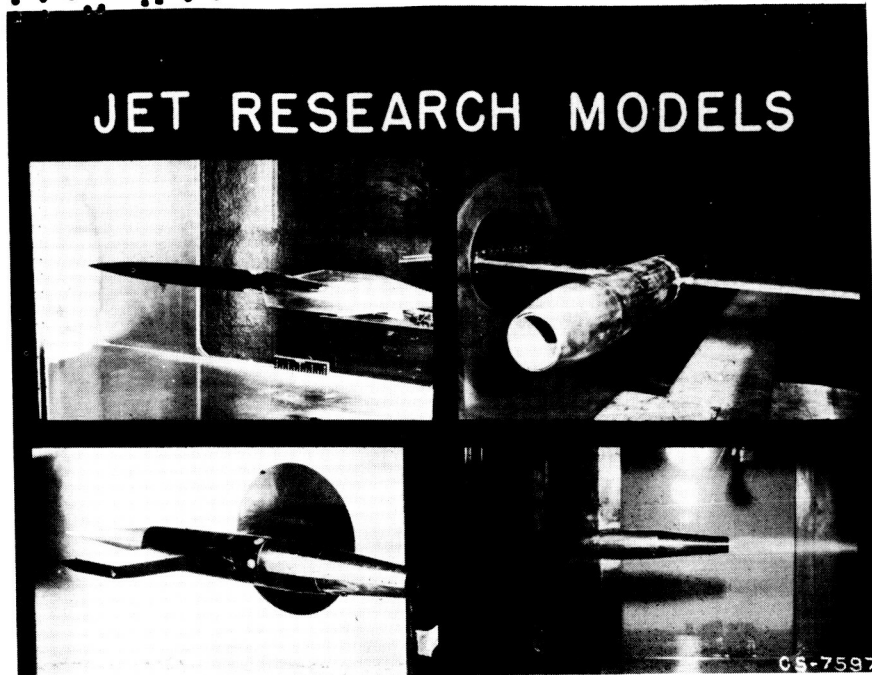


Figure 1



PARAMETERS AND NOMENCLATURE

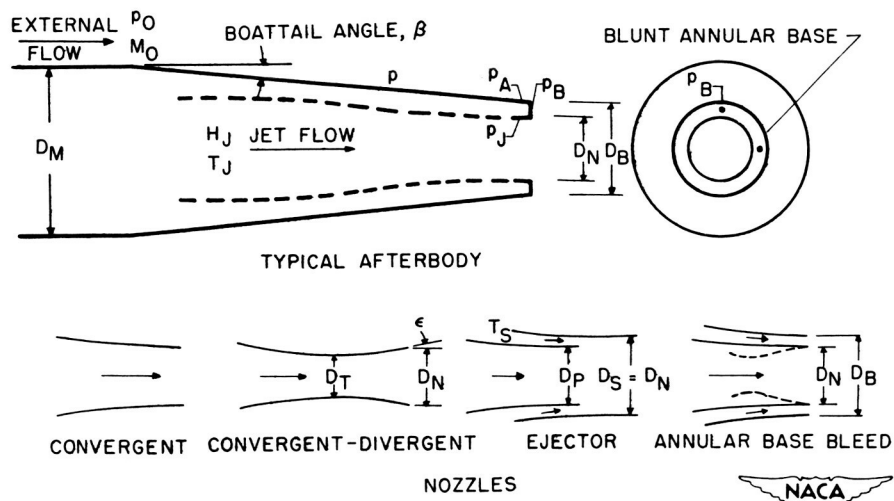


Figure 2

JET EFFECTS ON BOATTAIL PRESSURES

$M_0 = 1.9$
 $\beta = 5.6^\circ$

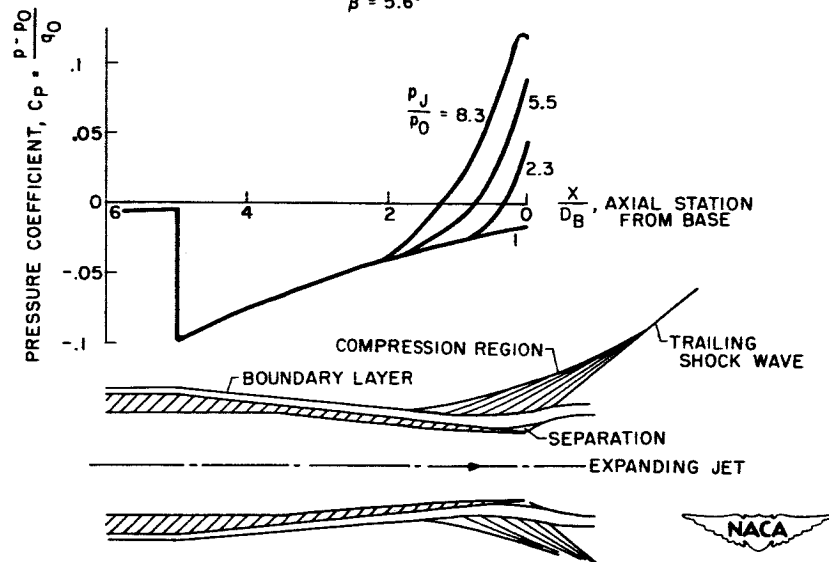
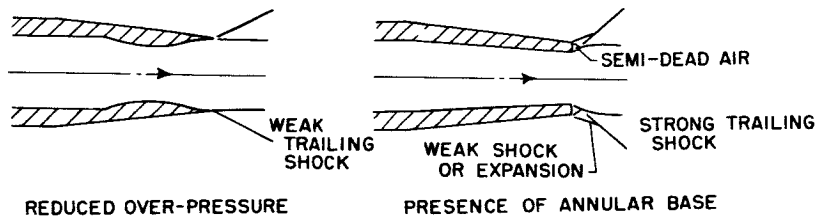


Figure 3

FACTORS MODIFYING JET EFFECTS ON BOATTAIL PRESSURES JET INTERFERENCE REDUCED BY



JET INTERFERENCE INCREASED BY

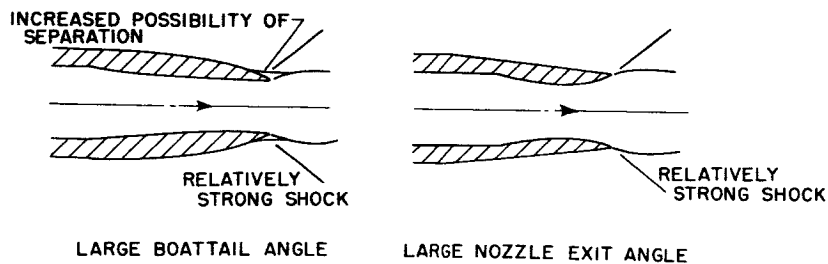


Figure 4

JET EFFECTS ON BOATTAIL PRESSURE DRAG

$$M_0 = 1.9-2.0$$

(a) EFFECT OF BOATTAIL SHAPE (b) EFFECT OF NOZZLE ANGLE

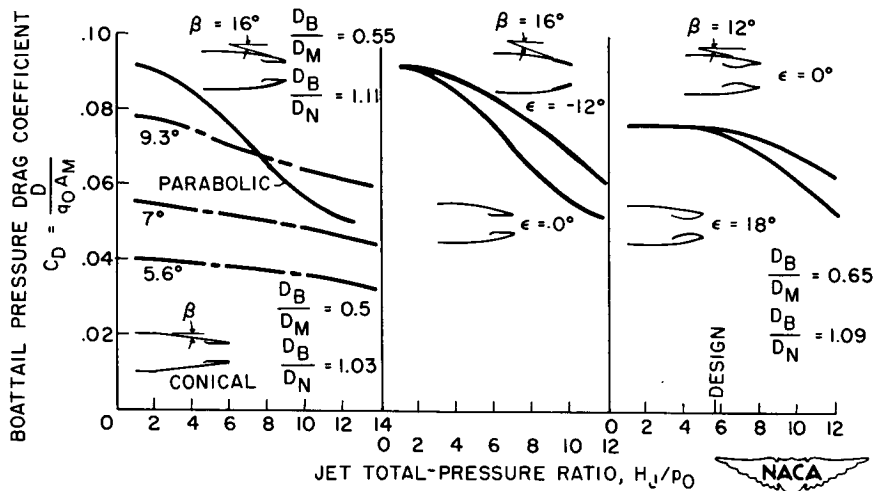


Figure 5

CRITICAL PRESSURE-RISE COEFFICIENT

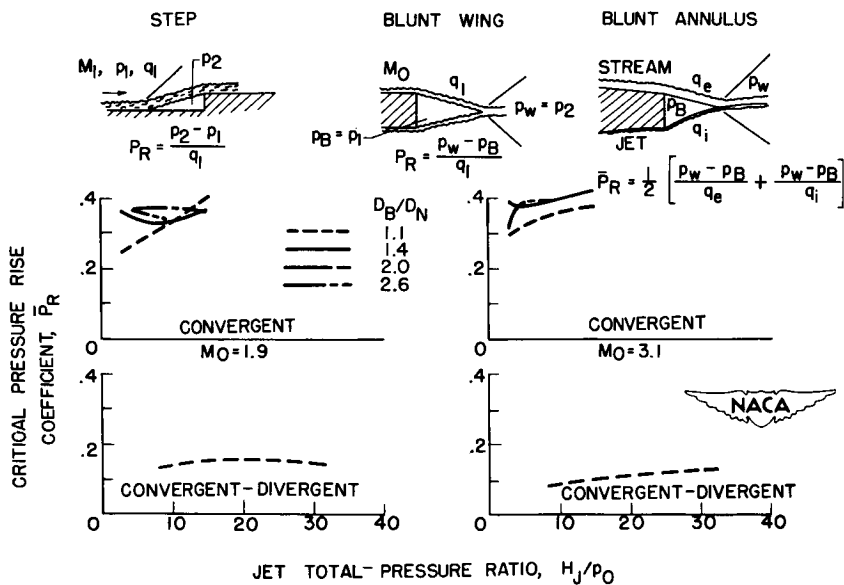


Figure 6

DECLASSIFIED

JET EFFECTS ON BASE PRESSURE

$M_0 = 1.9$

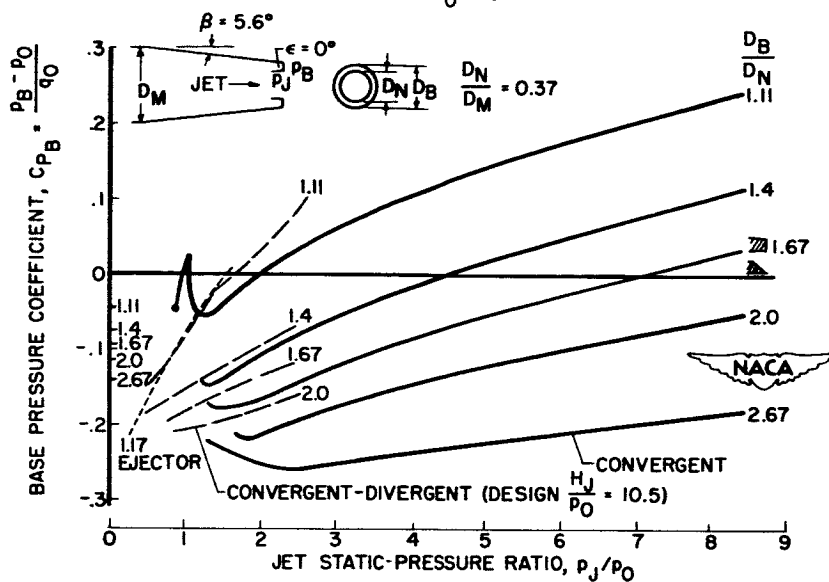


Figure 7

EFFECT OF STREAM MACH NUMBER

$\beta = 5.6^\circ$, $D_N/D_M = 0.37$

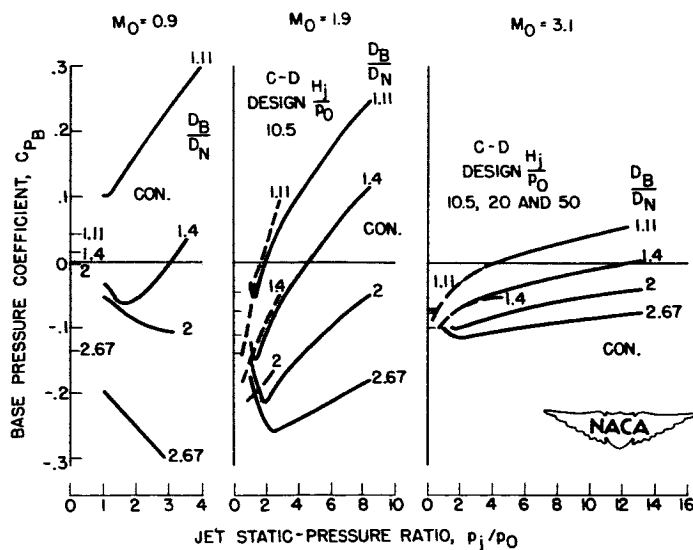


Figure 8

EFFECT OF AFTERBODY GEOMETRY $M_0 = 1.9$

CONVERGENT NOZZLE, $H_1/p_0 = 8$

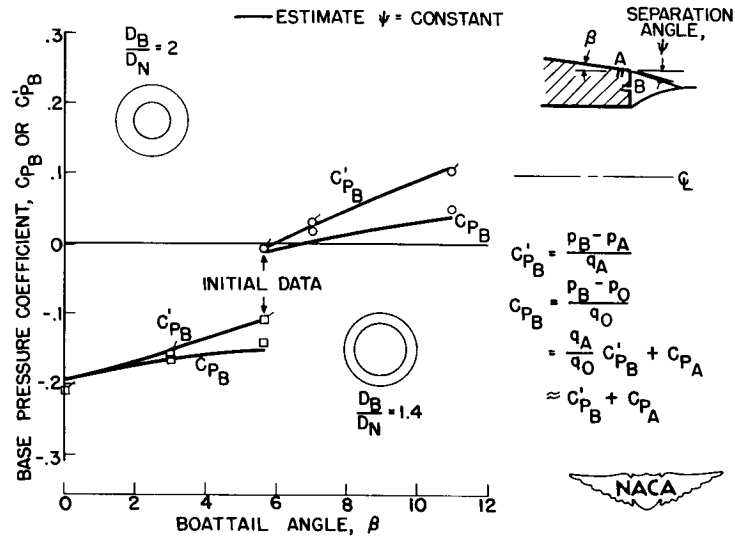


Figure 9

EFFECT OF NOZZLE EXIT ANGLE $M_0 = 1.6$

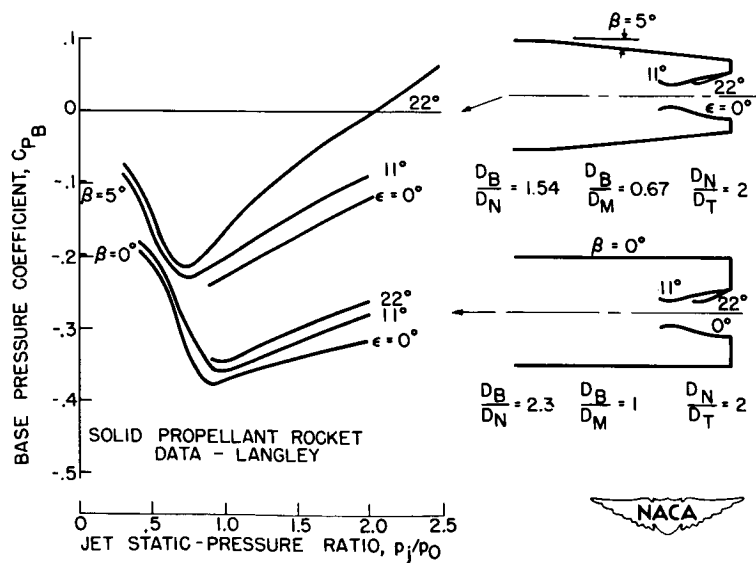


Figure 10

DECLASSIFIED

EFFECT OF JET TEMPERATURE

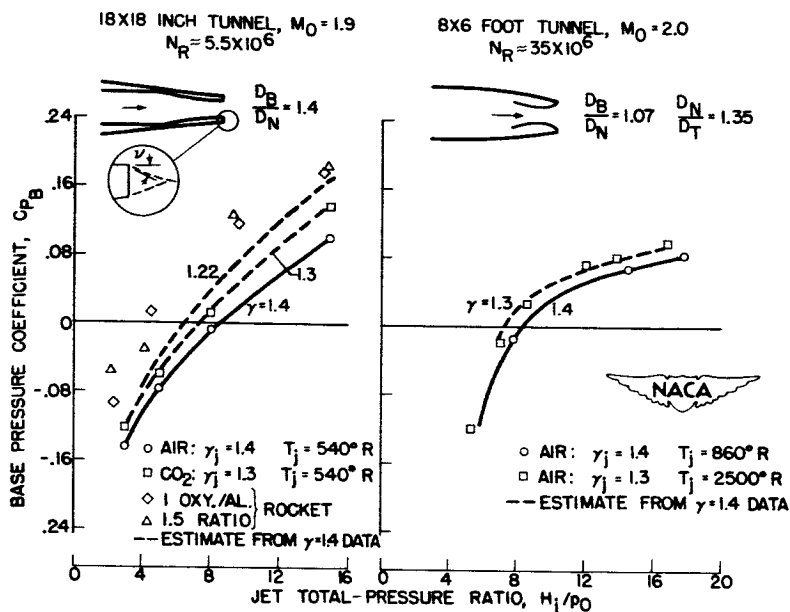


Figure 11

EFFECT OF REYNOLDS NUMBER

TURBULENT BOUNDARY LAYER

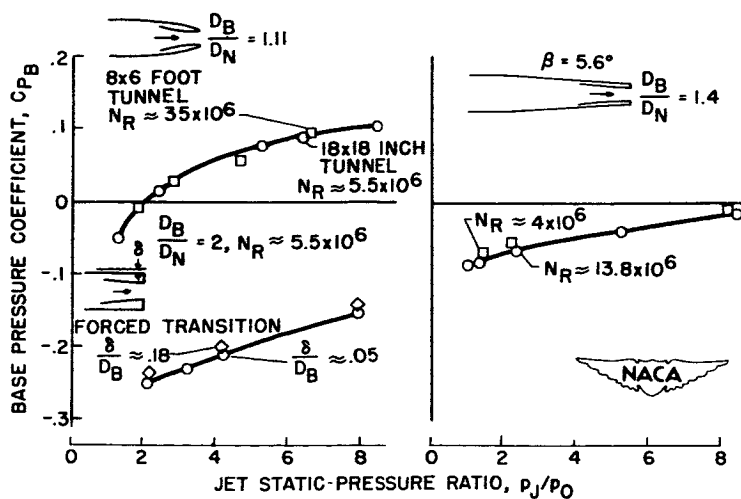
 $M_0 = 1.9-2.0$ $M_0 = 3.1$ 

Figure 12

EFFECT OF ANNULAR BASE BLEED

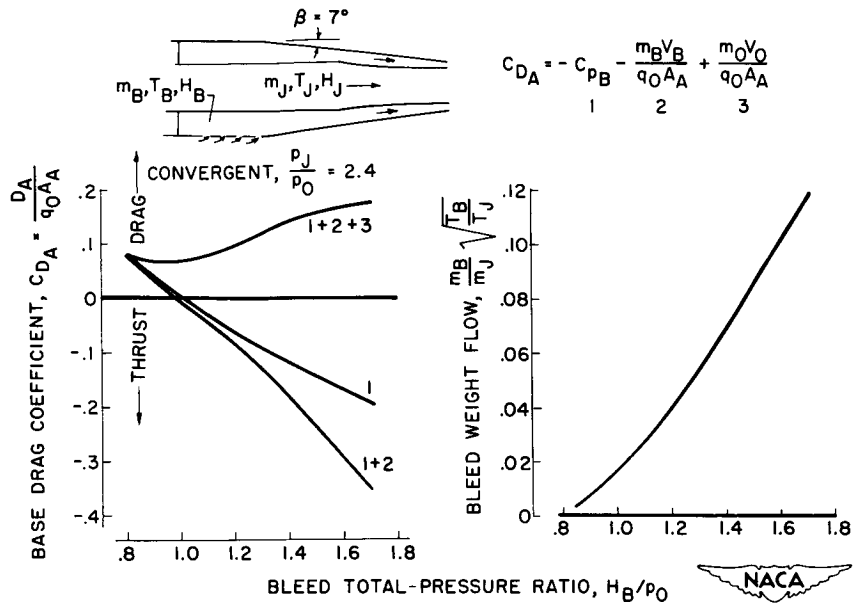
 $M_0 = 1.9$ 

Figure 13

OVERALL AFTERBODY DRAG CONSIDERATIONS

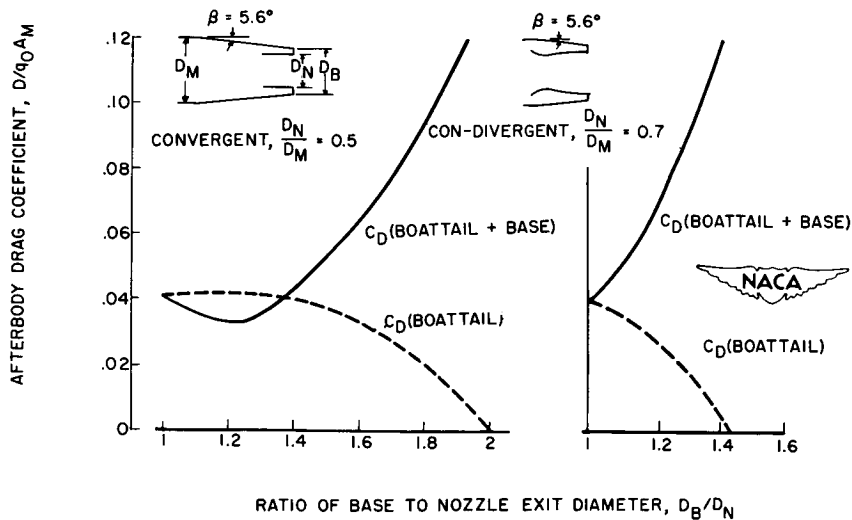
 $M_0 = 1.9, H_J/p_0 = 10$ 

Figure 14

CONFIDENTIAL

DECLASSIFIED

SOME EFFECTS OF A JET ON SURFACES DOWNSTREAM OF THE EXIT

By Maxime A. Faget and Carlos A. de Moraes


Langley Aeronautical Laboratory

It has been shown that a jet issuing from the rearward end of a body at supersonic speeds can have considerable effects on the pressures acting on the base annulus and in certain cases on the boattail. The induced forces produced by the jet on surfaces downstream of the jet exit can also be expected to be of major importance. Until recently, this problem has been avoided by designers because there was little information on these jet effects and because satisfactory aircraft configurations were obtainable without placing any surfaces in the vicinity of the jet blast. More recently, it has become desirable to have the jet exit in such a position that large surfaces are in the vicinity of the jet blast. An example may be an engine location well forward in the fuselage or a nacelle installation in which the jet exit is ahead of the wing trailing edge. In addition, there are configurations where a rear fuselage location is chosen, but a large portion of the fuselage extends beyond the jet exit for better fairing or other reasons. An example of this is a model of a delta-wing aircraft configuration recently tested by Langley Pilotless Aircraft Research Division and shown in figure 1. For this model, a specially modified solid-fuel rocket was used to simulate the characteristics of a turbojet exhaust.

Jet-effect results were obtained at Mach number 1.5. The effect of the jet was to induce negative pressures on the area behind the exit. A plot of the pressure coefficient on this area is shown. This negative pressure, of course, tended to pitch the nose of the model down.

In this case, there is little or no free-stream flow between the jet and the adjacent surface. The overexpansion of the jet causes the negative pressures on the surface. A more important case is where the jet boundary is not isolated from the external flow, and the interference of the jet on the external flow predominates in the aerodynamic effects produced. Some idea of this type of jet effect upon the surrounding flow field may be obtained from figures 2 to 4.

Figure 2 shows schlierens taken in the Langley 8-foot transonic tunnel and at $M = 1.1$. The jet stagnation temperature was 1000° F. This temperature was achieved by the combustion of ethylene and air. The model has a sonic exit and the pressure ratios (H_j/p_o) shown are 2, 4, and 5.5. At the lowest pressure ratio, the jet emerges with little or no disturbance upon the free stream. At higher pressure ratios, shocks are generated in the external flow. These shocks are caused by the



initial expansion of the jet and by the bulges produced in the jet boundary further downstream resulting from the Mach diamonds in the jet.

Figure 3 shows shadowgraphs taken at the preflight jet of the Langley Pilotless Aircraft Research Station at Wallops Island, Va., and are at a free-stream Mach number of 2.02. A sonic helium jet was used. Pressure ratios (H_j/p_o) shown are 3, 5, and 7. Two shocks in the free stream which originate at the jet can be seen. These shocks are caused by the original expansion bulge and the bulge caused by the first diamond. It should be noted that the second shock moves rearward as the pressure ratio is increased.


Figure 4 shows schlierens taken in a 9-inch blowdown jet at the Langley laboratory. These schlierens are for Mach number 3 and use a sonic, unheated air jet. The model is at an angle of attack of 8° . Pressure ratios (H_j/p_o) shown are 11.4, 22.7, and 38.0. It can be seen that the shock wave in the external flow caused by the initial expansion of the jet starts well forward on the lee side of the boattail because of the separated boundary layer.

In order to study the effect of a jet on adjacent surfaces in the external flow, an investigation using the preflight jet of the Langley Pilotless Aircraft Research Station at Wallops Island, Va., has been initiated. Preliminary results from this investigation are presented in this paper.

In this investigation, made at $M = 2.02$, a model simulating a turbojet nacelle was mounted in the vicinity of a flat surface simulating a wing as shown in figures 5 and 6. The nacelle was tested in the four vertical positions shown. These were 0.93, 1.45, 2.39, and 3.40 jet diameters below the wing surface. Static pressures were measured on the wing surface at the various positions shown. The measured pressures were used to determine the forces induced on the wing. The tests were conducted at approximately sea-level free-stream conditions.

In these tests it was desired to simulate the jet of an afterburning turbojet with a sonic exit. Since it was impractical to use hot gases in these tests, simulation of a turbojet exhaust was attempted by using light gases which would have high sonic velocities.

In order to determine whether it was necessary to duplicate the jet velocity of the turbojet, tests were made with three gases at ambient temperature for the jet. These were air, helium, and a mixture of 58 percent CO_2 and 42 percent H_2 . Properties of these gases and the resulting jet properties are given in the following table. This comparison is made for a sonic exit area of 5 square feet and a gross thrust of 15,500



Declassified

at 35,000 feet. The properties of a typical afterburning turbojet are also listed for comparison.

Condition	Air	He	58% CO ₂ + 42% H ₂	Turbojet
γ	1.4	1.66	1.4	1.26
R (gas constant)	533	367	342	537
Stagnation temperature, °R	520	520	520	3400
Mass flow, lb/sec	320	130	126	125
Total pressure, lb/sq ft	2840	2770	2840	2880
Static pressure, lb/sq ft	1500	1343	1500	1593
Velocity, ft/sec	1020	2760	2590	2520
Density, slugs/cu ft	0.00202	0.00029	0.00030	0.00031

Figure 7 gives a comparison of the jet effect of the three artificial jets on the row of static pressures which were measured directly in line with the jet axis. This comparison was made with the nacelle in the highest position, that is, with the exit located 0.93 diameters below the wing surface.

The important differences in the three gases were in γ (which would set the shape of the jet boundary if there were no mixing) and the jet-velocity-to-free-stream-velocity ratio (which will determine the amount of decay of the jet boundary due to mixing). The jet velocity for He and the H₂-CO₂ mixture was approximately 20 percent greater than the free-stream velocity, whereas the jet velocity for air was less than half the free-stream velocity.

In figure 7, the pressure coefficients produced by the jet for a jet pressure ratio of $8 \left(\frac{H_j}{P_o} = 8 \right)$ is plotted against the downstream distance from the exit in jet diameters. Two pressure peaks, produced by two shock waves in the free stream by the disturbance of the jet are shown. The upstream shock originates at the jet exit and is generated by the initial expansion of the jet gases. The farther downstream shock wave is generated by the second expansion of the jet as it forms its first diamond.


When the three curves are compared, it will be noticed that, whereas there are slight differences between the profiles produced by the light gas jets, the profile produced with the air jet is noticeably different in the region of the second shock. In view of the differences in the properties of these gases, some differences in these pressure profiles should not be unexpected.

Although the H_2-CO_2 mixture is thought to duplicate more closely the turbojet gas, the remainder of the tests were conducted with helium since both these gases essentially produced the same results. By using helium, which is a pure gas, standardization of the jet properties was assured.

In figure 8 are shown the results from tests with the nacelle located in four vertical positions. These results are for a pressure ratio $\left(\frac{H_j}{P_o}\right)$ of 8 with a helium jet. Pressure coefficients on the wing directly above the nacelle are again plotted against the distance downstream from the exit in exit diameters. Two curves are shown corresponding to the power-on and power-off condition. The difference in these curves will thus be an indication of the pressures induced by the jet flow. It should be noted that, as the nacelle is moved downward away from the wing, the pressure peaks move rearward and decrease slightly. However, the general pattern remains essentially unchanged. These pressures induced on the wing can therefore be attributed to shocks produced in the external flow by the shape of the jet boundary. This conclusion has been substantiated by the examination of shadowgraph pictures.

Figure 9 shows the pressure profiles measured to the side, as well as directly above the exit, when the nacelle was tested in position B. It should be noted that pressure peaks diminish only slightly and move rearward for the outboard positions. This result is in agreement with the expected location and strength of the shock waves generated by the jet in the external flow.

It might be expected that these disturbances on the wing could be somewhat alleviated by directing the jet axis away from the wing. This effect was investigated by making a test with the nozzle axis deflected 10° down. The results from this test are shown in figure 10. It should be noted that in order to obtain this deflection the nacelle center line was abruptly turned 10° two exit diameters ahead of the exit. Thus, although these results are for the exit in position B, the nacelle itself is in a higher position than the undeflected exit nacelle location. When comparison of the flow field for the 10° deflected exit and the undeflected exit is made, it can be seen that no apparent alleviation from the strength of the shock waves has been obtained. The first pressure peak for the deflected jet is not only farther forward but is stronger. Study



SECRET

of shadowgraph pictures reveals that in this case the shock originates slightly ahead of the exit where the flow appears to separate on the upper surface of the boattail. The fact that the nacelle for the deflected case has been bent and is located in a higher position probably accounts for this difference as well as for some other differences in the flow fields shown. For instance, in the case of the deflected jet, lower pressures ahead of the first peak are shown.

In these tests only a limited area of the wing surface was surveyed, as can be seen by looking at the orifice locations again (fig. 11). Qualitative results, however, can be obtained for the induced lift and center of pressure for that area in the region of the pressure orifices. Figure 12 shows the results obtained for the undeflected jet tested in the four vertical positions. The lower curve shows the induced lift (that is, integrated lift from pressure coefficients with power-on minus the lift from pressure coefficients with power-off) divided by the gross thrust of the jet plotted against jet pressure ratio $\left(\frac{H_j}{P_o}\right)$. The upper curve shows center-of-pressure locations for the induced lifting force. The center of pressure is located as the number of jet diameters downstream of the jet exit. It can be seen that induced lift equal to the gross thrust was encountered at low jet pressure ratios. The lift-to-thrust ratio decreases with increase in jet pressure ratio. There appears to be no definite trend in the lift-to-thrust ratio for the different vertical nacelle locations. This result can be attributed to the limited surface area for which the pressures were integrated. Probably, if the integration of the induced lift were made over a sufficiently large area, there would be no noticeable difference in lift in going from one location to the next. The center of the induced pressure is shown to be farthest rearward for the lowest nacelle position, the intermediate nacelle positions having intermediate center-of-pressure locations.

It has been shown that considerable forces can be induced on nearby surfaces by a jet issuing in a supersonic free stream. The underexpanded jet expands abruptly at the exit and acts as a strong disturbance from which shock waves are generated. Additional disturbances are produced downstream by the Mach diamonds in the jet. Since deflecting the jet does not appear to lessen the strength of the shocks, the only way that induced aerodynamic forces from an underexpanded jet can be completely avoided is not to have aerodynamic surfaces within the shock field of the jet. At Mach number 1 this condition would mean that the jet exit would have to be at the rear of the aircraft. However, it has been shown that these jet effects are beneficial to the extent that an underslung nacelle exit will provide additional induced lift. The effect of the jet disturbance on the drag is yet to be investigated. However, since the underexpanded jet acts like a strong source, it appears likely that

03710281030

considerable drag reduction might be obtained if the jet exit is properly located with respect to the changes in cross-sectional areas defined by the "area rule."

[REDACTED]

CONFIDENTIAL

DECLASSIFIED

7

PRESSURE DISTRIBUTION DOWNSTREAM OF JET EXIT

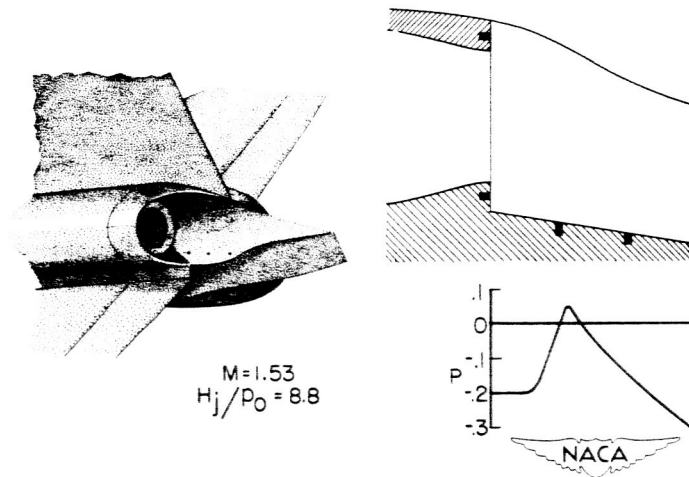


Figure 1

$M_j=1.0; M_0=1.1; \alpha=0^\circ$

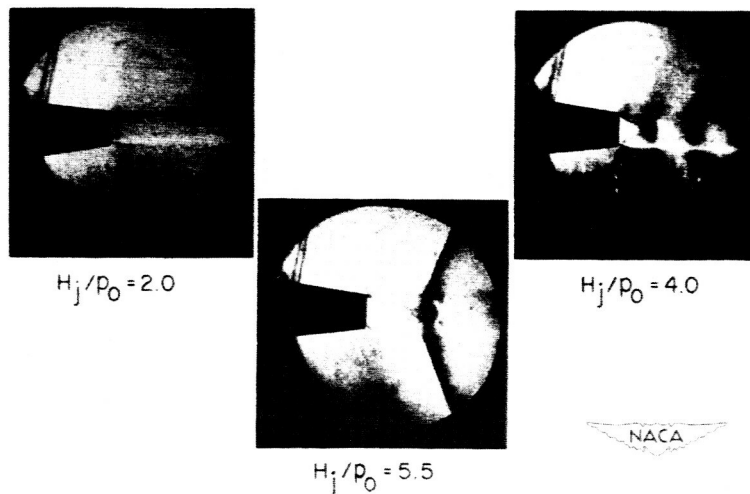


Figure 2

03171229.1030

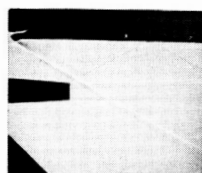
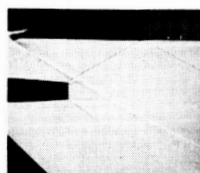
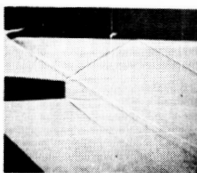
 $M_j = 1.0$; $M_0 = 2.02$; $\alpha = 0^\circ$  $H_j/p_0 = 3.0$  $H_j/p_0 = 5.0$  $H_j/p_0 = 7.0$ 

Figure 3

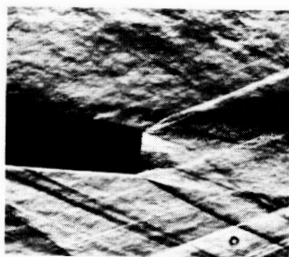
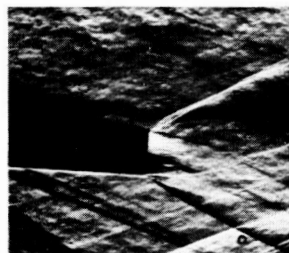
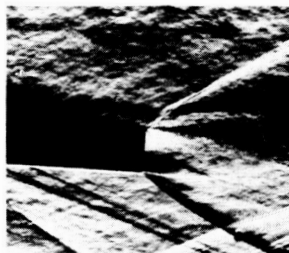
 $M_j = 1.0$; $M_0 = 3.03$; $\alpha = 8^\circ$  $H_j/p_0 = 11.46$  $H_j/p_0 = 22.72$  $H_j/p_0 = 38.00$ 

Figure 4

DECLASSIFIED

TEST SETUP
(SIDE VIEW)

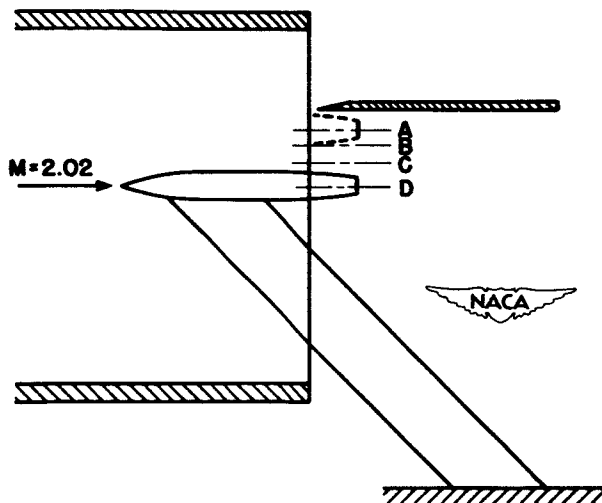


Figure 5

ORIFICE LOCATIONS
(BOTTOM VIEW)

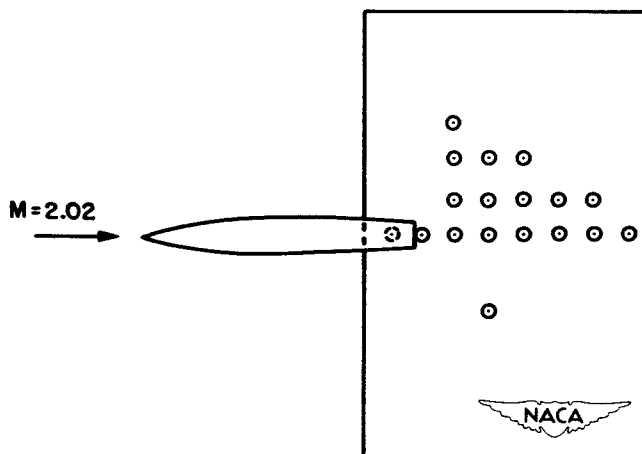


Figure 6



03:12:28.10:38

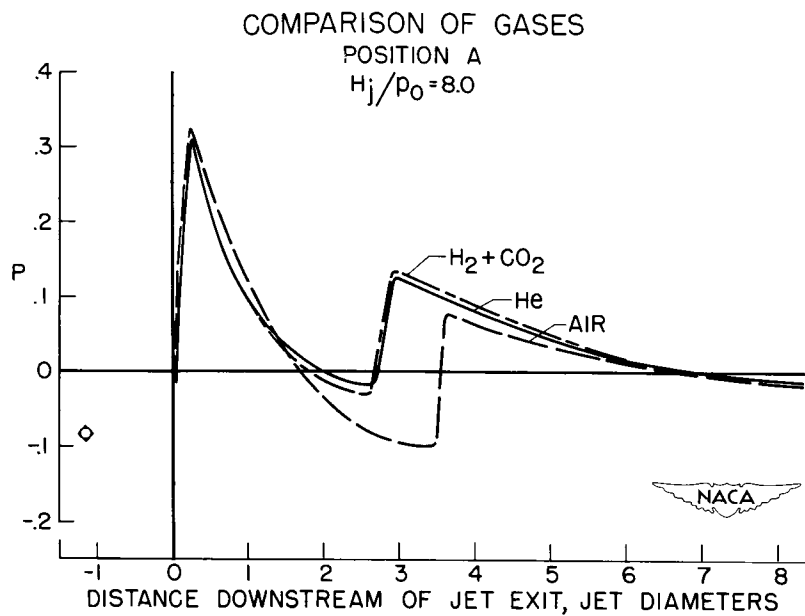


Figure 7

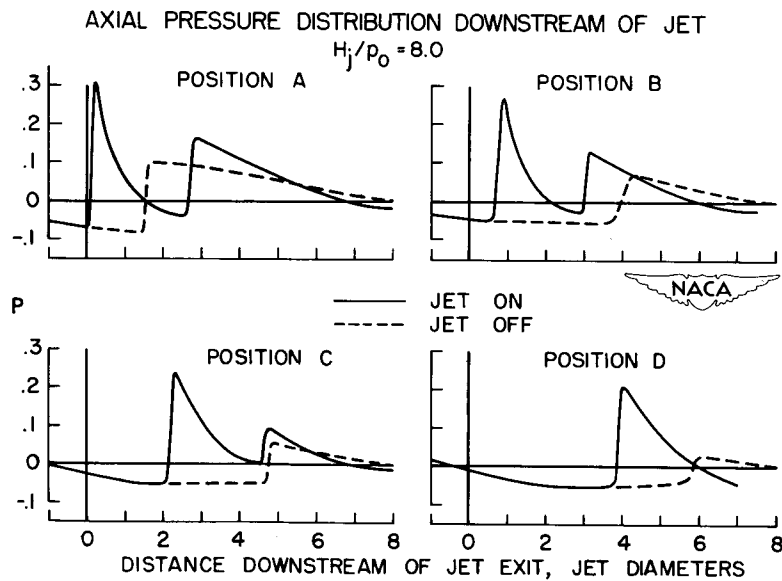


Figure 8

PRESSURE FIELD ON WING WITH NACELLE IN POSITION B
 $H_j/p_0 = 8.0$

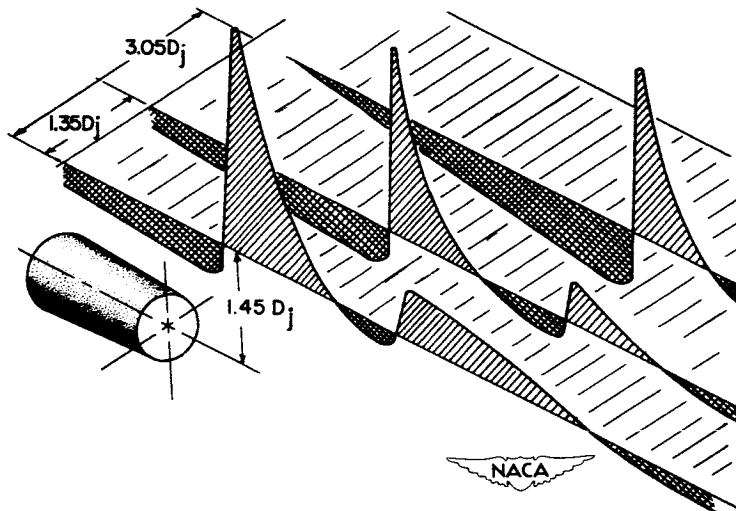


Figure 9

PRESSURE FIELD ON WING WITH NACELLE IN
POSITION B AND CANTED 10° DOWN
 $H_j/p_0 = 8.0$

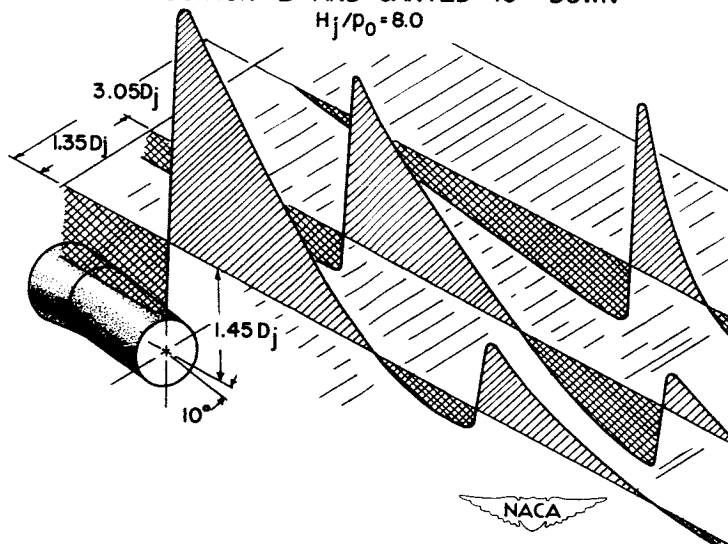


Figure 10

0371228.103

INTEGRATED AREA USED IN OBTAINING LIFT AND C.P. POSITION

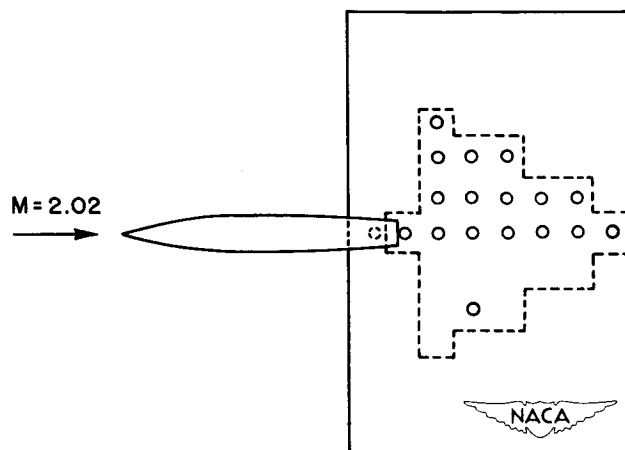


Figure 11

INTEGRATION OF DIFFERENCE IN PRESSURE COEFFICIENTS, POWER-ON AND POWER-OFF

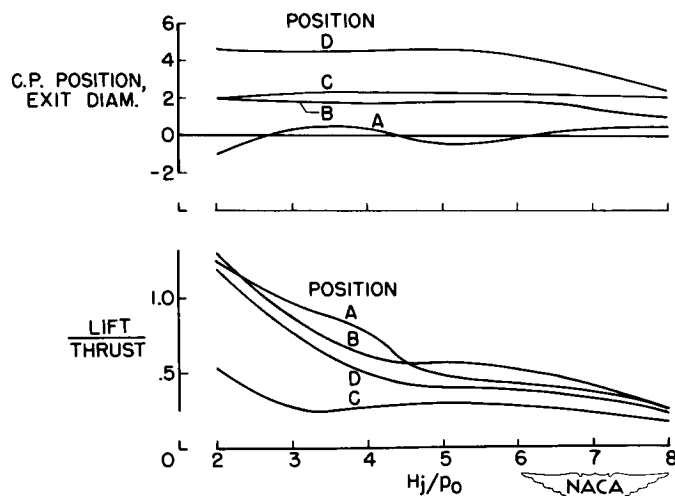


Figure 12

CONFIDENTIAL

SECRET

THE EFFECTS OF OPERATING PROPELLERS ON AIRPLANE

STABILITY AND PERFORMANCE


By Robert M. Crane

Ames Aeronautical Laboratory

The use of turbine-propeller powerplants for high-performance airplanes, especially those designed for long-range operations at high subsonic speeds, has been suggested by many design studies made by the NACA and by other agencies. One deterrent to the development of such airplanes has been the imperfect knowledge of the effects of propeller operation on the low-speed stability and control and on the high-speed performance. While these power effects have had to be contended with in the past in the design of propeller-driven airplanes, there has been a hesitancy to apply the results of our past research to the case where the engine powers are greater by a factor of about 5 and the propeller disk loadings are increased by a factor of as much as 8. In order to achieve the high-speed performance desired of such airplanes, wing sweep is indicated and little if any knowledge has been available of the effect of a propeller slipstream on the flow over a swept wing at either high or low speeds.

It is the purpose of this paper to summarize some of the results obtained from NACA studies of the effects of propeller operation at large engine powers on the aerodynamic characteristics of a single-engine and of a multiengine swept-wing airplane including data at Mach numbers up to 0.90. The case of a twin-engine tractor installation on a straight-wing airplane has recently been reported in reference 1. Analysis of the wind-tunnel data for the cases of the swept-wing configurations is not yet complete, but certain trends are indicated which are felt to be of general interest.

The half-span powered model of a four-engine swept-wing airplane arrangement which was tested in the Ames 12-foot pressure wind tunnel is shown in figure 1. The wing has 40° of sweep and an aspect ratio of 10. The nacelles are located at 25 and 50 percent of the semispan and house electric motors driving single-rotation supersonic propellers. If the model is assumed to be 1/12 scale, the wing area is 2000 square feet, the propeller diameter is 14 feet, and the power conditions simulated at high Mach numbers are as large as 5000 horsepower per engine at an altitude of 40,000 feet or 20,000 horsepower per engine at sea level. A complete description of the model and the results of tests without operating propellers will be found in references 2, 3, 4, and 5.




In the following discussion of this airplane arrangement, the propeller thrust coefficient and the amount of engine power simulated are based on the measured thrust and efficiency of the propeller installed on an isolated nacelle and operating at the same propeller blade angle, advance ratio, Mach number, Reynolds number, and angle of attack as on the complete powered model. The propeller characteristics and the measured upwash at the propeller planes have been reported in references 6 and 7.

The effect of propeller operation on the static longitudinal stability at high Mach numbers can be seen from figure 2. On the left of the figure is the tail incidence required for trim as a function of Mach number and on the right is the tail incidence for trim as a function of normal acceleration at a Mach number of 0.80. Comparison is made between the condition of propellers operating at the power required for level flight at an altitude of 40,000 feet and the condition of propellers removed. Operation of the propellers is destabilizing as evidenced by the reduced variation of tail incidence with both Mach number and normal acceleration. These effects of propeller operation on longitudinal stability are small at these high speeds and the low-speed data must be examined to assess this particular factor.

Before the low-speed power effects on stability are discussed, however, there is another possible effect of propeller operation at high Mach numbers which should be examined. This is the effect of the propeller slipstream on the drag of the wing-nacelle-fuselage combination both as it affects the total drag and the Mach number for drag divergence. Since the velocity in the slipstream is higher than the free-stream velocity, some decrease might be expected in drag-divergence Mach number due to operating propellers. Figure 3 shows the variation with Mach number, at a lift coefficient of 0.40, of the increment in drag coefficient above its value at a Mach number of 0.70 for several different values of propeller thrust coefficient and with propellers removed. At a Mach number of 0.80, a T_c of 0.03 corresponds to 5000 horsepower per engine at 40,000 feet. The Mach number for drag divergence was little affected by operation of the propellers; but, at supercritical Mach numbers, the drag rise with increasing Mach number was reduced a considerable amount with increase in propeller thrust coefficient. This reduction is due, in part, to the fact that operating the propellers at a thrust coefficient as large as 0.03 increases the wing lift-curve slope about 10 percent. The same lift coefficient can thus be obtained at a lower angle of attack which tends to reduce the shock-induced separation on the outer portions of the wing for this airplane configuration.

Consider now the low-speed data on this same model. Figure 4 shows the variation of pitching-moment coefficient with lift coefficient for




the model with propellers removed and for two different power conditions: power required for level flight and 10,000 horsepower per engine. Lines of constant angle of attack are shown on the figure to indicate the large gains in lift-curve slope accompanying operation of the propeller. With the propellers absorbing 10,000 horsepower per engine, the negative slope of the pitching-moment curve has decreased a considerable amount compared with that for propellers off, indicating a decrease in the static longitudinal stability due to propeller operation and a corresponding decrease in the variation of stick position with airspeed. This condition of constant power corresponds to the case of a wave-off or balked landing and the power effects are much more destabilizing than for trimmed flight at a constant airspeed. For example, at any constant value of thrust, the decrease in stability due to propeller operation is only 25-percent of the decrease observed with full power.

The effects of propeller operation on longitudinal stability can be divided into four individual components which we can then study separately. These four components are the pitching moment due to propeller thrust, the pitching moment due to propeller normal force, the pitching moment due to slipstream on the wing, and that due to slipstream on the horizontal tail. Special consideration will be given to the condition of 10,000 horsepower per engine, since from the standpoint of longitudinal stability and control it is more critical than the condition of constant thrust. Some of the data shown in the subsequent figures are actual experimental data but a large part of the data is calculated from the measured power effects for the single airplane arrangement which was investigated. The scale to which the pitching moments are plotted in figures 5, 6, 7, and 8 has been expanded to show more clearly the individual power effects.

The pitching moment contributed by the propeller thrust is shown in figure 5. It is obvious that this moment contribution is proportional to the vertical distance from the thrust axis to the airplane center of gravity. This effect is shown for the three airplane arrangements noted in the figure. Since at a lift coefficient of 1.6 the propellers are producing over 50,000 pounds of thrust, this pitching moment increment can become quite large and destabilizing if the thrust axis is very far below the airplane center of gravity. The advantage of a high wing design in this respect is obvious.

The pitching-moment contribution due to propeller normal force is shown in figure 6. The magnitude of the propeller normal force is a function of the size and shape of the propeller and the propeller loading or thrust coefficient. Little control is possible over the magnitude of the normal force but the moment it produces can be controlled by changing the longitudinal distance from the propeller disks to the airplane center of gravity as shown in the figure. For the original model, propeller normal force was very destabilizing as indicated by the large positive




slope of ΔC_m against C_L . Moving the powerplants farther out along the span as shown by the other two airplane arrangements reduces this destabilizing moment to less than half its original value. Instead of moving the powerplants outward, the same effect can be achieved by moving the propellers closer to the wing leading edge.

The moment contribution due to propeller slipstream on the wing is shown in figure 7 for the original powerplant arrangement and for two alternate locations of the nacelles. The high disk loadings associated with the large power of the turboprop engine and the small diameter of the supersonic propeller make for extremely high dynamic pressures in the slipstream at low forward speeds. The incremental wing lift due to slipstream is thus quite large and, if the center of pressure of this lift increment is ahead of the center of gravity, a destabilizing pitching moment will result. This was the case for the original configuration with nacelles at 25 and 50 percent of the semispan. Moving the powerplants farther from the plane of symmetry permits this destabilizing moment to be reduced or made stabilizing as shown by the other two airplane arrangements in the figure.

The fourth moment contribution to be considered is the effect of the propeller slipstream on the flow at the horizontal tail. This effect may be stabilizing or destabilizing depending on the location of the tail with respect to the slipstream and the amount of lift being carried by the tail. The effect of vertical height of the horizontal tail for the model configuration under discussion is shown in figure 8. It would be expected that this slipstream contribution would depend to some extent on the mode of rotation of the propellers. Because the tests were made on a reflection-plane model, the conditions simulated are the same as if the airplane had right-hand propellers on the right wing and left-hand propellers on the left wing. Attempts to calculate this tail contribution and the effects of slipstream rotation on it have not been too successful. If the powerplants are moved further out along the span to reduce the destabilizing moments due to propeller normal force and slipstream on the wing, it may be that the slipstream will pass outboard of the horizontal tail and thus have little effect on its contribution to the airplane stability.

The effect of propeller operation on the longitudinal characteristics of the model with the flaps deflected is shown in figure 9. The flaps extended from the fuselage to the inner side of the outboard nacelle. As can be seen, the effects of propeller operation were extremely large and destabilizing. Also note the large increment in lift due to operation of the propeller. The largest single destabilizing contribution due to the propeller with the flaps deflected is that due to the slipstream on the wing and on the tail. Removing the portion of flap between the inner nacelle and the fuselage, as shown in figure 10, and adding a small-span flap outboard of the outer nacelle greatly reduces




the instability. For this case, the reduction in stability resulting from application of 10,000 horsepower per engine is about the same as for the original model with the flaps retracted. As was the case with flaps retracted, moving the powerplants outward will further reduce the destabilizing effect of power and in the extreme case a stabilizing effect can be obtained.

Reviewing the case of a four-engine, swept-wing tractor configuration it appears that power effects on longitudinal stability can be minimized by maintaining a high wing design, placing the powerplants fairly well out along the span, and keeping the propeller disk as close to the wing leading edge as propeller stress considerations will allow. An area-increasing or high-lift-producing flap so immersed in the slipstream that the center of pressure of its lift is ahead of the center of gravity should be avoided. A fairly small tail span in conjunction with an outboard nacelle location can be used to advantage to minimize the effect of the slipstream on the tail contribution to stability.

So far only the effects of power on the longitudinal characteristics have been discussed. The lateral disposition of nacelles indicated as desirable from the standpoint of longitudinal stability and control will make more critical the lateral and directional control following power failure. Additional study of this problem is required before the best airplane arrangement can be selected.

In addition to the study of the multiengine airplane configuration made at the Ames Laboratory, a similar investigation of a model of a single-engine tractor airplane has been made at low speed in the Langley 300 MPH 7- by 10-foot tunnel. The wing had 40° of sweepback and an aspect ratio of 3.5. A three-blade, single-rotation supersonic propeller was used and the power simulated on the model corresponds to 7000 horsepower on the airplane at sea level. The effects of power on the longitudinal characteristics are shown in figure 11. Note here that the comparison is for a condition of constant power with a condition of zero propeller thrust instead of with the propeller removed as in the previous figures. A large part of the propeller normal force is present at zero thrust so that the stability change will be somewhat less than if the propellers-off condition had been selected as a reference. As can be seen from the data in figure 11, operation of the propeller decreased the static margin but resulted in acceptable longitudinal stability characteristics. The large increase in lift due to operation of the propeller is noted in the figure.

This model was also tested with a horizontal tail mounted lower on the vertical tail as indicated by the dotted line on the airplane side view in figure 11. For this configuration, the model with the flaps retracted became longitudinally unstable for either power condition or with propeller off at a lift coefficient of about 0.80 and with the




flaps deflected became neutrally stable at a lift coefficient of about 1.0. In general the power-on longitudinal stability was largely dependent on the power-off characteristics of the model. Leading-edge chord extensions, slats, and wing fences which improved the power-off characteristics showed comparable improvements with the propeller operating.

The effects of operating propellers on the lateral and directional characteristics of an airplane of this type with a single-rotation propeller are particularly severe. This result is due primarily to the large amount of power being absorbed and not to the fact that it is a swept-wing airplane. For the subject model, full aileron deflection of $\pm 18^\circ$ and rudder deflection of -25° were not sufficient to balance the airplane in the take-off condition with full power.

Both of these deficiencies were in large part a result of using a single-rotation propeller. Because of the rotation in the slipstream, flow separation at the higher angles of attack was accelerated on the left wing behind the up-going propeller blade and was delayed on the right wing behind the down-going blade. This effect resulted in a large asymmetry of the separated flow and consequently a large rolling moment. Differential deflection of the wing flaps was found to provide an extremely powerful lateral control for the take-off condition and, in conjunction with the ailerons, was capable of balancing the airplane laterally at take-off up to angles of attack of about 15° . As the angle of attack was increased above 15° with take-off power, the roll-off became violent and uncontrollable. Extension of partial-span leading-edge slats increased the angle of attack at which lateral control could be maintained to slightly over 19° .

The inability of the rudder to balance the airplane directionally was largely a result of the flow angularity at the vertical tail brought about by slipstream rotation. A small triangular retractable fin behind the canopy, set at an angle of 10° to counteract the slipstream rotation, was found to be extremely effective in reducing the sidewash at the vertical tail. With the addition of this device and a moderate increase of rudder area, the airplane could be balanced directionally at take-off with sufficient excess rudder power to control the airplane in steady sideslips.

In summary, it appears that high powered turbopropeller powerplants can be mounted as tractor installations on swept-wing airplane without severe aerodynamic compromises. Compared to a turbojet airplane, the size of the vertical tail and rudder may have to be increased and the lateral control provided by conventional ailerons may have to be augmented in order to provide for control following power failure of a multiengine design or to provide control at take-off for a single-engine design with a single-rotation propeller. As a result of the theoretical work and the




CONFIDENTIAL

SECRET

7

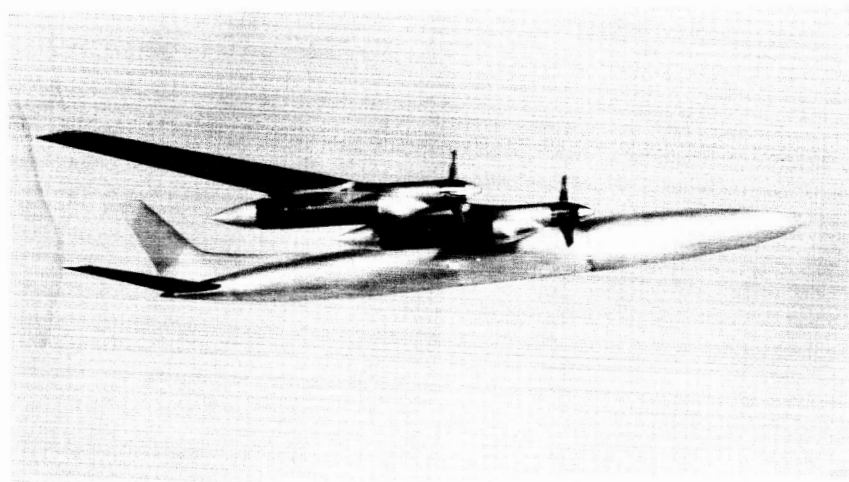
wind tunnel investigations now being made by the NACA of propeller-powered models, methods of computing the propeller effects are being studied and evaluated for power conditions representative of modern turboprop engines. These investigations are being extended to high subsonic Mach numbers and the airplane configurations under consideration are capable of flight at these high Mach numbers. In studies made to date, stability and control problems have been found to be greater only in degree from those previously encountered on conventional propeller-driven airplanes.

REFERENCES

1. Sleeman, William C. Jr., and Linsley, Edward L.: Low-Speed Wind-Tunnel Investigation of the Effects of Propeller Operation at High Thrust on the Longitudinal Stability and Trim of a Twin-Engine Airplane Configuration. NACA RM L52D04, 1952.
 2. Edwards, George G., Tinling, Bruce E., and Ackerman, Arthur C.: The Longitudinal Characteristics at Mach Numbers Up to 0.92 of a Cambered and Twisted Wing Having 40° of Sweepback and an Aspect Ratio of 10. NACA RM A52F18, 1952.
 3. Tinling, Bruce E.: The Longitudinal Characteristics at Mach Numbers Up to 0.9 of a Wing-Fuselage-Tail Combination Having a Wing With 40° of Sweepback and an Aspect Ratio of 10. NACA RM A52I19, 1952.
 4. Boltz, Frederick W., and Shibata, Harry H.: Pressure Distribution at Mach Numbers Up to 0.90 on a Cambered and Twisted Wing Having 40° of Sweepback and an Aspect Ratio of 10, Including the Effects of Fences. NACA RM A52K20, 1953.
 5. Tinling, Bruce E., and Lopez, Armando E.: The Effects of Nacelles and of Extended Split Flaps on the Longitudinal Characteristics of a Wing-Fuselage-Tail Combination Having a Wing With 40° of Sweepback and an Aspect Ratio of 10. NACA RM A53D06, 1953.
 6. Demele, Fred A., and Otey, William R.: Investigation of the NACA 1.167-(0)(03)-058 and NACA 1.167-(0)(05)-058 Three-Blade Propellers at Forward Mach Numbers to 0.92 Including Effects of Thrust-Axis Inclination. NACA RM A53F16. (Prospective NACA paper.)
 7. Lopez, Armando E., and Dickson, Jerald K.: The Effects of Compressibility on the Upwash at the Propeller Planes of a Four-Engine Tractor Airplane Configuration Having a Wing With 40° of Sweepback and an Aspect Ratio of 10. NACA RM A53A30a, 1953.
- 

CONFIDENTIAL

POWERED MODEL TESTED IN AMES 12-FOOT TUNNEL



NACA

Figure 1

EFFECT OF PROPELLERS AT HIGH SUBSONIC SPEEDS

40,000 ft, $\frac{W}{S} = 65$ lbs /sq ft

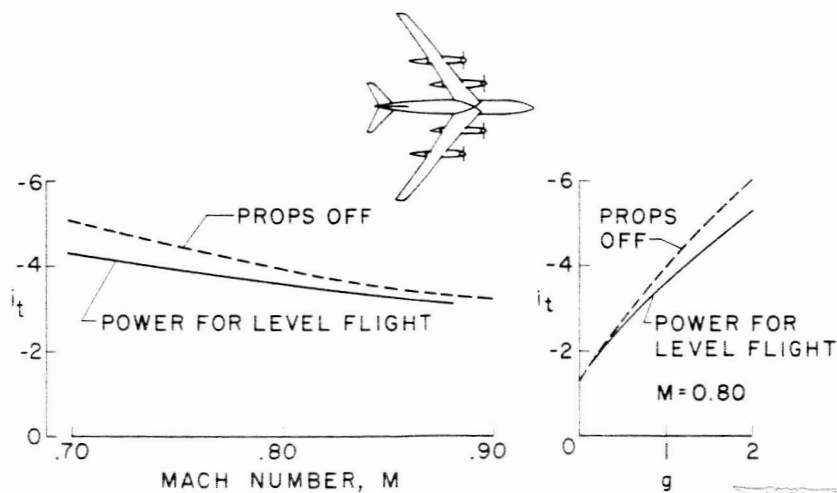


Figure 2

EFFECT OF PROPELLERS ON HIGH SPEED DRAG

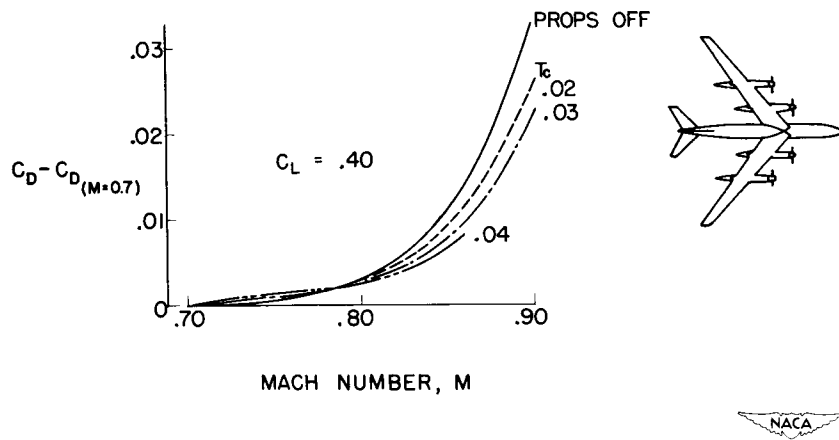


Figure 3

EFFECT OF PROPELLERS ON PITCHING MOMENT

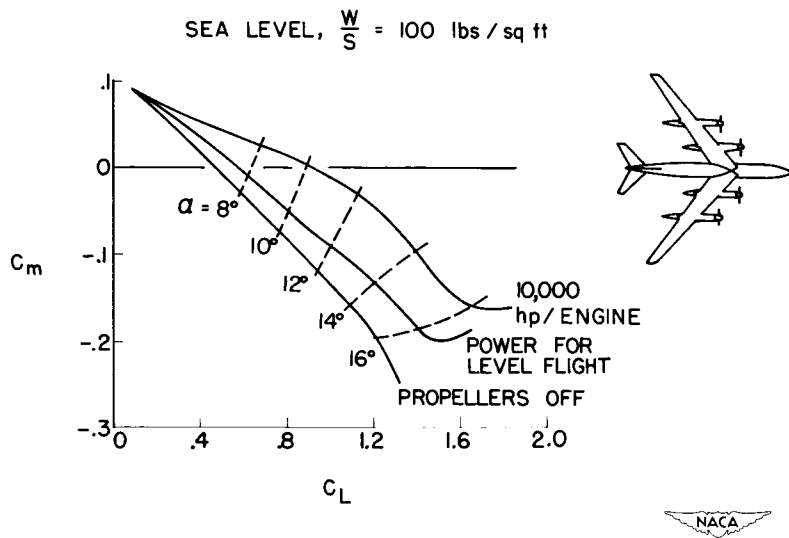


Figure 4

PITCHING MOMENT DUE TO PROPELLER THRUST

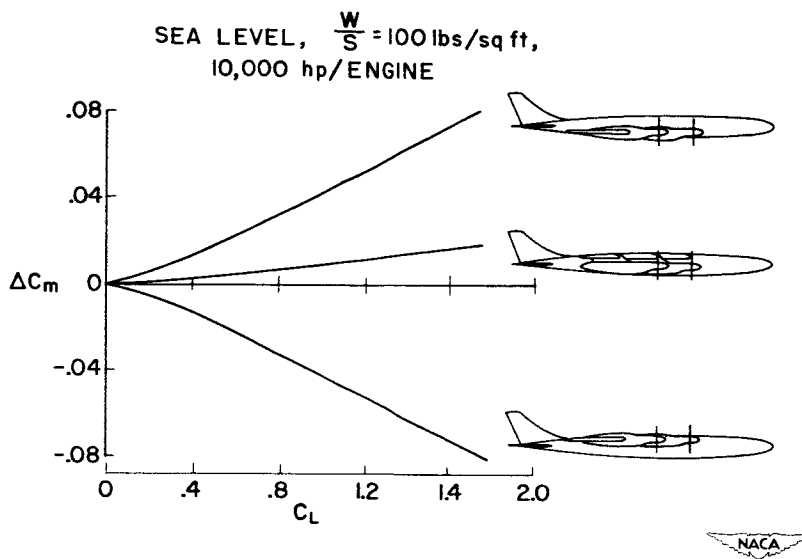


Figure 5

PITCHING MOMENT DUE TO PROPELLER NORMAL FORCE

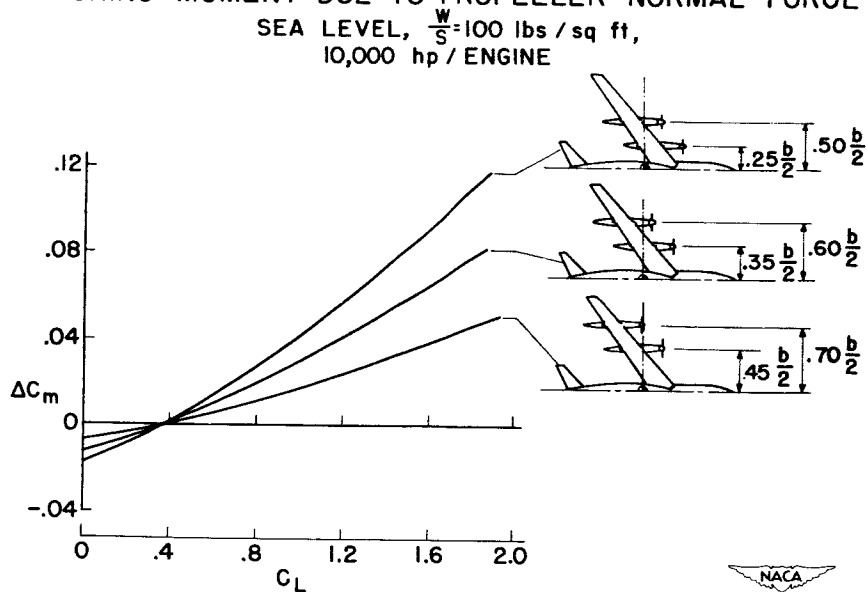


Figure 6

PITCHING MOMENT DUE TO SLIPSTREAM ON WING

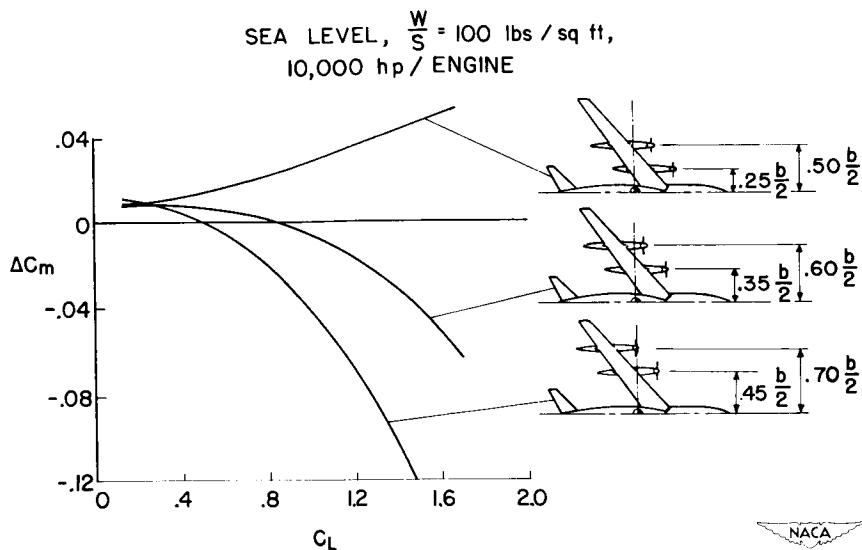


Figure 7

PITCHING MOMENT DUE TO SLIPSTREAM ON HORIZONTAL TAIL

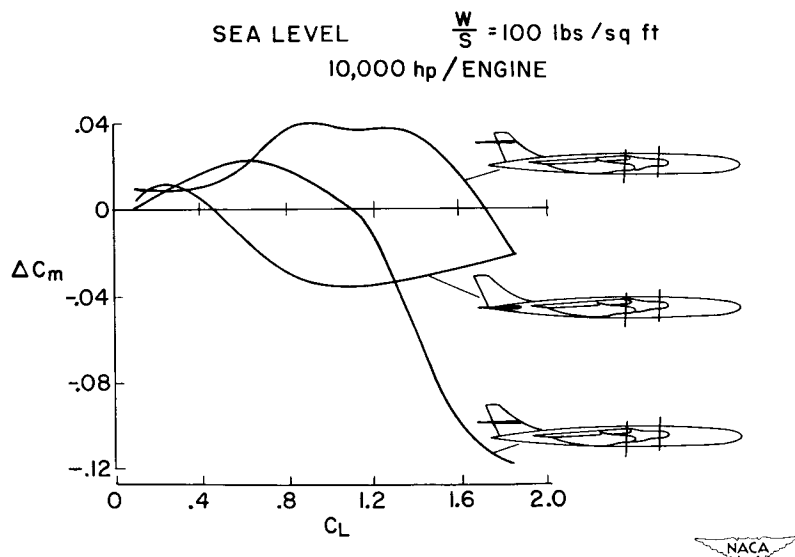


Figure 8

EFFECT OF PROPELLERS WITH FLAPS DEFLECTED 30°

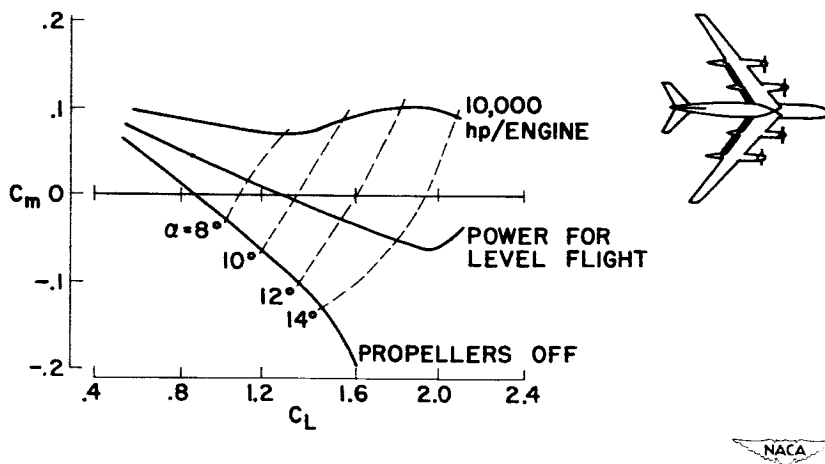
SEA LEVEL $\frac{W}{S} = 100 \text{ lbs/sq ft}$ 

Figure 9

EFFECT OF PROPELLERS WITH REVISED FLAP DEFLECTED 30°

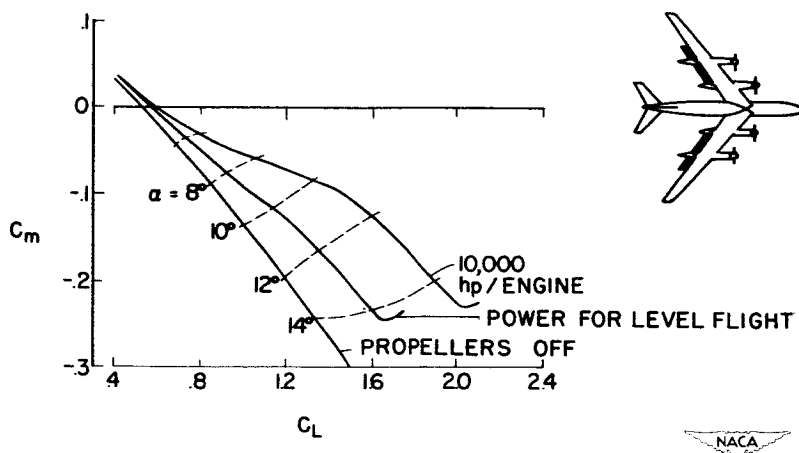
SEA LEVEL, $\frac{W}{S} = 100 \text{ lbs / sq ft}$ 

Figure 10

EFFECT OF PROPELLER ON PITCHING MOMENT

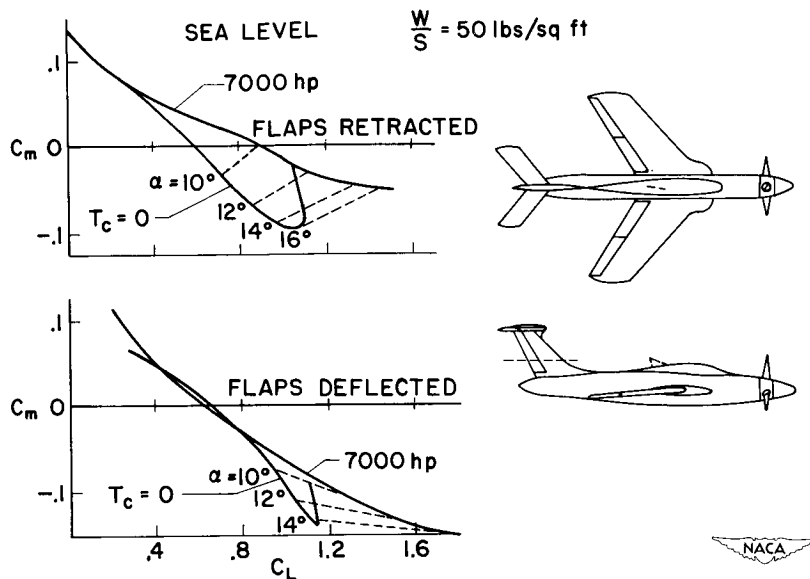


Figure 11

CONFIDENTIAL

SOME FREE-FLIGHT MEASUREMENTS OF TURBULENT SKIN FRICTION AND HEAT TRANSFER AT HIGH SUPERSONIC SPEEDS

By Alvin Seiff, Simon C. Sommer, and Barbara J. Short


Ames Aeronautical Laboratory

Turbulent skin friction has always been of interest to aircraft designers because of the large drag term which it represents. This remains true at high supersonic speeds, particularly for thin wings and slender bodies. However, there is another very important reason for interest in turbulent skin friction at high supersonic speeds, namely, the direct relation between skin-friction coefficient and heat-transfer coefficient which was first proposed by Osbourne Reynolds.

For these reasons, a large amount of experimental work has been done in recent years to define the variation of turbulent-skin-friction coefficient with Mach number. Some of the more recent data (refs. 1, 2, and 3), obtained by direct measurement of the skin-friction force, are shown in figure 1, where the ratio of skin-friction coefficient to the corresponding incompressible value is plotted against Mach number in the conventional manner. Several of the theories, including the original estimate of Von Kármán, agree reasonably well with the data but, as pointed out by Chapman, do not provide a sound basis for extending the data precisely beyond a Mach number of 4.5.

It should be emphasized that all these data were obtained at or near zero heat transfer, a condition that is not apt to occur in free flight at high supersonic speeds. The effect of large rates of heat transfer on these results is, therefore, a question of great practical importance. As the heat transfer is varied, a marked change in the boundary-layer temperature and density profiles occurs. The variation in skin friction with Mach number at zero heat transfer is primarily due to variation in the temperature and density profiles so it might well be expected that the skin friction will also vary with heat transfer.

Some theoretical estimates have been made of this effect. Of the theorists represented in the first figure, only Van Driest (ref. 4) has estimated the effect of heat transfer. However, Monaghan (ref. 5) has extended Cope's theory to include heat transfer and Clemmow (ref. 6) has applied the Von Kármán mixing length expression used by Wilson to the heat-transfer case. Also, Von Kármán's original method of estimating the Mach number effect (ref. 7), namely evaluating the density and viscosity in the incompressible-skin-friction formula at the wall temperature, can be readily applied to estimate the effect of heat transfer as can that of Tucker (ref. 8) who used the mean of wall temperature and



SEIFF, SOMMER
& SHORT


free-stream temperature for evaluating density and viscosity. Figure 2 shows these five estimates of the effect of heat transfer on skin friction at Mach numbers of 3.9 and 7.25. The ratio of skin-friction coefficient to the corresponding incompressible coefficient is plotted against the difference between recovery temperature T_r and wall temperature T_w divided by the temperature at the edge of the boundary layer T_1 , a parameter which is proportional to the heat-transfer rate.

There are several interesting things about these curves. First, all of the theories predict that the skin friction increases with increasing heat-transfer rate. But, they disagree as to how much, the rises ranging from just over 20 percent to more than 100 percent. Also, three of these estimates show, for the heat-transfer condition corresponding to equal wall temperature and free-stream temperature, no reduction in skin-friction coefficient with increasing Mach number.

The experiments which are the subject of this paper were conducted then for two reasons: to measure the turbulent skin friction under a condition of large heat transfer and to extend the Mach number range for which skin-friction data are available. The data were obtained in free flight using gun-launched, spin-stabilized models of the type shown in figure 3. The models were thin-walled tubes, flown with their axes parallel to the stream, with diameters of about $1\frac{1}{2}$ inches and wall thicknesses of 0.03 inch. The leading edges were symmetrically beveled with a half-angle of 10° . Figure 4 is a shadowgraph picture of a test model in free flight at a Mach number of 3.9. The shock patterns associated with the inside and outside flows can be seen, as well as the annular wake and the Mach waves produced by the turbulent boundary layer.

Tests were conducted at a Mach number of 3.9 by firing through still air at 1 atmosphere pressure and at a Mach number of 7.25 by firing upstream through a Mach number 2 air stream. The surface temperature rise during flight was estimated theoretically, assuming conservatively that the heat transfer occurred at the maximum initial rate. Temperature gradients within the model were accounted for. It was found that the temperature rise in the 1/100-second duration of the flight was 35° F. Thus, the wall-to-free-stream-temperature ratios were found to be 1.06 and 1.82 for the tests at $M = 3.9$ and 7.25, respectively. The calculated turbulent recovery temperatures at the two Mach numbers were 2000° R and 4000° R, indicating the large rates of heat transfer which occurred.

The test procedure was as follows. A test model and a tare model were fired under the same test conditions and their drag coefficients were computed from deceleration data. The difference in drag is, except for small correction terms, a measure of the skin friction of the aft part of the test model. Thus the tare model takes care of some of the



drag terms which are not susceptible to accurate calculation, including the drag of the boundary-layer trip, that of the laminar flow over the wedge and trip, and the base drag. Corrections were applied for the differences in base drag (using the data obtained by Chapman) and for the small differences in model geometry that inevitably occur. In this connection, an interesting point is that the leading-edge thickness, although always less than 0.001 inch, had to be measured very carefully, since differences of 0.0001 inch caused appreciable scatter at $M = 7.25$.

The matter of the boundary-layer trip was treated with great care in an effort to avoid artificial thickening of the turbulent boundary layer at the trip. Trip strength was varied until the least disturbance which caused turbulence to occur on or near the trailing edge of the roughened region was found. Transition was then assumed to occur at the trailing edge of the trip and the turbulent origin was estimated from theoretical considerations of the relative rates of growth of laminar and turbulent boundary layers. These considerations were then applied to the determination of the Reynolds number limits required in computing the incompressible skin friction. The Kármán-Schoenherr equation was used throughout in computing the incompressible friction.


The results of these experiments are shown in figure 5. The test point at $M = 3.9$ was obtained at a Reynolds number of 5×10^6 and is the mean of 12 results which had a root-mean-square deviation of 1.3 percent from the mean. At $M = 7.25$, tests were conducted at a Reynolds number of 5×10^6 , and the mean of 12 results obtained is the upper of two test points shown. Because of the reduced ratio of skin friction to total drag, a large scatter occurred, with values of the friction drag ranging from 0.3 to 0.4 of the total drag. Therefore, as a check, additional tests at a Reynolds number of 7.5×10^6 were run, and the mean of the six results then obtained agreed closer than was expected with the point at a Reynolds number of 5×10^6 , as shown by the two test points in the figure.

At $M = 3.9$, the present data lie 37 percent above the no-heat-transfer data. When plotted against heat-transfer rate as in figure 6, the data do not agree consistently with any of the theories. In addition to the test points shown for $M = 3.9$, an additional value of C_f/C_{f_1}

at an intermediate heat-transfer condition can be obtained from the data of figure 5 by interpolation, since the curve for $T_w/T_1 = 1.8$ must cross the zero-heat-transfer curve at $M = 2.1$. The interpolated value at $M = 3.9$ was used to define the shape of the dashed experimental curve which turns out to be qualitatively similar to that predicted by some of the theories.

Turning now to the question of turbulent heat transfer, it is well to start with some mention of Reynolds analogy, which has been the most powerful theoretical tool available in this field. This analogy states that the heat-transfer coefficient, when nondimensionalized with respect to the heat capacity, density, and velocity of the stream to form the Stanton number, is equal to one-half the skin-friction coefficient. Recent theoretical work by Rubesin (ref. 9) and others suggests that the ratio of Stanton number to skin-friction coefficient may be closer to 0.6 than one-half, but that this ratio is relatively unaffected by Mach number and Reynolds number. Within the limits of accuracy of this theory, the experimental skin-friction curves of figure 5 also represent the rate of fall of heat-transfer coefficient with increasing Mach number. But, it is very important to compare this prediction with experimental data. In the remainder of this paper, some free-flight experiments dealing with this question will be described, after which a collection of the available data will be shown.

In the aforementioned experiments, slender, fin-stabilized bodies of revolution of fineness ratio 30 were gun launched through still air at 1 atmosphere pressure at a Mach number of 3.2. The approximate temperature conditions of the flight were as follows: wall temperature, 540°R ; turbulent recovery temperature, 1500°R ; and $T_w/T_1 = 1.02$. The boundary layers were tripped by sand blasting the model tips and a flash interferometer picture was taken of the model in flight. One of the pictures obtained is shown as figure 7. The fringe shift in the boundary layer was about 0.6 of the fringe space and was carefully read by different observers with an accuracy of about 0.03 fringe. Refraction errors which plague two-dimensional boundary-layer interferometry were carefully calculated and found to be negligible because of the short path length in the disturbed flow. It was found that adjacent fringes did not give identical fringe shift data, but that the differences between fringes could be repeated within the scatter of measurement by different observers. These differences from fringe to fringe are believed due to spatial variations in the density distribution of the turbulent boundary layer. The fringe data were reduced to density distribution assuming axial symmetry, and the density data were converted to temperature data assuming uniform static pressure in the boundary layer. The data so obtained are shown at the left in figure 8. The large scatter is partly due to real differences between the fringes and partly due to errors in reading the fringes. The filled-in points were reduced from fringe measurements of a second observer and can be used as a measure of the scatter due to reading. The mean of the experimental data is plotted at the right and compared with the theory of Van Driest and with the Crocco equation relating temperature profile to velocity profile as applied to a $1/9$ th power velocity profile. An interesting feature of these profiles is that the cold wall holds the air temperature ratio below 1.4 whereas the recovery temperature ratio is 2.8. The recovery




temperature is not a good index of the maximum air temperature in the presence of a cold wall.

Very near the wall, the temperature ratio drops sharply to the wall value, 1.02. A suggestion of this reversal appears in the interferograms, but it is not detailed enough to permit measurements. The extent along y of this sharp temperature rise can be estimated from the heat-transfer coefficient, which gives the slope of the temperature profile at the wall as 1.2×10^6 OF/inch, at which rate the temperature would rise from the wall value to meet the curve at $y/\delta = 0.002$.

The temperature profile data can be used to estimate the average-heat-transfer coefficient by means of an energy-balance calculation analogous to the momentum-loss method of measuring skin friction. In this calculation, the kinetic energy lost by the model through the action of the skin-friction force is examined. Part of this energy appears as increased thermal and kinetic energy of the boundary-layer air, and the remainder appears as heat in the body. In evaluating the increased energy of the boundary layer, a velocity profile is required. To this


end, it was assumed that a law of the form $u/u_1 = (y/\delta)^{1/n}$ would hold and n was evaluated from the skin-friction and density-profile data in a momentum-loss integral. Values of n of 8.2 and 8.4 were calculated. Thus, it was possible to compute all of the energy terms and obtain the rate of heat input to the body. The results of this calculation are shown in figure 9, where the variation of Stanton number with Mach number is plotted. The experimental skin-friction curves presented earlier are replotted here and compared with collected heat-transfer data. The present data are represented by the two diamond points at a Mach number of 3.2 and should, if Reynolds analogy holds, compare with the upper curve. The wind-tunnel data of Pappas and Rubesin (ref. 10) and that of Fallis (ref. 11), being obtained near zero heat transfer, should compare with the lower curve. The measurements of Fischer and Norris (ref. 12) were made in free flight on the nose cone of a V-2 rocket. The temperature ratios were between 1.2 and 1.4 so the data should fall between the curves but closer to the upper one. The same is true of the data of Chauvin and deMoraes, obtained from free-flight tests of an NACA RM-10. (See ref. 13.) The data of Monaghan and Cooke (ref. 14) were obtained under hot-wall conditions, with the wall temperature well above the boundary-layer recovery temperature. They would therefore be expected to fall below the zero-heat-transfer curve. Within the limited framework of available data, it appears that there is a correlation between skin-friction and heat-transfer coefficients, both following the same trends with changing wall temperature.

It should be pointed out that the data shown here were modified from those originally given in three cases, namely, the experiments presented in references 11, 12, and 13. The principal modification was the




measurement of Reynolds number from the turbulent origin rather than the leading edge or nose. Determination of the transition point is one of the most uncertain factors in some of the experiments. An additional modification was required in the case of the V-2 experiments to correct the data from cone to flat plate using the theoretical correction of Van Driest.


In summary, theory and the present experiments indicate that a significant increase in turbulent-skin-friction coefficient occurs as the heat transfer is increased from zero toward values which may occur in free flight. Furthermore, the limited data now available indicate the correctness of Reynolds analogy as a means of estimating turbulent heat transfer.



REFERENCES

1. Chapman, Dean R., and Kester, Robert H.: Measurements of Turbulent Skin Friction on Cylinders in Axial Flow at Subsonic and Supersonic Velocities. Paper presented at 21st Annual Meeting, I.A.S. (New York), Jan. 26-29, 1953. (Preprint No. 391.)
 2. Coles, Donald, and Goddard, Frank E., Jr.: Direct Measurement of Skin Friction on a Smooth Flat Plate at Supersonic Speeds. Paper presented at Eighth International Congress on Theoretical and Applied Mechanics, Istanbul, Turkey, Aug. 22, 1952.
 3. Dhawan, Satish: Direct Measurements of Skin Friction. NACA TN 2567, 1952.
 4. Van Driest, E. R.: The Turbulent Boundary Layer for Compressible Fluids on a Flat Plate With Heat Transfer. Rep. No. AL-1006, North American Aviation, Inc., Feb. 20, 1950.
 5. Monaghan, R. J.: A Review and Assessment of Various Formulae for Turbulent Skin Friction in Compressible Flow. Tech. Note Aero. 2182, British R.A.E., Aug. 1952.
 6. Clemmow, D. M.: The Turbulent Boundary Layer Flow of a Compressible Fluid Along a Flat Plate. Rep. No. 50/6, Director of Guided Weapons Research and Development, Aug. 1950.
 7. Von Kármán, Th.: The Problems of Resistance in Compressible Fluids. Galcit Pub. No. 75, 1936. (From R. Accad. D'Italia, Cl. Sci. Fis., Mat. e Nat., vol. XIV, 1936.)
 8. Tucker, Maurice: Approximate Calculation of Turbulent Boundary-Layer Development in Compressible Flow. NACA TN 2337, 1951.
 9. Rubesin, Morris W.: A Modified Reynolds Analogy for the Compressible Turbulent Boundary Layer on a Flat Plate. NACA TN 2917, 1953.
 10. Pappas, Constantine C., and Rubesin, Morris W.: Heat Transfer in the Compressible Turbulent Boundary Layer on a Flat Plate. Heat Transfer and Fluid Mechanics Institute, U.S.C., Los Angeles, June 1953.
 11. Fallis, W. B.: Heat Transfer in the Transitional and Turbulent Boundary Layers of a Flat Plate at Supersonic Speeds. Rep. No. 19, Univ. of Toronto, Institute of Aerophysics, May 1952.
 12. Fischer, W. W., and Norris, R. H.: Supersonic Convective Heat-Transfer Correlation From Skin-Temperature Measurements on a V-2 Rocket in Flight. Trans. A.S.M.E., vol. 71, no. 5, July 1949, pp. 457-469.
- 

CONFIDENTIAL

13. Chauvin, Leo T., and deMoraes, Carlos A.: Correlation of Supersonic Convective Heat-Transfer Coefficients From Measurements of the Skin Temperature of a Parabolic Body of Revolution (NACA RM-10). NACA RM L51A18, 1951.
 14. Monaghan, R. J., and Cooke, J. R.: The Measurement of Heat Transfer and Skin Friction at Supersonic Speeds. Part III - Measurements of Overall Heat Transfer and of the Associated Boundary Layers on a Flat Plate at $M_1 = 2.43$. Tech. Note Aero. 2129, British R.A.E., Dec. 1951.
 15. Van Driest, E. R.: Turbulent Boundary Layer on a Cone in a Supersonic Flow at Zero Angle of Attack. Jour. Aero. Sci., vol. 19, no. 1, Jan. 1952, pp. 55-57, 72.
- 

EFFECT OF MACH NUMBER ON TURBULENT SKIN - FRICTION AT ZERO HEAT TRANSFER

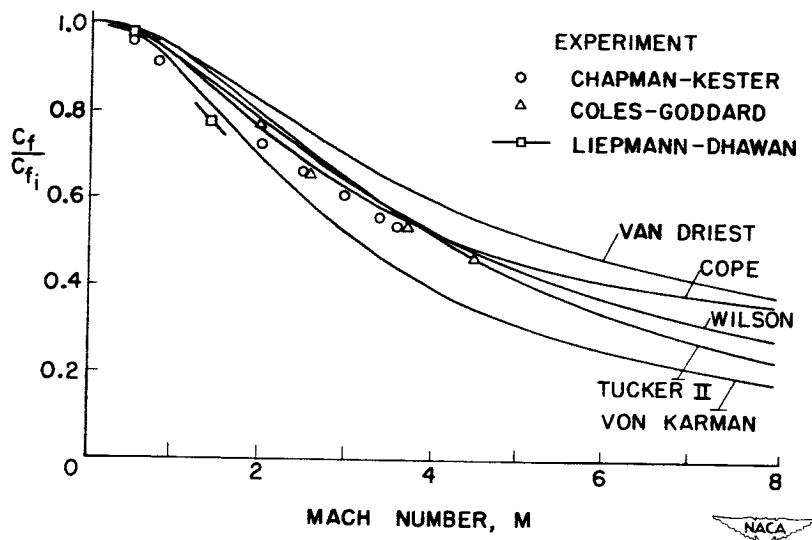


Figure 1

PREDICTED EFFECT OF HEAT TRANSFER ON SKIN FRICTION

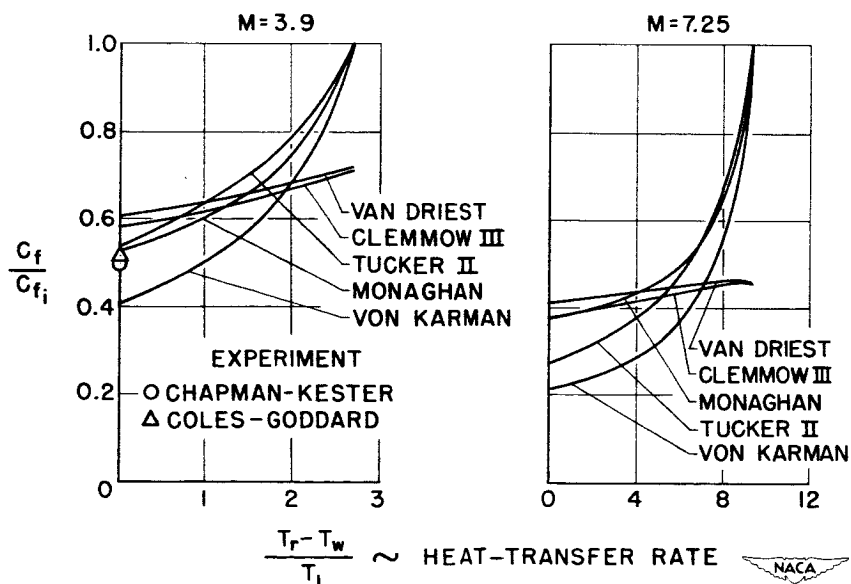


Figure 2

MODELS

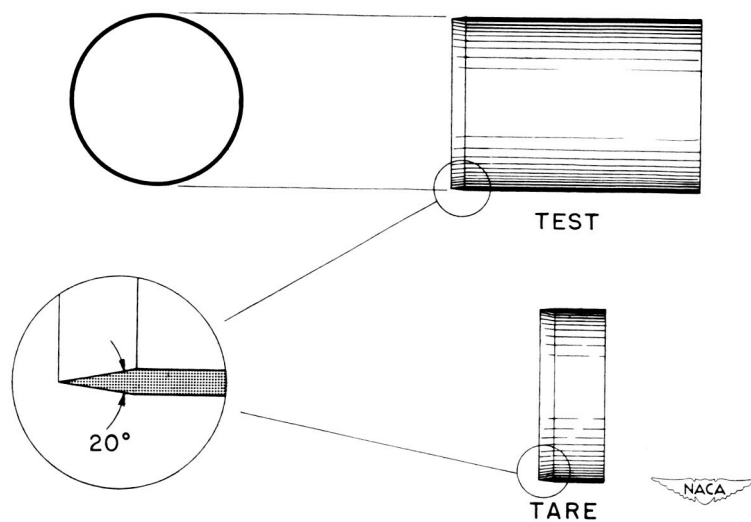


Figure 3

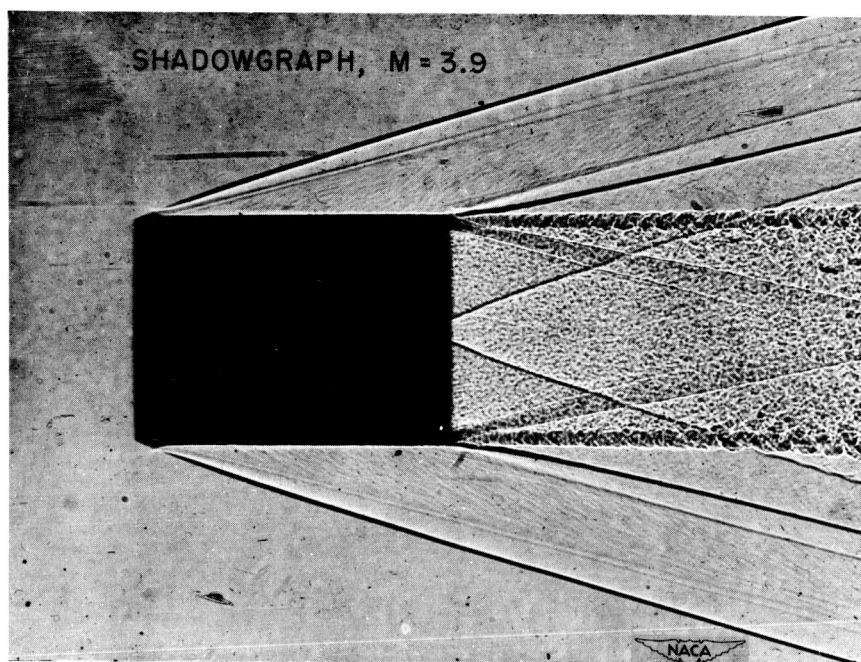


Figure 4

PRESENT DATA COMPARED WITH ZERO-HEAT-TRANSFER DATA

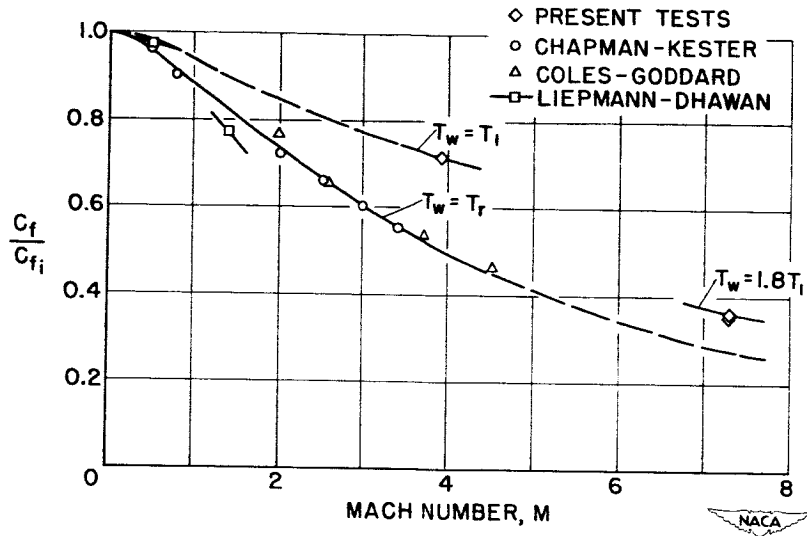


Figure 5

COMPARISON OF DATA WITH THEORETICAL EFFECT OF HEAT TRANSFER

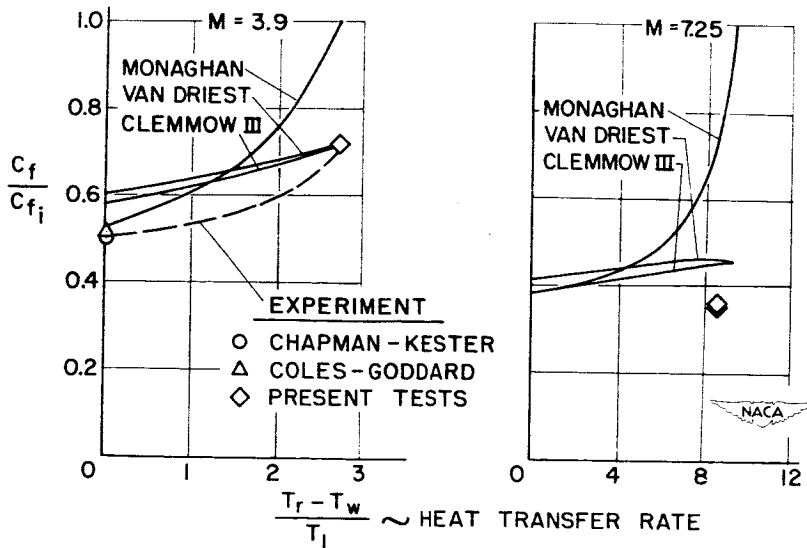


Figure 6

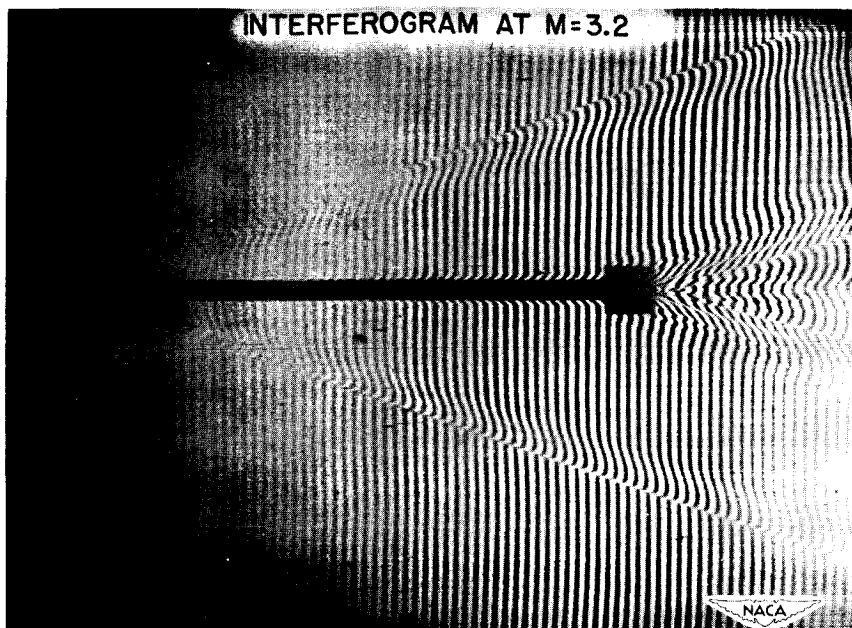


Figure 7

TEMPERATURE PROFILES IN TURBULENT
BOUNDARY LAYER

M = 3.2

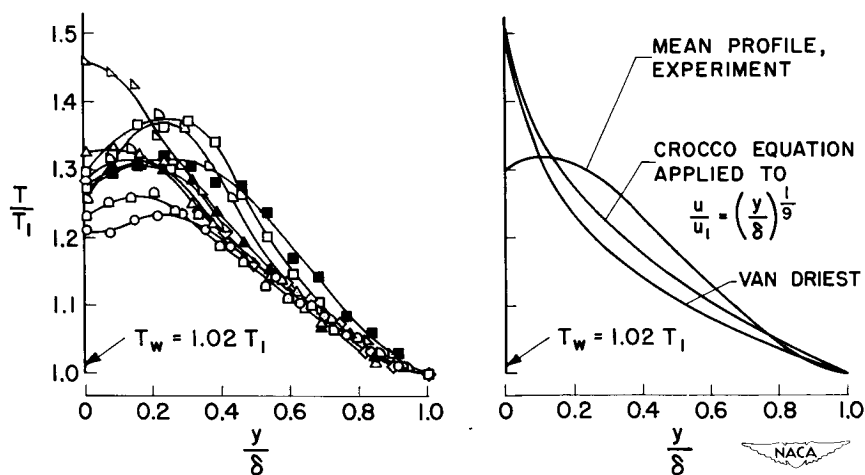


Figure 8

VARIATION OF HEAT-TRANSFER COEFFICIENT WITH MACH NUMBER

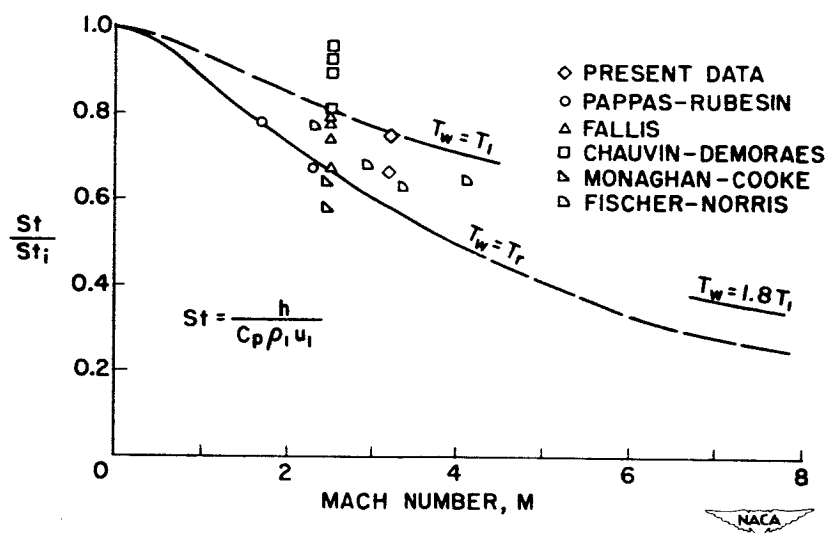


Figure 9

CONFIDENTIAL

FACTORS AFFECTING TRANSITION AT SUPERSONIC SPEEDS


By K. R. Czarnecki and Archibald R. Sinclair

Langley Aeronautical Laboratory

With the advent of flight at supersonic speeds there has been renewal of interest in the subject of boundary-layer transition. Whereas experience has shown that extensive runs of laminar flow cannot be obtained under practical field operating conditions at subsonic speeds, both theory and practical considerations indicate a more favorable outlook at supersonic speeds. For example, it has been demonstrated that longer runs of laminar flow can be obtained by cooling the boundary layer and that the cooling can be obtained by taking advantage of the natural heat capacity of a missile, at least in the initial phases of the flight. Also, since the missile is intended to make but a single flight, the construction and maintenance of a smooth surface is simplified. Further, such large reductions in drag and aerodynamic-heating rate are possible with laminar flow that reexamination of the problem of transition is imperative. This paper surveys the available material to summarize what is known to date about boundary-layer transition at supersonic speeds.

The bulk of our current information on supersonic transition comes from wind tunnels. As in subsonic tunnels, the transition results obtained are critically dependent on the quality of the airstream. It is necessary, therefore, in any analysis of tunnel transition data to first ascertain whether the results are unduly affected by wind-tunnel disturbances. Indications have been found that supersonic transition data are affected by local shocks and angularity of the tunnel airstream as well as by turbulence level. Because it is difficult to evaluate the quality of supersonic tunnel flows by direct measurement of these factors, the NACA is conducting comparative transition tests with zero heat transfer on a particular body shape, a 10° cone, in many of its supersonic facilities. In figure 1 are shown some of the results obtained to date. The Reynolds number of transition R_t based on distance from the nose, is plotted against M and also against R per foot. Both abscissas are used here simply to define the test conditions and not to indicate that they are significant parameters affecting transition.

This figure is presented only to show the wide range of transition Reynolds numbers obtained in different tunnels under comparable test conditions and hence the wide variation in the quality of the airstreams in these wind tunnels. Some of the facilities have sufficiently small disturbances to permit extensive laminar flows, for example, the Langley 9-inch and 4-foot supersonic tunnels.


CZARNECKI
& SINCLAIR

In the remainder of this paper the bulk of the tunnel data used are from these two tunnels having the high transition Reynolds numbers. In addition, transition data from model flight tests in still air at the U.S. Naval Ordnance Laboratory and at the Ames Aeronautical Laboratory are used.

The effect of Mach number on transition on smooth bodies at supersonic speeds is considered in figure 2. The data presented at the lower Mach numbers, $M = 5$ or less, are for zero or essentially zero heat transfer. The data at the higher Mach numbers include some boundary-layer cooling. The point at $M = 0$ is the transition Reynolds number for a flat plate at low speeds for a wind-tunnel turbulence level of less than 0.1 percent (ref. 1). For the lower Mach number tests, R_t generally corresponds to transition at the model base, hence there are no changes in pressure gradient to be considered. The arrow at $M = 5.8$ (data from ref. 2), incidentally, indicates that the exact value of R_t is not known but is greater than the value plotted.

In general, the results in figure 2 for M less than 5 indicate a decrease in R_t with increasing Mach number except for the cone-cylinder when M is less than 2. It may be remarked here that the rate of decrease in transition Reynolds number with increase in Mach number may be affected somewhat by changes in tunnel-flow characteristics that occur with changes in test section Mach number. From these data one might expect to obtain very little laminar flow at higher Mach numbers and this was the picture until recently. Recent hypersonic wind-tunnel results, however, show the relatively high values of R_t indicated by the points for $M \approx 6$ and 7. These relatively high values of R_t are believed to be due partly to favorable heat-transfer effects which may usually be expected at hypersonic speeds and partly to favorable shock—boundary-layer interactions at the nose of the models which result in a favorable local pressure gradient (ref. 3). The important conclusion that can be drawn is that values of R_t of the same order of magnitude as those obtained at low supersonic speeds can be obtained in practical cases at hypersonic speeds.

Figure 3 shows the effect of surface pressure gradient on smooth bodies at a Mach number of 1.61. The sketches in the upper part of the figure indicate the types of bodies tested and their pressure distributions. The curves in the lower part of the figure are a plot of the measured skin friction based on wetted-surface area. At the point where the experimental skin-friction curve leaves the theoretical laminar curve, transition has appeared at the base of the body and is beginning to move forward.



CONFIDENTIAL


The results indicate that the parabolic body with a moderately favorable pressure gradient over the length of the body had the largest value of R_t , about 11×10^6 . The cone-cylinder with the least amount of favorable pressure gradient showed the lowest value, about 2.75×10^6 . From these results, it is apparent that pressure gradient has a strong effect on transition at the lower supersonic Mach numbers just as at subsonic speeds. In order to obtain high values of R_t , it is apparently desirable to maintain a favorable pressure gradient where the boundary layer is most susceptible to instability - in these tests a favorable pressure gradient toward the rear of the body. Regions to the left of the curves indicate either a theoretically stable or experimentally laminar boundary layer. At higher test Reynolds numbers, when transition has moved forward on the bodies, both the ogive-cylinder and cone-cylinder show larger runs of laminar flow than the parabolic body because of the more favorable pressure gradients on the ogive or at the cone shoulder.

Some additional results showing the effects of pressure gradient are presented in figure 4. In this case the pressure gradient was altered by changing the shape of the body progressively from that shown at the upper left to that at the upper right. The transition results are plotted against the ratio of base area to maximum cross-sectional area, which is a rough index of the increase in length of favorable pressure gradient. It may be noted that increasing the run of favorable pressure gradient resulted in a reduction in the rate of falling pressure. Transition in these tests always occurred at the base.

The results indicate a large increase in R_t with increase in length of favorable pressure gradient at both Mach numbers investigated. The reverse in the curves at the lowest area ratio is due to laminar separation at the model base. The reason for the discontinuity in the Mach number 1.93 curve near $A_{\text{base}}/A_{\text{max}} = 0.7$ is not known.

An analysis of the data from which the curves of figures 3 and 4 were obtained and of other results available at supersonic speeds shows a tendency for the favorable effects of a falling pressure to decrease as the boundary layer becomes thin as near the nose of a body or at very high test Reynolds numbers. In addition, theoretical calculations by Lees (ref. 4) and by Weil (ref. 5) predict a decrease in the effects of pressure gradient as M is increased; although, as yet, there is no reliable experimental verification.

The possibility of a large stabilizing effect due to cooling of the laminar boundary layer at supersonic speeds in the case of the Tollmien-Schlichting type of boundary-layer instability was predicted theoretically in the well-known work of Lees in 1947 (ref. 6). Recent studies, particularly those in the Langley 4- by 4-foot supersonic pressure tunnel



CONFIDENTIAL

(refs. 7 and 8) and in flight (ref. 9), have confirmed the existence of this effect. In figure 5, the chart on the right compares the theoretical effect of heat transfer on the stability of the boundary layer on a flat plate (ref. 10) with the experimental effect of heat transfer on transition on the RM-10 parabolic body. The parameter R_t is plotted against T_w/T_∞ , the ratio of wall temperature to free-stream temperature. At a value of this ratio of 1.05 theory indicates that the boundary layer will be stable for all Reynolds numbers. The trends of the curves are in good agreement. A part of the displacement between curves occurs because of the comparison between two- and three-dimensional bodies, a part because of the additional length of surface required for the disturbance in the boundary layer to amplify sufficiently to break down the laminar flow, and another part because of the favorable pressure gradient on the body. The highest value of R_t obtained in the tunnel tests was about 28.5×10^6 (ref. 8). The highest value of R_t measured to date with cooling is about 90×10^6 and was obtained at White Sands Proving Ground in flight on the conical nose of a V-2 rocket (ref. 9). Thus, if transition can be limited to the apparently Tollmien-Schlichting type, boundary-layer cooling will be of great aid in obtaining long runs of laminar flow.

In the chart on the left the experimental results for the parabolic body have been replotted against $\Delta T/T_{stag}$, an index of the amount of heating or cooling relative to the stagnation temperature. In addition are shown some results typical of the earlier experiments in other wind tunnels in which low adiabatic transition Reynolds numbers were obtained.

An analysis of the results shows that when the transition Reynolds number for zero heat transfer is low, the effects of heat transfer are small, and, when R_t for the adiabatic case is high, the effects of heat transfer are large. The low effectiveness of heat transfer on transition in the earlier tests is usually derived from the fact that transition is generally influenced by surface roughness, boundary-layer separation due to adverse pressure gradients, or tunnel effects. These types of transition do not appear to be strongly influenced by heat transfer.

Because of its importance, the next type of transition to be studied is that due to surface roughness. In figure 6 is presented a plot of $R_t/R_{t_{k=0}}$, the ratio of Reynolds number of transition with single-element surface roughness to Reynolds number of transition for a smooth body, against the parameter k/δ_k^* , the ratio of roughness height to boundary-layer displacement thickness at the roughness. The solid line is the low-speed correlation obtained by Dryden (ref. 1) on the basis of transition data for Reynolds numbers less than 2×10^6 . For this case, the


results show that for a roughness-height ratio of less than 0.1 single-element surface roughness has no effect on transition. Results for bodies having values of R_t greater than 2×10^6 do not extend to sufficiently low values of $k/\delta^*_{k_1}$ to establish the validity of this conclusion for cases with longer runs of laminar flow.

Only one approximate point is available for plotting for the supersonic speeds. This point indicates a somewhat higher value of roughness ratio required to effect transition than in the subsonic case, but the point may be within the range of scatter obtained in the subsonic correlation. A somewhat larger amount of data is available for comparison with subsonic results if the Reynolds number for transition itself is plotted against roughness ratio as is indicated by the chart on the left in figure 7. The three data points for the parabolic body at $M = 1.61$ appear to fall within the same range as the low-speed airfoil data for similar single-element roughness. The steep rise in R_t as the roughness ratio is reduced in the supersonic case compares closely to the trends obtained at high Reynolds numbers of transition subsonically.

In the chart on the right is presented a plot of R_t against the parameter $\frac{k}{\delta}$ for distributed surface roughness on an ogive-cylinder body. When the roughness is distributed over an area it is not clear what value of boundary-layer thickness should be used as an index of the roughness effect; hence, an arbitrary value of boundary-layer thickness, δ for $R = 10^6$, was chosen for this chart. The tests were made with a wall-to-free-stream temperature ratio of about 1.04, thus indicating that the tests were within the region for infinite Tollmien-Schlichting boundary-layer stability for a flat plate. The results show trends similar to those determined for single-element roughness. Other preliminary data indicate that, for equivalent roughness heights, transition will occur at lower Reynolds numbers for distributed roughness than for single-element roughness when the leading edges of the roughnesses are at the same location.

An investigation of effects of heat transfer on transition due to roughness was made on the parabolic body at $M = 1.61$ (refs. 7 and 8) but few of the data were susceptible to the present type of analysis. A study of the trends, however, shows that the effect of heat transfer on the critical roughness parameter may be small. In particular, however, the results showed that whenever transition was significantly affected by surface roughness or, for that matter, by any other type of finite disturbance, then boundary-layer cooling was ineffective in extending the length of the laminar run.

If the results that have been presented on surface roughness are interpreted to mean that the Mach number effects on the correlations




are small, then for constant Reynolds number the allowable roughness height before transition is effected should increase with Mach number because of the growth of boundary-layer thickness with Mach number. At $M = 5$ the allowable roughness should be increased by 2.5 and at $M = 10$ by a factor of 6 (fig. 8, left plot).

In addition, as the altitude is increased or the pressure decreased, the molecular mean free path becomes relatively large compared to the protuberance height and continuum flow will not exist and the effects of surface roughness may conceivably disappear. Calculations indicate that for all cases where surface roughness effects could be detected the roughness was considerably greater than 100 times the length of the molecular mean free path (fig. 8, right plot). The calculations also show that, even on the basis of this criterion, the allowable surface roughness will be greater than 200 microinches at 100,000 feet and 7000 microinches, or 0.007 inch, at 200,000 feet altitude. The shaded area in figure 8 indicates the usual range of maximum surface roughness encountered on wind-tunnel and flight-test models.

Up to now all data that have been presented have been for bodies only and for zero angle of attack. Airplanes and missiles, however, usually have wings and fly at some angle of attack. There are insufficient data on wing transition to present any type of correlation; hence, this phase will not be discussed. Figure 9, however, has been prepared to show the effect of α on R_t for two bodies, each at a different Mach number. The tests of the parabolic body were made in a wind tunnel without heat transfer and transition was obtained from force tests and boundary-layer surveys. The results thus correspond to transition at the base of the body. The tests of the slender ogive-cylinder were made in the Ames free-flight tunnel and include a large amount of cooling. In this case transition was obtained by means of shadowgraph studies and is shown for the upper surface only since this is the more critical surface. The latter tests were also limited to a Reynolds number of 11×10^6 .

Both sets of data, which include differences in Mach number and heat-transfer conditions, indicate similar trends: a decrease in R_t as α is increased. For the parabolic body, a change in α from 0° to 2° reduces R_t by 60 percent. Both curves are not too well defined for α less than 1° , but the trends appear to indicate that transition will be sensitive to α even at very low angles.

In conclusion, first, boundary-layer transition should be of the Tollmien-Schlichting type if favorable effects of pressure gradient and heat transfer are to be realized. Maximum transition Reynolds numbers of about 28×10^6 in wind-tunnel tests of a parabolic body and 90×10^6




CONFIDENTIAL

SECRET

in flight tests of a cone have been obtained with boundary-layer cooling. The effects of surface roughness at supersonic speeds appear similar to those at subsonic speeds, and the allowable-roughness-height parameters are of about the same magnitude as at subsonic speeds. Hence, to avoid transition due to roughness, the roughness size should be limited to about $1/10$ the boundary-layer displacement thickness. Finally, for the longest possible runs of laminar flow, the body should be closely aligned with the flow.

[REDACTED]

REFERENCES

1. Dryden, Hugh L.: Laminar and Turbulent Flows and Heat Transfer. Laminar and Turbulent Flows. Transition From Laminar to Turbulent Flow. Vol. IV of High Speed Aerodynamics and Jet Propulsion, pt. 1, D, Aeronautics Publication Program, Princeton Univ.
 2. Nagamatsu, Henry T.: Hypersonic Wind Tunnel Bimonthly Progress Summary - December 1, 1952 to February 1, 1953. GALCIT Memo. Army Ordnance and Air Force Contract No. DA-04-495-Ord-19.
 3. McLellan, Charles H.: Exploratory Wind-Tunnel Investigation of Wings and Bodies at $M = 6.9$. Jour. Aero. Sci., vol. 18, no. 10, Oct. 1951, pp. 641-648.
 4. Lees, Lester: Stability of the Supersonic Laminar Boundary Layer With a Pressure Gradient. Rep. No. 167, Princeton Univ., Aero. Eng. Lab., Nov. 20, 1950.
 5. Weil, Herschel: Effects of Pressure Gradient on Stability and Skin Friction in Laminar Boundary Layers in Compressible Fluids. Jour. Aero. Sci., vol. 18, no. 5, May 1951, pp. 311-318.
 6. Lees, Lester: The Stability of the Laminar Boundary Layer in a Compressible Fluid. NACA Rep. 876, 1947. (Supersedes NACA TN 1360.)
 7. Czarnecki, K. R., and Sinclair, Archibald, R.: Preliminary Investigation of the Effects of Heat Transfer on Boundary-Layer Transition on a Parabolic Body of Revolution (NACA RM-10) at a Mach Number of 1.61. NACA RM L52E29a, 1952.
 8. Czarnecki, K. R., and Sinclair, Archibald, R.: An Extension of the Investigation of the Effects of Heat Transfer on Boundary-Layer Transition on a Parabolic Body of Revolution (NACA RM-10) at a Mach Number of 1.61. NACA RM L53B25, 1953.
 9. Sternberg, Joseph: A Free-Flight Investigation of the Possibility of High Reynolds Number Supersonic Laminar Boundary Layers. Jour. Aero. Sci., vol. 19, no. 11, Nov. 1952, pp. 721-733.
 10. Van Driest, E. R.: Calculation of the Stability of the Laminar Boundary Layer in a Compressible Fluid on a Flat Plate With Heat Transfer. Jour. Aero. Sci., vol. 19, no. 12, Dec. 1952, pp. 801-812.
- 

COMPARISON OF WIND-TUNNEL TRANSITION
RESULTS ON 10° CONE

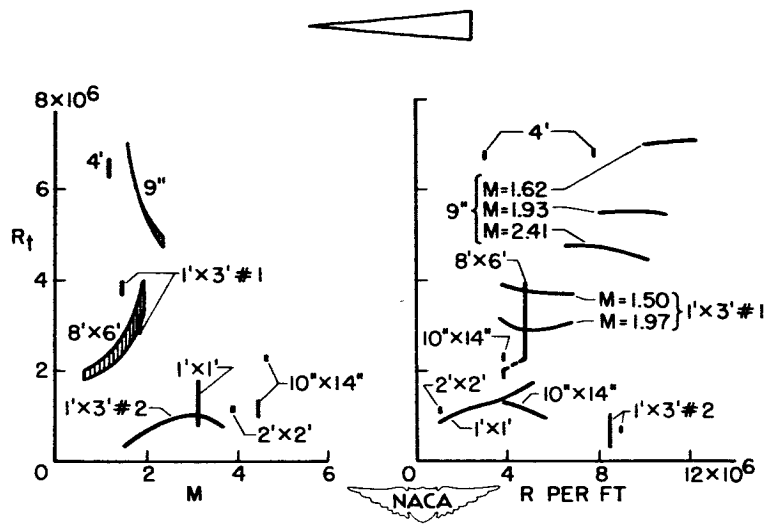


Figure 1

EFFECT OF MACH NUMBER ON TRANSITION

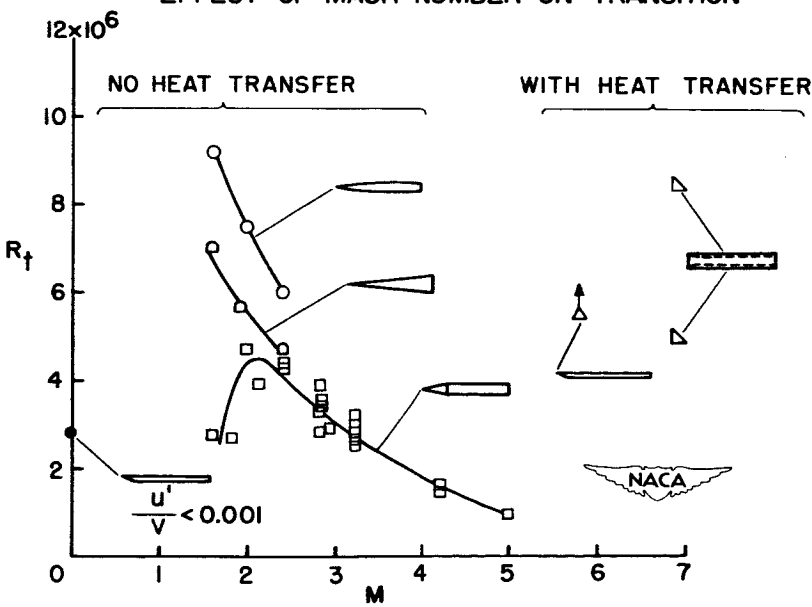


Figure 2

EFFECT OF PRESSURE GRADIENT ON TRANSITION

$M=1.61$; $L/D=12.2$; $\alpha=0^\circ$; NO HEAT TRANSFER

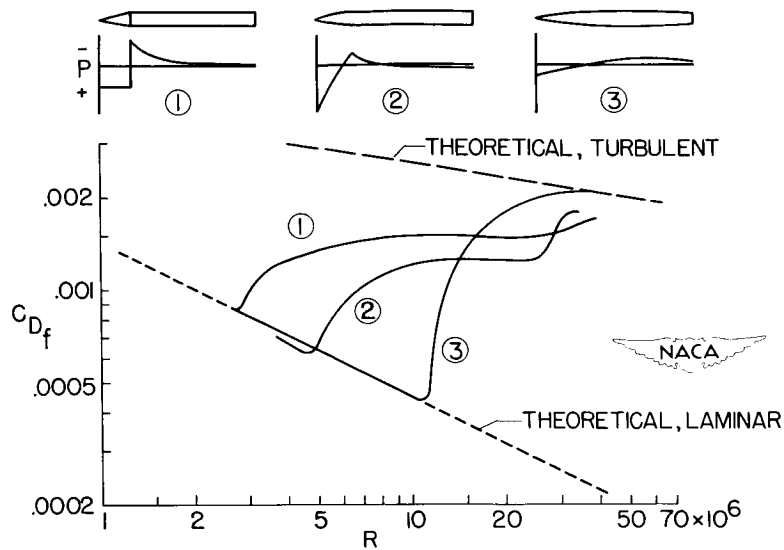


Figure 3

EFFECT OF PRESSURE GRADIENT ON TRANSITION

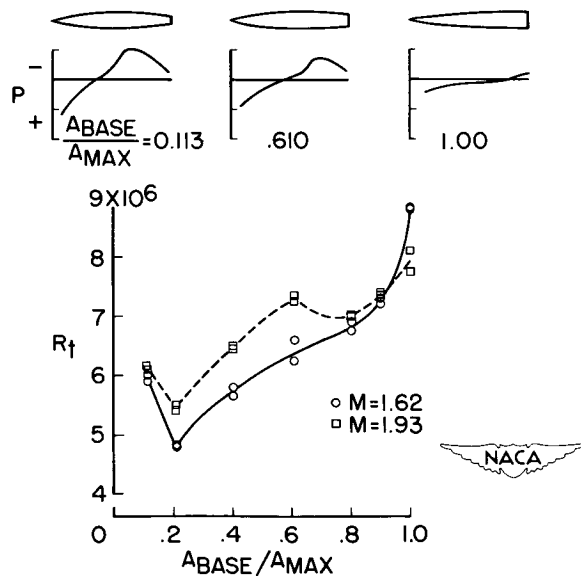


Figure 4

EFFECT OF HEAT TRANSFER ON TRANSITION

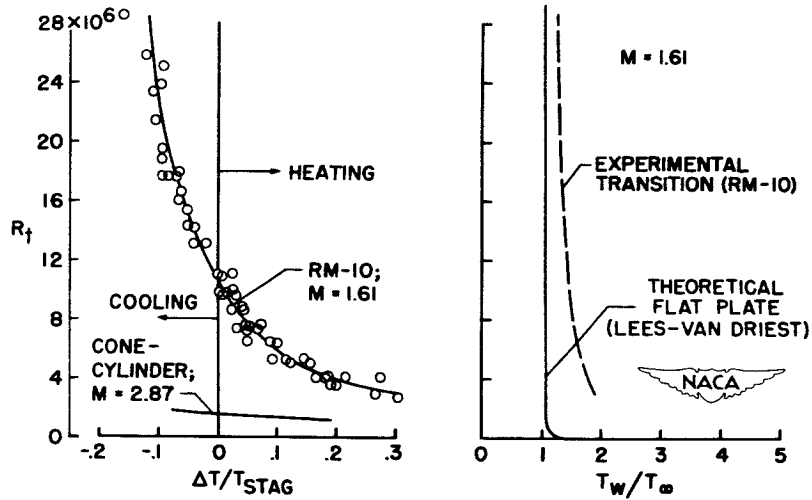


Figure 5

COMPARISON OF ROUGHNESS EFFECTS AT SUBSONIC AND SUPERSONIC SPEEDS NO HEAT TRANSFER

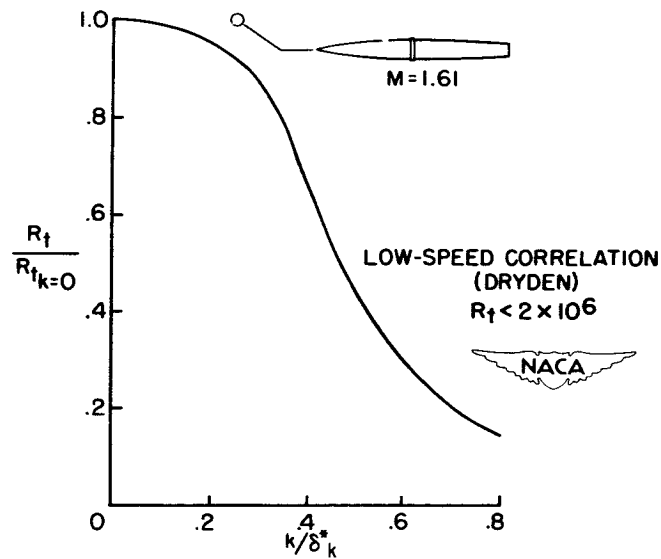


Figure 6

EFFECT OF ROUGHNESS ON TRANSITION AT SUPERSONIC SPEEDS

SINGLE-ELEMENT ROUGHNESS

DISTRIBUTED ROUGHNESS

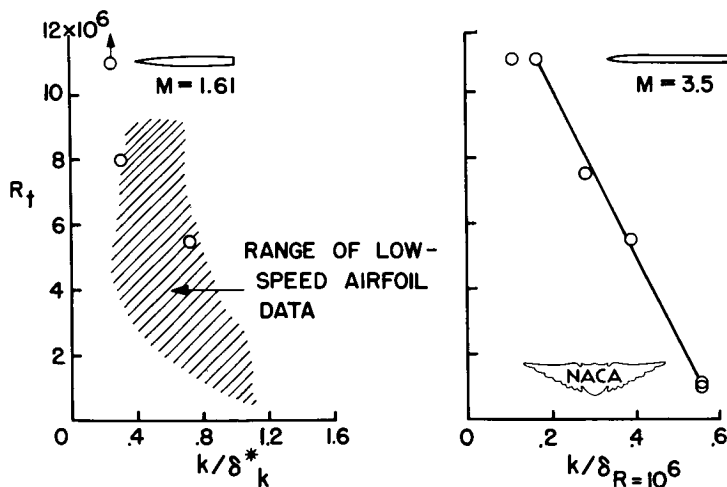


Figure 7

EFFECT OF MACH NUMBER AND ALTITUDE ON TRANSITION DUE TO ROUGHNESS

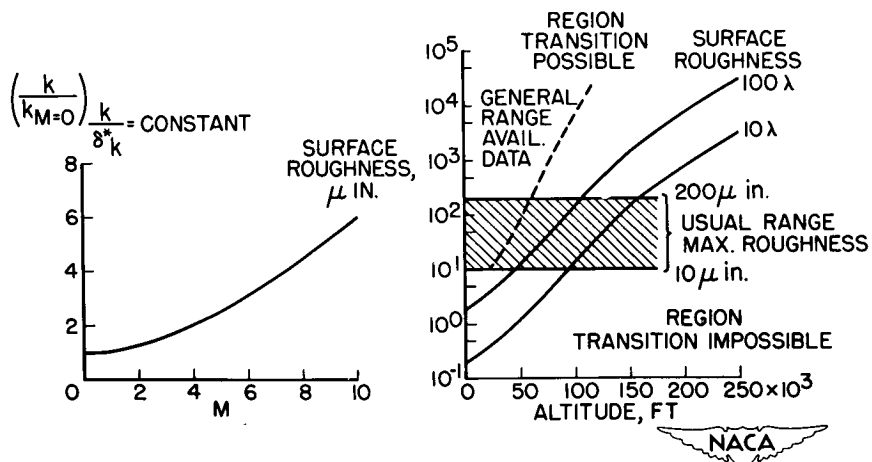


Figure 8

EFFECT OF ANGLE OF ATTACK ON BODY TRANSITION

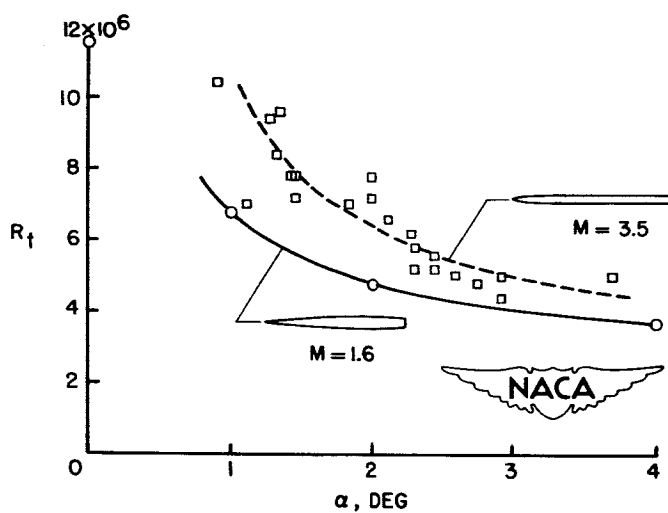


Figure 9

CONFIDENTIAL

REF ID: A50715

COMMENTS PERTAINING TO THE PREDICTION OF SHOCK-INDUCED
BOUNDARY-LAYER SEPARATION

By Roy H. Lange

Langley Aeronautical Laboratory

INTRODUCTORY REMARKS

One of the fundamental problems that appears in the investigation of supersonic flow over a surface is that of the phenomena associated with the interaction of shock waves and boundary layers. The problem of whether a given shock wave will cause boundary layer separation is one which occurs in all cases where a pressure increase is to be obtained as a result of the retardation of the flow. Such problems occur, for example, in the flow in supersonic diffusers and air inlets and in the flow at the rear of airfoils and bodies. Shock-induced boundary-layer separation generally results in poor aerodynamic efficiency in the former case and in undesirable airfoil characteristics in the latter case and, therefore, this problem is of considerable practical significance. The purpose of this paper is to discuss the status of information relative to the prediction of shock-induced boundary-layer separation. In order to study the fundamental features of the problem, the discussion is concerned principally with data obtained on flat plates in two-dimensional flow.

Prandtl has discussed separation of the incompressible boundary layer under the influence of a positive pressure gradient (refs. 1 and 2). The approximate methods such as those of Von Kármán, Pohlhausen, and Buri for predicting separation were derived on the assumption that the boundary layer has time to adjust itself to a prescribed pressure distribution. The Von Kármán-Pohlhausen approximation for a laminar boundary layer is:

$$\frac{\delta}{q_1} \frac{dp}{dx} = K_1 R_\delta^{-1} \quad (1)$$

and Buri's approximation for a turbulent boundary layer is:

$$\frac{\delta}{q_1} \frac{dp}{dx} = K_2 R_\delta^{-1/4} \quad (2)$$

LANGE

where

δ boundary-layer thickness

$\frac{dp}{dx}$ streamwise pressure gradient

q_1 free-stream dynamic pressure

K_1, K_2 empirical constants

R_δ Reynolds number based on distance δ

Experience with the use of these approximations has shown that the occurrence of separation depends chiefly upon the pressure gradient dp/dx , and that the turbulent boundary layer can withstand a much greater pressure increase before separation than can a laminar boundary layer. When the influence of a shock wave on a boundary layer is considered, it is evident that, if the infinite free-stream pressure gradient which the shock wave represents could extend all the way to the wall, then separation would certainly result; however, as shown in the sketch of figure 1, it is known that the pressure difference across the shock is spread out in the lower levels of the boundary layer. (See refs. 3 to 7.) The work of Liepmann and Ackeret has shown that the amount of spread of the pressure rise at the wall depends upon the state of the boundary layer, that is, whether the boundary layer is laminar or turbulent (refs. 3 and 6). Thus, the pressure gradient appearing at the wall boundary is fixed by the physical properties of the boundary layer and by the strength of the shock wave. It seems logical to assume, then, that the occurrence of separation in this case depends principally upon the pressure rise $p_2 - p_1$ through the shock wave. It was further anticipated that as the pressure rise across the shock was decreased there would be one shock strength below which no separation of the boundary layer would occur. This concept was advanced by Beastall and Eggink (ref. 8) and, later, a simplified dimensional analysis presented in reference 9 indicated that the critical pressure rise across the shock $\Delta p/q_1$ which just causes separation of the boundary layer should be proportional to the local skin-friction coefficient, c_f . These approximations are extended to the case for flat plates in terms of the Reynolds number based on x . Thus, for a laminar boundary layer,

$$\frac{\Delta p}{q_1} \propto c_f \propto R_\delta^{-1} \propto R_x^{-1/2} \quad (3)$$

SECRET


and for a turbulent boundary layer

$$\frac{\Delta p}{q_1} \propto c_f \propto R_\delta^{-1/4} \propto R_x^{-1/5} \quad (4)$$

It should be emphasized that the relationships given in equations (1) to (4) are only approximations. For incompressible flow more refined methods have been developed (refs. 10 to 13); however, the applications of these methods for predicting separation have met with only limited success. A collection of the available data for supersonic flow (ref. 9) appeared to bear out the predictions shown by equations (3) and (4) at the time they were first derived; however, since that time, more experimental data have come to light, especially for the turbulent boundary layer, which show that the problem must be reexamined. The discussion of these data forms the subject of this paper which now follows for both laminar and turbulent boundary layers.

LAMINAR BOUNDARY LAYER

The available data for shock-induced separation for laminar boundary layers on flat plates are given in figure 2, where the critical pressure rise Δp across the shock divided by the free-stream dynamic pressure q_1 is plotted against Reynolds number on logarithmic scales. The Reynolds number is based on the distance from the leading edge of the plate to the point of intersection of the shock wave and the boundary layer. The sources of these data are given at the top of the figure. (See refs. 3, 6, 8, 14, 15, and 16.) It can be seen that the available data are rather limited in scope and, therefore, are not conclusive; however, there are some trends in the data which should be mentioned. For example, at free-stream Mach numbers M_1 of 1.93, 2.00, 2.05, and 2.48 the Reynolds number effect on the critical pressure coefficient appears to follow the inverse square root of the Reynolds number as denoted by the dashed lines on the figure. Except for the data at Mach numbers of 1.40 and 1.44, the critical pressure coefficient also decreases with increasing Mach number. These trends of Reynolds number and Mach number agree with the predictions of equation (3); however, the magnitude of the Mach number effect shown, especially between Mach numbers of 1 and 2, is much greater than that which would be predicted by reference 9. Recent data obtained at the Ames Laboratory in the separated region ahead of a forward-facing step show an increase in $\Delta p/q_1$ with increase in Reynolds number; thus the configuration appears to have a large effect on laminar separation. Stewartson (ref. 17) has made a detailed analysis of the interaction



process which leads to the inference that the dimensionless pressure rise required to produce laminar separation would be proportional to $R_x^{-2/5}$. Also shown in figure 2 is a curve which traces the criterion of separation advanced by Pabst (ref. 18) in a recent Argentine paper; however, this criterion cannot account for the Mach number effect and does not correlate with any of the experimental data shown.


TURBULENT BOUNDARY LAYER

Investigations of shock—boundary-layer interaction for the turbulent boundary layer have shown that a given shock wave may or may not separate the boundary layer. Data are now available from a number of sources in which turbulent boundary-layer separation has been investigated by three methods: (1) the forward-facing-step technique, (2) the wedge technique, and (3) the incident-shock technique.

In order to remove all doubt as to whether the turbulent boundary layer has been separated, several investigators have forced separation by means of a forward-facing step mounted on a flat plate (see refs. 8, 9, 19, and 20). Typical data for this type of configuration are given in figure 3 which shows the pressure distribution along the surface and (to the same scale) a sketch of the flow field in the interaction region as determined from shadowgraphs. These data were obtained in a blowdown jet of the Langley gas dynamics laboratory at a Mach number of 3.03. The flow diagram at the top of the figure shows that a wedge-shaped separation region is formed ahead of the step and is bounded on its upstream edge by the shock wave. The direction of the circulatory flow within the separated region is shown by the arrows.

The pressure coefficients on the plate first reach a maximum value, noted herein as the first peak, at a point about halfway between the location of the shock wave and the location of the step. This distance is roughly the equivalent of 8 boundary-layer thicknesses or 133 momentum thicknesses, on the assumption of a $1/7$ -power velocity distribution in the boundary layer just ahead of the shock. The pressures then dip slightly behind the first peak and subsequently rise sharply, showing the large influence of the circulatory flow. Also pertinent to the discussion of the flow in the separated region are the pressure coefficients measured along the front vertical face of the step given in figure 4.

The three isolated points at a Reynolds number of 4×10^6 were obtained at $M_1 = 1.86$ (ref. 21), and the data for Reynolds numbers ranging from 12×10^6 to 32×10^6 were obtained at $M_1 = 3.03$. The pressure orifices were located at the base of the step and at two other vertical locations



above the surface of the plate as denoted by z/h . The data at $M_1 = 3.03$ show no significant Reynolds number effect on the pressure coefficients. The results show that there is one stagnation point at the foot of the step and one near the top of the step, and calculations based on the data at $M_1 = 3.03$ and utilizing the incompressible Bernoulli equation show that the velocity downward along the vertical face is about $1/4$ the free-stream velocity; whereas the velocity along the plate in a direction opposite to the main flow is about $1/3$ the free-stream velocity. Thus the separated region cannot be treated as a dead-air space as is commonly assumed. The results at both Mach numbers also show that a considerable error would result if the pressures on the front face of the step were assumed to be the same as that obtained on the plate surface ahead of the step in the separated region. The first peak pressure coefficients obtained ahead of the step are shown by the dashed lines at both Mach numbers for comparative purposes in this case. This result may be changed when the step height is very large compared to δ . It is clear then, from the results given in figures 3 and 4, that the first peak pressure coefficient is obtained as a result of the mutual effects of the shock on the boundary layer and of the circulatory flow in the separated region and should not be interpreted as the value of the pressure rise across the minimum strength of shock wave which just causes separation of the boundary layer.

A summary of the available data obtained from the use of the step technique for forcing boundary-layer separation is given in figure 5 which shows $\Delta p/q_1$ taken at the first peak plotted against Reynolds number on a logarithmic scale. The Reynolds number is based on the distance from the leading edge of the plate to the point of intersection of the shock wave with the boundary layer. All the data were obtained from pressure distributions (see refs. 8, 14, 20, 22, and 23), and the sources are given at the top of the figure. The Mach number range of the data is from 1.55 shown by the long string of points at the top of the data to 3.65 shown by the lowest data points. The pressure distribution data at $M_1 = 3.03$ given by the circles are new data which have not been published. The data given in reference 9 (TN 2770) for $M_1 = 3.03$ represented by the dashed line which varies as $R_x^{-1/5}$ were obtained by measuring shock angles close to the point of intersection of the shock wave and the boundary layer, where, as shown previously, the pressures on the plate are changing rapidly; therefore this method for obtaining pressure coefficients is too crude and the data should be ignored. It is apparent from the mass of data that, except for the data at Mach numbers of 1.86 and 2.48, the Reynolds number effect on the value of $\left(\frac{\Delta p}{q_1}\right)_{1st \text{ peak}}$ is very slight. On the basis that there is

no Reynolds number effect, figure 6 has been prepared to show the decrease in $\left(\frac{\Delta p}{q_1}\right)_{1st\ peak}$ with increase in free-stream Mach number for Mach num-

bers between 1.55 and 3.65. All the data from the previous figure have been included in this plot, and the vertical lines connecting some of the symbols show the extent of the Reynolds number effect obtained. Included on this plot is the empirical relationship derived by Beastall and Eggink from a curve which best fit their data for both forward-facing steps and backward-facing steps (refs. 8 and 24). This approximation is independent of both Reynolds number and Mach number and, therefore, does not correlate well with the available experimental data for forward-facing steps.

The second technique for producing turbulent boundary-layer separation is the use of wedges of different angles mounted on flat plates, and a limited amount of data is available. (See refs. 20 and 25.) This configuration is analogous to the deflection of a flap or a control surface. Typical data obtained at a Mach number of 3.03 are given in figure 7 which shows the pressure distribution along the plate and on the wedge and above it a sketch of the flow phenomena as determined by shadow-graphs. A double scale is given along the abscissa of the pressure distribution - one which gives x in inches measured from the leading edge of the wedge and one which gives a measure of the boundary-layer thickness, x/δ . As shown in the flow picture, the separation in the corner produced by this particular wedge angle results in a weak shock wave, which projects ahead of the main shock, and an inflection point is obtained in the pressure distribution on the surface. Downstream of this point the pressure coefficient continues to rise and levels off at a value somewhat less than that calculated from oblique-shock theory for this wedge angle in the absence of a boundary layer. In general, the limited available data at a given Mach number show that, for wedge angles greater than a certain value, the pressure distribution has an inflection point similar to that shown in figure 7; moreover, the value of $\Delta p/q_1$ measured at the inflection point remains almost constant with further increases in wedge angle. The data at $M_1 = 3.03$ also show that the value of $\Delta p/q_1$ obtained at the inflection point is essentially constant for Reynolds numbers ranging from 12×10^6 to 32×10^6 . Results are available from tests utilizing the third technique in which shock waves of varying strength are made to impinge upon the boundary layer on a flat plate. (See refs. 16 and 26.) In these tests inflection points are obtained in the pressure distributions along the plate surface somewhat similar to those in the wedge tests, and these inflection points are also associated with local separation of the turbulent boundary layer. The tests of Gadd and Holder at a Mach number of 2 show no significant effect of Reynolds number on the value of $\Delta p/q_1$ obtained at the inflection point for Reynolds

numbers ranging from about 0.8×10^6 to 10×10^6 . In figure 8 $\Delta p/q_1$ is plotted against Mach number, where the inflection-point pressure coefficients obtained in the wedge tests are given by the open symbols and the inflection-point pressure coefficients obtained by the incident-shock technique are given by the solid symbols. Also shown on this figure is the curve representing the data obtained by the forward-facing-step technique. The data given on this figure, therefore, constitute all information available at present on turbulent boundary-layer separation. The spread in $\Delta p/q_1$ obtained at $M_1 = 1.80$ in the wedge tests represents a Reynolds number effect, although, as mentioned previously, no such Reynolds number effect was obtained at $M_1 = 3.03$. The spread in $\Delta p/q_1$ at $M_1 = 2$ in the incident-shock tests represents the maximum scatter in the data. Although the available data are rather limited in scope, the results show that the inflection-point pressure coefficients obtained from both techniques generally have the same range of values with increasing Mach number and that on the average these values are about 20 percent lower than those obtained using the step technique. The application of these data for predicting separation should, therefore, be limited to these particular configurations, at least for the present. For example, the data from the incident-shock technique represent conditions of local separation of the flow and, because the experiments are performed on flat plates, the flow reattaches downstream of the separation point. This reattachment may be changed somewhat for conditions where a back pressure exists - for example, for conditions near the trailing edge of an airfoil. Also, flight data for a wing in transonic flow indicate that the $\Delta p/q_1$ for separation is predicted more accurately by the step data if extrapolated to the lower supersonic Mach numbers obtained in the flight tests (ref. 27). These data are useful, then, in providing a first approximation to the pressure coefficient for which separation is likely to be encountered.

CONCLUDING REMARKS

In conclusion, the present status of information relative to the prediction of shock-induced boundary-layer separation indicates that, although no universal value of pressure-rise coefficient which causes incipient separation of the boundary layer has been found, there is a fairly narrow band of pressure coefficients from which predictions of turbulent separation can be made with an accuracy probably sufficient for engineering purposes. On the basis of these results the following tentative conclusions are given:

1. The data obtained with forward-facing steps, wedges, and incident shock waves indicate that there is a dependency of the pressure

coefficient for separation on Reynolds number for the laminar boundary layer but little, if any, dependency on Reynolds number for the turbulent boundary layer. There is a dependency of this pressure coefficient on Mach number for both laminar and turbulent boundary layers.

2. For the particular case of the spoiler, the available data obtained by the forward-facing-step technique permit calculations of the loading on the surface ahead of the spoiler, the pressure on the front face of the spoiler, and the separation point ahead of the spoiler for a Mach number range of from 1.55 to 3.65 for the turbulent boundary layer.

3. For application to supersonic diffusers or scoop inlets, the available data from incident-shock-wave tests provide a first approximation to the minimum strength of shock which will separate the turbulent boundary layer for Mach numbers between 2 and 3.

4. From the data available from the wedge tests, a first approximation to the pressure coefficient for which separation becomes appreciable as a result of flap deflection can be made for a surface with a turbulent boundary layer for Mach numbers between 1.75 and 3.03.

5. Caution should be exercised in attempting to predict the separation or loading on configurations which differ considerably from those for which experimental data are available. For example, fair success has been obtained in predicting base pressure coefficients by the use of the forward-facing-step data, but reasons for this success are not at present fully understood.

REFERENCES

1. Prandtl, L.: On the Role of Turbulence in Technical Hydrodynamics. World Eng. Cong. (Tokyo).
2. Prandtl, L.: The Mechanics of Viscous Fluids. Vol. III of Aerodynamic Theory, div. G, W. F. Durand, ed., Julius Springer (Berlin), 1935, pp. 34-208.
3. Liepmann, H. W., Roshko, A., and Dhawan, S.: On Reflection of Shock Waves From Boundary Layers. NACA Rep. 1100, 1952. (Supersedes NACA TN 2334.)
4. Liepmann, Hans Wolfgang: Investigations of the Interaction of Boundary Layer and Shock Waves in Transonic Flow. Tech. Rep. No. 5688, ATI No. 34705, Air Materiel Command, U. S. Air Force, Feb. 9, 1948; The Interaction Between Boundary Layer and Shock Waves in Transonic Flow. Jour. Aero. Sci., vol. 13, no. 12, Dec. 1946, pp. 623-638.
5. Liepmann, H. W.: Boundary-Layer Shock-Wave Interaction. Symposium on Experimental Compressible Flow, June 29, 1949. NOLR 1133, U. S. Naval Ord. Lab., May 1, 1950, pp. 39-66.
6. Ackeret, J., Feldmann, F., and Rott, N.: Investigations of Compression Shocks and Boundary Layers in Gases Moving at High Speed. NACA TM 1113, 1947.
7. Fage, A., and Sargent, R. F.: Shock-Wave and Boundary-Layer Phenomena Near a Flat Surface. Proc. Roy. Soc. (London), ser. A, vol. 190, no. 1020, 1947, pp. 1-20.
8. Beastall, D., and Eggink, H.: Some Experiments on Breakaway in Supersonic Flow (Part I). TN No. Aero. 2041, British R.A.E., June 1950.
9. Donaldson, Coleman duP., and Lange, Roy H.: Study of the Pressure Rise Across Shock Waves Required to Separate Laminar and Turbulent Boundary Layers. NACA TN 2770, 1952.
10. Von Kármán, Th., and Millikan, C. B.: On the Theory of Laminar Boundary Layers Involving Separation. NACA Rep. 504, 1934.
11. Von Doenhoff, Albert E.: A Method of Rapidly Estimating the Position of the Laminar Separation Point. NACA TN 671, 1938.
12. Tetervin, Neal, and Lin, Chia Chiao: A General Integral Form of the Boundary-Layer Equation for Incompressible Flow With an Application to the Calculation of the Separation Point of Turbulent Boundary Layers. NACA Rep. 1046, 1951. (Supersedes NACA TN 2158.)

13. Rubert, Kennedy F., and Persh, Jerome: A Procedure for Calculating the Development of Turbulent Boundary Layers Under the Influence of Adverse Pressure Gradients. NACA TN 2478, 1951.
14. Mueller, James N.: Investigation of Spoilers at a Mach Number of 1.93 To Determine the Effects of Height and Chordwise Location on the Section Aerodynamic Characteristics of a Two-Dimensional Wing. NACA RM L52L31, 1953.
15. Barry, F. W., Shapiro, A. H., and Neumann, E. P.: The Interaction of Shock Waves With Boundary Layers on a Flat Surface. Jour. Aero. Sci., vol. 18, no. 4, Apr. 1951, pp. 229-238.
16. Gadd, C. E., and Holder, D. W.: The Interaction of an Oblique Shock Wave With the Boundary Layer on a Flat Plate. Part I. Results for $M = 2$. F.M. 1714, British N.P.L. (Rep. No. 14,848, A.R.C.), Apr. 24, 1952.
17. Stewartson, K.: On the Interaction Between Shock Waves and Boundary Layers. Proc. Cambridge Phil. Soc., vol. 47, pt. 3, July 1951, pp. 545-553.
18. Pabst, Otto Ernesto: Criterio para el desprendimiento de la capa limite en presencia de chogues de compresion. Escuela Superior De Aerotenica, Cordoba. Comunicaciones e. Informes. C-4, Apr. 1952.
19. Moeckel, Wolfgang E.: Flow Separation Ahead of Blunt Bodies at Supersonic Speeds. NACA TN 2418, 1951.
20. Barry, F. W.: A Review of Experimental Results on Boundary Layer - Shock Wave Interaction. Rep. No. AL-1599, North American Aviation, Inc., Dec. 15, 1952.
21. Patterson, R. T.: The Characteristics of Trailing-Edge Spoilers. Part II - The Effects of Gap, Flap Deflection Angle, Thickness, and Sweep Angle on the Aerodynamic Characteristics of Two-Dimensional Spoilers, and the Pressure Distribution Near the Tip of a Partial-Span Trailing-Edge Spoiler, at a Mach Number of 1.86 - TED No. TMB DE-3109. Aero. Rep. 827, David W. Taylor Model Basin, Navy Dept., Dec. 1952.
22. Love, Eugene S.: The Base Pressure at Supersonic Speeds on Two-Dimensional Airfoils and Bodies of Revolutions (With and Without Fins) Having Turbulent Boundary Layers. NACA RM L53C02, 1953.

REF ID: A63715

23. Patterson, R. T.: The Characteristics of Trailing-Edge Spoilers. Part I - The Effects of Turbulent Boundary Layer Thickness on the Characteristics of Two-Dimensional Spoilers at Two Supersonic Mach Numbers - TED No. TMB DE 3109. Aero. Rep. 827, David W. Taylor Model Basin, Navy Dept., Aug. 1952.
 24. Beastall, D., and Eggink, H.: Some Experiments on Breakway in Supersonic Flow (Part II). R.A.E. TN No. Aero. 2061, British R.A.E., June 1950.
 25. Drougge, Georg: Experimental Investigation of the Influence of Strong Adverse Pressure Gradients on Turbulent Boundary Layers at Supersonic Speeds. Eighth International Cong. on Theoretical and Applied Mechanics, Istanbul, 1952.
 26. Bogdonoff, S. M., and Solarski, A. H.: A Preliminary Investigation of A Shockwave-Turbulent Boundary Layer Interaction. Rep. No. 184, Princeton Univ. Aero. Eng. Lab. (Contract N6-ori-270, Task Order No. 6) Nov. 30, 1951.
 27. Zalovcik, John A., and Luke, Ernest P.: Some Flight Measurements of Pressure-Distribution and Boundary-Layer Characteristics in the Presence of Shock. NACA RM L8C22, 1948.
- [REDACTED]

SHOCK WAVE ENTERING A BOUNDARY LAYER

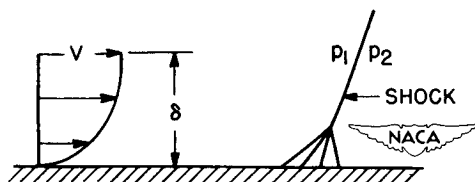


Figure 1

CRITICAL PRESSURE COEFFICIENTS FOR LAMINAR BOUNDARY LAYERS

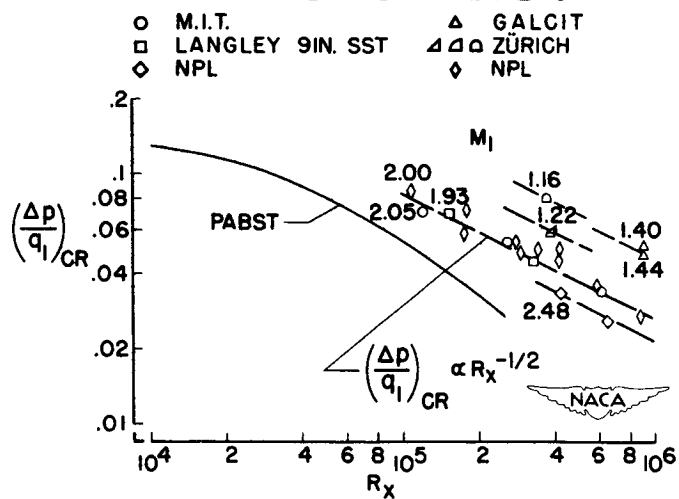


Figure 2

2. [REDACTED]

[REDACTED]

SEPARATION OF TURBULENT BOUNDARY LAYER BY STEP

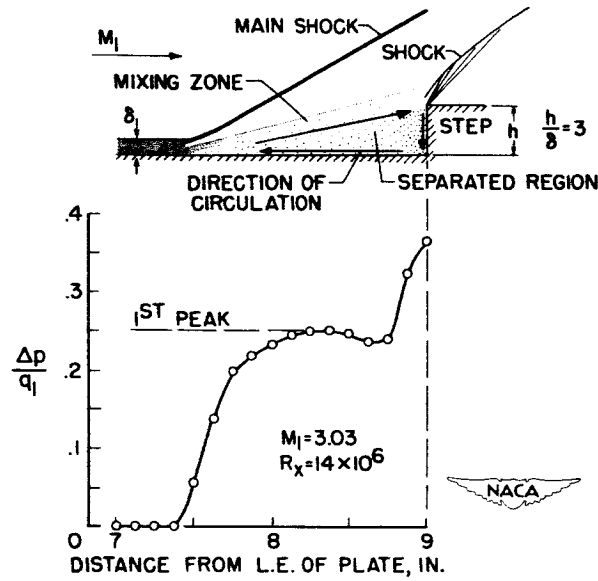


Figure 3

PRESSURE COEFFICIENTS ON VERTICAL FACE OF STEP

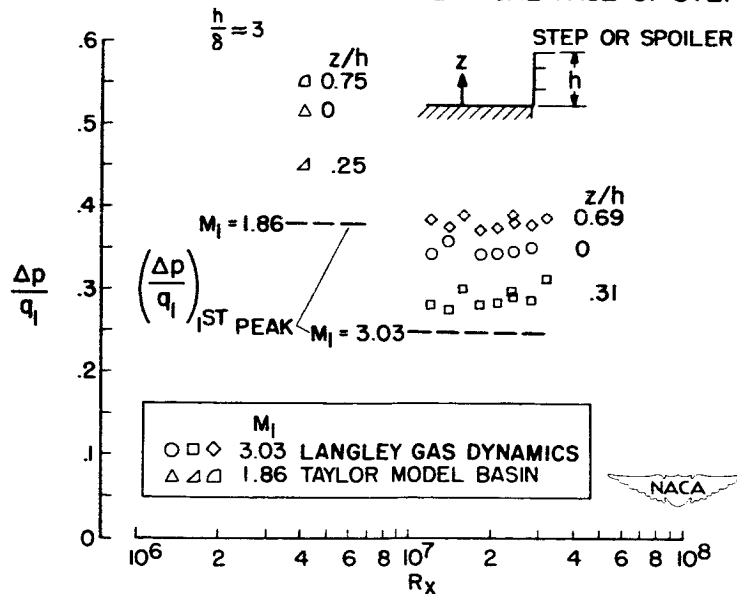


Figure 4

FIRST PEAK PRESSURE COEFFICIENTS AHEAD OF STEPS FOR
TURBULENT BOUNDARY LAYERS

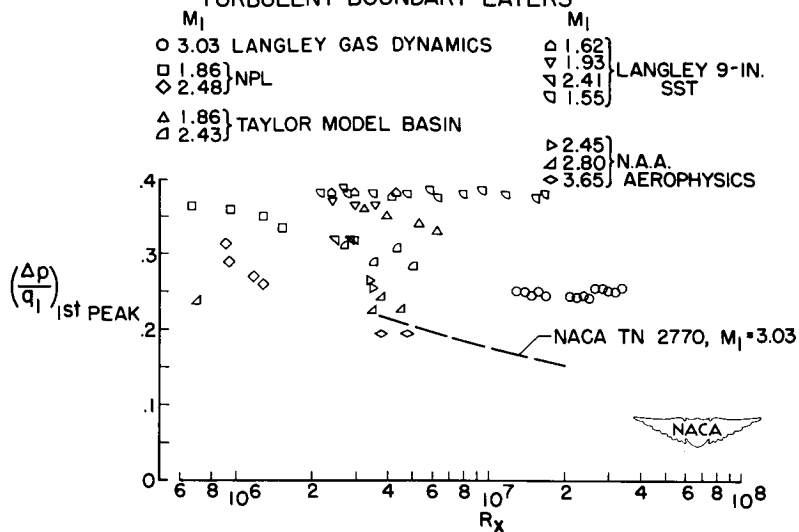


Figure 5

MACH NUMBER EFFECT ON PEAK PRESSURE COEFFICIENT
TURBULENT BOUNDARY LAYER

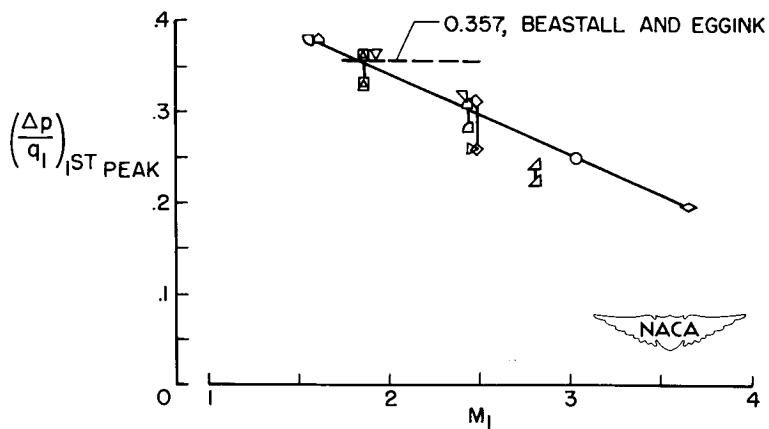


Figure 6

SEPARATION OF TURBULENT BOUNDARY LAYER BY WEDGE

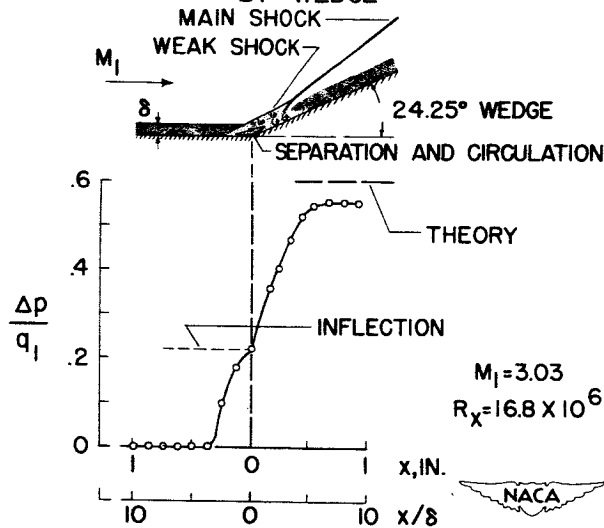


Figure 7

SEPARATION PRESSURE COEFFICIENTS FOR TURBULENT BOUNDARY LAYERS

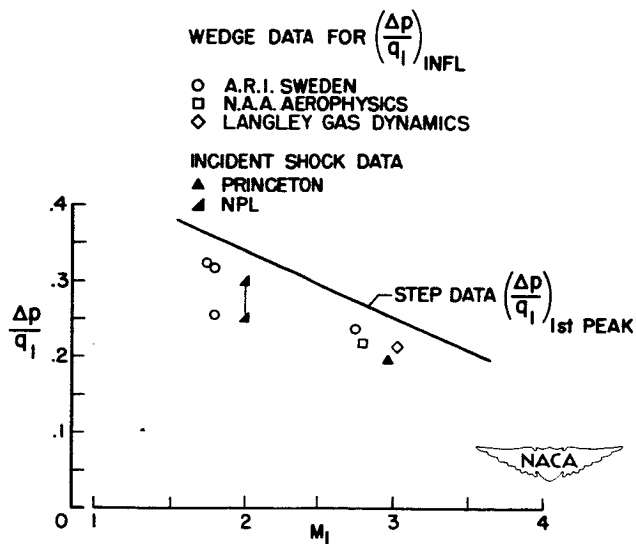


Figure 8

A STUDY OF THE MOTION AND AERODYNAMIC HEATING
OF MISSILES ENTERING THE EARTH'S ATMOSPHERE
AT HIGH SUPERSONIC SPEEDS

By H. Julian Allen

Ames Aeronautical Laboratory

In the design of long-range rocket missiles one of the most difficult phases of flight with which the designer must cope is the re-entry into the atmosphere. In the re-entry the rapidly increasing density with decreasing altitude can promote large drag forces which, in turn, can cause serious deceleration loads within the structure. More important, the air temperature in the boundary layer can reach values in the tens of thousands of degrees and this, combined with the high surface shear, will promote very great heat transfer to the surface.

The designer should know, then, what control he has over the missile characteristics which will permit a reduction of the problems associated with the motion and, particularly, the aerodynamic heating. The motion and heating of missiles, of course, has been given considerable attention by all designers of high-speed, long-range rockets, but these analyses have been made for individual designs and so have not been too instructive in giving an over-all view of the problems. In this paper, which is a condensation of reference 1, we shall discuss a generalized analytical approach, purposely simplified so that the salient features of the problems will be made clear in order that successful solutions of the problems will suggest themselves.

Consider first, the motion of a ballistic missile entering the atmosphere shown in figure 1. The equations of motion expressing the deceleration in vertical and horizontal directions are, respectively,

$$\frac{d^2y}{dt^2} = -g + \frac{\rho V^2 C_D A}{2m} \sin \theta$$

$$\frac{d^2x}{dt^2} = \frac{\rho V^2 C_D A}{2m} \cos \theta$$

where

ρ air density



V velocity

θ flight-path angle to horizontal

C_D drag coefficient

A reference area for drag evaluation

m mass


t time

x,y horizontal and vertical distances from impact point (0,0)

Analytical solutions of these equations would be extremely difficult since the density is a function of altitude, while the drag coefficient, the velocity, and the flight-path angle are functions of both x and y . However, the greatest stumbling block in solution of these equations results from the presence of the gravity term, $-g$. For very high speed missiles it would be expected that the gravity term would be small and might be neglected in the range of altitude in which the deceleration and heating are intense.

To investigate this possibility, consider the descent of a 1-foot-diameter solid iron ball entering the atmosphere vertically at 10,000 feet per second. It is known that for spheres the drag coefficient is essentially constant and equal to unity. In figure 2, the solid curves show the velocity and deceleration as a function of altitude as obtained by step-by-step integration of the motion equation which includes the gravity term. The dashed curves represent a similar solution neglecting the gravity term. The close agreement shows that at the high flight speeds considered here, the gravity term may be ignored without too serious error. When this gravity term is neglected, the flight-path angle, θ , becomes constant and equal to the entrance angle, θ_E . That is, the trajectory is a straight line so that the drag coefficient, air density, and velocity may be expressed as functions of x or y , and analytical solution of the equations of motion becomes feasible.

As a second step in obtaining analytical solutions, it is necessary to express the density-altitude relation in analytic form. In figure 3 is shown a logarithmic plot of the NACA standard atmosphere variation of density with altitude indicated by the solid line. The dashed line represents an approximation to the density-altitude relation using the exponential type of variation, $\rho = \rho_0 e^{-\beta y}$ with ρ_0 set at 0.0034 slug per cubic foot and β set at $(1/22,000)$ feet⁻¹. In figure 4, the solid curve shows the deceleration calculated by the step-by-step method, neglecting the gravity-acceleration term, for the vertically descending solid iron ball previously considered. The dashed curve shows the deceleration obtained from an analytical solution, neglecting gravity



acceleration, using the exponential expression for the density as a function of altitude. It is clear that such an exponential density relation gives satisfactory results when the constants are so chosen as to give a good "fit" in the altitude range for which the deceleration is large.

If it is assumed in the equations of motion that the gravity term is negligible and that the exponential density relation is applicable, it can be shown that for a missile with constant drag coefficient entering the atmosphere with the velocity V_E at the flight-path angle θ_E , the velocity at any altitude y is

$$V = V_E e^{-\frac{C_D \rho_0 A}{2\beta m \sin \theta_E} e^{-\beta y}}$$

and the corresponding deceleration is

$$-\frac{dV/dt}{g} = \frac{C_D \rho_0 A V_E^2}{2mg} e^{-\beta y} e^{-\frac{C_D \rho_0 A}{\beta m \sin \theta_E} e^{-\beta y}}$$

The maximum deceleration can, then, be shown to be

$$-\left(\frac{dV/dt}{g}\right)_1 = \frac{\beta V_E^2 \sin \theta_E}{2ge}$$

which occurs when the velocity is

$$V_1 = e^{-1/2} V_E \approx 0.61 V_E$$

and the altitude is

$$y_1 = \frac{1}{\beta} \log_e \frac{C_D \rho_0 A}{\beta m \sin \theta_E}$$

A strange feature of this solution is that the maximum deceleration is independent of the physical characteristics of the body (that is, the weight, size, and drag coefficient of the missile). It is a function

only of the entrance speed and the entrance angle. Moreover, this maximum deceleration occurs at 61 percent of the entrance speed, again regardless of the physical characteristics. On the other hand, the altitude at which the maximum deceleration occurs is independent of the entrance velocity but is a function of the body characteristics and of the flight-path angle. As a demonstration of these points, let us consider three solid iron balls, having diameters of 1/10 foot, 1 foot, and 10 feet, entering the atmosphere at a speed of 20,000 feet per second at a 45° flight-path angle. In figure 5 are shown the decelerations of these three spheres. There are several important points to note here. Not only is the maximum deceleration the same for each missile, but the deceleration curves are identical except for the fact that they are shifted vertically, the smallest sphere reaching its maximum deceleration at the highest altitude. The 10-foot sphere happens to be of just such weight as to reach its maximum flight deceleration just above sea level. Any larger sphere would, of course, reach its maximum flight deceleration at sea level and that deceleration would be less than that shown here. Nevertheless, it should be noted that the sphere sizes shown in this figure represent a tremendous variation in weight, from 1/4 pound for the smallest to 250,000 pounds for the largest. Hence it should be clear that for missiles of usual weight, this maximum deceleration will be reached in the descent except in the cases for which the drag coefficient is exceptionally low.

It was noted previously that the solutions given are applicable only where the drag coefficient is constant, and one might expect that such a solution would not be a satisfactory one except for very blunt bodies, such as the spheres considered here. It can readily be shown, however, that this is not the case. In figure 6 is shown the deceleration and velocity for a 40° conical missile having a base area of 10 square feet and a weight of 5,000 pounds. The entrance velocity is 10,000 feet per second and the entry flight path is 30° . The constant drag coefficient assumed in this analysis is that corresponding to conditions at the altitude for maximum deceleration. In figure 7 are shown the total and frictional drag coefficients calculated at each altitude for the Mach and Reynolds number corresponding to this altitude-velocity relation. It is seen that in spite of the large changes in Mach number and Reynolds number, the drag characteristics are nearly constant in the altitude range where deceleration is large. This near constancy results from the fact that while the effect of decreasing Mach number with altitude is to increase the drag coefficients, the effect of increasing Reynolds number with altitude is to decrease the drag coefficients, and these effects are very nearly compensating.

In figures 8 and 9 are shown similar results for a missile identical to the one just described except that the cone angle is 10° . Again we see that the frictional and total drag coefficients are nearly constant in the altitude range where the deceleration is large. In the heating analysis to follow, the assumption of constant frictional drag



DECLASSIFIED

coefficient is permissible then, since, as will be seen later, the heating rate is proportional to the deceleration.

Let us next consider the far more serious problems resulting from aerodynamic heating. For high-speed ballistic rockets, the heat input is very great, and, hence, a means of cooling must be provided to prevent destruction of the essential elements of the missile. It is a characteristic of rockets that for every pound of material which is carried to "burn out," many pounds of fuel are required in the booster to obtain the flight range. Hence, it is clear that the amount of material which is added to protect the warhead from overheating must be minimized to keep the take-off weight to a practicable value. Thus, the first heating problem of interest concerns the total heat input since this input determines the coolant weight. We will confine this discussion to a comparison of the heat input of a missile of one shape with that of another to determine what shape characteristics reduce the heating. Hence, we will be interested in relative rather than absolute heating so that the analysis will be simplified by the following assumptions:

First, we will consider only convective heating, that is, we ignore radiation to or from the body. Ignoring the radiation from the air to the body is certainly permissible at the lower speeds, say of the order of 10,000 feet a second, although it may become inadmissible as the speed is increased, say to the escape speed. Radiation from the missile will certainly occur but since for any given missile design the surface will be allowed to get as hot as structurally permissible, the radiation from two designs considered will be very nearly the same and, hence, because our interests are relative rather than absolute, the assumption is satisfactory. The second assumption which is made is that imperfect gas characteristic effects are ignored - in particular, dissociation. This is again done on the basis that relative rather than absolute values are of interest since for a given entrance speed the dissociation of the air will be roughly comparable for two designs. The third assumption which is made is that there is no interaction between shock waves and the boundary layer. Such an assumption is a good one at the lower speeds but the work of Lees and Probstein (ref. 2) and Li and Nagamatsu (ref. 3) would indicate that at very high speeds serious effects of such interaction can occur. Fourth, it is assumed that Reynolds analogy holds. A recent examination of the effect of compressibility on the adequacy of the Reynolds analogy by Rubesin (ref. 4) has indicated that the analogy is a satisfactory assumption, at least in the speed ranges of the interest of this paper, say the order of 10,000 feet per second. Finally, it will be assumed that the Prandtl number is unity. This assumption is justified, again on the basis that relative rather than absolute values are of interest.

The heat-transfer equation which must be solved is



$$\frac{dH}{dt} = -V \frac{dH}{dy} \sin \theta_E = h(T_R - T_W)$$

Here H is the heat transfer per square foot of surface at any local point on the surface of the missile and its change with time or with altitude can be expressed as the product of the local heat-transfer coefficient, h , and the difference between the recovery temperature and the wall temperature, $T_R - T_W$. The heat-transfer coefficient

$$h \sim C_f' \rho V c_p$$

is proportional to the velocity, density, specific heat, and the equivalent frictional drag coefficient, C_f' , which is, in turn, proportional to the frictional drag coefficient. As noted earlier, we will assume the frictional drag coefficient to be constant.

As regards the temperature difference

$$(T_R - T_W) = T + \frac{\gamma-1}{2} M^2 T - T_W$$

an important simplification which can be made at very high speeds is that the recovery temperature due to high Mach number is so large that the temperature, $T - T_W$, can be assumed to be negligible by comparison to $\frac{\gamma-1}{2} M^2 T$, so that the temperature difference can be expressed as

$$(T_R - T_W) = \frac{\gamma-1}{2} M^2 T = \frac{V^2}{2c_p}$$

If we now substitute the velocity and density as determined from the motion analysis into the heating equation, the equation can be integrated to give the total heat input which is

$$Q = \frac{1}{4} \left(\frac{C_f' S}{C_D A} \right) m V_E^2 \left[1 - e^{-\frac{C_D \rho_0 A}{\beta m \sin \theta_E}} \right]$$

Here, the factor Q is the total heat input over the wetted area S . Let us consider now the case of a missile which is relatively heavy.



By this, we mean that in the exponent $C_D \rho_0 A / \beta m \sin \theta_E$, the denominator is very large compared to the numerator. In this case the bracket term can be expanded in series and, if we retain only the first term, we find the total heat input is approximately

$$Q \approx \frac{C_f' S \rho_0 V_E^2}{4 \beta \sin \theta_E}$$

This equation indicates that the least heating will occur for the relatively heavy missile when the frictional drag is a minimum. This is the usual expectation. On the other hand, if we have a relatively light missile, that is, one for which the numerator of the above exponent is large with respect to the denominator, then it can be shown that the total heat input is approximately

$$Q \approx \frac{1}{2} m V_E^2 \left(\frac{C_f' S}{2 C_D A} \right)$$

For this case we see a very interesting result that the heating will be decreased by increasing the total drag, provided the frictional drag does not increase proportionately as rapidly. This may at first seem somewhat perplexing but we note that making the drag coefficient in the exponential relation large or the mass small is equivalent to making the terminal speed very low with respect to the entrance speed. This means that all the kinetic energy, $\frac{1}{2} m V_E^2$, must be converted to thermal energy - that is, to heating both the atmosphere and the missile.

By making $C_D A$ large compared to $C_f' S$ the maximum amount of heat is delivered to the atmosphere and hence the missile is heated the least. Thus, it appears that the optimum solution as regards the total heat input depends upon the missile drag coefficient. To look into this matter further let us consider the heating of conical-shaped missiles entering the atmosphere at 10,000 feet a second at a 30° flight-path angle. For each of these missiles a constant base area of 10 square feet will be assumed. In figure 10 is shown the total heat input, as a function of cone angle, for missiles of 1000, 5000, and 10,000 pounds weight and, as a matter of interest, a hypothetical missile of infinite weight. We note, here, that the minimum which occurs for the small cone angles is that corresponding to a minimum value of $C_f' S$, while the low heating for the large cone angles is a result of making $C_f' S / C_D A$ a minimum. The minimum which we see here for the small cone angle is not very pronounced since at the lower speeds the equivalent frictional drag coefficient does not change rapidly with cone angle, but, as is shown in figure 11, as the speed is increased this minimum


is more accentuated and the advantage of the large cone angles less apparent. Nevertheless, in general, it has been found that giving the missile a high drag coefficient is nearly always the best for the most usual weights of interest.

Let us now turn to another heating problem of serious importance. As pointed out previously the time rate of heat input can be great for these high-speed missiles. Many missiles are designed to absorb the heat within the solid surface of the missile shell or to transmit it through the shell to a coolant. For these missiles an excessively large time rate of heat input may promote such large thermal stresses as to cause spalling of the surface (and therefore result in a loss of heat absorbent material) or even structural failure. The time rate of heat input is also important for sweat-cooled missiles since it will determine the required surface porosity and the liquid coolant pumping rate.

The designer is interested in the maximum time rate of heat input to an average surface element - since this is proportional to the average thermal shell stress and, therefore, determines the structural strength of the missile as a whole - and the maximum time rate of heat input at the surface elements of maximum heating - since this determines the local strength at these "hot spots."

Consider, first, the maximum time rate of heat transfer to an average surface element. Analysis has shown that in this case, it is better to make either the frictional drag coefficient a minimum or the ratio of the frictional drag coefficient to the total drag per unit dynamic pressure a minimum. In figure 12 it is seen that, considering the same conical missiles as before at an entrance speed of 10,000 feet per second, small-cone-angle and large-cone-angle missiles have the least maximum time rate of heat input for an average surface element.

Consider, next, the maximum time rate of heating at hot spots. The local surface elements for which the heat-transfer rates are greatest in practically every case will be those which first meet the air, for then the boundary-layer thickness is least and, hence, the shear is greatest. For the missile body this element is the nose and it should be noted at the outset that truly pointed bodies should be avoided, for at the point the heat-transfer rate is tremendously high while the point itself has no capacity for absorbing heat. Therefore, let us consider only the case of a rounded-nose missile with a nose radius, σ , and discuss the heating at the stagnation point. For such a body, the bow shock wave is detached and is a normal shock on the stagnation stream line. Thus, the high supersonic speed is converted to a low subsonic speed flow after the shock. Accordingly, we may determine the heating at the stagnation point by use of a low-speed analysis such as that given by Sibulkin (ref. 5). The results of this analysis show that the maximum heat-transfer rate is inversely proportional to the square




root of the nose radius which indicates that the largest possible nose radius should be employed. Let us now alter each of the conical missiles previously considered to have a hemispherical nose of small but arbitrary radius, σ . In figure 13 is shown the product of the square root of the nose radius times the maximum heat-transfer rate at the stagnation point as a function of the cone angle. Here we see that the minimum local heating is obtained by using the largest possible cone angle; that is, the missile having the highest drag per unit dynamic pressure is always the optimum as regards the heating at hot spots. We should also note, in addition, that we have not considered wings or wing-like tail surfaces for these missiles. It is the general experience of designers that stabilizer surfaces or wings should not be used for these very high-speed missiles since such surfaces are almost impossible to cool.

Now let us look back from the designer's point of view on the results which have been obtained. First, from the results of the motion analysis we have seen that for long-range ballistic rockets of usual weights the maximum deceleration, except for missiles having unusually low drag shapes, is constant and independent of the shape. Thus, shapes having very high drag coefficients are not inferior to those of more usual design. Second, as far as total heat input is concerned, the missiles having the least ratio of frictional to total drag are generally the optimum. These are, of course, high-drag-coefficient shapes. Third, as regards the maximum time rate of heat input to an average surface element, either the very low drag or the very high drag shapes are best, but, fourth, as regards the local heating rate at hot spots, local heating is always decreased by increasing the drag coefficient.

One shape, then, which would appear to have considerable promise is a sphere for it has the following advantages: It is a very high drag shape and its frictional drag is only a few percent of its total drag. It has a maximum volume for its surface area; its continuously curved surface is inherently stiff and strong. The large stagnation point radius significantly assists in reducing the maximum thermal stress in the shell. Aerodynamic forces are not sensitive to attitude and, hence, there is no problem of stabilization. Because of this insensitivity to attitude, the sphere may be purposely rotated in a random manner to subject all surface elements to about the same amount of heating and thereby approach uniform shell heating. On the other hand, a spherical missile may be unacceptable since it will have a low terminal speed and, hence, may permit effective countermeasures. Also, the lower average speed of descent will increase the wind-drift error at the target.

These possible disadvantages of very high drag shapes might be alleviated by using variable geometry arrangements. To illustrate such an arrangement, consider the missile shown in figure 14. Here it is assumed that the warhead is contained within the high-fineness-ratio



forebody and that the afterbody is an extensible skirt acting as an air brake which is flared to large angles, and therefore high drag, when the missile enters the atmosphere. As the air density increases with decreasing altitude, the skirt flare is decreased so as to keep the missile from decelerating to too small a terminal speed. The examples considered are, of course, only to demonstrate some of the means available to the designer to diminish some of the aerodynamic heating problems for such high-speed missiles.

REFERENCES

1. Allen, H. Julian, and Eggers, A. J., Jr.: A Study of the Motion and Aerodynamic Heating of Missiles Entering the Earth's Atmosphere at High Supersonic Speeds. NACA RM A53D28, 1953.
2. Lees, Lester, and Probstein, Ronald F.: Hypersonic Viscous Flow Over a Flat Plate. Rep. No. 195, Princeton Univ., Aero. Eng. Lab., Apr. 20, 1952.
3. Li, Ting-Yi, and Nagamatsu, H. T.: Shock Wave Effects on the Laminar Skin Friction of an Insulated Flat Plate at Hypersonic Speeds. GALCIT Memo. No. 9, (Contract No. DA-04-495-Ord-19), July 1, 1952.
4. Rubesin, Morris W.: A Modified Reynolds Analogy for the Compressible Turbulent Boundary Layer on a Flat Plate. NACA TN 2917, 1953.
5. Sibulkin, M.: Heat Transfer Near the Forward Stagnation Point of a Body of Revolution. Jour. Aero. Sci. (Readers' Forum), vol. 19, no. 8, Aug. 1952, pp. 570-571.

[REDACTED]

MISSILE TRAJECTORY COORDINATE SYSTEM

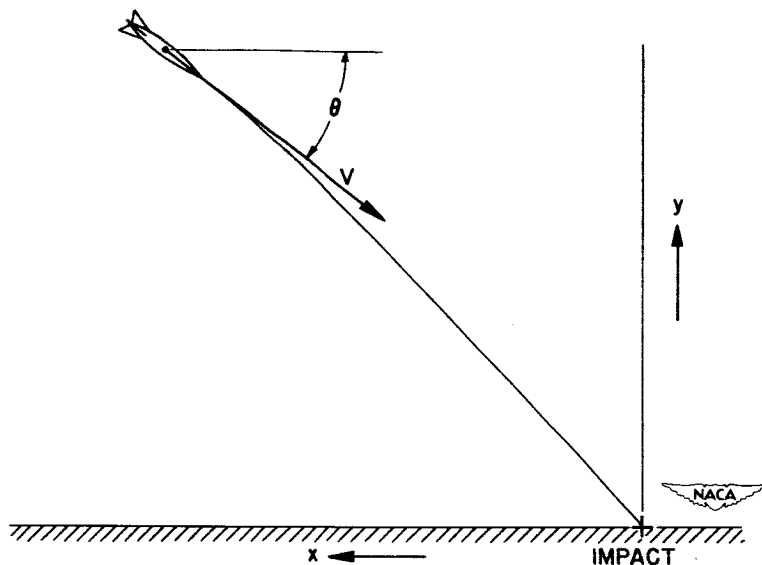


Figure 1

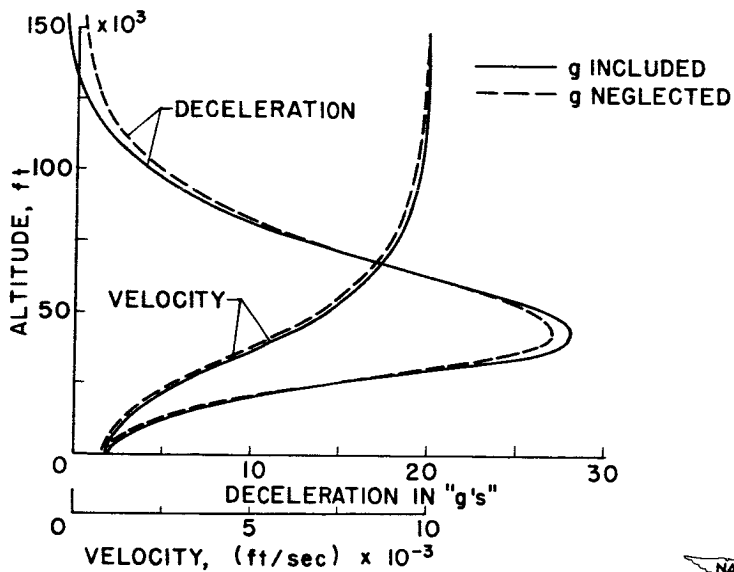
VERTICAL FALL OF A ONE-FOOT-DIAMETER IRON BALL
EFFECT OF GRAVITY

Figure 2

AIR-DENSITY VARIATION WITH ALTITUDE

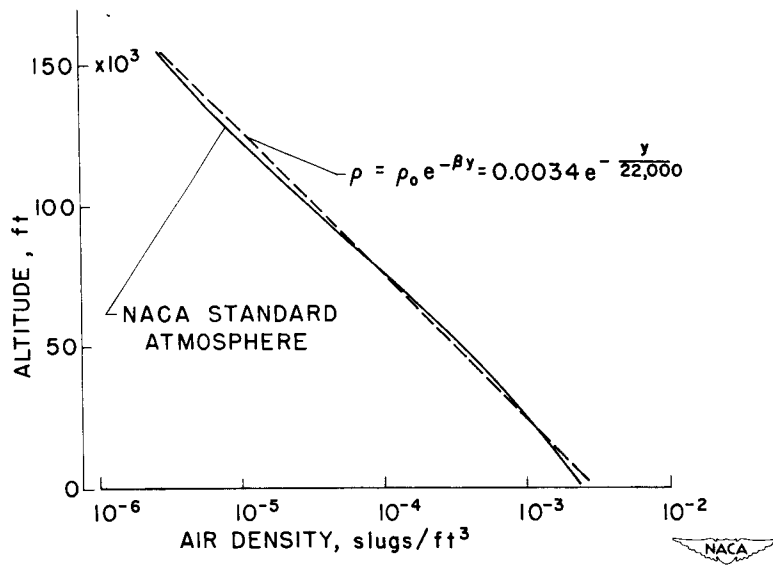


Figure 3

VERTICAL FALL OF A ONE-FOOT-DIAMETER IRON BALL EFFECT OF AIR DENSITY-ALTITUDE RELATION

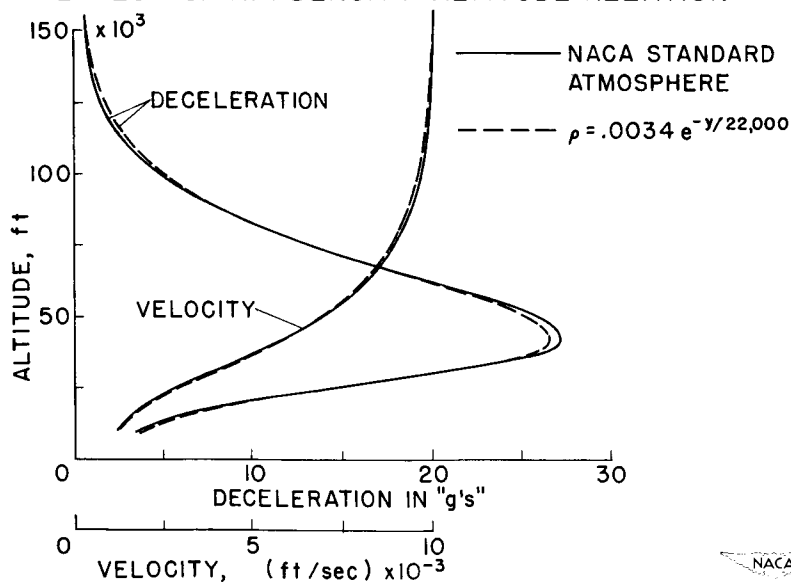


Figure 4

DESCENT OF IRON BALL

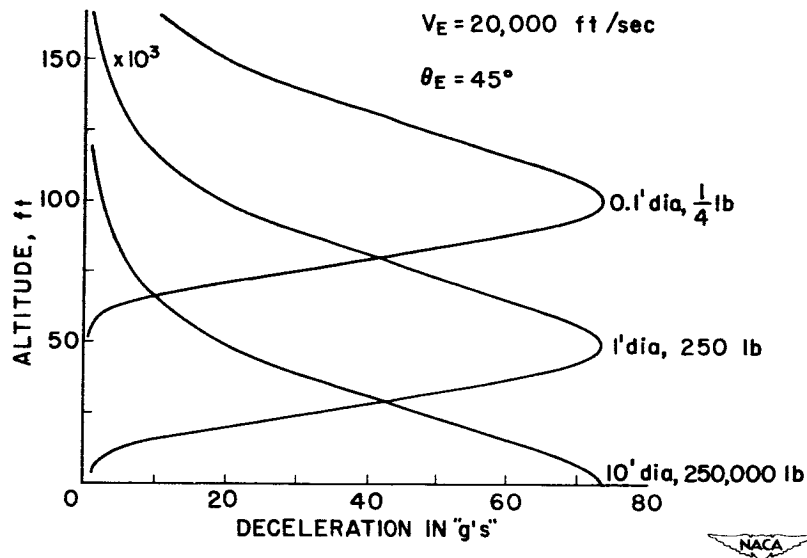


Figure 5

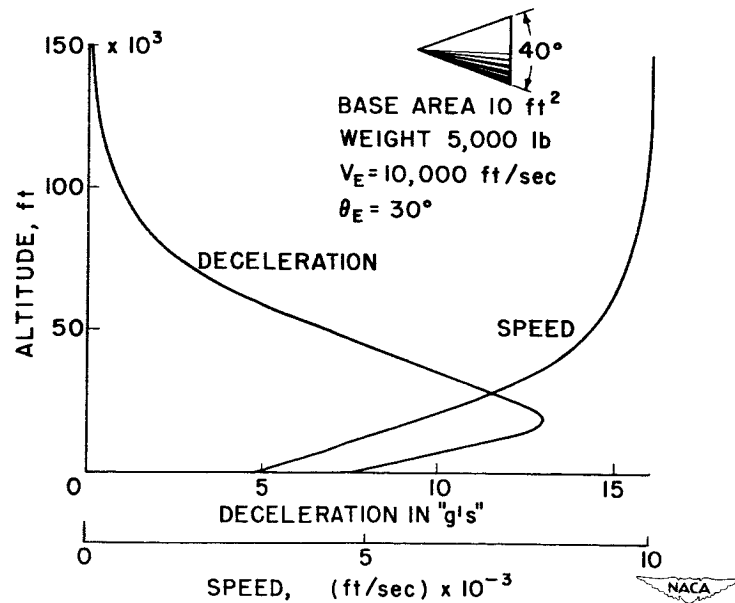
SPEED AND DECELERATION OF 40° CONICAL MISSILE

Figure 6

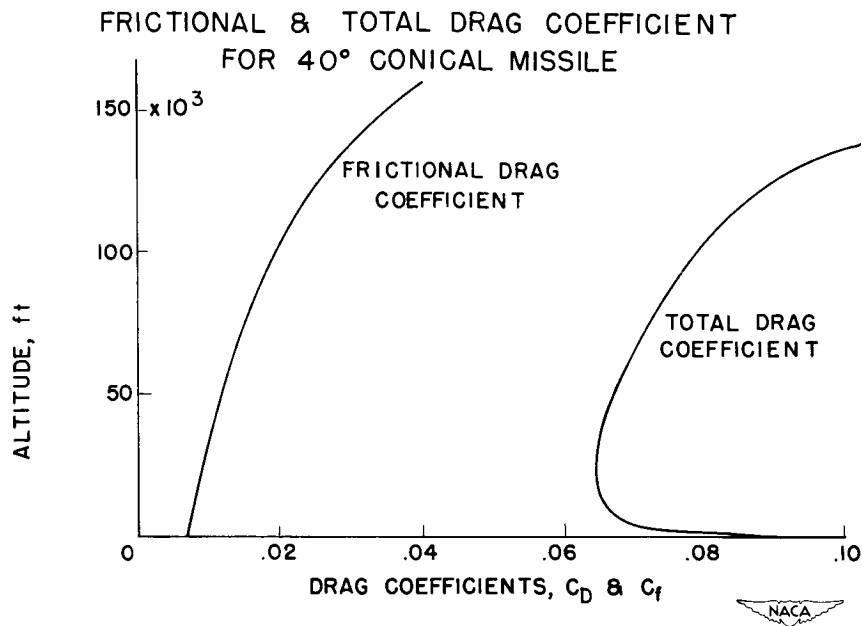


Figure 7

SPEED AND DECELERATION OF 10° CONICAL MISSILE

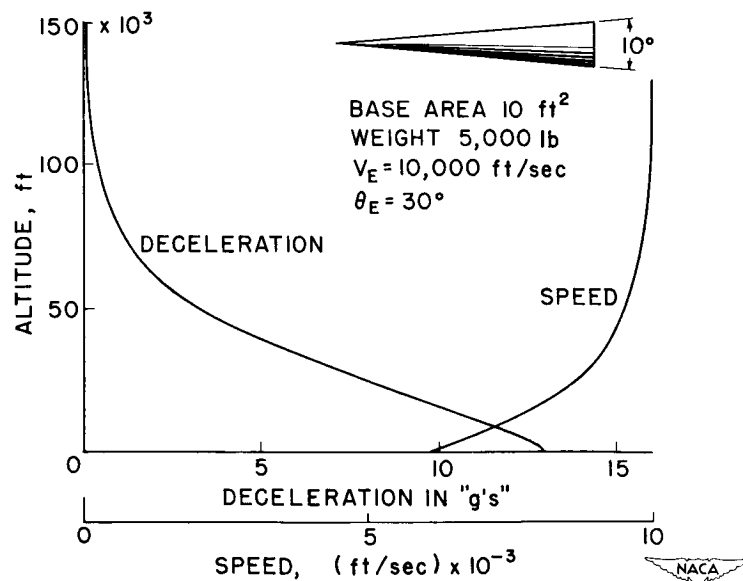


Figure 8

FRictional & TOTAL DRAG COEFFICIENT FOR 10° CONICAL MISSILE

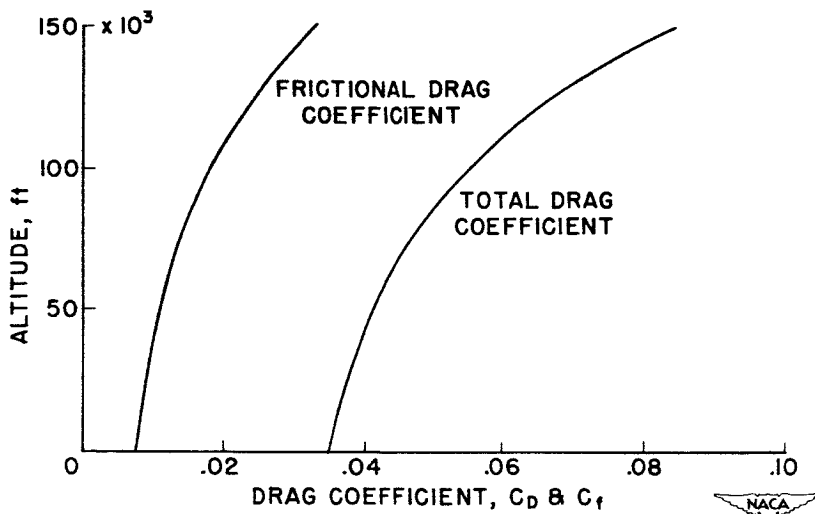


Figure 9

TOTAL HEAT INPUT

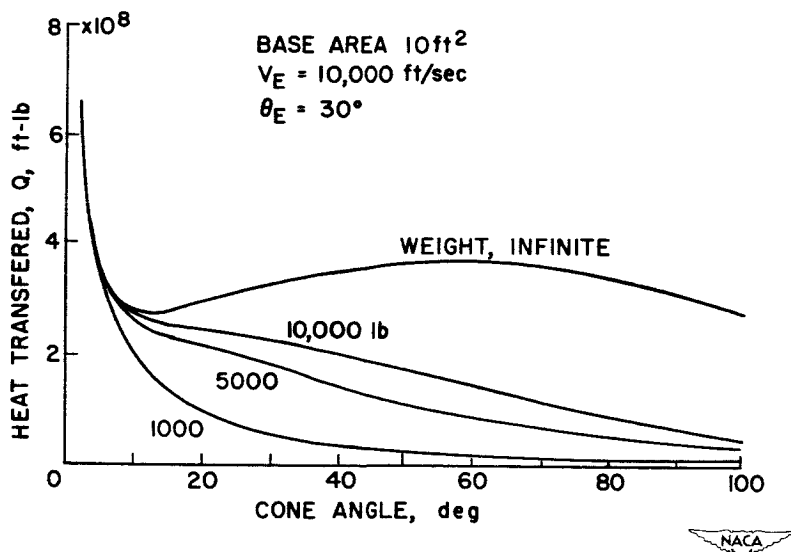


Figure 10

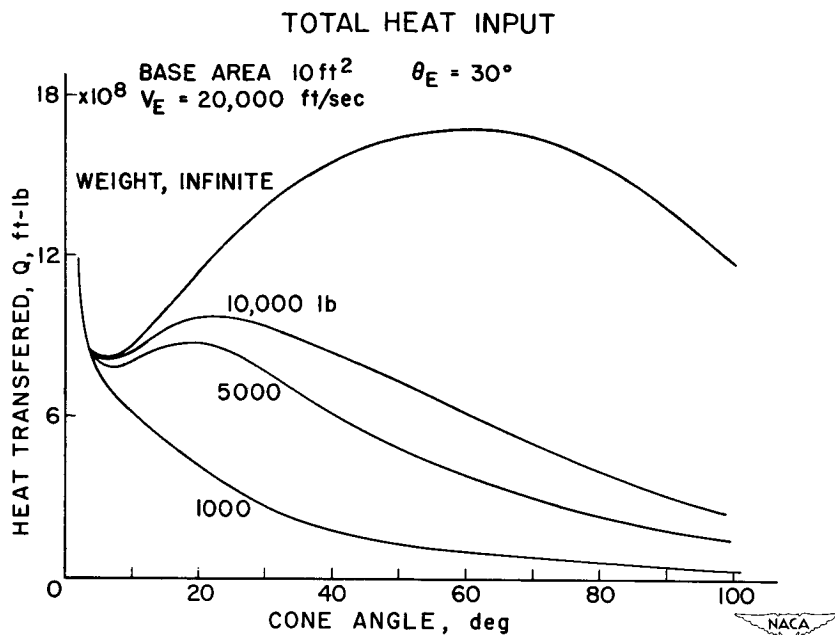


Figure 11

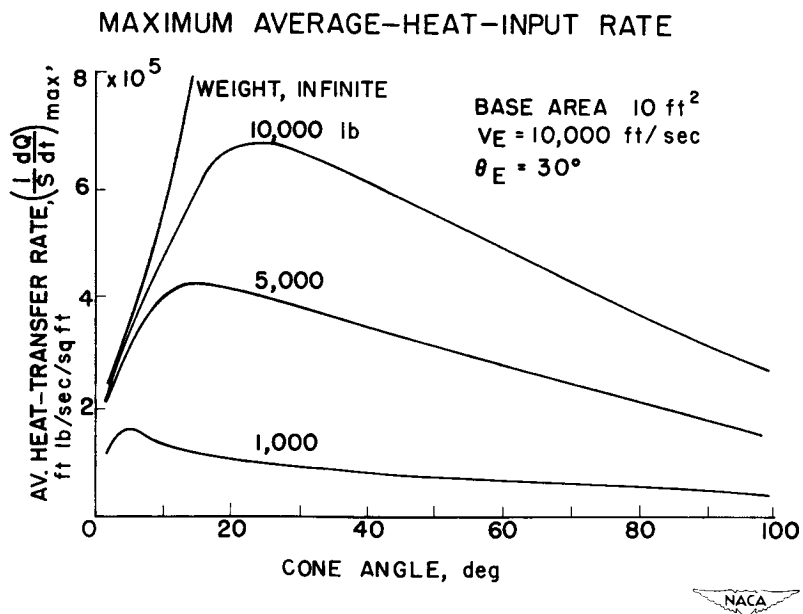


Figure 12

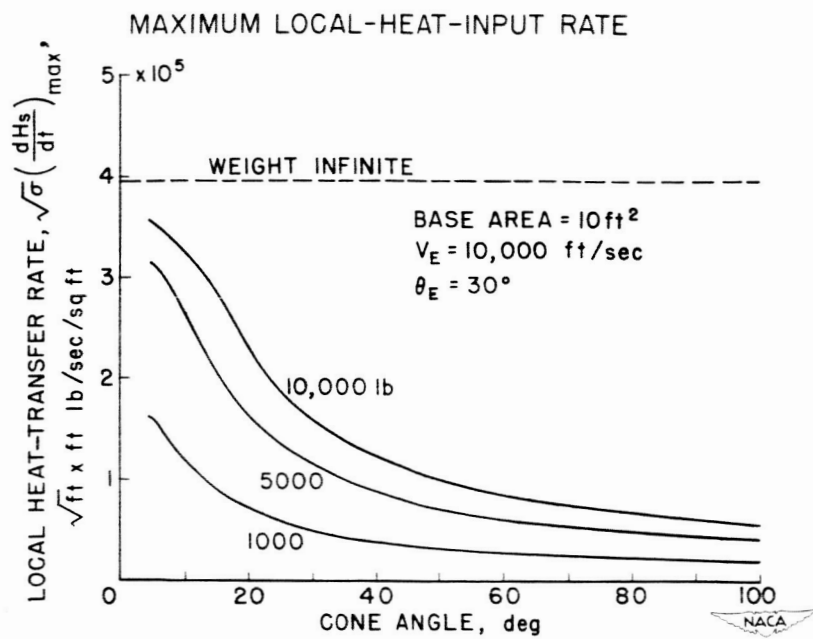


Figure 13

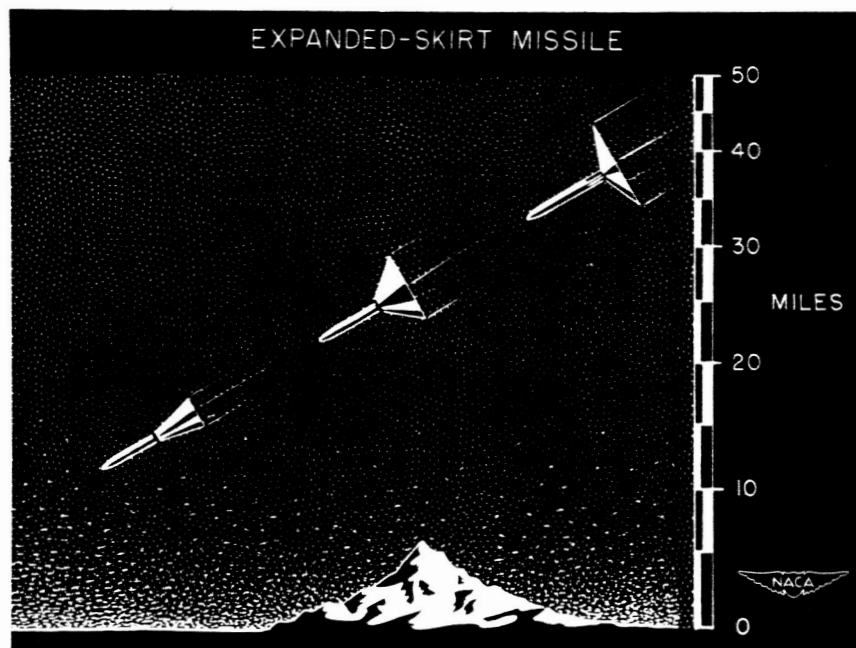


Figure 14

PROBLEMS AND INITIAL EXPERIMENTS ON HEAT TRANSFER AT HYPERSONIC SPEEDS

By A. J. Eggers, Jr., and A. C. Charters, Jr.

Ames Aeronautical Laboratory

The significance of aerodynamic heating in hypersonic flight is perhaps best demonstrated by the fact that solution of the heating problem may in large part dictate the choices of aircraft structure and power-plant. The preceding paper by H. Julian Allen on missiles penetrating the earth's atmosphere provides substantial evidence to this effect. Moreover, it points out that there are many gaps in the existing knowledge of hypersonic heat transfer. One of the foremost of these gaps concerns the behavior of air at the high temperatures encountered in hypersonic flight. It is this matter with which the present paper is chiefly concerned, and, following a brief review of the subject, it is undertaken to describe a novel apparatus and the results of initial experiments aimed at determining hypersonic heat transfer to objects under conditions of pressure and, especially, temperature actually found in the atmosphere.

First, it is instructive to obtain some idea of the magnitude of the boundary-layer temperatures in hypersonic flight. Figure 1 shows the maximum temperature in the laminar boundary layer on a flat plate as a function of Mach number assuming an insulated wall and assuming a wall temperature equal to an ambient temperature of 500° R. These results were obtained from the calculations of Van Driest for a constant Prandtl number of 0.75 and neglecting effects of dissociation and other phenomena which may occur at the higher temperatures (see ref. 1). Ordinarily the wall temperature of a missile would not be expected to fall below ambient temperature; hence it is concluded that air in the hypersonic boundary layer is heated to temperatures in the thousands of degrees. In this light it is not surprising that heat is transferred very rapidly to a hypersonic missile with any reasonably low surface temperature.

The heat-transfer process is complicated, however, by the fact that basic physical properties of air such as the specific heats, viscosity, and thermal conductivity may be profoundly altered, especially if appreciable dissociation occurs at these high temperatures. Considerable uncertainty exists at present as to the extent of these alterations. For example, the variations with temperature of the specific heat at a pressure of 1 atmosphere are shown in figure 2. The upper boundary is for the case of dissociation equilibrium and was obtained by using the enthalpy calculations of Krieger and White (see ref. 2). The lower boundary is for the case of no dissociation. If the kinetics of dissociation were well-understood, an estimate of the specific heat could be made for a particular

flow, and it would probably lie somewhere between these two curves. The kinetics of the rate process are not well-understood, however; thus it must be concluded that at the higher temperatures, the specific heat may be in doubt, even in order of magnitude. Knowledge of thermal conductivity and viscosity at the high temperatures encountered in the hypersonic boundary layer is also limited. As a result, different predictions of heat transfer can be obtained. This point is illustrated in figure 3 which shows, for a cool sphere, the ratio of stagnation-point heat-transfer rate for dissociation equilibrium to that for no dissociation, both rates being calculated by the incompressible-flow method of Sibulkin (ref. 3) in combination with the results of Hansen (ref. 4). It is predicted that, as the Mach number increases above 5 in air of 500° R static temperature, the ratio increases and reaches a value of about 2.5 at a Mach number of 15. Recent studies at the Langley and Ames Laboratories indicate that the effects of dissociation may be more compensating if variations in fluid properties are considered, with the result that the over-all increase in heat transfer, due to dissociation, may not be as large as shown in figure 3.¹ In any case, however, the flow process is not well-understood.


In view of the magnitude of the heat-transfer problem in hypersonic flight, it seems fair to conclude from these considerations that experiments must be conducted which will explore aerodynamic heating on a properly scaled model. Attention is given next, therefore, to experimental methods of obtaining a "hot" hypersonic air stream.

The continuous-flow wind tunnel appears to be unsuited for this purpose because of the extreme difficulties of heating and cooling the air and, of preventing structural failure. Rather, then, some more novel type of equipment appears to be required.

In this connection, the shock tube is an attractive apparatus, especially when employed after the method of Hertzberg (see ref. 7). As is well-known, however, this apparatus tends to assume very large proportions if running times in excess of milliseconds are desired. Longer running times are, of course, desirable from the standpoint of making heat-transfer measurements.

With these points in mind, a search was made for a rapid compression process which would create a reservoir of air at high pressure and, especially, at high temperature. For this purpose, irreversible adiabatic compression deserves attention, since it can, by means of shock waves,


¹ Moore (ref. 5) and Crown (ref. 6) have found in their analyses of the flat-plate case that here also there is noteworthy compensation of dissociation effects. The degree of compensation is open to question, however, inasmuch as both of these analyses appear to be in some error (see ref. 4).



produce a large temperature rise with a large pressure rise. In fact, the more inefficient or irreversible the compression process, the larger the temperature and the larger the final volume of the compressed air. This characteristic is desired because the large temperature coupled with high pressure suggests that with the aid of a nozzle a hypersonic air stream can be generated having the same free-stream temperature and pressure as are encountered in the atmosphere. Furthermore, with the relatively large volume of the compressed air, it is suggested that this stream can be made of substantial duration, thereby facilitating heat-transfer measurements.

In order to investigate these possibilities, an apparatus, compressing air in the irreversible adiabatic manner and then exhausting it through a hypersonic nozzle, has been developed at the Ames Laboratory. This apparatus is termed a hypersonic gun tunnel and is shown schematically in figure 4. In the upper part of this figure is shown the gun tunnel as it appears before firing. The nozzle extends laterally from the gun tube and is isolated from the interior of the barrel by a valve. Air on both sides of this valve is fixed at a pressure of 10 atmospheres and at ambient temperature. The compressor piston is of light weight and is located in the position normally occupied by the projectile for the gun. When the gun is fired, this piston is accelerated rapidly to high velocity and sends out strong shock waves which compress and heat the air in the gun barrel. These waves strike the valve piston covering the nozzle and set it into motion toward the muzzle end of the gun, forcing the air between this piston and the muzzle out through the port. Because of the strong damping in the compression process, the system returns to equilibrium very rapidly, requiring only several hundredths of a second. The equilibrium configuration is shown in the lower portion of this figure. The powder is now in the gaseous state and the trapped air has been compressed to a pressure of about 300 atmospheres. Assuming conservatively an irreversible adiabatic process with the working pressure equal to the final pressure, the final air temperature would be estimated to be about 5,000° R. Inasmuch as the nozzle is now open, this air passes out through the nozzle and forms a hypersonic stream about the model - the stream duration is of the order of 1 second. At the same time, the powder gases are allowed to leak out of the gun barrel at a slower rate through the exhaust port at the breech end of the barrel.

A heavy-wall 20-mm smooth-bore gun was employed in the test apparatus which is shown in figures 5 and 6. Figure 5 is a photograph of the complete assembly; the gun mounted on an I-beam fastened to the wall of the test chamber can be seen stretching diagonally across the center of the picture with its breech at the right and muzzle at the left. The nozzle extends vertically down from the muzzle to the vacuum tank. The vacuum tank and pump can be seen placed on the floor of the test chamber to the left of the gun installation. Figure 6 is an enlargement of the nozzle unit and shows the windows of the working section and the outline of the principal




schlieren objective mirror attached to the wall behind the working section. The compressor piston was a 1/2-caliber nylon cylinder and the valve piston was a 3-caliber nylon cylinder. The nozzle air passage was conical in shape and had a throat diameter of 0.021 inch, a length of 6 inches, and a test-section diameter of 1 inch. Models were located at the exit of the nozzle and were sting supported from below.

Initial experiments included firings with the hypersonic nozzle and nozzle valve removed from the barrel. Several schlieren photographs of the flow from the muzzle port are shown in figures 7(a) and 7(b). One millisecond after firing the gun, a long tongue of incandescent gas can be seen extending approximately 1 foot to the right from the muzzle port. Two milliseconds after firing, the incandescence has disappeared and the jet seems almost to be erupting. Six milliseconds after firing, the flow has steadied down considerably, although there is observed a second surge of incandescent gas, somewhat smaller in extent than the first. There is some indication that these surges occur each time a strong shock or series of shocks collides with the muzzle cap. In any case, after about 50 milliseconds have elapsed, flow from the muzzle port takes on the familiar steady character with more or less equally spaced shock systems. From this time on, until all the air has been exhausted from the gun, there is no apparent change in the flow from the muzzle port. This was the first experimental evidence that the duration of the nonsteady compression process would be short compared to the 1-second duration of flow from the hypersonic nozzle. Also, these experiments confirmed the need for the nozzle valve to protect the nozzle and test models from the initial surges of extremely high-temperature, high-pressure air.

Preliminary calibration of the nozzle was undertaken in the following manner: Pitot and static pressures were measured with conventional tubes connected to variable-capacitance gages. Using these two stream properties and the fact that pitot pressure is essentially twice the dynamic pressure in a hypersonic stream, the Mach number was found to be approximately 6.7. It is necessary to know at least one other property of the stream in order to fix the state of the gas with reasonable certainty. Therefore a direct measurement of stream velocity was made. For this purpose a spark discharge was created near the exit of the nozzle. The resulting pressure disturbance was photographed as it passed through the test section. The velocity of the center of the disturbance was determined from measurements of the distance traveled by the center and the time of travel. This velocity closely approximates the stream velocity and was found to be about 8,200 ft/sec.


The stream velocity and the dynamic pressure determine the stream density, and the stream temperature can be computed from the stream density and the static pressure, provided the gas constant is known. The magnitude of the gas constant depends of course not only on the air temperature, but also on how nearly the air, in expanding out through the



nozzle, has achieved a state of thermal equilibrium, especially as regards dissociation. It is believed that dissociation is negligible, except in the disturbed flow about models in the present tests. This opinion is held because the stagnation pressures appear to be too large by conservative estimate to permit appreciable dissociation in the reservoir. It was tentatively assumed, therefore, that the usual value for the gas constant applied, and this value was used to calculate the stream static temperature. A temperature of 670°R was obtained, which value is low enough to support the initial assumption regarding the gas constant. It should be noted that this temperature is, as desired, equal to those ordinarily encountered in the earth's atmosphere. Also, an effective stagnation temperature of about $6,700^{\circ}\text{R}$ is indicated by these results, which is not out of line with the estimated value of $5,000^{\circ}\text{R}$.


Several measurements were made of each of the stream properties just discussed, and it was found that they varied by less than 10 percent from one run to another. It was therefore undertaken to make preliminary measurements of heat transfer in this stream. In particular, measurements of the temperature rise at the stagnation point of a hemisphere and of the temperature rise of a cylinder were made. Results of measurements for the hemisphere are shown in figure 8. Results of measurements for the cylinder are shown in figure 9. The hemisphere was a copper shell of 0.2-inch diameter with a 0.01-inch thick wall. The shell was one leg of a thermocouple. The other leg was a constantan wire attached to the inside of the shell at the stagnation point. The test conditions are as indicated, the equivalent pressure altitude being about 115,000 feet. A schlieren photograph of flow about the model is also shown in figure 8. In addition to experimental data, the temperature-rise rates calculated by the method of Sibulkin are shown for the cases of equilibrium dissociation and no dissociation (see refs. 2, 3, and 4). These calculated rates bracket the experimental rate initially, being $6,300^{\circ}\text{R}$ per second for no dissociation and $15,000^{\circ}\text{R}$ per second for dissociation equilibrium - the corresponding heat-transfer rates are $280\text{ Btu/ft}^2\text{-sec}$ and $660\text{ Btu/ft}^2\text{-sec}$, respectively. These results suggest that in the present tests the time of passage through the bow wave and past the stagnation point was too short for the air to achieve thermal equilibrium.

Considering now the cylinder tests, the model in this case was an iron-constantan cylinder 0.040 inch in diameter. The thermocouple joint of the two materials was located on the nozzle center line. The initial temperature-rise rate of the cylinder is about $2,500^{\circ}\text{R}$ per second and the corresponding heat-transfer rate is $110\text{ Btu/ft}^2\text{-sec}$. This rate is substantially lower than that measured at the stagnation point of the hemisphere, which result is attributable in good part to the very high heat-transfer rates at the stagnation point. This matter was discussed in the previous paper by H. Julian Allen.



In analyzing the hemisphere and cylinder data, only the initial heat-transfer rates have been considered and, in fact, the experimental data for only the first 0.1 second of flow have been presented. It is observed that even in this short period of time the measured temperature-rise rates have decreased significantly. This result is attributed primarily to transfer of heat through the models, away from the locations at which temperatures were measured, and is not thought to be indicative of a large reduction in the rate of heat transfer into the models.

In summary, it is pointed out that existing information on the behavior of air at the high temperatures encountered in hypersonic flight is both meager and in some cases conflicting. This situation seriously limits knowledge of hypersonic heat transfer. An apparatus termed the hypersonic gun tunnel has therefore been developed with the specific purpose of providing data on hypersonic heat transfer to objects under conditions of pressure and, especially, temperature found in the atmosphere. Results have been presented which indicate that the apparatus is a workable device for producing a "hot" hypersonic air stream. Finally, preliminary heat-transfer data have been obtained for a cylinder and at the stagnation point of a hemisphere immersed in this stream.



CONFIDENTIAL

DECLASSIFIED

REFERENCES

1. Van Driest, E. R.: Investigation of Laminar Boundary Layer in Compressible Fluids Using the Crocco Method. NACA TN 2597, 1952.
2. Krieger, F. J., and White, W. B.: The Composition and Thermodynamic Properties of Air at Temperatures From 500 to 8000°K and Pressures From 0.00001 to 100 Atmospheres. U. S. Air Force Project RAND Rep. R-149, the RAND Corp., Apr. 15, 1949.
3. Sibulkin, M.: Heat Transfer Near the Forward Stagnation Point of a Body of Revolution. Jour. Aero. Sci. (Readers' Forum), vol. 19, no. 8, Aug. 1952, pp. 570-571.
4. Hansen, C. Frederick: Note on the Prandtl Number for Dissociated Air. (To be published in Jour. Aero. Sci. (Readers' Forum).)
5. Moore, L. L.: A Solution of the Laminar Boundary-Layer Equations for a Compressible Fluid With Variable Properties, Including Dissociation. Jour. Aero. Sci., vol. 19, no. 8, Aug. 1952, pp. 505-518.
6. Crown, J. C.: The Laminar Boundary Layer at Hypersonic Speeds. NAVORD Rep. 2299, U. S. Naval Ord. Lab. (White Oak, Md.), Apr. 15, 1952.
7. Hertzberg, A.: Shock Tubes for Hypersonic Flow. Rep. No. AF-702-A-1, Cornell Aero. Lab., Inc., May 1951.

MAXIMUM TEMPERATURE IN LAMINAR BOUNDARY LAYER ON FLAT PLATE

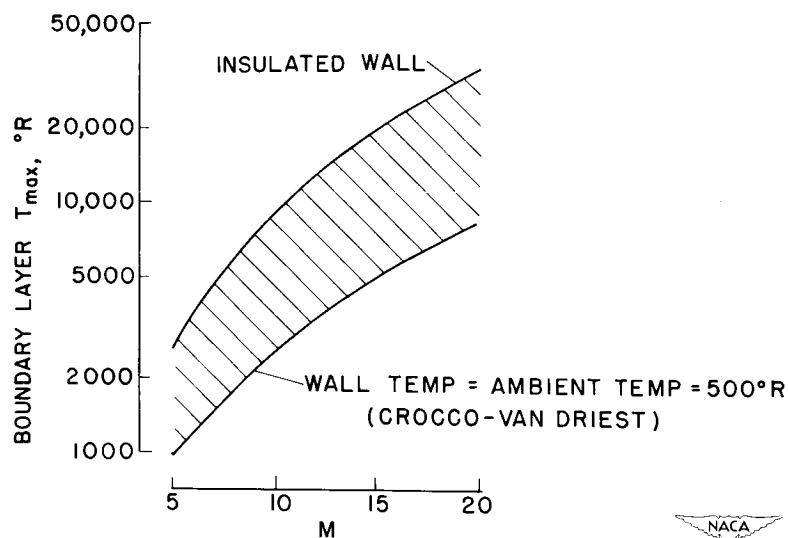


Figure 1

EFFECT OF TEMPERATURE ON SPECIFIC HEAT OF AIR

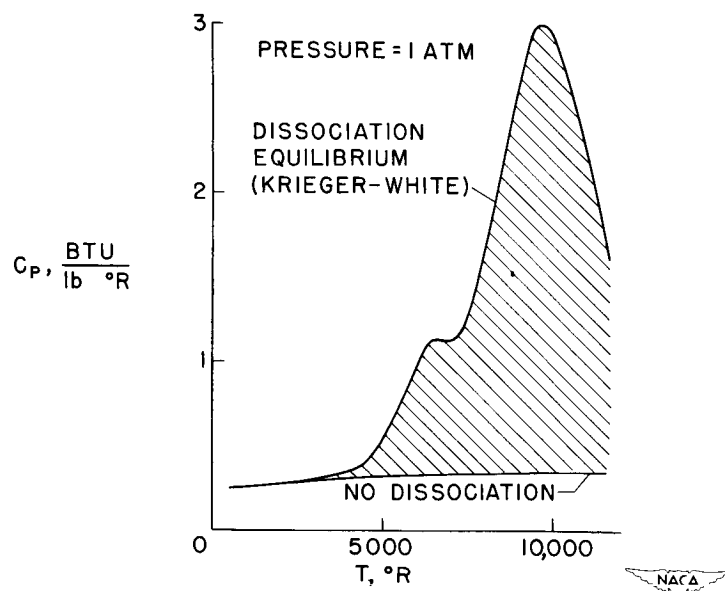


Figure 2

EFFECT OF DISSOCIATION ON HEAT TRANSFER TO STAGNATION POINT OF A SPHERE

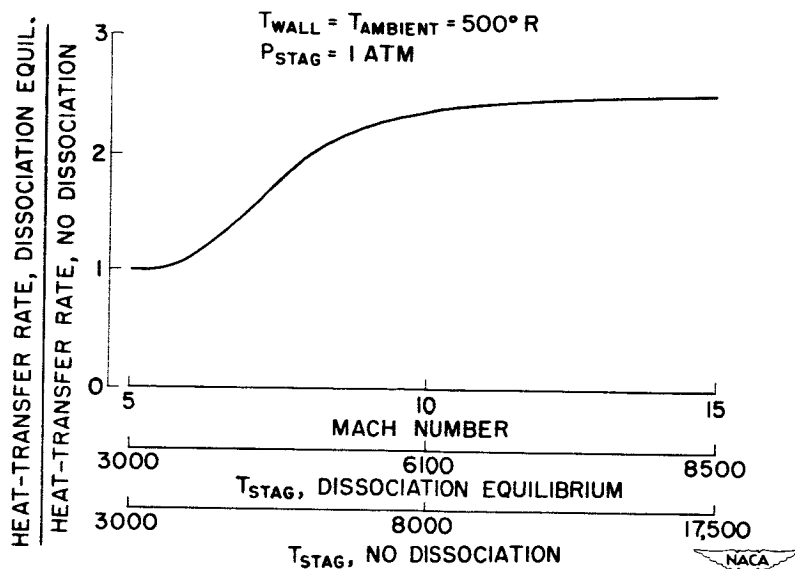


Figure 3

HYPERSONIC GUN TUNNEL

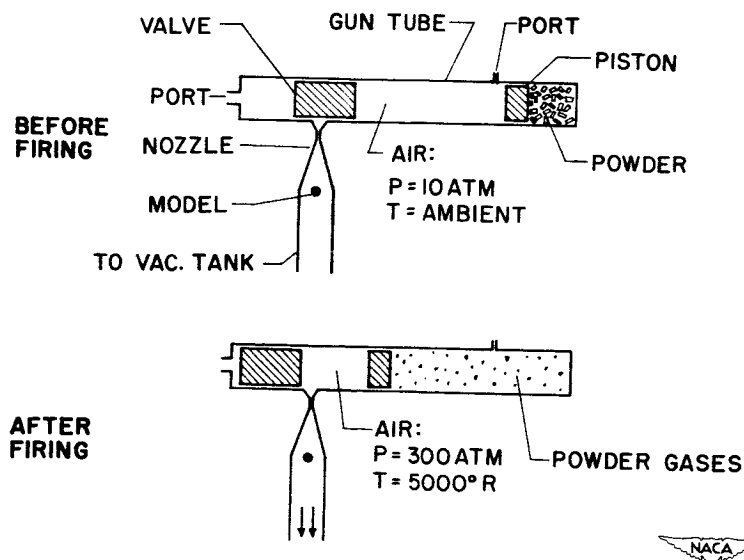


Figure 4

THE 20 MM HYPERSONIC GUN TUNNEL

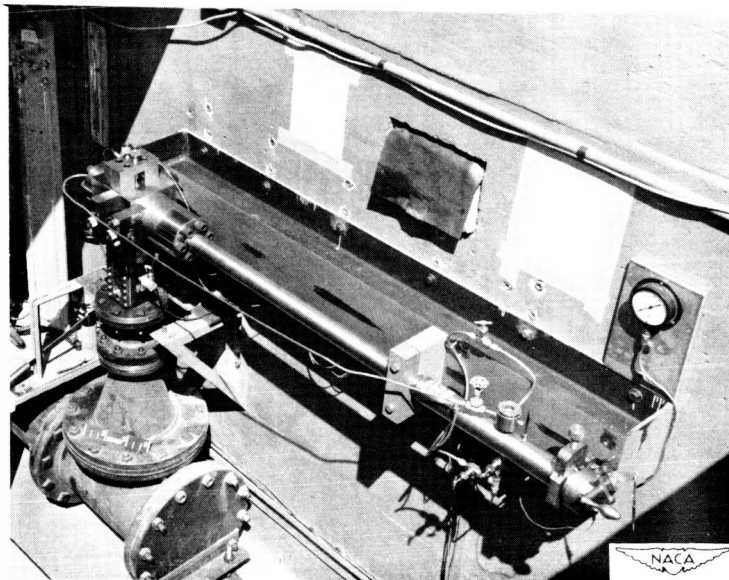


Figure 5

WORKING SECT. OF THE 20 MM HYPERSONIC GUN TUNNEL

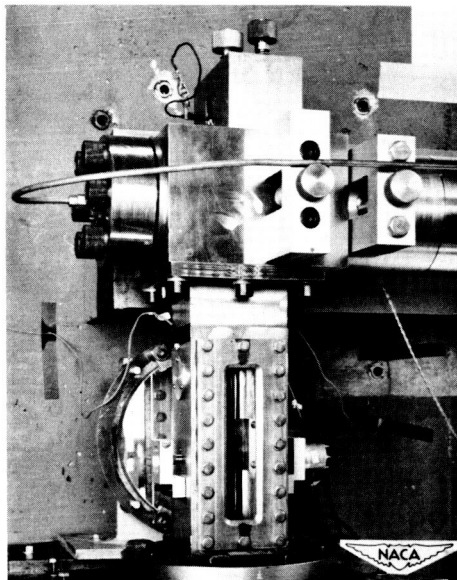


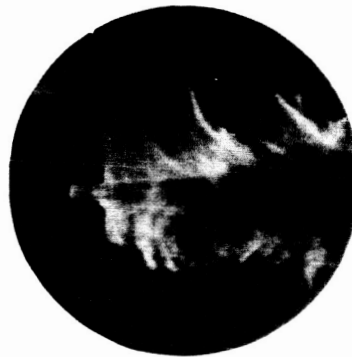
Figure 6



FLOW FROM MUZZLE PORT



1 MILLISECOND
AFTER FIRING



2 MILLISECONDS
AFTER FIRING

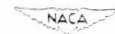
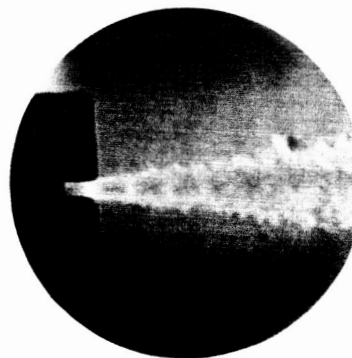


Figure 7(a)

FLOW FROM MUZZLE PORT



6 MILLISECONDS
AFTER FIRING



56 MILLISECONDS
AFTER FIRING



Figure 7(b)



TEMPERATURE RISE AT STAGNATION POINT OF HEMISPHERE

MODEL: COPPER SHELL, 0.2" dia, .01" thick

TEST CONDITIONS: $V=8,200$ ft/sec, $M=6.7$

$P=11$ lb/ft², $q=290$ lb/ft²

$T=670$ °R

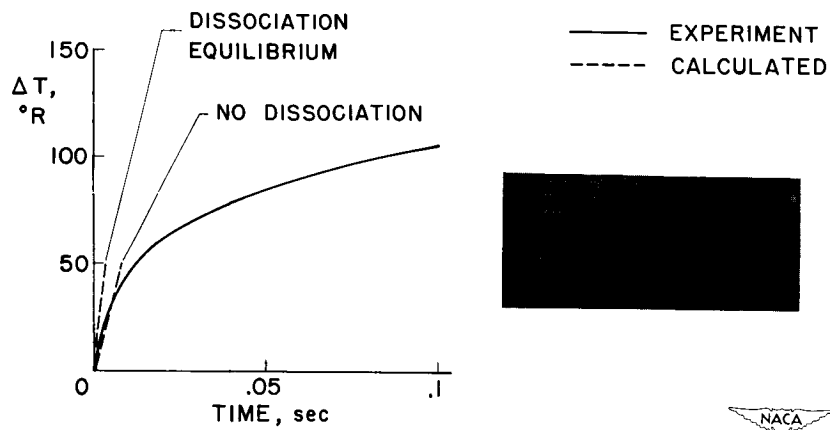


Figure 8

TEMPERATURE RISE OF A TRANSVERSE CYLINDER

MODEL .04 in dia IRON-CONSTANTAN CYLINDER

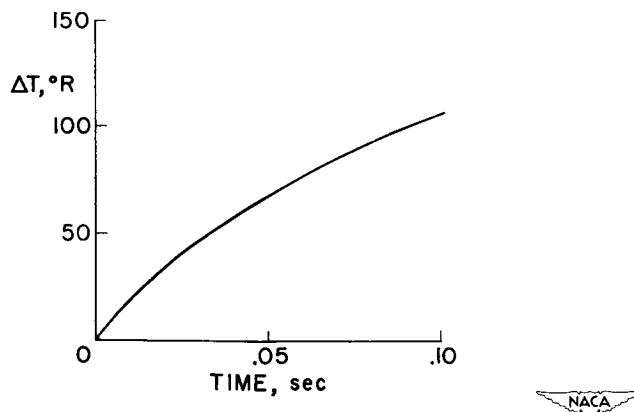


Figure 9

EXPLORATORY TESTS OF THE ALLEVIATION OF AERODYNAMIC HEATING BY WATER TRANSPIRATION COOLING

AT MACH NUMBER 2

By William J. O'Sullivan, Jr., Leo T. Chauvin,
and Charles B. Rumsey

Langley Aeronautical Laboratory

In the last few years the phenomenon of aerodynamic heating in supersonic flight has been investigated, correlated with theory, and its destructive effects upon aircraft structures recognized and demonstrated (for example, refs. 1 to 4). Gas and liquid transpiration cooling have been proposed and are being investigated as a means of cooling turbojets, rocket motors, and their nozzles (for example, refs. 5 to 7). This paper deals with recent exploratory tests (ref. 8) of water transpiration cooling as a means of alleviating aerodynamic heating of aircraft structures at supersonic speeds.

Shown schematically in figure 1 is a conical model of 8° total apex angle equipped with transpiration cooling and installed in a free-air jet. The cooling water entered through the base of the model and emerged through the porous band. Means were provided for measuring the temperature of the entering water and its mass rate of flow. Twenty-eight thermocouples were installed in the skin of the model back of the porous band to measure skin temperatures. The length of the model from apex to rearmost thermocouple was 10.6 inches. The air jet had a Mach number of 2.05 and approximately sea-level temperature and static pressure for a hot day.

Tests were first made without water to measure the dry recovery factors and heat-transfer coefficients on the cone.

In figure 2 the measured recovery factors plotted against distance along the cone back of the porous band are shown as circled points. For comparison, the theoretical recovery factors for a laminar and a turbulent boundary layer, based on the Prandtl number just outside the boundary layer (refs. 9 and 10), are shown as solid curves. The measured recovery factors are in close agreement with the theoretical turbulent value.


The measured heat-transfer coefficients are presented in figure 3 in terms of dimensionless parameters for comparison with theory. The ordinate is the Nusselt number, which contains the heat-transfer coefficient, divided by the cube root of the Prandtl number. The abscissa

is the Reynolds number. These dimensionless parameters are based upon conditions just outside the boundary layer and distance from the apex of the cone. The thermal ratio is the skin temperature T_w divided by the temperature just outside the boundary layer T_1 . Experimental points are shown for thermal ratios of 1.48, 1.52, and 1.56. For comparison, Van Driest's theoretical curve for a thermal ratio of 1.52 (ref. 11) is drawn through the experimental points. The theoretical curves for thermal ratios of 1.48 and 1.56 would lie, respectively, upon the upper and lower edges of the curve shown. Also shown is the experimental flat-plate laminar-boundary-layer curve (ref. 12) corrected to a cone by the theory of Mangler (ref. 13). The heat-transfer measurements agree with the recovery-factor measurements in indicating a turbulent boundary layer.

In figure 4 the steady skin temperature maintained with 52° F cooling water at a mass-flow rate of 0.01 pound of water per second is plotted against position along the model back of the porous band. The entire model skin back of the porous band was uniformly cooled to about 125° F, and cooling extended an unknown distance beyond the end of the model. For comparison the skin temperature of 500° F that would have existed without cooling as determined from the dry tests is shown. The temperature difference is 375° F.


The temperature contours measured when the cooling-water flow rate was reduced to the point where uniform cooling did not occur over the entire length of the model are shown in figure 5 upon a development of the model's surface. The skin temperature was held to between 115° F and 125° F back to nearly the third band of thermocouples and thereafter rose rapidly, except for a cool strip, toward the temperature of 498° F which would have been the skin temperature without cooling. The cool strip may be due to slight angle of attack of the model. The cooling water entered the model at 50° F at a mass-flow rate of 0.0025 pound per second. If the cool strip is disregarded and only the uniformly cooled area forward of the 125° F contour is considered, the water expenditure rate is 2.72 pounds or 0.33 gallon per minute per square foot of cooled surface. An ideal water jacket attached to the under surface of the skin would require about four times as much water to produce the same skin temperature.

An attempt has been made to calculate the skin temperature produced by water-transpiration cooling. The process was visualized as one of evaporation of the water from the model surface into the bottom of the boundary layer producing saturation of the lowermost layer of air. The cooling is thus assumed analogous to the cooling of the wet bulb of the familiar wet and dry bulb sling psychrometer used for the measurement of humidity. Accordingly, the cooled-skin temperature can be conveniently calculated by use of a variation of the sling psychrometer chart





shown in figure 6. The ordinate is temperature and the abscissa is the absolute humidity or pounds of water contained in 1 pound of air. Drawn across the graph is the saturation curve for the particular total air pressure upon the surface of the conical model, which was approximately 1 atmosphere. The air at the surface of the model is considered to be initially at the dry adiabatic wall temperature and therefore is practically dry. Evaporation of water is assumed to take place into the air until saturation occurs. The air temperature is thereby lowered, but the enthalpy or total heat content must remain constant. In reading the chart, start with the dry-air adiabatic wall temperature, proceed along a curve of constant enthalpy until the saturation curve is reached, and there read the temperature of the air-water vapor mixture adjacent to the water film on the model. Under steady cooling, this temperature must also be the temperature of the water film and hence the skin temperature. When the dry adiabatic wall temperature of 500°F employed in the tests is used, the calculated skin temperature is found to be 124°F ; this value agrees almost exactly with the measured skin temperature.

These exploratory tests show that water-transpiration cooling produces large reductions in equilibrium skin temperature at Mach number 2 at high Reynolds numbers. These tests show that on an 8° cone in axially symmetric flow the cooling is nearly uniform for a considerable distance downstream of the point of water release; therefore, the entire cooled surface need not be porous, and heavy and expensive double-wall construction associated with a continuous porous skin may not be required. The physical process of the cooling phenomenon has been visualized as that of evaporation, and the degree of cooling so calculated was found to agree with experiment. Although one is tempted to proceed to the prediction of the skin temperature under transpiration cooling at other Mach numbers, altitudes, and with other cooling liquids, it is considered that further tests should be performed before confidence could be placed in such predictions.



REFERENCES

1. Chauvin, Leo T., and de Moraes, Carlos A.: Correlation of Supersonic Convective Heat-Transfer Coefficients From Measurements of the Skin Temperature of a Parabolic Body of Revolution (NACA RM-10). NACA RM L51A18, 1951.
 2. Donaldson, Coleman duP.: Heat Transfer and Skin Friction for Turbulent Boundary Layers on Heated or Cooled Surfaces at High Speeds. NACA RM L52H04, 1952.
 3. Heldenfels, Richard R., Rosecrans, Richard, and Griffith, George E.: Tests of an Aerodynamically Heated Multiweb Wing Structure (MW-1) in a Free Jet at Mach Number 2. NACA RM L53E27, 1953.
 4. Heldenfels, Richard R., and Rosecrans, Richard: Preliminary Results of Supersonic-Jet Tests of Simplified Wing Structures. NACA RM L53E26a, 1953.
 5. Kinney, George R., Abramson, Andrew E., and Sloop, John L.: Internal-Liquid-Film-Cooling Experiments With Air-Stream Temperatures to 2,000° F in 2- and 4-Inch-Diameter Horizontal Tubes. NACA Rep. 1087, 1952. (Supersedes NACA RM E50F19 by Kinney and Sloop, NACA RM E51C13 by Kinney and Abramson, and NACA RM E52B20 by Kinney.)
 6. Wheeler, H. L., Jr.: Heat Transfer in Nitrogen and Hydrogen Sweat-Cooled Tubes. Progress Rep. No. 20-160, Jet Propulsion Lab., C.I.T., 1952.
 7. Zucrow, M. J., Beighley, C. M., and Knuth, E.: Progress Report on the Stability of Liquid Films for Cooling Rocket Motors. PROJECT SQUID Tech. Rep. No. 23 (N6-ORI-104, Task Order I NR 220-042, Phase 7, Dept. Navy Dept. Air Force), Purdue Univ., Nov. 30, 1950. (Preprint from Jour. Am. Rocket Soc.)
 8. O'Sullivan, William J., Jr., Chauvin, Leo T., and Rumsey, Charles B.: Exploratory Investigation of Transpiration Cooling To Alleviate Aerodynamic Heating on an 8° Cone in a Free Jet at $M = 2.05$. (Prospective NACA paper.)
 9. Wimbrow, William R.: Experimental Investigation of Temperature Recovery Factors on Bodies of Revolution at Supersonic Speeds. NACA TN 1975, 1949.
 10. Squire, H. B.: Heat Transfer Calculations for Aerofoils. R. & M. No. 1986, British A.R.C., 1946.
- 

11. Van Driest, E. R.: Turbulent Boundary Layer on a Cone in a Supersonic Flow at Zero Angle of Attack. Jour. Aero. Sci., vol. 19, no. 1, Jan. 1952, pp. 55-57, 72.
 12. Johnson, H. A., and Rubesin, M. W.: Aerodynamic Heating and Convective Heat Transfer - Summary of Literature Survey. Trans. A.S.M.E., vol. 7, no. 5, July 1949, pp. 447-456.
 13. Mangler, W.: Compressible Boundary Layers on Bodies of Revolution. Rep. and Trans. No. 47, British M.A.P. Völkenrode, Mar. 15, 1946.
- 

SCHEMATIC ARRANGEMENT OF 8° CONE TEST MODEL

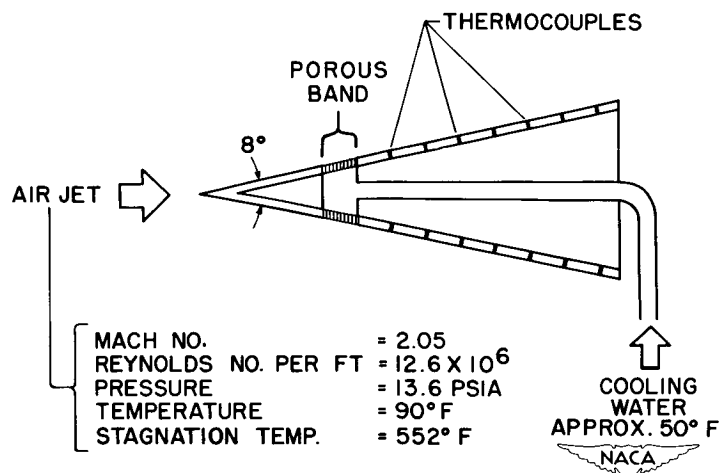


Figure 1

TEMPERATURE RECOVERY FACTOR ON DRY CONE

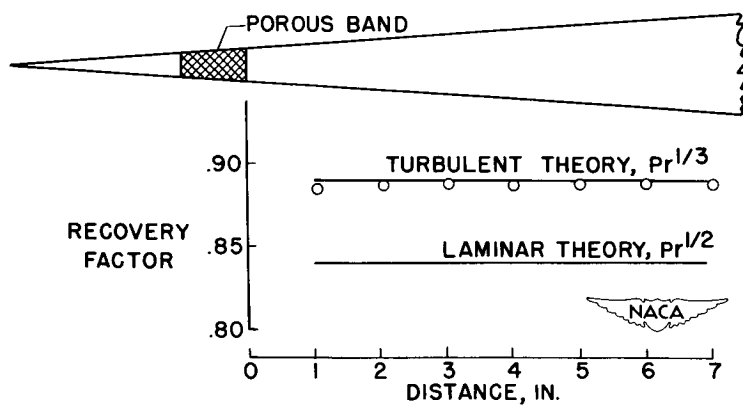


Figure 2

HEAT TRANSFER ON DRY CONE

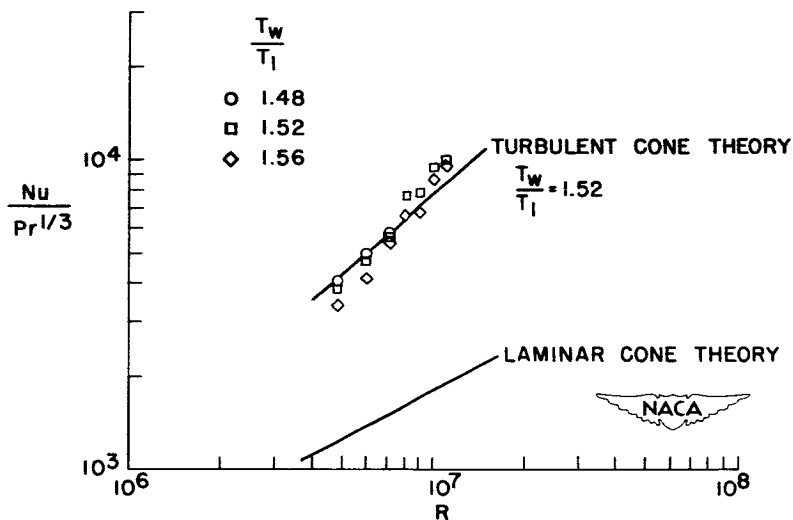


Figure 3

EFFECT OF COOLING ON TEMPERATURE

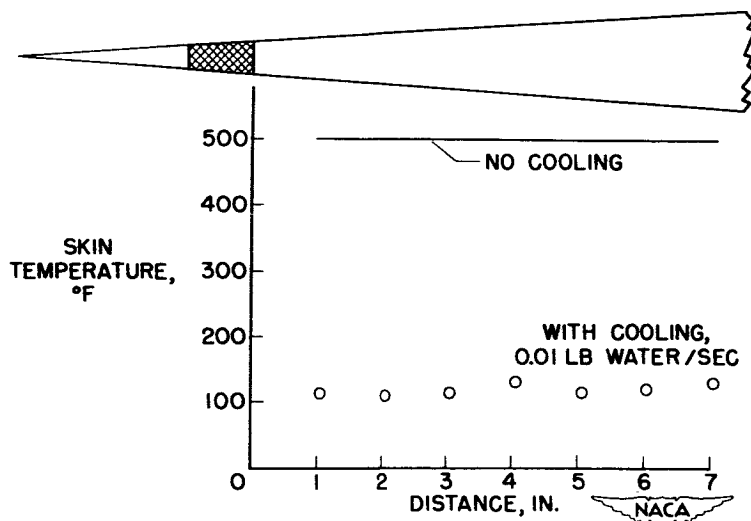


Figure 4

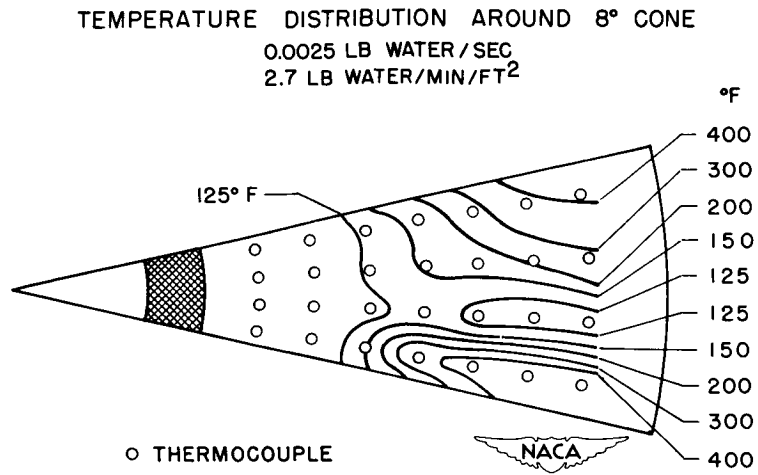


Figure 5

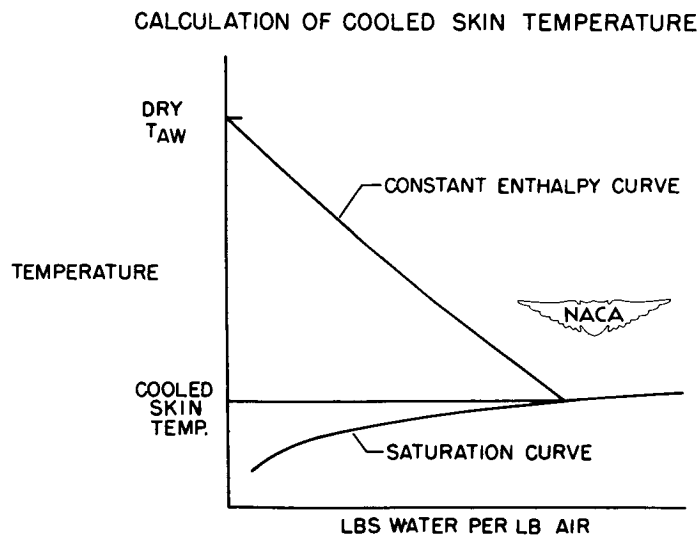


Figure 6

MODEL EXPERIMENTS OF BOMB RELEASES AT SUPERSONIC SPEEDS

By Robert W. Rainey

Langley Aeronautical Laboratory

INTRODUCTION

A recent problem of major concern with regard to supersonic bomber-type aircraft is the attainment of successful release and breakaway characteristics of bombs or stores. For the release and breakaway to be successful, certain essential performance requirements must be met which concern both the aircraft and the bomb or store. Insofar as the aircraft is concerned, the bomb must not strike or endanger the aircraft or its equipment; with regard to the bomb, it not only must clear the aircraft but, because of possible instrumentation within the bomb, it must also avoid rapid accelerations and decelerations and, consequently, appreciable angles of pitch and yaw. It becomes apparent that the interference factors which might cause the bomb to diverge from a near-level attitude during release and breakaway must be minimized.

In an effort to shed some light on this release problem, drop tests have been made in the Langley 9-inch supersonic tunnel at a Mach number of 1.62 of four bomb shapes released from several fuselage bomb-bay configurations and from several pylons beneath a swept wing. These tests were primarily of an exploratory nature to determine what first-order detrimental interference effects are involved. In these tests the breakaway characteristics and initial trajectories were observed and recorded. Approximately 230 drop tests have been made to date.

MODEL CONFIGURATIONS

As shown in figure 1, the four bomb configurations consisted of a 1/30-scale model of the 500-pound Douglas Aircraft Co. store shape having a fineness ratio of about 8.6, the same body shape but with enlarged and modified tail fins, and two models having fineness ratios of 5 and 7 which were equipped with the same enlarged fins. The forebodies and afterbodies of each of the two latter configurations consisted of circular arcs of revolution joined tangentially at 40 percent of the body length. The actual body length of all models was about the same and was approximately $3\frac{1}{2}$ inches.

In figure 2 are presented five of the fuselage—bomb-bay configurations, and their designations, from which bomb-drop tests were made.

The fuselage was mounted from the tunnel side wall beneath a wing having a rectangular plan form and wedge leading and trailing edges. The bombs were held in place in a 45° roll attitude by a spring-loaded wire and were released mechanically in a manner which did not disturb the bomb; at the same time the drop was photographed with a high-speed motion-picture camera which took approximately 1000 frames per second.

In figure 3 is presented a typical bomb-wing-pylon installation. The wing was mounted on the tunnel side wall and was an untapered, 30° swept wing having an NACA 65-009 airfoil section normal to the leading edge. The majority of the drop tests to determine the effects of variation in simulated altitude and chordwise and vertical location of the bomb installation were made from the 80-percent-semispan station. Here again the bombs were released manually, and their release characteristics were recorded by a high-speed motion-picture camera.

SIMILARITY RELATION

Because the Mach number had to be duplicated and because of the limitations of tunnel operation and tunnel size, complete simulation of prototype conditions is impossible and simulation is restricted to dynamic pressure and bomb mass. Therefore, the ratio of the drag to the gravitational force is simulated:

$$\left(\frac{\text{Drag}}{\text{Gravity force}} \right)_{\text{prototype}} = \left(\frac{\text{Drag}}{\text{Gravity force}} \right)_{\text{model}}$$

This means that the path of the model center of gravity essentially duplicates the path of the prototype center of gravity.

This drag—gravitational-force ratio reduces to the form:

$$\left(\frac{C_D q l^2}{w l^3} \right)_{\text{prototype}} = \left(\frac{C_D q l^2}{w l^3} \right)_{\text{model}}$$

where C_D is the drag coefficient, q is the dynamic pressure, l is a representative length, and w is the average bomb density. For these tests, $C_{D_{\text{prototype}}}$ was assumed equal to $C_{D_{\text{model}}}$; therefore,

$$\left(\frac{q}{w l} \right)_{\text{prototype}} = \left(\frac{q}{w l} \right)_{\text{model}}$$




For these tests the prototype was assumed to be a 500-pound Douglas Aircraft Co. store which establishes $l_{\text{prototype}}$ and $w_{\text{prototype}}$ which is given in the following table along with the average bomb densities for three other bombs:

Bomb		Average bomb density, w , lb/cu ft
500-lb	Douglas Aircraft Co. store	91
500-lb	General-purpose M-43	151
1,000-lb	General-purpose M-44	158
10,000-lb	Standard	131

Altitudes were assumed to vary from about sea level to about 40,000 feet which established $q_{\text{prototype}}$. Limitations in tunnel size determined l_{model} ; and, in order to fulfill the similarity relation, q_{model} divided by w_{model} had to be of small magnitude. Therefore, the tunnel was operated at low stagnation pressures, and the models were constructed of lead. Variations in prototype altitude were simulated through variations in tunnel stagnation pressure and, consequently, tunnel dynamic pressure. For a given simulated altitude, the tunnel dynamic pressure was the same for all models, and the shape of the trajectory at one simulated altitude might be essentially the same as that for the same bomb configuration with a different density and at a different altitude.

The inadequacy of the unavoidably low Reynolds numbers of the tests is recognized; however, as shown in figure 4 which presents results from reference 1, the bomb configurations are stable about their centers of gravity in the upper Reynolds number range of these drop tests. Schlieren photographs also presented in reference 1 indicated that, in the upper limit of the Reynolds number range of these drop tests, the flow separated at the maximum diameters of the models; therefore, center-of-pressure shifts, if any, would be expected to be small at lower Reynolds numbers. Further, there are no forward center-of-pressure shifts as a result of increasing the Reynolds number to 10×10^6 , and rearward shifts are small, with the possible exclusion of the Douglas Aircraft Co. store. The Reynolds number inadequacy can, therefore, be discarded as having any overshadowing effect in the drop tests. Attention is drawn to the large shift in center of pressure which results from enlarging and modifying the fins on the Douglas Aircraft Co. store shape.

As previously stated, it was assumed that the prototype drag coefficient is the same as the model drag coefficient in the similarity relation; however, as also presented in reference 1, the model drag



coefficients were considerably lower than the prototype drag coefficients, and this would show up as an increase in simulated altitude.


Because the moment-of-inertia requirements for simulation are not met, the model attitude is representative of prototype attitude in level or near-level drops only; however, it is emphasized that the purpose of these tests is to achieve level or near-level drops. In order to assess the release characteristics of these bomb drops, the film records have been plotted in the form of trajectory diagrams to show the attitude and position of the bombs every $1/120$ second. As a matter of convenience in presenting the results, each release has been classified as good, marginal, or unacceptable. It should be remembered that, because moment of inertia is not simulated, these classifications primarily specify the relative severity of the interference effects upon the bomb. An example of each of the three classifications is presented in figure 5. These releases were made from the fuselage with the conventional box-type bomb bay.

A release classified as good always cleared the aircraft and maintained a near-level attitude. Such model releases should be applicable to the prototype conditions because moment-of-inertia simulation is not required for the near-level drops. All other releases involved changes in attitude; therefore, the extent to which these releases simulate the prototype conditions is doubtful. It is possible to separate these remaining releases into two categories; one, classified as marginal, in which only moderate interference effects appear evident and the model bomb did not undergo extreme changes in attitude and cleared the fuselage in good fashion, and, two, classified as unacceptable, in which large interference effects appear evident and the model bomb undergoes large changes in attitude and also might endanger the fuselage. The boundaries of these two categories are arbitrary and subject to individual interpretation.

RESULTS AND DISCUSSION

Bomb Releases From Fuselage

In analyzing the bomb releases made from the conventional box-type bomb bay (see table I and fig. 6), it was found that the nose-down tendency, shown in figure 5, could be lessened through an increase in body size or a decrease in fin size. Tuft studies of the flow within the bomb bay indicated that a strong counterclockwise circulation of flow was present similar to that noted previously during a subsonic bomb-drop investigation in the Langley 300 MPH 7- by 10-foot tunnel and reported in reference 2. Apparently the increase in body size, accomplished by a reduction in fineness ratio, restricted and weakened this




flow circulation, thereby reducing the nose-down attitude of the bomb during release. Likewise, the smaller fins on the Douglas Aircraft Co. store resulted in a smaller increment of interference lift at the tail and lessened the nose-down pitching-moment increment. Increases in simulated altitude generally improved the release characteristics, and good releases were obtained with the Douglas Aircraft Co. store and the bomb of fineness ratio 5 at a simulated altitude of 40,000 feet only.

Efforts to lessen the nose-down tendency during the release phases of the Douglas Aircraft Co. store at lower altitudes included the installation of solid and perforated spoilers at the front of the bomb bay, setting the fuselage at positive and negative angle of attack of 4° and setting the bomb at a positive angle of incidence of 4° with the fuselage at 0° angle of attack. Improvement of the release characteristics was obtained only in the case of the fuselage at a negative angle of attack of 4° , and good releases were obtained at simulated altitudes of 30,000 and 40,000 feet. It was also found that the installation of three baffles across the interior of the bomb bay would alter the flow within the bomb bay sufficiently to obtain good drops with all bombs over a relatively wide range of simulated altitudes.

Removal of the forward and rearward inner portions of the fuselage modified the box-type bomb bay into a complete channel (see fig. 2). This alleviated the aforementioned flow circulation and removed most of the nose-down tendency; the small nose-down tendency which remained was probably due to the flow blockage and pressure increase between the top of the channel and the forward portions of the bombs (see fig. 6). Changes in bomb configurations or simulated altitude had little effect upon the releases, all of which were marginal or good (see table I).

The bomb releases from the semiexternal bomb bay showed strong nose-up tendencies, and the only good releases obtained were with the bombs of fineness ratio 8.6 at 30,000 feet (see table I and fig. 7). It is believed that the bomb cavity deflected the flow downward onto the afterportions of the bomb during the initial release phases and caused the nose-up tendency. Suspending the bomb on struts 0.2 bomb length below the fuselage (see the semiexternal bomb bay with struts in figs. 2 and 7) did not remove the bomb far enough from the cavity to improve the release characteristics. However, removing the cavity, as in the case of the external bomb bay, did alleviate the situation, and good drops were obtained over a relatively wide range of altitudes for the large-finned bombs. In using these three latter bomb bays, increases in static margin of the bomb or simulated altitude were beneficial to the release characteristics (see table I).




Bomb Releases From Wing Pylons

The majority of the wing-pylon releases, as shown in figure 3, were made from the 80-percent-semispan station using a short-chord pylon at 20,000 and 30,000 feet simulated altitudes. The Douglas Aircraft Co. store was not used in these tests. Because the flow beneath the wing impinged on the forward portions of the bombs, unacceptable nose-down tendencies were evident for all bombs released from position I (see fig. 8), and the fins gouged into the lower wing surface. Shifting the bombs to position II or III did not relieve the condition appreciably; however, at position IV the nose-down tendency was replaced by nose-up tendencies for the bombs of fineness ratio 5 and 7 resulting in marginal releases. Good releases were obtained with the bomb of fineness ratio 8.6. A summary of the wing-pylon releases is presented in table II. In an effort to alleviate the fin gouging noted during the releases of the bombs at position I, the trailing edge of the pylon was extended to the rear of the bomb so that during the nose-down portion of the release, the rotation would take place about the rear of the bomb. This pylon is designated the long-chord pylon in figure 8. This scheme was effective in eliminating the fin gouging of all bombs; and, in the case of the bombs of fineness ratio 7 and 8.6, the release characteristics were marginal at all simulated altitudes as compared to unacceptable for the short-chord-pylon releases.

Two additional releases were made from the 40-percent-semispan station using the bomb of fineness ratio 7 at position III. No changes in the release characteristics were evident as a result of moving the bomb-release station inboard.

CONCLUSIONS

As a result of these bomb-drop tests at a Mach number of 1.62, the following conclusions are indicated:

1. The effects of increasing altitude were, in most cases, beneficial to the release characteristics of a bomb; these effects were never detrimental.
 2. In making releases from an internal box-type bomb bay of the type common to subsonic bombers, it appears beneficial to reduce the flow circulation within the bomb bay by reducing the clearance around the bomb or by using baffles.
 3. In general, the release characteristics of bomb drops from the complete channel, the external bomb bay, and the box-type bomb bay with baffles were superior throughout a wide range of altitudes to the releases from the other bomb bays.
- 

4. In making releases from semiexternal or external mounts below the fuselage and from pylons beneath the wing, an increase in static margin improves the release characteristics.

5. The bomb position which results in the best releases from the wing-pylon mount appears to be very close to that which gives the least drag rise due to the addition of a similar bomb-pylon installation as indicated in reference 3.

REFERENCES

1. Rainey, Robert W.: Effects of Variations in Reynolds Number on the Aerodynamic Characteristics of Three Bomb or Store Shapes at a Mach Number of 1.62 With and Without Fins. NACA RM L53D27, 1953.
2. Kuhn, Richard E., and Polhamus, Edward C.: Wind-Tunnel Investigation of Bomb-Bay Configurations Intended to Minimize the Tumbling of Light-Weight Bombs. NACA RM L7D11, 1947.
3. Jacobsen, Carl R.: Effects of Spanwise, Chordwise, and Vertical Location of an External Store on the Aerodynamic Characteristics of a 45° Sweptback Tapered Wing of Aspect Ratio 4 at Mach Numbers of 1.41, 1.62, and 1.96. NACA RM L52J27, 1953.

TABLE I. - SUMMARY CHART OF RELEASES FROM FUSELAGES

Bomb-bay configurations	Bomb fineness ratio	*Release characteristics at simulated altitudes of -				Bomb motion for M and U classifications
		10,000 ft	20,000 ft	30,000 ft	40,000 ft	
Conventional box type	5 7 8.6 8.6 (D.A.C.)	U	M U U U	M U U M	G M U G	Nosed down
Conventional box type with 3 baffles	5 7 8.6 8.6 (D.A.C.)	M G G	G G G			Slight nose-up, then nose-down
Complete channel	5 7 8.6 8.6 (D.A.C.)	M M M M	M M M M	M M G M		Nosed down slightly
Semiexternal	5 7 8.6 8.6 (D.A.C.)	U	U U M	U M G G		Nosed up
Semiexternal with struts	5 7 8.6 8.6 (D.A.C.)	U M M U	U M M	U M G G		Nosed up
External	5 7 8.6 8.6 (D.A.C.)	M G G U	M G G M	G G G G		Nosed up

* G = Good.
M = Marginal.
U = Unacceptable.



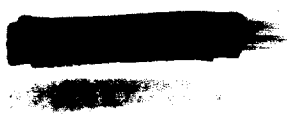
[REDACTED]

TABLE II.- SUMMARY CHART OF WING-PYLON RELEASES

Bomb position	Bomb fineness ratio	^a Release characteristics at simulated altitudes of -		Bomb motion for M and U classifications
		20,000 ft	30,000 ft	
SHORT-PYLON RESULTS				
I	5 7 8.6	U U U	U U U	Nosed down
II	5 7 8.6	U U M	U U M	Nosed down
III	5 7 8.6	U U U	U U U	Nosed down
IV	5 7 8.6	U U bG	M M G	Nosed up
LONG-PYLON RESULTS				
I	5 7 8.6	U bM bM	U M M	Nosed down

^aG = Good
M = Marginal
U = Unacceptable.

^bRelease characteristics were marginal at 10,000 feet.



BOMB CONFIGURATIONS TESTED

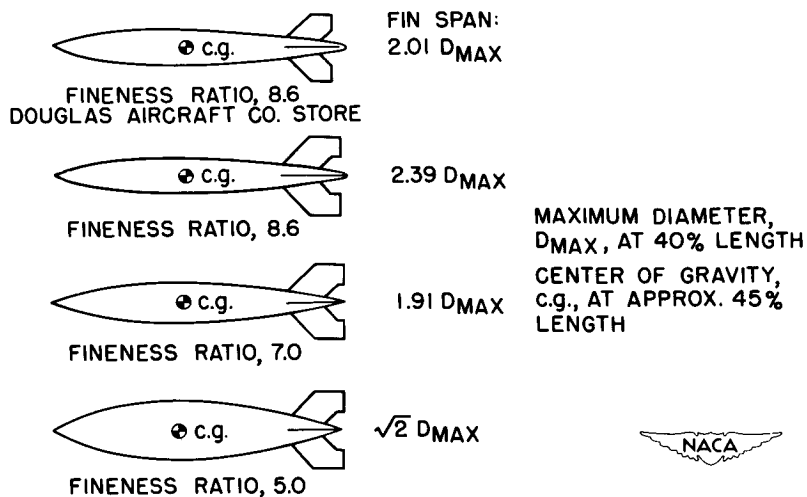


Figure 1

BOMB-BAY CONFIGURATIONS

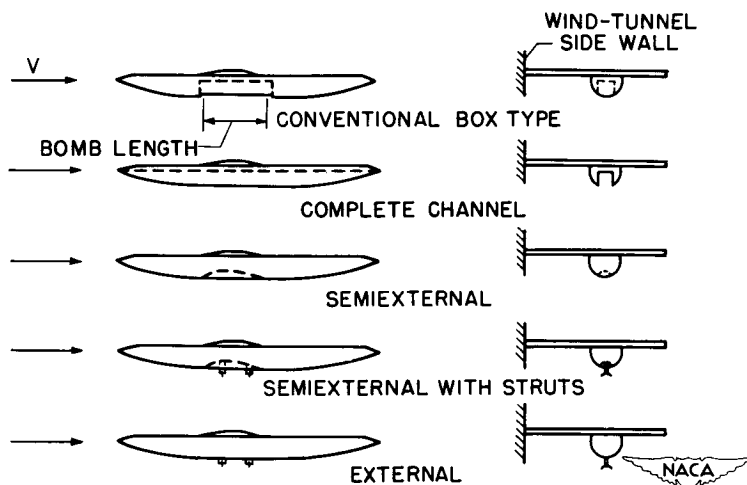


Figure 2

[REDACTED]

[REDACTED]

TYPICAL BOMB-WING-PYLON INSTALLATION

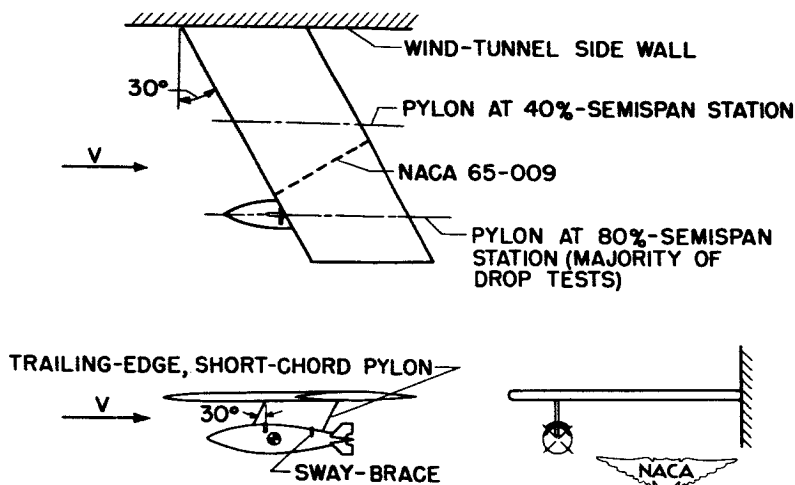


Figure 3

CENTER-OF-PRESSURE POSITION OF BOMBS AT $\alpha=0^\circ$

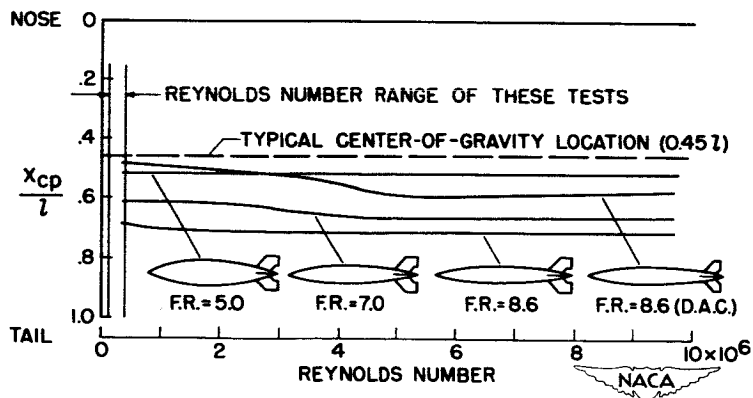


Figure 4

EXAMPLES OF GOOD, MARGINAL, AND UNACCEPTABLE BREAKAWAY CHARACTERISTICS

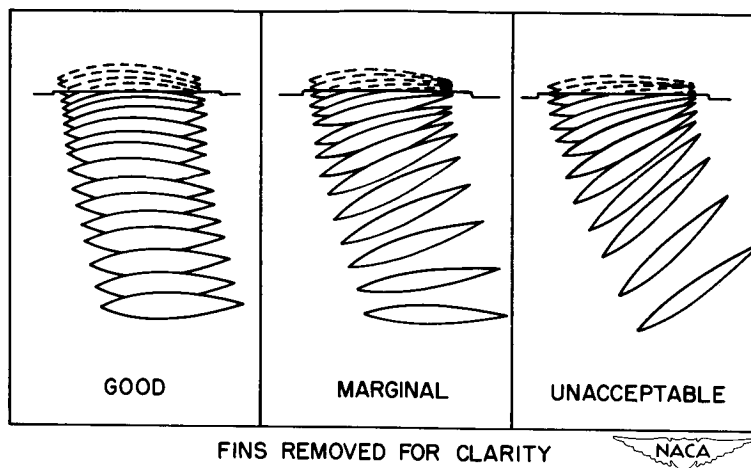
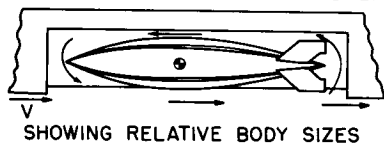


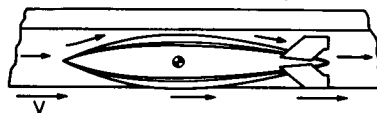
Figure 5

INTERNAL BOMB-BAY CONFIGURATIONS

CONVENTIONAL BOX-TYPE BOMB BAY



COMPLETE CHANNEL



SHOWING RELATIVE FIN SIZES
ON FINENESS-RATIO-8.6 BOMBS



Figure 6



EXTERNAL BOMB-BAY CONFIGURATION FINENESS-RATIO-5 BOMB

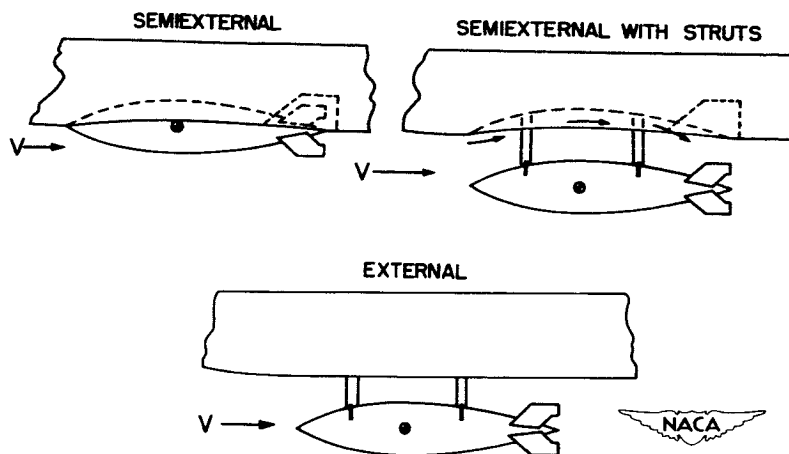


Figure 7

BOMB LOCATIONS FOR WING-PYLON RELEASES

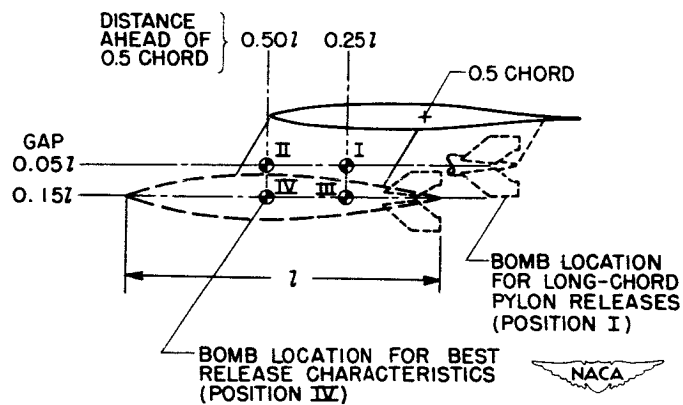


Figure 8

DECLASSIFIED

CONFIDENTIAL

CONSIDERATIONS AFFECTING HYDRO-SKI AIRPLANE DESIGN

By Kenneth L. Wadlin


Langley Aeronautical Laboratory

Several methods of basing and operating airplanes become possible when the airplanes are equipped with hydro-skis. This paper, however, will be concerned only with the fully water-based hydro-ski airplane that starts at rest in the water and makes the complete take-off and landing run on the water. An airplane of this type is shown in figure 1. Before discussing the hydrodynamic performance of this type of airplane, it may be well to consider how the application of hydro-skis affects supersonic configurations. Such details as the location of the wing, tail, air intakes, and jet exhaust must be examined with reference to the peculiarities of water operation.

The airplane shown in figure 1 was derived from the D-558-II research airplane. The location of the air intakes of the D-558-II on the under side of the fuselage is an example of how water operation influences the aerodynamic configuration. This location is obviously not suitable for the water-based hydro-ski airplane since the intakes would be submerged when the airplane is at rest and at low speeds. The air intakes were, therefore, moved to the upper portion of the fuselage. Also, the jet and rocket exhausts were inverted to keep the jet exhaust as high as possible. Tests have shown that air intakes in this position can be kept clear of water by the use of small strips placed along the fuselage center line below the intakes and extending forward to the nose.

For airplanes of this type, portions of the aerodynamic surfaces may be wetted or even be under water at rest and at low speeds and be subjected to hydrodynamic loads. The dynamic pressure of the water at these low speeds, however, is of the same order as the dynamic pressure of the air at supersonic speeds. For example, the dynamic pressure of the water at 45 fps is comparable to that encountered in the air at a Mach number of 1.2. Hydro-skis normally raise most of the airplane clear of the water at speeds under 45 fps; therefore, airplanes that operate at supersonic airspeeds will, because of aerodynamic requirements, normally be designed to a strength of the order of that necessary for the water loads encountered by aerodynamic surfaces.

In considering the take-off performance of the hydro-ski airplane, water resistance is generally one of the first problems to arise. A typical water-resistance curve for a hydro-ski airplane is presented in figure 2. As the water speed is increased, the resistance rises rapidly to a peak value or "hump." This rapid rise occurs when the fuselage is carrying most of the load. The hump occurs in the speed range where



WADLIN


the skis are emerging from the submerged to the planing condition. As the speed increases further, the hydrodynamic load is transferred entirely to the skis and the resistance decreases because of inherent decreases in load and angle of attack. Also included in this figure are the resistance of the fuselage alone and of the planing skis alone when the fuselage and the skis are operating under the same load conditions. These two components are the primary sources of the hydrodynamic resistance. However, for a hydro-ski airplane when the load is divided between the fuselage and the skis, other factors, such as the hydrodynamic resistance of the supporting struts and wetted portions of the wing, spray, and interference effects, influence the total hydrodynamic resistance. These factors result in the over-all resistance differing from the dashed-line curves shown for the two principal components.

The resistance of the fuselage rises rapidly and indefinitely with speed while the planing resistance of the skis decreases as the speed is increased and becomes zero, of course, when the skis leave the water at take-off. If the fuselage were not lifted clear of the water, the resistance would continue to rise and the airplane would not take off. It is necessary, therefore, for the skis to raise the fuselage clear of the water before the take-off resistance of the airplane exceeds the available thrust. The characteristics of the skis selected must be such that the intersection of the separate resistance curves for the fuselage and the skis occurs at an acceptable value of resistance.

The remainder of this paper summarizes hydrodynamic investigations by the National Advisory Committee for Aeronautics of fuselages, hydro-skis, and struts and how the results of these investigations may be used to assist in the design of hydro-ski airplanes. Investigations on complete configurations are reported in references 1 to 11. The scope of the available NACA information is shown in figures 3 and 4. Data have been obtained for three streamline bodies of revolution having fineness ratios of 6, 9, and 12, for a body having a fineness ratio of 9 but modified to increase the longitudinal curvature, and for a fuselage having a fineness ratio of 9 with the aft end modified to accommodate a jet exhaust (refs. 12 to 15).

At speeds where the skis are submerged, the struts supporting the skis contribute to the total resistance. The resistance of the struts at preemergence speeds, which are generally below the inception of cavitation, is estimated to be less than 5 percent of the total hydrodynamic resistance. Surface-piercing struts at zero yaw have been investigated at speeds up to 80 fps at several depths of immersion, with zero rake and raked 30° forward and aft (ref. 16). NACA 66-series airfoil sections of 12 and 21 percent thickness were used.

The range of ski shapes covered is shown in figure 4. The plan forms for which planing data have been obtained include rectangular and



triangular forms, and rectangular forms with triangular aft ends. The triangular aft ends have been found to be of interest because of their improved stability and lower landing loads as compared with rectangular aft ends. The cross sections include curved-bottom shapes, flat and V-bottom shapes with several dead-rise angles and flared and vertical chines (refs. 17 to 22). Planing data have been obtained for a flat ski with taxiing wheels of several sizes and cross sections located at a variety of positions with respect to the ski (refs. 23 and 24). In addition, data have been obtained in the submerged condition for flat plates having length-beam ratios of 8, 4, and 1.

From fuselage data (refs. 12 to 15), it is possible to determine the maximum speed which a fuselage can attain before exceeding a specified value of resistance. Figure 5 presents such data as a plot of the lift-resistance ratio of several fuselages against the Froude number. The Froude number is the speed divided by the square root of the product of the gravitational constant and the wetted length. It is usually the governing parameter when, as in the case of the fuselage, wave-making resistance is predominant. When plotted in this manner, the data for each fuselage at various speeds and loads fall along a single curve. From these curves the speed at which the fuselage must clear the water to attain a given lift-resistance ratio can be estimated.


Since in the low-speed range the hydrodynamic lift supports nearly all the weight of the airplane and since the resistance cannot exceed the thrust available for take-off, the minimum allowable lift-resistance ratio is determined by the ratio of weight to thrust of the airplane. The thrust of recent high-speed airplanes has been such that the required lift-resistance ratio falls between 2.5 and 4. In this range of lift-resistance ratios, fuselages in general would have to be lifted clear of the water at a Froude number of approximately 1.3, which corresponds to a speed of 45 fps if the fuselage is 40 feet long, or 65 fps if 80 feet long. A hydro-ski that will lift the fuselage from the water at this speed can be selected by using data similar to that given in figures 6 and 7.

Figure 6 presents the variation of hydrodynamic lift coefficient with angle of attack (where the lift coefficient is based on the wetted area) for a flat ski, a curved-bottom ski suitable for flush retraction into a streamline fuselage, and for a curved ski with vertical chine strips equal to 10 percent of the beam. The data shown are for a wetted length-beam ratio of 4. These lift curves are nonlinear as for low-aspect-ratio airfoils. The convex ski has lower lift at all angles of attack than the flat-bottom ski. The addition of vertical chines to the curved-bottom ski, however, increases the lift to values larger than for the flat ski.

Figure 7 presents the variation of lift-resistance ratio with lift coefficient for the same three skis. The flat-bottom ski and the convex-bottom ski have approximately the same maximum lift-resistance ratio, whereas the convex-bottom ski with the vertical chines has a lower maximum. These maximum lift-resistance ratios occur at low lift coefficients. For ease of retraction and for limiting landing loads, hydro-skis are preferably small and must, therefore, operate at high lift coefficients in the critical region of ski emergence. At the higher lift coefficients, the lift-resistance ratio of the curved-bottom ski is considerably lower than that for the flat-bottom ski. The addition of the vertical chine strips, however, increases the lift-resistance ratio to a value higher than that of the flat-bottom ski. In the higher range of lift coefficients, the lift-resistance ratio is primarily determined by the resistance due to lift, and the ski with the greatest lift for a given angle of attack will generally also have the highest lift-resistance ratio as shown in figures 6 and 7.

The planing data were obtained at relatively low speeds in the towing tanks and the question of their validity at the high speeds involved in the take-off and landing of present high-speed airplanes is an obvious question. In view of this condition, the NACA has been investigating methods of obtaining data at higher speeds. A small blow-down water jet has been employed for an exploratory investigation. Tests of small planing surfaces at speeds up to 200 fps have been made in this jet. Figure 8 shows a schematic diagram of the apparatus. A high-pressure air supply is used to force water from a tank through a nozzle. The nozzle has an elliptical profile and produces a rectangular stream 3 inches wide and $3/4$ inch deep. The model is supported in the stream by a strain-gage balance that measures lift, resistance, and trimming moment which are recorded on an oscillograph simultaneously with the pressure at the nozzle. A limited quantity of high-pressure air is admitted to the water tank. As water is forced out of the tank, the speed of the jet stream decreases because of the decreasing pressure of the expanding air. In this way data are obtained at speeds from 200 fps down to about 70 fps in a single run.

Figure 9 presents some of the lift data obtained with this apparatus and corresponding data obtained at lower speeds in Langley tank no. 1. The data in both cases are for a rectangular flat plate having a wetted length-beam ratio of 4. An experimentally determined boundary-correction factor has been applied to the data obtained in the jet, no correction being required for the towing tank data. The data shown by the untagged points were obtained in the jet; the tagged points are towing tank data. The upsweep at low speeds is due to buoyancy effects which decrease rapidly with speed and are not a consideration at the speeds in question. Except for a slight upsweep at the highest speeds, which is believed to be at least in part due to the boundary conditions imposed by the method of testing, there is no appreciable variation in lift coefficient with speed. The data that have been obtained up to the present time are



somewhat limited and have not as yet been completely analyzed; however, indications are that there is no significant effect of speed on the lift of prismatic planing surfaces, and the trends indicated by data obtained at towing tank speeds can be expected to hold at the higher speeds encountered during landing and take-off of full-scale airplanes. For complex surfaces, however, where negative pressures may be present, this effect is not necessarily the case.


The considerations so far have been concerned with meeting the take-off requirements; however, the required ski size is also influenced by the landing-load requirements. The beam of the ski and the flight-path angle at a given landing speed are the primary factors influencing the landing load on the ski. Figure 10 shows the theoretical variation of landing load factor with ski beam for a 20,000 pound airplane equipped with twin flat-bottom rectangular skis (ref. 25). The variation for flight-path angles of 3° and 6° are presented. It can be seen that for a given flight-path angle the load factor increases with increasing beam. Therefore, the beam of the ski to meet a specified load factor is limited. The trend of decreasing load factor with decreasing beam points out the structural advantage of the hydro-ski with its relatively narrow beam as compared with that of a typical flying-boat hull. Although figure 10 is limited to rectangular skis, similar theoretical information for skis with triangular aft ends is also available in references 26 and 27. Since triangular skis present smaller wetted beams during the initial phases of a landing, they will have correspondingly lower loads as indicated in figure 10.

If the size of ski required for take-off is not compatible with the landing load requirements, other load-alleviating features such as variable area or variable dead rise may be used. Shock absorbers may also be used to reduce the load factor, and thereby allow more freedom in the selection of ski proportions that will meet both take-off and landing requirements.

The forces on the submerged hydro-ski or on its supporting struts do not generally have a major effect on the selection of the ski size. Force data on struts and submerged skis are, however, useful in determining design loads when the ski is submerged. They are also useful in calculations to assess the relative hydrodynamic performance of different configurations. Submerged ski data indicate a basic stability problem encountered in the transition from the submerged to the planing condition. This condition is illustrated in figure 11 where the lift of a flat rectangular ski is plotted against the distance of the leading edge of the ski from the water surface measured in ski length, that is, z/l where l is the ski length and z is the distance of the leading edge from the water surface. For the submerged condition, z is taken as positive and indicates the draft of the ski leading edge; for the planing condition, z is negative and indicates the vertical distance that the ski protrudes above the water.


Figure 11 shows that, for a fixed angle of attack, as the ski approaches the water surface, the lift drops rapidly to a planing lift that is only about one-half the lift obtained in the deeply submerged condition. This decrease in lift will cause the ski to resubmerge when it breaks the water surface and rise again when the flow is reestablished. The ski will oscillate between planing and deep submergence. One obvious way to avoid such an oscillation is to increase the angle of attack sufficiently to obtain planing lift equal to the submerged lift. Fortunately, ski-airplane configurations that have been considered have usually provided an inherent increase in ski angle of attack because of rotation of the airplane about the aft end of the fuselage as the ski lifts itself toward the water surface. Configurations that do not provide an inherent increase in angle of attack with ski emergence may still merit consideration if means for manual control of angle of attack by the pilot can be provided.

In summarizing, it may be stated that, although the many interrelated variables involved preclude the complete design of a hydro-ski airplane without tank tests of models of complete configurations, sufficient data are available to make some first approximations that will assist in preliminary design and to establish trends that minimize the number of tests required to arrive at a final design.



REFERENCES


1. Dawson, John R., and Wadlin, Kenneth L.: Preliminary Tank Tests of NACA Hydro-Skis for High-Speed Airplanes. NACA RM L7104, 1947.
2. Wadlin, Kenneth L., and Ramsen, John A.: Tank Spray Tests of a Jet-Powered Model Fitted With NACA Hydro-Skis. NACA RM L8B18, 1948.
3. Ramsen, John A.: The Effect of Rear Chine Strips on the Take-Off Characteristics of a High-Speed Airplane Fitted With NACA Hydro-Skis. NACA RM L9B10a, 1949.
4. Fisher, Lloyd J.: Model Ditching Investigations of Three Airplanes Equipped With Hydro-Skis. NACA RM L9K23, 1950.
5. Wadlin, Kenneth L., and Ramsen, John A.: Tank Investigation of the Grumman JRF-5 Airplane Fitted With Hydro-Skis Suitable for Operation on Water, Snow, and Ice. NACA RM L9K29, 1950.
6. Ramsen, John A., and Gray, George R.: Tank Investigation of the Grumman JRF-5 Airplane With a Single Hydro-Ski and an Extended Afterbody. NACA RM L51E21, 1951.
7. McKann, Robert E., Coffee, Claude W., and Arabian, Donald D.: Hydrodynamic Investigation of a $\frac{1}{13}$ -Scale Model of the Consolidated Vultee Skate 7 Seaplane Equipped With Twin Hydro-Skis - TED No. NACA DE 342. NACA RM SL51F07a, Bur. Aero., 1951.
8. Hoffman, Edward L., and Fisher, Lloyd J.: Yawed-Landing Investigation of a Model of the Convair Y2-2 Airplane - TED No. NACA DE 363. NACA RM SL51H17a, Bur. Aero., 1951.
9. Ramsen, John A., Wadlin, Kenneth L., and Gray, George R.: Tank Investigation of the Edo Model 142 Hydro-Ski Research Airplane. NACA RM SL51I24, U.S. Air Force, 1951.
10. Ramsen, John A., and Gray, George R.: Tank Investigation of the Grumman JRF-5 Airplane Equipped With Twin Hydro-Skis - TED No. NACA DE 357. NACA RM SL52D17, Bur. Aero., 1952.
11. Fisher, Lloyd J., and Hoffman, Edward L.: A Brief Hydrodynamic Investigation of a $1/24$ -Scale Model of the DR-77 Seaplane - TED No. NACA DE 353. NACA RM L53F04, 1953.

12. Weinflash, Bernard: The Effect of Air Jets Simulating Chines or Multiple Steps on the Hydrodynamic Characteristics of a Streamline Fuselage. NACA RM L8J21, 1949.
 13. Weinflash, Bernard, Christopher, Kenneth W., and Shuford, Charles L., Jr.: The Effect of Air-Jet and Strip Modifications on the Hydrodynamic Characteristics of the Streamline Fuselage of a Transonic Airplane. NACA RM L9D20, 1949.
 14. Weinflash, Bernard, Shuford, Charles L., Jr., and Christopher, Kenneth W.: Hydrodynamic Force Characteristics of a Streamline Fuselage Modified by Either Breaker Strips or Rows of Air Jets Simulating Chines. NACA RM L9L21a, 1950.
 15. Weinflash, Bernard, and Shuford, Charles L., Jr.: Investigation of the Hydrodynamic Stability and Resistance of Two Streamline Fuselages. NACA RM L52B11, 1952.
 16. Coffee, Claude W., Jr., and McKann, Robert E.: Hydrodynamic Drag of 12- and 21-Percent-Thick Surface-Piercing Struts. (Prospective NACA paper.)
 17. Wadlin, Kenneth L., and McGehee, John R.: Planing Characteristics of Three Surfaces Representative of Hydro-Ski Forms. NACA RM L9C03, 1949.
 18. Wadlin, Kenneth L., and McGehee, John R.: Planing Characteristics of Six Surfaces Representative of Hydro-Ski Forms. NACA RM L9L20, 1950.
 19. Kapryan, Walter J., and Weinstein, Irving: The Planing Characteristics of a Surface Having a Basic Angle of Dead Rise of 20° and Horizontal Chine Flare. NACA TN 2804, 1952.
 20. Blanchard, Ulysse J.: The Planing Characteristics of a Surface Having a Basic Angle of Dead Rise of 40° and Horizontal Chine Flare. NACA TN 2842, 1952.
 21. Chambliss, Derrill B., and Boyd George M., Jr.: The Planing Characteristics of Two V-Shaped Prismatic Surfaces Having Angles of Dead Rise of 20° and 40° . NACA TN 2876, 1953.
 22. Weinstein, Irving, and Kapryan, Walter J.: The High-Speed Planing Characteristics of a Rectangular Flat Plate Over a Wide Range of Trim and Wetted Length. NACA TN 2981, 1953.
 23. Land, Norman S., and Fontana, Rudolph E.: Preliminary Tank Tests of Some Hydro-Ski—Wheel Combinations in the Planing Condition. NACA RM L52H15, 1952.
- 

DECLASSIFIED

CONFIDENTIAL

9

24. Land, Norman S., and Pelz, Charles A.: Force Characteristics in the Submerged and Planing Condition of a $\frac{1}{5.78}$ -Scale Model of a Hydro-Ski-Wheel Combination for the Grumman JRF-5 Airplane. NACA RM L52B28, 1952.
 25. Schnitzer, Emanuel: Theory and Procedure for Determining Loads and Motions in Chine-Immersed Hydrodynamic Impacts of Prismatic Bodies. NACA TN 2813, 1952.
 26. Smiley, Robert F.: The Application of Planing Characteristics to the Calculation of the Water-Landing Loads and Motions of Sea-planes of Arbitrary Constant Cross Section. NACA TN 2814, 1952.
 27. Miller, Robert W.: Water-Landing Investigation of a Flat-Bottom V-Step Model and Comparison With a Theory Incorporating Planing Data. NACA TN 2932, 1953.
- 

HYDRO-SKI AIRPLANE CONFIGURATION

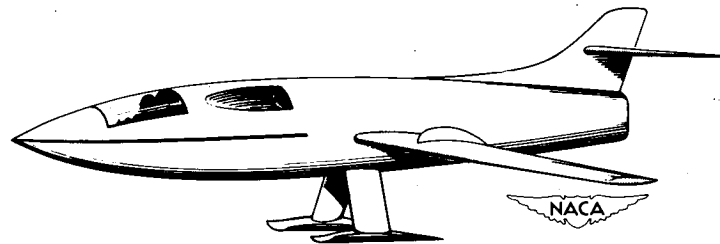


Figure 1

HYDRODYNAMIC RESISTANCE OF HYDRO-SKI AIRPLANE

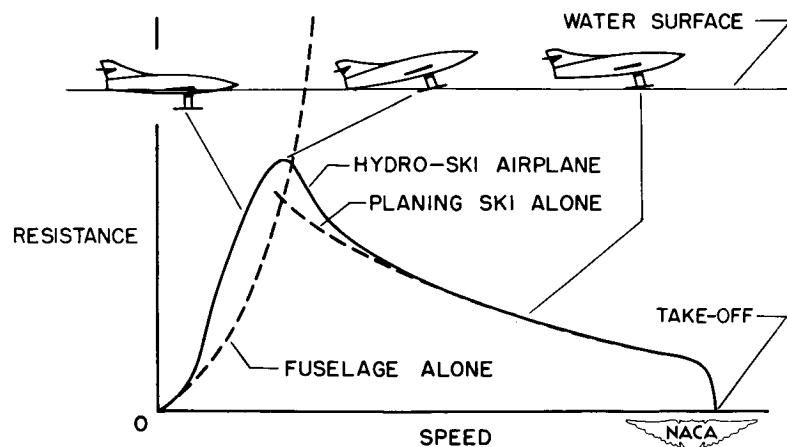


Figure 2

SCOPE OF INVESTIGATION - FUSELAGES AND STRUTS

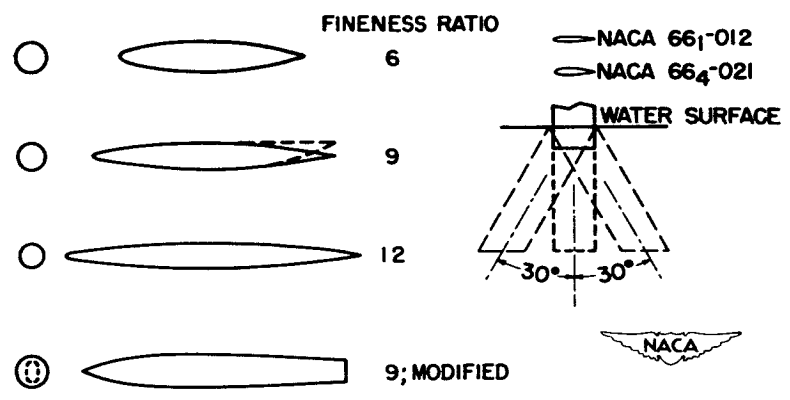


Figure 3

SCOPE OF INVESTIGATION - SKIS

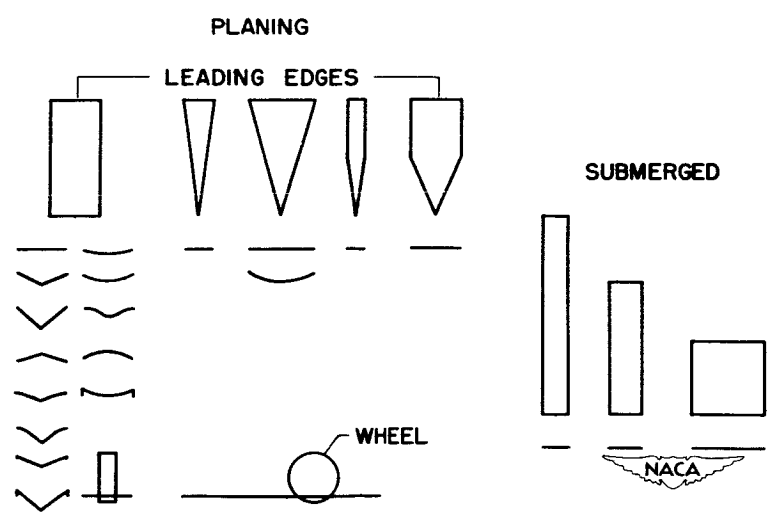


Figure 4

HYDRODYNAMIC LIFT-RESISTANCE RATIO OF FUSELAGES

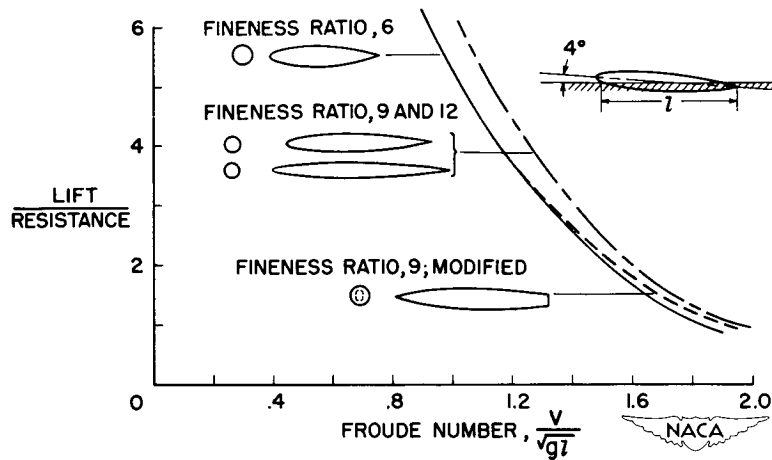


Figure 5

HYDRODYNAMIC LIFT OF SKI SHAPES

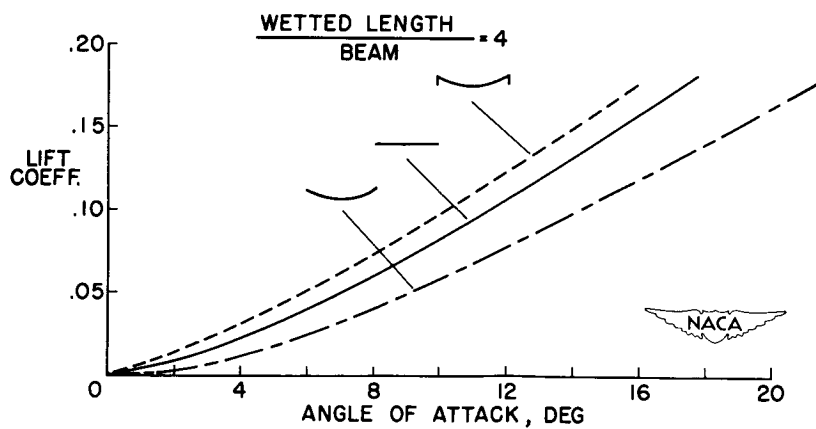


Figure 6

HYDRODYNAMIC LIFT-RESISTANCE RATIO OF SKI SHAPES

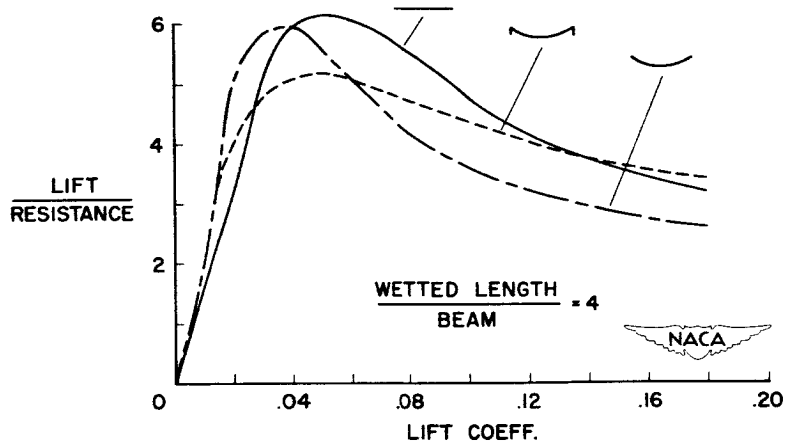


Figure 7

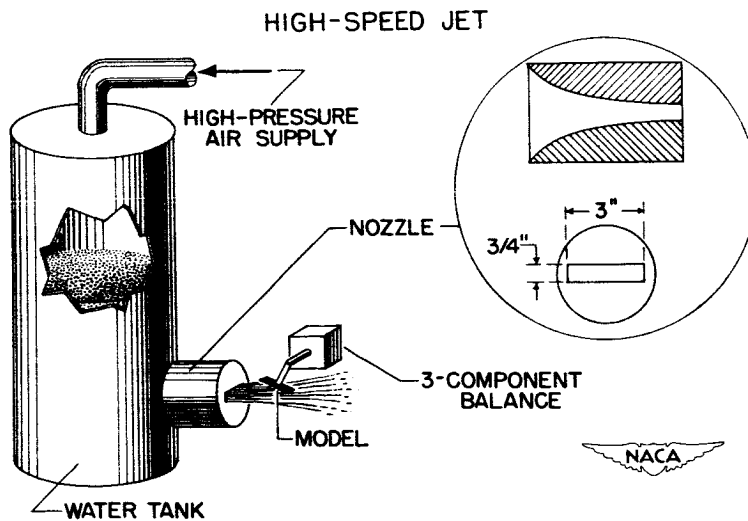


Figure 8

EFFECT OF SPEED ON HYDRODYNAMIC LIFT COEFFICIENT

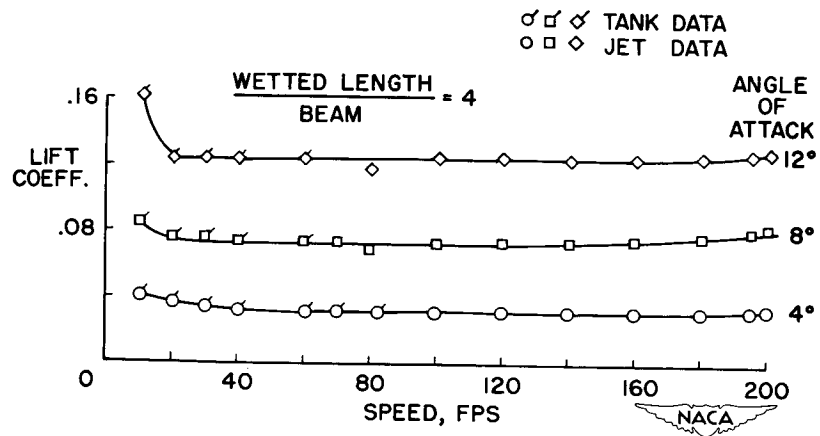


Figure 9

EFFECT OF SKI BEAM ON LANDING LOAD FACTOR

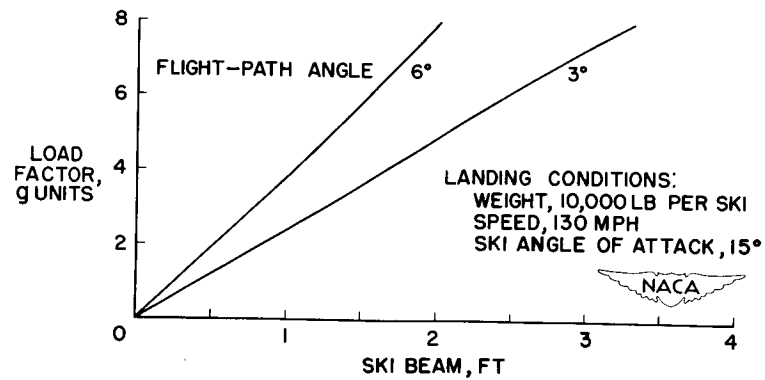


Figure 10

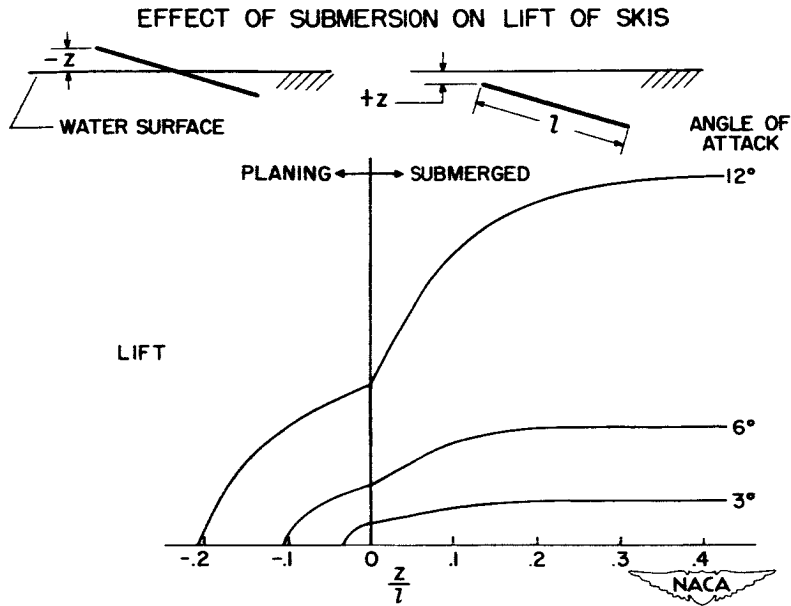


Figure 11

SOME DESIGN CONSIDERATIONS PERTINENT TO THE ROUGH-AIR

BEHAVIOR OF AIRPLANES AT LOW ALTITUDE

By Philip Donely and Clarence L. Gillis

Langley Aeronautical Laboratory


INTRODUCTION

There are certain types of military operations that will require flights of 1 or 2 hours duration at altitudes of 1,000 feet or less at high subsonic speeds, speeds that must be maintained. Rough air is encountered about 30 to 40 percent of the time at low altitudes, and the National Advisory Committee for Aeronautics in a study found that turbulence is of importance not only for structural strength but also in regard to the precision of flight and also in regard to the crew's efficiency and well-being. The study indicated that even moderately rough air would be troublesome and the problems of flight precision and crew reactions can be considered as new problems that may modify the design of the airplane.

It is the purpose of this discussion to examine some of the design variables that have a bearing on the problem. After treating the question of what happens to an airplane and the conditions that appear desirable, the direct effects of turbulence will be considered followed by a discussion of the influence of some variables affecting the motions of the airplane.

SYMBOLS

W	weight, lb
V	forward speed, fps
U	gust velocity, fps
$dC_L/d\alpha$	slope of lift curve, per radian
Λ	sweep angle, deg
S	wing area, sq ft
ρ	air density, slugs/cu ft



Δn	acceleration increment, g
\bar{c}	wing mean aerodynamic chord, ft
c'	wing mean geometric chord, ft
A	aspect ratio
$\Delta\theta$	pitch-angle increment
μ_g	mass ratio, $2W/\rho g \frac{dC_L}{d\alpha} Sc'$
f	frequency, cps
Ω	frequency, radians/ft
ϕ_i	power density, (ft/sec) ² ft
L	scale of turbulence, ft
$T_{1/2}$	time to damp to half-amplitude, sec
$C_{1/10}$	cycles to damp to 1/10 amplitude
p	period, sec
dC_m/dC_L	slope of pitching-moment curve

RESULTS AND DISCUSSION

Airplane reactions of concern as to the precision of flight and crew's reactions are illustrated in figure 1 by these short samples of acceleration and direction records from flight at a Mach number of only 0.60 at an altitude of 1,500 feet. Although this flight is in moderate to severe rough air, the acceleration record indicates that the crew was being continually jolted. The heading record is of interest in that while the crew was being jolted, the airplane developed a yawing oscillation with a period of about 3 seconds with an amplitude of $\pm 1.3^\circ$, an oscillation not present in smooth air. This amplitude would correspond to a miss distance of 22 feet at a 1,000-foot range or 22 mils. Similar behavior has been noted for other airplanes, as for example the X-5 with the wings swept 59° .

The feelings of the crew will depend on both the acceleration intensity and the frequency. Figure 2 is another example of the jolting that can be experienced. This acceleration record is a 12-second section from a 2-minute flight (21 miles) at 1,500 feet with an F-86 airplane

flying at $M \approx 0.85$. The complete run shows accelerations up to $1.5g$ while this particular section shows small rapid oscillations at about 3 or 4 per second with peaks of about $0.2g$. While the pilot had made many runs at Mach numbers of 0.4 and 0.8, he noted that this run of 2 minutes was about his limit. He felt that, at this speed and altitude, the degree of concentration and effort required to control the airplane was so great as to jeopardize the safety of the airplane if such flights were continued.

The decision as to how much the reactions of the airplane should be reduced is a difficult one since it is subjective and little factual information is available. From the short runs made with the F-86 airplane, it appears that moderate rough air results in a ride that is near the safety limit. For flights of 1 or 2 hours in rough air, a substantial reduction in the acceleration level would appear to be required; perhaps, a reduction to about 30 percent of the level shown. McFarland in his book on human factors in air transport design (see ref. 1) indicates that the work of Reihe and Meister showed that although accelerations of $\pm 0.2g$ at 3 to 5 cps would be dangerous, a level of $0.04g$ at these frequencies would be merely disagreeable. This is a reduction to 20 percent of the level shown on the F-86 records and assumes that a disagreeable ride would be tolerable. In regard to airplane motions, a deviation of 5 mils is considered satisfactory; thus, the motions of the B-45 airplane at 22 mils would have to be decreased to about 25 percent of that value to be useful under the conditions specified for this mission. Since all considerations indicate a reduction to about 20 or 30 percent, the acceleration record for the F-86 airplane will be used as a standard, and a reduction by a factor 3 in acceleration or to 30 percent will be the criterion of satisfactory behavior for moderately rough air used herein.

The factors that are pertinent for obtaining the desired reduction are indicated in the following relationship:

$$\Delta n \approx \frac{\rho UV}{2} \frac{dC_L/d\alpha}{W/S} \pm \frac{\rho V^2}{2} \frac{dC_L/d\alpha}{W/S} \Delta\theta \quad (1)$$

The acceleration can be considered as composed of two effects: the direct effect of the gust consisting of such quantities as airspeed, air density, lift-curve slope, and wing loading which determine the magnitude of the disturbance of the airplane and the indirect effects due to the resulting airplane motions which are represented by the pitch angle $\Delta\theta$. Since the speed, air density, and gust velocity are specified in this problem, the major elements at the disposal of the designer are changes in lift-curve slope, wing loading, and the disturbed airplane motions.

What can be accomplished by working on the lift-curve slope and wing loading will be taken up first. The remainder of the discussion will be concerned with the second term representing the influence of airplane motion. The indirect effects of various factors such as, sweep, static margin, lack of a tail surface, and artificial damping will be touched on.

Direct Effects

Three methods of obtaining a low lift-curve slope are to reduce the aspect ratio, sweep the wing, or introduce flexibility particularly for a sweptback wing. The effect of aspect ratio and sweep are used in combination many times. Gust-tunnel investigations, references 2 and 3, have indicated the effectiveness of both quantities and figure 3 shows that these investigations are borne out by flight experience. Figure 3 indicates that, if an unswept-wing airplane encountered a given value of acceleration, then the ordinate represents the acceleration that a swept-wing airplane would experience in the same rough air with equal frequency. To obtain the line of circle test points labeled 35° , an F-80 and an F-86 airplane were flown side by side in the same rough air at a Mach number of about 0.6. In this case, the F-80 with about the same wing loading and aspect ratio as the F-86 was used as the reference, and the acceleration increments for equal frequency of occurrence were plotted. The square test points labeled 59° were obtained from go-and-return flights of the X-5 airplane in rough air at a Mach number of about 0.7. Alternate runs with the wings swept 20° and 59° were made. The X-5 data for 20° sweep corrected slightly to 0° were the reference conditions to obtain the square test points. The solid lines represent the relation between accelerations for the airplanes if the lift-curve slope is assumed to be the only factor. As can be noted, the agreement is fairly good.

Figure 3 indicates that reducing the lift-curve slope through the use of sweep is quite effective. Since the F-86 acceleration record is the basis for the reduction desired, it can be seen that, if the wings were swept to 60° by rotation, the acceleration could be reduced from say 0.6g to about 0.4g, 30 percent or about half the desired reduction. If this same 30-percent reduction were to be obtained by reducing aspect ratio, the aspect ratio would have to be decreased say from 6.0 to 2.0. Unless extreme values of sweep or aspect ratio are utilized, it does not appear practical to obtain the reduction to 30 percent in this way. As a matter of fact, the relation given indicates that for aspect ratio below about 1.5 the effect of sweep is not significant.

Flexibility utilizing washout under load is the third way of obtaining low lift-curve slopes. About the only experimental evidence is contained in reference 4. This gust-tunnel investigation of a 45°

sweptback wing, hinged at the root, showed that a 21-percent reduction in acceleration could be obtained if the airplane did not pitch. The wing deflection corresponded to 20 inches per g at the tip of a wing with a span of 100 feet. Unfortunately these tests also indicated that adverse pitch due to forward movement of the aerodynamic center as the wings deflected canceled half the gain. It is apparent, therefore, that while the introduction of flexibility can be of benefit the net gain may depend on the induced airplane motions to a high degree and these motions may require careful consideration. So far no full-scale experimental results are available to assess this phase of the problem.

The effect of wing loading on accelerations due to a gust are well-known, reference 2, but for convenience are shown in figure 4 for wings of various sweep. Simple calculations for a single gust encounter have been made for a 20-fps gust (about the maximum experienced by the F-86) and a flight speed of 1,000 fps. Values of the acceleration increment for wing loadings from 50 to 300 lb/sq ft are shown for sweeps of 0°, 50°, and 60°. A delta wing of 60° would follow the 60° line quite closely. The curves indicate that for the wings shown, the wing loading for an unswept-wing airplane would have to be increased from 50 to about 200 lb/sq ft to reduce the acceleration to 30 percent. If a shift is made from an unswept wing to one swept 60°, the wing loading would have to be increased to only 100 lb/sq ft to achieve the reduction.

Indirect Effects

What can be done by modifying the second term of equation (1), which represents in principle the effect of airplane motion, is not so obvious. The subject of airplane motions is complex but the magnitude of changes in acceleration have been studied since the equation indicates this term may increase or decrease the acceleration. Since continuous rough air is being dealt with, generalized harmonic analysis for random disturbances, references 5 and 6, has been utilized in the subsequent studies.

The remainder of the discussion deals with possible benefits of modifying the stability of stable well-damped airplanes, the influence of adverse moments due to sweep on the benefits just indicated, comparison of tailed and tailless configurations, and the use of artificial damping for poorly damped motions. Although it was found that most factors were not significant in the problem under consideration, the study of configuration and artificial damping indicated that some adverse effects could be eliminated or reduced.

Input spectrum.- For the analyses of the effects of modifying the stability of well-damped airplanes and the effect of adverse moments due to sweep, the input spectrum shown in figure 5 was used. The curve of

CONFIDENTIAL

power density Φ_i as a function of frequency is based primarily on air-speed fluctuation data obtained on an L-5 airplane operating in moderately rough air at an altitude of 400 feet. These data which are in agreement with other samples were used to arrive at a fitted curve for isotropic turbulence. The curve shown in figure 5 is for a scale length L of 300 feet.

For the study of tailed and tailless configurations and artificial damping, spectra were for a lower level of turbulence. Since the basic investigation involved experimental studies with rocket models, it was more convenient to utilize the associated analyses. Since in this study relative effects on models are being assessed, the actual intensity is not significant.

Unswept-wing airplanes.- Figure 6 and table I give the characteristics of the airplane family used to study changes in dynamic stability obtained by varying the moment-curve slope dC_m/dC_L and the mass ratio μ_g . The moment-curve slope dC_m/dC_L was varied from -0.03 to -0.08 and the mass ratio was varied from 10 to 200. The airplanes had a weight of 100,000 pounds and were geometrically similar with a flight speed of 1,118 fps. Figure 6 indicates that the heavily loaded airplane had a short period from 5.6 to 3.1 seconds, damping to half-amplitude in 0.9 seconds, whereas the lightly loaded airplane has an infinite short period and is heavily damped. Some of these airplanes represent extreme variations.

The response transforms were obtained by computing the step function according to methods of reference 7 and then transforming the results to the frequency plane. Although flight at high Mach number is assumed, two-dimensional incompressible unsteady-lift functions and low-speed lift-curve slopes were used. This was done since the available evidence, reference 8 and other studies, is very inconclusive as to the proper functions for gust calculations at high Mach number. Also, the airplanes were assumed to be rigid; therefore, structural vibrations are not included in the response calculations.

The response transforms were then multiplied by the input spectrum of figure 5 to obtain output spectra. As noted in reference 5, the area under the output spectrum is the mean square acceleration and the square root of this quantity, the root-mean-square acceleration increment, will be used as a measure of the airplane behavior.


The results are given in figure 7 as a function of wing loading with dC_m/dC_L as the parametric variable. For comparison, the root-mean-square acceleration increment for the F-86 record of which figure 2 is a portion was 0.21 so the criterion of reduction used herein would imply that a satisfactory value would be about 0.07. As previously noted the direct effect of wing loading seems to be the dominant factor and the

influence of stability is small and unimportant for the problem at hand. It might be noted that at low wing loadings the effect of stability was negligible, whereas at high wing loadings a reduction in stability tends to reduce the accelerations slightly. Other studies have shown similar results; but, it has been found that, depending on the mass ratio and geometry, the effect of increased stability is sometimes favorable as indicated in reference 9.

Swept-wing airplanes.- Since the root section of a swept wing penetrates a gust before the wing tips, an adverse pitching moment is produced similar to that mentioned earlier for the flexible sweptback wing. An analysis was made, therefore, to see if this factor might cancel the direct benefits obtained through reducing the lift-curve slope. The airplane characteristics are given in figure 8 and table II. As in the previous case the weight was kept at 100,000 pounds, the mass ratio was varied from 10 to 200, and the sweep was varied from 0° to 60° with the aspect ratio kept unchanged. Strip theory was used to modify the unsteady-lift functions to account for sweep. The speed was the same as for the unswept-wing family. The airplanes were assumed to be neutrally stable (aperiodic), and, as indicated, the time to damp to half-amplitude varied from 0.12 second to about 0.90 second as the wing loading increased.

In figure 9, the root-mean-square acceleration increment is again shown as a function of wing loading. The lowest curve, indicated by the diamond symbols, indicates the direct effect of lift-curve slope. This curve was obtained by multiplying the root-mean-square acceleration for 0° sweep by the ratio of lift-curve slopes for the 60° and 0° sweep cases. The difference between this curve and the 60° curve with triangle symbols is used as a measure of the influence of pitch. At low wing loadings, the three curves coincide indicating that the pitch had effectively canceled the effect of reduced lift-curve slope. As the wing loading increases, the influence of pitch is decreased so that most of the benefit of sweep is realized. At a wing loading of 160 lb/sq ft, the adverse pitch increases the acceleration 14 percent. Such adverse effects indicate increased angular motions of the airplane that might require modification for gunnery or bombing considerations.

Airplane configuration and artificial damping.- So far all configurations had well-damped motions; but, of considerable concern, are low-damped airplane motions such as illustrated by the heading record shown in figure 1. A configuration that may well have low damping in pitch is one without a horizontal tail. For such configurations, the motions of the airplanes are significant in their own right and can also lead to increased accelerations that cancel any benefits of increased wing loading or reduced lift-curve slope as for the cases just discussed.




The NACA has initiated exploratory studies of the problem by means of rocket models and analysis. The results that bear on the specific mission will now be discussed preceded by a brief comparison of experiment and calculation to provide a measure of the validity of this and the preceding analyses.

Figure 10 gives the configurations tested and their dynamic characteristics. The models consisted of the same forebody and wing but, as indicated by the dashed lines, in one case the body was extended and a horizontal tail added. The inset figures for period and cycles to damp to $1/10$ amplitude indicate that both models were very stable but the damping was poor when compared with the criterion of one cycle to damp to $1/10$ amplitude.

The output spectra with the corresponding calculated curves are shown in figure 11 for $M \approx 0.81$ while the corresponding values of root-mean-square acceleration increment are given in figure 12. The discrepancy between calculation and experiment represents the combined effects of errors in calculating the motion and accounting for the temporal character of the input spectra during a rocket flight. The spectra shown represent about the greatest discrepancy found and the agreement is considered fairly good. Figure 12 gives an over-all picture of the results and indicates that, considering all the experimental samples, the tailless model gave excellent results (owing in part to the fact that stability derivatives were available from tests of similar models) and the calculated values were a little low for the tailed model.

For the purpose of this paper, the experiments were not used directly but analyses with the two configurations adjusted to give the same natural frequency were made. In addition to the calculation for the configurations, the effect of adding rate damping to both models was also analyzed. The damping systems assumed control deflections proportional to angular velocity and the black areas on the models (fig. 13(b)) indicate that a trailing-edge flap was used for the tailless model and an all-moving tail for the tailed model. For the tailless model the flap had a chord of $0.25c$ and the system would respond to 14 cps. The frequency response of the control system for the tailed model was the same.

The calculated output spectra, in figure 13, show by comparing the solid curves that adding a tail reduced the root-mean-square acceleration increment 20 percent. Although this gain is significant it is not as great as might be expected and does not rule out tailless configurations. Comparison of the dashed and solid curves, figure 13, indicates that the use of artificial damping leads to very significant gains. With damping, the output spectra are very flat and the root-mean-square acceleration increments were reduced about 50 percent.



The effect of added damping is shown in a different form in figure 14 where the calculated frequency distributions are plotted for the four cases as the number of peaks per mile as a function of the acceleration increment. Inspection of figure 14 indicates that the added damping has increased the number of small acceleration peaks for both models by increasing the response somewhat at high frequencies. At high acceleration, the benefit of the tail and of the use of artificial damping show up quite clearly, with the damped tailed model having the lowest acceleration at 10 per mile and the damped tailless model next. It is obvious from these results that, for low-damped motions, the use of artificial damping can reduce the accelerations due to airplane motion so that the direct benefits can be utilized if high wing loading and reduced lift-curve slope lead to such motions. It might be noted that the large gains are made only for poorly damped configurations as tests of a rate autopilot in a subsonic stable airplane indicated a reduction of only 7 per cent, reference 10.


CONCLUDING REMARKS

In conclusion the discussion has indicated that if a reduction in airplane response in rough air by a factor of 3 is required for high-subsonic-speed low-altitude flight:

(a) Increasing the wing loading and reducing the lift-curve slope through sweep, reduced aspect ratio, or increased flexibility will be the major factors.

(b) The effect of moderate changes in stability for airplanes with satisfactory characteristics does not appear significant. For configurations using swept wings and those involving low damping of airplane motions, adverse angular displacements may cancel the benefits of other changes but the adverse effects can be significantly reduced by artificial damping.

It might be noted in closing that solution of the gust problem for this mission may introduce other serious problems in regard to handling qualities or increased landing and take-off speeds.



0371238 1038

10

CONFIDENTIAL

REFERENCES

1. McFarland, Ross A.: Human Factors in Air Transport Design. McGraw-Hill Book Co., Inc., 1946.
2. Donely, Philip: Summary of Information Relating to Gust Loads on Airplanes. NACA Rep. 997, 1950. (Supersedes NACA TN 1976.)
3. Pierce, Harold B.: Gust-Tunnel Investigation of a Wing Model With Semichord Line Swept Back 60°. NACA TN 2204, 1950.
4. Reisert, Thomas D.: Gust-Tunnel Investigation of a Flexible-Wing Model With Semichord Line Swept Back 45°. NACA TN 1959, 1949.
5. Press, Harry, and Mazelsky, Bernard: A Study of the Application of Power-Spectral Methods of Generalized Harmonic Analysis to Gust Loads on Airplanes. NACA TN 2853, 1953.
6. Liepmann, H. W.: An Approach to the Buffeting Problem From Turbulence Considerations. Rep. No. SM-13940, Douglas Aircraft Co., Inc., Mar. 13, 1951.
7. Mazelsky, Bernard, and Diederich, Franklin W.: A Method of Determining the Effect of Airplane Stability on the Gust Load Factor. NACA TN 2035, 1950.
8. Binckley, E. T., and Funk, Jack: A Flight Investigation of the Effects of Compressibility on Applied Gust Loads. NACA TN 1937, 1949.
9. Funk, Jack, and Binckley, Earle T.: A Flight Investigation of the Effect of Center-of-Gravity Location on Gust Loads. NACA TN 2575, 1951.
10. Payne, Chester B.: A Flight Investigation of Some Effects of Automatic Control on Gust Loads. NACA RM L53E14a, 1953.

CONFIDENTIAL

TABLE I
CHARACTERISTICS OF UNSWEPT WING AIRPLANES
[Gross weight, 100,000 lb]

	$\frac{dC_m}{dC_L} = -0.03$			$\frac{dC_m}{dC_L} = -0.05$			$\frac{dC_m}{dC_L} = -0.08$		
	10	80	200	10	80	200	10	80	200
Mass ratio									
Pitching moment of inertia slug-ft ²	2,889,000	718,500	395,200	2,889,000	718,500	395,200	2,889,000	718,500	395,200
Air density, slugs/cu ft	0.00238	0.00238	0.00238	0.00238	0.00238	0.00238	0.00238	0.00238	0.00238
Forward velocity, fps	1,118	1,118	1,118	1,118	1,118	1,118	1,118	1,118	1,118
Wing aspect ratio	3.1	3.1	3.1	3.1	3.1	3.1	3.1	3.1	3.1
Wing lift-curve slope, per radian	3.65	3.65	3.65	3.65	3.65	3.65	3.65	3.65	3.65
Wing mean aerodynamic chord, ft	30.5	15.2	11.3	30.5	15.2	11.3	30.5	15.2	11.3
Gross wing area, sq ft	2,512	625	343	2,512	625	343	2,512	625	343
Wing loading, lb/sq ft	39.8	160.0	291.5	39.8	160.0	291.5	39.8	160.0	291.5
Horizontal distance from center of gravity of air-plane to aerodynamic center of wing, ft	5.02	2.50	1.86	4.44	2.21	1.64	3.54	1.76	1.31
Tail lift-curve slope, per radian	3.57	3.57	3.57	3.57	3.57	3.57	3.57	3.57	3.57
Tail mean aerodynamic chord, ft	12.5	6.23	4.62	12.5	6.23	4.62	12.5	6.23	4.62
Gross tail area, sq ft	469	117	64	469	117	64	469	117	64
Horizontal distance from center of gravity of air-plane to aerodynamic center of tail, ft	84.3	42.0	31.2	85.0	42.4	31.4	86.0	42.8	31.8
Distance between trailing edge of wing mean aerodynamic chord to leading edge of tail mean aerodynamic chord, ft	54.1	27.0	20.0	54.1	27.0	20.0	54.1	27.0	20.0
Tail efficiency factor	0.8	0.8	0.8	0.8	0.8	0.8	0.8	0.8	0.8
Downwash factor	0.5	0.5	0.5	0.5	0.5	0.5	0.5	0.5	0.5

NACA

TABLE II

CHARACTERISTICS OF SWEEP WING AIRPLANES

[Gross weight, 100,000 lb; $dc_m/dc_L = 0$]

	$\Lambda = 0^\circ$			$\Lambda = 45^\circ$			$\Lambda = 60^\circ$		
	10	80	200	10	80	200	10	80	200
Mass ratio									
Pitching moment of inertia slug-ft ²	2,594,000	653,000	355,600	2,814,000	708,200	382,700	3,261,000	815,100	439,800
Air density, slugs/cu ft	0.00238	0.00238	0.00238	0.00238	0.00238	0.00238	0.00238	0.00238	0.00238
Forward velocity, fps	1,118	1,118	1,118	1,118	1,118	1,118	1,118	1,118	1,118
Wing aspect ratio	3.0	3.0	3.0	3.0	3.0	3.0	3.0	3.0	3.0
Wing lift-curve slope, per radian	3.6	3.6	3.6	3.18	3.18	3.18	2.56	2.56	2.56
Wing mean aerodynamic chord, ft	28.9	14.5	10.7	30.1	15.1	11.1	32.4	16.2	11.9
Gross wing area, sq ft	2,507	627	340	2,724	681	370	3,147	787	427
Wing loading, lb/sq ft	39.9	159.5	294.1	36.7	146.8	270.3	31.8	127.1	234.2
Horizontal distance from center of gravity of air-plane to aerodynamic center of wing, ft	6.42	3.21	2.37	6.70	3.35	2.47	7.20	3.60	2.65
Tail lift-curve slope, per radian	3.6	3.6	3.6	3.18	3.18	3.18	2.56	2.56	2.56
Tail mean aerodynamic chord, ft	12.9	6.46	4.76	13.5	6.74	4.96	14.5	7.24	5.34
Gross tail area, sq ft	501	125	68.1	544	136	73.9	629	157	85.4
Horizontal distance from center of gravity of air-plane to aerodynamic center of tail, ft	80.3	40.2	29.6	83.7	41.8	30.8	90.0	45.0	33.1
Distance between trailing edge of wing mean aerodynamic chord to leading edge of tail mean aerodynamic chord, ft	61.8	30.9	22.8	76.9	38.5	28.3	92.5	46.3	34.1
Tail efficiency factor	0.8	0.8	0.8	0.8	0.8	0.8	0.8	0.8	0.8
Downwash factor	0.5	0.5	0.5	0.5	0.5	0.5	0.5	0.5	0.5

NACA

TIME HISTORIES FOR B-45 AIRPLANE IN ROUGH AIR
M \approx 0.60; ALTITUDE, 1,500 FT

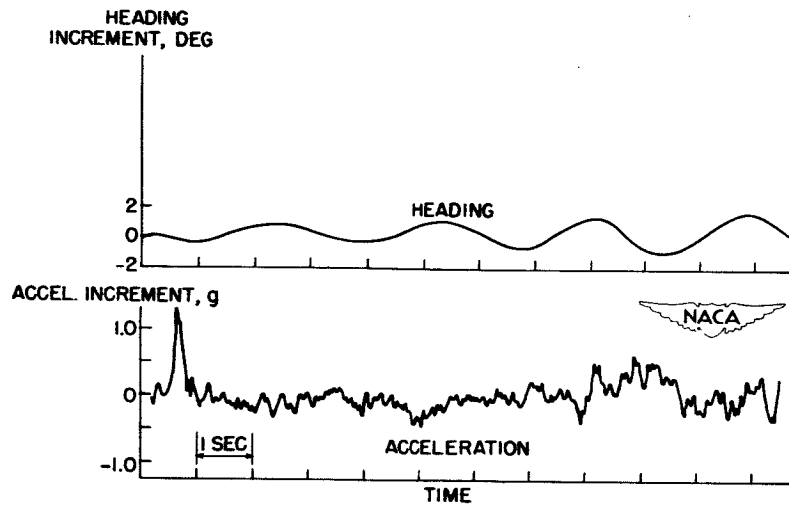


Figure 1

ACCELERATION RECORD FOR F-86 AIRPLANE
IN ROUGH AIR
M \approx 0.85; ALTITUDE, 1,500 FT

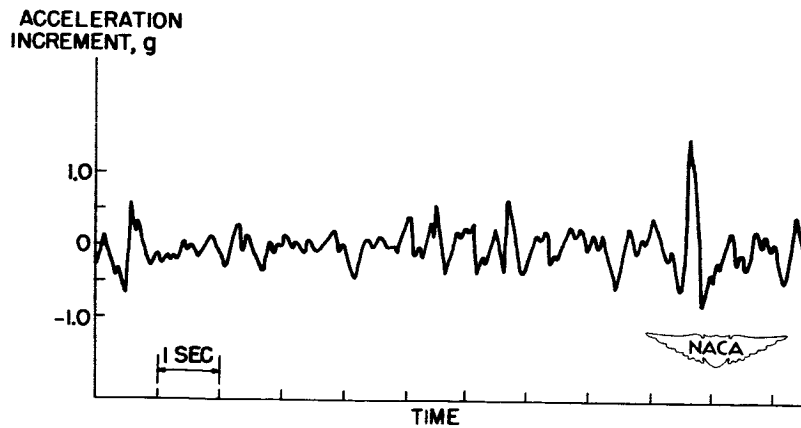


Figure 2

FLIGHT TEST RESULTS ON SWEEP-WING AIRPLANES

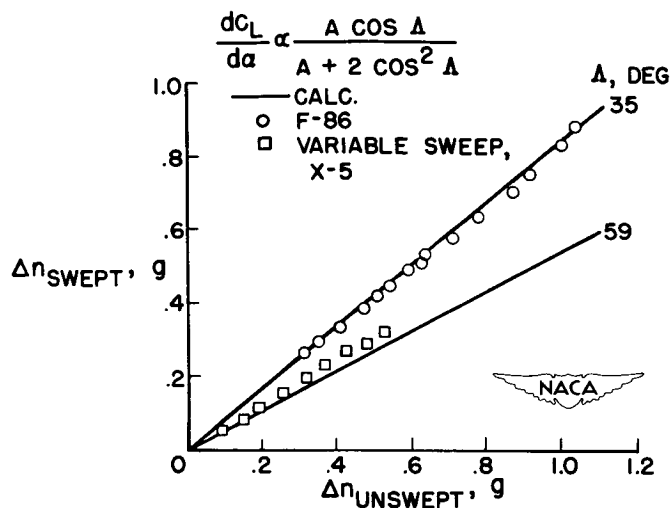


Figure 3

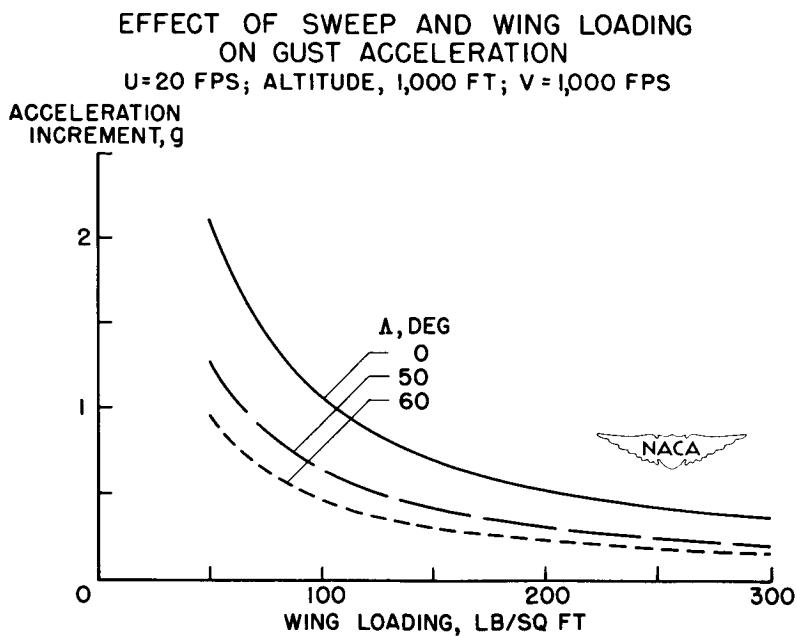


Figure 4

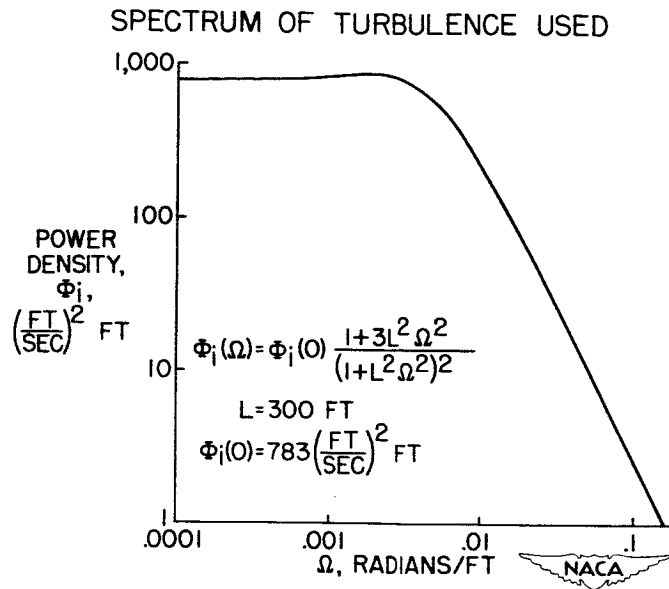
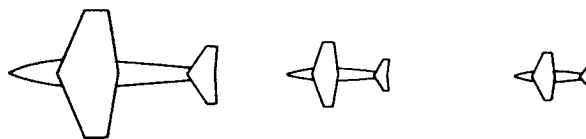


Figure 5

AIRPLANE CHARACTERISTICS
UNSWEEP WINGS



$\frac{dC_m}{dC_L}$	$\mu g = 10$ W/S = 40 LB/SQ FT		$\mu g = 80$ W/S = 160 LB/SQ FT		$\mu g = 200$ W/S = 292 LB/SQ FT	
	P, SEC	$T_{1/2}$, SEC	P, SEC	$T_{1/2}$, SEC	P, SEC	$T_{1/2}$, SEC
-0.03	—	0.13	5.0	0.51	5.6	0.92
-.05	—	.12	3.7	.50	4.0	.91
-.08	—	.12	2.8	.49	3.1	.90



Figure 6

EFFECT OF STABILITY ON GUST ACCELERATIONS

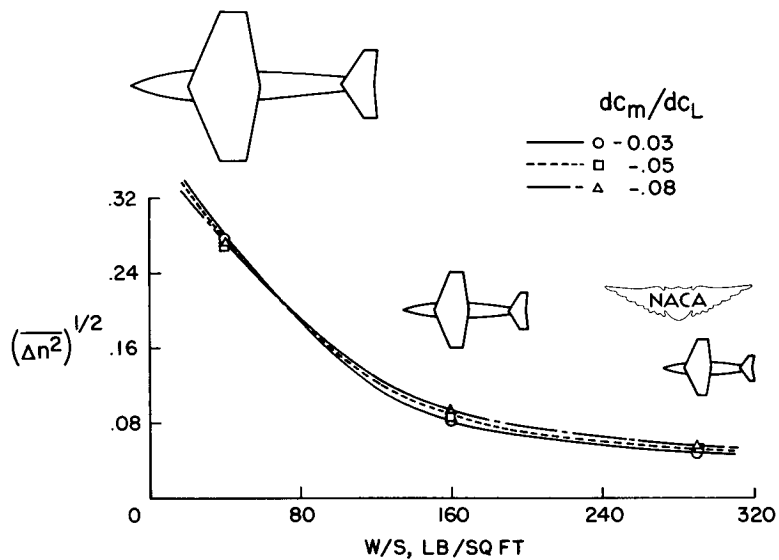
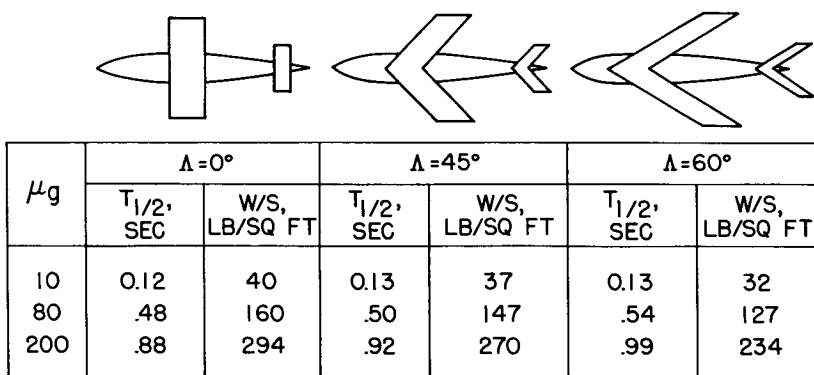


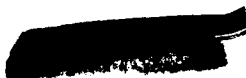
Figure 7

AIRPLANE CHARACTERISTICS SWEPT WINGS



NACA

Figure 8



EFFECT OF PITCH ON GUST ACCELERATIONS FOR SWEEP-WING AIRPLANES

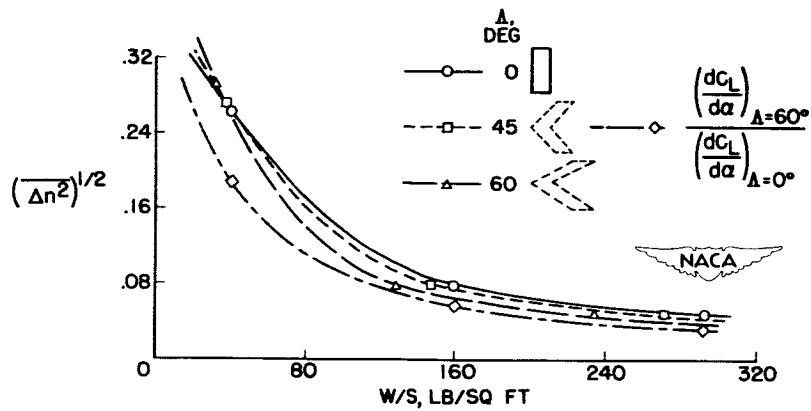


Figure 9

MODEL CHARACTERISTICS

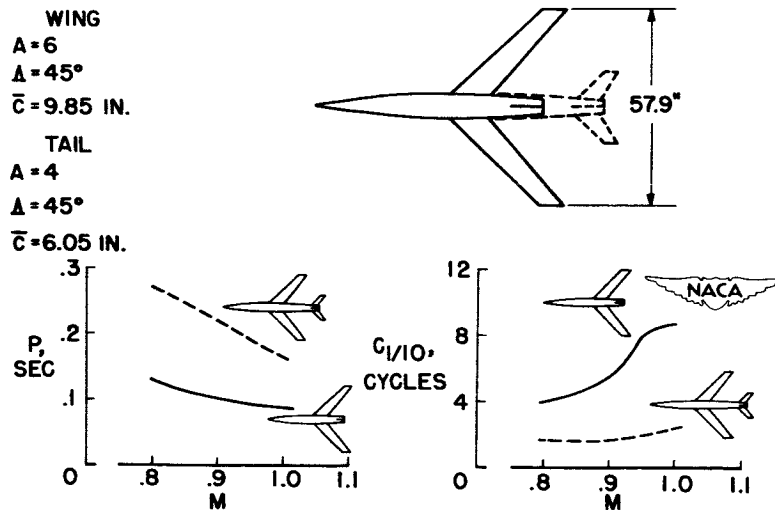


Figure 10

CALCULATED AND MEASURED POWER SPECTRUMS

$M \approx 0.81$

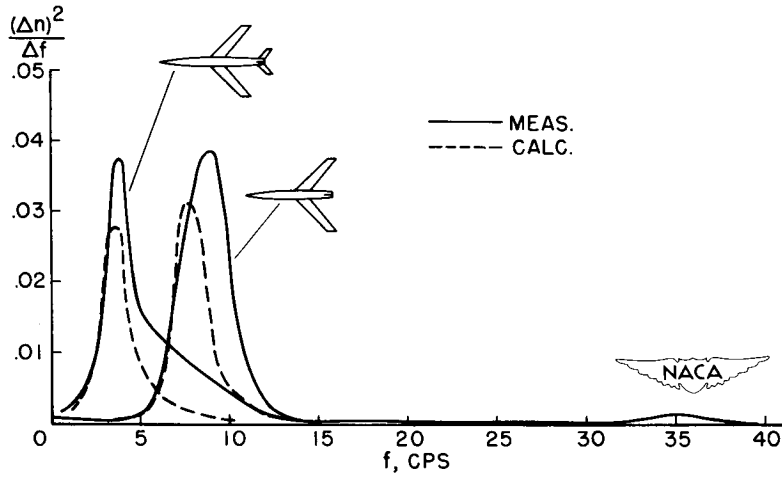


Figure 11

COMPARISON OF MEASURED AND CALCULATED RESULTS

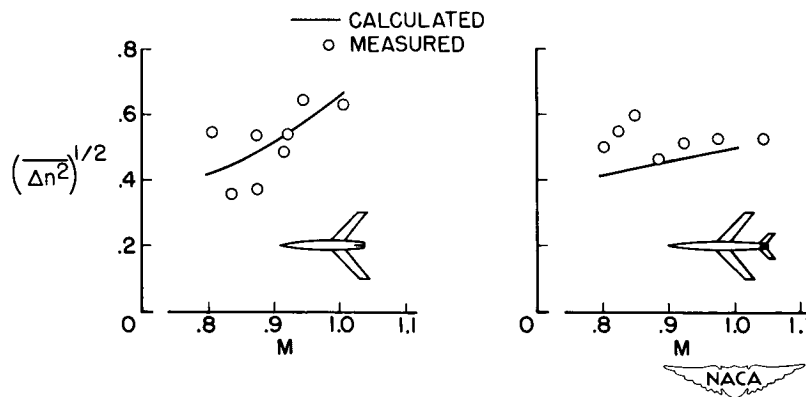


Figure 12

EFFECT OF CONFIGURATION

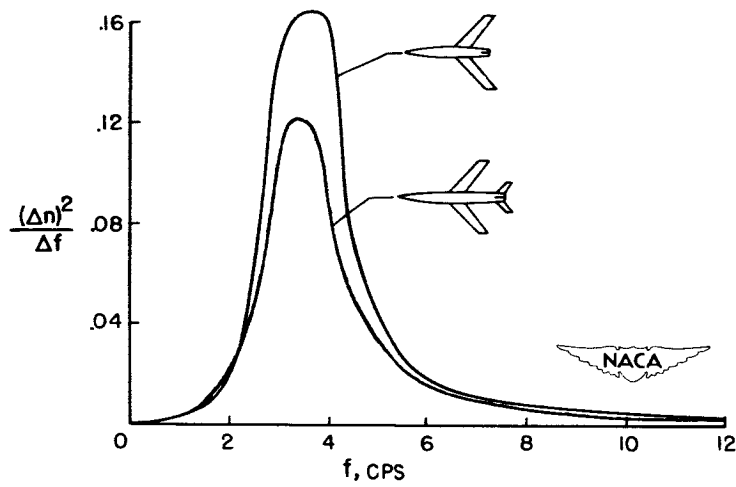


Figure 13(a)

EFFECT OF ARTIFICIAL DAMPING

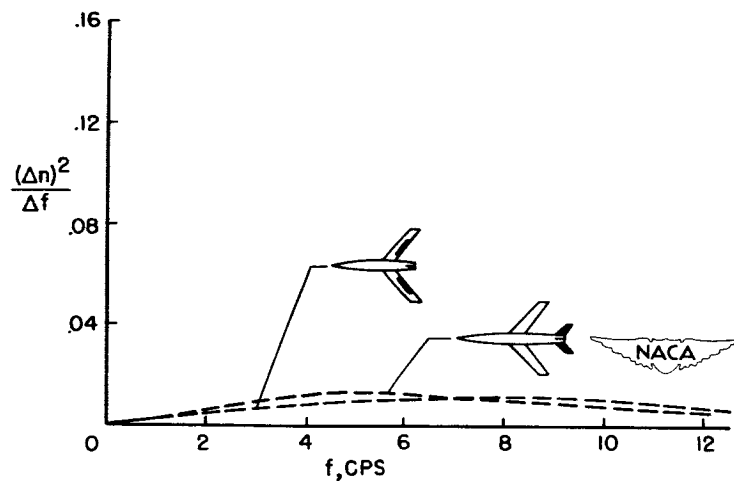


Figure 13(b)

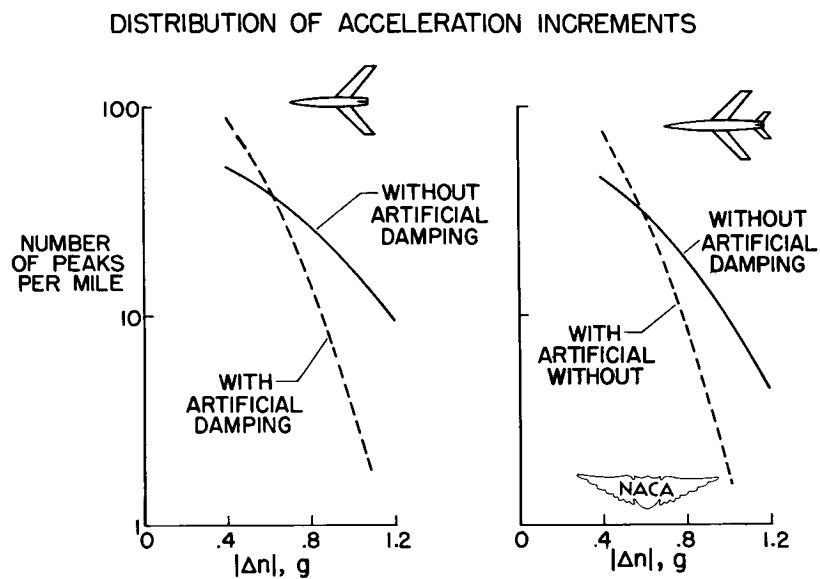


Figure 14

DECLASSIFIED

**STABILITY
AND CONTROL**

DECLASSIFIED

CONFIDENTIAL


ADDITIONAL INVESTIGATION OF THE HANDLING QUALITIES
OF AIRPLANES AT HIGH SPEEDS

By A. Scott Crossfield, Hubert M. Drake, Jack Fischel,
and Joseph A. Walker

NACA High-Speed Flight Research Station

In a paper by W. C. Williams and A. S. Crossfield (ref. 1), some characteristics of research and tactical airplanes were compared with the handling-qualities requirements. An evaluation of these characteristics was made with regard to danger, limits to usefulness of the airplanes, and possible needs for review of the handling-qualities requirements. A major effort to investigate these characteristics during the past year and a half has served to clarify some of the problems and has brought to light additional problems. This paper is concerned with those characteristics which appear to be of major importance that were investigated with the research airplanes. The research airplanes have sweep, wing loading, tail volume, and tail placement similar to most current and near-future tactical airplanes. No direct comparison with handling-qualities requirements is attempted because this paper is restricted to problems which are all in flagrant violation of the requirements. The troublesome area of major importance is still the transonic region because airplanes are flying and being manufactured to fly in this area. It is here that the most serious problems concerning buffeting, stability and trim changes, drag changes, and dynamic stability are encountered.

In reference 1 the accelerated flight pitch-up characteristics of the D-558-II, the X-4, and the F-86A are described and evaluated. A number of fixes which wind-tunnel investigations indicated might be promising have since been tried on the D-558-II. Figure 1 shows the types of fixes attempted and the characteristic elevator-angle-of-attack variations for Mach numbers of 0.7 and 0.87. These fixes apply only to the wing and none of these changes resulted in tolerable behavior; however, some reduction in divergence rates was noted with full slats and chord-extensions below a Mach number of 0.80. For a Mach number of 0.7 with slats fully extended, D and E, the airplane retrimmed after a typical pitch. The chord-extensions G showed similar trends but buffeting intensities reached extreme values of 2g total amplitude. None of the modifications provided measurable improvement between Mach numbers of 0.8 and 0.95, the upper limit of the tests, and all were characterized by an abrupt change in stability at the pitch-up. It has been concluded that with the tail configuration of the D-558-II ($h_t = 69$ percent \bar{c}) a real cure of the pitch-up is not feasible.




CROSSFIELD, DRAKE,
FISCHEL & WALKER

A word of caution regarding the interpretation of these data is in order. Above the abrupt change in stability there are unbalanced moments and pitching-acceleration contributions, and, therefore, caution should be taken in static evaluation of data at angles of attack above the change. A stable slope above the stability change may or may not represent a severe pitch-up. All of these cases are pitch-ups with severity roughly in proportion to the abruptness of the stability change. If pitch-ups are permitted to develop without corrective control, violent rolling often results.

Although the stability results are somewhat negative, these investigations have had considerable value in determining how to interpret flight and wind-tunnel data. In earlier investigations the problem was not clearly understood and, therefore, fixes selected on the basis of wind-tunnel evaluation were tried that would not be tried now. Representation on the basis of C_M against C_L is obscured by the nonlinear character of the higher portion of the lift-curve slope which changes with the fixes. In addition, these investigations brought to light that the pitch-up maneuver is of dynamic character. The type of maneuver used, that is, a slow continuing rate turn at constant speed, is similar to a tactical maneuver, except that the rate is low enough to permit static-data evaluation before pitch-up. The pilot approaches the stability change with a finite amount of pitching momentum which is, however, usually less than that in a typical tactical maneuver. Compiled tactical information indicates that military pilots are going to use all of the lift capabilities they can handle in order to line up with the target, regardless of buffeting. Only test pilots have the fortunate circumstance of being able to concentrate on approaching difficulties.

The stability boundaries as influenced by normal-force coefficient and Mach number for the D-558-II, the X-4, and the F-86A were published in reference 1. In figure 2 the D-558-II boundary has been extended into the supersonic region. The character of the pitch-up encountered below a Mach number of 1.3 is similar to the transonic case with the added difficulty that the transonic troublesome area is traversed before recovery can be made at subsonic speeds. At a Mach number of about 1.6, the rates of pitch or severity tended to diminish to much more controllable values. It is suspected that the pitch-up character begins to change at about 1.3 where the Mach cone angle approaches the leading-edge sweep angle.

Also shown in figure 2 are the stability boundaries for the X-5 with 60° sweep and the XF-92A. In addition, the limit of C_{NA} reached in tests is shown for these airplanes as well as for the X-3. The swept- and delta-wing airplanes exhibit similar trends of decreasing C_{NA} for pitch-up with speed. The delta-wing XF-92A exhibited the lowest boundary. The boundaries of the X-5 at 45° and 20° sweep have not been fully



explored at the present time but the indications are that the boundaries for these sweep angles are similar to those for the 60° case shown. The large amount of unusable normal-force capability above the boundaries should be noted.

Flight-test results on the relatively thick straight-winged X-1 envelope have been published previously and virtually blanket figure 2 except at extremely high speeds. No static longitudinal difficulties were encountered. The X-3 with a thin low-aspect-ratio straight wing is being demonstrated by the Douglas Aircraft Company and thus far has been maneuvered to normal-force coefficients shown without static longitudinal difficulty. Notice that a normal-force coefficient of 0.6 has been reached at a Mach number of 0.93.

Approaching and penetrating the region of stability change with the XF-92A leaves the pilot with two distinct impressions. The first is the extreme drag due to lift which sometimes requires a loss of 10,000 feet in an effort to maintain speed. The other impression is a periodic behavior indicated in figure 3 which is a time history of a wind-up turn at constant Mach number to the point of instability. Instability occurred at $10\frac{1}{2}$ seconds and was followed by a longitudinal oscillation which is felt to be the result of static divergence between two stable regions. Little rolling and yawing occurs. Notice that the mean control position during the oscillation is about that required to penetrate the unstable regions. In a similar maneuver when the control was reversed rapidly, the acceleration went from $7\frac{1}{2}g$ at the peak of the pitch-up to $-4\frac{1}{2}g$. This 12g change was in $1/2$ second and resulted in structural damage. An additional note may be added here with respect to fixes.

Fences were added to the XF-92A at 60 percent of the semispan from the leading edge to the flap hinge line. The fence height was equal to the wing maximum thickness at this span station. The fences, as a first estimate, were selected from tests of a delta-wing airplane having a thinner airfoil. Below a Mach number of 0.70, the stability boundary was raised to nearly maximum normal-force coefficient where pitching rates were encountered similar to those before but with very small increases in lift. Of interest is a maneuver at a Mach number of 0.6 and below where the airplane retrimmed at 40° angle of attack with full elevon deflection. It descended nearly vertically with full power losing speed.

Above a Mach number of 0.80, no apparent improvement resulted from the fences during the initial divergence. However, the previously described oscillation appeared in a more erratic form with less amplitude.

Another type of pitch-up requires some discussion of trim and apparent stability variations with Mach number

Transonic longitudinal trim characteristics are discussed in reference 1 and those of the X-5 and XF-92A have been determined since that time. These two airplanes exhibit the usual trim variations with speed but to a lesser extent than the airplanes having less sweep.


The longitudinal control effectiveness $d\delta_e/dC_{N_A}$ of these airplanes follows the usual pattern. The apparent reduction in elevator power for the XF-92A results, however, primarily from increased airplane stability from Mach numbers of 0.85 to 0.92. Above a Mach number of 0.92, a loss in flap effectiveness becomes apparent.

The second type of static instability is experienced when decelerating through this speed range where there are changes in trim and apparent stability. This condition occurs with all airplane configurations. The severity of this type of pitch-up is aggravated in low-aspect-ratio configurations where drag due to lift is high.

Figure 4 shows an example of an XF-92A maneuver during which, in a dive at a Mach number of 0.95, the pilot pulled up to the instability boundary as evidenced at 8 seconds. Then the speed was permitted to decrease, and from 14 to $19\frac{1}{2}$ seconds the control was fixed. However, the acceleration continued to increase because of trim change and decreased the apparent stability until the instability boundary was reentered at about $19\frac{1}{2}$ seconds at a Mach number of 0.85. Notice the high response to corrective control. During another similar maneuver at lower altitude and lower C_{N_A} , acceleration increased from 4g to 7g in 4 seconds with no control motion.

The pilot's attitude toward pitch-up is strongly influenced by the stick-free stability of the airplane. Stick-free instability contributes to the violence of the pitch-up. The D-558-II was made stick-free stable for one speed for the slats-out case and the severity of the pitch-up was only slightly alleviated. Provisions of more tail power for control of pitch-up, as has been proposed, in turn make it much easier to get into the unstable region at transonic speeds, and hence the difficulty is not materially improved.

The pilot's attitude is also strongly influenced by pitching rates. The current B-47A has a static instability as shown in figure 5 and is compared with the D-558-II; however, since divergence rates were of the order of one-fifth or less than those of fighter-weight airplanes, the pilot felt it was controllable to a large degree. Pitching rates of the B-47A are well below 0.1 radian/sec, whereas the research airplanes experience rates from above 0.3 to nearly 1 radian/sec.




A further influence on pilot's attitude toward the pitch is colored by the additional difficulty he may experience after entering the changing stability region. The amount of additional g acquired before control of the airplane is regained, deteriorating lateral directional stability at high lift, and the accelerated spinning characteristics, all of which incidentally arise from the same source, tend to cause the pilot to dislike approaching the unstable region, especially if he is thinking about it.

Now, assume that the pilot has traversed the transonic region through the narrow corridor at low lift without much difficulty and he attempts a maneuver at supersonic speed. Figure 6 illustrates the change in C_{NA} with Mach number of the D-558-II performing a turn at 50,000 feet. The turn is initiated with adequate power for a Mach number of 1.15 and, after only 20° of turn, the airplane enters the unstable, high-buffeting, high-drag, low-control region. Some of the most violent and uncontrollable maneuvers recorded have been made when the transonic region was entered from the high-speed side. Recognize that, at 60,000 feet and above, C_{NA} for 1 g flight is deep in the troublesome area.

At the other end of the speed scale the landing problems seem to reflect the transonic problems of basic wing plan forms. However, these low-speed longitudinal troubles respond nicely to various fixes like fences and slats. Also, the XF-92A with 30 lb/sq ft wing loading lands above 140 mph, which is about the speed for landing other research airplanes of twice or more wing loading. However, this speed falls at about 15 percent above the speed for maximum lift with full elevon deflection, about minimum wave-off speed and close to minimum ground clearance speed. There is, however, a landing difficulty arising from unique lateral-directional characteristics. Four pilots have described what appears to them to be directional instability while landing. The airplane literally flies sideways. This condition has been observed by the pilots and by ground and air observers. No explanation of this behavior has been determined up to the present time and investigations are continuing. Also, the high dihedral of the XF-92A requires careful coordination of approach turns because it overpowers the ailerons at small angles of sideslip.

Another lateral characteristic observed since publication of reference 1 is that, like other airplanes, the X-5 at 59° sweep has a transonic wing heaviness. Because the X-5 aileron effectiveness is sustained through the transonic region, the wing heaviness is more easily controlled.

The ailerons present a difficulty with the X-5 because of nonlinearity of aileron hinge moments with Mach number and lift. This difficulty is manifested in a lightening of the control forces at Mach numbers above 0.92 in straight flight and in aileron "snatch" or overbalance at high lift. The ailerons have large sealed internal balances. These changes in



[illegible]

100

—

[REDACTED]

constant values of angle of attack with either or both rudder and ailerons fixed or both controls available to the pilot.

Figure 8 shows a run at an angle of attack of -1° during which, with use of all controls, the pilot could prevent divergence of the oscillations. The motion has shown a similar but less divergent nature with power off as is also illustrated and this case is used to show the observed effect of angle of attack. In the same speed range as with power on, a pull-up is started at a Mach number of 1.7 with power off, and the oscillation is damped rapidly. Figure 9 shows the variation of the magnitude of the yawing oscillation with angle of attack for two speeds. The magnitude varies with speed and power, but the trend with angle of attack is the same with either power on or power off. It is felt that the influence of angle of attack results primarily from the change of the inclination of the principal axis of inertia because only slight changes in lateral derivatives occur in this angle-of-attack range.

Another lateral-directional problem has been experienced with the X-5 which exhibits a directional divergence at lifts above the longitudinal-stability boundary. This directional divergence has led to some startling maneuvers. Figure 10 is a time history of a push-down--pull-up maneuver where the longitudinal-stability boundary was penetrated. The airplane pitched, then diverged in sideslip to about 30° and a violent spin resulted during which the rolling record went off scale at 3 radians/sec. The airplane continued in a horizontal accelerated spin for several seconds before a conventional spin resulted and recovery was made. A pitch-up will not serve as a warning for the directional divergence at a higher lift but instead will probably assure its occurring. A directional divergence of the type experienced by the X-5 is intolerable and dangerous. The D-558-II has encountered a similar divergence at high lift.

To summarize the preceding comments, the following conclusions are indicated:

1. In general, the transonic region of heavy buffeting, high drag, instability, trim effectiveness, stability changes, and dynamic stability still warrants major attention.

2. Also, in general, the pitch-up, roll-off, and directional divergence have their origin in local changes of spanwise lift distribution at moderate to high lifts. With swept-wing airplanes these considerations are manifested with moment changes about all three axes. Wind-tunnel data indicate these phenomena but flight tests have been necessary to interpret the wind-tunnel information.

3. The specific problems fall into two categories. The first is the group of characteristics that are potentially dangerous or in any event intolerable. These characteristics are presented as follows:



(a) With fixes which apply only to the wing, no real solution has been found for the intolerable and dangerous pitch-up behavior of swept-wing airplanes of the configurations tested at transonic and low supersonic speeds.

(b) Directional divergence of the type experienced by the X-5 assumes importance equal to that of pitch-up.

(c) The severe roll-off which is related to pitch-up and directional divergence in its cause is wholly as dangerous and intolerable. Its addition to the two preceding characteristics compounds the difficulty presented to the pilot.

The second category is concerned with problems which are not particularly dangerous but still do not approach the minimum handling-qualities requirements. These problems are presented as follows:

(a) Trim and stability changes of any airplane may become important when they induce severe pitch-up.

(b) Low-rate pitch-ups characterized by the B-47 reduce the danger aspect of an otherwise intolerable behavior.

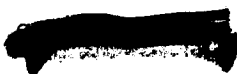
(c) The sideslipping behavior in straight flight of the XF-92A may explain its poor landing behavior.

(d) High effective dihedral of severely swept wings adversely affects handling qualities.

(e) The supersonic lateral motions of the D-558-II which decrease with increased angle of attack apparently are influenced by the change in inclination of the principal axis of inertia with angle of attack.

REFERENCE

1. Williams, W. C., and Crossfield, A. S.: Handling Qualities of High-Speed Airplanes. NACA RM L52A08, 1952.



CONFIDENTIAL

CLASSIFIED

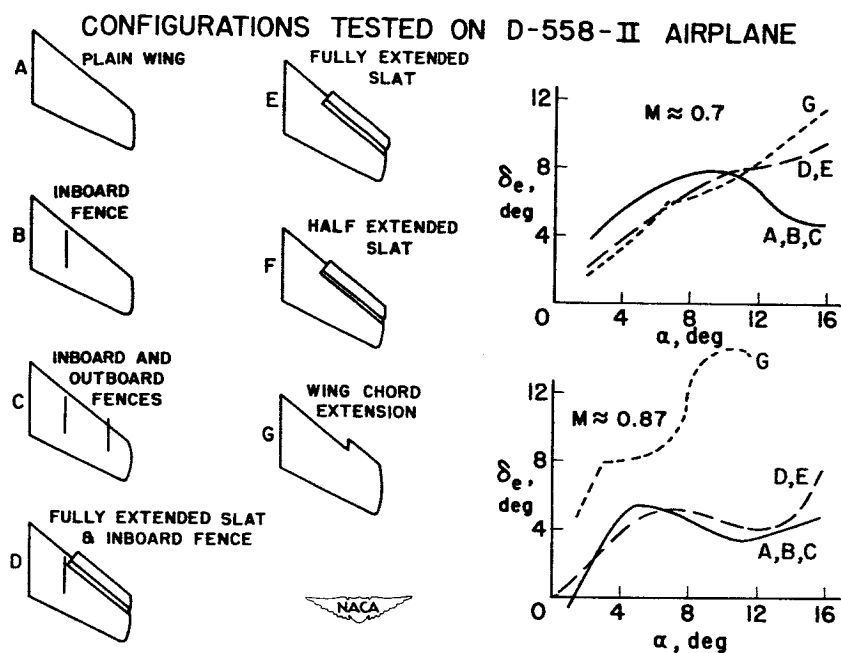


Figure 1

BOUNDARY FOR DECAY OF STICK-FIXED LONGITUDINAL STABILITY

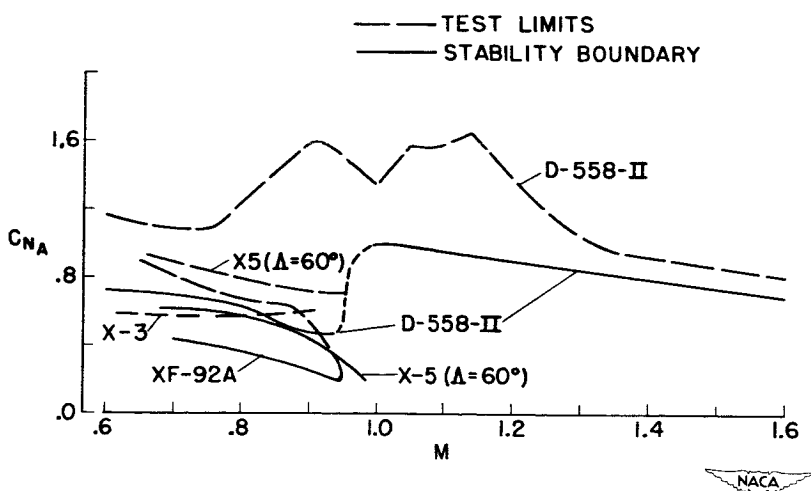


Figure 2

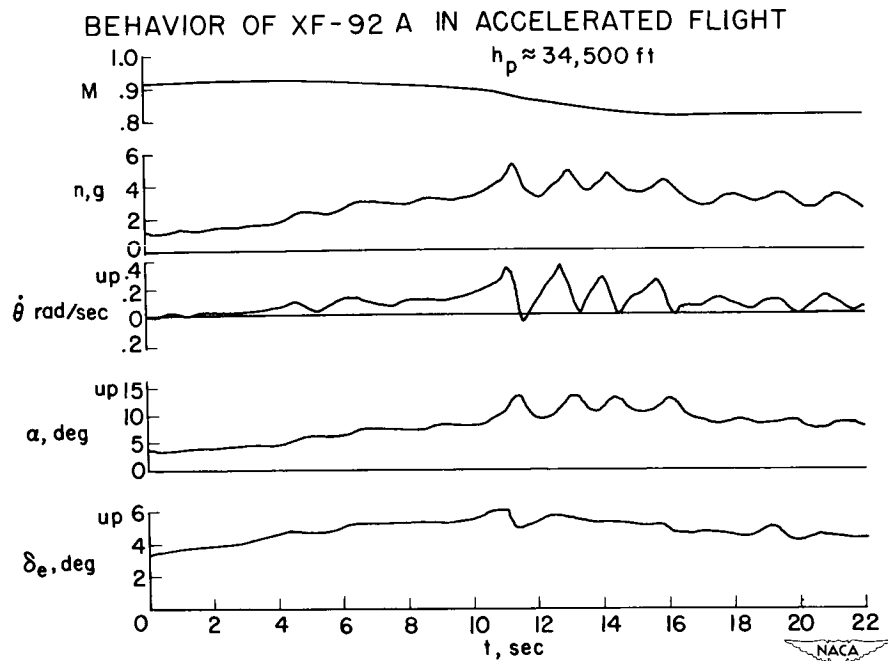


Figure 3

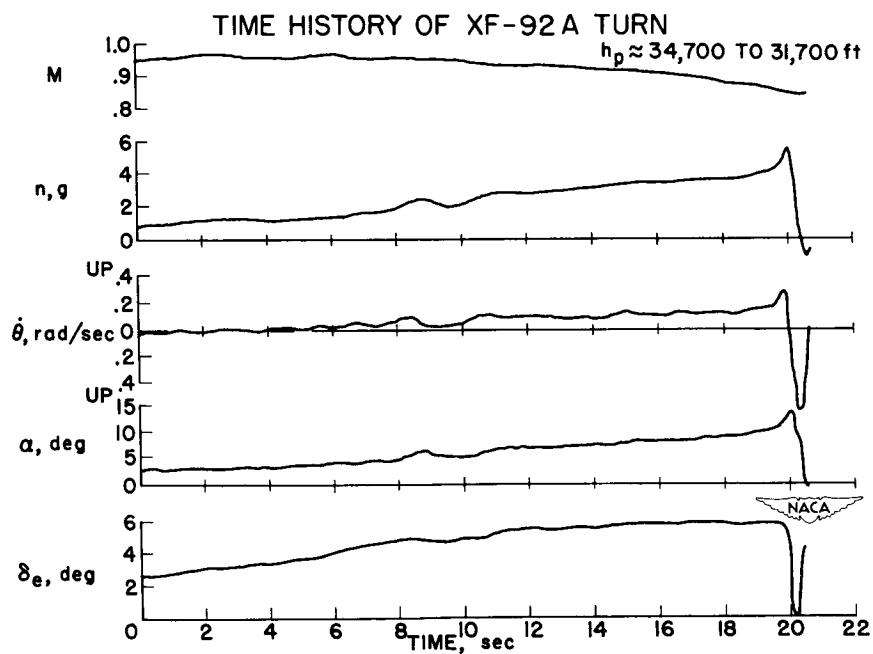


Figure 4

EXAMPLES OF PITCH-UP

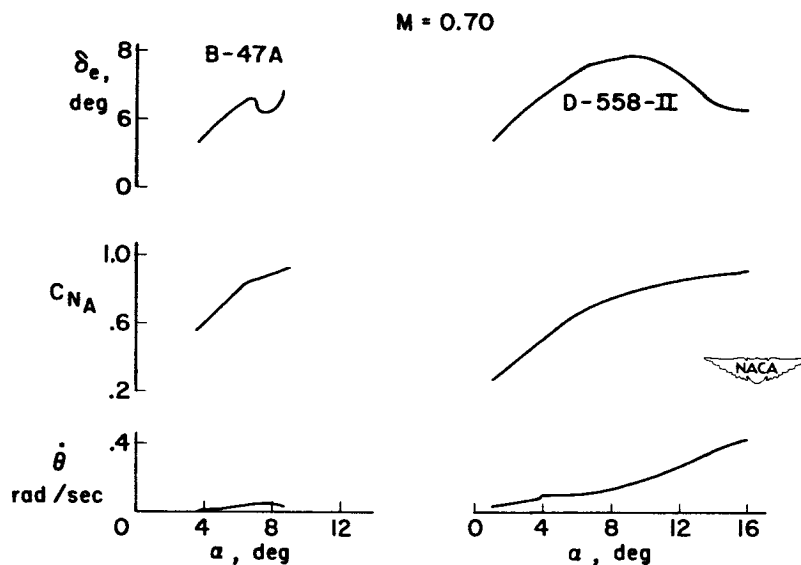


Figure 5

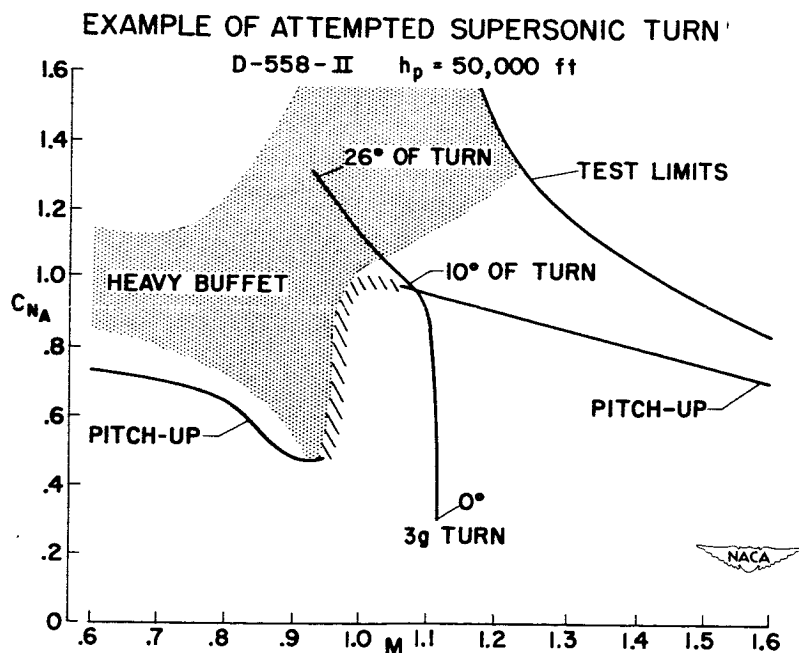


Figure 6

X-5 GYROSCOPIC COUPLING

$M = 0.85$; $h_p = 40,000$ ft

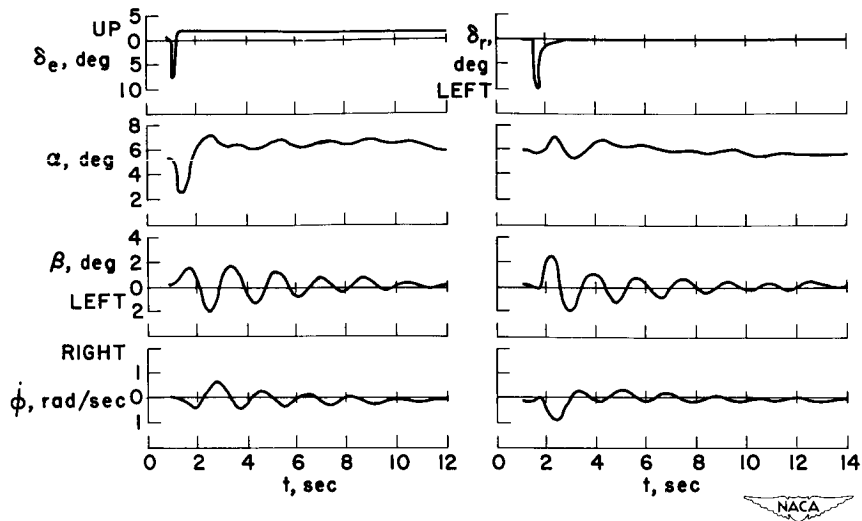


Figure 7

SUPERSONIC OSCILLATION OF D-558-II

$H_p \approx 63,000$ ft

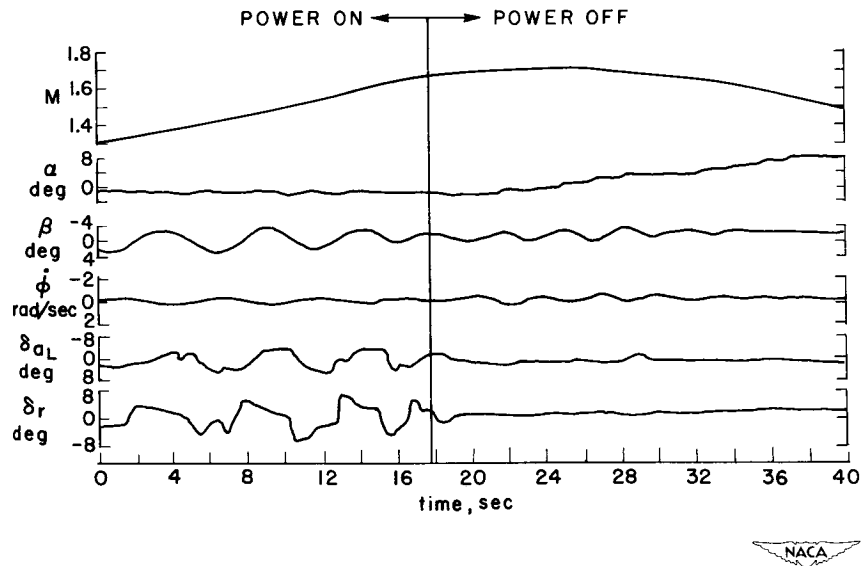


Figure 8

AMPLITUDE OF LATERAL OSCILLATION D-558-II

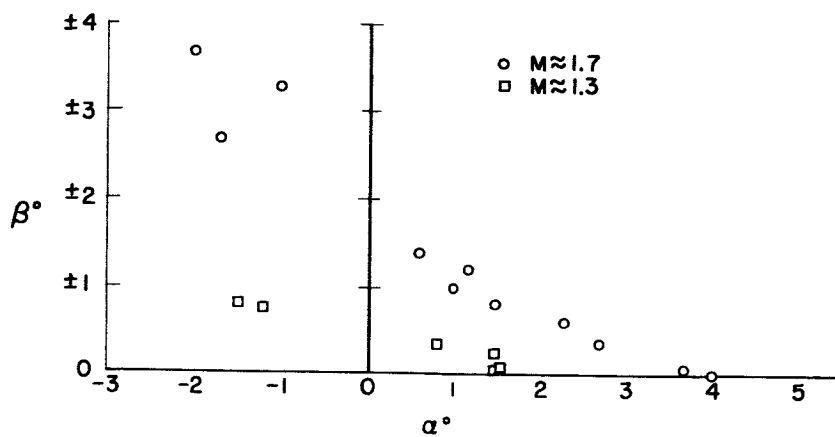


Figure 9

X-5 DIRECTIONAL DIVERGENCE FOLLOWED BY SPIN

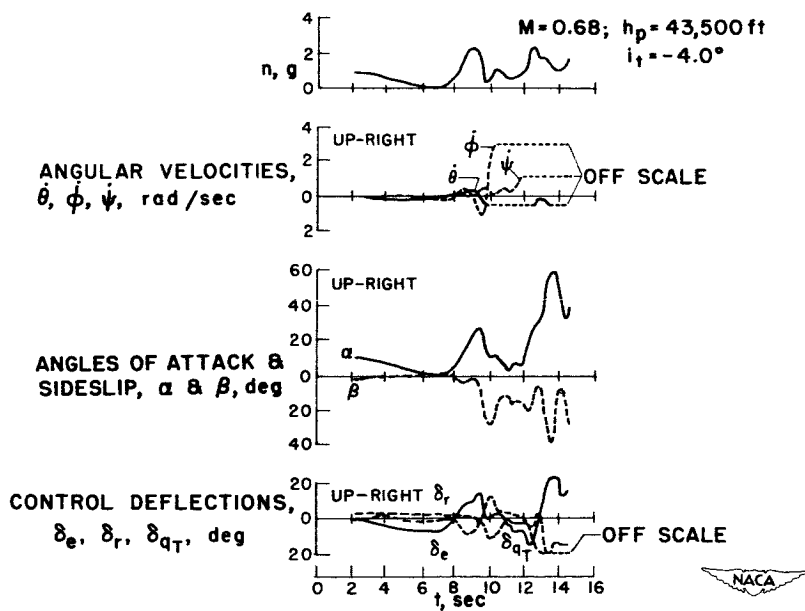


Figure 10

CONFIDENTIAL

RELASIFIED

RELATION BETWEEN FLIGHT BEHAVIOR AND STALL

PROGRESSION ON SWEPT WINGS

By Steven E. Belsley and Seth B. Anderson

Ames Aeronautical Laboratory

INTRODUCTION

Previous papers have pointed out the existence of erratic moments on an airplane when large areas of separation exist on the wing due either to stalling or shock separation. On sweptback wings the areas of separation begin over the outer part of the wings near the wing tips and must be controlled if smooth flight is to be accomplished at high values of lift. Although completely satisfactory control of separation over the Mach number range has not yet been accomplished, it has been possible to provide some improvements. It is the purpose of this paper to point out the degree to which pilots' opinions are affected by changes in nonlinear variations of aerodynamic parameters.

TEST EQUIPMENT

In figure 1 are shown a number of modifications designed to control separation which were flight tested on the F-86A airplane. These are the normal airplane with slats, cambered leading edge, extended leading edge plus fence, and blunt trailing-edge ailerons. In this paper evaluation of the modifications themselves is not the primary concern - but rather the effect the modifications have in altering the airplane behavior as far as the pilot is concerned.

RESULTS AND DISCUSSION

Characteristics at Low Speeds

Pitching-moment characteristics with a sharp break.- The effect of the shape of the pitching-moment curve will be discussed first. While the stable break shown in figure 2 by the solid curve is to be desired, it is possible that an unstable break (shown by the dashed curve) near maximum lift coefficient can be tolerated, provided the airplane does not pitch to large attitude. The stable break is for the F-86A with the slats open while the dashed curve was obtained by replacing the


BELSLEY &
ANDERSON

slats with a cambered leading edge. These data were obtained from reference 1. Note that the elevator-angle variation for trim obtained from flight tests was very similar for both cases. The pilot was aware of the nose-down behavior of the aircraft at the stall for the slats-open case; however, for the cambered leading edge, the pilot was not conscious of a pitch-up. Examination of the time histories indicated that the airplane actually did attain a nose-up pitching velocity of 0.2 radians per second; however, this occurred after $C_{L_{max}}$ and therefore was accom-

plished by a decrease in normal acceleration. It is believed that the pilots' insensitivity to the pitch-up associated with this type of pitching-moment break is primarily due to the absence of any inadvertent increase in normal acceleration. This is in contrast to the results obtained at higher speeds which will be covered later in this paper.

Rolling-moment characteristics.- For the airplane with the cambered leading edge, the pilot was aware of a severe roll-off. This prompted a closer study of the wind-tunnel measured characteristics which would be indicative of such a roll-off. In general, the only guide for anticipating this type of stall behavior from wind-tunnel tests has been from an inspection of the relative sharpness of lift-curve peaks coupled with tuft studies of stall progression on the wing. A sharp lift-curve peak is usually indicative of a rapid stall progression and large rolling moments. With this in mind, note in figure 3 the lift curves and rolling moments near maximum lift taken from full-scale wind-tunnel tests for the normal airplane with slats open and with the cambered leading edge. For the normal airplane the lift-curve peak is fairly smooth and well-rounded while for the cambered leading edge the lift-curve peak has a sharp break. It is seen that for the normal slats-open case the rolling moments through the stall are fairly small; however, for the cambered leading edge the rolling-moment variation above the stall is of large magnitude.

Stalls in flight indicated a correlation between the pilot's opinion of the suitability of the stall and the magnitude of the rolling motions (ref. 2), in that the objectionable stall was accompanied with large rolling motions. If these results were able to be interpreted simply in terms of static wind-tunnel measurements, some insight would be had into what to look for in the wind tunnel. Considering only gross effects leads one to believe that the objectionable airplane rolling motions must be due to the large rolling moments indicated previously. A comparison of pilots' opinions of the suitability of the stall with the rolling moments at the stall obtained from static wind-tunnel measurements at zero sideslip for a number of configurations yielded the results presented in figure 4 (ref. 3). These magnitudes were not a function of the asymmetry of the airplane since similar magnitudes of rolling-moment coefficient were obtained when the airplane was stalled at various



CONFIDENTIAL

REF ID: A55755

constant values of sideslip. It is shown that a reasonable correlation can be achieved, indicating that if the rolling-moment coefficient at the stall is kept below 0.01 the chance is very good that the stalling characteristics will be considered satisfactory, while values above 0.03 will be unsatisfactory. The correlation is good enough to be used as a guide during wind-tunnel tests of a prototype or for comparisons between various schemes designed to increase the maximum lift capabilities of the aircraft where good stalling characteristics are necessary. It should be noted that the rolling-moment criteria shown in figure 4 are limited to the type and size of aircraft tested. In addition these results were obtained at flight values of Reynolds number.

Pitching-moment characteristics with a gradual break. - In this section the gradual break in pitching moment will be covered in contrast to the sharp pitching-moment break previously discussed. An example of this type of pitching-moment variation is shown in figure 5 for the RF-84F at low speeds (ref. 4). Note that the pitching-moment variations depart from linearity well before maximum lift. For the unmodified airplane shown by the solid curve, the pilot was well aware of longitudinal instability in approaching the stall. Although there was little or no tendency to roll-off, the stall was considered unsatisfactory because of the necessity of applying continually increasing down-elevator as the speed was reduced and the possibility of running out of elevator control to check any dynamic maneuvers. The elevator angle required for trim for this condition is also shown in figure 5. These results are for a wings-level straight-flight stall. This pitching-moment characteristic was particularly objectionable at higher speeds, such as in an approach turn, because of the uncontrolled increase in normal acceleration. Addition of a blunt leading edge over the outboard part of the wing plus a fence changed the pitching-moment variation to that shown by the dashed curve. To the pilot this resulted in an improvement over the unmodified airplane in the approach to the stall. This is reflected in the variation of elevator angle with airspeed which indicates an over-all increased stability in approaching the stall. Although a pitch-up is still evident with this improvement and would be unacceptable under the Air Force flying-qualities requirements, it was not considered violent, was easily controlled by the pilots, and was preceded by adequate warning in the form of buffet (ref. 5). In addition, it is felt that the effectiveness of the longitudinal control would greatly influence pilot opinion of the controllability of an airplane with this type of pitching-moment variation. A very effective control would result in smaller stick movements, and hence the instability apparent to the pilot would be reduced.

Characteristics at High Speeds


Normal airplane characteristics.- Going now to higher speeds, the effects of Mach number in modifying the shape of the pitching-moment curves for the F-86A aircraft are shown in figure 6. It will be noted that the pitching-moment variation with C_N goes from a gradual break at a Mach number of 0.80 to a more abrupt break at a Mach number of about 0.90. These pitching-moment variations are reflected in the elevator angle and elevator control-force variation with g , showing gradual variations for trim at 0.80 Mach number and more abrupt variations at 0.90 Mach number (ref. 6). At high altitude the pilot felt that the pitch-up at 0.80 Mach number was rather mild but still objectionable, while at 0.90 Mach number the pitch-up was very abrupt and considered extremely unsatisfactory. At 35,000 feet the pitch-up may result in an overshoot of about $1g$ and a positive pitching velocity of about 0.3 radian per second at 0.80 Mach number and as much as $3g$ overshoot and 0.6 radian per second at 0.90 Mach number. As far as the pilot is concerned, the pitch-up at high Mach numbers is mainly a longitudinal disturbance although lateral unsteadiness or roll-off may precede the pitch-up and be troublesome in precise maneuvers such as in a tracking run.

Effect of modifications.- Obviously the pitch-up at high Mach numbers is undesirable, and various modifications have been flight tested in an attempt to eliminate or modify it. Shown in figure 7 are tuft patterns obtained in flight at 0.82 Mach number. Also shown in figure 7 is the wing-fuselage pitching moment. Note first, for the normal airplane, the separation starting at midchord, spreading rearward and outboard with increase in C_N . Note also the pitching-moment changes accompanying the separation growth. Now inspect the right-hand side of the figure where results are shown for a 15-percent chord-extension plus an outboard fence. Here it is shown that separation starts at the midspan position and spreads predominantly inboard with increase in C_N . The wing-fuselage pitching-moment changes accompanying this separation spread show a stable variation with increase in C_N . Although the pilot felt that he had improved control at the higher values of lift for the configuration with the extended leading edge, he was not completely satisfied. The reason for this is reflected in the data presented in figure 8, which show the total airplane pitching-moment curves and the elevator and stick-force variations with g for the normal and modified airplanes. It was found that the pilot objected to the region of neutral stability which occurred too close to level flight C_N values at high altitude. In summing up the effect of modifications at this lower Mach number region near 0.80, it is interesting to note that the use of outboard slats also resulted in improved pitching-moment characteristics while the use of fences alone did not provide any improvement (ref. 7).

In the Mach number range around 0.90 a different type of separation pattern was evident from tuft studies taken in flight and are shown in figure 9. Looking first at the normal airplane it can be observed that initial separation takes place along the trailing-edge part of the wing following the severe adverse pressure gradient which fans out from the juncture of the fuselage and the wing trailing edge. Note how the pitching-moment changes are more abrupt - reflecting the large, predominantly outboard growth of separation. Now on the right-hand side of the figure note for the leading-edge extension and fence how the tuft patterns remain substantially similar to the normal airplane, the pitching moments indicating only a slightly higher C_N value before the unstable break. This postponement of the pitch-up was noticeable but not particularly appreciated by the pilot, since the abruptness of the pitch-up remained unchanged and at high altitude the acceleration at which the pitch-up occurred was below the structural limit of the airframe.

Another modification which was particularly effective in the Mach number range around 0.90 was the addition of a blunt trailing edge to the ailerons. Although the pilot felt that this was the best modification tested on the F-86 airplane in the Mach number range around 0.90, the reasons for his feelings were not particularly evident from the data. Shown in figure 10 are the airplane pitching-moment curves and control variations for the normal airplane and the airplane with the blunt trailing-edge ailerons. For the blunt trailing-edge configuration the pilot noted a marked improvement in control at the higher values of lift. It can be seen that by comparing with the normal airplane, the departure from linearity in the pitching moment occurs at the same C_N value and the over-all change in stability is about the same; however, for the blunt trailing-edge configuration the pitching-moment variation after the break is less unstable. This suggests that a particularly bad pitch-up may be mitigated by flying at a more forward center-of-gravity position, resulting in a stable rotation of the pitching-moment curves. Another factor appreciated by the pilots for the configuration with the blunt trailing-edge ailerons was the complete absence of a roll-off or wing dropping for level flight lift values over the extent of the tests to 1.06 Mach number.


One factor influencing the pilots' opinion of the pitch-up behavior is the adequacy of the longitudinal control. Considering control by elevator and all-movable tail, the stick-force variations per g are shown in figure 11 for 35,000 feet altitude for a given airplane stability shown by this pitching-moment variation at 0.90 Mach number. With this reduced variation in stick force offered by the all-movable tail, the pitch-up was just noticeably apparent to the pilot. However, even with this apparent improvement in control, the pilot's tracking ability remained poor in the pitch-up region.



It should be noted that in this paper, reference has been made primarily to steady-state conditions and the pilot's reactions thereto. Since pilot reaction may be affected also by angular accelerations experienced in the transient, unbalanced phase of a maneuver, application of our results to other airplanes should consider not only differences in pitching-moment variations but also differences in the ratio of aerodynamic moments to inertia moments.


CONCLUSIONS

The results of this paper can be summarized as follows:

1. Unstable low-speed longitudinal-stability changes occurring at or beyond maximum lift were not noticed by the pilot because of a decrease in normal acceleration accompanying the pitch-up.
 2. Satisfactory stalling characteristics are indicated if the rolling-moment coefficient at stall is less than 0.01.
 3. Although a linear pitching-moment variation to maximum lift is desired by the pilot, an airplane possessing a slow forward neutral point shift with increase in C_N may be tolerable.
 4. At high speeds presence of any pitch-up was considered undesirable; however, improvements were appreciated. Regions of reduced stability were not as objectionable as long as the airplane was stable near maximum load factor. The use of a powerful longitudinal control device such as an all-movable tail reduces apparent instability and provides improved control in the pitch-up region, but the pilot's tracking remained poor.
 5. Various modifications to change the pitch-up characteristics are roughly correlated with the separation patterns measured in flight.
- 

CONFIDENTIAL

REFERENCES

1. Maki, Ralph L.: Full-Scale Wind-Tunnel Investigation of the Effects of Wing Modifications and Horizontal-Tail Location on the Low-Speed Static Longitudinal Characteristics of a 35° Swept-Wing Airplane. NACA RM A52B05, 1952.
 2. Anderson, Seth B., Matteson, Frederick H., and Van Dyke, Rudolph D., Jr.: A Flight Investigation of the Effect of Leading-Edge Camber on the Aerodynamic Characteristics of a Swept-Wing Airplane. NACA RM A52L16a, 1953.
 3. Anderson, Seth B.: Factors Influencing the Roll-Off Characteristics of a 35° Swept-Wing Aircraft in Low-Speed Stalls. (Prospective NACA paper.)
 4. Hunton, Lynn W., Griffin, Roy N., Jr., and James, Harry A.: Wind-Tunnel Investigation of the Low-Speed Static Longitudinal Characteristics of the Republic RF-84F Airplane. NACA RM SA52H04, U. S. Air Force, 1952.
 5. Phillips, Alfred D., and Stephens, R. L.: Phase II Performance & Stability Tests of the YRF-84F Airplane USAF No. 51-1828. AF Tech. Rep. No. AFFTC 52-32, Air Force Flight Test Center (Edwards, Calif.), Jan. 16, 1953.
 6. Anderson, Seth B., and Bray, Richard S.: A Flight Evaluation of the Longitudinal Stability Characteristics Associated With the Pitch-Up of a Swept-Wing Airplane in Maneuvering Flight at Transonic Speeds. NACA RM A51I12, 1951.
 - 7 Bray, Richard S.: The Effects of Fences on the High-Speed Longitudinal Stability of a Swept-Wing Airplane. NACA RM A53F23. (Prospective NACA paper.)
- 

MODIFICATIONS TESTED ON F-86A

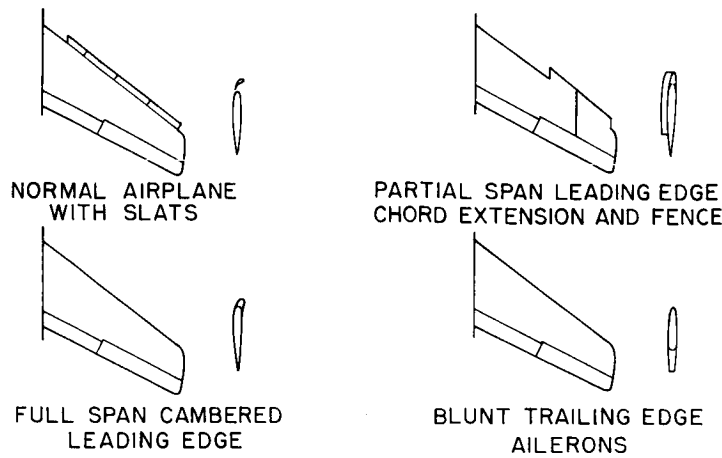


Figure 1

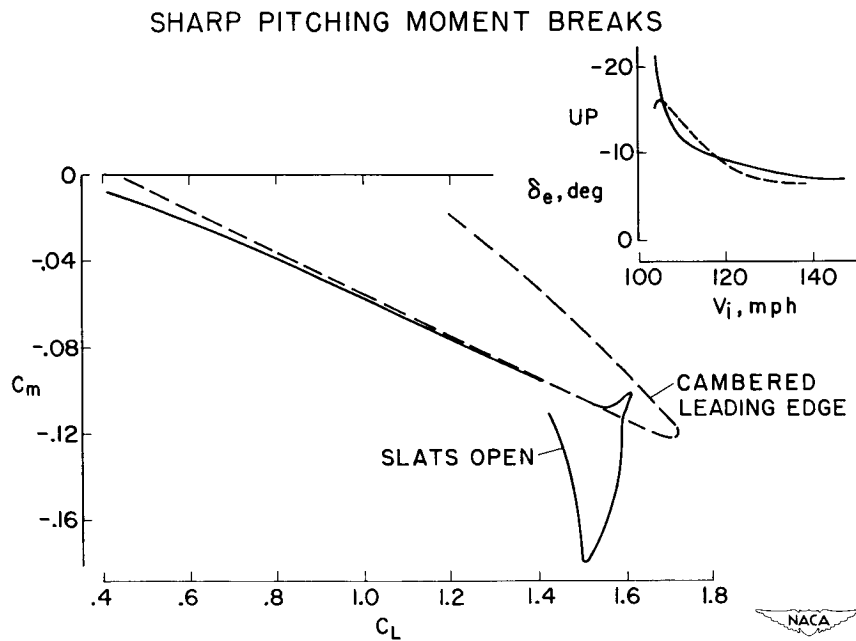


Figure 2

[REDACTED]

COMPARISON OF LIFT AND ROLLING MOMENT BREAKS

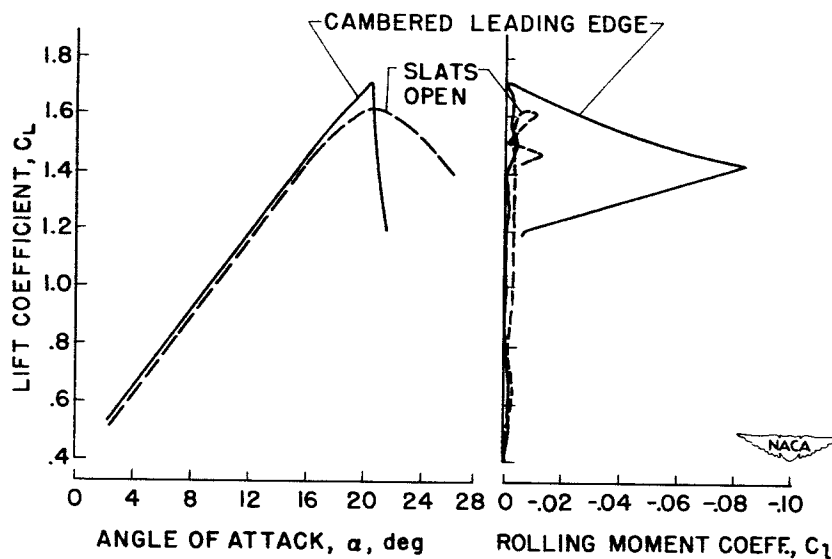


Figure 3

WIND TUNNEL ROLL-OFF CRITERION

PILOTS' COMMENTS ON STALL

- UNSATISFACTORY
- UNSATISFACTORY TO MARGINALLY SATISFACTORY
- MARGINALLY SATISFACTORY
- SATISFACTORY TO MARGINALLY SATISFACTORY
- SATISFACTORY

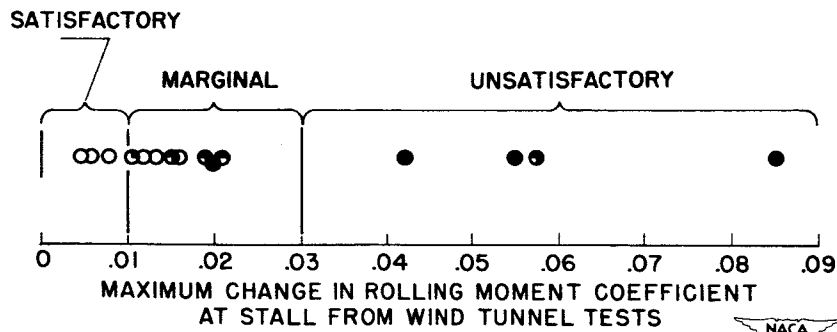


Figure 4

GRADUAL PITCHING MOMENT BREAKS

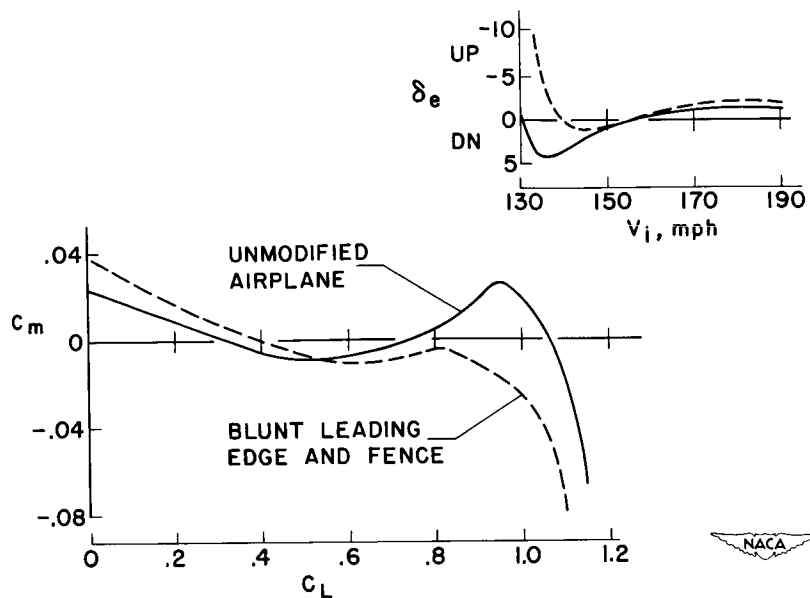


Figure 5

MACH NUMBER EFFECTS

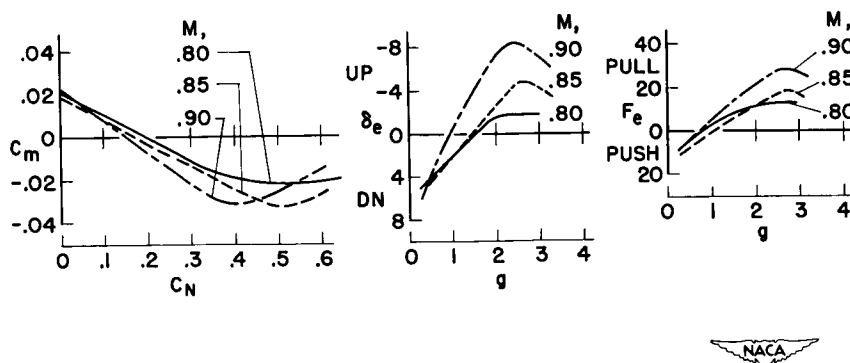


Figure 6

[REDACTED]

DECLASSIFIED

SEPARATION PATTERN AFFECTED BY L.E. EXTENSION

M, 0.82

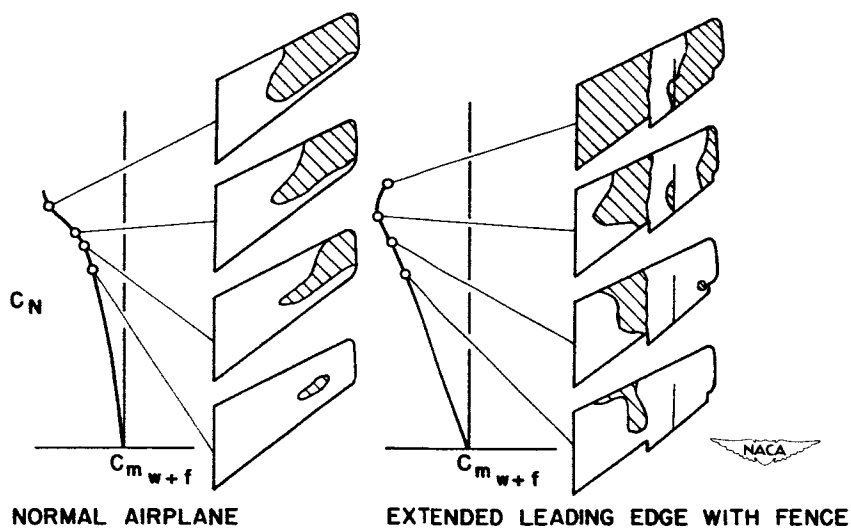


Figure 7

EFFECT OF LEADING EDGE EXTENSION

M, .80

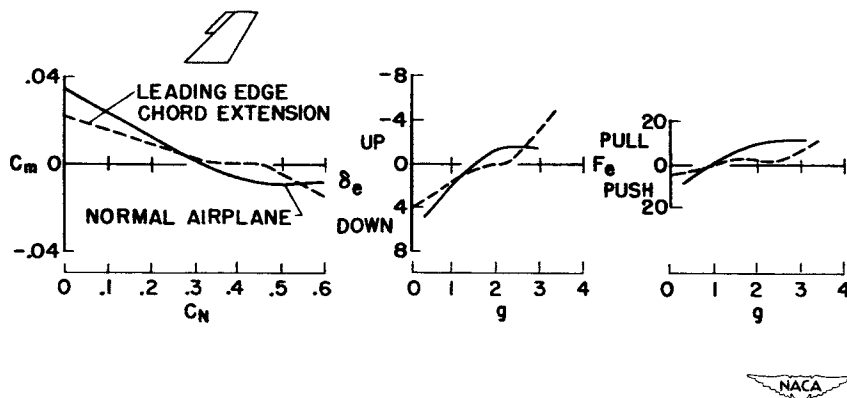


Figure 8

SEPARATION PATTERN AFFECTED BY L.E. EXTENSION

$M, 0.91$

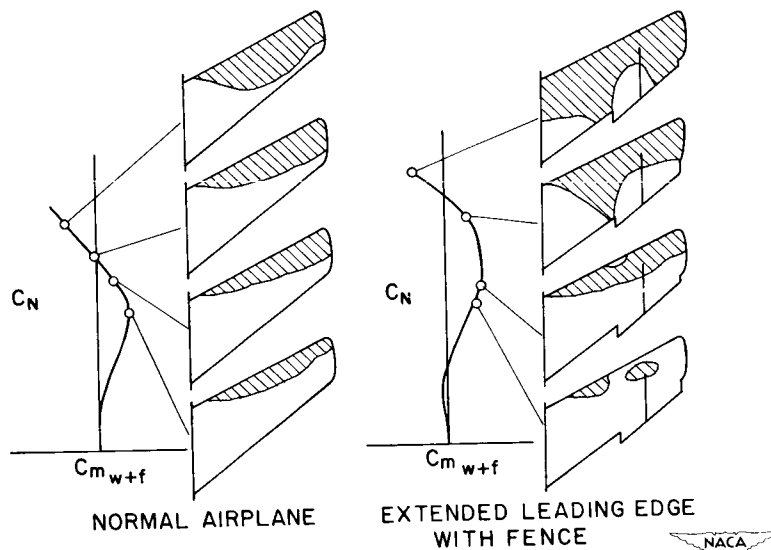


Figure 9

EFFECT OF BLUNT TRAILING EDGE

$M, .90$

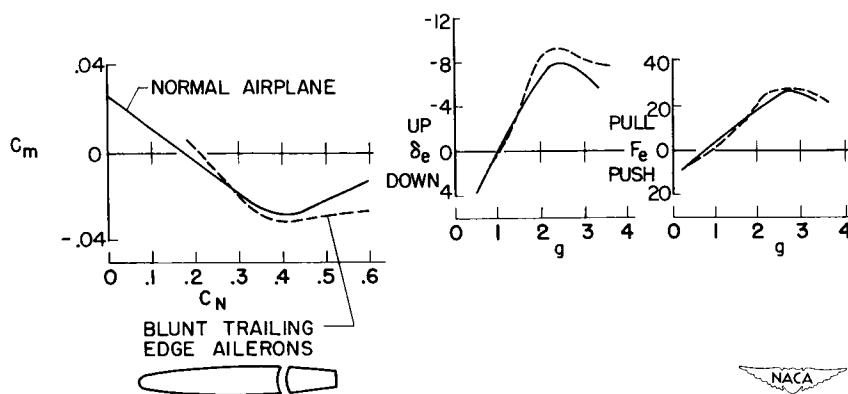


Figure 10

EFFECT OF ALL-MOVING TAIL

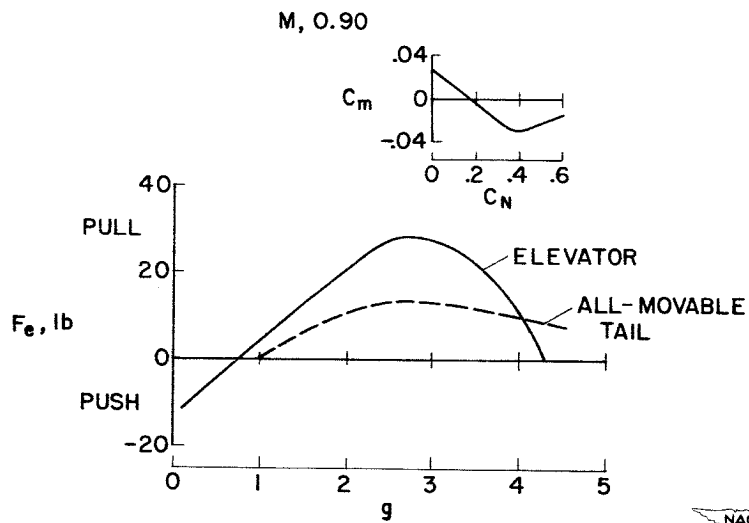


Figure 11

STALL PROGRESSION ON SWEEPED WINGS AT LOW AND HIGH SPEEDS

By Charles W. Harper and Robert M. Crane

Ames Aeronautical Laboratory

STALL PROGRESSION AT LOW SPEEDS

The need for some design procedure which will enable the designer of swept wings to obtain desired stalling characteristics without recourse to extensive trial-and-error testing is very apparent. In undertaking the development of a procedure, the most logical starting point seemed to be the procedure developed to a useful point by Anderson and others (e.g., refs. 1 to 3) for the case of the unswept wing. A factor which has made this procedure especially useful is that span-loading and section characteristics are handled independently. This can be done when it is assumed that each section operates independently except for the induced upwash variations across the span. In order to extend the method to swept wings while maintaining this usefulness, it is necessary (1) to use an applicable span-loading procedure, (2) to choose that section on the swept wing the characteristics of which can best be approximated from section tests, and (3) to continue to assume independence of the sections. With regard to the first point, several methods, of varying degrees of accuracy, are available. With regard to the second point, it is assumed in this paper that the most appropriate choice, in that the greatest understanding, and hence control, of the stall will result therefrom, is to consider the effective section to be that one lying normal to the quarter-chord line of the wing; this assumption follows directly from the theory of sweep.


Thus as shown in figure 1, by modifying Anderson's basic method, it is possible to predict the wing lift coefficient and location on the span at which the first section will stall (refs. 4 and 5), as is done by Anderson for the straight wing (ref. 1). Also shown in this figure are the force-test results for this wing. Stall was predicted at a C_L of 0.38 and at a span location such that a nose-up pitching moment would result. The force tests show no effects of stall until about $0.5C_L$ and no evidence of a nose-up moment until about $0.6C_L$.

Similar results have been found when applying the method to other wings in that an increment in lift is almost always realized before the wing-force characteristics show the effect of stall. The magnitude of this increment is as yet an unpredictable factor but the fact that it is not much changed for a given wing plan form by modifications to the

airfoil sections and the fact that it seems to vary regularly with wing plan-form changes, and so can be empirically accounted for, enables practical use to be made of the method. For instance, as shown in figure 2, the predicted effects of adding to the wing just considered a partial-span nose flap in order to raise the maximum lift of the outboard sections are a slight increase in wing lift before stall and a reduced degree of instability after stall because of the inboard shift of initial stall. Pitching-moment variations show that both effects were realized and that the lift increment due to the flap was very well predicted.

In another case, illustrated by figure 3, it was desired to reach a wing C_L of 1.4 at an angle of attack of 14° before stall was encountered in the landing condition. Allowing for its conservatism, empirically determined in this case to be $0.15C_L$, the method was used to choose flaps and leading-edge slats from available two-dimensional data. Shown in the figure are the predicted (ref. 6) span-load distributions for the C_L at which stalling begins for the modified wing and also the measured moment characteristics; these measured moment characteristics indicate that the design requirement was met.

The direct approach to the control of swept-wing stall illustrated by the two cases just shown may prove adequate in many cases, provided it can be reasoned that there will exist an upper limit to the angle of attack or lift coefficient reached in normal operation and hence airplane characteristics beyond this point are of no interest. Even accepting this provision, however, it is doubtful whether enough control of the stall can be realized by section modification alone to make this approach sufficient in all cases. This is due to the conflict between requirements for good low-speed and good high-speed section characteristics and to the lack of information regarding control of section stall at high speed where the pitch-up problem is also serious. Therefore, in many cases it is necessary to devise means of controlling the spread of stall in the lift-coefficient range between the first appearance of stall or separation and maximum lift. Although, in the case of the unswept wing, Anderson's method (ref. 1) can be used successfully to design for a desired stalling progression, the modified method proposed herein for swept wings fails completely in this regard. Figure 4 shows why this failure occurs and indicates that wing sweep introduces a new factor which has a profound effect on section stalling characteristics. It is clear that the factor of major importance in producing observed stall progressions on swept wings is the increasing value of maximum lift realizable by sections as they are placed more inboard (ref. 7). At all stations the maximum lift exceeds that measured for the same section in two-dimensional tests. Similar data have been obtained for many wings and throughout the subsonic Mach number range.



Rather simple reasoning, which can be presented with the aid of figure 5, indicates a possible source of this effect of sweep although as yet no proof exists. Consider first the case of the infinite yawed wing. Assume that the maximum lift of any section will be governed by the stability of the turbulent boundary layer as it flows normal to the isobars which in this case are exactly parallel to the wing leading edge. Assume further that the stability of the boundary layer against an adverse pressure gradient is not materially affected by the shearing resulting from the spanwise component of the free-stream velocity. This assumption would imply also that the boundary-layer thickness measured either parallel to or normal to the isobars would be constant along any chordwise line, as indicated by arrow length. Under these conditions, the section maximum lift coefficient will be unaffected by the angle of yaw as long as the reference section is chosen normal to the wing leading edge and the reference velocity is that component of free-stream velocity normal to the wing leading edge. Making this infinite yawed wing semi-infinite by forming a tip in the downstream portion will not appreciably alter the conditions just described. However, making it a finite wing by placing a barrier in the upstream portion will markedly change the conditions. As the boundary layer is carried away from the downstream face of the barriers, it can no longer be replaced and hence a thinning should take place, as indicated by the reduced arrow length. The thinning should be evident whether boundary-layer thickness is measured parallel or normal to the isobars. This thinning is, in effect, boundary-layer control and should increase the maximum lift of these sections above the value reached without the barrier and hence above the value for the section in the purely two-dimensional case. It is easy to see that some degree of thinning will be felt along the entire span, being greatest at the root and least at the tip. This variation in thinning agrees with the observed variation in section maximum lifts. Thus, despite the fact that this reasoning ignores many factors, which means that it could be correct in only the grossest sense, it is believed to outline the major factor controlling the stall progression of swept wings and has been extremely useful in guiding the direction of research to control stall progression. In particular, it emphasizes the fact that, if desirable stall progression is to be realized, some means of adjusting this boundary-layer control must be available. Further, in order to satisfactorily refine the method discussed previously, some quantitative measure must eventually be made of this effect.


One obvious way to control stall progression is to redistribute the boundary-layer-control effect so that maximum lift coefficients typical of the root can be realized near the tip and vice versa. Establishing barriers, such as fences, to the boundary-layer flow would be expected to do this since just outboard of them the boundary-layer control should be as large as that of the root while just inboard it should be as little as that of the tip. Hence, at lift coefficients above that for initial stall on the unmodified wing, the addition of

barriers should unstuff the area just outboard of them and produce stall just inboard. The increased loading thus realized outboard plus the decreased loading inboard are, of course, the changes which would be adjusted to produce satisfactory pitching-moment characteristics.

Figure 6 shows the measured effect of fences on the distribution of section lift and wing stall on a low-aspect-ratio swept wing at a wing lift coefficient well above the first appearance of stall. The resemblance of the measured effect to that proposed indicates that the reasoning is sound; the major redistribution of lift and stall indicates that the effect is great. As shown in figure 7, very similar results with regard to the redistribution of section lift have been found on a high-aspect-ratio wing when fences were installed (ref. 8). Shown here also is the magnitude of the pitching-moment change which can be realized from these span-loading changes.

It also has been found that an aerodynamic fence can be effective in controlling the boundary-layer drain. Such a fence is in the form of a vortex lying just above the wing surface and rotating so as to sweep the boundary layer inboard. A vortex of this nature can be created by a discontinuity at the wing leading edge such as formed by a partial-span extended slat. Figure 8 shows the effectiveness of such a device in shifting the point of initial stall to control the pitching moment of a 45° swept wing (ref. 9). Note that when the discontinuity was moved far inboard, it was unable to overcome the boundary-layer drain and initial stall appeared at the tip. It has been observed that increasing the sweep, which increases the boundary-layer control at the inboard sections, restricts the effectiveness of such a device closer to the tip, thus indicating that at some sweep a leading-edge discontinuity and probably also a fence will become incapable of controlling, to any useful degree, the stall progression.

Some other points in connection with leading-edge extensions are of interest. Smoothly fairing the discontinuity into the wing leading edge sharply reduces its effectiveness, as would be expected from the reduction in vortex strength. Reversing the discontinuity so that a sudden reduction in chord is encountered when moving toward the tip entirely cancels the effect of a discontinuity, as would be expected since in this case the vortex rotates so as to enforce the boundary-layer drain. This statement does not apply to notches which have an entirely different geometry. Finally, in comparing the effectiveness of fences and leading-edge discontinuities, it must be remembered that these discontinuities are often formed by the inboard end of a device designed to increase the maximum lift of tip sections; in this way two means of increasing tip section $C_{L_{max}}$ are used, giving greater control over stall than may be realized by either one alone.



The foregoing discussion has attempted to present, for the low Mach number case, a brief description of the stalling of swept wings and the operation of devices used to control this stall. The whole picture is exceedingly complex, however, and much research with regard to the effects of plan form, airfoil section, Mach number, and so forth, is required before a wholly quantitative analysis can be made. To illustrate the progress being made in one field, the next section discusses the effects of Mach number on the stall progression.


EFFECTS OF MACH NUMBER ON STALL PROGRESSION

The basic method, described in the preceding section of this paper, of calculating the lift coefficient for initial separation on a swept wing can be applied at supercritical speeds as well as at low Mach numbers as long as the shock waves that exist on the wing are due to the flow over the wing profile and are not a result of the three-dimensional flow field. This is shown in figure 9 which compares the measured pitching moments on a 45° swept wing of aspect ratio 5 (ref. 10) with the lift coefficient for separation predicted from section data. At Mach numbers up to 0.85 the predicted value of lift coefficient agrees well with that at which nonlinearities are evident in the pitching-moment data.

At transonic Mach numbers, shock waves usually exist which cannot be correlated with the section characteristics of the wing. The shock wave emanating from the wing-fuselage juncture and the shock wave associated with deceleration of the entire three-dimensional flow field are examples of disturbances of this type. The data shown at a Mach number of 0.92 are typical of this Mach number range. Areas of separated flow are evident at lift coefficients above about 0.20 although the value of lift coefficient for separation predicted from section data is about 0.40. Under these conditions, section data cannot be used to predict the wing lift coefficient at which initial separation will occur, and recourse must be made to experimental data on the three-dimensional wing.

A second example of the use of section data at high Mach numbers is shown in figure 10. In this case a section modification was made to the leading edge of a 35° swept wing in an effort to increase the lift coefficient for pitch-up (ref. 11). Section data obtained at low speeds had indicated the large gains possible by increasing the airfoil leading-edge radius and introducing camber on the forward part of the airfoil.

At higher Mach numbers and a Reynolds number of 2×10^6 , the section data indicated that the leading-edge modification would be ineffective, the maximum lift coefficient of the section with forward camber




decreasing rapidly as the Mach number was increased and actually becoming less than that of the basic section at a section Mach number of 0.65 corresponding to a wing Mach number of 0.80. That the predicted trend was correct is evidenced by the experimental data on the swept wing which show that the section modification did not increase the lift coefficient for pitch-up at the Mach numbers above about 0.80.

This adverse effect of compressibility on the maximum lift of the cambered airfoil appears to be peculiar to airfoils which have their camber concentrated near the leading edge. When the camber is distributed over the chord, such as with the $a = 1.0$, $a = 0.8$, or even $a = 0.4$ mean lines, the lift increment due to camber is maintained to high section Mach numbers.

The data shown in figure 10 emphasize a factor which was pointed out earlier in this paper. In order to utilize section data for the prediction of the lift coefficient for initial stall on a swept wing, the section data must be at the Mach number and Reynolds number corresponding to the component of velocity normal to the sweep of the wing. For example, on the cambered wing shown in this figure, increasing the Reynolds number at low speeds from 2×10^6 to 11×10^6 increased the lift coefficient for pitch-up from 0.80 to 1.2. Similar Reynolds number effects were evident in the section data. Just how important the Reynolds number is at the higher Mach numbers has not been firmly established but there are experimental data on swept wings, especially those having large thickness-chord ratios or cambered sections, which show large effects of Reynolds number on the lift coefficient for pitch-up at Mach numbers as high as 0.94.

The effectiveness of fences and of leading-edge discontinuities in delaying or modifying the pitch-up is much diminished at high transonic Mach numbers. An example is shown in figure 11 which shows the effect of a fence on the pitching-moment characteristics of a wing-fuselage combination having a 35° swept wing of aspect ratio 4.5 (ref. 12). At Mach numbers less than about 0.82, initial separation occurred along the leading edge of the wing and the fence was effective in improving the pitching-moment characteristics of the wing-fuselage combination. It did this not by delaying separation on the wing, but by redistributing the separated regions along the span so that the initial stalled area and its subsequent growth was such as to produce a nose-down moment. At Mach numbers of 0.85 and above, tuft studies showed that flow separation occurred on the outer sections of the wing behind a line that was approximately normal to the plane of symmetry. Pressure data are not available but it is believed that the disturbance causing this separation was a shock wave emanating from the wing-fuselage juncture. There was no spanwise flow in the region of the fence and the force tests showed the fence to be completely ineffective as would be deduced from the tuft studies.



In contrast to this result, figure 12 shows the effect of adding fences to a cambered 40° swept wing having an aspect ratio of 10 (ref. 13). In this case, both pressure data and tuft studies showed separation starting from the trailing edge and at the higher Mach numbers a shock wave was evident which produced local separation along a line approximately parallel to the wing leading edge. In this case, the tuft studies showed spanwise flow in the region of shock-induced separation and although the fences were not as effective as they were at a Mach number of 0.25, they still afforded considerable improvement in the pitching-moment characteristics at Mach numbers of 0.80 and 0.90.

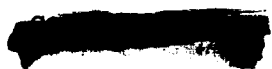
That this is not the usual case can be seen from inspection of data from the Langley high-speed 7- by 10-foot tunnel and 16-foot transonic tunnel (refs. 14 to 17) which show little, if any, effect of fences on the pitching-moment characteristics of thin 45° swept wings of aspect ratio 4 at Mach numbers between 0.90 and 0.98. It is believed that these cases are similar to that shown for the 35° swept wing in which the shock-induced separation is not associated with the wing section but rather with the entire three-dimensional flow field.

The effects of a leading-edge chord-extension and of a partial-span slat on a thin 45° swept wing of aspect ratio 4 and shown in figures 13 and 14 (refs. 17 and 18). Both the slat and the chord-extension tend to modify the stall progression over the wing by providing an aerodynamic barrier to spanwise flow. In addition the slat increases the lift-carrying potential of the outer section of the wing. Inspection of the data reveals that the slat and the leading-edge extension were about equally effective in delaying the pitch-up at Mach numbers up to 0.85. However, at Mach numbers between 0.90 and 0.98, the slat lost only part of its effectiveness while the leading-edge extension was almost completely ineffective. The data shown at a Mach number of 0.94 are typical for this range of Mach number. In general, the effectiveness of leading-edge chord-extensions and slats diminishes at transonic speeds. As was the case with fences, the leading-edge devices do not appear to be powerful enough to have much effect on the initial location and subsequent growth of separation induced by strong shock waves. When properly located along the span, however, these devices do maintain effectiveness to a higher Mach number than do fences and can afford some improvement in the pitching-moment characteristics throughout the entire speed range.


In this paper it has been demonstrated that a fairly successful method has been developed for predicting and controlling the first appearance of stall on a swept wing through use of span-loading theories and section data. The method can be applied at supercritical Mach numbers as well as at low speeds providing the shock waves that exist are due to the flow over the wing profile and are not a result of the


three-dimensional flow field. The lift-coefficient range above the point of initial stall has been examined and conclusions have been drawn as to the important factors affecting stall progression in this region.

Several different types of stall-control devices for swept wings have been examined and it has been demonstrated that their action is essentially that of modifying, either by terminating or reinforcing, the automatic boundary-layer control action which is inherent on a swept wing. There is a range of transonic Mach numbers on swept wings at which the lift coefficient for initial separation cannot be predicted from section data. The lower limit of this Mach number range is the Mach number at which strong shocks from the wing-fuselage combination predominate over the section characteristics of the wing in causing separation. The actual value of Mach number at which this condition first exists is a function of the wing sweep, aspect ratio, thickness-chord ratio, and the wing-body interference. In this same Mach number range, wing fences and leading-edge extensions are almost completely ineffective.



REFERENCES

1. Anderson, Raymond F.: The Experimental and Calculated Characteristics of 22 Tapered Wings. NACA Rep. 627, 1938.
 2. Pearson, Henry A., and Anderson, Raymond F.: Calculation of the Aerodynamic Characteristics of Tapered Wings With Partial-Span Flaps. NACA Rep. 665, 1939.
 3. Sivells, James C., and Neely, Robert H.: Method for Calculating Wing Characteristics by Lifting-Line Theory Using Nonlinear Section Lift Data. NACA Rep. 865, 1947. (Supersedes NACA TN 1269.)
 4. DeYoung, John, and Harper, Charles W.: Theoretical Symmetric Span Loading at Subsonic Speeds for Wings Having Arbitrary Plan Form. NACA Rep 921, 1948.
 5. Maki, Ralph L.: The Use of Two-Dimensional Section Data to Estimate the Low-Speed Wing Lift Coefficient at Which Section Stall First Appears on a Swept Wing. NACA RM A51E15, 1951.
 6. DeYoung, John: Theoretical Symmetric Span Loading Due to Flap Deflection for Wings of Arbitrary Plan Form at Subsonic Speeds. NACA Rep. 1071, 1952. (Supersedes NACA TN 2278.)
 7. Hunton, Lynn W.: Effects of Finite Span on the Section Characteristics of Two 45° Swept-Back Wings of Aspect Ratio 6. NACA RM A52A10, 1952.
 8. Boltz, Frederick W., and Shibata, Harry H.: Pressure Distribution at Mach Numbers up to 0.90 on a Cambered and Twisted Wing Having 40° of Sweepback and an Aspect Ratio of 10, Including the Effects of Fences. NACA RM A52K20, 1953.
 9. James, Harry A.: Low-Speed Aerodynamic Characteristics of a Large-Scale 45° Swept-Back Wing With Partial-Span Slats, Double-Slotted Flaps, and Ailerons. NACA RM A52B19, 1952.
 10. Johnson, Ben H., Jr., and Shibata, Harry H.: Characteristics Throughout the Subsonic Speed Range of a Plane Wing and of a Cambered and Twisted Wing, Both Having 45° of Sweepback. NACA RM A51D27, 1951.
 11. Demele, Fred A., and Sutton, Fred B.: The Effects of Increasing the Leading-Edge Radius and Adding Forward Camber on the Aerodynamic Characteristics of a Wing With 35° of Sweepback. NACA RM A50K28a, 1951.
- 

12. Selan, Ralph, and Bandettini, Angelo: The Effects of Leading-Edge Extensions, a Trailing-Edge Extension, and a Fence on the Static Longitudinal Stability of a Wing-Fuselage-Tail Combination Having a Wing With 35° of Sweepback and an Aspect Ratio of 4.5. NACA RM A53E12, 1953.
 13. Edwards, George G., Tinling, Bruce E., and Ackerman, Arthur C.: The Longitudinal Characteristics at Mach Numbers up to 0.92 of a Cambered and Twisted Wing Having 40° of Sweepback and an Aspect Ratio of 10. NACA RM A52F18, 1952.
 14. Goodson, Kenneth W., and Few, Albert G., Jr.: Effect of Leading-Edge Chord-Extensions on Subsonic and Transonic Aerodynamic Characteristics of Three Models Having 45° Sweptback Wings of Aspect Ratio 4. NACA RM L52K21, 1953.
 15. Spreemann, Kenneth P., and Alford, William J., Jr.: Investigation of the Effects of Leading-Edge Chord-Extensions and Fences in Combination With Leading-Edge Flaps on the Aerodynamic Characteristics at Mach Numbers From 0.40 to 0.93 of a 45° Sweptback Wing of Aspect Ratio 4. NACA RM L53A09a, 1953.
 16. Hieser, Gerald: An Investigation at Transonic Speeds of the Effects of Fences, Drooped Nose, and Vortex Generators on the Aerodynamic Characteristics of a Wing-Fuselage Combination Having a 6-Percent-Thick, 45° Sweptback Wing. NACA RM L53B04, 1953.
 17. West, F. E., Jr., Liner, George, and Martz, Gladys S.: Effect of Leading-Edge Chord-Extensions on the Aerodynamic Characteristics of a 45° Sweptback Wing-Fuselage Combination at Mach Numbers of 0.40 to 1.03. NACA RM L53B02, 1953.
 18. Runckel, Jack F., and Steinberg, Seymour: Effects of Leading-Edge Slats on the Aerodynamic Characteristics of a 45° Sweptback Wing-Fuselage Configuration at Mach Numbers of 0.4 to 1.03. NACA RM L53F23, 1953.
- 

PREDICTION OF THE FIRST APPEARANCE OF STALL ON A SWEEP WING

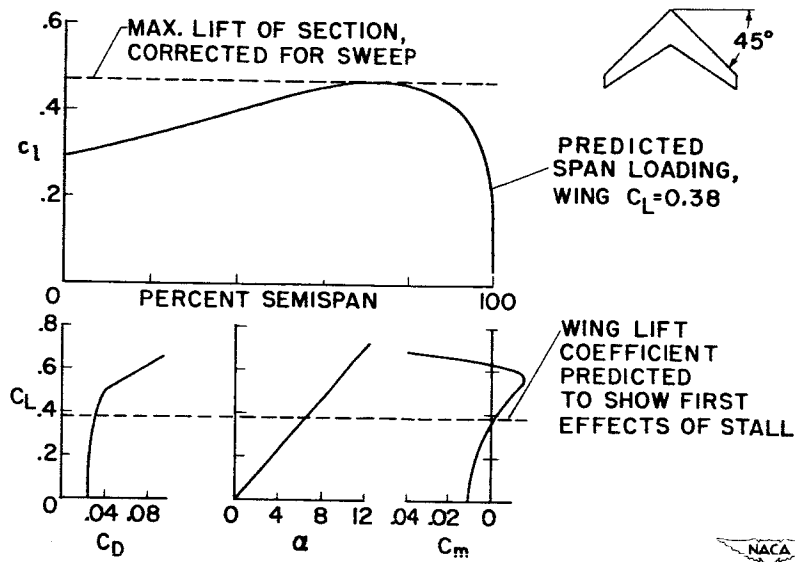


Figure 1

EFFECTS OF LEADING-EDGE FLAP ON FIRST STALL

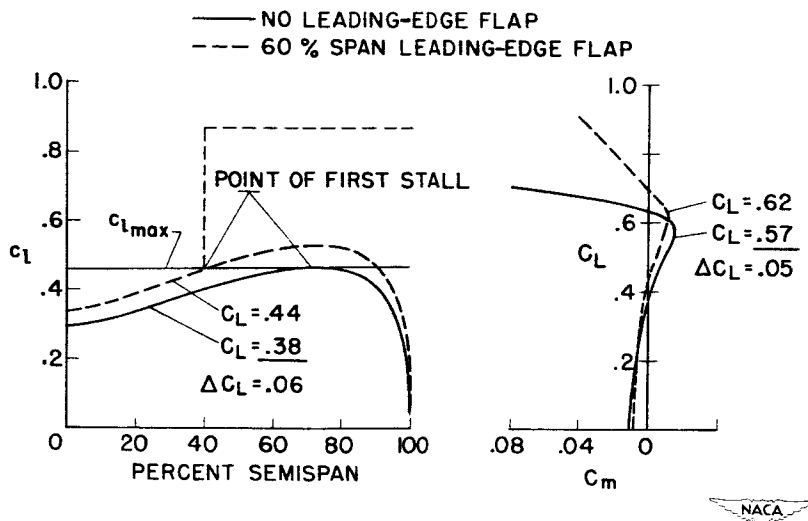


Figure 2

METHOD USED TO DESIGN FOR GIVEN CONDITION

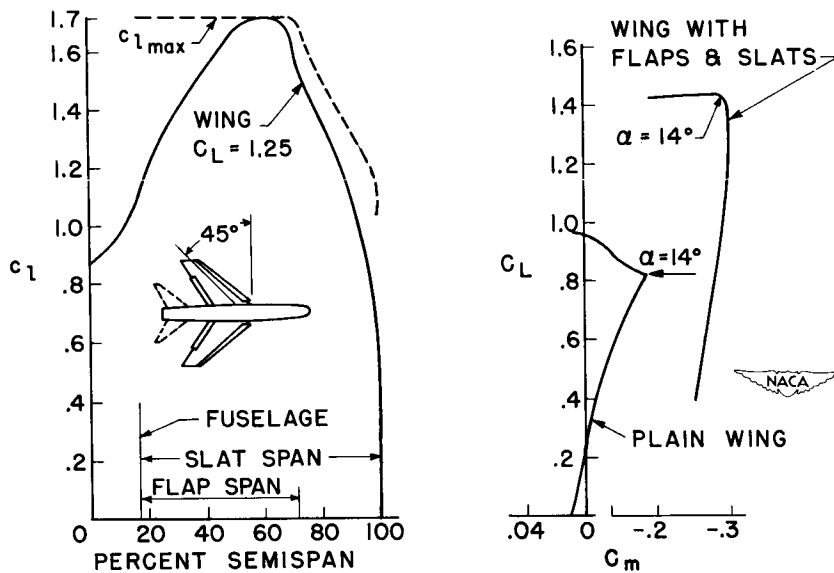


Figure 3

EFFECT OF SWEEP ON SECTION MAXIMUM LIFT

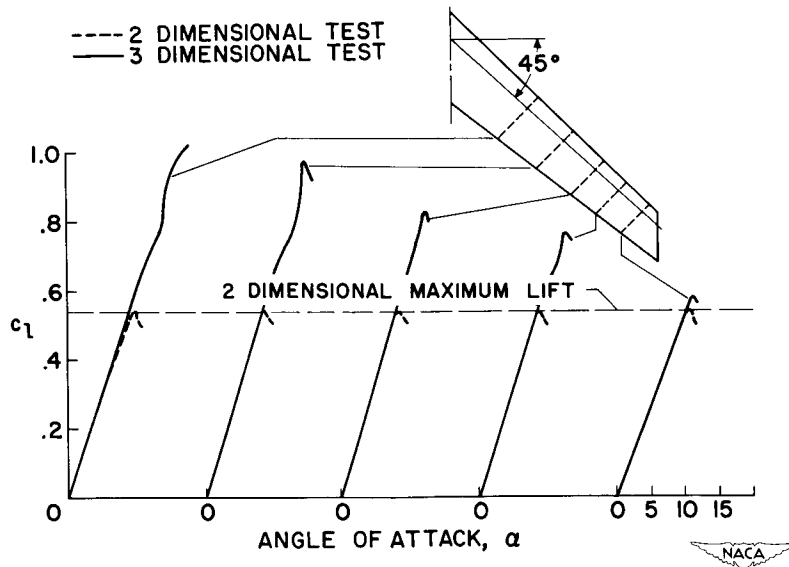


Figure 4

SPANWISE BOUNDARY-LAYER FLOW ON A YAWED WING

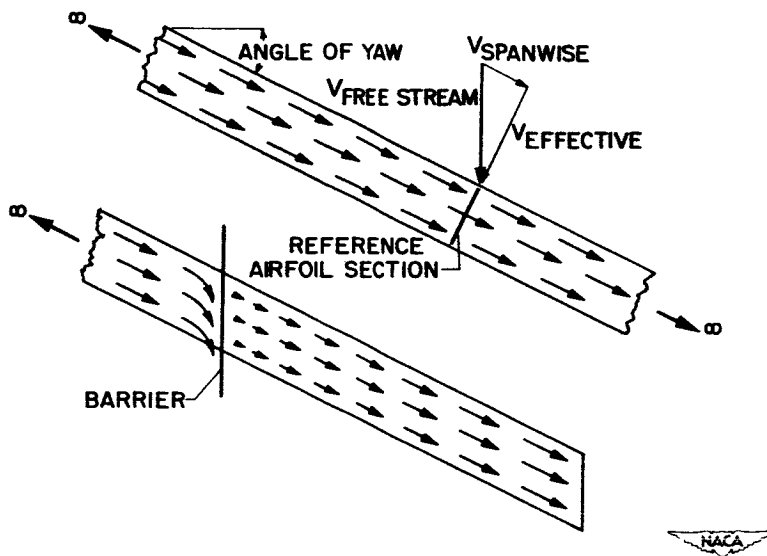


Figure 5

MEASURED EFFECT OF FENCES

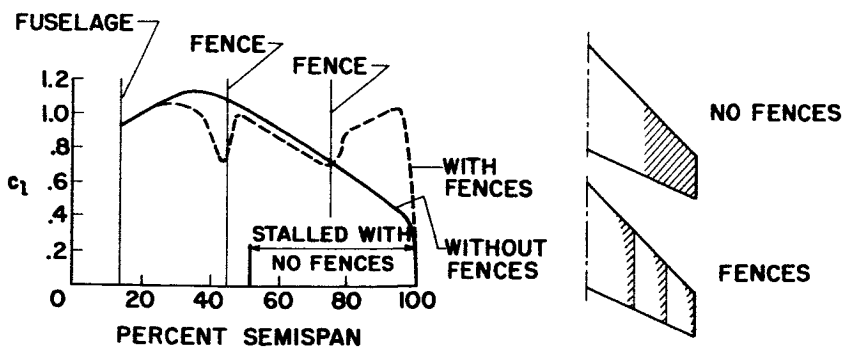
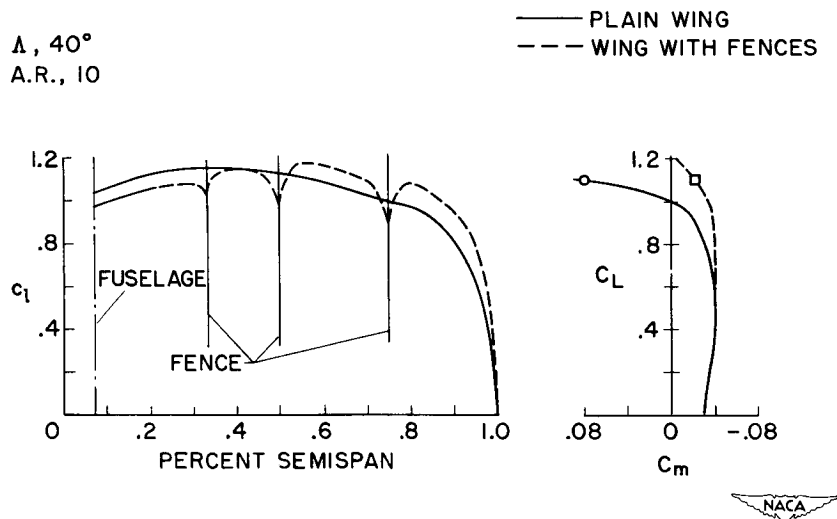
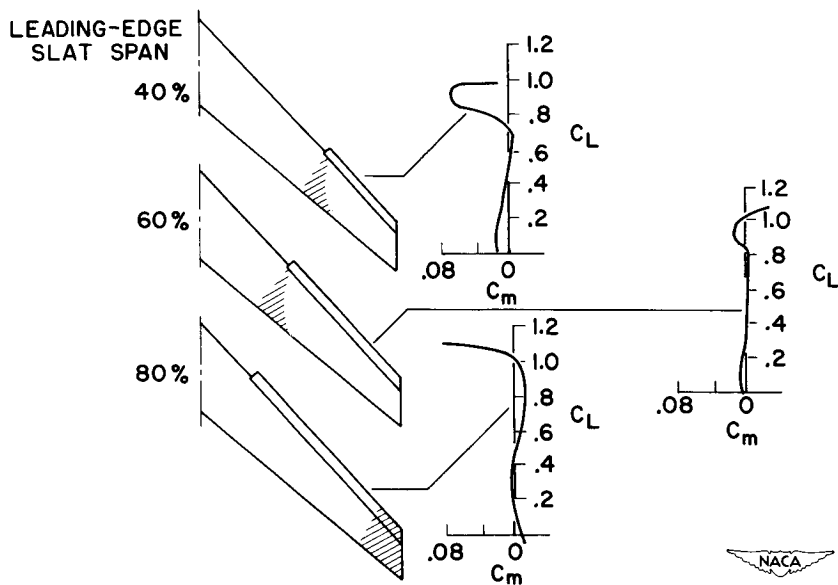


Figure 6

EFFECT OF FENCES ON A HIGH-ASPECT-RATIO SWEEPED WING



EFFECT OF SLAT SPAN ON SWEEPED-WING STALL PATTERNS



COMPARISON OF MEASURED & PREDICTED SECTION STALL
SWEEP, 45° A.R., 5.0

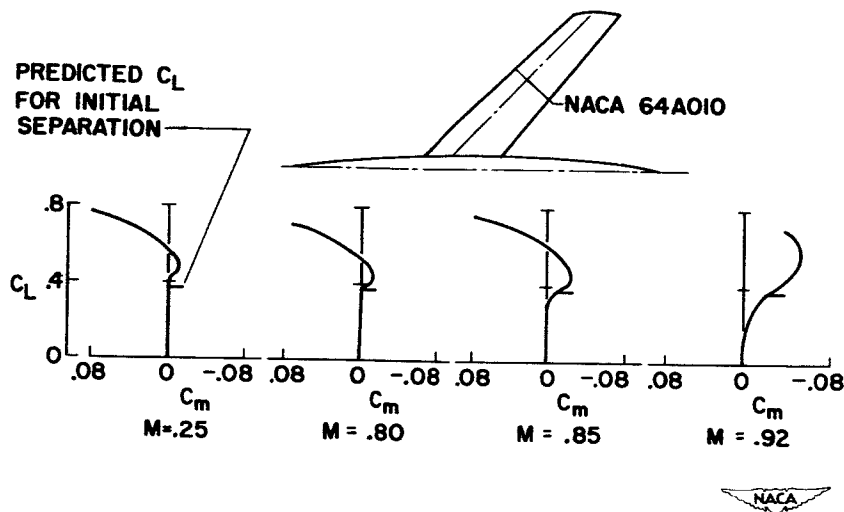


Figure 9

EFFECT OF LEADING-EDGE MODIFICATION ON PITCH-UP
SWEEP, 35°; A.R., 4.5

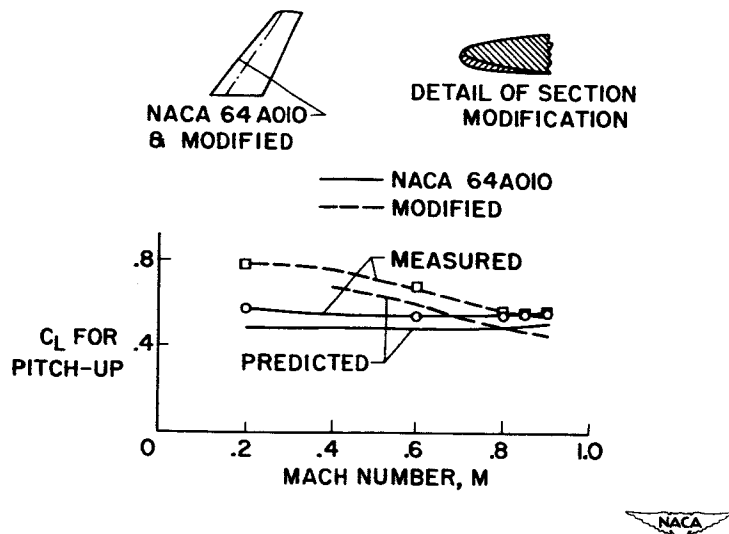


Figure 10

EFFECTS OF FENCE ON PITCH-UP
SWEEP, 35°; A. R., 4.5

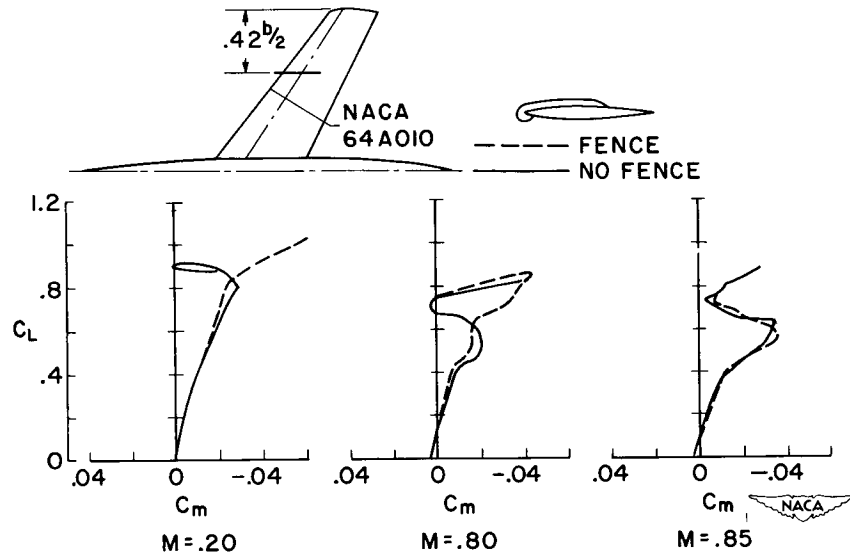


Figure 11

EFFECTS OF FENCES ON PITCH-UP
SWEEP, 40°; A. R., 10.0

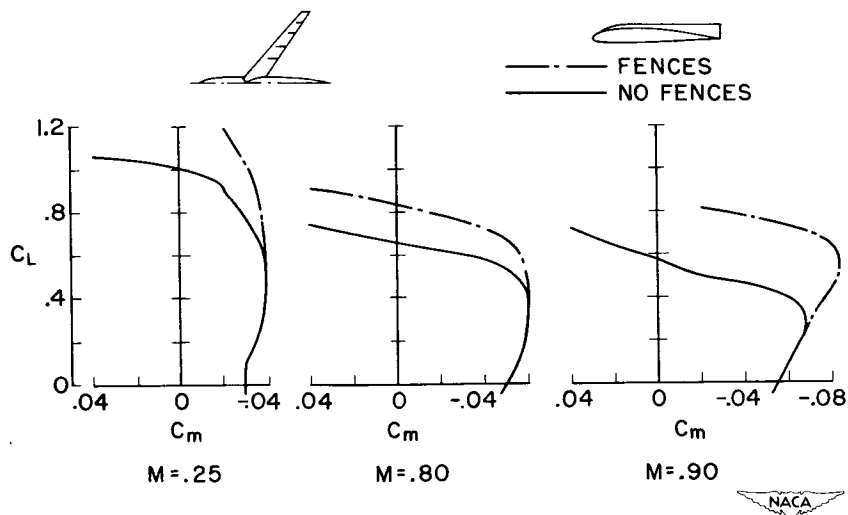


Figure 12

EFFECTS OF LEADING-EDGE CHORD EXTENSION ON PITCH-UP
SWEEP, 45° ; A.R., 4

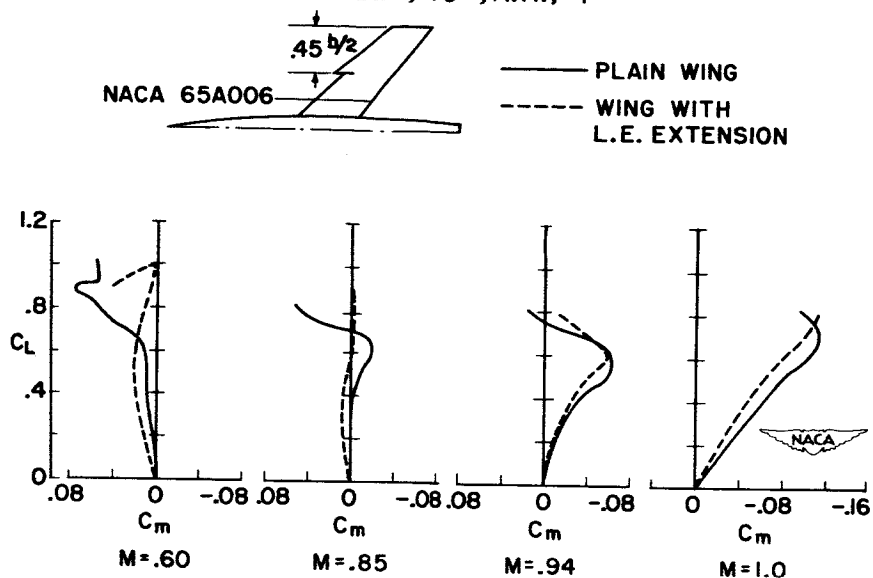


Figure 13

EFFECTS OF LEADING-EDGE SLAT ON PITCH-UP
SWEEP, 45° ; A.R., 4

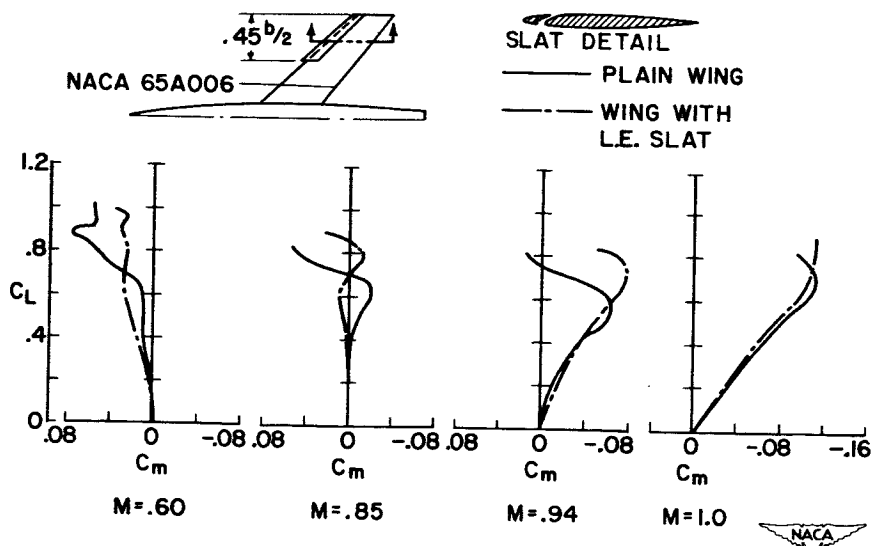


Figure 14

CONFIDENTIAL

DECLASSIFIED

RECENT DESIGN STUDIES DIRECTED TOWARD ELIMINATION OF PITCH-UP

By Joseph Weil and W. H. Gray

Langley Aeronautical Laboratory

INTRODUCTORY REMARKS

A previous paper by Thomas A. Toll has evaluated the status of wing research relative to the pitch-up problem. Other papers have discussed the nature of the flow phenomena responsible for pitch-up and presented flight experience with configurations having pitch-up. The function of the present paper is to present the results of recent design studies of complete configurations expressly directed toward elimination of high-speed pitch-up.


Before proceeding with the discussion it should be stated that methods are available from which arbitrary nonlinear aerodynamic characteristics can readily be converted into calculated time histories of representative flight maneuvers. (See ref. 1.) Such calculations obviously do not have the value of flight tests but nevertheless are very useful in serving as a guide in interpreting wind-tunnel data and in studying the importance of the various factors affecting the over-all problem.

The application of the calculation method to evaluate the effectiveness of corrective control for a given pitching-moment shape is illustrated in figure 1.

The particular pitching-moment curve used had a region of neutral stability. A ramp stabilizer input was applied at one degree per second. It was assumed the pilot desired to arrest the motion at $\alpha = 8^\circ$; however, because of reaction time delay and control lag it was further assumed that there was a 0.5-second delay before either the control motion was stopped or 4-degrees-per-second corrective control applied.

An important factor in determining the controllability of an overshoot is a term proportional to the ratio of the aerodynamic moment to the airplane moment of inertia. For a value of this dynamic response factor of 16 (representative of an airplane primarily loaded along the fuselage and flying at altitude at transonic speeds), it is evident that corrective control was instrumental in appreciably reducing the overshoot although the peak angle reached was still about 5° greater than would have been attained with a linear pitching-moment curve and therefore undesirable.

For a dynamic response factor of 64 (representative of an airplane primarily loaded along the wings), the motion builds up so rapidly that corrective control is completely ineffective in reducing the overshoot.



It should be noted that the interpretation of some of the results to be presented in this paper are based on calculations such as these where flight experience with configurations having similar characteristics was not available.

The problem of tail location (from the stability standpoint) is one of matching the stability contribution of the tail to the wing-fuselage characteristics. The manner in which the choice of tail location might be affected by three different types of simplified wing-fuselage pitching-moment curves is shown in figure 2.

With a tail-off curve characterized by a stable break at moderate angle of attack, location of the tail so that it approaches the wing wake with reduced tail contribution to stability in the moderate α range will tend to linearize the stability characteristics of the complete configuration. For a wing-fuselage curve with a mild destabilizing break, the use of a somewhat lower tail with the tail contribution to stability shown might be desired. When the wing-fuselage curve indicates a large unstable change at moderate angle of attack, the only possibility of securing an acceptable complete configuration lies in the use of a tail low enough so that its emergence from the wing wake and resulting increased stability contribution will overcome the tail-off instability.

SCOPE

The scope of the complete configurations to be discussed in this presentation is shown in figure 3. The configurations studied were conceived as having all-movable tails and the tail lengths varied from 1.2 to 1.4 wing semispans. Stability information showing effects of changes in tail height is presented for these configurations in subsequent figures. The Reynolds numbers of the data were generally of the order of from 3×10^6 to 4×10^6 . Most of the investigations were made at high subsonic Mach numbers, the range in which the most serious pitch-up is usually encountered.

DISCUSSION

The effect of varying tail height on the pitching-moment characteristics of an aspect-ratio-3 wing having an unswept 50-percent-chord line is shown in figure 4. The wing had a taper ratio of 0.2 and a 4-percent-thick airfoil. Data are presented at a Mach number of 0.80 and 0.90 for tail heights of 0, 32, and 64 percent of the wing semispan above the wing chord plane extended. A reference center-of-gravity location has been

DECLASSIFIED

chosen for each tail height such that an initial slope $\frac{\partial C_m}{\partial C_L} = -0.12$

was obtained at $M = 0.80$. (See table I.) The lift curve is shown for reference purposes.

It is seen that, at $M = 0.80$, some overshoot would be experienced at high C_L for either of the two higher tails. Although the highest tail shows an abrupt instability, it is not thought that this instability would seriously limit the usefulness of the airplane because the pitch-up tendency is preceded by a pronounced stable break in the moment curve which would serve as a warning to the pilot and occurs at an angle of attack considerably above the severe break in the lift curve and therefore probably well into the heavy buffet region. No pitch-up problem is indicated for the lift range obtained at $M = 0.90$. Somewhat similar results were obtained from an investigation of an unswept wing of aspect ratio 4 and taper ratio 0.6. (See fig. 5.)


The effects of reducing the aspect ratio of a moderately swept wing from 4 to 3 are presented in figure 6. Inasmuch as the lower-aspect-ratio wing was formed by cutting off the tips of the aspect-ratio-4 configuration, the taper ratio increased from 0.60 to 0.68. Data are presented for a Mach number of 0.90 for a tail located approximately 15 percent semispan above and below the wing chord plane extended.

For the tail located above the fuselage, a pitch-up tendency is shown for either aspect ratio wing coincident with an abrupt break in the lift curve. For the aspect-ratio-4 wing, the severity of the C_m break would indicate a fairly severe pitch-up. Reducing the aspect ratio to 3 delayed the onset of pitch-up by about $0.1C_L$ and the importance of the much milder pitch-up tendency indicated is questionable in view of the probable presence of appreciable buffet.

With the tail located below the fuselage, no pitch-up tendency is shown for either aspect ratio.

Figure 7 illustrates the effect of taper ratio on the stability characteristics of configurations having an aspect ratio of 3 and quarter-chord sweep of 30° . Data are presented at Mach numbers of 0.92 and 1.06 for a tail located on the chord plane extended and 64 percent of the wing semispan above the chord plane extended.

At $M = 0.92$, regardless of tail height and taper ratio, a jog is present in the moment curve at moderate lift coefficient. The destabilizing tendencies, however, occur at a lift coefficient about 0.2 higher for the wing having 0.5 taper and would appear to be somewhat less severe.



For either taper ratio, an abrupt instability is present at extremely high α as the high tail approaches the wake. At a Mach number of 1.06, no pitch-up problem is indicated in the lift range obtained.


The effect of tail height on the stability characteristics of a 45° delta wing with tips clipped to form a wing with an aspect ratio of 3 are given in figure 8. The taper ratio was 0.14 and the quarter-chord sweep, 36.8° . Of the three tail positions investigated, the middle tail was clearly the worst. For the high tail, the lift coefficient at which a pronounced instability exists at $M = 0.80$ was delayed to an angle of attack of 18° or well beyond the abrupt break in the lift curve. The chord-plane tail had fairly acceptable characteristics at both Mach numbers. Thus for this arrangement, it is obvious that a low tail or a very high tail represents the best choice of tail location from the pitch-up standpoint.

The effect of Mach number on the stability characteristics of a configuration having a 47° swept wing of aspect ratio 3.5 is shown in figure 9 for tail heights of 6 and 56 percent of the wing semispan above the wing chord plane. Figure 9 shows that, although the instability was less pronounced for the lower tail, neither configuration had acceptable pitch-up characteristics. Furthermore, the results show that the onset of pitch-up is delayed to a progressively higher lift coefficient as the Mach number is increased from 0.90 to 1.04. For the lower tail it is also evident that the severity of the pitch-up tendency is considerably reduced at the highest Mach number.

The effect of tail height on the stability characteristics of a 45° swept wing of aspect ratio 4 at a Mach number of 0.90 is shown in figure 10. The wing-fuselage characteristics are such that, even when the tail is placed $0.14b/2$ below the fuselage, undesirable pitching-moment characteristics are retained.

The effect of a leading-edge modification on the stability characteristics of the 45° wing at $M = 0.90$ is presented in figure 11. The leading-edge modification used consisted of a 10-percent chord-extension from 65 percent semispan to the wing tip and a full-span 20-percent-chord nose flap. The combination was drooped 6° streamwise and hinged about the 20-percent chord line. Such an arrangement has been shown to have favorable performance characteristics at high subsonic speeds. See reference 2.

For a tail location above the fuselage, the use of the modified wing delayed the onset of pitch-up by about $0.1C_L$. The severity of the pitch-up, however, would not appear to be altered. When the tail is placed below the fuselage it would appear that the use of the modification would result in fairly acceptable pitching-moment characteristics. See reference 3.



REF ID: A66515

The importance of localized inboard plan-form modifications on the tail contribution to stability at $M = 0.90$ is illustrated in figure 12. The inboard modifications were added to the configuration having nose droop and chord-extensions. Pitching-moment and tail contribution to the stability $(C_{m\alpha})_t$ are plotted against angle of attack.

On the left-hand side of figure 12 is shown the effect of adding a trailing-edge extension inboard of the 40-percent-semispan station. The tail height was $0.26b/2$ above the chord plane extended. It is evident that the addition of the extension increased the severity of the instability. The reason for this increase is traceable to the highly destabilizing effect of the trailing-edge extension on the tail contribution to the stability.


On the right-hand side of figure 12 is shown the effect of a root indentation extending inboard of the 30-percent-semispan station intersecting the fuselage at about the 30-percent-chord line. A tail height of 14-percent semispan above the chord plane was used for this study. A significant improvement in the stability characteristics is shown for the configuration with root indentations. The reason for this improvement is traceable to the stabilizing effect of the indentation on the tail contribution to stability.

The effects of more extreme plan-form modifications are summarized in figures 13 and 14. Data are presented for the basic 45° wing of aspect ratio 4, for a cranked wing with inboard sections swept 45° and outboard 40-percent-semispan sections unswept, and for an M-plan-form wing with inboard 40-percent-semispan sections swept forward 45° and outboard sections swept back 45° . Results are presented at Mach numbers of 0.80 and 0.90 and for tail heights of 0, 27, and 55 percent above the chord plane.

For the basic swept wing it has been previously shown that, because of the nature of the tail-off characteristics, no tail location produced acceptable stability characteristics.

From the results with the cranked wing it would appear that somewhat better characteristics were obtained for the low tail than for the corresponding swept-wing configuration. Although the high tail investigated would not be acceptable, there was a definite improvement over the results obtained with the swept wing and the use of an extremely high tail should not be ruled out. The mid-tail showed essentially no improvement and had by far the worst stability characteristics.

For the M-plan-form wing, no pitch-up is indicated for the chord-plane tail. For the high tail, the lift coefficient at which pitch-up is indicated is almost twice that for the swept wing at $M = 0.80$ and substantial gains over the swept wing are also shown at $M = 0.90$. A somewhat



higher tail location than that tested would, however, in this instance also be desirable. The characteristics of the mid-tail were considerably improved over the comparable swept-wing configuration but this tail location still appears the least desirable of the three locations investigated.

SUMMARY OF RESULTS

Figure 15 is used as an aid in summarizing the results and is essentially a high-speed counterpart of the Shortal-Maggin boundary for wing and wing-fuselage configurations. The configurations have been evaluated in the Mach number range from 0.80 to 0.95, the speed range for which the most serious pitch-up can be expected for many configurations. The points plotted are for simple wing and wing-fuselage combinations having thicknesses from 3 to 6 percent streamwise. The open symbols define the combination of aspect ratio and sweep that produce pitching-moment characteristics that would not of themselves constitute a pitch-up problem whereas the solid symbols represent configurations having unacceptable tail-off pitching-moment characteristics. The half-filled symbols define configurations which, when combined with a fairly constant tail contribution to stability, would produce marginal pitch-up characteristics. The boundary region represents wings having more or less marginal characteristics.

For configurations having wings falling on the left side of the boundary, caution must be exercised to avoid placing the tail in a region of unfavorable flow characteristics. For the aspect-ratio-3, essentially unswept wing investigated, it was not considered that a serious pitch-up problem existed; however, for a range of high tail positions a pitch-up tendency would be encountered at extremely high angles of attack.

For configurations falling in the boundary area, the tail must be located so as not to aggravate but, if possible, to improve the wing characteristics. For these wings it was generally found that a moderately high tail location produced the most serious pitch-up tendency. A very high or moderately low tail would give more marginal results and only a very low tail produced good characteristics.

For wings falling above the boundary, the tail must overcome the undesirable wing characteristics. For the rather thoroughly investigated 45° swept aspect-ratio-4 wing, undesirable pitch-up would probably be present at all rational tail positions. The use of wing "fixes" combined with a very low tail produced an acceptable configuration for this wing. The use of localized plan-form modifications and composite plan forms offers the possibility of greater latitude in tail location for wings of this type and warrant further study.

DECLASSIFIED

Finally, it should be remembered that only the constant-speed pitch-up has been treated in this paper. Large and abrupt changes in pitching moment with Mach number, however, can also produce severe pitch-up and should be avoided if possible.

REFERENCES

1. Campbell, George S., and Weil, Joseph: The Interpretation of Nonlinear Pitching Moments in Relation to the Pitch-Up Problem. (Prospective NACA paper.)
2. Spreemann, Kenneth P., and Alford, William J., Jr.: Investigation of the Effects of Leading-Edge Chord-Extension and Fences in Combination With Leading-Edge Flaps on the Aerodynamic Characteristics at Mach Numbers From 0.40 to 0.93 of a 45° Sweptback Wing of Aspect Ratio 4. NACA RM L53A09a, 1953.
3. Morrison, William D., Jr., and Alford, William J., Jr.: Effects of Horizontal-Tail Height and a Wing Leading-Edge Modification Consisting of a Full-Span Flap and a Partial-Span Chord-Extension on the Aerodynamic Characteristics in Pitch at High Subsonic Speeds of a Model With a 45° Sweptback Wing. NACA RM L53E06, 1953.

TABLE I.- REFERENCE CENTER-OF-GRAVITY LOCATIONS

$$\left[\frac{\partial C_m}{\partial C_L} = -0.12 \text{ at } M = 0.8; \text{ low } C_L \right]$$

Figure	Aspect ratio	$\Lambda_c/4$, deg	λ	Remarks	$h_t/b/2$	Reference center of gravity
4	3	12.6	0.20		0	0.04c
4	3	12.6	.20		0.32	.13c
4	3	12.6	.20		.64	.21c
5	4	0	.60		0	.14c
5	4	0	.60		.27	.16c
5	4	0	.60		.55	.25c
6	4	32.6	.60		-.14	.24c
6	4	32.6	.60		.14	.23c
6	3	32.6	.68		-.17	.25c
6	3	32.6	.68		.17	.22c
7	3	30	.20		0	.17c
7	3	30	.20		.64	.36c
7	3	30	.50		0	.13c
7	3	30	.50		.64	.32c
8	3	36.8	.14		0	.19c
8	3	36.8	.14		.32	.28c
8	3	36.8	.14		.64	.32c
9	3.5	47	.20		.06	.35c
9	3.5	47	.20		.56	.40c
10	4	45	.30		-.14	.36c
10	4	45	.30		.14	.34c
10	4	45	.30		.26	.37c
11	4	45	.30	Chord extension and nose droop	-.14	.36c
11	4	45	.30	Chord extension and nose droop	.14	.30c
12	4	45	.30	Inboard modification	.14	.36c
12	4	45	.30	Inboard modification	.26	.33c
13	4	45	.30	} Fuselage differs slightly from that used in figures 10-12 {	0	.29c
13	4	45	.30		.27	.34c
13	4	45	.30		.55	.40c
13	4	45° inboard; 0° outboard	.30	Cranked plan form	0	.11c
13	4	45° inboard; 0° outboard	.30	Cranked plan form	.27	.18c
13	4	45° inboard; 0° outboard	.30	Cranked plan form	.55	.24c
14	4	-45° inboard; 45° outboard	.30	M plan form	0	.04c
14	4	-45° inboard; 45° outboard	.30	M plan form	.27	.11c
14	4	-45° inboard; 45° outboard	.30	M plan form	.55	.17c

CONFIDENTIAL

DECLASSIFIED

EFFECT OF CORRECTIVE CONTROL IN TIME HISTORY OF PULL-UP

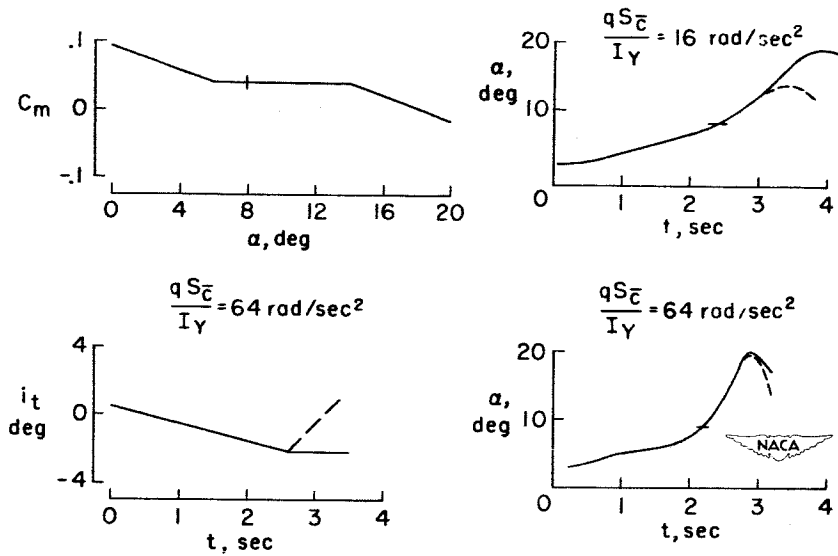


Figure 1

ILLUSTRATION OF PROBLEM

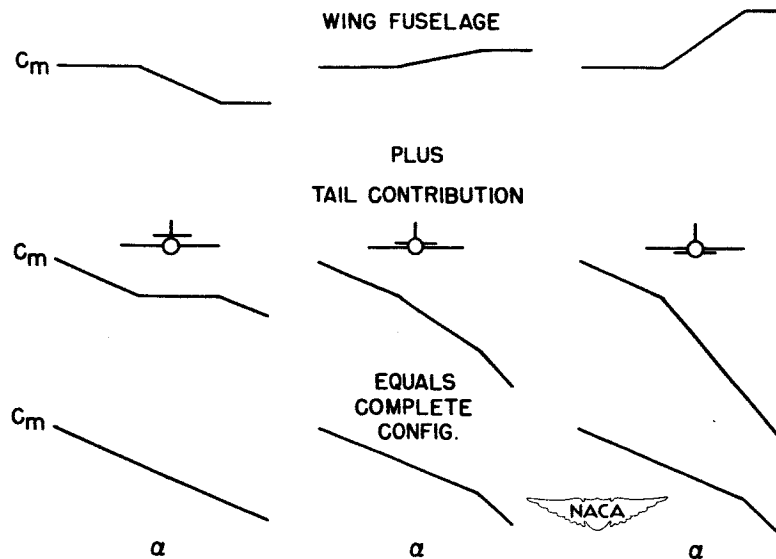


Figure 2

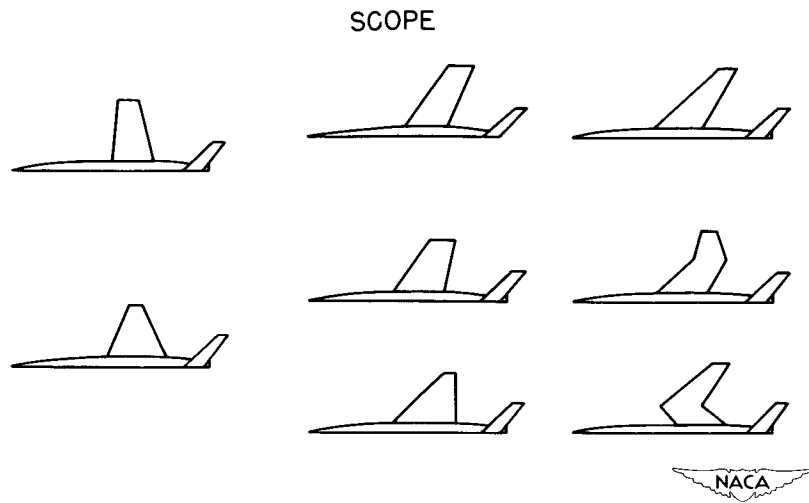


Figure 3

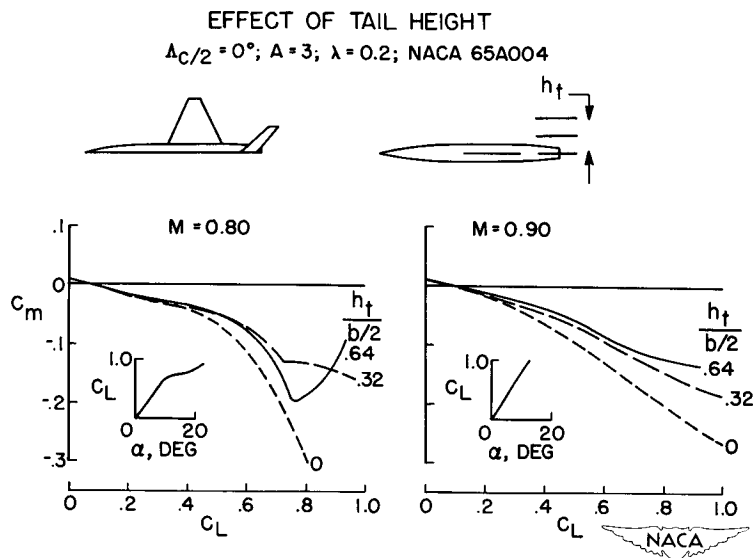


Figure 4

EFFECT OF TAIL HEIGHT

$\Delta C/4 = 0^\circ$; $A = 4$; $\lambda = 0.6$; NACA 65A006

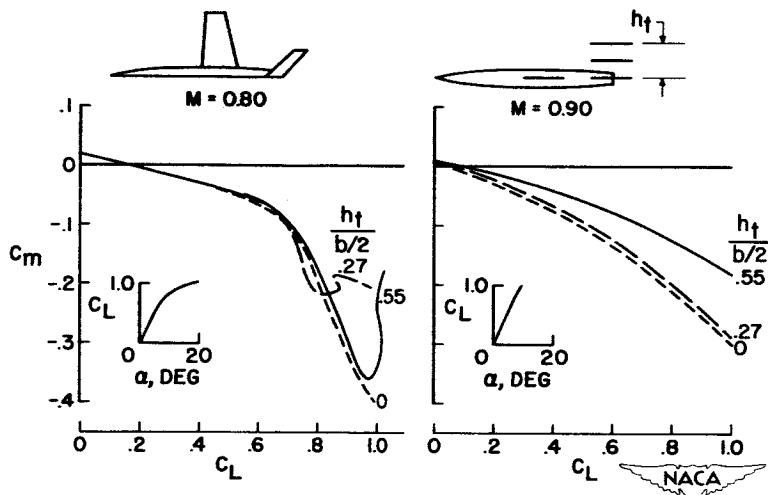


Figure 5

EFFECT OF ASPECT RATIO, $\Delta C/4 = 32.6^\circ$

NACA 65A006; $M = 0.90$

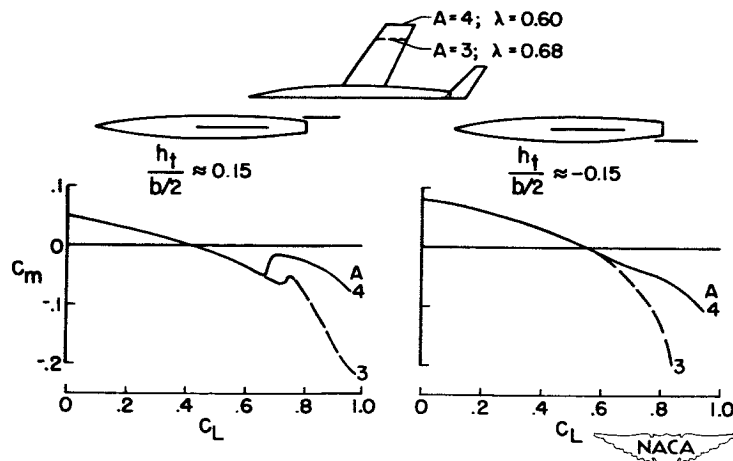


Figure 6

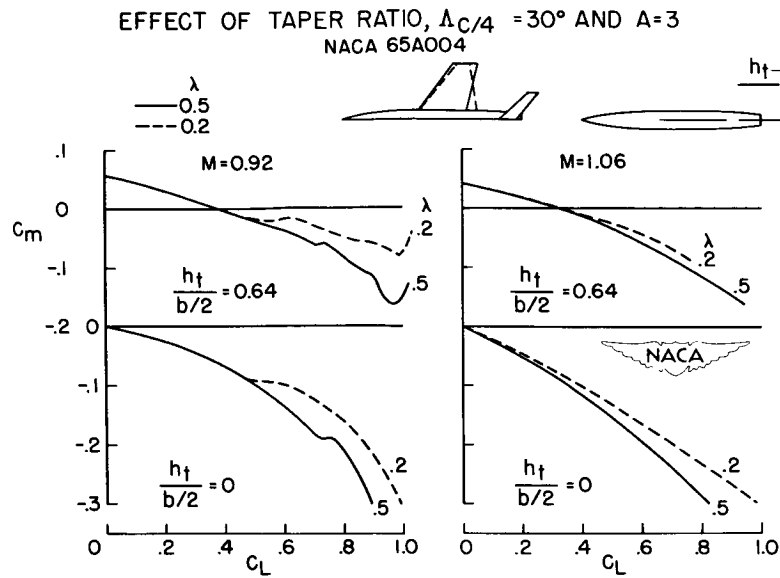


Figure 7

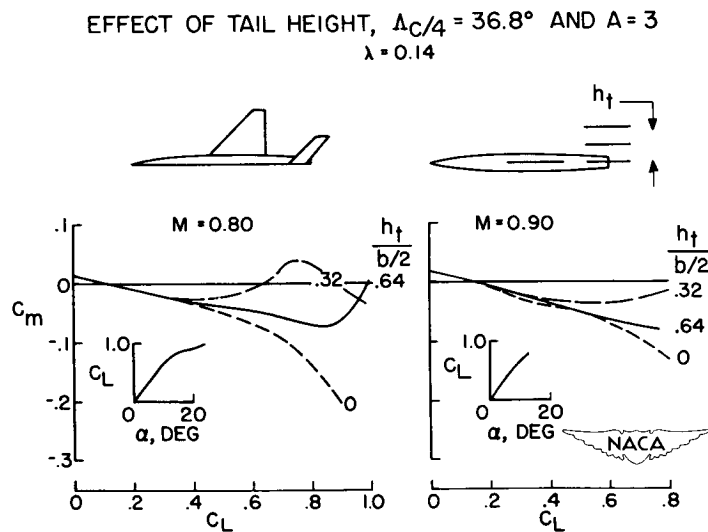


Figure 8

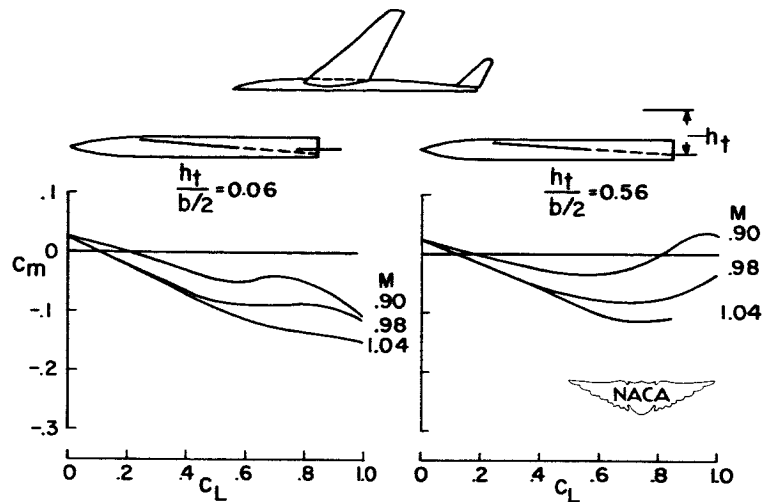
EFFECT OF MACH NUMBER, $\Delta C/4 = 47^\circ$ AND $A = 3.5$ $\lambda = 0.2$; $t/c = 0.055$ 

Figure 9

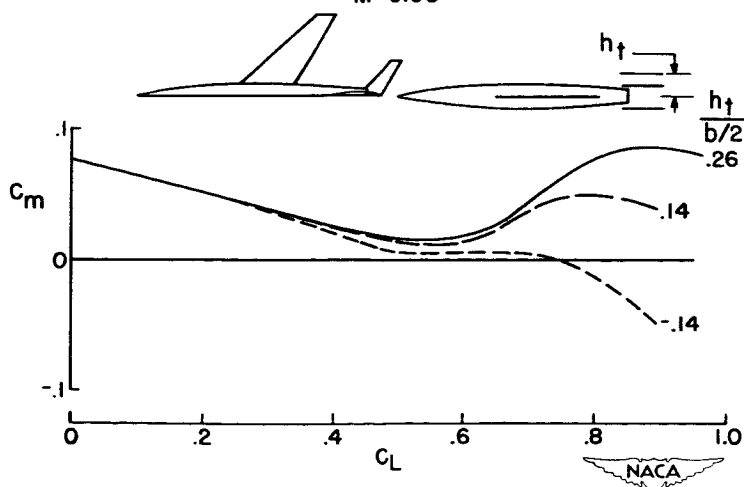
EFFECT OF TAIL HEIGHT, $\Delta C/4 = 45^\circ$ AND $A = 4$ $\lambda = 0.3$; NACA 65A006 $M = 0.90$ 

Figure 10

COMBINED EFFECT OF CHORD-EXTENSION AND NOSE DROOP

M=0.90

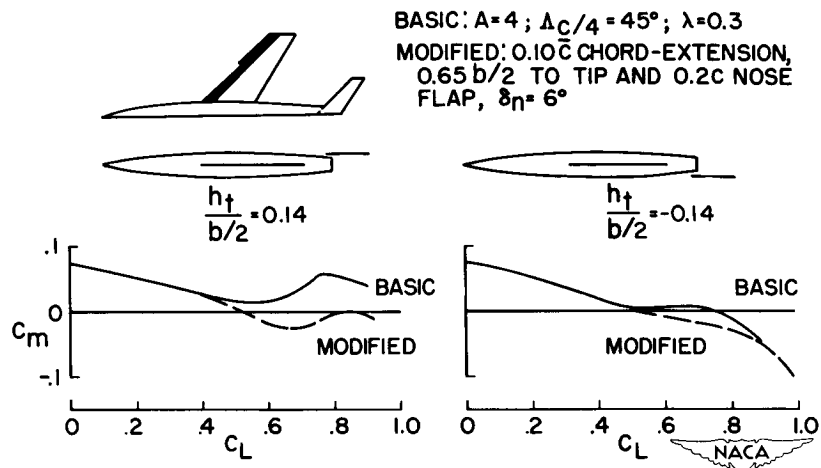


Figure 11

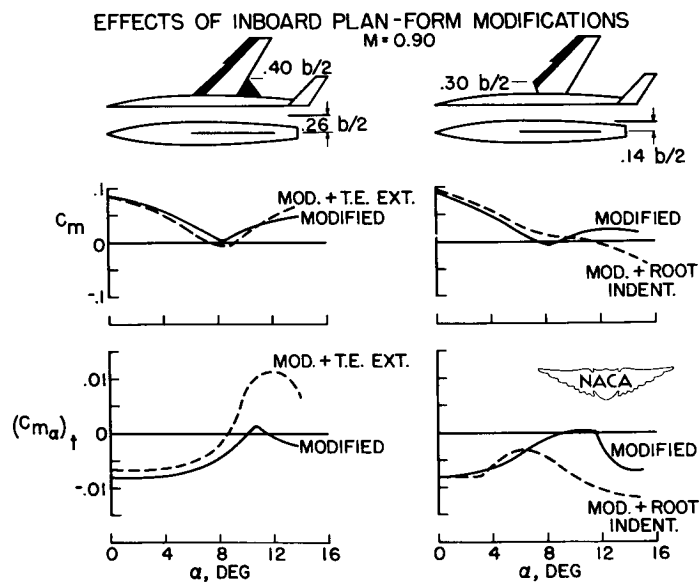


Figure 12

EFFECT OF TAIL HEIGHT FOR COMPOSITE PLAN FORMS
A=4; NACA 65A006

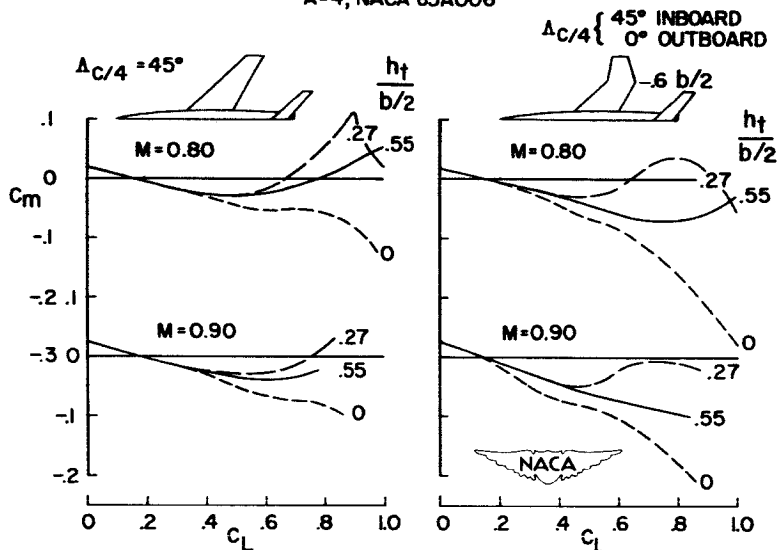


Figure 13

EFFECT OF TAIL HEIGHT FOR COMPOSITE PLAN FORM
A=4; NACA 65A006

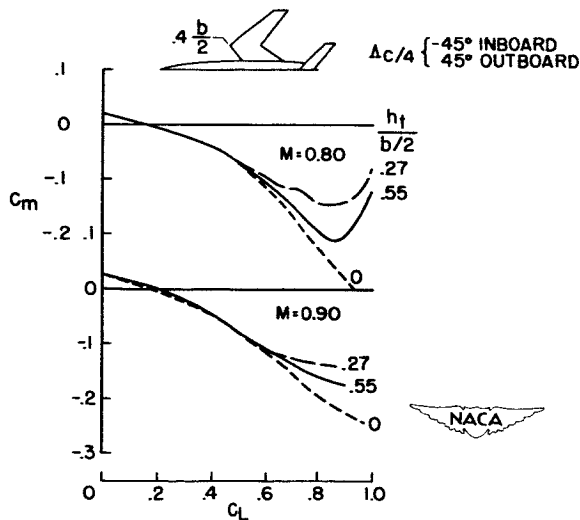


Figure 14

HIGH-SPEED WING-FUSELAGE STABILITY BOUNDARY
 $M=0.80$ TO 0.95 ; $t/c=0.03$ TO 0.06 ; $\lambda=0$ TO 0.7

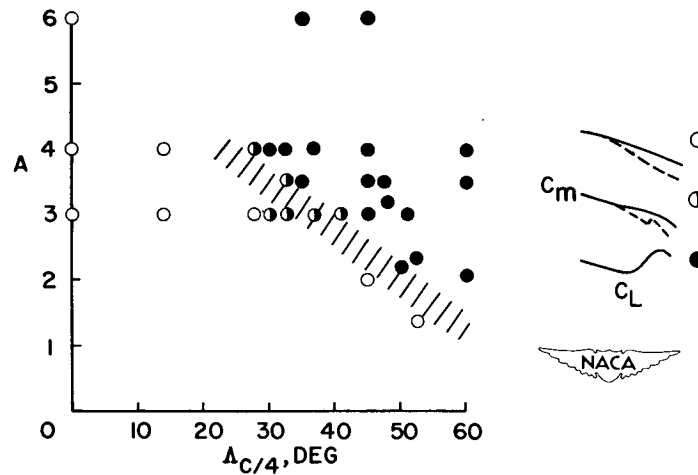


Figure 15

CONFIDENTIAL

DECLASSIFIED

SOME AERODYNAMIC CONSIDERATIONS GOVERNING THE STATIC

STABILITY OF CRUCIFORM MISSILES

By Donald D. Baals, M. Leroy Spearman, and David G. Stone

Langley Aeronautical Laboratory

INTRODUCTION


The static stability and control requirements governing the design of cruciform missiles are broad and complex, but, in general, there are two basic requirements of overriding importance: the first, to maintain linearity of the pitching or yawing moments to sufficiently high angles of incidence and, second, to minimize the induced rolling moment resulting from roll attitude or control deflection. This paper presents some of the available methods for predicting missile stability characteristics and will endeavor to indicate how to minimize adverse aerodynamic effects.

At the 1951 NACA Conference on Aerodynamic Design Problems of Supersonic Guided Missiles, a rather complete coverage of the basic problems of the stability of cruciform missiles was presented wherein it was shown that the longitudinal and induced roll characteristics are largely understandable and predictable on the basis of existing aerodynamic theory. For missile configurations the assumption was made that the vortex sheet trailing the forward surfaces is completely rolled up in the region of the tail. The resulting vortex locations and tail loads can then be predicted by existing techniques.

This general approach has not changed significantly. Recent work has added to the knowledge of missile vortex fields (ref. 1), and limited advances in simplifying assumptions and calculative techniques have been made. It now appears possible by rather simple techniques to predict the general variation and the order of magnitude of the pitching and induced rolling moments for a relatively wide range of missile configurations.

LONGITUDINAL CHARACTERISTICS

Figure 1 is an illustration of the simplified flow model considered in the analysis which follows. It is assumed that the basic-body, body-wing, and body-tail characteristics can be estimated by slender-body and linear theory. In order to determine the interference effects of the forward wing on the trailing surface, the assumption is made that the



BAALS, SPEARMAN
& STONE

trailing vortex sheet behind each wing panel is concentrated into one discrete vortex. The position of each vortex with respect to the tail is approximated for zero roll by simply assuming that the vortex trails in the streamwise direction. It is then possible to calculate the downwash distribution in the plane of the tail and the corresponding tail loads. This procedure has been systematized and compared with experiment in reference 2.


The procedure assumed is of necessity over-simplified and embodies the inherent limitations of slender-body and linear theory along with known discrepancies in the assumption of the vortex field. It is known, for example, that the body-alone characteristics are nonlinear and are predicted by slender-body theory only for bodies at low angles of attack. In calculating wing-tail interference, the assumption that one fully rolled up vortex is discharged from each wing panel holds in the majority of configurations. The work of Spahr and Dickey (ref. 1), however, shows that for panels of high aspect ratio the flow behind the panel may consist of a flat sheet of several vortices; and for high angles of attack, body vortices appear in the flow. In spite of the rather gross assumptions involved, however, the results provide, for moderate angles of attack, a qualitative picture which fits the pattern of experiment.

Figure 2 shows the range of missile configurations investigated. It includes configurations with the smaller surfaces forward or rearward and considers both subsonic and supersonic characteristics.

Figure 3 shows the center-of-pressure variation with angle of attack for a representative group of missile configurations from figure 2. The circles are experimental results and the dashed lines are calculated results based on the aforementioned procedures. It will be noted that the correlation is relatively good - especially with relation to the center-of-pressure shift with angle of attack.

With the simplified flow model and the calculative techniques as a basis, it is possible to propose missile configuration requirements for minimizing the longitudinal center-of-pressure travel with angle of attack. An analysis of results indicates that one of the most important parameters governing the center-of-pressure shift is the ratio of the spans of the two lifting surfaces.

In figure 4 is shown, as a function of span ratio, the experimental variation of center-of-pressure shift in terms of body length for an angle-of-attack increment of 10° . The "span ratio" here is defined as the ratio of the small to the large surface. The numbers within the symbols refer to the configurations in figure 2. Configurations 1 to 8 are limited to subsonic characteristics; configurations 9 to 21 are for Mach numbers in the range from approximately 1.3 to 2.0. The center-of-pressure shift is rearward except for those symbols with flags. It will



be noted that the largest center-of-pressure shift occurs for span ratios near unity.

Figure 5 shows the calculated center-of-pressure shifts corresponding to the experimental results of figure 4. It will be noted that the calculated results correlate very well with the experimental values, and the same general effects of span ratio are noted. Also shown in this figure is the calculated center-of-pressure variation for a missile configuration in which the span ratio is systematically varied. The calculations are made for wing and tail with 60° delta plan form at a Mach number of 2.0. Note that the peak center-of-pressure travel occurs when the rear surface is about 0.9 of the span of the forward surface or, in other words, when the tail span is approximately equal to the vortex span.

Although span ratio appears to be the primary parameter from the standpoint of center-of-pressure shift, the scatter at any one value of span ratio indicates the importance of other parameters. From analysis of experimental data and use of the simplified calculative techniques, these parameters are indicated to be:

- (a) Panel aspect ratio and plan form
- (b) Ratio of body diameter to wing span
- (c) Relative distances between the forward and rear surfaces
- (d) Fineness ratio of the body alone

In general, for a given configuration holding span ratio and aspect ratio constant, the effect of plan form on center-of-pressure shift is relatively small. The effective panel aspect ratio βA does have a significant influence, the larger center-of-pressure shifts occurring for the lower values of effective aspect ratio.

There appears to be an effect of spacing between the forward and rearward surfaces associated with the displacement of the vortex at the tail. The maximum center-of-pressure shift for span ratios near 1 appears to occur for a wing-tail spacing of about 2 to 3 spans. Shorter spacings can reduce the center-of-pressure shift but at a sacrifice in tail efficiency.

Another parameter to be considered is the ratio of body diameter to wing span. If this ratio is large, the position of the wing trailing vortices are greatly influenced by body cross-flow characteristics; and secondly, the nonlinear force characteristics of the body alone become evident in the complete configuration characteristics.

For configurations where the wing-tail interference effects are small, the body-alone characteristics may be the primary factor governing

the center-of-pressure shift. In a previous paper, Edward W. Perkins and David H. Dennis have considered the nonlinear body characteristics with angle of attack and have shown that these are a function of nose shape and fineness ratio, along with other factors. Related characteristics have been considered in reference 3.


The pitching-moment characteristics of a series of ogive cylinders of fineness ratio from 14.8 to 19.1 are shown in figure 6 from tests in the Langley 4- by 4-foot supersonic pressure tunnel at a Mach number of 2.0 (ref. 4). The Reynolds number based on body diameter was 750,000. The pitching-moment coefficient is based on the chord and area of a typical wing that was added later to provide a complete missile. The center of moments has been adjusted for each fineness-ratio body to provide the same low angle-of-attack stability. Note that the linearity of the moment curve is greatly influenced by fineness ratio, and that the shortest body (fineness ratio of 14.8) has the least departure from the low angle-of-attack stability.

Figure 7 shows the stability characteristics of a canard missile configuration utilizing the various fineness-ratio bodies shown in figure 6. The wing and controls had leading-edge sweeps of 70° with a span ratio of 0.46. This would result in low canard-wing interference. Data are presented for control deflections of 0° and 10° . The center of moments has been adjusted such that each configuration has the same static stability at low angles of attack. Note that the long body is linear only to about 10° and has zero moment at approximately 20° angle of attack. The short body (fineness ratio of 14.8) has the most linear characteristics and is stable throughout the test angle-of-attack range.

The change in the complete model stability for these configurations stems basically from the body-alone characteristics. The canard-wing interference was negligible as found by agreement between the complete-configuration tests and summation of the individual components.

In figure 8 is shown the control characteristics for the fineness-ratio-15.7 configuration at a Mach number of 2.0. Note that, for a control deflection of 30° , the pitching-moment variation with angle of attack is linear up to a trim angle of 12° . The corresponding α/δ curve shows a gradual decrease in control effectiveness with no severe nonlinearities. For the fineness-ratio-14.8 configuration, which basically has the most linear moment characteristics, a 30° control deflection will trim the model at approximately 18° angle of attack. The static stability was adjusted in each case to give the highest usable trim angle of attack. Thus, if the basic configuration has sufficiently linear characteristics, high trim angles may be obtained with relatively small controls.

The Mach number characteristics of some free-flight missile configurations with low span ratios are shown in figure 9. The aerodynamic-



center location through the Mach number range is shown for a series of missiles of two different fineness ratios with the control surfaces either forward or rearward. The short bodies show the least center-of-pressure travel. The only significant center-of-pressure travel is noted for the longest body in the transonic speed range.

To summarize the situation with relation to the longitudinal characteristics of missile configurations, it has been shown possible for a rather wide range of configuration to predict for zero roll the general variation of the nonlinear moment characteristics for moderate angles of attack. The most important parameter governing the nonlinearities is the span ratio of the lifting surfaces. In general, the span ratio should not be near unity. That is, the tail span should not be of the same order as the wing vortex span. The effect of body-alone characteristics is shown to be of importance. If the body diameter is large with relation to the wing span, the body-alone characteristics can govern the complete configuration.

LATERAL CHARACTERISTICS

The discussion thus far has been limited to the longitudinal characteristics of missile configurations. From the symmetry conditions of a cruciform missile, however, the same general analysis and conclusions will apply for the characteristics in the side-force plane. There remains, however, the problem of induced roll produced by the reaction of the trailing wing to the vorticity shed by the forward control surfaces.

Sherman Edwards and Katsumi Hikido of the Ames Aeronautical Laboratory, in an unpublished analysis, have attacked the problem of induced roll with essentially the same basic approach that has been used in the analysis of the longitudinal characteristics, but with the difference that the load distribution on the tail resulting from the vortex field is integrated to give tail rolling moment. The basic aerodynamic model here assumes a deflection of the vertical control surfaces with the unyawed model at an angle of attack.

Because the induced roll is critical to the spanwise load distribution on the tail and because of the fact that the vortices in the angle-of-attack plane trail in a complex path to the rear, a more precise method is employed in establishing the position of the vortices in relation to the tail. A step-by-step graphical analysis is made which includes image vortices in the body and considers the movement of the four free vortices due to mutual interference and to the potential cross-flow around the body.

Figure 10 shows the calculated values and the experimental results for the tail rolling moment for a wide variety of different missile configurations with the control surfaces forward. Looking from the rear, this




figure shows the calculated position of the vortices in the plane of the tail for increments in angle of attack of 4° . For these vortex positions, the induced tail rolling-moment coefficients based on tail area and span have been calculated and are shown by the dashed curve. Good agreement is shown with the experimental values of tail rolling moment represented by the symbols.

It will be noted for the two configurations on the right that, when the body diameter is large with relation to the vortex span, the vortex on the underside quickly passes around the body and becomes located in the second quadrant. For such conditions, the rolling-moment coefficient reverses direction and tends toward positive values for the configuration analyzed. It should be noted that the induced roll is small for configurations where the span ratio is small. In addition, there has been found an effect of longitudinal spacing between the forward and rear surfaces. The shorter spacing reduces the displacements of the vortices at the tail and tends to minimize the induced roll.

The linearity of the rolling-moment-coefficient curve is not important in itself. The major problem, however, is whether the magnitude of the induced rolling moments is sufficiently small to be within the rolling power of the ailerons.

Figure 11 is an experimental contour plot showing lines of constant rolling-moment coefficient for conditions of combined pitch and yaw for zero control deflection. These data are from tests in the Langley 4- by 4-foot supersonic pressure tunnel at a Mach number of 2.0 of a delta-canard configuration (fineness ratio of 15.7) utilized in reference 4. The rolling moment is zero when $\alpha = \beta$ (a roll angle of 45°) since the configuration is then symmetrical with respect to the relative wind. The maximum roll occurs for a roll angle of approximately $22\frac{1}{2}^\circ$ - approximating a sine wave variation.

A 20° differential deflection of the two tip ailerons (see ref. 5 for wing aileron configuration) of this configuration produces a rolling-moment coefficient of about 0.01 for the range of α and β considered. For the untrimmed condition assumed ($\delta_H = \delta_V = 0$), the rolling moment produced by the ailerons is sufficient to overcome the induced roll for all combinations of α and β except for the small shaded area shown.

Figure 12 shows the experimental variation of induced rolling moment that occurs when the vertical canards are deflected while the angle of attack is varied at zero sideslip. The results show that the induced roll due to control deflection can be either positive or negative and of the same order of magnitude as for the controls undeflected.

[REDACTED]


[REDACTED]

This indicates regions where the induced roll may be zero or may be beyond the range of some types of roll control.


Recent experimental information is available to show the effect of combined pitch and yaw with controls deflected. Figure 13 shows the experimental effects of sideslip on the induced roll variation with angle of attack for the 10° vertical canard deflection shown in figure 12. The nature of the induced roll is shown to vary considerably in sign and magnitude as the sideslip angle is changed. These large and varied changes in induced roll for cases of combined pitch and yaw are indicative of the complex control problems that exist for canard cruciform missiles, even though the canard surfaces are small.

These induced roll problems for configurations with controls forward might possibly be circumvented through the use of trailing-edge controls on the rear panel or through the use of tail rearward designs in contrast to a canard configuration. Any gains to be had by these means, however, might result in other problems such as a decrease in longitudinal control effectiveness or maximum trim angles attainable.

In summary, the problem of induced roll for cruciform missile configurations is important, for rolling moments can be produced which are beyond the range of roll control. The simple case of induced roll due to the deflection of forward controls with the body incidence limited to one plane appears to be understood and can be adequately predicted. The practical problem of induced roll for conditions of combined pitch and yaw using control deflections required to trim is more complex. This problem merits considerable further experimental and analytical study.



REFERENCES

1. Spahr, J. Richard, and Dickey, Robert R.: Wind-Tunnel Investigation of the Vortex Wake and Downwash Field Behind Triangular Wings and Wing-Body Combinations at Supersonic Speeds. NACA RM A53D10, 1953.
 2. Nielsen, Jack N., Kaattari, George E., and Anastasio, Robert E.: Calculative Method for Estimating the Lift and Center of Pressure of Wing-Body-Tail Combinations at Subsonic, Transonic and Supersonic Speeds. (Prospective NACA paper.)
 3. Allen, H. Julian, and Perkins, Edward W.: Characteristics of Flow Over Inclined Bodies of Revolution. NACA RM A50L07, 1951.
 4. Spearman, M. Leroy: Aerodynamic Characteristics in Pitch for a Series of Canard-Type Cruciform-Wing Missiles at a Mach Number of 2.01. (Prospective NACA paper.)
 5. Spearman, M. Leroy, and Robinson, Ross B.: Wind-Tunnel Investigation of a Ram-Jet Canard Missile Model Having a Wing and Canard Surfaces of Delta Plan Form With 70° Swept Leading Edges. Longitudinal and Lateral Stability and Control Characteristics at a Mach Number of 1.60. NACA RM L52E15, 1952.
- 

SIMPLIFIED VORTEX MODEL

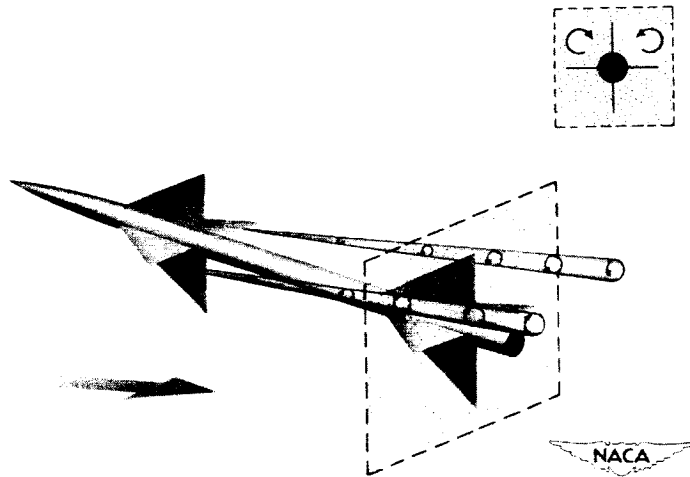


Figure 1

EXPERIMENTAL MISSILE CONFIGURATIONS

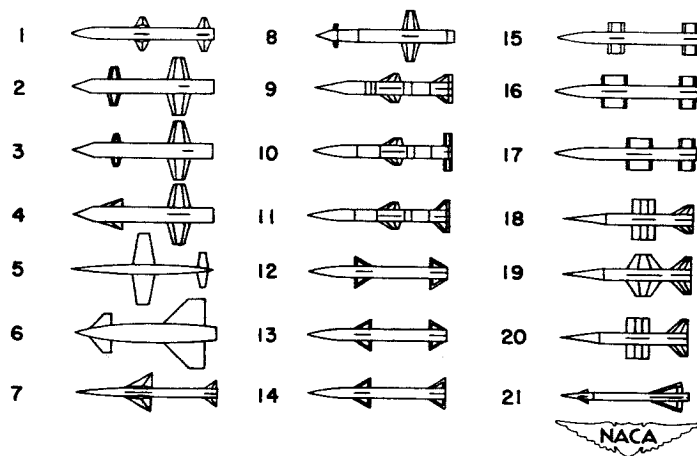


Figure 2

TYPICAL CENTER-OF-PRESSURE VARIATIONS WITH ANGLE OF ATTACK

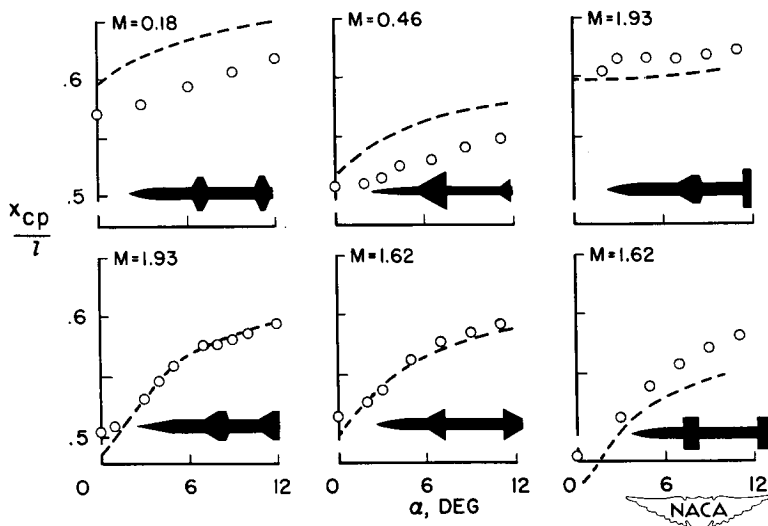


Figure 3

EXPERIMENTAL EFFECT OF SPAN RATIO

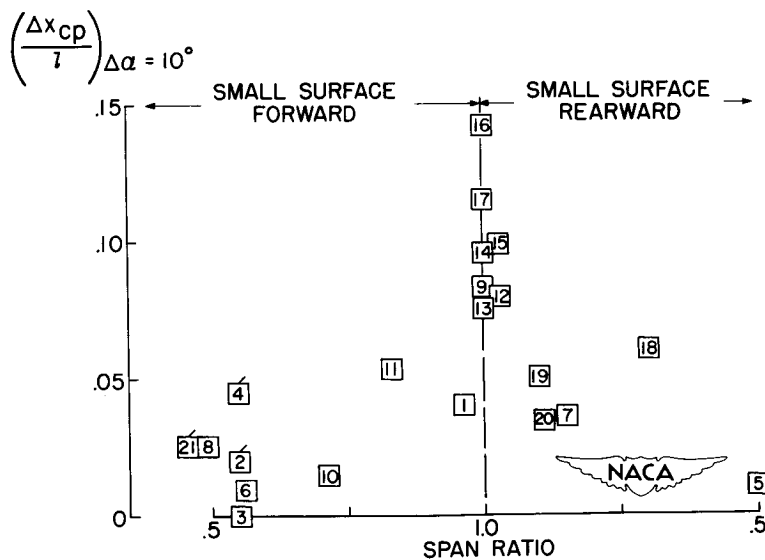


Figure 4

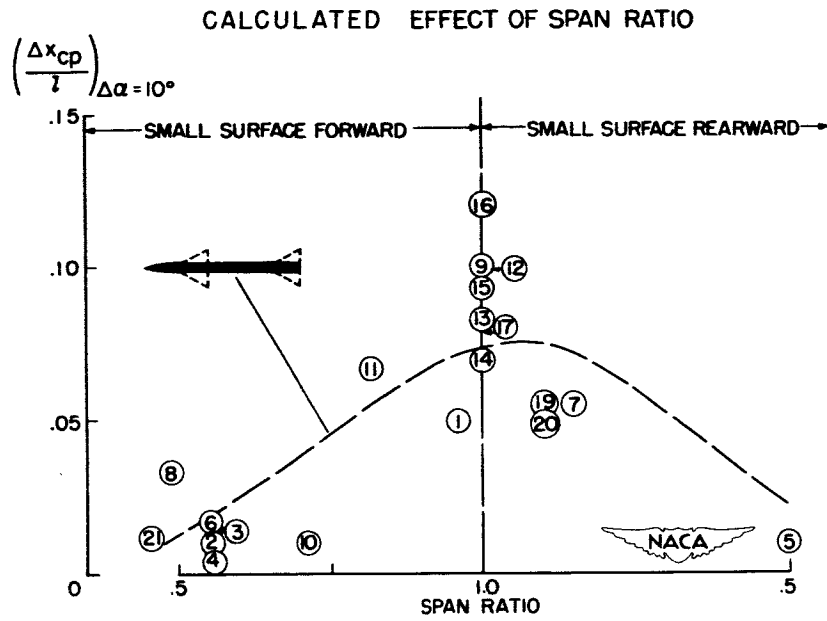


Figure 5

EFFECT OF BODY FINENESS RATIO ON C_m
M = 2.0

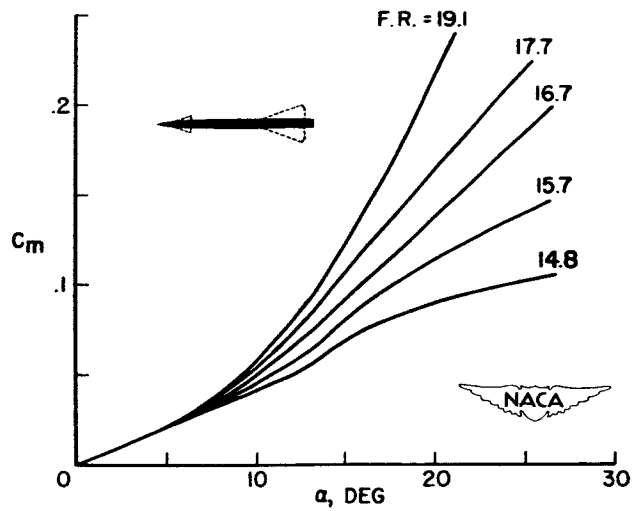


Figure 6

STABILITY CHARACTERISTICS FOR MISSILES OF VARIOUS FINENESS RATIOS

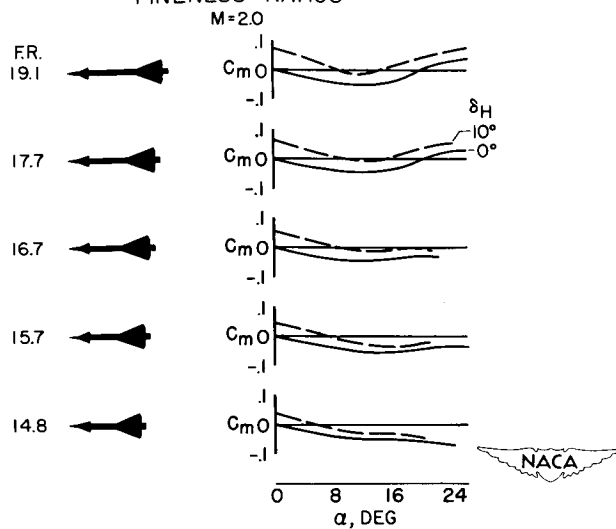


Figure 7

TRIM CHARACTERISTICS OF CANARD CONFIGURATION

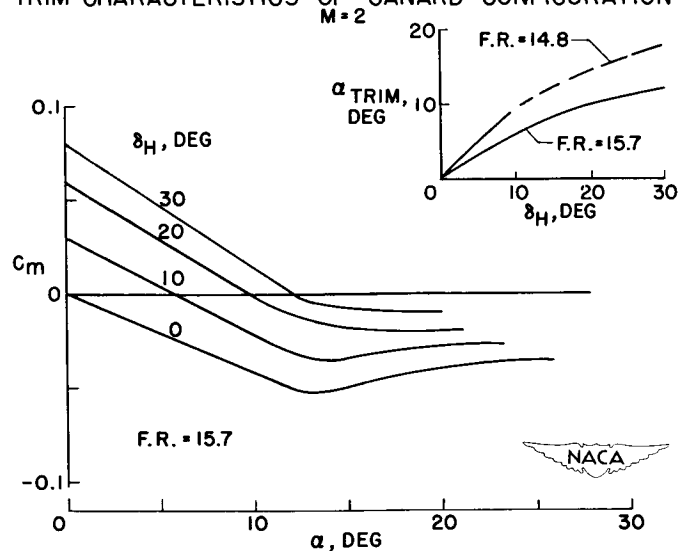


Figure 8

MACH NUMBER CHARACTERISTICS OF MISSILE CONFIGURATIONS

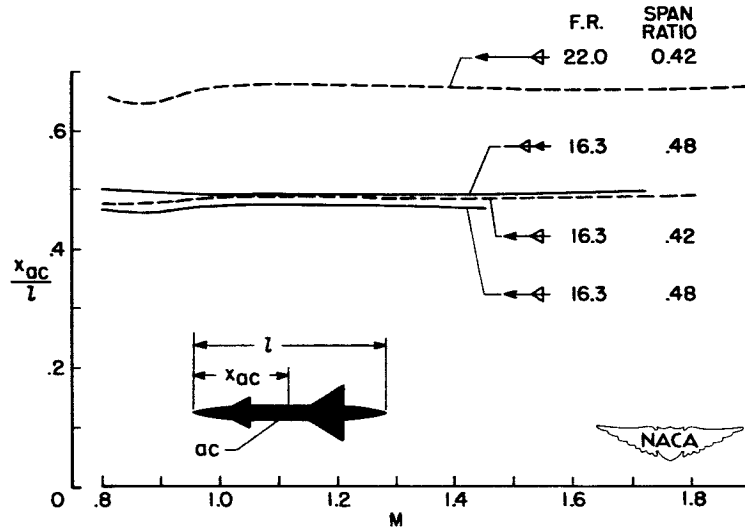


Figure 9

INDUCED-ROLL CHARACTERISTICS OF CRUCIFORM MISSILES

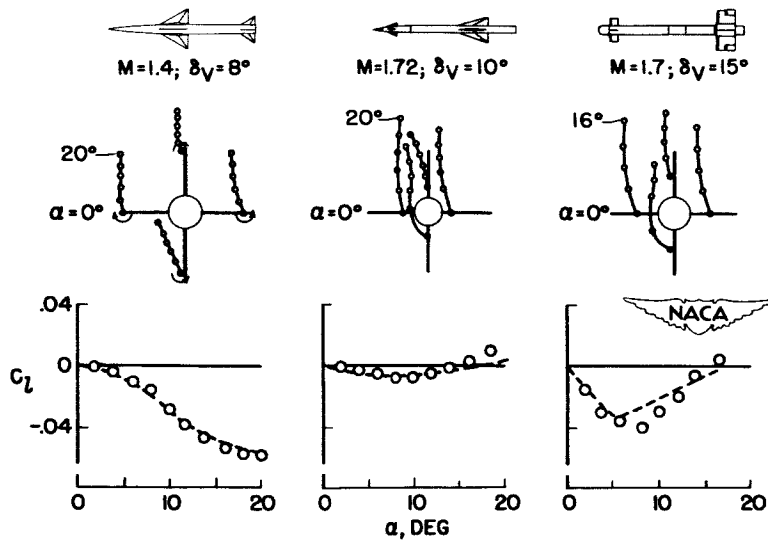


Figure 10

ROLLING-MOMENT VARIATION FOR COMBINED α AND β

$M=2.0$; $F.R.=15.7$; $\delta_V=\delta_H=0^\circ$

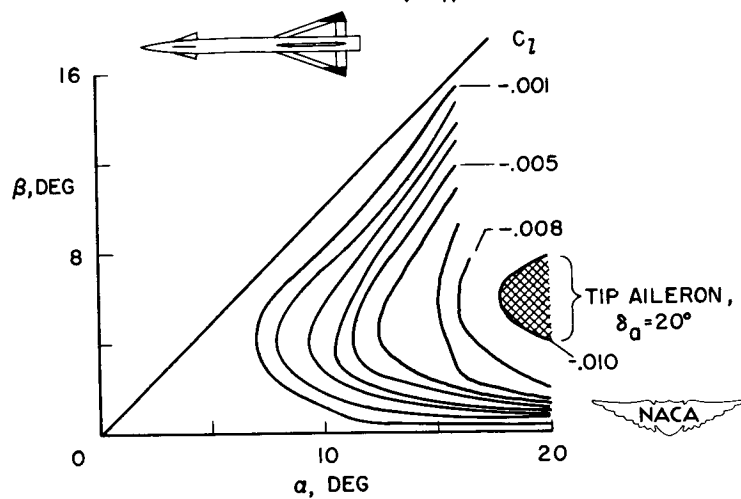


Figure 11

EFFECT OF CONTROL DEFLECTION ON INDUCED ROLL

$M=2.0$; $F.R.=15.7$; $\delta_H=0^\circ$

$\beta=0^\circ$

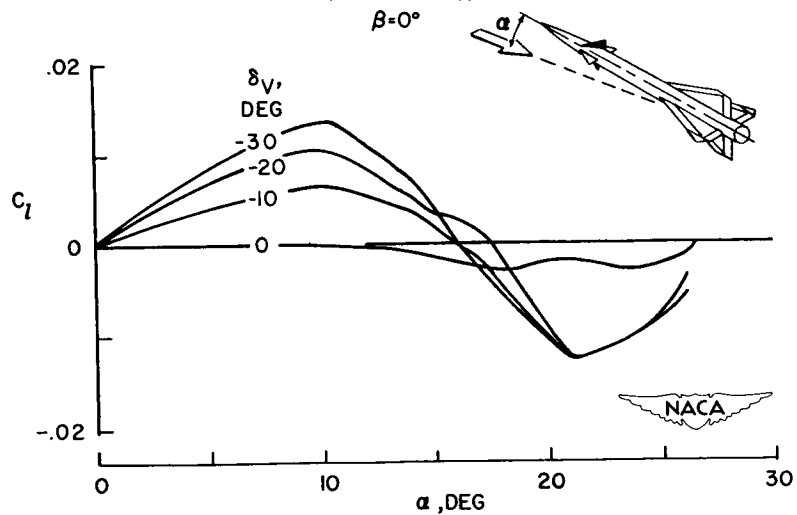


Figure 12

EFFECT OF β ON INDUCED-ROLL VARIATION WITH α
 $\delta_V = -10^\circ$; $M=2.0$; F.R. = 15.7

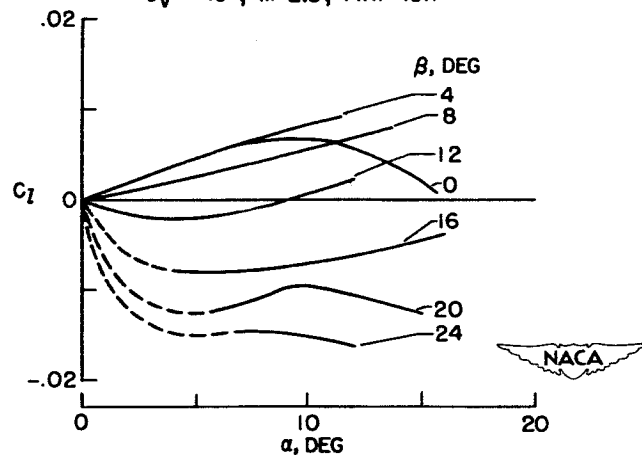


Figure 13

DECLASSIFIED

EXAMINATION OF RECENT STABILITY DERIVATIVE DATA

By Frank S. Malvestuto, Jr., and Richard E. Kuhn

Langley Aeronautical Laboratory


INTRODUCTION

A number of previous papers have reported on the effects of various aerodynamic parameters on the longitudinal motions of airplanes and missiles. In the present paper attention is directed to the aerodynamic parameters, the so-called stability derivatives that affect the lateral behavior of airplanes and missiles. The discussion is centered on three important quantities $C_{l\beta}$, the effective-dihedral derivative, $C_{n\beta}$, the directional-stability derivative, and C_{lp} , the damping-in-roll derivative. These quantities are considered for a large angle-of-attack range at subsonic speeds. A few remarks will also be made on the sideslip derivatives at zero lift in the supersonic speed range.

DISCUSSION

For the subsonic speed range, the lateral-stability derivatives have been the subject of intensive research by the Langley high-speed 7- by 10-foot tunnel. Particular attention has been paid to the variation with Mach number in the high angle-of-attack range that is representative of flyable attitudes of many high-speed airplanes. The effective-dihedral and the directional-stability derivatives of the three complete models sketched in figure 1 are presented in figures 2 and 3. Model I is equipped with a 30° sweptback wing of aspect ratio 3; model II has a 45° swept wing of aspect ratio 4; and model III (representing the X-5 airplane) is equipped with a 60° swept wing of aspect ratio 2. To the right of each sketch in figure 1 is a plot of the model lift coefficient against angle of attack for two available Mach numbers indicative of the low and high subsonic speed range.

The effective dihedral derivative $C_{l\beta}$, expressed here in radians, for the three models is presented in figure 2 for the range of angle of attack and the Mach numbers indicated in figure 1. It is important to note the highly nonlinear variation of this derivative with angle of attack and the pronounced effect of Mach number on these variations. This nonlinear behavior is strongly dependent upon the separation of flow from the wings, particularly in the vicinity of the tips, and



commences at angles of attack at which these swept wings by no means completely stalled. Note that model I retains its positive effective dihedral (that is, $-C_{l_\beta}$) through the angle-of-attack range and increasing

Mach number tended to increase this quantity at the higher angles.

Models II and III have the more typical variation of C_{l_β} with angle of

attack and show the decrease to zero and to negative effective dihedral at the higher angles. Configurations having this latter type of variation of C_{l_β} , and the variation of the derivative C_{n_β} to be discussed

later, could easily be flying at angles at which one or the other of these derivatives become zero. The manner in which these zero values affect the lateral motions of airplanes will be discussed in the following paper by John P. Campbell with emphasis on the C_{n_β} derivative. The point to be

observed from the data presented here is that increasing Mach number may change the angle of attack at which derivatives become zero. As an illustration, the results of model II show that increasing Mach number increased the angle at which C_{l_β} and C_{n_β} become zero; whereas, for model III, the

Mach number effect is reversed; that is, increasing Mach number decreases the angle of attack at which zero values occur.

The effects of angle of attack and Mach number on the companion derivative C_{n_β} are shown in figure 3. At the higher angles the varia-

tion of this derivative depends not only upon the tail effectiveness, that is, the difference between the tail-on and tail-off results, but also may be greatly influenced by the variation of the wing-body characteristics. As an example, for models I and II the increase in the stability of the wing-body combination at the higher Mach number tends to compensate for the reduction in tail effectiveness shown by the decrease in the increment between the tail-on and tail-off results. For model III, however, although the tail effectiveness remains appreciably constant up to large angles of attack, the decrease in the stability of the wing-body combination causes a reduction in C_{n_β} for the complete model and is the

primary cause of this reduction. It is also of interest to point out for this model that the angle of attack at which C_{l_β} and C_{n_β} tend to zero

is approximately the same and decreases with increasing Mach number. This similarity of the action of Mach number on C_{l_β} and C_{n_β} is not surprising


since for this model the wing-body characteristics, which in the main usually control C_{l_β} , are also the controlling influence for C_{n_β} as was

indicated previously. These results emphasize the need for having, through the Mach range, not only proper tail effectiveness, but equally important, proper wing-body design, incorporating satisfactory directional characteristics.

The effects of horizontal-tail height on the directional-stability derivative $C_{n\beta}$ and also on the effective-dihedral derivative $C_{l\beta}$ for model I are shown in figures 4 and 5. The curves on the left of each figure represent horizontal tail-off data; the next set of curves are for the horizontal tail in the low position. This arrangement is the one considered in the previous figures. The data to the right are for the horizontal tail in high position. The expected increase in the directional-stability derivative with the tail in the high position is clearly evident from these results. For the effective-dihedral derivative $C_{l\beta}$, the relocation of the tail from the low to the high position produced again, as expected, an increase in the negative value of the derivative.

There is one additional point related to the sideslip derivatives that deserves consideration. In attempts to devise "optimum fixes" to alleviate the pitch-up conditions for various airplanes, consideration has also been given to the effect of these same fixes on the lateral derivatives. The results available so far are very limited and no specific conclusion can be made. The data of figure 6, however, illustrate for one configuration, model III, the effect of a leading-edge chord-extension on the $C_{n\beta}$ and $C_{l\beta}$ derivatives. At the lower Mach number the effect of chord-extensions in producing a linear pitching-moment variation is clearly evident, but the effect of these chord-extensions on the corresponding $C_{n\beta}$ and $C_{l\beta}$ derivatives are relatively insignificant. At the higher Mach number, although unfortunately the available chord-extension-on data are somewhat incomplete, the small effect of these chord-extensions on the derivatives is still evident, the trend for the higher Mach number being almost identical to that shown for the lower Mach number. It should be remembered, of course, that $C_{l\beta}$ did not show any pronounced breaks until angles of attack approaching stall were reached.

So far, the discussion of the lateral derivatives for the subsonic speed range has been directed toward the static effects. Recently, the characteristics in steady roll of several wings at high angles of attack in the subsonic speed range have been investigated experimentally. For a 45° swept-wing-body arrangement, the variation of the damping-in-roll parameter C_{lp} with angle of attack and Mach number is shown in figure 7, together with the corresponding lift variations. It can be seen that at a Mach number of 0.2 the wing maintains a reasonable amount of damping at all angles of attack up to the stall. However, as the Mach number is increased, the damping-in-roll ability of the wing seriously diminishes until at a Mach number of 0.91 instability in roll is indicated at an angle of attack of 11° . Note also that this result occurs although the lift is still increasing at this angle of attack. Similar effects occur



for wings of other plan forms as indicated in figure 8. It will be noted here that all these wings indicate a serious loss in damping effectiveness in about the same angle-of-attack range. Note also that, with the exception of the unswept wing, this loss occurs although the over-all lift coefficients of the wings are still increasing. For the unswept wing, this loss in damping occurs at angles of attack corresponding to the stall, as would be expected.

One additional important point connected with these regions of poor damping is that the variation of rolling moment with rolling velocity may be very irregular as shown in figure 9. Under these conditions it is difficult to determine a representative value of the damping coefficient. The data shown in figure 9 are for a Mach number of 0.85. The variation of the rolling-moment coefficient with rolling velocity shown by the dashed curve is representative of the linear stable slope characteristic of the low angle-of-attack range. At an angle of attack of 11° , however, the variation is nonlinear and, in the case of the 32.6° swept wing, it is unstable over a very wide range of $pb/2V$. The hysteresis shown in the data for the unswept wing and the 60° triangular wing would certainly give rise to some undesirable dynamic-stability characteristics and possibly complicate the design of any automatic stabilizing equipment. The instability at small values of $pb/2V$ and the associated hysteresis loops also may have some relationship to the wing-dropping problem.

Some consideration has been given to the use of fences in an attempt to reduce the loss of damping in roll. Since a loss in damping is associated with tip stalling, which is also a contributing factor in producing pitch-up, tests were made to determine whether devices which are known to alleviate pitch-up would also improve the damping in roll. The effect of a fence on the damping characteristics of the 45° swept wing is shown in figure 10. The fences were full chord and were located at the $0.65 b/2$ station. For the Mach number of 0.85, the fences delayed the pitch-up by some 5° and decidedly improved the damping. At a Mach number of 0.91, however, the effect of the fences on either the damping or the pitch-up decreased considerably. Reference 1 contains a more complete discussion of the damping-in-roll characteristics of swept wings at high angles of attack and high subsonic speeds. Included also in this report is a simple procedure for estimating the load distribution in roll provided the corresponding angle-of-attack load distribution is known.

The preceding discussion of the lateral-stability derivatives at high angles of attack has of necessity been based wholly on experimental data. This discussion has been confined to the subsonic speed range. In the supersonic speed range, recent theoretical work applied to three complete configurations has demonstrated the ability of theory to predict the lateral-stability derivatives at low angles of attack. The variations of the derivatives C_{l_β} and C_{n_β} with Mach number for these three

configurations are shown in figures 11 and 12. The theoretical results are presented for the complete arrangement, vertical-tail alone, and body or wing-body alone. The experimental results, the dark circles, are for the complete arrangement. The comparison of theory and experiment indicates that the level and trend of the experimental variations are predicted by the theory. For one of these airplanes a thorough study and prediction of all the major longitudinal and lateral derivatives has been made and is reported in reference 2.

CONCLUDING REMARKS


It has not been possible to consider all the recent information on lateral-stability derivatives. However, a bibliography of papers containing lateral-stability-derivative data has been attached. Reference 3 also contains a large number of references not included here. The following remarks are offered as an indication of the present general status of the stability-derivative field.

At low angles of attack within the subsonic speed range below the critical Mach number, it is felt that available theory permits fairly reliable predictions of the lateral-stability derivatives.

At the higher angles of attack in the subsonic and transonic ranges, the unpredictable, nonlinear characteristics of the derivatives stress the necessity for determining experimentally for a particular configuration the derivatives needed in the estimation of stability.

In the supersonic range at low angles of attack, combined theoretical and experimental studies have produced useful aerodynamic-derivative data. For the complete configurations so far considered, derivative estimates made for these conditions have met with a good measure of success.

In the supersonic range at high angles of attack there are no data available.



REFERENCES

1. Kuhn, Richard E.: Notes on Damping in Roll and Load Distributions in Roll at High Angles of Attack and High Subsonic Speed. NACA RM L53G13a. (Prospective NACA paper.)
2. Margolis, Kenneth, and Bobbitt, Percy J.: Theoretical Calculations of the Stability Derivatives at Supersonic Speeds for a High-Speed Airplane Configuration. NACA RM L53G17. (Prospective NACA paper.)
3. Campbell, John P., and McKinney, Marion O.: Summary of Methods for Calculating Dynamic Lateral Stability and Response and for Estimating Lateral Stability Derivatives. NACA Rep. 1098, 1952. (Supersedes NACA TN 2409.)

BIBLIOGRAPHY

THEORETICAL STUDIES AND ESTIMATING PROCEDURES

- Purser, Paul E.: An Approximation to the Effect of Geometric Dihedral on the Rolling Moment Due to Sideslip for Wings at Transonic and Supersonic Speeds. NACA RM L52B01, 1952.
- Margolis, Kenneth, Sherman, Windsor L., and Hannah, Margery E.: Theoretical Calculation of the Pressure Distribution, Span Loading, and Rolling Moment Due to Sideslip at Supersonic Speeds for Thin Sweptback Tapered Wings With Supersonic Trailing Edges and Wing Tips Parallel to the Axis of Wing Symmetry. NACA TN 2898, 1953.
- Robinson, A., and Hunter-Tod, J. H.: The Aerodynamic Derivatives With Respect to Sideslip for a Delta Wing With Small Dihedral at Supersonic Speeds. Rep. No. 12, College of Aero., Cranfield (British), Dec. 1947.
- Nonweiler, T.: Theoretical Stability Derivatives of a Highly Swept Delta Wing and Slender Body Combination. Rep. No. 50, College of Aero., Cranfield (British), Nov. 1951.
- Jacobs, Willi: Lift and Moment Changes Due to the Fuselage for a Yawed Aeroplane With Unswept and Swept Wings. Rep No. 34, Aero. Res. Inst. of Sweden (Stockholm), 1950.
- Ksoll, R.: Theoretical Investigations on the Rolling Moment Due to Side Slip of Wing and Fuselage Arrangements With a Fuselage of Pear Shaped Cross Section. Repts. and Translations No. 134, British M.O.S.(A) Völkenrode, Aug. 1946.

CONFIDENTIAL

DECLASSIFIED

- Martin, John C., and Malvestuto, Frank S., Jr.: Theoretical Force and Moments Due to Sideslip of a Number of Vertical Tail Configurations at Supersonic Speeds. NACA TN 2412, 1951.
- Riley, Donald R.: Effect of Horizontal-Tail Span and Vertical Location on the Aerodynamic Characteristics of an Unswept Tail Assembly in Sideslip. NACA TN 2907, 1953.
- Coale, Charles W.: Restoring Moment in Yaw Due to Interference Between the Vertical Stabilizer and Fuselage at Supersonic Velocities. Rep. No. SM-13496, Douglas Aircraft Co., Inc., Feb. 7, 1949.
- Owen, P. R., and Andersen, R. G.: Interference Between the Wings and the Tail Surfaces of a Combination of Slender Body, Cruciform Wings and Cruciform Tail Set at Both Incidence and Yaw. Rep. No. Aero. 2471, British R.A.E., June 1952.
- Tscherfing, W., and Decker, J. L.: Directional Stability Characteristics of Tee-Tails. Eng. Rep. No. 4797, The Glenn L. Martin Co., Feb. 20, 1952.
- Falkner, V. M.: Rotary Derivatives in Yaw. Aircraft Engineering, vol. XXIII, no. 264, Feb. 1951, pp. 44-50, 54.
- Hunter-Tod, J. H.: The Aerodynamic Derivatives With Respect to Rate of Yaw for a Delta Wing With Small Dihedral at Supersonic Speeds. Rep. No. 28, College of Aero., Cranfield (British), March 1949.
- Ribner, Herbert S.: On the Effect of Subsonic Trailing Edges on Damping in Roll and Pitch of Thin Sweptback Wings in a Supersonic Stream. NACA TN 2146, 1950.
- Ribner, Herbert S.: Damping in Roll of Cruciform and Some Related Delta Wings at Supersonic Speeds. NACA TN 2285, 1951.
- Martina, Albert P.: Method for Calculating the Rolling and Yawing Moments Due to Rolling for Unswept Wings With or Without Flaps or Ailerons by Use of Nonlinear Section Lift Data. NACA TN 2937, 1953.
- Diederich, Franklin W.: A Simple Approximate Method for Calculating Spanwise Lift Distributions and Aerodynamic Influence Coefficients at Subsonic Speeds. NACA TN 2751, 1952.
- Diederich, Franklin W., and Zlotnick, Martin: Theoretical Spanwise Lift Distributions of Low-Aspect-Ratio Wings at Speeds Below and Above the Speed of Sound. NACA TN 1973, 1949.

Co

Diederich, Franklin W.: A Plan-Form Parameter for Correlating Certain Aerodynamic Characteristics of Swept Wings. NACA TN 2335, 1951.

DeYoung, John: Theoretical Antisymmetric Span Loading for Wings of Arbitrary Plan Form at Subsonic Speeds. NACA Rep. 1056, 1951. (Supersedes NACA TN 2140.)

Moeckel, W. E., and Evvard, J. C.: Load Distributions Due to Steady Roll and Pitch for Thin Wings at Supersonic Speeds. NACA TN 1689, 1948.

Bleviss, Zegmund O.: Some Roll Characteristics of Cruciform Delta Wings at Supersonic Speeds. Jour. Aero. Sci., vol. 18, no. 5, May 1951, pp. 289-297.

Bleviss, Zegmund O.: Some Roll Characteristics of Plane and Cruciform Delta Ailerons and Wings in Supersonic Flow. Rep. No. SM-13431, Douglas Aircraft Co., Inc., June 1949.

Lagerstrom, P. A., and Graham, Martha E.: Some Aerodynamic Formulas in Linearized Supersonic Theory for Damping in Roll and Effect of Twist for Trapezoidal Wings. Rep. No. SM-13200, Douglas Aircraft Co., Inc., March 12, 1948.

Graham, Ernest W.: A Limiting Case for Missile Rolling Moments. Jour. Aero. Sci., vol. 18, no. 9, Sept. 1951, pp. 624-628.

Miles, John W.: A Note on the Damping in Roll of a Cruciform Winged Body. Quarterly Appl. Math., vol. X, no. 3, Oct. 1952, pp. 276-277.

Adams, Gaynor J., and Dugan, Duane W.: Theoretical Damping in Roll and Rolling Moment Due to Differential Wing Incidence for Slender Cruciform Wings and Wing-Body Combinations. NACA Rep. 1088, 1952.

Van Meter, J. T.: Damping in Roll of Triangular Planform Wings in Supersonic Flow. Meteor Rep. UAC-34, United Aircraft Corp., June 1949.

Lehrian, Doris E.: Calculation of the Damping for Rolling Oscillations of a Swept Wing. C. P. No. 51, British N.P.L. (Tech. Rep. 13,448, A.R.C.), 1951.

Bobbitt, Percy J., and Malvestuto, Frank S., Jr.: Estimation of Forces and Moments Due to Rolling for Several Slender-Tail Configurations at Supersonic Speeds. NACA TN 2955, 1953.

Martin, John C., and Gerber, Nathan: On the Effect of Thickness on the Damping in Roll of Airfoils at Supersonic Speeds. Rep. No. 843, Ballistic Res. Labs., Aberdeen Proving Ground, Jan. 1953.



Nicolaides, John D., and Bolz, Ray E.: On the Pure Rolling Motion of Winged and/or Finned Missiles in Varying Supersonic Flight. Rep. No. 799, Ballistic Res. Labs., Aberdeen Proving Ground, March 1952.

Steinmetz, Harold F.: Wing-Body Interference Effects on the Tail Contribution to the Damping-in-Roll of Supersonic Missiles. Preprint No. 384, S.M.F. Fund Paper, Inst. Aero. Sci.

EXPERIMENTAL STUDIES

Wing and Wing-Fuselage Data

Letko, William, and Wolhart, Walter D.: Effect of Sweepback on the Low-Speed Static and Rolling Stability Derivatives of Thin Tapered Wings of Aspect Ratio 4. NACA RM L9F14, 1949.

Brewer, Jack D., and Fisher, Lewis R.: Effect of Taper Ratio on the Low-Speed Rolling Stability Derivatives of Swept and Unswept Wings of Aspect Ratio 2.61. NACA TN 2555, 1951. (Supersedes NACA RM L8H18.)

Letko, William, and Jaquet, Byron M.: Effect of Airfoil Profile of Symmetrical Sections on the Low-Speed Static-Stability and Yawing Derivatives of 45° Sweptback Wing Models of Aspect Ratio 2.61. NACA RM L8H10, 1948.


Jaquet, Byron M., and Brewer, Jack D.: Low-Speed Static-Stability and Rolling Characteristics of Low-Aspect-Ratio Wings of Triangular and Modified Triangular Plan Forms. NACA RM L8L29, 1949.

Neumark, S.: Lateral Characteristics of Wings of Small Aspect Ratio From Some German Model Tests. Tech. Note No. Aero. 1917, British R.A.E., Sept. 1947.

Wolhart, Walter D.: Wind-Tunnel Investigation at Low Speed of the Effects of Symmetrical Deflection of Half-Delta Tip Controls on the Damping in Roll and Yawing Moment Due to Rolling of a Triangular-Wing Model. NACA RM L51B09, 1951.

Lichtenstein, Jacob H.: Effect of High-Lift Devices on the Low-Speed Static Lateral and Yawing Stability Characteristics of an Untapered 45° Sweptback Wing. NACA TN 2689, 1952. (Supersedes NACA RM L8G20.)

Lichtenstein, Jacob H., and Williams, James L.: Effect of High-Lift Devices on the Static-Lateral-Stability Derivatives of a 45° Sweptback Wing of Aspect Ratio 4.0 and Taper Ratio 0.6 in Combination With a Body. NACA TN 2819, 1952.



Fisher, Lewis R.: Low-Speed Static Longitudinal and Lateral Stability Characteristics of Two Low-Aspect-Ratio Wings Cambered and Twisted To Provide a Uniform Load at a Supersonic Flight Condition. NACA RM L51C20, 1951.

Salmi, Reino J., and Fitzpatrick, James E.: Yaw Characteristics and Side-wash Angles of a 42° Sweptback Circular-Arc Wing With a Fuselage and With Leading-Edge and Split Flaps at a Reynolds Number of 5,300,000. NACA RM L7I30, 1947.

Salmi, Reino J.: Yaw Characteristics of a 52° Sweptback Wing of NACA 64₁-112 Section With a Fuselage and With Leading-Edge and Split Flaps at Reynolds Numbers From 1.93×10^6 to 6.00×10^6 . NACA RM L8H12, 1948.

McCormack, Gerald M., and Walling, Walter C.: Aerodynamic Study of a Wing-Fuselage Combination Employing a Wing Swept Back 63° . Investigation of a Large-Scale Model at Low Speed. NACA RM A8D02, 1949.

Hunton, Lynn W., and Dew, Joseph K.: Measurements of the Damping in Roll of Large-Scale Swept-Forward and Swept-Back Wings. NACA RM A7D11, 1947.

Cole, Henry A., Jr., and Ganzer, Victor M.: Experimental Investigation of Rolling Performance of Straight and Sweptback Flexible Wings With Various Ailerons. NACA TN 2563, 1951.


Adler, Alfred A.: A Correlation of Theory With Experiment for Low-Aspect-Ratio Wings at Subsonic Speeds. Rep. No. AF-743-A-4 (Air Res. and Dev. Command Contract No. AF 33(038)-17397 E.O. No. 460-31-12-12 SR 1g), Cornell Aero. Lab., Inc., Dec. 1952.

Thiel, G.: Rolling Balance Measurements. Part II - Results of Tests on Two Tapered Wings. British Ministry of Supply Translation No. GDC 10/451(11)T (R.A.E. Library Trans. 379, pt. 2), Sept. 1951.

Halliday, A. S., Cox, D. K., and Skelton, W. C.: Measurement of Rolling Moment on an Elliptic Wing on the N.P.L. Whirling Arm. Rep. 10,935, British A.R.C. (S. & C. 2161), Oct. 16, 1947.

Halliday, A. S., and Cox, D. K.: The Measurement of Yawing Moment on an Elliptic Wing on the Whirling Arm. Rep. 12,497, British A.R.C. (S. & C. 2320), Aug. 2, 1949.

Kuhn, Richard E., and Fournier, Paul G.: Wind-Tunnel Investigation of the Static Lateral Stability Characteristics of Wing-Fuselage Combinations at High Subsonic Speeds. Sweep Series. NACA RM L52G11a, 1952.



Fournier, Paul G., and Byrnes, Andrew L., Jr.: Wind-Tunnel Investigation of the Static Lateral Stability Characteristics of Wing-Fuselage Combinations at High Subsonic Speeds. Aspect-Ratio Series. NACA RM L52L18, 1953.

Wiggins, James W., and Fournier, Paul G.: Wind-Tunnel Investigation of the Static Lateral Stability Characteristics of Wing-Fuselage Combinations at High Subsonic Speeds. Taper-Ratio Series. NACA RM L53B25a, 1953.

Wiggins, James W.: Wind-Tunnel Investigation at High Subsonic Speeds of the Static-Longitudinal and Static-Lateral Stability Characteristics of a Wing-Fuselage Combination Having a Triangular Wing of Aspect Ratio 2.31 and an NACA 65A003 Airfoil. NACA RM L53G09a. (Prospective NACA paper.)

Fournier, Paul G.: Wind Tunnel Investigation of the Aerodynamic Characteristics in Pitch and Sideslip at High Subsonic Speeds of a Wing-Fuselage Combination Having a Triangular Wing of Aspect Ratio 4. NACA RM L53G14a. (Prospective NACA paper.)

Kuhn, Richard E., and Draper, John W.: Wind-Tunnel Investigation of the Effects of Geometric Dihedral on the Aerodynamic Characteristics in Pitch and Sideslip of an Unswept- and a 45° Sweptback-Wing-Fuselage Combination at High Subsonic Speeds. NACA RM L53F09, 1953.

Johnson, Harold S.: Wind-Tunnel Investigation at Low Transonic Speeds of the Effects of Number of Wings on the Lateral-Control Effectiveness of an RM-5 Test Vehicle. NACA RM L9H16, 1949.

Lockwood, Vernard E.: Damping-in-Roll Characteristics of a 42.7° Sweptback Wing As Determined From a Wind-Tunnel Investigation of a Twisted Semispan Wing. NACA RM L9F15, 1949.

Lockwood, Vernard E.: Effects of Sweep on the Damping-in-Roll Characteristics of Three Sweptback Wings Having an Aspect Ratio of 4 at Transonic Speeds. NACA RM L50J19, 1950.

Kuhn, Richard E., and Myers, Boyd C., II: The Effect of Tip Tanks on the Rolling Characteristics at High Subsonic Mach Numbers of a Wing Having an Aspect Ratio of 3 With Quarter-Chord Line Swept Back 35° . NACA RM L9J19, 1950.

Myers, Boyd C., II, and Kuhn, Richard E.: High-Subsonic Damping-in-Roll Characteristics of a Wing With the Quarter-Chord Line Swept Back 35° and With Aspect Ratio 3 and Taper Ratio 0.6. NACA RM L9C23, 1949.

Kuhn, Richard E., and Myers, Boyd C., II: Effects of Mach Number and Sweep on the Damping-in-Roll Characteristics of Wings of Aspect Ratio 4. NACA RM L9E10, 1949.

Stone, David G.: A Collection of Data for Zero-Lift Damping in Roll of Wing-Body Combinations As Determined With Rocket-Powered Models Equipped With Roll-Torque Nozzles. NACA RM L53E26, 1953.

Bland, William M., Jr., and Dietz, Albert E.: Some Effects of Fuselage Interference, Wing Interference, and Sweepback on the Damping in Roll of Untapered Wings As Determined by Techniques Employing Rocket-Propelled Vehicles. NACA RM L51D25, 1951.

Sanders, E. Claude, Jr., and Edmondson, James L.: Damping in Roll of Rocket-Powered Test Vehicles Having Swept, Tapered Wings of Low Aspect Ratio. NACA RM L51G06, 1951.

Sanders, E. Claude, Jr.: Damping in Roll of Straight and 45° Swept Wings of Various Taper Ratios Determined at High Subsonic, Transonic, and Supersonic Speeds With Rocket-Powered Models. NACA RM L51H14, 1951.

Sanders, E. Claude, Jr.: Damping in Roll of Models With 45° , 60° , and 70° Delta Wings Determined at High Subsonic, Transonic, and Supersonic Speeds With Rocket-Powered Models. NACA RM L52D22a, 1952.

Edmondson, James L.: Damping in Roll of Rectangular Wings of Several Aspect Ratios and NACA 65A-Series Airfoil Sections of Several Thickness Ratios at Transonic and Supersonic Speeds As Determined With Rocket-Powered Models. NACA RM L50E26, 1950.

Stone, David G., and Sandahl, Carl A.: A Comparison of Two Techniques Utilizing Rocket-Propelled Vehicles for the Determination of the Damping-in-Roll Derivative. NACA RM L51A16, 1951.

Edmondson, James L., and Sanders, E. Claude, Jr.: A Free-Flight Technique for Measuring Damping in Roll by Use of Rocket-Powered Models and Some Initial Results for Rectangular Wings. NACA RM L9I01, 1949.

Dietz, Albert E., and Edmondson, James L.: The Damping in Roll of Rocket-Powered Test Vehicles Having Rectangular Wings With NACA 65-006 and Symmetrical Double-Wedge Airfoil Sections of Aspect Ratio 4.5. NACA RM L50B10, 1950.

Bland, William M., Jr., and Sandahl, Carl A.: A Technique Utilizing Rocket-Propelled Test Vehicles for the Measurement of the Damping in Roll of Sting-Mounted Models and Some Initial Results for Delta and Unswept Tapered Wings. NACA RM L50D24, 1950.

Hopko, Russell N.: A Flight Investigation of the Damping in Roll and Rolling Effectiveness Including Aeroelastic Effects of Rocket-Propelled Missile Models Having Cruciform, Triangular, Interdigitated Wings and Tails. NACA RM L51D16, 1951.

CONFIDENTIAL

Strass, H. Kurt, and Marley, Edward T.: Rolling Effectiveness of All-Movable Wings at Small Angles of Incidence at Mach Numbers From 0.6 to 1.6. NACA RM L51H03, 1951.

Bland, William M., Jr.: Effect of Fuselage Interference on the Damping in Roll of Delta Wings of Aspect Ratio 4 in the Mach Number Range Between 0.6 and 1.6 As Determined With Rocket-Propelled Vehicles. NACA RM L52E13, 1952.

Martz, C. William, and Church, James D.: Flight Investigation at Subsonic, Transonic, and Supersonic Velocities of the Hinge-Moment Characteristics, Lateral-Control Effectiveness, and Wing Damping in Roll of a 60° Sweptback Delta Wing With Half-Delta Tip Ailerons. NACA RM L51G18, 1951.

Brown, Clinton E., and Heinke, Harry S., Jr.: Preliminary Wind-Tunnel Tests of Triangular and Rectangular Wings in Steady Roll at Mach Numbers of 1.62 and 1.92. NACA RM L8L30, 1949.

McDearmon, Russell W., and Heinke, Harry S., Jr.: Investigation of the Damping in Roll of Swept and Tapered Wings at Supersonic Speeds. NACA RM L53A13, 1953.

Chubb, Robert S.: Experimental Investigation of the Static Aerodynamic and Dynamic Damping-in-Roll Characteristics of an 8-CM Aircraft Rocket With Solid and Slotted Fins. NACA RM A52C04, 1952.

Spearman, M. Leroy, and Hilton, John H., Jr.: Aerodynamic Characteristics at Supersonic Speeds of a Series of Wing-Body Combinations Having Cambered Wings With an Aspect Ratio of 3.5 and a Taper Ratio of 0.2. Effects of Sweep Angle and Thickness Ratio on the Static Lateral Stability Characteristics at $M = 1.60$. NACA RM L51K15a, 1952.

Hamilton, Clyde V.: Aerodynamic Characteristics at Supersonic Speeds of a Series of Wing-Body Combinations Having Cambered Wings With an Aspect Ratio of 3.5 and a Taper Ratio of 0.2. Effects of Sweep Angle and Thickness Ratio on the Static Lateral Stability Characteristics at $M = 2.01$. NACA RM L52E23, 1952.

Lessing, Henry C.: Aerodynamic Study of a Wing-Fuselage Combination Employing a Wing Swept Back 63° - Effect of Sideslip on Aerodynamic Characteristics at a Mach Number of 1.4 With the Wing Twisted and Cambered. NACA RM A50F09, 1950.

Scherrer, Richard, and Dennis, David H.: Lateral-Control Characteristics and Dihedral Effect of a Wing-Body Combination With a Variable-Incidence Triangular Wing and Wing-Tip Ailerons at a Mach Number of 1.52. NACA RM A50H10, 1951.

0370201030 Complete

Campbell, John P., and Toll, Thomas A.: Factors Affecting Lateral Stability and Controllability. NACA RM L8A28a, 1948.

Fisher, Lewis R., and Michael, William H., Jr.: An Investigation of the Effect of Vertical-Fin Location and Area on Low-Speed Lateral Stability Derivatives of a Semitailless Airplane Model. NACA RM L51A10, 1951.

Letko, William, and Riley, Donald R.: Effect of an Unswept Wing on the Contribution of Unswept-Tail Configurations to the Low-Speed Static- and Rolling-Stability Derivatives of a Midwing Airplane Model. NACA TN 2175. 1950.

Goodman, Alex: Effects of Wing Position and Horizontal-Tail Position on the Static Stability Characteristics of Models With Unswept and 45° Sweptback Surfaces With Some Reference to Mutual Interference. NACA TN 2504, 1951.

Bird, John D., Lichtenstein, Jacob H., and Jaquet, Byron M.: Investigation of the Influence of Fuselage and Tail Surfaces on Low-Speed Static Stability and Rolling Characteristics of a Swept-Wing Model. NACA TN 2741, 1952. (Supersedes NACA RM L7H15.)

Letko, William: Effect of Vertical-Tail Area and Length on the Yawing Stability Characteristics of a Model Having a 45° Sweptback Wing. NACA TN 2358, 1951.


Bird, John D., Jaquet, Byron M., and Cowan, John W.: Effect of Fuselage and Tail Surfaces on Low-Speed Yawing Characteristics of a Swept-Wing Model As Determined in Curved-Flow Test Section of the Langley Stability Tunnel. NACA TN 2483, 1951. (Supersedes NACA RM L8G13.)

Goodman, Alex, and Wolhart, Walter D.: Experimental Investigation of the Low-Speed Static and Yawing Stability Characteristics of a 45° Swept-back High-Wing Configuration With Various Twin Vertical Wing Fins. NACA TN 2534, 1951.

Jaquet, Byron M., and Brewer, Jack D.: Effects of Various Outboard and Central Fins on Low-Speed Static-Stability and Rolling Characteristics of a Triangular-Wing Model. NACA RM L9E18, 1949.

Goodman, Alex: Effect of Various Outboard and Central Fins on Low-Speed Yawing Stability Derivatives of a 60° Delta-Wing Model. NACA RM L50E12a, 1950.

— 40 —

- Bird, John D., Fisher, Lewis R., and Hubbard, Sadie M.: Some Effects of Frequency on the Contribution of a Vertical Tail to the Free Aerodynamic Damping of a Model Oscillating in Yaw. NACA TN 2657, 1952.
- Fisher, Lewis R., and Wolhart, Walter D.: Some Effects of Amplitude and Frequency on the Aerodynamic Damping of a Model Oscillating Continuously in Yaw. NACA TN 2766, 1952.
- Wolhart, Walter D.: Influence of Wing and Fuselage on the Vertical-Tail Contribution to the Low-Speed Rolling Derivatives of Midwing Airplane Models With 45° Sweptback Surfaces. NACA TN 2587, 1951.
- Letko, William: A Low-Speed Experimental Study of the Directional Characteristics of a Sharp-Nosed Fuselage Through a Large Angle-of-Attack Range at Zero Angle of Sideslip. NACA TN 2911, 1953.
- Jaquet, Byron M., and Fletcher, H. S.: Lateral Oscillatory Characteristics of the Republic F-91 Airplane Calculated by Using Low-Speed Experimental Static and Rotary Derivatives. NACA RM L53G01. (Prospective NACA paper.)
- Hunton, Lynn W., and Dew, Joseph K.: An Investigation of the Wing and the Wing-Fuselage Combination of a Full-Scale Model of the Republic XP-91 Airplane in the Ames 40- by 80-Foot Wind Tunnel. NACA RM SA8F09, U. S. Air Force, 1948.
- Queijo, M. J., and Wells, Evalyn G.: Wind-Tunnel Investigation of the Low-Speed Static and Rotary Stability Derivatives of a 0.13-Scale Model of the Douglas D-558-II Airplane in the Landing Configuration. NACA RM L52G07, 1952.
- Queijo, M. J., Wolhart, W. D., and Fletcher, H. S.: Wind-Tunnel Investigation at Low Speed of the Static Longitudinal and Lateral Stability Characteristics of a 1/9-Scale Powered Model of the Convair XFY-1 Vertically Rising Airplane - TED No. NACA DE 373. NACA RM SL53B20, Bur. Aero., 1953.
- Queijo, M. J., Wolhart, Walter D., and Fletcher, H. S.: Wind-Tunnel Investigation at Low Speed of the Rolling Stability Derivatives of a 1/9-Scale Powered Model of the Convair XFY-1 Vertically Rising Airplane - TED No. NACA DE 373. NACA RM SL53E13, Bur. Aero., 1953.
- Queijo, M. J., Wolhart, W. D., and Fletcher, H. S.: Wind-Tunnel Investigation at Low Speed of the Yawing Stability Derivatives of a 1/9-Scale Powered Model of the Convair XFY-1 Vertically Rising Airplane. TED No. NACA DE 373. NACA RM SL53D01, Bur. Aero., 1953.
- 

Johnson, Joseph L.: Damping in Yaw and Static Directional Stability of a Canard Airplane Model and of Several Models Having Fuselages of Relatively Flat Cross Section. NACA RM L50H30a, 1950.

Bates, William R.: Low-Speed Static Lateral Stability Characteristics of a Canard Model Having a 60° Triangular Wing and Horizontal Tail. NACA RM L9J12, 1949.

Delany, Noel K., and Hayter, Nora-Lee F.: Low-Speed Investigation of a 0.16-Scale Model of the X-3 Airplane - Lateral and Directional Characteristics. NACA RM A51A16, 1951.

Rose, Leonard M.: Low-Speed Investigation of a Small Triangular Wing of Aspect Ratio 2.0. III - Static Stability With Twin Vertical Fins. NACA RM A8C03, 1948.

McCormack, Gerald M.: Aerodynamic Study of a Wing-Fuselage Combination Employing a Wing Swept Back 63° . Aerodynamic Characteristics in Side-slip of a Large-Scale Model Having a 63° Swept-Back Vertical Tail. NACA RM A9F14, 1949.

Anderson, Adrien E.: An Investigation at Low Speed of a Large-Scale Triangular Wing of Aspect Ratio Two. III. Characteristics of Wing With Body and Vertical Tail. NACA RM A9H04, 1949.


Koenig, David G.: Tests in the Ames 40- by 80-Foot Wind Tunnel of an Airplane Configuration With a Variable-Incidence Triangular Wing and an All-Movable Horizontal Tail. NACA RM A53D21, 1953.

Koenig, David G.: Tests in the Ames 40- by 80-Foot Wind Tunnel of an Airplane Configuration With an Aspect Ratio 3 Triangular Wing and an All-Movable Horizontal Tail - Longitudinal and Lateral Characteristics. NACA RM A52L15, 1953.

Graham, David, and Koenig, David G.: Tests in the Ames 40- by 80-Foot Wind Tunnel of an Airplane Configuration With an Aspect Ratio 2 Triangular Wing and an All-Movable Horizontal Tail - Lateral Characteristics. NACA RM A51L03, 1952.

Marino, Alfred A., and Mastrocola, N.: Wind-Tunnel Investigation of the Contribution of a Vertical Tail to the Directional Stability of a Fighter-Type Airplane. NACA TN 2488, 1952. (Supersedes NACA RM L7K03.)

Falkner, V. M., and Nixon, H. L.: Wind Tunnel Tests on the Yawing Moment of a Meteor Model. Rep. No. 11,943, British A.R.C., Nov. 25, 1948.



Ross, J. G., and Lock, R. C.: Wind-Tunnel Measurements of Yawing Moment Due to Yawing (n_r) on a 1/5.5 Scale Model of the Meteor Mark F.III. R. & M. No. 2791, British A.R.C., 1947.

Kemp, W. B., and Polhamus, E. C.: Wind-Tunnel Tests of a 1/4-Scale Model of the Bell XS-1 Transonic Airplane (Army Project MX-653) II - Lateral and Directional Stability and Control. NACA MR L6E27, Army Air Forces and Bur. Aero., 1946.

Spearman, M. Leroy, and Becht, Robert E.: The Effect of Negative Dihedral, Tip Droop, and Wing Tip Shape on the Low-Speed Aerodynamic Characteristics of a Complete Model Having a 45° Sweptback Wing. NACA RM L8J07, 1948.

Goodson, Kenneth W., and Few, Albert G., Jr.: Low-Speed Static Longitudinal and Lateral Stability Characteristics of a Model With Leading-Edge Chord-Extensions Incorporated on a 40° Sweptback Circular-Arc Wing of Aspect Ratio 4 and Taper Ratio 0.50. NACA RM L52I18, 1952.

Schuldenfrei, Marvin, Comisarow, Paul, and Goodson, Kenneth W.: Stability and Control Characteristics of a Complete Airplane Model Having a Wing With Quarter-Chord Line Swept Back 40°, Aspect Ratio 2.50, and Taper Ratio 0.42. NACA TN 2482, 1951. (Supersedes NACA RM L7B25.)

Goodson, Kenneth W., and Comisarow, Paul: Lateral Stability and Control Characteristics of an Airplane Model Having a 42.8° Sweptback Circular-Arc Wing With Aspect Ratio 4.00, Taper Ratio 0.50, and Sweptback Tail Surfaces. NACA RM L7G31, 1947.


Polhamus, Edward C.: Wind-Tunnel Investigation of the Low-Speed Stability and Control Characteristics of a Model With a Sweptback Vee Tail and a Sweptback Wing. NACA RM L7K13, 1948.

Kemp, William B., Jr., and Becht, Robert E.: Stability and Control Characteristics at Low Speed of a 1/4-Scale Bell X-5 Airplane Model. Lateral and Directional Stability and Control. NACA RM L50C17a, 1950.

Polhamus, Edward C., and Becht, Robert E.: Low-Speed Stability Characteristics of a Complete Model With a Wing of W Plan Form. NACA RM L52A25, 1952.

Kuhn, Richard E., and Wiggins, James W.: Static Lateral Stability Characteristics of a 1/10-Scale Model of the X-1 Airplane at High Subsonic Mach Numbers. NACA RM L51F01a, 1951.

Donlan, Charles J., and Kuhn, Richard E.: Estimated Transonic Flying Qualities of a Tailless Airplane Based on a Model Investigation. NACA RM L9D08, 1949.



Polhanus, Edward C., and King, Thomas J., Jr.: High-Speed Wind-Tunnel Investigation of the Lateral Stability Characteristics of a 0.10-Scale Model of the Grumman XF9F-2 Airplane - TED No. NACA DE 301. NACA RM SL9G21a, Bur. Aero., 1949.

Wiggins, James W., Kuhn, Richard E., and Fournier, Paul G.: Wind Tunnel Investigation to Determine the Horizontal- and Vertical-Tail Contributions to the Static Lateral Stability Characteristics of a Complete-Model Configuration at High Subsonic Speeds. NACA RM L53E19, 1953.

Kuhn, Richard E., and Wiggins, James W.: Wind-Tunnel Investigation to Determine the Aerodynamic Characteristics in Steady Roll of a Model at High Subsonic Speeds. NACA RM L52K24, 1953.

Kuhn, Richard E., and Draper, John W.: Aerodynamic Characteristics in Pitch and Sideslip at High Subsonic Speeds of a 1/14-Scale Model of the Grumman XF10F Airplane With Wing Sweepback of 42.5° - TED No. NACA DE 354. NACA RM SL53G20, Bur. Aero., 1953.

Purser, Paul E., and Mitchell, Jesse L.: Miscellaneous Directional-Stability Data for Several Airplane-Like Configurations From Rocket-Model Tests at Transonic Speeds. NACA RM L52E06b, 1952.

Mitcham, Grady L., Blanchard, Willard S., Jr., and Hastings, Earl C., Jr.: Summary of Low-Lift Drag and Directional Stability Data from Rocket Models of the Douglas XF4D-1 Airplane With and Without External Stores and Rocket Packets at Mach Numbers From 0.8 to 1.38 - TED No. NACA DE 349. NACA RM SL52G11, Bur. Aero., 1952.

White, Maurice D.: Effect of Camber and Twist on the Stability Characteristics of Models Having a 45° Swept Wing As Determined by the Free-Fall Method at Transonic Speeds. NACA RM A52F16, 1952.

Gillis, Clarence L., and Mitchell, Jesse L.: Flight Tests at Transonic and Supersonic Speeds of an Airplane-Like Configuration With Thin Straight Sharp-Edge Wings and Tail Surfaces. NACA RM L8K04a, 1949.

D'Aiutolo, Charles T., and Mason, Homer P.: Preliminary Results of the Flight Investigation Between Mach Numbers of 0.80 and 1.36 of a Rocket-Powered Model of a Supersonic Airplane Configuration Having a Tapered Wing With Circular-Arc Sections and 40° Sweepback. NACA RM L50H29a, 1950.

Crabill, Norman L.: The Effects of Extensible Rocket Racks on Lift, Drag, and Stability of a 1/10-Scale Rocket-Boosted Model of the McDonnell XF3H-1 Airplane for a Mach Number Range of 0.60 to 1.34 - TED No. NACA DE 31. NACA RM SL53F15, Bur. Aero., 1953.

Blanchard, Willard S., Jr., and Mitcham, Grady L.: Longitudinal Stability and Estimated Flying Qualities of the Douglas XF4D-1 Airplane With and Without External Stores and Rocket Packets at Mach Numbers from 0.8 to 1.36 As Determined From Flight Tests of 0.10-Scale Rocket Models - TED No. NACA DE 349. NACA RM SL52K19a, Bur. Aero., 1952.

D'Aiutolo, Charles T., and Parker, Robert N.: Preliminary Investigation of the Low-Amplitude Damping in Pitch of Tailless Delta- and Swept-Wing Configurations at Mach Numbers From 0.7 to 1.35. NACA RM L52G09, 1952.

Spearman, M. Leroy, and Robinson, Ross B.: The Aerodynamic Characteristics of a Supersonic Aircraft Configuration With a 40° Sweptback Wing Through a Mach Number Range From 0 to 2.4 As Obtained From Various Sources. NACA RM L52A21, 1952.

Spearman, M. Leroy: An Investigation of a Supersonic Aircraft Configuration Having a Tapered Wing With Circular-Arc Sections and 40° Sweepback. Static Lateral Stability Characteristics at Mach Numbers of 1.40 and 1.59. NACA RM L50C17, 1950.

Hilton, John H., Jr., Hamilton, Clyde V., and Lankford, John L.: Preliminary Wind-Tunnel Investigation of a 1/20-Scale Model of the Convair MX-1554 at Mach Numbers of 1.61 and 2.01. NACA RM SL52L11a, U. S. Air Force, 1952.


Sherrer, Richard, and Dennis, David H.: Damping in Roll of a Missile Configuration With a Modified Triangular Wing and a Cruciform Tail at a Mach Number of 1.52. NACA RM A51A03, 1951.

Seaberg, Ernest C., and Geller, Edward S.: Flight Investigation of the Aerodynamic Derivatives and Performance of Control Systems of Two Full-Scale XASM-N-4 DOVE Bombs. NACA RM SL53E22, Bur. Ordnance, 1953.

Phelps, E. Ray, and Lazzeroni, Frank A.: Wind-Tunnel Investigation of the Aerodynamic Characteristics of 1/15-Scale Model of the Northrop MX-775A Missile. NACA RM A51E28, 1951.

Seaberg, Ernest C., and Geller, Edward S.: Flight Investigation of the Aerodynamic Derivatives and Performance of Control Systems of Two Full-Scale XASM-N-4 DOVE Bombs. NACA RM SL53E22, Bur. Ordnance, 1953.

Letko, William: Wind-Tunnel Investigation of the Low-Speed Static Stability and Control Characteristics of a Model of the Bell MX-776 (Rascal) in Combined Angle of Attack and Sideslip. NACA RM SL52D23, U. S. Air Force, 1952.



Wiley, Harleth G.: Wind-Tunnel Investigation of a Full-Scale Model of the Hughes MX-904 Missile. NACA RM SL9D28, U. S. Air Force, 1949.

Blalock, James E., and Broberg, Ralph F.: Wind-Tunnel Tests of a 1/3-Scale Model of the Turbojet Version XSUM-N-2 (Grebe) Pilotless Aircraft. Part I - Lateral Stability and Control Characteristics. Rep. C-156 Aero 759, David Taylor Model Basin, Navy Dept., Oct. 1948.

Spahr, J. Richard, and Robinson, Robert A.: Wind-Tunnel Investigation at Mach Numbers of 1.5 and 2.0 of a Canard Missile Configuration. NACA RM A51C08, 1951.

Darling, J. A., and DeMeritte, F. J.: Static Stability Measurements on 1/17th Scale Modified Shrike at Mach Number 1.87. NAVORD Rep. 2364 (Aeroballistic Res. Rep. 87), U. S. Naval Ord. Lab. (White Oak, Md.), June 10, 1952.

Turner, Robert L., and Lobrecht, Dorr, Jr.: Stability and Control Tests of a 0.135-Scale Sperry XAAM-N-2 Model at Mach Number 2.00. OAL Rep. 112-15, Ord. Aerophysics Lab. (Daingerfield, Tex.), May 12, 1951.

Darling, J. A., and DeMeritte, F. J.: Static Stability Measurements on Rascal Missile (MX-776) at Mach Number 1.56. NAVORD Rep. 2362 (Aeroballistic Res. Rep. 85), U. S. Naval Ord. Lab. (White Oak, Md.), June 11, 1952.


Clancy, Thomas M.: Wind-Tunnel Investigation of the RS-9 Meteor at Mach Numbers 1.56, 1.87, 2.16, 2.48, and 2.87. NAVORD Rep. 2414 (Aeroballistic Res. Rep. 94), U. S. Naval Ord. Lab. (White Oak, Md.), July 17, 1952.

Anderson, Arnold W., and Putnam, Russell H.: Wind-Tunnel Tests of a 0.65-Scale Model XKD5G-1 Pilotless Target Aircraft. Part III - Lateral and Directional Stability and Control Characteristics. Rep. C-413 Aero 799, The David W. Taylor Model Basin, Navy Dept., Mar. 1951.

Turner, Robert L., Jr., and Jackson, C. E.: Stability and Control Tests of a 0.135-Scale Sperry XAAM-N-2 Model at Mach Number 1.50. OAL Rep. 112-16, Ord. Aerophysics Lab. (Daingerfield, Tex.), June 22, 1951.

Turner, Robert L., Jr., and Jackson, C. E.: Stability and Control Tests of a 0.135-Scale Sperry XAAM-N-2 Model at Mach Number 2.50. OAL Rep. 112-17 (Contract NOrd-9028, Bur. Ord.), Ord. Aerophysics Lab. (Daingerfield, Tex.), June 25, 1951.

Spearman, M. Leroy, and Robinson, Ross B.: Wind-Tunnel Investigation of a Ram-Jet Canard Missile Model Having a Wing and Canard Surfaces of Delta Plan Form With 70° Swept Leading Edges. Longitudinal and Lateral Stability and Control Characteristics at a Mach Number of 1.60. NACA RM L52E15, 1952.



Hamilton, Clyde V., Driver, Cornelius, and Sevier, John R., Jr.: Wind-Tunnel Investigation of a Ram-Jet Missile Model Having a Wing and Canard Surfaces of Delta Plan Form With 70° Swept Leading Edges. Force and Moment Characteristics of Various Combinations of Components at a Mach Number of 1.6. NACA RM L53A14, 1953.

Watts, P. E.: Preliminary Force and Moment Measurements on a Cruciform Rectangular Wing-Body Combination at Mach Number 1.57. Tech. Memo. No. Aero 285, British R.A.E., June 1952.

Pfyll, Frank A.: Wind-Tunnel Investigation of the Aerodynamic Characteristics of a 0.07-Scale Model of the North American MX-770 Missile. NACA RM SA52E07, U. S. Air Force, 1952.

Krieger, Robert H.: Supersonic Wind Tunnel Tests of a Model of the North American Guided Missile MX 770 at Mach No. 1.72. Memo. Rep. No. 566, Ballistic Res. Labs., Aberdeen Proving Ground, Sept. 1951.

Beal, R. R.: Roll-Damping and Additional Roll-Control Characteristics of the Sparrow 14-B at $M = 2.50$ As Determined by Wind-Tunnel Tests of a 13.5-Percent-Scale Model. Rep. No. SM-14062 (Contract NOa(s)-51-513, Bur. Aero.), Douglas Aircraft Co., Inc., Dec. 18, 1951.

03712291030

THREE HIGH-SPEED MODELS

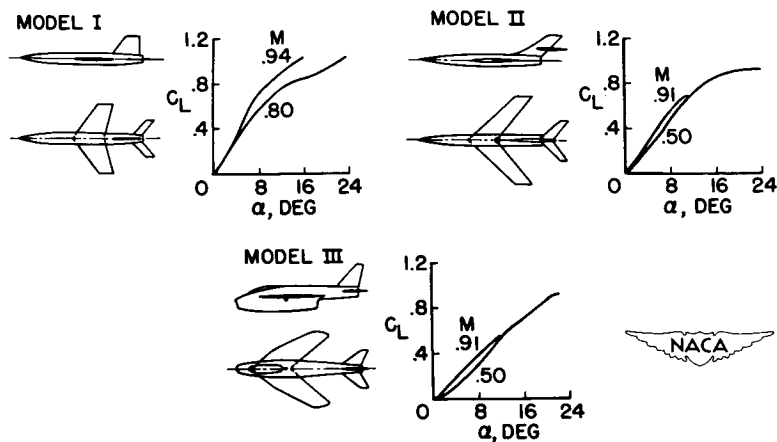


Figure 1

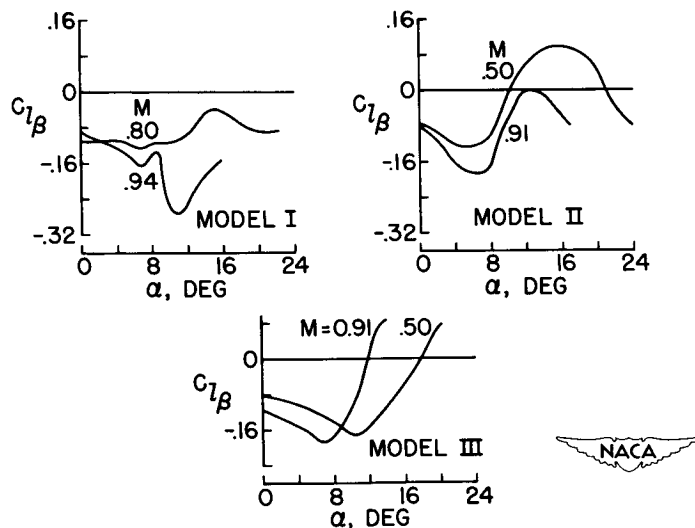
EFFECTIVE-DIHEDRAL DERIVATIVE $C_{l\beta}$
FOR THREE HIGH-SPEED MODELS

Figure 2

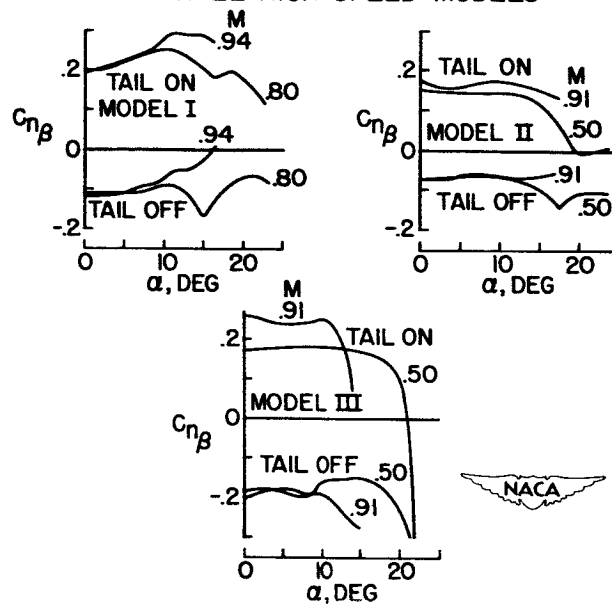
DIRECTIONAL-STABILITY DERIVATIVE $C_{n\beta}$
FOR THREE HIGH-SPEED MODELS

Figure 3

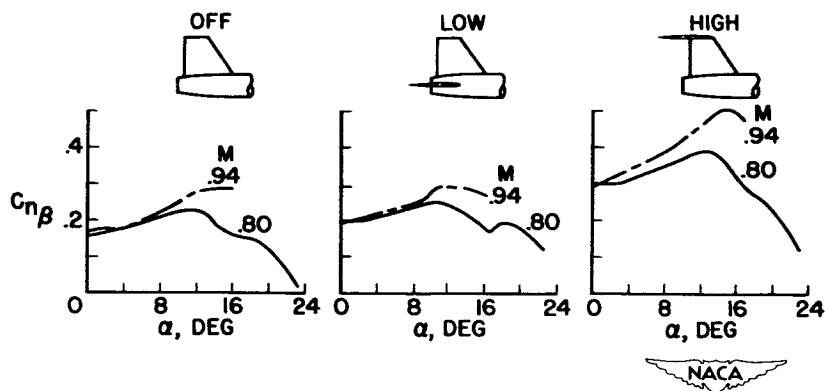
VARIATION OF DIRECTIONAL-STABILITY DERIVATIVE $C_{n\beta}$
WITH HORIZONTAL-TAIL HEIGHT

Figure 4

VARIATION OF EFFECTIVE-DIHEDRAL DERIVATIVE $C_{l\beta}$ WITH HORIZONTAL-TAIL HEIGHT

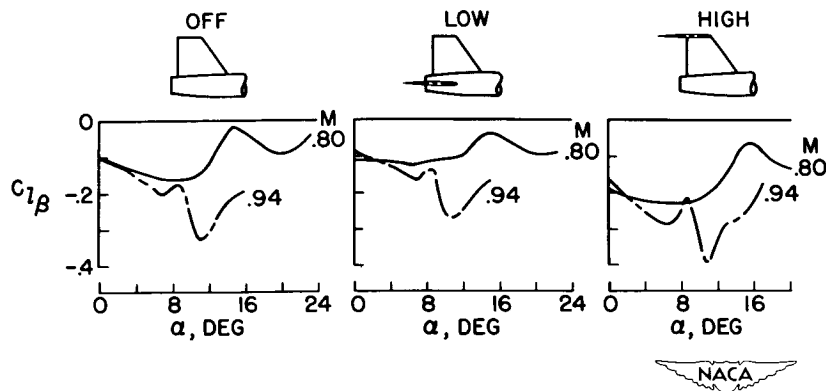


Figure 5

EFFECT OF CHORD-EXTENSIONS ON CHARACTERISTICS OF MODEL III

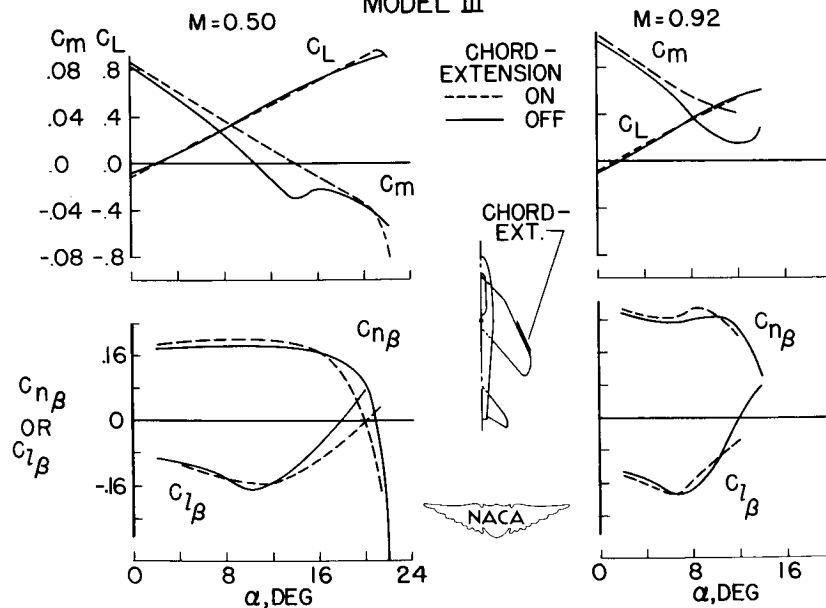


Figure 6

VARIATION OF THE DAMPING IN ROLL C_{lp} WITH MACH NUMBER
AND ANGLE OF ATTACK

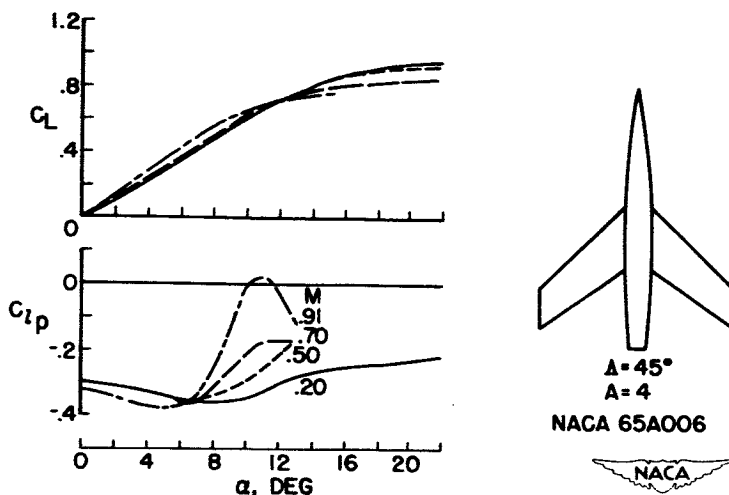


Figure 7

VARIATION OF THE DAMPING IN ROLL C_{lp} WITH
ANGLE OF ATTACK
 $M = 0.85$

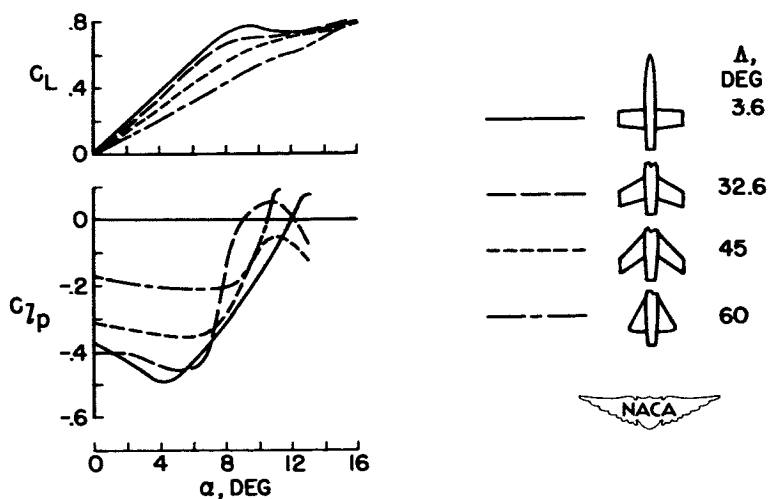


Figure 8

TYPICAL VARIATIONS OF THE ROLLING-MOMENT
COEFFICIENT C_l WITH RATE OF ROLL $\frac{pb}{2V}$

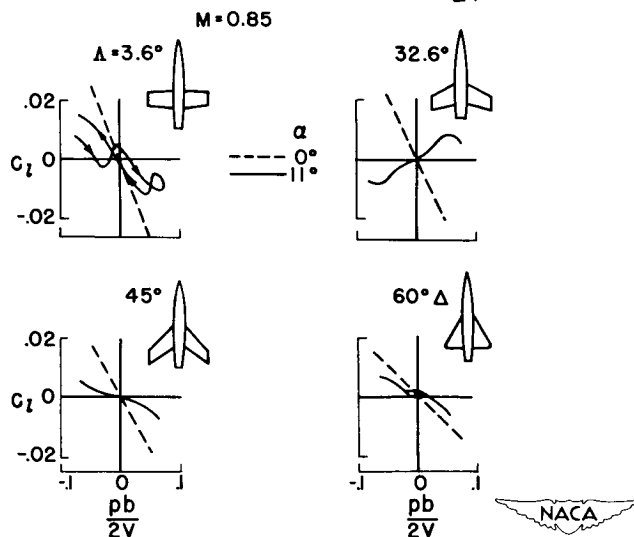


Figure 9

EFFECT OF FENCE ON CHARACTERISTICS
OF A 45° SWEEP WING

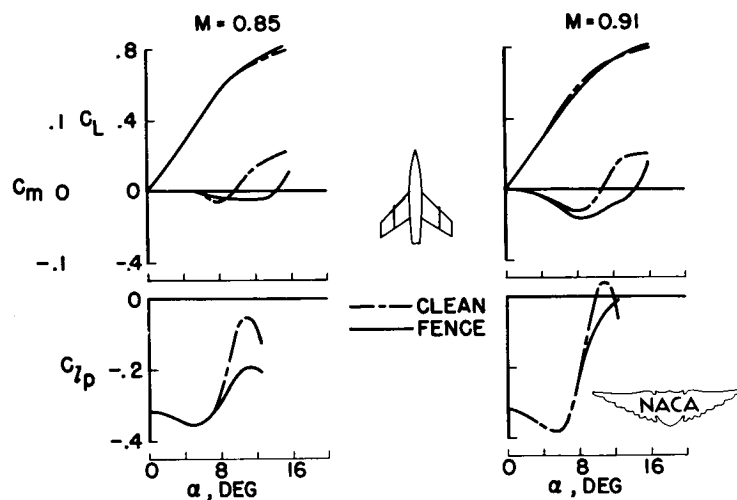


Figure 10

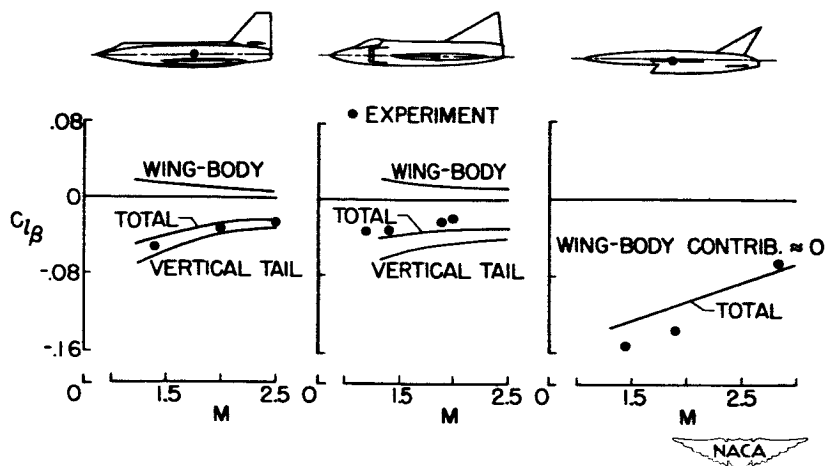
$C_{l\beta}$ DERIVATIVE FOR THREE HIGH-SPEED MODELS

Figure 11

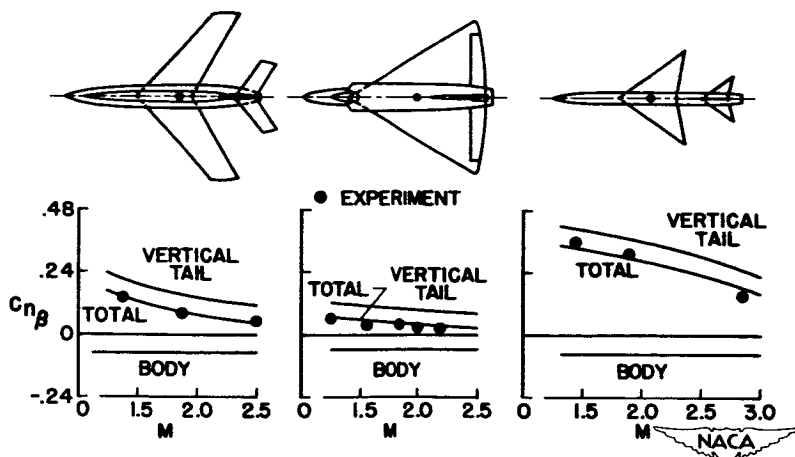
 $C_{n\beta}$ DERIVATIVE FOR THREE HIGH-SPEED MODELS

Figure 12

CONFIDENTIAL

DECLASSIFIED

DESIGN TRENDS IN RELATION TO AIRPLANE LATERAL STABILITY

By John P. Campbell

Langley Aeronautical Laboratory


INTRODUCTION

This paper deals with two lateral stability problems - unsatisfactory damping of the Dutch roll oscillation, which is common to practically all current high-speed airplanes; and the directional divergence at high angles of attack that has recently been encountered with some highly swept designs. In the discussion of the Dutch roll oscillation, one of the approaches now being made by the National Advisory Committee for Aeronautics to improve the damping is described. In the case of the new and relatively unfamiliar problem of directional divergence, the problem itself is described and some possible solutions to the problem are discussed.

DUTCH ROLL OSCILLATION

The existence of poorly damped Dutch roll oscillations for virtually every current high-speed airplane has led to increasing use of artificial stabilizing devices such as yaw dampers in an effort to provide adequate stability. In most cases, these devices have proved satisfactory, but their use has led to increases in cost, weight, complexity, and maintenance problems. The armed services and the airplane manufacturers are therefore becoming increasingly concerned about this problem and have expressed interest in means of obtaining satisfactory Dutch roll stability without resort to complicated artificial stabilizing devices.

One of the fundamental reasons for poor inherent stability seems to be that very little consideration is given to dynamic stability in the early stages of design. That is, the basic design of the airplane is determined from other considerations and attempts are made later to improve the dynamic stability by the minor changes in the configuration which are then permissible. The NACA is now making a study to determine how much improvement in Dutch roll stability might be obtained by incorporating in the basic design of an airplane features which are conducive to good stability. (See ref. 1.)



CAMPBELL

Effect of Wing Plan Form

As a preliminary step in this study, calculations were made to establish more clearly the causes of the poor Dutch roll stability of current designs. The configurations considered in the preliminary study are shown in figure 1. These configurations form a systematic series covering a range of sweep and aspect ratio.

Some of the results of stability calculations for these four configurations are shown in figure 2, which is a conventional plot of damping against period of the Dutch roll oscillation. The hatched line represents the present service requirement for damping, with values below the line being satisfactory. There are, of course, other factors such as roll-to-yaw ratio which must be considered in an over-all evaluation of lateral flying characteristics but for simplicity the present discussion will deal only with the period and damping.

Results are shown on this plot for each of the four configurations in three flight conditions: for a Mach number of 0.75 at sea level and at 50,000 feet and for a moderate lift coefficient at sea level. For the Mach number 0.75 sea-level condition, the four configurations have about the same period and damping because they were designed to have equal tail effectiveness and because, for the low lift coefficient involved (0.04), the changes in wing plan form do not appreciably alter most of the stability derivatives. As the lift coefficient is increased to a moderate value, however, the effects of wing plan form begin to become evident and the 45° swept-wing design is definitely less satisfactory than the other three. For this same lift coefficient at 50,000 feet (which corresponds to a Mach number of 0.75), all the designs are unsatisfactory and the swept designs are especially so.

Analysis has shown that the decrease in damping in going from the aspect-ratio-6 unswept design to the 45° sweptback design can be accounted for by changes in three or four of the more important stability derivatives. If the sweepback is held at 45°, only one of these derivatives can be modified appreciably by other changes in the geometry of the airplane. This derivative is $C_{l\beta}$, the rolling moment due to sideslip, which can be varied by changes in wing dihedral. Calculations for the 45° swept design showed that the sea-level conditions could be made satisfactory by the use of 5° negative wing dihedral but the damping for the altitude condition was still very unsatisfactory.

Effect of Mass Distribution

Since it did not appear feasible to obtain adequate damping by modifying the geometry of the 45° swept configuration to give it more favorable stability derivatives, attention was given to the possibility of altering the mass characteristics of the airplane to improve its stability. The pronounced effect of the product of inertia on Dutch roll stability has, of course, been known for some time. In order to get a large beneficial effect from this source, a configuration was laid out which would have a more favorable inclination of the principal axis of inertia and more favorable values of the rolling and yawing moments of inertia. A profile of the resulting design is shown on the right in figure 3, compared with the more conventional profile originally assumed for the 45° swept-wing design. For the conventional arrangement, the principal axis of inertia is inclined downward about 3° with respect to the wing because of the relatively high location of the tail assembly and fuselage at the rear of the airplane. This negative inclination of the principal axis of inertia tends to produce poor damping of the lateral oscillation. The modified arrangement has a 2° upward, or favorable, inclination of the principal axis of inertia brought about by the use of an underslung scoop inlet with the engine low at the rear and with a lower location of the rear end of the fuselage and tail surfaces. The rolling inertia factor k_x/b was reduced from 0.15 to 0.10 and the yawing inertia factor k_z/b was increased from 0.32 to 0.40 by shifting weight from the wing to the fuselage. The effect of these three changes on the stability of the 45° swept configuration for the two unsatisfactory flight conditions is shown in figure 4, which is another period-damping plot.

In figure 4, the two different mass distributions are indicated by the two profiles from figure 3. The original profile is dark and the modified profile light. The modified configuration has much better damping characteristics than the original configuration for both of these flight conditions and meets the present period-damping requirement. The figure also shows results for a third condition, Mach number 2 at 50,000 feet. These results show that the change in mass distribution also provided satisfactory stability for this supersonic-speed, high-altitude condition.

Of course, it should not be concluded from the results for this one hypothetical airplane that this procedure is a cure for the Dutch roll oscillation troubles of all designs; but the results do emphasize the fact that pronounced improvements in Dutch roll damping can be obtained in some cases by careful attention to mass distribution during the early stages of design.


DIRECTIONAL DIVERGENCE

Bell X-5 Research Airplane

Consider now the relatively new problem of directional divergence at high angles of attack. Such divergences were first noted in Langley free-flight tunnel tests of models of new highly swept fighter airplane designs. Recently, in full-scale flight tests of the Bell X-5 airplane with 60° sweep, directional divergences at high angles of attack were also encountered. (See ref. 2.) These divergences are directly related to the decrease in the directional-stability parameter $C_{n\beta}$ at high angles of attack discussed by Frank S. Malvestuto in the preceding paper. To illustrate this point let us take the case of the X-5 and see in figure 5 what the variation of $C_{n\beta}$ with lift coefficient is for this airplane with 60° sweep. Also plotted in figure 5 is the effective-dihedral parameter $-C_{l\beta}$ which is another important stability parameter affecting the directional divergence. There are other factors such as the yawing moment due to rolling C_{n_p} and the yawing moment due to aileron deflection, which affect the directional characteristics, but these parameters $C_{n\beta}$ and $-C_{l\beta}$ appear to be the most important ones affecting the directional divergence. Both the directional stability and the effective dihedral are positive over the low and moderate lift range but both drop to zero at a lift coefficient about 0.1 below the stall, and at the stall $C_{n\beta}$ is highly negative or unstable. The directional divergences encountered in flight tests of the X-5 occurred at lift coefficients approximately where these parameters dropped to zero.

In the preceding paper, Frank S. Malvestuto showed that for the X-5 airplane both $C_{n\beta}$ and $-C_{l\beta}$ dropped to zero at progressively lower angles of attack as the Mach number was increased. Presented in figure 6 are some flight-test data for the X-5 airplane which verify those force-test results. In this figure the angle of attack at which directional divergence was encountered in flight tests of the airplane is plotted against Mach number (circles). The solid line, which represents the angles of attack at which $C_{n\beta}$ dropped to zero according to force tests of the X-5, is in general agreement with the flight data. These results indicate that the directional-divergence problem for the X-5 becomes more serious at the higher Mach numbers.

Presented in figure 7 is a flight record for a divergence that occurred at a Mach number of 0.66. In this figure, the angle of attack (solid line) and the angle of sideslip (dashed line) are plotted against



REF ID: A63115

time in seconds. The maneuver which the pilot was to perform during this test was a 2g push-over, pull-up maneuver. First, a push-over to about zero g was made, then the pull-up. Because of the pitch-up tendency of the X-5, the airplane reached a higher angle of attack than had been intended. At this high angle of attack, the airplane suddenly diverged in sideslip to an angle of about 30° and then rolled off into a spin.


Delta-Wing Configuration

As another example of the directional-divergence problem, let us now take the case of a 60° delta-wing configuration tested in the Langley free-flight tunnel. The stability parameters for this model are shown in figure 8. For this model, the effective-dihedral parameter $-C_{l_p}$ remained positive over the lift range and even at the stall; a characteristic which should reduce any tendency toward directional divergence. The static directional stability or C_{n_β} characteristics of this model, however, were very poor. The parameter C_{n_β} was low at low and moderate lift coefficients and became negative at a lift coefficient well below the stall. Another unsatisfactory characteristic that cannot be seen from a plot of this type was the variation of yawing-moment coefficient with sideslip angle for this configuration.

In order to illustrate this point, let us take the condition where C_{n_β} is zero and see in figure 9 what the variation of yawing-moment coefficient with sideslip angle looks like. For small angles of sideslip, the model is neutrally stable, but at about 5° sideslip, a sharp destabilizing break occurs. This nonlinearity is apparently associated with the vortex flow from the wing-fuselage combination. When the model sideslips, the vertical tail moves into an unfavorable sidewash field created by the vortex flow and loses effectiveness. In flight tests of this model at high angles of attack, violent directional divergences were obtained.

In figure 10 are shown the results of some of the attempts made to eliminate this divergence for the delta-wing model. Figure 10 is the plot of yawing-moment coefficient against angle of sideslip for the basic design (solid line) and for various modified arrangements (dashed lines).

The first modification considered was an increase in tail size as shown by the dotted lines in the sketch. This large tail provided stability at low angles of sideslip but a sharp destabilizing break still occurred at about 5° sideslip; so the model was about as unstable in this range as before. In flight tests of the model with this large tail, the



directional divergence was delayed to a higher angle of attack but it still occurred at angles of attack below the stall. The further addition of midspan leading-edge slats provided a small improvement at low angles of sideslip and a large improvement at high angles of sideslip so that the over-all effect was a stable and fairly linear variation of yawing-moment coefficient with sideslip over the sideslip range. The slat apparently interrupted the vortex flow which was causing the destabilizing break in the yawing-moment curve. In flight tests of the model with both the large tail and the leading-edge slat, no directional divergences were encountered, even at the stall.

CONCLUDING REMARKS

The recent NACA work on the problems of unsatisfactory damping of Dutch roll oscillations and of directional divergence at high angles of attack can be summarized briefly as follows:

1. Improvements in damping of Dutch roll oscillations can be obtained without resort to artificial stabilizing devices by careful attention to mass distribution during the early stages of design.
2. The directional divergences at high angles of attack associated with highly swept designs can be eliminated in some cases by the use of adequate-size vertical tails and perhaps some flow-control device such as leading-edge slats.

REFERENCES

1. Campbell, John P., and McKinney, Marion O., Jr.: A Preliminary Study of the Problem of Designing High-Speed Airplanes With Satisfactory Inherent Damping of the Dutch Roll Oscillation. (Prospective NACA paper.)
2. Finch, Thomas W., and Walker, Joseph A.: Static Longitudinal Stability of the Bell X-5 Research Airplane With 59° Sweepback. NACA RM L53A09b, 1953.

CONFIGURATIONS USED IN CALCULATIONS

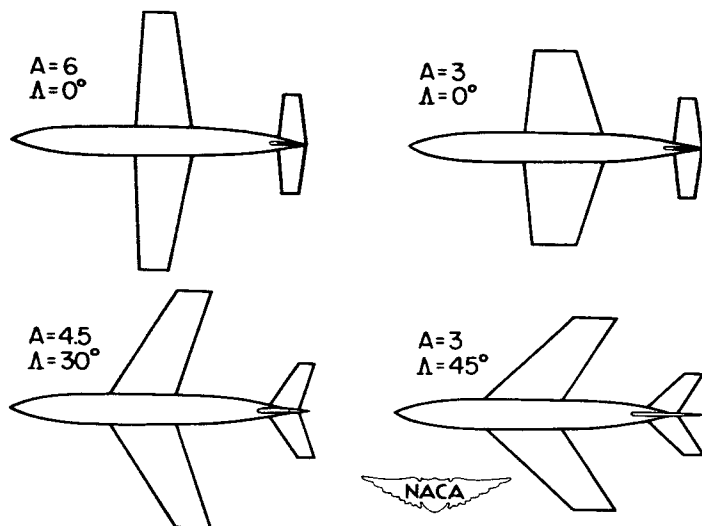


Figure 1

EFFECT OF WING PLAN FORM ON DAMPING

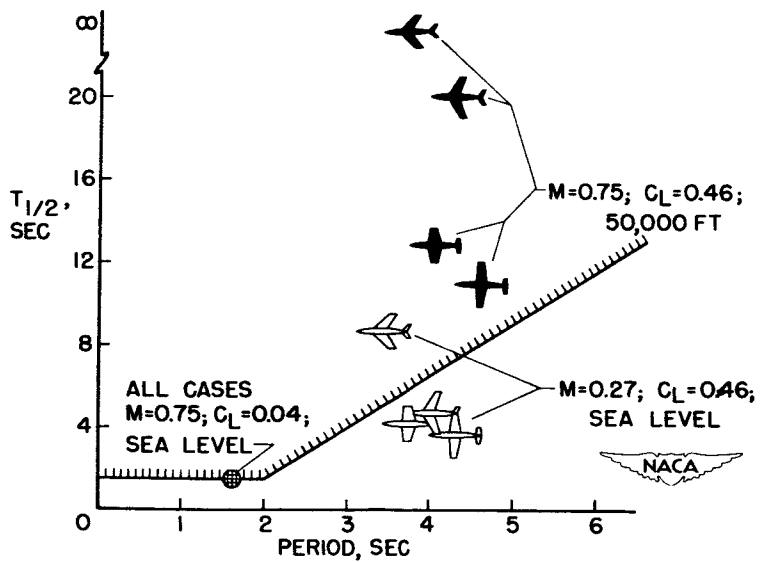
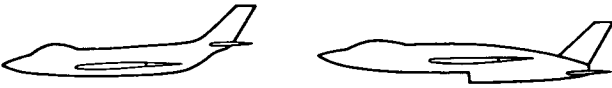


Figure 2

MASS DISTRIBUTION OF TWO DESIGNS



INCLINATION OF PRINCIPAL AXIS, ϵ	-3°	2°
ROLLING INERTIA FACTOR, k_{x_0}/b	0.15	0.10
YAWING INERTIA FACTOR, k_{z_0}/b	0.32	0.40




Figure 3

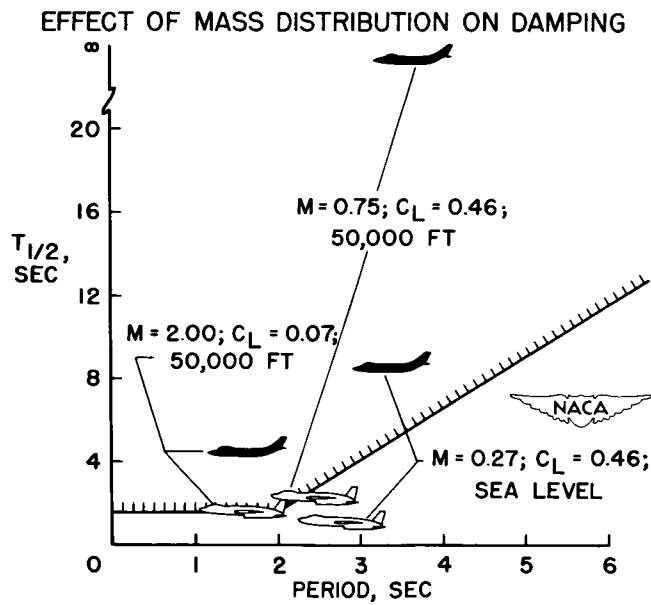


Figure 4

CONFIDENTIAL

UNCLASSIFIED

STABILITY PARAMETERS FOR X-5 AIRPLANE 60° SWEEP

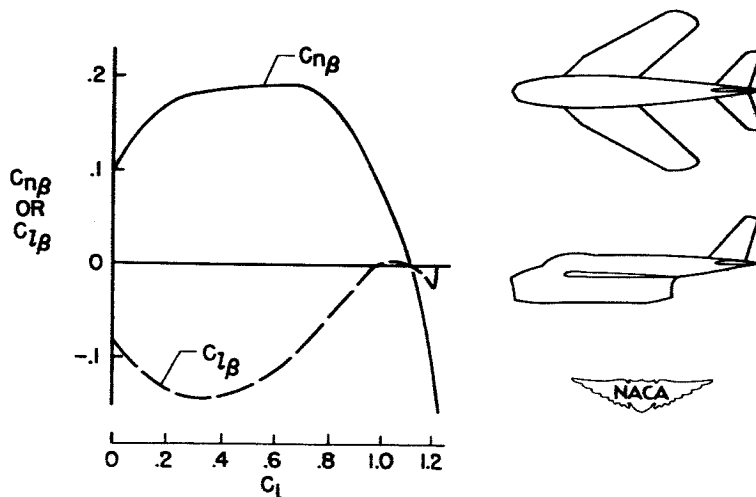


Figure 5

EFFECT OF MACH NUMBER ON DIRECTIONAL DIVERGENCE OF X-5 AIRPLANE WITH 60° SWEEP

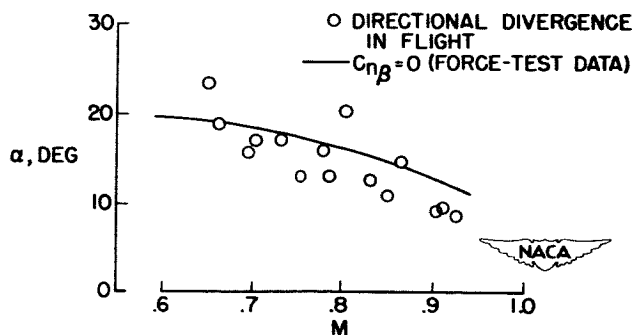


Figure 6

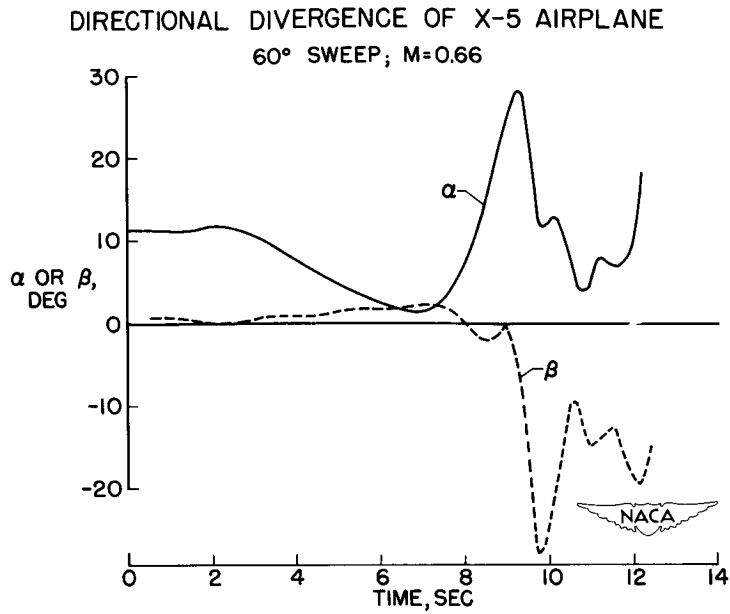


Figure 7

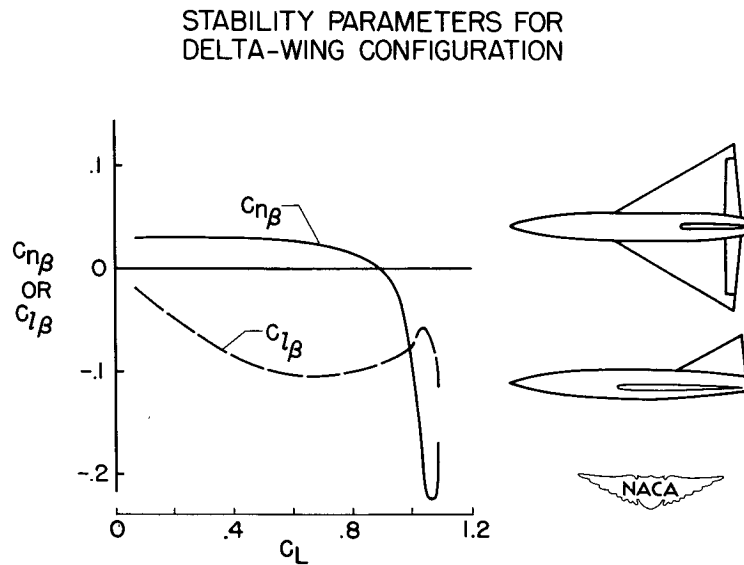


Figure 8

DIRECTIONAL STABILITY OF DELTA-WING MODEL
 $C_{n\beta} = 0 (\beta < 5^\circ)$

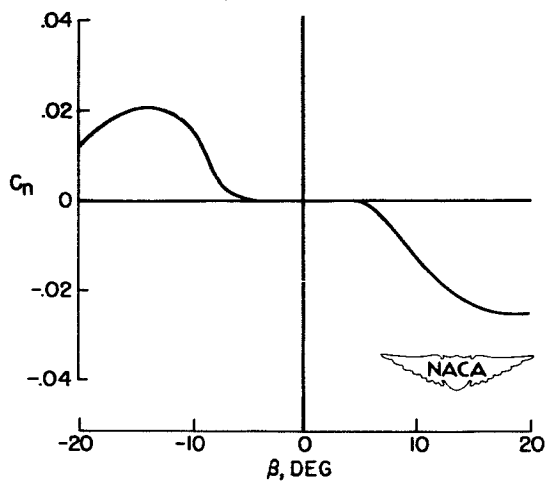


Figure 9

DIRECTIONAL STABILITY OF DELTA-WING
 MODEL, MODIFIED

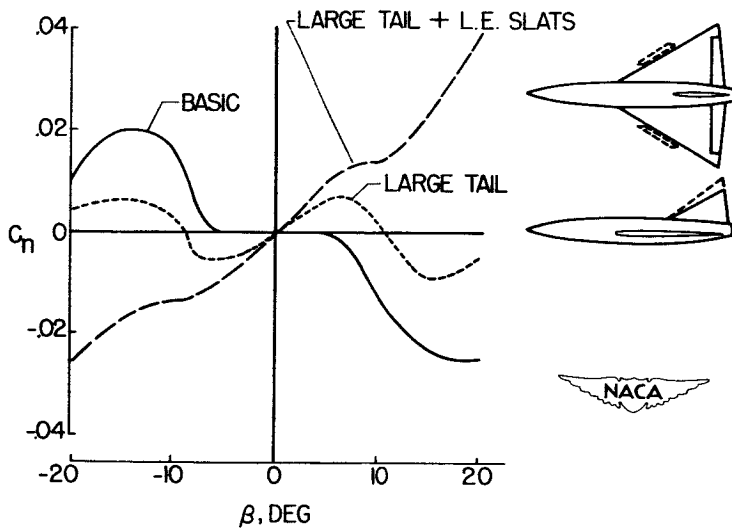


Figure 10

CONFIDENTIAL

DECLASSIFIED

THE EFFECT OF STABILITY AND CONTROL CHARACTERISTICS ON THE TRACKING EFFECTIVENESS OF AIRPLANES

By George A. Rathert, Jr.

Ames Aeronautical Laboratory


INTRODUCTION

Three major factors affect the "kill probability" of a fighter: the tracking of the target by the pilot, the fire-control-system computations, and the ballistics. This paper is a discussion of the factor of direct concern to the aerodynamicist, the effect of the airplane stability and control characteristics on the pilots' tracking accuracy.

Flying-qualities specifications have always been based to a certain extent on the pilots' opinion of the airplane as a gun platform. The preceding papers remind us, however, that, as airplane speeds and altitudes increase and weapons systems become more complicated, these specifications can become very difficult and expensive to meet. It is increasingly important, therefore, to examine the stability and control requirements rigorously using measured tracking performances as a guide. Both the Langley and Ames Laboratories are conducting flight tests to study this problem (refs. 1 to 3), either by correlating the tracking performances of existing fighters with their flying qualities, or by testing airplanes equipped to vary significant stability parameters in flight.

TEST METHOD

The flight-test maneuver used at the Ames Laboratory to measure tracking ability is shown in figure 1. From an initial lateral displacement the tracker swings in behind the target, tracks in level flight, and attempts to follow as the target abruptly enters a steady turn. The maneuver provides, at a selected Mach number and altitude, 45 seconds of tracking in level flight, 1 to 10 seconds of tracking under transition conditions where the normal acceleration is changing as rapidly as possible, and 45 seconds of tracking in a steady accelerated turn. The tracking accuracy will be indicated by the aim wander, the standard deviation from the mean, in mils. To give this number more meaning, the aiming point would be within a circle of a radius equal to the aim wander approximately 70 percent of the time.



RATHERT

DISCUSSION

Typical World War II Fighters

The aim wander in level flight and steady accelerated turns is discussed first. Figure 2 shows the yaw and pitch aim wanders as functions of normal acceleration for two typical World War II fighters, the North American F-51H and the Grumman F8F-1, tested with fixed sights and visual target presentation. The shaded areas contain 120 test runs per airplane made by three pilots. The points were obtained throughout the range of normal operating conditions: normal accelerations up to the buffet boundaries, Mach numbers from 0.4 to 0.7, and altitudes of 10,000 and 20,000 feet. There were no significant changes with flight conditions or pilots. The average values by airplane were 1.6 and 1.3 mils for the F-51H and 1.9 and 1.6 mils for the F8F-1. These values are similar to the results of gunnery tests of the Grumman F9F-2 and McDonnell F2H-2 airplanes made at the U. S. Naval Air Test Center at Patuxent River, Md. (refs. 4 and 5). It is interesting to note that they are also comparable to the accuracies ascribed to current models of each of the other two major components of the weapons system, 2 to 3 mils for a 50-calibre machine gun and 3 mils for a disturbed-reticle sight computer. Aim wanders less than 4 mils appear to represent reasonably good tracking.

Typical High-Performance Fighters

With the World War II fighter data as a basis for comparison, the effects of extending the ranges of performance and stability and control characteristics covered to values typical of current operational day fighters were examined by testing the North American F-86A and F-86E airplanes. Both the F-86A and the F-86E were tested to investigate the effects of changing from a conventional power-assisted elevator control with aerodynamic stick forces to an irreversible, all-movable tail with completely artificial stick-force feel. The aim-wander data are presented in figure 3. The shaded regions include 86 and 130 test runs, respectively, by two pilots and cover the normal operating conditions: normal accelerations up to the buffet boundary, Mach numbers from 0.7 to 0.97, and altitudes of 10,000 and 35,000 feet. Within the normal operating envelope there again were no significant changes with flight conditions. The average values were 2.6 and 2.7 mils for the F-86A and 2.6 and 2.5 mils for the F-86E; these values are somewhat higher than but still comparable with those for the World War II fighters.

Looking now at the individual test points, contrary to the case with the World War II fighters it was possible to operate the swept-wing fighters at accelerations significantly higher than their buffet boundaries. In this partially stalled regime they were subject to three problems which affect

CONFIDENTIAL

SECRET

the tracking effectiveness: buffeting, lateral unsteadiness (either a mild roll-off or an aileron over-controlling tendency), and the longitudinal pitch-up discussed in the preceding papers. Further discussion of these problems is presented in references 6 and 7. By correlating the pilots' notes with particular test points it has been deduced that the amount of buffeting and the lateral unsteadiness present before the pitch-up made tracking more difficult but did not result in aim wanders above 4 mils. The initial pitch-up tendency produced the errors of 6 to 12 mils shown in the figure, whereas the fully developed pitch-up introduced such gross errors that tracking was impossible. The equally large errors for the F-86A and F-86E show that the change in longitudinal control to the all-movable tail with artificial stick-force feel was not an acceptable solution to the pitch-up problem from a tracking standpoint, despite the favorable opinion of the pilot.

Abruptly Maneuvering Conditions

The two comparisons presented, that between the World War II and the swept-wing fighters and that between the two different control systems, indicate that the ranges of airplane characteristics covered so far do not significantly affect the ability to track in level flight or steady turns. However, if it can be assumed that the sight mechanism can compute the correct lead angle rapidly enough, then the tracking under transition conditions shown in figure 4 is also of interest. The small sketch indicates the transition region where the target airplane is changing normal acceleration as abruptly as possible.

The table shows the average aim wanders by airplane for both the steady turns and the transition region, and the ratio between the two. For the World War II fighters the average radial aim wanders under transition conditions were 1.4 times greater than those in steady accelerated turns. For the high-performance fighters they were 1.8 to 2.2 times greater.

Sources of Aim Wander

The sources of aim errors in both steady accelerated turns and in the transition region were identified by analyzing the frequency content of the aim-wander records. There were two predominant frequencies in the aim wander, indicating two predominant sources of error: first, the frequency of the movements of the control surfaces and, second, the short-period oscillatory frequencies of the airframe. In steady turns (figs. 5(a) and 5(b)) the aim wanders identified with the control movements were generally much more significant than those identified with the oscillatory characteristics. In the transition region (fig. 6) the effects of the oscillatory characteristics became equally prominent, apparently due to

CONFIDENTIAL

CONFIDENTIAL

increased excitation of airplane oscillations by the necessary control movements. This explains the increased aim wanders in the transition region noted in figure 4. The transition aim wanders were largest for the more lightly damped high-performance fighters.

The frequency analysis suggests that a closer scrutiny of the effects of the control system and of the oscillatory characteristics of the airframe, including extrapolations to values typical of future designs, is necessary.

Longitudinal Control Characteristics

With regard to control characteristics, the effects of changing the longitudinal control sensitivity have been studied on an F-51H modified to vary the stick gearing and stick-force gradients in flight (see ref. 8). Figure 7 shows the ranges of angular stick movement per g and stick force per g which have been tested. Including the four existing fighters, stick-force gradients from 32 pounds per g have been tested on the F-86A to 0.15 pound per g on the modified F-51H and stick-movement gradients from 9° per g on the F-86A to 0.1° per g on the modified F-51H. The pilot has been able to track with aim wanders of 3 mils or less with every system set up, including systems that were completely unacceptable for formation, instrument, or even cross-country flying. The pilot effort or work required to track accurately is greater with the very sensitive systems but the time spent in flight actually tracking is less than that for the other types of flying for which the configurations are already rated unacceptable by the pilot. At least for fixed sights and visual target sighting, it must be concluded that the longitudinal-control requirements needed to insure effective tracking are less severe than those already imposed for formation and instrument flying (ref. 9).

Lateral Oscillatory Characteristics

The other significant sources of aim wander indicated by the frequency analysis - the short-period oscillations - have also been investigated in the lateral case with variable-stability airplanes, a Grumman F6F and a North American F-86 at Ames and a Lockheed TV-2 at Langley. The ranges of lateral oscillatory characteristics which have been tested are indicated in figure 8; the period, the time to damp to half amplitude, and the Air Force specifications defining the boundary between satisfactory and unsatisfactory characteristics are shown. The intensely shaded region shows the range of period and damping covered by the four existing fighters for which the tracking effectiveness already has been shown. Note that the tests included configurations that did not meet the flying-qualities requirements. The right-hand large lightly shaded region indicates the

CONFIDENTIAL

CONFIDENTIAL

001453715

extension to regions of very poor damping at periods from 2 to $4\frac{1}{2}$ seconds which was accomplished by using a variable-stability F6F airplane. The left-hand cross-hatched area indicates the extension to low periods, of the order of 1 second, achieved on the variable-stability F-86A. The tests of the variable-stability TV-2 made at Langley (ref. 3) were extended to zero damping at periods of 1.5 to 2.5 seconds.

The effects of the oscillatory characteristics in smooth air are summarized on the left-hand side of figure 9. The yaw aim wander is shown as a function of period for two degrees of damping. The shaded region marked "high damping" is the envelope of all the test points for a time to damp to half amplitude of approximately 1 second. The region marked "low damping" is the envelope of test points for times to damp to half amplitude of 5 to 14 seconds.

All the test points are below 4 mils, including the points in the low-damping region representing configurations unsatisfactory for formation and instrument flying. As with the longitudinal control characteristics, the lateral oscillatory characteristics are not critical with regard to tracking effectiveness in smooth air. In addition to the period and damping, the effect of the roll-to-yaw ratio was investigated and a similar conclusion was reached. It should be noted that, although the 4-mil wanders appear reasonably good with present fire-control equipment and armament, these values can be further reduced if necessary by providing better damping.

All the data examined up to this point were taken in normally smooth air considered by the pilots to be typical of air-to-air gunnery at the test altitudes of 10,000 to 35,000 feet. For lower altitudes and air-to-ground gunnery, the effects of operating in rough air become of considerable importance, as shown on the right-hand side of figure 9. The magnitude of the rough air in which the runs were made is best expressed by the yaw angle of the resulting airplane motions if the controls were held fixed. Since the magnitude of the response depends on the stability parameters (ref. 10), the range of responses for the F6F will be given. The standard deviation of the yawing motions ranged from 14.1 mils at a period of 4.5 seconds and time to damp to half amplitude of 1.4 seconds to 128.5 mils at a period of 2.3 seconds and 11.5 seconds to damp to half amplitude. A considerably amplified discussion of these tests is presented in reference 2.

It is apparent that moderately rough air introduces unacceptably large tracking errors for the points corresponding to the combination of short periods and low damping. The short periods become impossible for the pilot to control; the low damping is identified with large excitations of the airplane in response to gusts. The tracking is satisfactory, or at least marginally so, for points representing either long, controllable periods or high damping. The importance of providing good yaw damping in future fighters is strikingly illustrated by the aim wanders at a period

of 1 second; the aim wander was reduced from 14 mils to 4 mils simply by making the variable-stability gear act in effect as a yaw damper and increase the damping in yaw C_{nr} .

Computing Gunsight

The effects of the stability and control characteristics on the pilots' ability to track with a fixed sight have been examined; it is now of interest to determine to what extent the conclusions formed would be affected by adding the dynamic characteristics of a typical disturbed-reticle computing sight to the system. Figure 10 shows the tracking performance with the A-1 sight in the F-86A airplane which was tested previously with a fixed sight. As shown by the small diagram, it is necessary to consider two aim wanders, the sight-line error which represents the tracking error of the pilot, and the control-line or gun-bore-axis wander which is a measure of the disturbances the pilot has to impose on the guns in order to track. It should be emphasized that the gun-axis wander or motion is being considered, not the pointing error.

For the normal A-1 sight at the 1,000-foot range corresponding to the fixed-sight tests, both the sight-line and the gun-bore-axis wanders are of the same accuracy as the fixed-sight results; therefore, the previous conclusions regarding the effects of the airplane stability and control characteristics should apply.

Since this type of sight is also being used with similar airframes but more advanced weapons, results were also obtained at a range of 3,000 feet. The sight-line wander is still comparable with the fixed-sight results but the gun-bore-axis wander is significantly higher. A frequency analysis of this wander indicates that it occurs primarily at very low frequencies, 0.1 cycle per second or less. It is believed to be caused by the fact that the pilot handles the airplane much more slowly and smoothly when correcting errors in order to avoid exciting unwanted disturbances of the computing reticle.

An additional investigation of tracking with a computing sight in an F9F-3 under various maneuvering conditions is presented in reference 11.

CONCLUSIONS

The results of these investigations may be summarized as follows:

1. The aim wanders for fighter airplanes typical of those from World War II up to current types were 4 mils or less throughout their normal ranges of operating conditions except under very abruptly maneuvering conditions.

CONFIDENTIAL

CONFIDENTIAL

SECRET

2. Tracking errors were excessive for current swept-wing fighters above their buffet boundaries in the pitch-up regime. Provision of an all-movable tail with artificial stick-force feel was not a remedy from the tracking standpoint.

3. The frequencies present in the aim wanders corresponded primarily to the frequencies at which the control surfaces were operated and secondarily to the short-period oscillatory frequencies of the airframe.


4. Detailed investigations of these two sources, including extrapolations to values typical of future fighters, showed that:

(a) The longitudinal control-system characteristics were less critical for tracking than for instrument and formation flying which are covered by the flying-qualities specifications already imposed.

(b) The lateral oscillatory characteristics were critical only in rough air at low periods in combination with poor damping. By providing good yaw damping, it was possible to track reasonably well with periods as low as 1 second. Otherwise the lateral-oscillatory-characteristics requirements for good tracking also would be less severe than those imposed for good formation and instrument-flying handling qualities.

5. The addition of a normal disturbed-reticle computing sight did not affect the tracking accuracy at normal ranges and the preceding conclusions should apply.

[REDACTED]

1. Rathert, George A., Jr., Gadeberg, Burnett L., and Ziff, Howard L.: An Analysis of the Tracking Performance of Two Straight- and Two Swept-Wing Fighter Airplanes With Fixed Sights in a Standardized Test Maneuver. (Prospective NACA paper.)
 2. McNeill, Walter E., Drinkwater, Fred J., III, and Van Dyke, Rudolph D., Jr.: A Flight Study of the Effects on Tracking Performance of Changes in the Lateral Oscillatory Characteristics of a Fighter Airplane. (Prospective NACA paper.)
 3. Kuehnelt, Helmut A., Beckhardt, Arnold R., and Champine, Robert A.: A Flight Investigation of the Effects of Varied Lateral Damping on the Effectiveness of a Fighter Airplane as a Gun Platform. NACA RM L53F08a, 1953.
 4. Davis, W. V., Jr.: Determination of Tracking Error for F9F-2 and F2H-2 Using Fixed Optical Sight. Letter Report No. 1 - Final Report. Project TED No. PTR-AR-6024, Armament Test Div., U. S. Naval Air Test Center (Patuxent River, Md.), Oct. 12, 1951.
 5. Davis, W. V., Jr.: Determination of Tracking Error for F2H-2 Using Fixed Optical Sight on a Maneuvering Target. Letter Report No. 1 - Final Report. Project TED No. PTR AR 6024.1, Armament Test Div., U. S. Naval Air Test Center (Patuxent River, Md.), Feb 21, 1952.
 6. Anderson, Seth B., and Bray, Richard S.: A Flight Evaluation of the Longitudinal Stability Characteristics Associated With the Pitch-Up of a Swept-Wing Airplane in Maneuvering Flight at Transonic Speeds. NACA RM A51I12, 1951.
 7. McFadden, Norman M., Rathert, George A., Jr., and Bray, Richard S.: The Effectiveness of Wing Vortex Generators in Improving the Maneuvering Characteristics of a Swept-Wing Airplane at Transonic Speeds. NACA RM A51J18, 1952.
 8. Abramovitz, Marvin, Schmidt, Stanley F., and Van Dyke, Rudolph D., Jr.: Investigation of the Use of a Stick Force Proportional to Pitching Acceleration for Normal-Acceleration Warning. NACA RM A53E21. (Prospective NACA paper.)
 9. Anon.: Flying Qualities of Piloted Airplanes. USAF Spec. No. 1815-B, June 1, 1948.
- 

CONFIDENTIAL

DECLASSIFIED

10. Bird, John D.: Some Calculations of the Lateral Response of Two Airplanes to Atmospheric Turbulence With Relation to the Lateral Snaking Problem. NACA RM L50F26a, 1950.
11. Cheatham, Donald C., Mathews, Charles W., and Harper, John A.: A Study of Visual Interception Attacks on a Nonmaneuvering Airplane Target. NACA RM L53E01, 1953.

STANDARD TEST MANEUVER

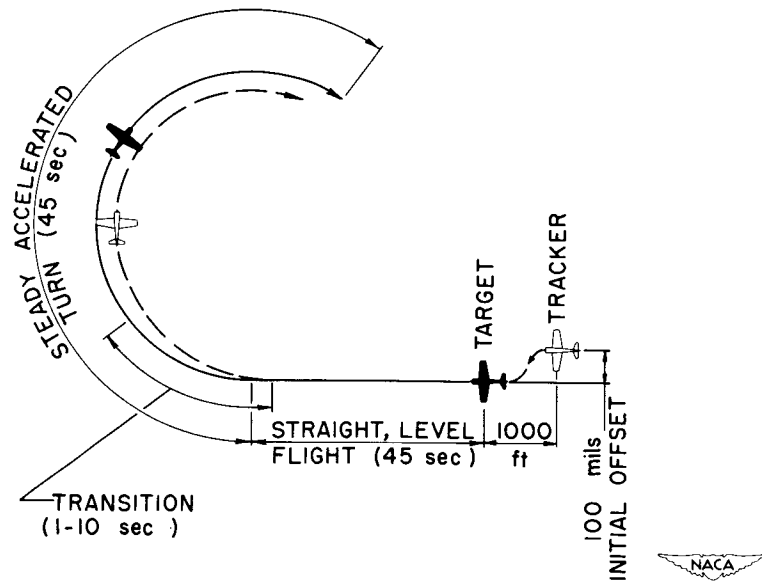


Figure 1

AIM WANDER OF WORLD WAR II FIGHTERS

RANGE OF TEST CONDITIONS

1 TO 4 g AND 0.4 TO 0.5 MACH NUMBER AT 10,000 ft
1 TO 4 g AND 0.4 TO 0.7 MACH NUMBER AT 20,000 ft

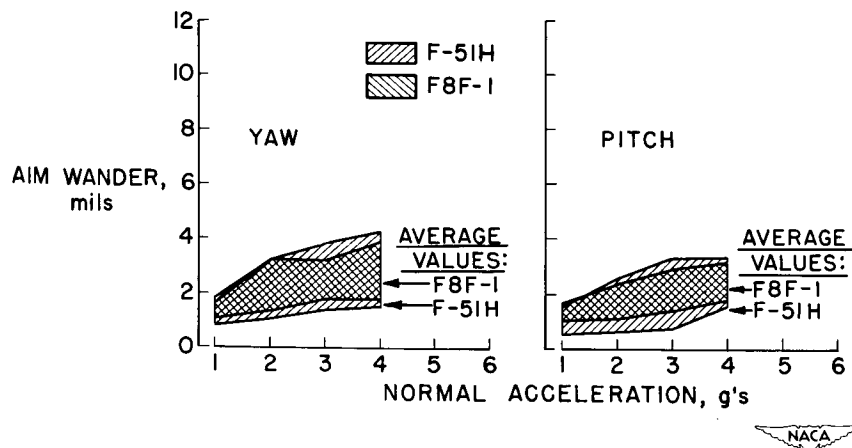


Figure 2

AIM WANDER OF SWEEP-WING FIGHTERS

RANGE OF TEST CONDITIONS

1 TO 5g AND 0.7 TO 0.90 MACH NO. AT 10,000 ft
 1 TO 3g AND 0.7 TO 0.97 MACH NO. AT 35,000 ft

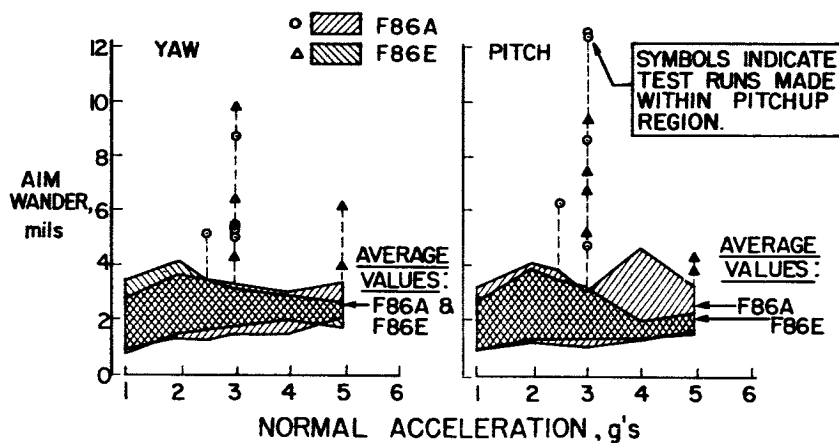


Figure 3

TRACKING ERRORS WITH RAPIDLY MANEUVERING TARGET

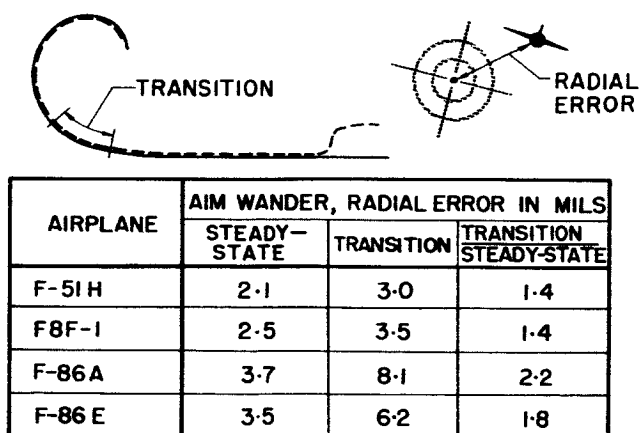


Figure 4

FREQUENCY ANALYSIS OF AIM WANDER AND CONTROL MOTION

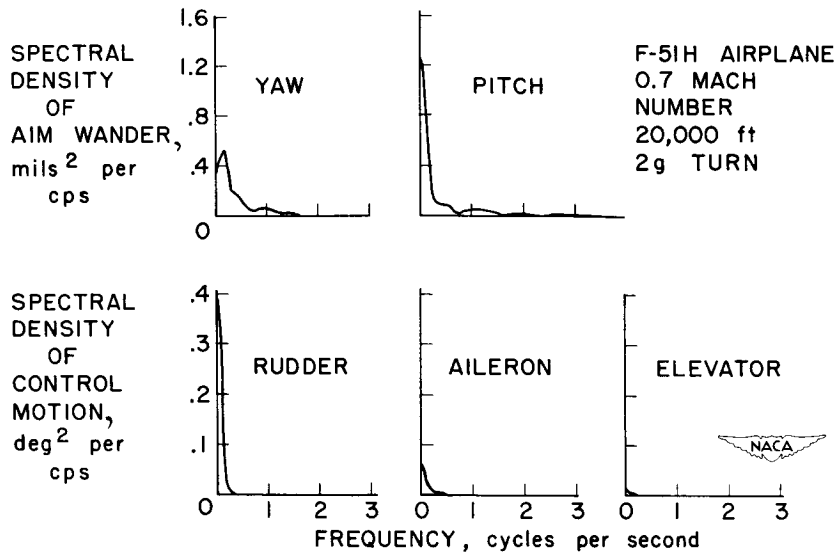


Figure 5(a)

FREQUENCY ANALYSIS OF AIM WANDER & CONTROL MOTION

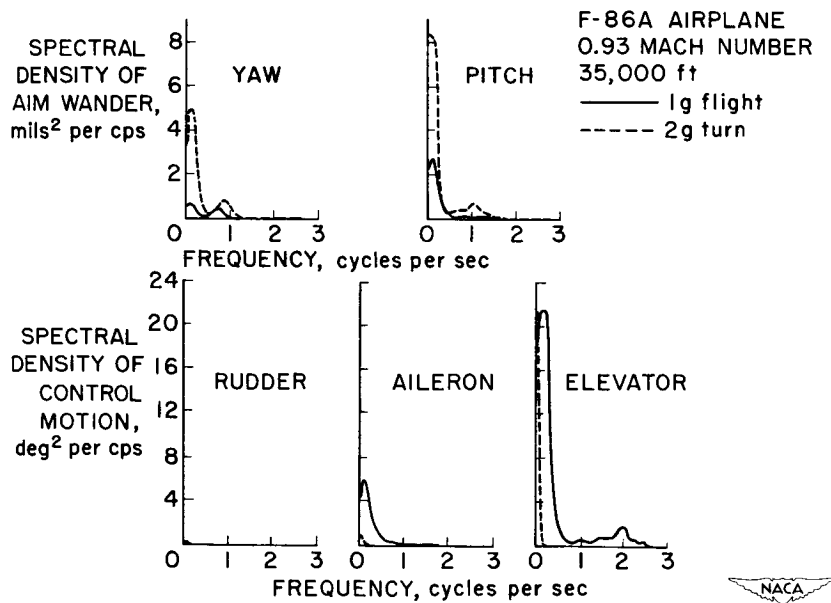


Figure 5(b)

CONFIDENTIAL

DECLASSIFIED

FREQUENCY ANALYSIS OF TRANSITION REGION AIM WANDER

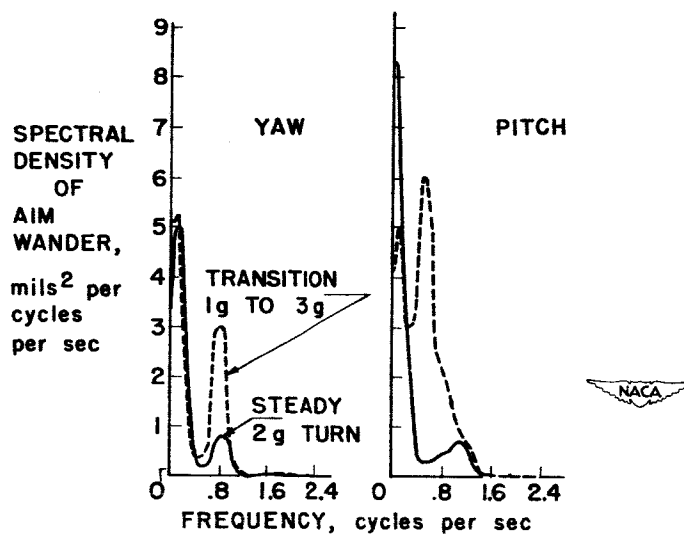


Figure 6

LONGITUDINAL-CONTROL SENSITIVITIES TESTED

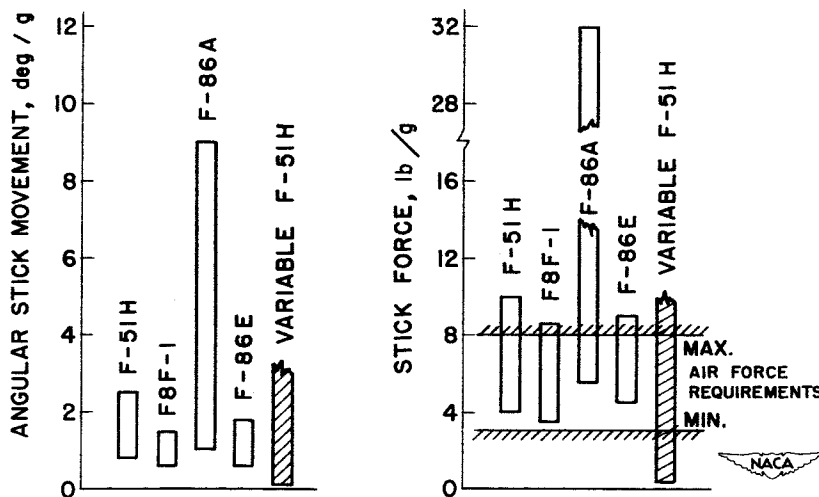


Figure 7

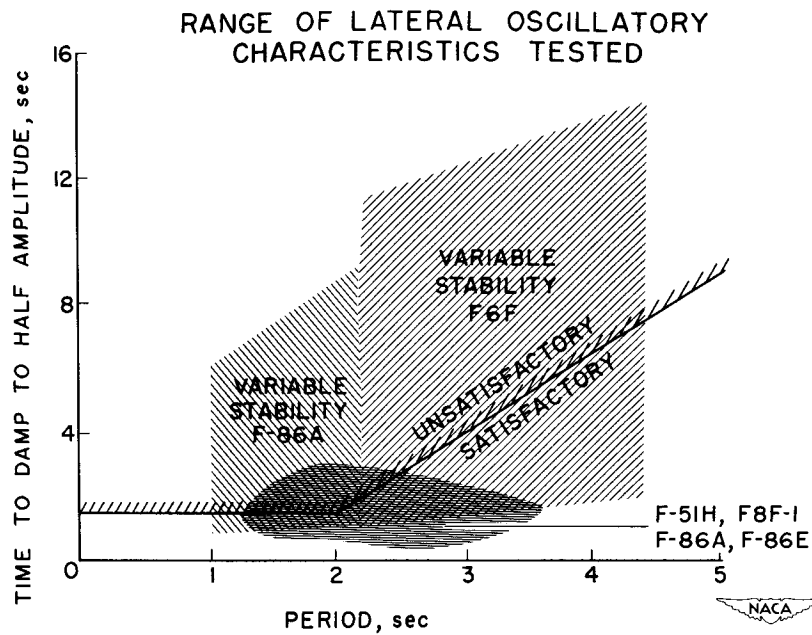


Figure 8

EFFECT OF LATERAL OSCILLATORY CHARACTERISTICS

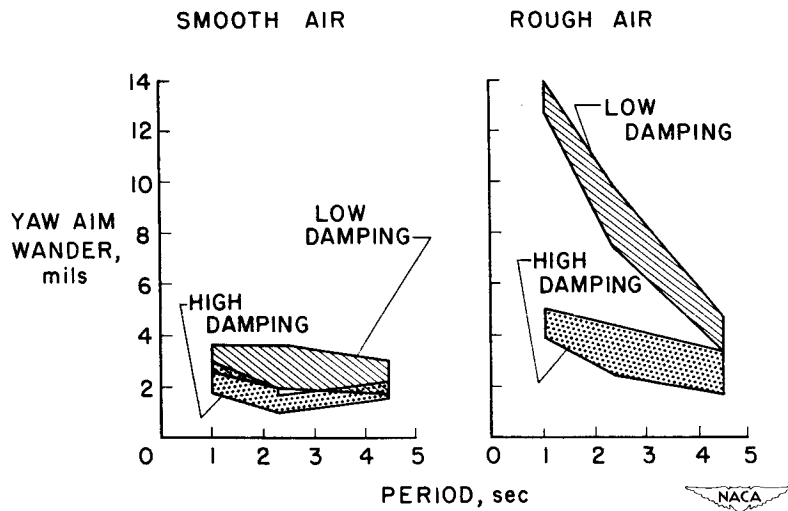


Figure 9

TRACKING WITH NORMAL COMPUTING GUNSIGHT

F86A AIRPLANE, A-1 SIGHT

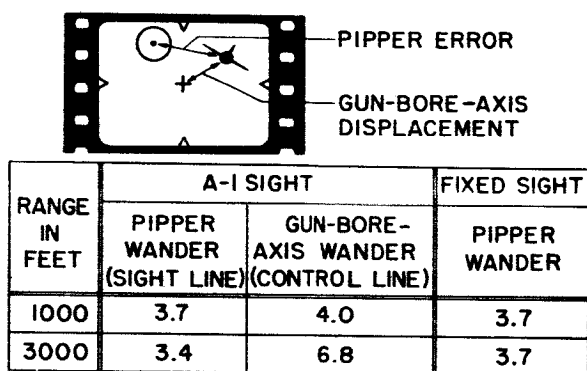


Figure 10

CONFIDENTIAL

DECLASSIFIED

DATA ON SPOILER-TYPE AILERONS


By John G. Lowry

Langley Aeronautical Laboratory

Interest in spoiler-type ailerons has been intensified recently mainly because they give high reversal speeds for the thin, flexible wings now being used. For the purpose of this paper the term "spoiler" will be applied to many different aileron configurations that obtain their effectiveness by reducing the lift on one wing. For the sake of completeness, a bibliography on spoiler-type controls is included; these papers are arranged according to date of publication.

Examination of spoiler data given in the bibliography indicates that spoilers can be designed to provide adequate effectiveness at subsonic, transonic, and supersonic speeds but at subsonic and transonic speeds plain spoilers do not, in general, provide linear variation of effectiveness with projection, particularly at the lower velocities. In addition, recent data on thin wings (6 percent thick or less) show that a region of ineffectiveness exists at high angles of attack. Using a slot through the wing behind the deflected spoiler (see refs. 1 to 5) alleviates the ineffectiveness associated with both low projections and high angles of attack.

Figure 1 illustrates the effect of the slot. On the left, the rolling-moment coefficient C_l is plotted against spoiler projection δ_s for a plain and a slotted spoiler on an unswept wing (unpublished data). For projections of less than 1 percent the plain spoiler is seen to be ineffective. If a slot is added behind the spoiler and, in this case, a deflector is added to the lower surface, the effectiveness is almost linear with projection and considerably greater than for the plain spoiler. The nonlinearity of control effectiveness of the plain spoiler can be masked to some extent by providing aileron-stick deflections that will rapidly deflect the spoiler near neutral. Although this nonlinear stick-aileron motion may provide satisfactory control for this condition, the control effectiveness will not be satisfactory at high angles of attack as shown by the right-hand portion of figure 1. Here C_l is plotted against angle of attack α for a spoiler on a 30° swept wing of aspect ratio 4 (unpublished data). The plain spoiler is ineffective above an angle of attack of about 13° . The addition of the slot and deflector increases the effectiveness at all angles of attack and provides control up to 24° . This ineffectiveness at high angles of attack results from flow separation at the wing leading edge and is almost independent of spoiler projection. It is, however, alleviated to some extent by decreases in the wing taper ratio and wing sweep, and by increases in the Reynolds number.




The use of leading-edge devices to delay leading-edge separation would be expected to improve the effectiveness of a spoiler aileron. Figure 2 shows the effect of one such device - a drooped leading edge and chord-extension - on the effectiveness of both a plain and slotted spoiler on a 6-percent-thick, 45° sweptback wing of aspect ratio 4 and taper ratio 0.3 (unpublished data). For both the plain spoiler and the spoiler-slot-deflector, where the deflector projection δ_d is three-fourths of the spoiler projection δ_s , the addition of the leading-edge modification improved the spoiler effectiveness, particularly at moderate angles of attack. These data indicate that modifications necessary from a longitudinal-stability point of view should be beneficial if they delay or eliminate the leading-edge separation.

Since the slots are desirable for almost all configurations and necessary in many cases at subsonic speeds, their effectiveness at supersonic speeds is of interest. Figure 3 shows the variation of rolling-moment coefficient with angle of attack for both a plain spoiler and a spoiler-slot-deflector on a swept and an unswept wing at a low supersonic speed, $M = 1.20$ (unpublished data). The addition of the slot and deflector increased the effectiveness of the plain spoiler at all angles of attack for both wings. Some preliminary results at a Mach number of 1.6 indicate the same trends as do these data at $M = 1.20$. Thus, the slots that are so desirable at subsonic speeds are also beneficial at supersonic speeds.

In order to realize the advantages of low twisting moment and resulting high reversal speed, the wing structure with the spoiler must be as stiff as with other types of ailerons. Fortunately, spoilers should be located well to the rear of the wing and, for most spoiler and spoiler-slot configurations, slots through the wing or breaks in the skin can be located behind the torque box and should not seriously reduce the torsional stiffness of the wing.

The next part of the discussion is concerned with the location of spoilers on wings of different plan forms. Figure 4 shows the most satisfactory location for spoiler ailerons on swept wings. The results of many investigations at subsonic, transonic, and supersonic speeds (refs. 5 to 21 and unpublished data) have indicated that for best effectiveness the spoilers should be located in the shaded area. The forward or chord-wise limit has been established from two considerations: (1) ineffectiveness at low projections (since this ineffectiveness increases with distance from trailing edge) and (2) unacceptable lag at low speeds. For configurations that do not operate at low speeds (for example, supersonic missiles), the lag may not be a determining factor as it decreases with increases in speed. The chord positions referred to are shown schematically on the right of figure 4. The spoiler location is considered



CONFIDENTIAL

DECLASSIFIED


as the point of highest deflection. The spanwise limits y_1 and y_0 are a function of the wing sweep.

Figure 5 shows the effect of sweep on these spanwise limitations. On the left is a typical example of the variation of effectiveness with aileron span for ailerons starting at the wing tips. For the unswept wing (unpublished data), the inboard 25 percent of the span does not give any appreciable rolling moment and, for the 50° swept wing (ref. 18), the outboard 15 percent is ineffective. From several similar investigations at both subsonic and supersonic speeds, the approximate variation with sweep for the inboard end y_1 and the outboard end y_0 has been established as shown on the right in figure 5. This plot shows that, as the sweep of the wing is increased, the spoiler should be moved inboard for best effectiveness.

Figures 6 and 7 show the most satisfactory locations for spoilers on 60° delta wings. The only limitation, based on the available data (refs. 22 and 23 and unpublished data), is the forward location of the spoilers. This limitation is based on ineffectiveness at small angles of attack at subsonic speeds. Figure 7 gives a typical example of the effect of chordwise location. The effectiveness C_l is plotted against projection at $M = 0.85$ for spoilers located at 60 percent root chord in the unsatisfactory region and at 93 percent root chord in the satisfactory region on a delta wing at zero angle of attack. It can be seen that the forward location is ineffective in producing rolling moment up to about 10 percent projection. The rearward location gives effectiveness throughout the deflection range. As the angle of attack is increased the forward spoiler tends to become more effective and has substantially the effectiveness of the rearward spoiler at 12° angle of attack.

A further restriction is necessary if the delta wing is equipped with a double slotted flap (ref. 23). In this case, the spoiler should be located on the flap (fig. 6). The right-hand portion of figure 7 shows the rolling-moment coefficient plotted against spoiler projection for a spoiler located ahead of the flap - the position found to be most satisfactory for relatively thick straight and swept wings - and for a spoiler located on the flap. It is obvious that when the spoiler is located ahead of the flap there is an undesirable variation of effectiveness with projection while the spoiler located on the flap provides sufficient control and has an almost linear variation with projection.


Now that the desirable location for spoilers on wings has been established to some extent, the next problem is to determine how big the spoilers have to be. At subsonic and transonic speeds experimental results must be relied on almost entirely. The results of configurations close to the desired one can then be adjusted to the desired configuration by using standard aileron design methods (refs. 24 to 26). The



effect of any changes in spoiler configuration must be obtained from existing experimental data. In general, flap-type spoilers will have about 10 percent less effectiveness than spoilers projected normal to the wing surface. An analysis of existing data has indicated that to provide adequate control spoilers should have a span of from 50 to 70 percent of the wing semispan and a projection of 7 to 10 percent of the mean chord. At supersonic speeds some helpful information is available concerning spoilers projected normal to the surface. Using a shock-expansion-separation theory the pressures ahead of the spoilers can be estimated and with the aid of empirical relationships the pressures behind the spoiler can be obtained (refs. 20 and 27). Thus for plain spoilers at supersonic speeds the effectiveness may be estimated with some degree of accuracy.

In the design of any control system it is necessary to know the operating forces of the control. The hinge-moment results for spoilers are not nearly so extensive at high speeds as are effectiveness data. The few data available do, however, show the general trends that are to be expected. Figure 8 shows the hinge-moment characteristics of flap-type spoilers on a 60° delta wing. The results (unpublished data) are presented as the variation of hinge-moment coefficient C_h with rolling-moment coefficient C_l , so that a comparison with a flap-type aileron of about the same size can be made. It can be seen that the hinge moments for this type of spoiler are of about the same magnitude as those of the flap at both subsonic and transonic speeds. At the subsonic speed, $M = 0.62$, a nonlinearity is present at low projections for the spoiler-type control - a phenomenon typical of this type of control (ref. 5).

When a spoiler-slot-deflector arrangement is used, the hinge moments of the deflector would be expected to reduce the hinge moments of the spoiler since the deflector should be unstable and tend to open because of its rear hinge location. Figure 9 shows the results of a recent investigation (unpublished) of a spoiler-slot-deflector on a 6-percent-thick 35° swept wing at $M = 0.85$. The hinge-moment coefficient C_h is plotted against spoiler projection δ_s for a plain flap-type spoiler and for a spoiler-slot-deflector when the deflector projection δ_d is one-half the spoiler projection. The deflector appreciably reduces the hinge moments of the spoiler particularly in the spoiler-deflection range from 1 to 4 percent chord. The curves are not faired from 0 to 1 percent projection since no data are available and reversals similar to those shown in figure 8 might be expected. Variation of the ratio δ_s/δ_d will allow one means of adjusting the hinge moments of this type of control and appears to offer promise of a control of good effectiveness and reasonably low hinge moments.




DECLASSIFIED 50

As would be expected, the hinge moments of thin-plate or circular-arc spoilers are small compared to those of flap-type spoilers since the hinge moments can be developed only on the top and bottom edges of the spoiler. Results at low speeds on relatively thick wings (refs. 5 and 28) and on a swept wing at transonic speeds (ref. 29) confirm the low hinge moments but show that they are very nonlinear. This nonlinearity can probably be tolerated since they give forces about one-thirtieth as large as do flap-type ailerons on a typical fighter at transonic speeds.

These low hinge moments are all very well, provided that the necessary 10 percent projection can be incorporated in a 4-percent-thick wing. Figure 10 shows two ways of doing this along with a typical flap-type spoiler. The top sketch is the flap-type spoiler where the projection is limited only by the chord of the flap and the deflection. The center sketch shows a form of circular-arc spoiler (ref. 30). In this case three circular-arc spoilers, one behind the other, are linked so that the rear spoiler deflects 3 times as fast as the front spoiler and at full deflection provides a solid spoiler of the desired height. The bottom sketch is the so-called semaphore spoiler and consists of several flat plates hinged in the chord plane and deflected similar to semaphore train signals. At full deflection, they can form an almost solid spoiler of considerable deflection as shown in the figure. The number and length of the individual arms will depend on the deflection desired and the wing thickness. These last two types can be made to have relatively low hinge moments while still providing the desired projection.

Another means of providing spoiler control with low operating forces is that of using a jet of air to replace the spoiler (refs. 31 to 33). Figure 11 shows some preliminary results of a jet control utilizing stagnation pressure on a 35° swept wing. For these tests a very short span spoiler was used but the variation of effectiveness with span should be the same as for a conventional spoiler. With stagnation-pressure air, the jet is as effective as a 3-percent-chord spoiler and does not show the loss in effectiveness at large angles of attack. This, of course, is not sufficient for a fighter-type airplane but could be used as emergency control if normal control were obtained by using air at high pressure where roll is obtained both from jet thrust and from changing circulation around the wing. In order to vary the rolling effectiveness C_l , the slot width can be varied. The right-hand portion of figure 11 shows the variation of C_l with gap width δ_g ; an almost linear varia-

tion is indicated for the jet alone. One means of increasing the effectiveness is to deflect a spoiler ahead of the jet. The curve for this configuration shows that considerably more effectiveness is obtained. In this case, the total spoiler projection, 3 percent chord, could be fitted as a simple circular-arc spoiler within the wing.



6 13710241030

CONFIDENTIAL

In addition to the effectiveness and hinge moments of a control system, its effect on the rest of the airplane is of importance. Any obstruction such as a spoiler that causes separation of flow behind it will create turbulent flow over parts of the airplane. This turbulent flow may result in buffeting or shaking of the airplane. The few data that are available (unpublished) on flow fluctuations behind a spoiler are too sketchy to provide any reliable indication of either the magnitude or frequency of the air flow. A survey of the airplanes using spoilers at high subsonic speeds indicates, however, that about one-half of them have had no trouble from buffeting. Although not much can be done as far as predicting buffeting, it is known that perforating the face of the spoiler or otherwise breaking up the solid blocking will reduce any tendency of buffeting but that this will also cause some reduction in effectiveness, the magnitude of the reduction depending on the amount of area removed.


Another point of concern in the use of spoiler-type ailerons is the drag penalty associated with their use. Figure 12 shows the drag coefficient due to control deflection ΔC_D for both flap-type ailerons and spoiler ailerons that produce the same rolling-moment coefficient. The left-hand portion is for a swept wing at subsonic speeds (unpublished data) and the right-hand portion is for an unswept wing at supersonic velocities (refs. 15 and 34). It can be seen that there is a large drag associated with spoilers at low angles of attack but that the drag increment decreases rapidly with increased angle of attack and at angles of attack of about 8° the spoiler and aileron produce the same drag. In order to give some idea of the seriousness of these relatively high drags associated with spoilers at low angles of attack, calculations were made for a modern fighter making a 90° bank in 1 second at 30,000 feet and at a Mach number of 0.85. These calculations show that the speed of the airplane will be decreased only 2 miles per hour. If the maneuver is assumed to be an entry into a turn, even less loss in speed would be obtained since the angle of attack increases during the maneuver.


In conclusion, in general, there should be a slot through the wing behind the deflected spoiler. The spoiler should be located to the rear of the wing in the center portion of the wing semispan. Satisfactory spoiler configurations can be designed that will have reasonably low operating forces.

CONFIDENTIAL

CONFIDENTIAL



REFERENCES

1. Vogler, Raymond D.: Wind-Tunnel Investigation at High Subsonic Speeds of a Spoiler-Slot-Deflector Combination on an NACA 65A006 Wing With Quarter-Chord Line Swept Back 32.6° . NACA RM L53D17, 1953.
 2. Hammond, Alexander D., and Watson, James M.: Lateral-Control Investigation at Transonic Speeds of Retractable Plug-Type Spoiler-Slot Ailerons on a Tapered 60° Sweptback Wing of Aspect Ratio 2. Transonic-Bump Method. NACA RM L52F16, 1952.
 3. Watson, James M.: Low-Speed Lateral-Control Investigation of a Flap-Type Spoiler Aileron With and Without a Deflector and Slot on a 6-Percent-Thick, Tapered, 45° Sweptback Wing of Aspect Ratio 4. NACA RM L52G10, 1952.
 4. Hammond, Alexander D., and McMullan, Barbara M.: Chordwise Pressure Distribution at High Subsonic Speeds Near Midsemispan of a Tapered 35° Sweptback Wing of Aspect Ratio 4 Having NACA 65A006 Airfoil Sections and Equipped With Various Spoiler Ailerons. NACA RM L52C28, 1952.
 5. Fischel, Jack, and Ivey, Margaret F.: Collection of Test Data for Lateral Control With Full-Span Flaps. NACA TN 1404, 1948.
 6. Hammond, Alexander D.: Lateral-Control Investigation of Flap-Type and Spoiler-Type Controls on a Wing With Quarter-Chord-Line Sweepback of 60° , Aspect Ratio 2, Taper Ratio 0.6, and NACA 65A006 Airfoil Section. Transonic-Bump Method. NACA RM L50E09, 1950.
 7. Schneider, Leslie E., and Watson, James M.: Low-Speed Wind-Tunnel Investigation of Various Plain-Spoiler Configurations for Lateral Control on a 42° Sweptback Wing. NACA TN 1646, 1948.
 8. Fischel, Jack, and Tamburello, Vito: Investigation of Effect of Span, Spanwise Location, and Chordwise Location of Spoilers on Lateral Control Characteristics of a Tapered Wing. NACA TN 1294, 1947.
 9. Fischel, Jack, and Hammond, Alexander D.: Investigation of Effect of Span and Spanwise Location of Plain and Stepped Spoiler Ailerons on Lateral Control Characteristics of a Wing With Leading Edge Swept Back 51.3° . NACA RM L9K02, 1950.
 10. Graham, Robert R., and Koven, William: Lateral-Control Investigation of a 37° Sweptback Wing of Aspect Ratio 6 at a Reynolds Number of 6,800,000. NACA RM L8K12, 1949.
- 

11. Spooner, Stanley H., and Woods, Robert L.: Low-Speed Investigation of Aileron and Spoiler Characteristics of a Wing Having 42° Sweepback of the Leading Edge and Circular-Arc Airfoil Sections at Reynolds Numbers of Approximately 6.0×10^6 . NACA RM L9A07, 1949.
12. Bollech, Thomas V., and Pratt, George L.: Effect of Plain and Step Spoiler Location and Projection on the Lateral Control Characteristics of a Plain and Flapped 42° Sweptback Wing at a Reynolds Number of 6.8×10^6 . NACA RM L9L20a, 1950.
13. Pasamanick, Jerome, and Sellers, Thomas B.: Low-Speed Investigation of the Effect of Several Flap and Spoiler Ailerons on the Lateral Characteristics of a 47.5° Sweptback-Wing-Fuselage Combination at a Reynolds Number of 4.4×10^6 . NACA RM L50J20, 1950.
14. Graham, Robert R.: Lateral-Control Investigation at a Reynolds Number of 5,300,000 of a Wing of Aspect Ratio 5.8 Sweptforward 32° at the Leading Edge. NACA RM L9H18, 1950.
15. Conner, D. William, and Mitchell, Meade H., Jr.: Effects of Spoiler on Airfoil Pressure Distribution and Effects of Size and Location of Spoilers on the Aerodynamic Characteristics of a Tapered Unswept Wing of Aspect Ratio 2.5 at a Mach Number of 1.90. NACA RM L50L20, 1951.
16. Strass, H. Kurt: Summary of Some Effective Aerodynamic Twisting-Moment Coefficients of Various Wing-Control Configurations at Mach Numbers From 0.6 to 1.7 As Determined From Rocket-Powered Models. NACA RM L51K20, 1952.
17. Schult, Eugene D., and Fields, E. M.: Free-Flight Measurements of Some Effects of Spoiler Span and Projection and Wing Flexibility on Rolling Effectiveness and Drag of Plain Spoilers on a Tapered Sweptback Wing at Mach Numbers Between 0.6 and 1.6. NACA RM L52H06a, 1952.
18. Kindell, William H.: Effects of Span and Spanwise and Chordwise Location on the Control Effectiveness of Spoilers on a 50° Sweptback Wing at Mach Numbers of 1.41 and 1.96. NACA RM L53B09, 1953.
19. Jacobsen, Carl R.: Control Characteristics of Trailing-Edge Spoilers on Untapered Blunt Trailing-Edge Wings of Aspect Ratio 2.7 With 0° and 45° Sweepback at Mach Numbers of 1.41 and 1.96. NACA RM L52J28, 1952.
- 


20. Mueller, James N.: Investigation of Spoilers at a Mach Number of 1.93 To Determine the Effects of Height and Chordwise Location on the Section Aerodynamic Characteristics of a Two-Dimensional Wing. NACA RM L52L31, 1953.
 21. Wagner, Herbert A.: Bars as Trailing-Edge Control Surfaces. Tech. Memo. Rep. No. 52, U. S. Naval Air Missile Test Center (Pt. Mugu, Calif.), Oct. 15, 1951.
 22. Wiley, Harleth G., and Solomon, Martin: A Wind-Tunnel Investigation at Low Speeds of the Aerodynamic Characteristics of Various Spoiler Configurations on a Thin 60° Delta Wing. NACA RM L52J13, 1952.
 23. Croom, Delwin R.: Characteristics of Flap-Type Spoiler Ailerons at Various Locations on a 60° Delta Wing With a Double Slotted Flap. NACA RM L52J24, 1952.
 24. DeYoung, John: Theoretical Antisymmetric Span Loading for Wings of Arbitrary Plan Form at Subsonic Speeds. NACA Rep. 1056, 1951. (Supersedes NACA TN 2140.)
 25. DeYoung, John: Spanwise Loading for Wings and Control Surfaces of Low Aspect Ratio. NACA TN 2011, 1950.
 26. Lowry, John G., and Schneider, Leslie E.: Estimation of Effectiveness of Flap-Type Controls on Sweptback Wings. NACA TN 1674, 1948.
 27. Czarnecki, K. R., and Lord, Douglas R.: Load Distributions Associated With Controls at Supersonic Speeds. NACA RM L53D15a, 1953.
 28. Ashkenas, I. L.: The Development of a Lateral-Control System for Use With Large-Span Flaps. NACA TN 1015, 1946.
 29. Fikes, Joseph E.: Hinge-Moment and Other Aerodynamic Characteristics at Transonic Speeds of a Quarter-Span Spoiler on a Tapered 45° Sweptback Wing of Aspect Ratio 3. NACA RM L52A03, 1952.
 30. Rogallo, Francis M., Lowry, John G., and Fischel, Jack: Lateral-Control Devices Suitable for Use With Full-Span Flaps. Jour. Aero. Sci., vol. 17, no. 10, Oct. 1950.
 31. Göthert, B.: Effectiveness of a Spoiler at High Subsonic Speeds. Reps. and Translations No. 364, British M.O.S. (A) Völkenrode, Feb. 1947.
 32. Stein H.: "Moeve Project" Die Erzeugung von Querkraften an Luftdurchflossenen Flubein. (Guided Projectiles - Trials on Wing Using Jet Methods for Increasing Lift.) British Ministry of Supply, TPA 3/TIB Translation No. [REDACTED] 947.
- [REDACTED]

CONFIDENTIAL

33. Wieghardt, K.: Zum Ersatz von Spreizklappen durch Ausblasen von Luft. FB Nr. 1849, Deutsche Luftfahrtforschung (Braunschweig), 1943.
34. Mitchell, Meade H., Jr.: Effects of Varying the Size and Location of Trailing-Edge Flap-Type Controls on the Aerodynamic Characteristics of an Unswept Wing at a Mach Number of 1.9. NACA RM L50F08, 1950.
- 
- 

CONFIDENTIAL

BIBLIOGRAPHY

- Weick, Fred E., and Shortal, Joseph A.: Wind-Tunnel Research Comparing Lateral Control Devices, Particularly at High Angles of Attack. V - Spoilers and Ailerons on Rectangular Wings. NACA Rep. 439, 1932.
- Weick, Fred E., and Wenzinger, Carl J.: Preliminary Investigation of Rolling Moments Obtained With Spoilers on Both Slotted and Plain Wings. NACA TN 415, 1932.
- Hübner, Walter, and Pleines, Wilhelm: The D.V.L. Gliding-Angle Control (W. Hübner Design). NACA TM 697, 1932.
- Shortal, J. A.: Effect of Retractable-Spoiler Location on Rolling- and Yawing-Moment Coefficients. NACA TN 499, 1934.
- Soulé, H. A., and McAvoy, W. H.: Flight Investigation of Lateral Control Devices for Use With Full-Span Flaps. NACA Rep. 517, 1935.
- Weick, Fred E., and Jones, Robert T.: Résumé and Analysis of N.A.C.A. Lateral Control Research. NACA Rep. 605, 1937.
- Rogallo, F. M.: Aerodynamic Characteristics of a Slot-Lip Aileron and Slotted Flap for Dive Brakes. NACA WR L-337, 1941. (Formerly NACA ACR, Apr. 1941.)
- Rogallo, Francis M., and Spano, Bartholomew S.: Wind-Tunnel Investigation of a Plain and Slot-Lip Aileron on a Wing With a Full-Span Slotted Flap. NACA WR L-375, 1941. (Formerly NACA ACR, Apr. 1941.)
- Rogallo, F. M., and Schuldenfrei, Marvin.: Wind-Tunnel Investigation of a Plain and a Slot-Lip Aileron on a Wing With a Full-Span Flap Consisting of an Inboard Fowler and an Outboard Slotted Flap. NACA WR L-421, 1941. (Formerly NACA ARR, June 1941.)
- Lowry, John G.: Power-Off Wind-Tunnel Tests of the 1/8-Scale Model of the Brewster F2A Airplane. NACA WR L-543, 1941. (Formerly NACA MR, June 21, 1941.)
- Lowry, John G.: Power-On Wind-Tunnel Tests of the 1/8-Scale Model of the Brewster F2A Airplane With Full-Span Slotted Flaps. NACA WR L-707, 1941. (Formerly NACA MR, Aug. 21, 1941.)
- Baker, Paul S.: The Development of a New Lateral-Control Arrangement. NACA ARR, Oct. 1941.
- 

Lowry, John G.: Additional Power-On Wind-Tunnel Tests of the 1/8-Scale Model of the Brewster F2A Airplane With Full-Span Slotted Flaps. NACA WR L-708, 1941. (Formerly NACA MR, Oct. 27, 1941.)

Anon.: Wind-Tunnel Investigation of Spoiler-Lateral-Control Devices - XP-61, Night Interceptor Pursuit. Rep. No. A-WT 7, Northrop Aircraft, Inc., Nov. 13, 1941.

Rogallo, Francis M., and Swanson, Robert S.: Wind-Tunnel Development of a Plug-Type Spoiler-Slot Aileron for a Wing With a Full-Span Slotted Flap and a Discussion of Its Application. NACA WR L-420, 1941. (Formerly NACA ARR, Nov. 1941.)

Rogallo, F. M., and Spano, Bartholomew S.: Wind-Tunnel Investigation of a Spoiler-Slot Aileron on an NACA 23012 Airfoil With a Full-Span Fowler Flap. NACA WR L-376, 1941. (Formerly NACA ARR, Dec. 1941.)

Wenzinger, Carl J., and Rogallo, Francis M.: Wind-Tunnel Investigation of Spoiler, Deflector, and Slot Lateral-Control Devices on Wings With Full-Span Split and Slotted Flaps. NACA Rep. 706, 1941.

Wenzinger, Carl J., and Bowen, John D.: Tests of Round and Flat Spoilers on a Tapered Wing in the NACA 19-Foot Pressure Wind Tunnel. NACA TN 801, 1941.

Lowry, John G., and Toll, Thomas A.: Power-On Longitudinal-Stability and Control Tests of the 1/8-Scale Model of the Brewster F2A Airplane Equipped With Full-Span Slotted Flaps and a New Horizontal Tail. NACA WR L-709, 1942. (Formerly NACA MR, Mar. 14, 1942.)


Lowry, John G. and Liddell, Robert B.: Wind-Tunnel Investigation of a Tapered Wing With a Plug-Type Spoiler-Slot Aileron and Full-Span Slotted Flaps. NACA WR L-250, 1942. (Formerly NACA ARR, July 1942.)


Wild, J. M.: Hinge-Moment Characteristics of a Plug-Type Spoiler-Slot Aileron - P-61 Night Interceptor Pursuit. Rep. No. A-WT-19, Northrop Aircraft, Inc., Aug. 1, 1942.

Clousing, Lawrence A., and McAvoy, William H.: Flight Measurements of the Lateral-Control Characteristics of an Airplane Equipped With a Combination Aileron-Spoiler Control System. NACA WR A-68, 1942. (Formerly NACA MR, Bur. Aero., Sept. 2, 1942.)


Turner William N., and Adams, Betty: Flight Measurements of the Effects of a Wing Leading-Edge Slot and Other Modifications on the Stability, Maximum Lift, and High Speed on an Observation Airplane. NACA WR A-88, 1943. (Formerly NACA MR, Bur. Aero., Jan. 19, 1943.)



- Spahr, J. Richard, and Christophersen, Don R.: Measurements in Flight of the Stability, Lateral-Control, and Stalling Characteristics of an Airplane Equipped With Full-Span Zap Flaps and Spoiler-Type Ailerons. NACA WR A-28, 1943. (Formerly NACA MR, Dec. 5, 1943.)
- Wetmore, Joseph W., and Sawyer, Richard H.: Flight Tests of F2A-2 Airplane With Full-Span Slotted Flaps and Trailing-Edge and Slot-Lip Ailerons. NACA WR L-272, 1943. (Formerly NACA ARR 3LO7.)
- Wieghardt, K.: Zum Ersatz von Spreizklappen durch Ausblasen von Luft. FB Nr. 1849, Deutsche Luftfahrtforschung (Braunschweig), 1943.
- Laitone, Edmund V.: An Investigation of the High-Speed Lateral-Control Characteristics of a Spoiler. NACA ACR 4C23, 1944.
- Laitone, Edmund V.: An Investigation of 0.15-Chord Ailerons on a Low- Drag Tapered Wing at High Speeds. NACA WR A-24, 1944. (Formerly NACA ACR 4I25.)
- Conner, D. W., Fairbanks, R. W., and Neely, R. H.: Tests of Spoilers as a Lateral-Control Device on a 1/8-Scale Model of the B-32 Airplane in the 19-Foot Pressure Tunnel. NACA MR L5A08, Army Air Forces, 1945.
- Nuber, Robert J., and Rice, Fred J., Jr.: Lift Tests of a 0.1536c Thick Douglas Airfoil Section of NACA 7-Series Type Equipped With a Lateral-Control Device for Use With a Full-Span Double-Slotted Flap on the C-74 Airplane. NACA WR L-641, 1945. (Formerly NACA MR L5C24a.)
- Purser, Paul E., and McKinney, Elizabeth G.: Comparison of Pitching Moments Produced by Plain Flaps and by Spoilers and Some Aerodynamic Characteristics of an NACA 23012 Airfoil With Various Types of Aileron. NACA WR L-124, 1945. (Formerly NACA ACR L5C24a.)
- Underwood, William J. and Fullmer, Felicien F., Jr.: Two-Dimensional Wind-Tunnel Investigation of Spoiler Aileron Flap Model for the Hughes XF-11 Airplane. NACA WR L-644, 1945. (Formerly NACA MR L5C29.)
- Laitone, Edmund V., and Summers, James L.: An Additional Investigation of the High-Speed Lateral-Control Characteristics of Spoilers. NACA WR A-21, 1945. (Formerly NACA ACR 5D28.)
- Weyl, A. R.: Tailless Aeroplane Control Systems. Aircraft Engineering, vol. XVII, no. 195, May, 1945, pp. 133-145.
- Holtzclaw, Ralph W.: Wind-Tunnel Investigation of the Effects of Spoilers on the Characteristics of a Low-Drag Airfoil Equipped With a 0.25-Chord Slotted Flap. NACA WR A-92, 1945. (Formerly NACA MR A5G23.)
- 

- Ashkenas, I. L.: The Development of a Lateral-Control System for Use With Large-Span Flaps. NACA TN 1015, 1946.
- Letko, William, and Goodman, Alex: Preliminary Wind-Tunnel Investigation at Low Speed of Stability and Control Characteristics of Swept-Back Wings. NACA TN 1046, 1946.
- Lowry, John G., and Turner, Thomas R.: Pressure Distribution Over a Plug-Type Spoiler-Slot Aileron on a Tapered Wing With Full-Span Slotted Flaps. NACA TN 1079, 1946.
- Soulé, Hartley A.: Influence of Large Amounts of Wing Sweep on Stability and Control Problems of Aircraft. NACA TN 1088, 1946.
- Spahr, J. Richard: Lateral-Control Characteristics of Various Spoiler Arrangements as Measured in Flight. NACA TN 1123, 1947.
- Fischel, Jack, and Tamburello, Vito: Investigation of Effect of Span, Spanwise Location, and Chordwise Location of Spoilers on Lateral Control Characteristics of a Tapered Wing. NACA TN 1294, 1947.
- Fitzpatrick, James E., and Furlong, G. Chester: Effect of Spoiler-Type Lateral-Control Devices on the Twisting Moments of a Wing of NACA 230-Series Airfoil Sections. NACA TN 1298, 1947.
- Holtzclaw, Ralph W., and Dods, Jules B., Jr.: Wind-Tunnel Investigation of Drooped Ailerons on a 16-Percent-Thick Low-Drag Airfoil. NACA TN 1386, 1947.
- Deters, Owen J., and Russell, Robert T.: Investigation of a Spoiler-Type Lateral Control System on a Wing With Full-Span Flaps in the Langley 19-Foot Pressure Tunnel. NACA TN 1409, 1947.
- Deters, Owen J.: Comparison of the Control-Force Characteristics of Two Types of Lateral-Control System for Large Airplanes. NACA TN 1441, 1947.
- Göthert, B.: Effectiveness of a Spoiler at High Subsonic Speeds. Reps. and Translations No. 364, British M.O.S.(A) Völkenrode, Feb. 1947.
- Silsby, Norman S., and Daum, Fred L.: The Effectiveness of a Trailing-Edge Spoiler on a Swept-Back Airfoil at Transonic Speeds From Tests by the NACA Wing-Flow Method. NACA RM L6K12a, 1947.
- Neely, Robert H., and Conner, D. William: Aerodynamic Characteristics of a 42° Swept-Back Wing With Aspect Ratio 4 and NACA 64₁-112 Airfoil Sections at Reynolds Numbers From 1,700,000 to 9,500,000. NACA RM L7D14, 1947.
- 

CONFIDENTIAL

- Schneider, Leslie E., and Ziff, Howard L.: Preliminary Investigation of Spoiler Lateral Control on a 42° Sweptback Wing at Transonic Speeds. NACA RM L7F19, 1947.
- Langley Research Staff (Compiled by Thomas A. Toll): Summary of Lateral-Control Research. NACA Rep. 868, 1947. (Formerly NACA TN 1245.)
- Stein H.: "Moeve Project" Die Erzeugung von Querkraften an Luftdurchflossenen Flubein. (Guided Projectiles - Trials on Wing Using Jet Methods for Increasing Lift.) British Ministry of Supply, TPA 3/TIB Translation No. UNT 329 T, 1947.
- Fischel, Jack, and Ivey, Margaret F.: Collection of Test Data for Lateral Control With Full-Span Flaps. NACA TN 1404, 1948.
- Schneider, Leslie E., and Watson, James M.: Low-Speed Wind-Tunnel Investigation of Various Plain-Spoiler Configurations for Lateral Control on a 42° Sweptback Wing. NACA TN 1646, 1948.
- Fischel, Jack, and Schneider, Leslie E.: High-Speed Wind-Tunnel Investigation of an NACA 65-210 Semispan Wing Equipped With Plug and Retractable Ailerons and a Full-Span Slotted Flap. NACA TN 1663, 1948.
- Hopkins, Edward J.: A Wind-Tunnel Investigation at Low Speed of Various Lateral Controls on a 45° Sweptback Wing. NACA RM A7L16, 1948.
- Sandahl, Carl A.: Free-Flight Investigation of the Rolling Effectiveness of a Wing-Spoiler Arrangement at High Subsonic, Transonic, and Supersonic Speeds. NACA RM L8A07, 1948.
- Turner, Thomas R., Lockwood, Vernard E., and Vogler, Raymond D.: Preliminary Investigation of Various Ailerons on a 42° Sweptback Wing for Lateral Control at Transonic Speeds. NACA RM L8D21, 1948.
- Fischel, Jack.: Wind-Tunnel Investigation of an NACA 65-210 Semispan Wing Equipped With Circular Plug Ailerons and a Full-Span Slotted Flap. NACA TN 1802, 1949.
- Fischel, Jack, and Vogler, Raymond D.: High-Lift and Lateral Control Characteristics of an NACA 65₂-215 Semispan Wing Equipped With Plug and Retractable Ailerons and a Full-Span Slotted Flap. NACA TN 1872, 1949.
- Ernst, G., and Kramer, M.: Development of Spoiler Controls for Remote Control of Flying Missiles. NACA TM 1210, 1949.
- Graham, Robert R. and Koven, William: Lateral-Control Investigation of a 37° Sweptback Wing of Aspect Ratio 6 at a Reynolds Number of 6,800,000. NACA RM L8K12, 1949.
- 

Schneider, Leslie E., and Watson, James M.: Wind-Tunnel Investigation at Low Speeds of Various Plug-Aileron and Lift-Flap Configurations on a 42° Sweptback Semispan Wing. NACA RM L8K19, 1949.

Spooner, Stanley H., and Woods, Robert L.: Low-Speed Investigation of Aileron and Spoiler Characteristics of a Wing Having 42° Sweepback of the Leading Edge and Circular-Arc Airfoil Sections at Reynolds Numbers of Approximately 6.0×10^6 . NACA RM L9A07, 1949.

Braslow, Albert L., and Visconti, Fioravante: Two-Dimensional Wind-Tunnel Investigation of Two NACA 7-Series Type Airfoils Equipped With a Slot-Lip Aileron, Trailing-Edge Frise Aileron, and a Double Slotted Flap. NACA RM L9B23, 1949.

Schneider, Leslie E., and Hagerman, John R.: Wind-Tunnel Investigation at High Subsonic Speeds of the Lateral-Control Characteristics of an Aileron and a Stepped Spoiler on a Wing With Leading Edge Swept Back 51.3° . NACA RM L9D06, 1949.

Newman, B. G.: The Re-Attachment of a Turbulent Boundary-Layer Behind a Spoiler. Rep. A. 64, Aero. Res. Lab. (Melbourne), Oct. 1949.

McLarren, Robert: Air Brakes: Standard Fighter Accessory. Aviation Week, vol. 51, no. 20, Nov. 14, 1949, pp. 21-28.

Lovell, Powell M., Jr., and Stassi, Paul P.: A Comparison of the Lateral Controllability With Flap and Plug Ailerons on a Sweptback-Wing Model. NACA TN 2089, 1950.

Riebe, John M., and Watson, James M.: The Effect of End Plates on Swept Wings at Low Speed. NACA TN 2229, 1950.


Lovell, Powell M., Jr.: A Comparison of the Lateral Controllability With Flap and Plug Ailerons on a Sweptback-Wing Model Having Full-Span Flaps. NACA TN 2247, 1950.

Graham, Robert R.: Lateral-Control Investigation at a Reynolds Number of 5,300,000 of a Wing of Aspect Ratio 5.8 Sweptforward 32° at the Leading Edge. NACA RM L9H18, 1950.

Fischel, Jack, and Hammond, Alexander D.: Investigation of Effect of Span and Spanwise Location of Plain and Stepped Spoiler Ailerons on Lateral Control Characteristics of a Wing With Leading Edge Swept Back 51.3° . NACA RM L9K02, 1950.

Bollech, Thomas V., and Pratt, George L.: Effect of Plain and Step Spoiler Location and Projection on the Lateral Control Characteristics of a Plain and Flapped 42° Sweptback Wing at a Reynolds Number of 6.8×10^6 . NACA RM L9L20a, 1950.

CONFIDENTIAL

- Olson, Robert N., and Mead, Merrill H.: Aerodynamic Study of a Wing-Fuselage Combination Employing a Wing Swept Back 63° . - Effectiveness of an Elevon as a Longitudinal Control and the Effects of Camber and Twist on the Maximum Lift-Drag Ratio at Supersonic Speeds. NACA RM A50A31a, 1950.
- Hammond, Alexander D.: Lateral-Control Investigation of Flap-Type and Spoiler-Type Controls on a Wing With Quarter-Chord-Line Sweepback of 60° , Aspect Ratio 2, Taper Ratio 0.6, and NACA 65A006 Airfoil Section. Transonic-Bump Method. NACA RM L50E09, 1950.
- Mitchell, Meade H., Jr.: Effects of Varying the Size and Location of Trailing-Edge Flap-Type Controls on the Aerodynamic Characteristics of an Unswept Wing at a Mach Number of 1.9. NACA RM L50F08, 1950.
- Weiburg, James A., and Carel, Hubert C.: Wind-Tunnel Investigation at Low Speed of a Wing Swept Back 63° and Twisted and Cambered for Uniform Load at a Lift Coefficient of 0.5 and With a Thickened Tip Section. NACA RM A50I14, 1950.
- Pasamanick, Jerome, and Sellers, Thomas B.: Low-Speed Investigation of the Effect of Several Flap and Spoiler Ailerons on the Lateral Characteristics of a 47.5° Sweptback-Wing-Fuselage Combination at a Reynolds Number of 4.4×10^6 . NACA RM L50J20, 1950.
- Davidson, Harold Wm.: Report of Additional (B) Wind-Tunnel Tests on a 15% Scale Model of the McDonnell XF3H-1 Airplane. GALCIT Rep. No. 550-B, Feb. 28, 1950.
- Holtby, K., and Seiler, R.: Development of Lateral Controls for Flexible Swept Wings (Model B-47). Doc. No. D-9458, Contract Nos. W33-038 ac-8429 and W33-038 ac-22413, Boeing Aircraft Co., Apr. 6, 1950.
- Rogallo, Francis M.: Lateral Control of Personal Aircraft at High Lift Coefficients. Aero. Eng. Rev., vol. 9, no. 8, Aug. 1950, pp. 18-22.
- Rogallo, Francis M., Lowry, John G., and Fischel, Jack: Lateral-Control Devices Suitable for Use With Full-Span Flaps. Jour. Aero. Sci., vol. 17, no. 10, Oct. 1950.
- Duddy, R. R.: Lift Spoilers for Lateral Control. Part I. Graduate and Student Sec., R.A.S., Apr. 1950.
- Fischel, Jack, and Watson, James M.: Investigation of Spoiler Ailerons for Use as Speed Brakes on Glide-Path Controls on Two NACA 65-Series Wings Equipped With Full-Span Slotted Flaps. NACA Rep. 1034, 1951. (Supersedes NACA TN 1933.)
- 

Kramer, Max, Zobel, Theodor W., and Esche, C. G.: Lateral Control by Spoilers at the DVL. NACA TM 1307, 1951.

Olson, Robert N., and Mead, Merrill H.: Aerodynamic Study of a Wing-Fuselage Combination Employing a Wing Swept Back 63° - Effectiveness at Supersonic Speeds of a 30-Percent Chord, 50-Percent Semispan Elevon as a Lateral Control Device. NACA RM A50K07, 1951.

May, Ellery B., Jr.: Investigation of the Effects of Leading-Edge Chord-Extensions on the Aerodynamic and Control Characteristics of Two Swept-back Wings at Mach Numbers of 1.41, 1.62, and 1.96. NACA RM L50L06a, 1951.

Conner, D. William, and Mitchell, Meade H., Jr.: Effects of Spoiler on Airfoil Pressure Distribution and Effects of Size and Location of Spoilers on the Aerodynamic Characteristics of a Tapered Unswept Wing of Aspect Ratio 2.5 at a Mach Number of 1.90. NACA RM L50L20, 1951.

Strass, H. Kurt, and Marley, Edward T.: Rocket-Model Investigation of the Rolling Effectiveness of a Fighter-Type Wing-Control Configuration at Mach Numbers From 0.6 to 1.5. NACA RM L51I28, 1951.

Gander, W. J.: Wind Tunnel Tests on the 1/7 Scale Model XF10F-1 Airplane Series 17A, 17B and 17C. G.W.T. Rep. No. 10, Grumman Aircraft Eng. Corp., Mar. 1951.

Visconti, F.: Wind Tunnel Tests on the 1/7 Scale Model XF10F-1 Airplane Series 19. G.W.T. Rep. No. 19, Grumman Aircraft Eng. Corp., Apr. 1951.


Maier, Norman M.: Wind Tunnel Tests on the 1/7 Scale Model XF10F-1 Airplane Series 19-A. G.W.T. Rep. No. 23 (Addendum No. 1 to G.W.T. Rep. No. 19), Grumman Aircraft Eng. Corp., Aug. 1951.

Wagner, Herbert A.: Bars as Trailing-Edge Control Surfaces. Tech. Memo. Rep. No. 52, U.S. Naval Air Missile Test Center (Pt. Mugu, Calif.), Oct. 15, 1951.

McLarren, Robert: Air Brakes. Aero Digest, vol. 63, no. 6, Dec. 1951, pp. 30-46.

Fischel, Jack, and Hagerman, John R.: Effect of Aspect Ratio and Sweep-back on the Low-Speed Lateral Control Characteristics of Untapered Low-Aspect-Ratio Wings Equipped With Retractable Ailerons. NACA Rep. 1091, 1952. (Supersedes NACA TN'S 2347 and 2348.)

Strass, H. Kurt: Summary of Some Effective Aerodynamic Twisting-Moment Coefficients of Various Wing-Control Configurations at Mach Numbers From 0.6 to 1.7 As Determined From Rocket-Powered Models. NACA RM L51K20, 1952.

- Vogler, Raymond D.: Wind-Tunnel Investigation at High Subsonic Speeds of Spoilers of Large Projection on an NACA 65A006 Wing With Quarter-Chord Line Swept Back 32.6° . NACA RM L51L10, 1952.
- Fikes, Joseph E.: Hinge-Moment and Other Aerodynamic Characteristics at Transonic Speeds of a Quarter-Span Spoiler on a Tapered 45° Swept-back Wing of Aspect Ratio 3. NACA RM L52A03, 1952.
- Maki, Ralph L.: Full-Scale Wind-Tunnel Investigation of the Effects of Wing Modifications and Horizontal-Tail Location on the Low-Speed Static Longitudinal Characteristics of a 35° Swept-Wing Airplane. NACA RM A52B05, 1952.
- Fitzpatrick, James E., and Woods, Robert L.: Low-Speed Lateral-Control Characteristics of an Unswept Wing With Hexagonal Airfoil Sections and Aspect Ratio 2.5 Equipped With Spoilers and With Sharp- and Thickened-Trailing-Edge Flap-Type Ailerons at a Reynolds Number of 7.6×10^6 . NACA RM L52B15, 1952.
- Hammond, Alexander D., and McMullan, Barbara M.: Chordwise Pressure Distribution at High Subsonic Speeds Near Midsemispan of a Tapered 35° Sweptback Wing of Aspect Ratio 4 Having NACA 65A006 Airfoil Sections and Equipped With Various Spoiler Ailerons. NACA RM L52C28, 1952.
- Lockwood, Vernard E., and Fikes, Joseph E.: Control Characteristics at Transonic Speeds of a Linked Flap and Spoiler on a Tapered 45° Swept-back Wing of Aspect Ratio 3. NACA RM L52D25, 1952.
- Hammond, Alexander D., and Watson, James M.: Lateral-Control Investigation at Transonic Speeds of Retractable Plug-Type Spoiler-Slot Ailerons on a Tapered 60° Sweptback Wing of Aspect Ratio 2. Transonic-Bump Method. NACA RM L52F16, 1952.
- Bandettini, Angelo: An Investigation at Subsonic Speeds of the Rolling Effectiveness of a Small Perforated Spoiler on a Wing Having 45° of Sweepback. NACA RM A52G02, 1952.
- Watson, James M.: Low-Speed Lateral-Control Investigation of a Flap-Type Spoiler Aileron With and Without a Deflector and Slot on a 6-Percent-Thick, Tapered, 45° Sweptback Wing of Aspect Ratio 4. NACA RM L52G10, 1952.
- Schult, Eugene D., and Fields, E. M.: Free-Flight Measurements of Some Effects of Spoiler Span and Projection and Wing Flexibility on Rolling Effectiveness and Drag of Plain Spoilers on a Tapered Sweptback Wing at Mach Numbers Between 0.6 and 1.6. NACA RM L52H06a, 1952.
- 

Fields, E. M.: Some Effects of Spoiler Height, Wing Flexibility, and Wing Thickness on Rolling Effectiveness and Drag of Unswept Wings at Mach Numbers Between 0.4 and 1.7. NACA RM L52H18, 1952.

Wiley, Harleth G., and Solomon, Martin: A Wind-Tunnel Investigation at Low Speeds of the Aerodynamic Characteristics of Various Spoiler Configurations on a Thin 60° Delta Wing. NACA RM L52J13, 1952.

Croom, Delwin R.: Characteristics of Flap-Type Spoiler Ailerons at Various Locations on a 60° Delta Wing With a Double Slotted Flap. NACA RM L52J24, 1952.

Jacobsen, Carl R.: Control Characteristics of Trailing-Edge Spoilers on Untapered Blunt Trailing-Edge Wings of Aspect Ratio 2.7 With 0° and 45° Sweepback at Mach Numbers of 1.41 and 1.96. NACA RM L52J28, 1952.

Anon. (M. de Selincourt, trans.): Investigation of Retractable Ailerons on Rectangular Wing of Profile S.O.2915. Library Trans. No. 407, Ministry of Supply, British R.A.E., May 1952.

Patterson, R. T.: The Characteristics of Trailing-Edge Spoilers. Part I - The Effects of Turbulent Boundary-Layer Thickness on the Characteristics of Two-Dimensional Spoilers at Two Supersonic Mach Numbers - TED No. TMB DE 3109. Aero Rep. 827, David W. Taylor Model Basin, Navy Dept., Aug. 1952. Part II - The Effects of Gap, Flap Deflection Angle, Thickness, and Sweep Angle on the Aerodynamic Characteristics of Two-Dimensional Spoilers, and the Pressure Distribution Near the Tip of a Partial-Span Trailing-Edge Spoiler, at a Mach Number of 1.86 - TED No. TMB DE-3109. Aero Rep. 827, David W. Taylor Model Basin, Navy Dept., Dec. 1952.

Pride, A. M.: Stall Characteristics Tests on an AD-4W Airplane With and Without Leading Edge Spoilers and Vortex Generators. Project TED No. PTR DE-331, Flight Test Div., U. S. Naval Air Test Center (Patuxent River, Md.), Aug. 14, 1952.

Henkels, W. J., Kuldell, P. D., and Brower, E. M.: Wind Tunnel Tests of a 2/9-Scale Half-Span Wing Model of the XWU-1 Airplane - TED No. TMB DE-3112. Aero. Rep. 826, David W. Taylor Model Basin, Navy Dept., Sept. 1952.

Mueller, James N.: Investigation of Spoilers at a Mach Number of 1.93 To Determine the Effects of Height and Chordwise Location on the Section Aerodynamic Characteristics of a Two-Dimensional Wing. NACA RM L52L31, 1953.

CONFIDENTIAL

CONFIDENTIAL

Kindell, William H.: Effects of Span and Spanwise and Chordwise Location on the Control Effectiveness of Spoilers on a 50° Sweptback Wing at Mach Numbers of 1.41 and 1.96. NACA RM L53B09, 1953.

Vogler, Raymond D.: Wind-Tunnel Investigation at High Subsonic Speeds of a Spoiler-Slot-Deflector Combination on an NACA 65A006 Wing With Quarter-Chord Line Swept Back 32.6° . NACA RM L53D17, 1953.

Czarnecki, K. R., and Lord, Douglas R.: Load Distributions Associated With Controls at Supersonic Speeds. NACA RM L53D15a, 1953.

Hammond, Alexander D., and West, Franklin E., Jr.: Loads Due to Flaps and Spoilers on Sweptback Wings at Subsonic and Transonic Speeds. NACA RM L53D29a, 1953.

EFFECT OF SLOT AND DEFLECTOR ON SPOILER EFFECTIVENESS

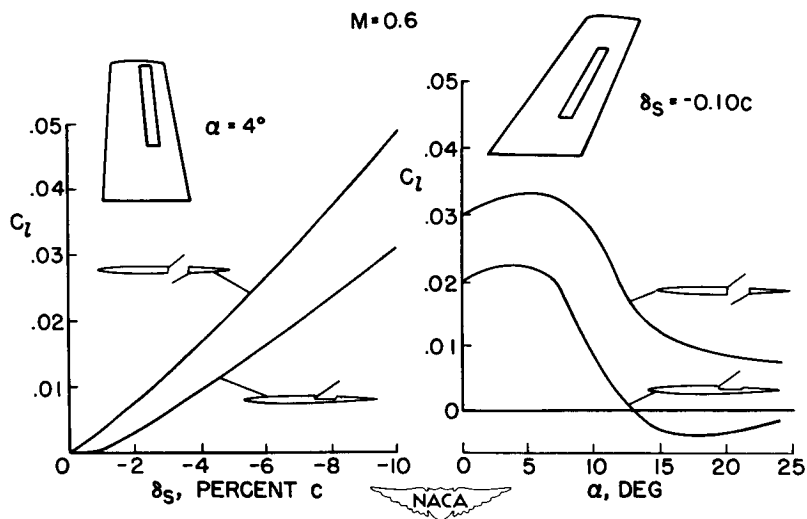


Figure 1

EFFECT OF DROOPED L. E. EXTENSION ON SPOILER EFFECTIVENESS

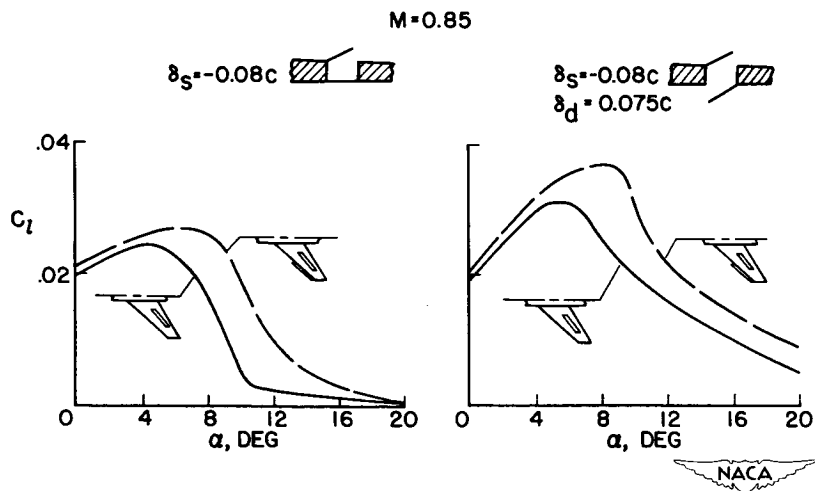


Figure 2

EFFECT OF SLOT AT LOW SUPERSONIC SPEEDS

M=1.20

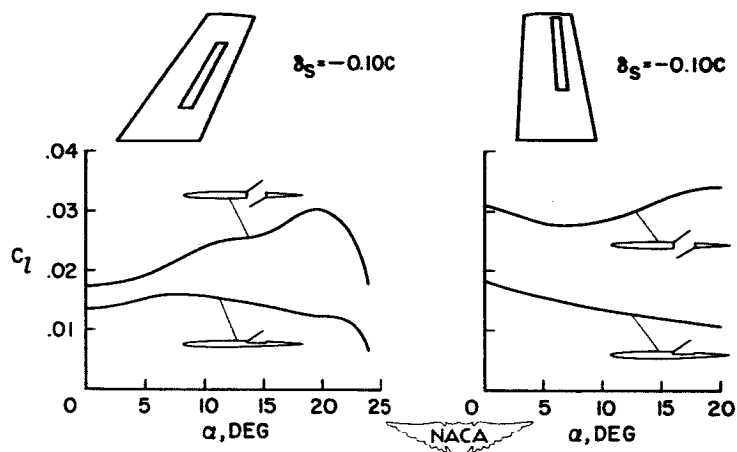


Figure 3

SATISFACTORY SPOILER LOCATION ON SWEEPED WINGS

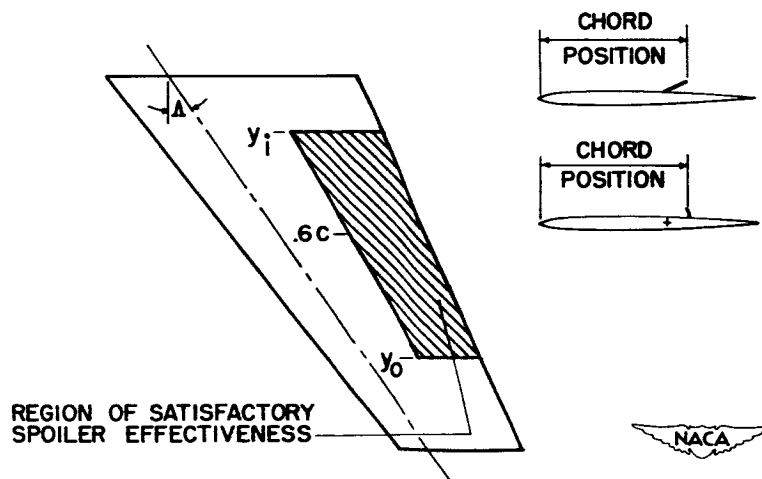


Figure 4

EFFECT OF SPANWISE SPOILER LOCATION ON SWEPT WINGS

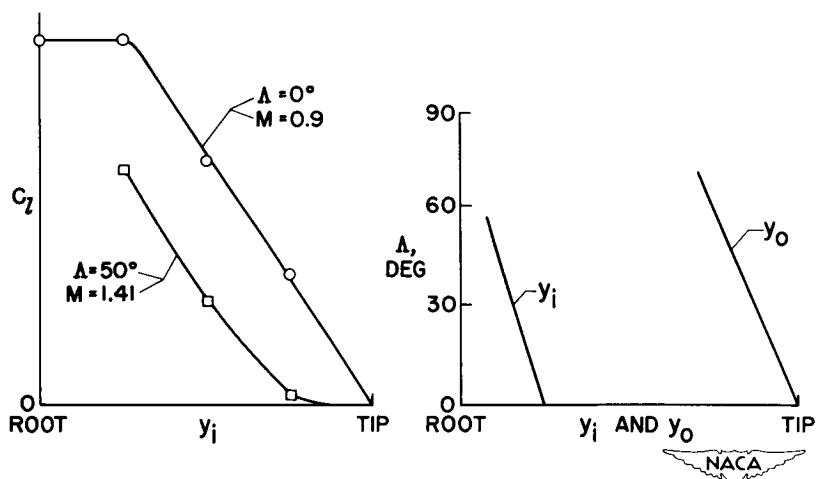


Figure 5

SPOILER LOCATION ON 60° DELTA WING

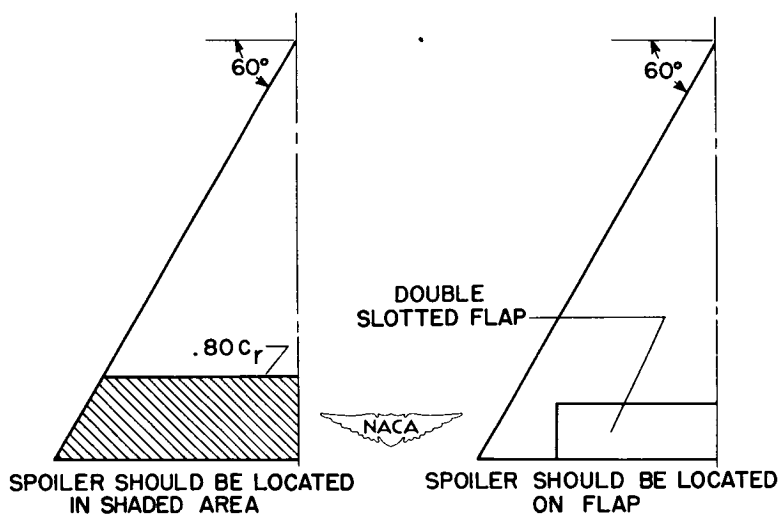


Figure 6

EFFECT OF CHORDWISE LOCATION OF SPOILERS ON 60° DELTA WING

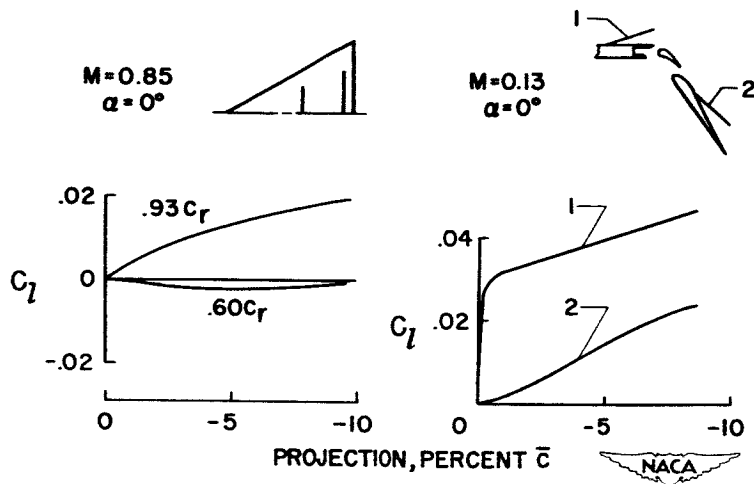


Figure 7

HINGE MOMENTS OF SPOILERAILERONS 60° DELTA WING

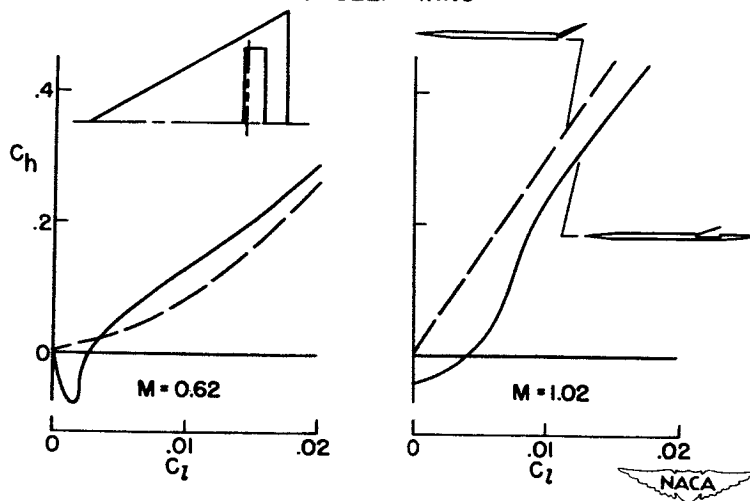


Figure 8

HINGE MOMENTS OF SPOILER-SLOT DEFLECTOR AILERONS $M=0.85$; $\alpha=4^\circ$

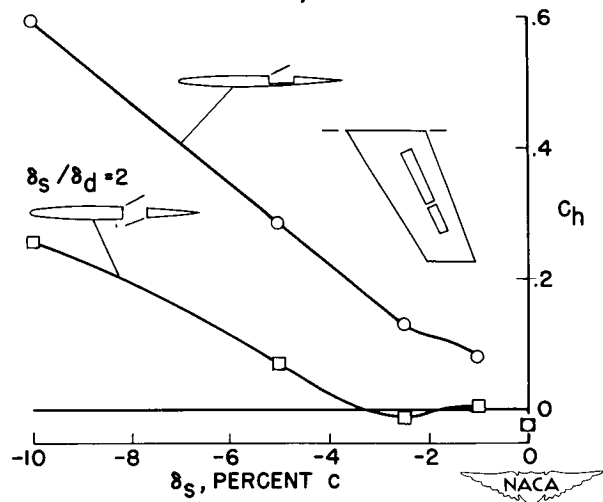


Figure 9

SPOILER CONFIGURATIONS ON A THIN WING

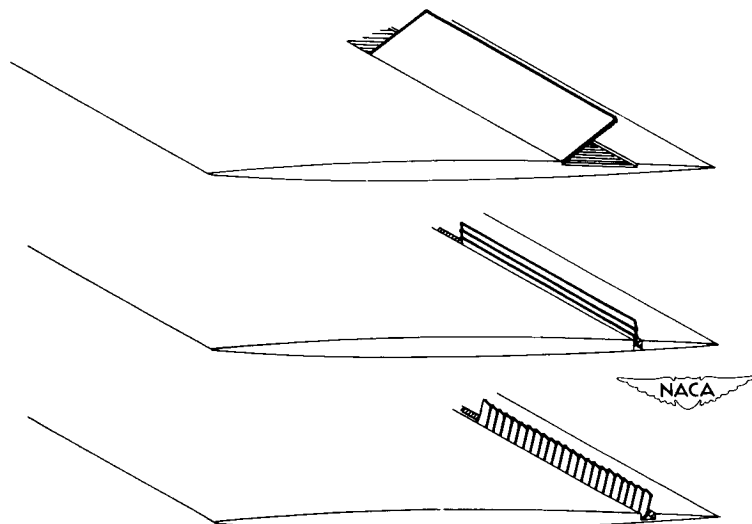


Figure 10

JET CONTROL UTILIZING AIR AT STAGNATION PRESSURE

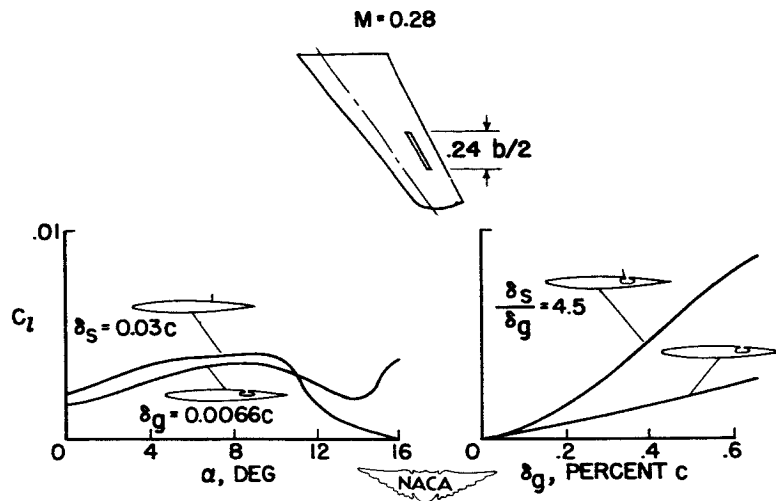


Figure 11

COMPARISON OF DRAG CHARACTERISTICS OF FLAPS AND SPOILERS

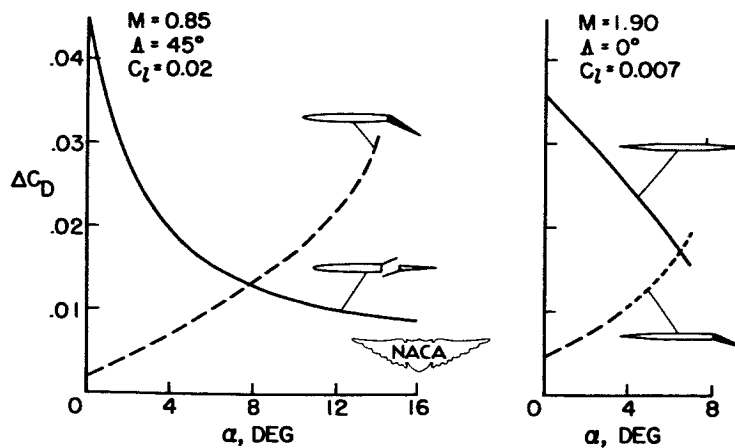


Figure 12

CONFIDENTIAL

RECENT INFORMATION ON FLAP AND TIP CONTROLS

By Douglas R. Lord and K. R. Czarnecki


Langley Aeronautical Laboratory

INTRODUCTION

In the past few years, research programs on controls have been expanded to include systematic transonic and supersonic investigations of new types of control devices and to adapt the controls developed through subsonic research to the supersonic regime. The results now available are sufficiently extensive to warrant an evaluation of the progress to date and to establish certain trends. The data presented in the present paper are used to outline these trends rather than to give a completely comprehensive summary of the available data. A bibliography of references, however, is included.


DISCUSSION

The fundamental requirement of a control, at any speed, is that it produce the necessary lift, pitching moment, or rolling moment to control the aircraft in flight. Considerable testing of controls at high speeds has shown that the desired effectiveness can usually be obtained without difficulty. Since the supersonic theory for predicting control effectiveness is cumbersome and the assumptions are often not well-supported by experiment, simpler methods of estimating the control effectiveness are desired. It is to be expected that, to a first order, the lift of a control is directly related to the area of the control, and the moment of the control forces about a given axis is directly related to the moment of the control area about that axis. This simple concept is substantiated by data presented in figures 1 and 2 which show the results of tests in the Langley 4- by 4-foot supersonic pressure tunnel at Mach number 1.61 of a delta wing and of a trapezoidal wing. In these figures, the slopes of the curves of lift, rolling-moment, and pitching-moment coefficients with control deflection are plotted as functions of the control area, control-area moment about the roll center, and control-area moment about the pitch center, respectively, for the control configurations tested. It is evident that to a first order it is possible to estimate from these correlations the effectiveness of any control on the wings shown, regardless of control plan form. Similar results have been obtained for wings of other plan forms (refs. 1 to 3). Some flight results (ref. 4) indicate that correlations may not be obtainable for some controls on high-aspect-ratio, highly swept wings.



In view of the fact that satisfactory control effectiveness can be obtained and usually can be estimated, a primary objective of research on controls at the present time is to develop methods for balancing the forces acting on the controls to improve the hinge-moment characteristics. In order to reduce the magnitude of the control hinge moments, several methods have been used, such as overhang nose balances, horn balances, tip controls, all-movable wings, tabs, and paddle balances. Until recently, very few data have been available on overhang balances at high speeds; however, recent transonic and supersonic tests of trailing-edge controls having various amounts of overhang nose balance have been made on the transonic bump in the Langley high-speed 7- by 10-foot tunnel and in the Langley 9- by 12-inch supersonic blowdown tunnel. Figure 3 shows the variation with Mach number of the hinge-moment-parameter slopes with control deflection and with angle of attack for the two extreme test configurations, one having no overhang balance and the other having 100-percent balance. Data for the configurations having a balance area between 0 and 100 percent fall between the curves shown. Throughout this paper, percent balance is defined as the ratio of control area ahead of the hinge line to control area behind the hinge line, expressed as a percentage. For this type of control, the hinge-moment-coefficient slopes, which are based on the moment of the control area behind the hinge line, have been converted to hinge-moment-parameter slopes, which are based on the moment of the total control area about the control leading edge, in order to make the data for the two controls directly comparable. It should be noted that all the tests were made with a rounded leading edge on the control and that the 9- by 12-inch-tunnel data were obtained on a wing mounted on a half-body, which may explain some of the discrepancies in the data from the two tests. In general, the data indicate that the nose balance is effective in changing the hinge moment due to control deflection throughout the speed range tested. The nose balance causes a much larger change in hinge moment due to wing angle of attack at supersonic speeds than at subsonic speeds. Since these slopes were obtained at a control deflection of 0° and an angle of attack of 0° , it appears that, in order to gain more insight into the effectiveness of the nose balance at subsonic and supersonic speeds, it will be necessary to consider the effect of control deflection and angle of attack.

Figure 4 shows for a Mach number of 0.60 and a Mach number of 1.96 the variation of the hinge-moment parameter with control deflection at an angle of attack of 0° and with angle of attack at a control deflection of 0° for the two control configurations discussed in the previous figure. In both the subsonic and supersonic cases, the unbalanced control, as designated by the solid curves, has fairly linear characteristics and for the Mach numbers shown there is only a small change in slope due to Mach number of the hinge-moment curve with control deflection near $\delta = 0^\circ$. For the 100-percent-balanced control, the subsonic curve shows a large balancing effect with increasing control deflection



at the small deflections. At supersonic speed, the 100-percent-balanced control shows less balancing action than it did at subsonic speed. Other data at angles of attack have shown that at supersonic speeds the balance is ineffective at positive control deflections when the nose of the control lies in the dead-air region behind the wing but has a strong balancing effect at negative control deflections when the control nose is exposed. At all the test angles of attack, the effect of the nose balance is less at subsonic than at supersonic speed when the control deflection is 0° .

Since at supersonic speeds the dead-air region from the wing seems to be important, it would appear that changes in wing section to minimize this region would improve the balancing effectiveness of this type of control. The results of two-dimensional tests in the Langley 9-inch supersonic tunnel at a Mach number of 2.40, in which changes in section were made, are shown in figure 5. The hinge-moment-parameter slopes, which were taken from fairly linear curves, are plotted as functions of the ratio of control balancing area to total control area. Models were tested for two of the sections with different balance-area ratios as shown by the curves. Models of all four sections for a balance-area ratio of 0.375 were tested. For these tests an area ratio of approximately 0.6 would be required to balance the hinge moment due to control deflection for the basic configuration (denoted by the solid curve); whereas a ratio of 0.4 is all that is required to balance the hinge moment due to angle of attack. The changes in section had only a minor effect on the hinge moment due to control deflection, contrary to what might have been expected, and had considerable effect on the hinge moment due to angle of attack.

In figure 6, pressure distributions are presented for a typical section modification, in this case wing bevel, to illustrate this phenomenon in more detail. The solid curves indicate the pressure variation along the chord on the upper surface and the dashed curves show the pressure variation on the lower surface. The left-hand side of the figure shows the effect of a change in section on the pressure distributions due to a large control deflection at an angle of attack of 2° . In this case, beveling the wing ahead of the control increased the load on the balancing portion of the control, but it also increased the load on the control behind the hinge line so that the net effect on the hinge moment was negligible.


The right-hand side of the figure shows the effect of a change in section on the pressure distribution due to an angle of attack of 8° with a control deflection of 0° . In this case, there is little change on the upper surface; however, the lower-surface peak-pressure point moves forward and increases in intensity. Behind the hinge line there is some forward shift in the center of pressure of the load. The resultant hinge moment is therefore much more positive because of the modification

of the wing section. Another way of increasing the balancing action of the overhang-nose-balance control is to increase the gap between the wing and the control so that the control behaves more like an isolated wing. However, such a modification results in a drag penalty, as do the modifications to the wing section.

A second method for reducing the hinge moments obtained on trailing-edge controls at supersonic speeds is to add a horn balance, ahead of the hinge line, to the outboard portion of the control. Figure 7 shows a correlation of hinge-moment-slope parameters at $M = 1.60$ obtained from recent tests of horn-balanced controls in the Ames 6- by 6-foot supersonic tunnel (ref. 5), tests in the C.I.T. Jet Propulsion Laboratory 12-inch supersonic tunnel (refs. 6, 9, and 16), and on a Langley Pilotless Aircraft Research Division rocket research model (refs. 17 and 18). The correlation with the ratio of control-balance area to total control area is approximately linear, even though both triangular horns and rectangular horns are included on delta wings having leading-edge sweeps from 60° to 75° . As compared to the overhang nose balance, the balancing horns are considerably more effective in reducing the hinge moments due to control deflection and angle of attack. A horn of only one-third the control area balances C_{h_δ} and a horn of only 15 percent of the control area balances C_{h_α} for this Mach number condition. With this type of control, it is of course impossible to balance both C_{h_δ} and C_{h_α} closely with one balance configuration.

Still another method of reducing the control hinge moments at supersonic speeds is to use tip controls, in which the hinge-line location may be chosen to balance the forces acting on the control. Figure 8 presents recent data on 60° half-delta tip controls on a 60° delta wing from Langley Pilotless Aircraft Research Division rocket tests (ref. 28) and tests in the Langley 9- by 12-inch supersonic blowdown tunnel (refs. 29 and 30), the Langley 4- by 4-foot supersonic pressure tunnel (ref. 13), the Langley 9- by 9-inch Mach number 4 blowdown jet, and the Langley 11-inch hypersonic tunnel. These data extend the speed range for which tip-control data were previously available to the hypersonic region and increase the range of balances tested. For comparative purposes, experimental curves are also shown for the hinge-moment-slope parameters of a 30-percent-chord trailing-edge control obtained from two-dimensional tests in some of the same test facilities (refs. 20 to 22). In general, the hinge-moment-slope parameters for the tip controls vary with shifts in the hinge-line location in a systematic manner, as would be expected. The linear-theory curve is shown for the 55-percent-balance condition, which corresponds to the square test points of the experimental data.

In view of the interest shown in data at the highest available Mach number, figure 9 shows in more detail the hinge-moment characteristics




with control deflection and angle of attack for the two types of controls tested at a Mach number of 6.90. The hinge-moment-coefficient scales are different for the two controls and the characteristics are not directly comparable because of the differences in moment areas on which the coefficients are based. The linear-theory curves are shown for the range of test angles, although the linear theory is obviously invalid at this Mach number except for very small angles and extremely thin wings.

The shock-expansion theory gives a reasonable prediction of the hinge-moment-coefficient variation with control deflection for the trailing-edge control and gives excellent prediction of the variation of hinge-moment coefficient with angle of attack. For the tip control, the shock-expansion theory, computed by assuming that the flow over the control was completely two-dimensional, provided an excellent prediction of the hinge-moment characteristics at the small angles. The linear-theory agreement with the shock-expansion theory at the small angles is fortuitous as a result of the section of the particular control tested.

The agreement between shock-expansion theory and experiment for the control hinge-moment coefficient due to control deflection, shown in this figure, tends to give an overly optimistic impression of our ability to predict the flow characteristics at this Mach number. Figure 10 shows the experimental and shock-expansion pressure distributions for the trailing-edge control, first with a control deflection of 16° and an angle of attack of 0° and second with an angle of attack of 16° and a control deflection of 0° . The prediction of the angle-of-attack effect is very good; however, the prediction of the control-deflection effect is poor. On the wing lower surface, the flow separates ahead of the hinge line and then gradually increases in pressure to the trailing edge. The effects on the hinge moment of the discrepancies between experimental and theoretical pressure distributions are of a compensating nature and therefore the experimental loss in hinge moment is considerably less than the experimental loss in lift. A similar investigation of the flow details for the tip-control case is needed to understand better the validity of the theoretical predictions at this Mach number.

To study more closely the effect of changes in tip-control hinge-line location and plan form at lower Mach numbers, extensive tests have been made in the Langley 4- by 4-foot supersonic pressure tunnel (ref. 13) and in the Langley 9- by 12-inch supersonic blowdown tunnel (refs. 29 and 30 and unpublished data). The correlation of the hinge-moment-slope parameters with area ratio at a Mach number of 1.6 for the 10 configurations tested is presented in figure 11. From this figure it is evident that the slope parameters correlate satisfactorily with area ratio, despite the secondary effects of plan form, which cause some scatter of the points. The tip controls may be balanced at this condition for an area ratio near 0.4, and the ratio for balancing $C_{h\delta}$ is very close to the ratio necessary to balance $C_{h\alpha}$.




The balancing of control hinge moments at a control deflection of 0° and an angle of attack of 0° is likely, however, to prove misleading in view of the effect of angle of attack and control deflection. The most closely balanced controls tend to have the most nonlinear hinge-moment characteristics. Figure 12 shows the hinge-moment-coefficient curves with control deflection at several angles of attack for a 55-percent-balanced control at a Mach number of 1.61. As the angle of attack is increased to 12° , the curves become increasingly nonlinear and in some regions the control is overbalanced. On the right-hand side of the figure, the hinge-moment curves for a control having less balance show an increased slope but no regions of overbalance with control deflection. In an attempt to reduce the nonlinearities, a fence was installed at the wing-control parting line to prevent crossflow through the angular gap due to deflection of the control (ref. 34). When this fence was installed, the average effect was an improvement in the linearity of the curves. A similar linearizing effect of the fence was also found in tip- and horn-balanced-control tests in the Langley 9- by 12-inch supersonic blowdown tunnel (refs. 30 and 14).

Other balancing devices which have been tested, but which are not discussed in detail here, are the paddle balances, tabs, and all-movable controls. The paddle balances (ref. 5) are very effective at supersonic speeds in reducing C_{h_g} and can be used alone to reduce C_{h_a} ; however, there is a very large drag penalty associated with their use. Tabs (refs. 33 and 34) are less effective at supersonic speeds than at subsonic speeds in balancing the hinge moments and require large deflections. All-movable delta controls appear encouraging at supersonic speeds because there is very little shift of the center of pressure with body angle of attack or wing deflection; however, there is a large shift in center of pressure through the transonic speed range and the method of mounting poses considerable problems.

CONCLUSIONS

Correlations have been obtained, on the basis of simple geometric parameters, which permit quick estimates of the effectiveness and hinge-moment characteristics of controls of any plan form or location on wings of many plan forms at supersonic speeds. Closely balanced controls tend to exhibit nonlinear hinge-moment characteristics with control deflection and angle of attack. On tip and horn-balanced controls, a fence installed at the wing-control parting line produces a linearizing effect.



CONFIDENTIAL

REFERENCES AND BIBLIOGRAPHY

Control Effectiveness

1. Mitchell, Meade H., Jr.: Effects of Varying the Size and Location of Trailing-Edge Flap-Type Controls on the Aerodynamic Characteristics of an Unswept Wing at a Mach Number of 1.9. NACA RM L50F08, 1950.
2. Jacobsen, Carl R.: Effects on Control Effectiveness of Systematically Varying the Size and Location of Trailing-Edge Flaps on a 45° Sweptback Wing at a Mach Number of 1.9. NACA RM L51I26, 1951.
3. Schult, Eugene D., Strass, H. Kurt, and Fields, E. M.: Free-Flight Measurements of Some Effects of Aileron Span, Chord, and Deflection and of Wing Flexibility on the Rolling Effectiveness of Ailerons on Sweptback Wings at Mach Numbers Between 0.8 and 1.6. NACA RM L51K16, 1952.
4. Strass, H. Kurt, Fields, E. M., and Schult, Eugene D.: Some Effects of Spanwise Aileron Location and Wing Structural Rigidity on the Rolling Effectiveness of 0.3-Chord Flap-Type Ailerons on a Tapered Wing Having 63° Sweepback at the Leading Edge and NACA 64A005 Airfoil Sections. NACA RM L51D18a, 1951.

Hinge Moments

Overhang-nose-balanced controls:

5. Boyd, John W., and Pfyl, Frank A.: Experimental Investigation of Aerodynamically Balanced Trailing-Edge Control Surfaces on an Aspect Ratio 2 Triangular Wing at Subsonic and Supersonic Speeds. NACA RM A52I04, 1953.
 6. Thomas, G. B.: Analysis of Supersonic Wind-Tunnel Tests of Balanced Aileron Configurations for the Nike Guided Missile. Rep. No. SM-13796, Douglas Aircraft Co., Inc., Sept. 29, 1950.
 7. Wiley, Harleth G.: Aerodynamic Characteristics at Transonic Speeds of a 60° Delta Wing Equipped With a Triangular Plan-Form Control Having a Skewed Hinge Axis and an Overhang Balance. Transonic-Bump Method. NACA RM L50L01, 1951.
 8. Mueller, James N., and Czarnecki, K. R.: Preliminary Data at a Mach Number of 2.40 of the Characteristics of Flap-Type Controls Equipped With Plain Overhang Balances. NACA RM L52F10, 1952.
-

CONFIDENTIAL

9. Mason, Maxwell, and Miller, Robert C.: Wind-Tunnel Test of 11 Per Cent Scale Semispan Models of the Douglas Nike 484 Missile. Rep. No. SWT 12-8, Jet Propulsion Lab., C.I.T., 1950.
10. Lockwood, Vernard E., and Hagerman, John R.: Aerodynamic Characteristics at Transonic Speeds of a Tapered 45° Sweptback Wing of Aspect Ratio 3 Having a Full-Span Flap Type of Control With Overhang Balance. Transonic-Bump Method. NACA RM L51L11, 1952.
11. Thompson, Robert F., and Moseley, William C., Jr.: Hinge-Moment and Control-Effectiveness Characteristics of an Outboard Flap With an Overhang Nose Balance on a Tapered 35° Sweptback Wing of Aspect Ratio 4. Transonic-Bump Method. NACA RM L52G08, 1952.
12. Croom, Delwin R., and Wiley, Harleth G.: Investigation of Transonic Speeds of the Hinge-Moment and Lift-Effectiveness Characteristics of a Single Flap and a Tandem Flap on a 60° Delta Wing. NACA RM L53E28a, 1953.

Horn-balanced controls:

References 5, 6, and 9.


13. Czarnecki, K. R., and Lord, Douglas R.: Hinge-Moment Characteristics for Several Tip Controls on a 60° Sweptback Delta Wing at Mach Number 1.61. NACA RM L52K28, 1953.
14. Guy, Lawrence D.: Control Hinge-Moment and Effectiveness Characteristics of a Horn-Balanced, Flap-Type Control on a 55° Sweptback Triangular Wing of Aspect Ratio 3.5 at Mach Numbers of 1.41, 1.62, and 1.96. NACA RM L52L15, 1953.
15. Wiley, Harleth G., and Zontek, Leon: Aerodynamic Characteristics at Transonic Speeds of a 60° Delta Wing Equipped With a Constant-Chord Flap-Type Control With and Without an Unshielded Horn Balance. Transonic-Bump Method. NACA RM L51H22, 1952.
16. Thomas, G. B.: Analysis of Additional Supersonic Wind-Tunnel Tests of Balanced Aileron Configurations for the Nike Guided Missile. Rep. No. SM-14290, Douglas Aircraft Co., Inc., Mar. 14, 1952.
17. Mitcham, Grady L., Crabill, Norman L., and Stevens, Joseph E.: Flight Determination of the Drag and Longitudinal Stability and Control Characteristics of a Rocket-Powered Model of a 60° Delta-Wing Airplane From Mach Numbers of 0.75 to 1.70. NACA RM L51I04, 1951.

CONFIDENTIAL

18. Mitcham, Grady L., Stevens, Joseph E., and Norris, Harry P.: Aerodynamic Characteristics and Flying Qualities of a Tailless Triangular-Wing Airplane Configuration As Obtained From Flights of Rocket-Propelled Models at Transonic and Low Supersonic Speeds. NACA RM L9L07, 1950.

Unbalanced controls:

References 5, 6, 9, 13, 15, and 16.

19. Boyd, John W.: Aerodynamic Characteristics of Two 25-Percent-Area Trailing-Edge Flaps on an Aspect Ratio 2 Triangular Wing at Subsonic and Supersonic Speeds. NACA RM A52D01c, 1952.
20. Czarnecki, K. R., and Mueller, James N.: Investigation at Mach Number 1.62 of the Pressure Distribution Over a Rectangular Wing With Symmetrical Circular-Arc Section and 30-Percent-Chord Trailing-Edge Flap. NACA RM L9J05, 1950.
21. Czarnecki, K. R., and Mueller, James N.: Investigation at Supersonic Speeds of Some of the Factors Affecting the Flow Over a Rectangular Wing With Symmetrical Circular-Arc Section and 30-Percent-Chord Trailing-Edge Flap. NACA RM L50J18, 1951.
22. Ulmann, Edward F., and Lord, Douglas R.: An Investigation of Flow Characteristics at Mach Number 4.04 Over 6- and 9-Percent-Thick Symmetrical Circular-Arc Airfoils Having 30-Percent-Chord Trailing-Edge Flaps. NACA RM L51D30, 1951.
23. Dunning, Robert W., and Ulmann, Edward F.: Aerodynamic Characteristics at Mach Number of 4.04 of a Rectangular Wing of Aspect Ratio 1.33 Having a 6-Percent-Thick Circular-Arc Profile and a 30-Percent-Chord Full-Span Trailing-Edge Flap. NACA RM L53D03, 1953.
24. Kolbe, Carl D., and Tinling, Bruce E.: Tests of a Triangular Wing of Aspect Ratio 2 in the Ames 12-Foot Pressure Wind Tunnel. III - The Effectiveness and Hinge Moments of a Skewed Wing-Tip Flap. NACA RM A8E21, 1948.
25. Sivells, James C., and Goin, Kenneth L.: Experimental and Calculated Hinge Moments of Two Ailerons on a 42.7° Sweptback Wing at a Mach Number of 1.9. NACA RM L8K24a, 1949.
26. Boatright, William B., and Rainey, Robert W.: Hinge-Moment Measurements of a Wing With Leading-Edge and Trailing-Edge Flaps at a Mach Number of 1.93. NACA RM L8K12a, 1949.
- 

CONFIDENTIAL

27. Conner, D. William, and Mitchell, Meade H., Jr.: Control Effectiveness and Hinge-Moment Measurements at a Mach Number of 1.9 of a Nose-Flap and Trailing-Edge Flap on a Highly Tapered Low-Aspect-Ratio Wing. NACA RM L8K17a, 1949.

Balanced tip controls:

References 13 and 16.


28. Martz, C. William, Church, James D., and Goslee, John W.: Rocket-Model Investigation To Determine the Force and Hinge-Moment Characteristics of a Half-Delta Tip Control on a 59° Sweptback Delta Wing Between Mach Numbers of 0.55 and 1.43. NACA RM L52H06, 1952.
29. Conner, D. William, and May, Ellery B., Jr.: Control Effectiveness Load and Hinge-Moment Characteristics of a Tip Control Surface on a Delta Wing at a Mach Number of 1.9. NACA RM L9H05, 1949.
30. Guy, Lawrence D.: Control Hinge-Moment and Effectiveness Characteristics of a 60° Half-Delta Tip Control on a 60° Delta Wing at Mach Numbers of 1.41 and 1.96. NACA RM L52H13, 1952.
31. Conner, D. William, and May, Ellery B., Jr.: Control Effectiveness and Hinge-Moment Characteristics of a Tip Control Surface on a Low-Aspect-Ratio Pointed Wing at a Mach Number of 1.9. NACA RM L9H26, 1949.
32. Wingrove, A. A., and Pindar, A. C. S.: Tests in High Speed Wind Tunnel on Half-Model of Delta Wing With Moving Tip Control. TN No. Aero. 2052, British R.A.E., May 1950.

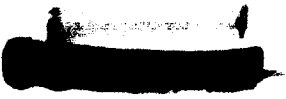
Paddle balances:

Reference 5.


Tab balances:

Reference 5.

33. Lockwood, Vernard E., and Fikes, Joseph E.: Preliminary Investigation at Transonic Speeds of the Effect of Balancing Tabs on the Hinge-Moment and Other Aerodynamic Characteristics of a Full-Span Flap on a Tapered 45° Sweptback Wing of Aspect Ratio 3. NACA RM L52A23, 1952.
- 

34. Czarnecki, K. R., and Lord, Douglas R.: Preliminary Investigation of the Effect of Fences and Balancing Tabs on the Hinge-Moment Characteristics of a Tip Control on a 60° Delta Wing at Mach Number 1.61. NACA RM L53D14, 1953.
35. Wegener: Preliminary Results of the Wind Tunnel Development of Control Surfaces With Tabs for the Control of the Wasserfall Device. Douglas Aircraft Co., Inc. translation of Archiv. No. 66/153, Wasserbau Exp. Inst. (Munich), Oct. 31, 1944.
- All-movable controls:
36. Conner, D. William: Aerodynamic Characteristics of Two All-Movable Wings Tested in the Presence of a Fuselage at a Mach Number of 1.9. NACA RM L8H04, 1948.
37. Johnson, M. C.: Wing Panel Hinge Moments for the Sparrow I Missile at a 45° Bank Angle. Rep. No. SM-14560, Douglas Aircraft Co., Inc., Jan. 8, 1953.
38. Johnson, M. C.: Analysis of Wing Panel Normal Force and Hinge Moment Characteristics From Wind Tunnel Tests of a 45-Percent-Scale Model of the Sparrow I Missile at Mach Numbers of 1.4 and 1.9. Rep. No. SM-14552, Douglas Aircraft Co., Inc., Jan. 16, 1953.
- Fences:
- References 14, 29, 30, and 34.
- Theory:
- Reference 34.
39. Lagerstrom, P. A., and Graham, Martha E.: Linearized Theory of Supersonic Control Surfaces. Jour. Aero. Sci., vol. 16, no. 1, Jan. 1949, pp. 31-34.
40. Goin, Kenneth L.: Equations and Charts for the Rapid Estimation of Hinge-Moment and Effectiveness Parameters for Trailing-Edge Controls Having Leading and Trailing Edges Swept Ahead of the Mach Lines. NACA Rep. 1041, 1951. (Supersedes NACA TN 2221.)
41. Frick, Charles W., Jr.: Application of the Linearized Theory of Supersonic Flow to the Estimation of Control-Surface Characteristics. NACA TN 1554, 1948.
42. Coale, Charles W.: Supersonic Characteristics of Rectangular Horn Balanced Ailerons. Rep. No. SM-13718, Douglas Aircraft Co., Inc., Mar. 31, 1950.
- 

CONFIDENTIAL

43. Tucker, Warren A., and Nelson, Robert L.: Theoretical Characteristics in Supersonic Flow of Two Types of Control Surfaces on Triangular Wings. NACA Rep. 939, 1949. (Supersedes NACA TN's 1600, 1601, and 1660.)
 44. Kainer, Julian H., and King, Mary Dowd: The Theoretical Characteristics of Triangular-Tip Control Surfaces at Supersonic Speeds. Mach Lines Behind Trailing Edges. NACA TN 2715, 1952.
 45. Kainer, Julian H., and Marte, Jack E.: Theoretical Supersonic Characteristics of Inboard Trailing-Edge Flaps Having Arbitrary Sweep and Taper. Mach Lines Behind Flap Leading and Trailing Edges. NACA TN 2205, 1950.
 46. Goin, Kenneth L.: Theoretical Analyses To Determine Unbalanced Trailing-Edge Controls Having Minimum Hinge Moments Due to Deflection at Supersonic Speeds. NACA RM L51F19, 1952.
 47. Morrisette, Robert R., and Oborny, Lester F.: Theoretical Characteristics of Two-Dimensional Supersonic Control Surfaces. NACA TN 2486, 1951. (Supersedes NACA RM L8G12.)
 48. Tucker, Warren A., and Nelson, Robert L.: Theoretical Characteristics in Supersonic Flow of Constant-Chord Partial-Span Control Surfaces on Rectangular Wings Having Finite Thickness. NACA TN 1708, 1948.
- 

DECLASSIFIED

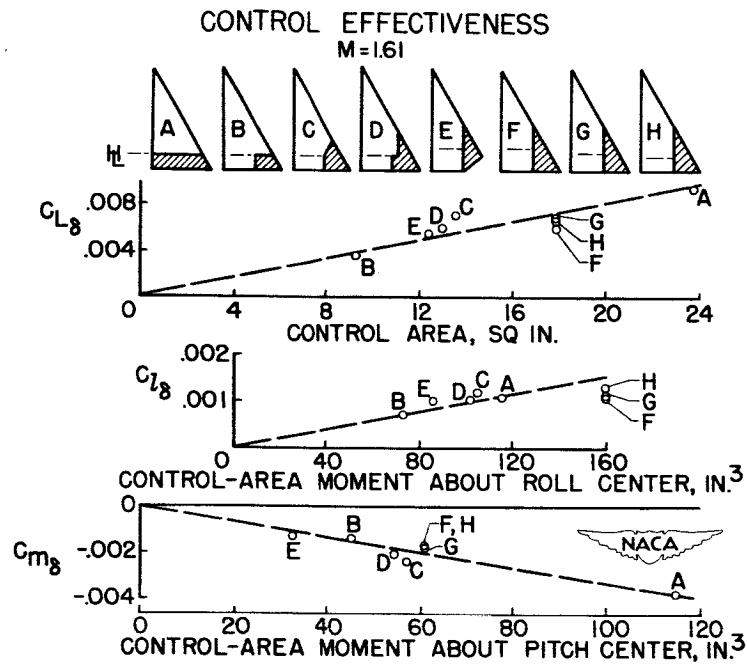


Figure 1

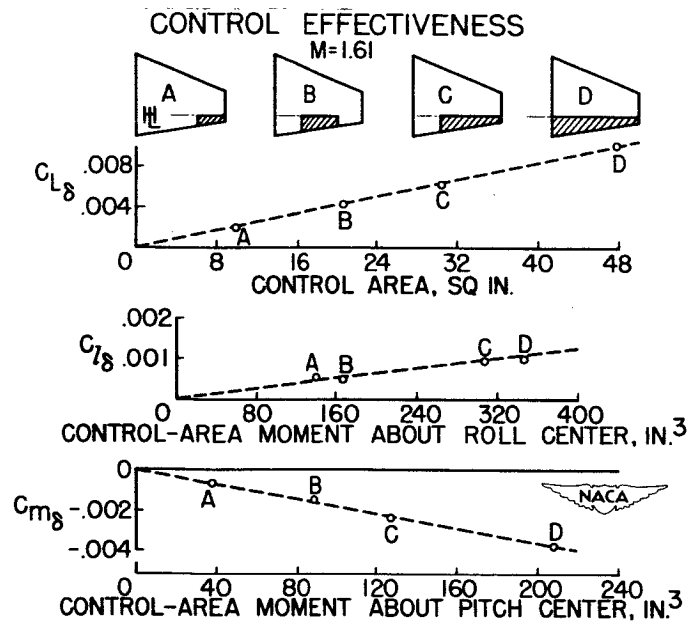


Figure 2

CONFIDENTIAL

OVERHANG NOSE-BALANCED CONTROLS

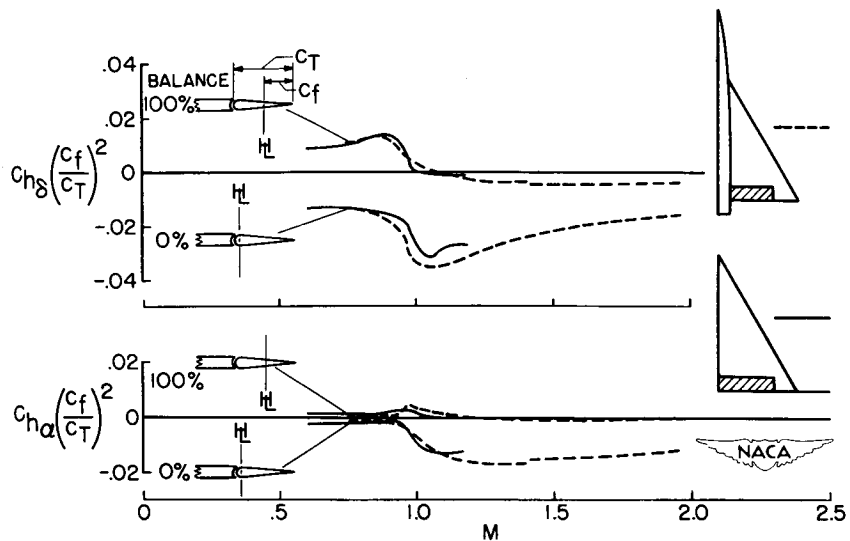


Figure 3

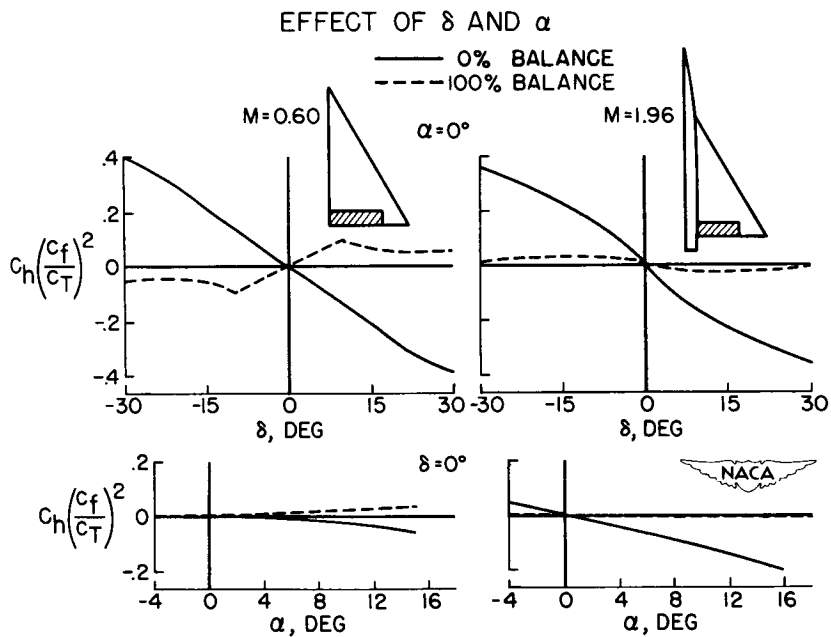


Figure 4

CONFIDENTIAL

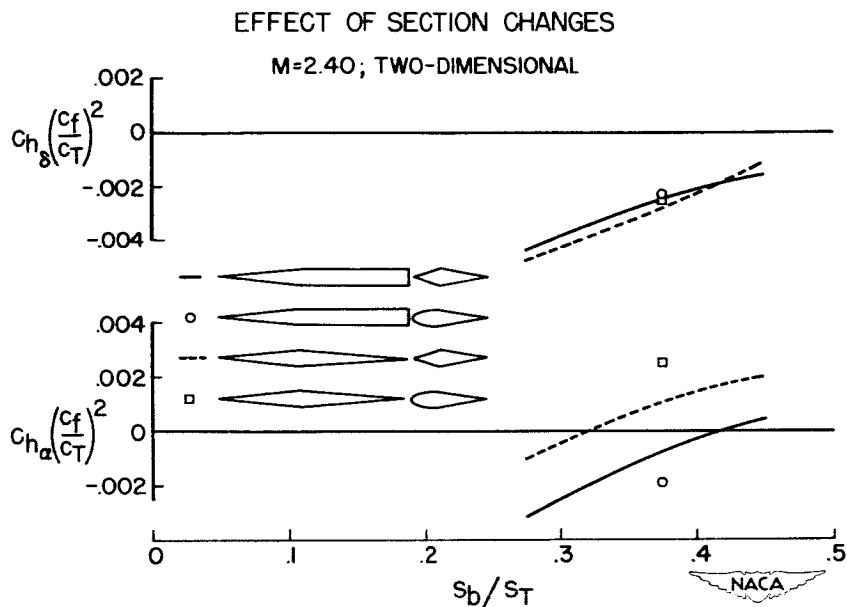


Figure 5

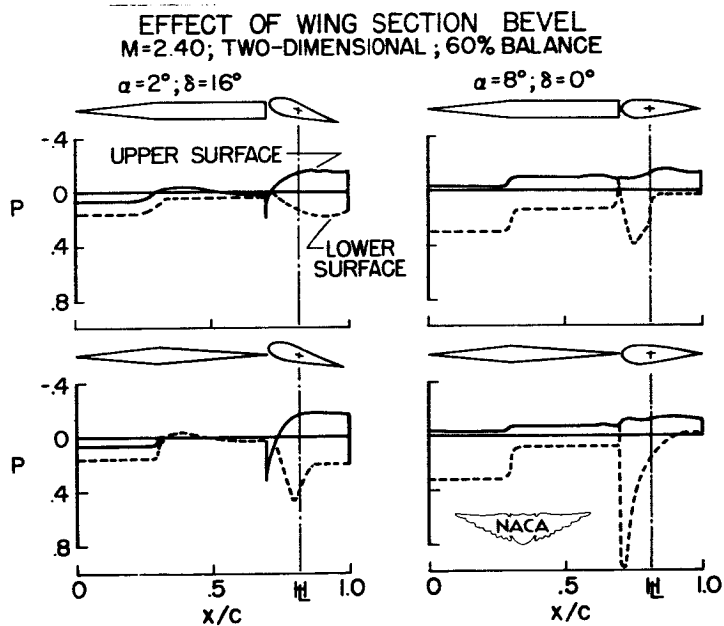


Figure 6

CONFIDENTIAL

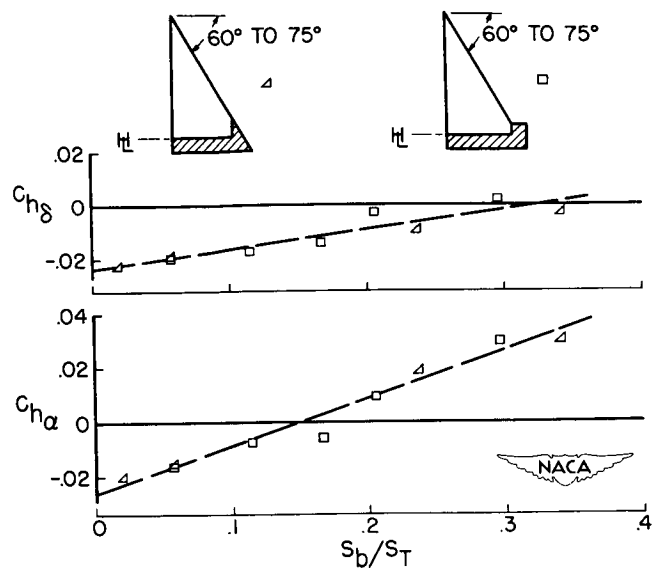
HORN-BALANCED CONTROLS
M=1.60

Figure 7

HALF-DELTA TIP CONTROL AND TRAILING-EDGE CONTROL

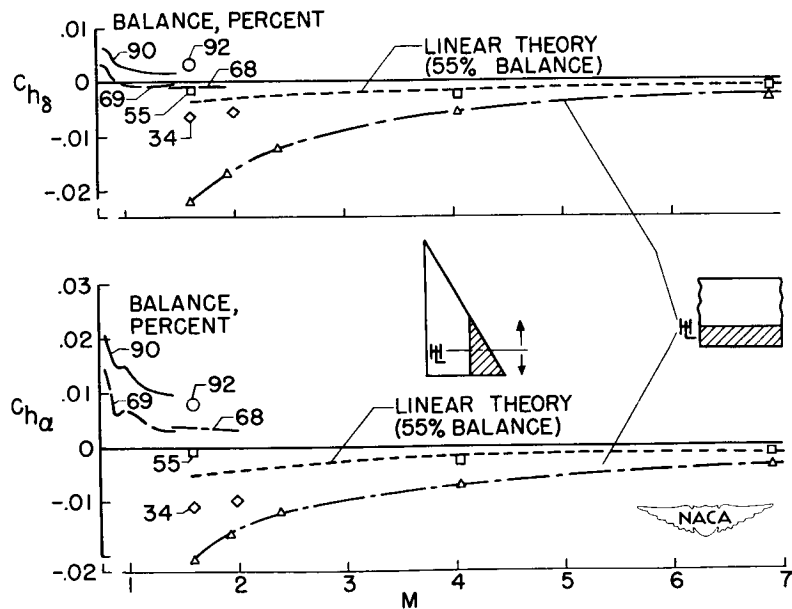


Figure 8

HIGH MACH NUMBER CHARACTERISTICS

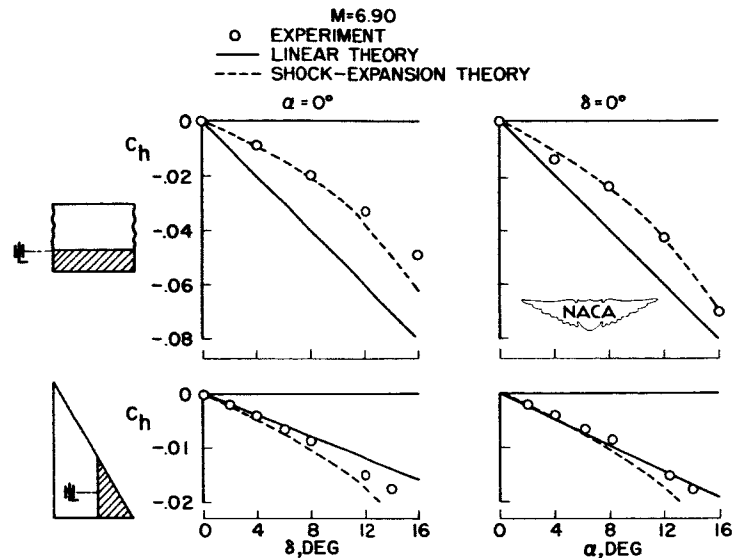


Figure 9

HIGH MACH NUMBER PRESSURE DISTRIBUTIONS

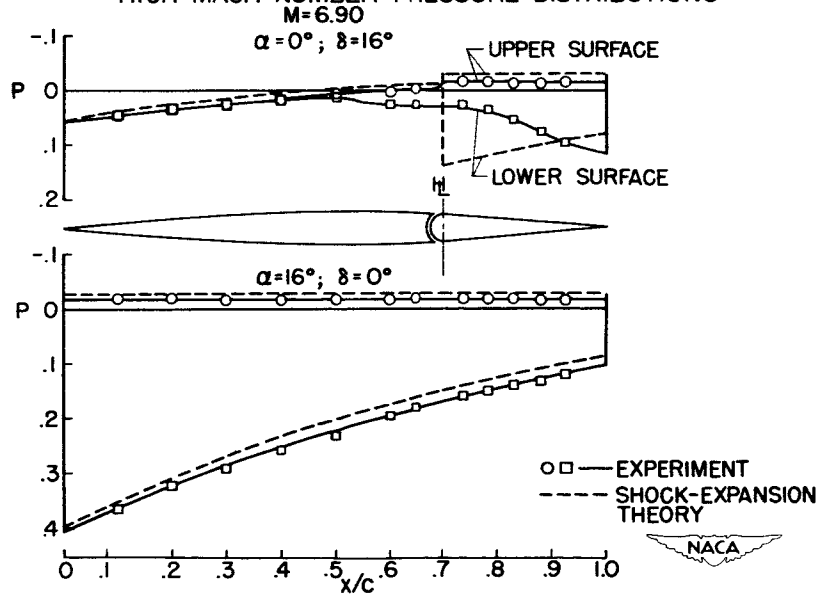


Figure 10

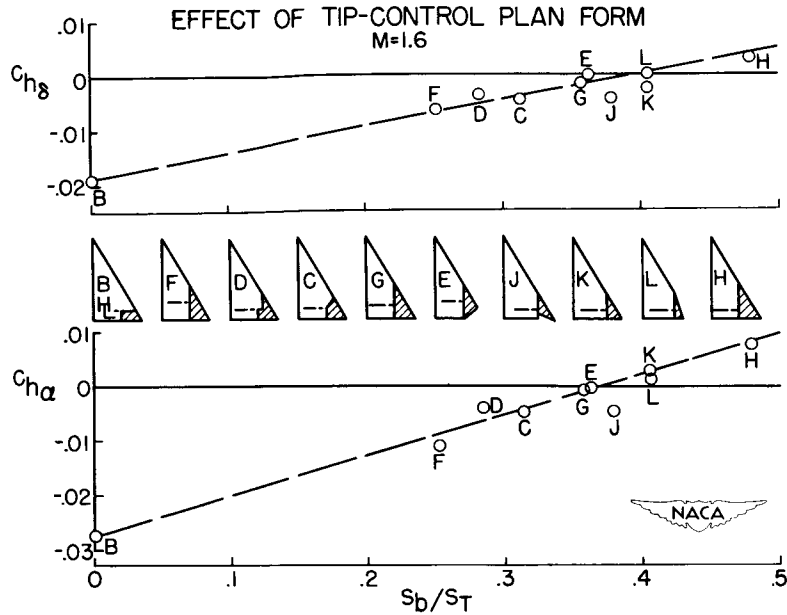


Figure 11

HINGE-MOMENT NONLINEARITIES FOR TIP CONTROLS

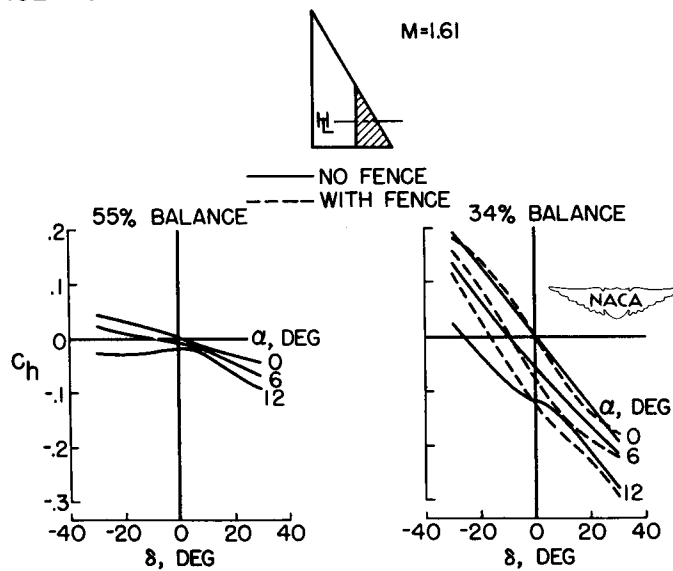


Figure 12

CONFIDENTIAL

DECLASSIFIED

SEVERAL FACTORS AFFECTING ROLL CONTROL SYSTEMS

OF INTERCEPTORS


By Leonard Sternfield

Langley Aeronautical Laboratory

One of the primary defense weapons of our country's air-defense system will be the manned all-weather interceptor, which is to be capable of flying at supersonic speeds and of operation to an altitude of 60,000 feet. During the attack phase of the interceptor's mission, which is started as soon as the interceptor establishes contact with the target, the radar continuously furnishes target data such as range and azimuth and elevation angles to the fire-control computer. These measured data are processed by the fire-control computer to obtain command signals to deflect the airplane's control surfaces. In order for the interceptor to maneuver toward the target, it must roll to turn. It is, therefore, necessary to incorporate an effective roll control system in the automatic guidance or tracking system of such airplanes. The purpose of this paper is to present the results of a theoretical investigation concerned with two different types of roll control systems.

Several recent design studies (ref. 1, for instance) for both longitudinal and lateral automatic-control systems have considered different types of compensating networks. The purpose of a compensating network is to cancel the effect of either one or more of the airplane's modes of motion from the response of the airplane to a command input. For example, the long-period longitudinal oscillation, the phugoid, may be canceled by a compensating network designed for an altitude control system, or the Dutch roll oscillation may be canceled by a compensating network designed for a lateral control system. A general study of compensating networks was undertaken and the first network studied was one designed to cancel the effect of the airplane dynamics, that is, all the lateral modes of motion, from the response of the airplane in roll. Thus, the first type of roll control system to be discussed is referred to as a compensating network system. In order to accomplish this cancellation, the compensating network is so designed that its transfer function is the inverse of the airplane's transfer function.

Figure 1 shows a block diagram of one type of compensating network incorporated in a roll control system. This system corresponds to a velocity command system that could control any one of a number of positional quantities such as the radar tracking error, airplane attitude, or, as in this case, controlling bank angle. An error in bank angle is immediately changed to a command in rolling velocity which passes through an integrator into the compensating network where $H(p)$ is the airplane's transfer



CONFIDENTIAL

function of rolling velocity due to an aileron deflection. The equation for $H(p)$ is given in figure 1. The output of the compensating network is fed into a hydraulic servomotor represented by a first-order time lag $1/(1+\tau_p)$ and results in an aileron deflection which causes the airplane to roll. It is seen that the compensating network is so designed that its transfer function includes the inverse of the airplane's transfer function $H(p)$. As would be expected, the closed-loop transfer function ϕ_o/ϕ_i of this system, presented in figure 1, is solely a function of the gains K_F and K_I and the time constant τ and does not include the airplane dynamics. The type of motion obtained for the aileron can be determined from the transfer function of δ_a/ϕ_i which is a product of two factors, the first being the closed-loop transfer function and the second, the inverse transfer function of the airplane where the denominator very closely represents the characteristics of one degree of freedom of the airplane in yaw. The aileron motion would, therefore, be a damped oscillatory motion, oscillating at a frequency which is approximately the airplane's natural frequency, and the damping of the oscillation is a direct function of the damping-in-yaw derivative C_{n_r} . Also, the motion in sideslip has the same period-damping relation as the aileron motion. However, the Dutch roll oscillation in the sideslip and aileron motions could be greatly reduced by using an automatic control system regulating sideslip and yawing velocity. Figure 2 shows the response in bank due to a step input command of 60° . The motion, corresponding to the closed-loop transfer function presented in figure 1 has good response characteristics and excellent stability.

With the compensating network just described, it appears obvious that the airplane dynamics could be eliminated from the motion in bank for a command input. There are, however, several problems of interest which were investigated. The transfer-function analysis of the system resulting in the expression shown in figure 1 assumes that the system is linear. The question arises as to how well the system behaves if nonlinearities of the type represented by limiting the maximum control deflection and maximum rate of control deflection are taken into account. Another problem directly related to compensating networks is the possibility of incomplete compensation occurring; that is, the transfer function of the compensating network will not cancel the airplane's transfer function. Incomplete compensation may be caused by designing a compensating network based on inaccurate estimates of the stability derivatives so that the airplane's transfer function in the compensating network is not the exact inverse of the true airplane's transfer function, or incomplete compensation may be due to the fact that the airplane assumes a flight condition different from the one for which the compensating network was designed. Also, one is concerned not only with knowing how well the compensating

network behaves as a command system but of equal importance one must determine the ability of the compensating network to stabilize the airplane motion if the airplane is disturbed by a gust.

Figure 3 illustrates the effect of limits in the velocity command system. Time histories of the motions in bank in response to a step input command are presented. These motions as well as all subsequent motions presented were obtained on a Reeves Electronic Analog Computer at Project Cyclone. The flight conditions correspond to an interceptor flying at 60,000 feet at $M = 2$. The upper plot shows the effect of limiting the maximum rate of control deflection $\dot{\delta}$ when the maximum control deflection δ is limited to 20° . The value of $\dot{\delta}$ for the solid-line curve is $100^\circ/\text{sec}$, whereas the dashed-line curve corresponds to a value of $\dot{\delta}$ of $40^\circ/\text{sec}$, the present requirement for powered controls. Although the rise time is not affected by reducing $\dot{\delta}$, the system becomes unstable. The lower plot in figure 3 shows the effect of limiting δ for a value of $\dot{\delta}$ of $100^\circ/\text{sec}$. The solid-line curve is for the condition of $\dot{\delta} = 100^\circ/\text{sec}$ and $\delta = 20^\circ$ and the dashed-line curve represents the case of the limited value of δ being reduced to 10° . Here again, the stability is decreased as δ is decreased. Thus, in general, a reduction in either the limiting value of $\dot{\delta}$ or δ decreases the stability of the system. If the error gain is decreased, the system becomes less critical to limiting but the response is much slower.

The other problem mentioned was the effect of small inaccuracies in the estimation of the stability derivatives in designing the compensating network, thereby resulting in incomplete cancellation of the airplane's transfer function. This problem was investigated by varying each derivative and several derivatives in combination. The results indicated that small variations of most of the derivatives had little effect on the motion. However, the estimation of the directional-stability derivative $C_{n\beta}$ was critical. Figure 4 shows the effect of inaccurately estimating $C_{n\beta}$ on the motion in bank for the velocity command system. The solid-line curve is for the case of complete cancellation where $C_{n\beta} = 0.28$. As $C_{n\beta}$ is increased to 0.32, indicated by the dashed-line curve, a slightly divergent oscillation is introduced. However, if the actual value of $C_{n\beta}$ were less than 0.28, a motion similar to the solid-line curve is obtained. The response for $C_{n\beta} = 0.24$ is shown in figure 4. It should be noted that, if rudder control is used to maintain zero sideslip during the maneuver, the roll control system may not be sensitive to the inaccurate estimate of $C_{n\beta}$.

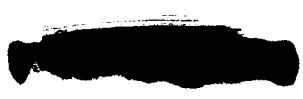
CONFIDENTIAL

Calculations made for the interceptor flying at $M = 1.4$ at 60,000 feet, where the stability derivatives corresponding to this new flight condition are different from those corresponding to the designed flight condition of the compensating network, show that the motion is unstable for the velocity command system but stable for a velocity-plus-acceleration command system. However, for this velocity-plus-acceleration command system, similar results on the effect of limiting and the inaccurate estimation of $C_{n\beta}$ were obtained as indicated for the velocity command system. If a displacement command system were used, it is expected that limiting would not have as pronounced an effect as shown in figure 3.

Thus far, the results presented were confined to a compensating network as a command system. In order to investigate how well the velocity command system stabilizes the airplane motion if the airplane is disturbed by a gust, the airplane was assumed to be disturbed from trim by step inputs of either $C_l = 0.005$ or $C_n = 0.005$. Figure 5 shows the results of these calculations. It is apparent from this figure that the Dutch roll oscillation does appear in the motion and, thus, the compensating network does not offer any improvement when the airplane is disturbed by a gust. The integrator in the system, which gives control proportional to the integral of the bank-angle error, reduces the steady-state error to zero. Additional calculations indicated that the response is improved for higher gains until limiting of δ and $\dot{\delta}$ takes place.

The second type of roll control system investigated is a conventional attitude control system with an integrator and rate and acceleration feedback. A block diagram of the system is shown in figure 6. The analysis considered three airplanes which had the characteristics shown in figure 7. The motions presented in figure 7 are the rolling velocity due to a step deflection of the aileron for each of the three airplanes. It is noted that, for airplanes B and C, the Dutch roll oscillation appears in the rolling motion, whereas for airplane A, the motion resembles the response obtained from considering the airplane in only one degree of freedom in roll. The corresponding sideslip motions will in all cases contain the Dutch roll characteristics. For these airplanes it was found that a yaw damper very effectively stabilized the sideslip motion but increased the steady-state sideslip angle to approximately 1° . Where the coupling between roll and sideslip is mainly a product of inertia effect, as in airplane B, a relatively larger amount of yaw damping is required to eliminate the Dutch roll from the rolling motion, thus resulting in a larger steady-state sideslip angle.

The results presented in the following figures indicate trends common to all three airplanes when equipped with a yaw damper and the roll control system outlined in the block diagram. The response of the airplane to a step-command input was very satisfactory without the integrator if the



CONFIDENTIAL

airplane has approximately neutral spiral stability. However, in analyzing the motion of the airplane after being disturbed by a gust, no satisfactory response was obtained as the gains of the system were varied; however, the integrator was required in particular to obtain zero steady-state error. Figure 8 shows the effect of varying the integrator constant K_I on the motion in bank when the airplane is disturbed from trim by a step input of $C_l = 0.01$. As K_I is increased, the airplane returns to its initial trimmed position much faster but, with further increase in K_I , the motion becomes oscillatory and will become unstable for larger values of the integrator constant. If, therefore, the integrator is an essential component of the system to obtain satisfactory response and reduces the steady-state error to zero when the airplane is disturbed by a gust, it is of interest to know the effect of the integrator on the airplane response to a step-command input. This effect is shown in figure 9. The solid-line curve in this figure represents the type of response obtained to a 60° bank-angle command without an integrator. In general, the response is excellent. With the integrator included in the system, the motion overshoots the commanded 60° bank angle and the response time, the time required for the motion to reach and remain within 5 percent of the steady-state value, is increased. This overshoot increases and the motion becomes oscillatory as the integrator gain is increased. In an attempt to improve the airplane response to a step-command input with an integrator present, the gains of the system were varied in order to obtain a more satisfactory response. First, more rate feedback was added to the system. For comparative purposes, in the lower part of figure 9 the dashed-line curve is replotted and compared with the solid-line curve which corresponds to a case which has double the rate feedback of the dashed-line curve. It is noted that the peak overshoot is not reduced and the time required for the motion to reach steady state is increased. The forward-loop gain was then varied. Figure 10 shows that a marked improvement in the command response can be realized by increasing the forward-loop gain. As the gain is increased, the overshoot is eliminated and satisfactory response is obtained. However, further increase in K_F causes the airplane to respond faster but once again introduces overshoot. This overshoot due to the forward-loop gain results from insufficient damping in the roll oscillation and can be eliminated by rate feedback. The lower part of figure 10 shows this effect. Thus, from a linear analysis of the problem, one can determine combinations of the gains in the system which will result in a very satisfactory response in bank.

The importance of taking into account the limits on control deflection and rate of control-surface deflection is shown in figure 11. As an example, the case which resulted in a satisfactory response in bank that was based on the linear analysis was selected. The solid-line curve corresponds to the case where δ is limited to 20° and $\dot{\delta}$ is limited to $120^\circ/\text{sec}$. If the maximum rate of control deflection is reduced to $40^\circ/\text{sec}$, the motion becomes oscillatory with a large amount of overshoot, although the rise time

031712Z JUL 68

is not seriously affected. If the limited value of δ is reduced to 5° , the stability is improved but the rise time is much slower. By knowing the maximum values of δ and $\dot{\delta}$ for which the airplane and hydraulic servomotor are designed, the values of gain constants could be selected to give good response in bank. For example, with limits on δ of 20° and on $\dot{\delta}$ of $40^\circ/\text{sec}$, the motion may be stabilized by introducing additional rate feedback into the system (see lower part of fig. 11).

In comparing the solid-line curve in the top plot with the solid-line curve in the lower plot, it is seen that the rise time for the system with a lower limited value of $\dot{\delta}$ and the proper gain values is slightly longer than for the higher limited value of $\dot{\delta}$ and the corresponding combination of gains for an input command or 60° bank angle. However, for smaller input command signals, the rise time for lower $\dot{\delta}$ is appreciably longer than the rise time obtained for higher $\dot{\delta}$. The reason is that for smaller inputs little limiting takes place and, thus, the system optimized for lower $\dot{\delta}$ has too much damping which tends to slow up the response.

Where limiting causes a lightly damped oscillation in the airplane motion, introducing acceleration feedback may have a pronounced stabilizing effect, particularly for airplanes that have a relatively low moment of inertia in roll.

In conclusion, the results of the preliminary study indicate that, for both roll control systems investigated, satisfactory response to command inputs is obtained, provided the rate and physical limits of control deflection are high. By taking account of the maximum value of control displacement and control rate, the system may be optimized by proper selection of the gains. However, the motion will be faster for all magnitudes of input command signals as the values of the limits are increased.

If the airplane is disturbed by a gust, the integrator present in both systems reduces the steady-state error to zero but the compensating network does not cancel the airplane dynamics from the response.

With a compensating network system, incomplete compensation will result if the estimated value of $C_{n\beta}$ used in designing the network is less than the actual $C_{n\beta}$ value of the airplane. However, if rudder control is used to maintain zero sideslip during the maneuver, the roll control system may not be sensitive to the inaccurate estimate of $C_{n\beta}$.

With a conventional attitude-roll control system, the Dutch roll oscillation present in the sideslip motion is effectively stabilized through use of a yaw damper but the steady sideslip angle is increased.

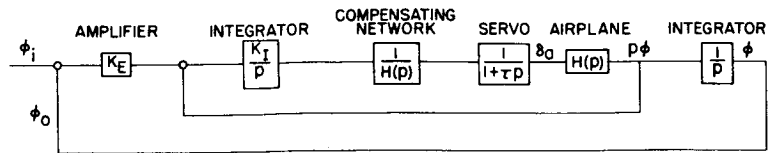
[REDACTED]

~~CONFIDENTIAL~~ 7

REFERENCE

1. Owen, J. C.: Report on Automatic Pilot for High Performance Aircraft. U.S.A.F. Exhibit MCREXELL-133, Contract AF-33(038)5700. Rep. No. 8, Eclipse-Pioneer Div. of Bendix Aviation Corp., Sept.-Oct. 1950, pp. 35-50.

BLOCK DIAGRAM FOR COMPENSATING NETWORK SYSTEM



$$H(p) = \frac{p(a_2 p^2 + a_1 p + a_0)}{b_4 p^4 + b_3 p^3 + b_2 p^2 + b_1 p + b_0}$$

$$\frac{\phi_o}{\phi_i} = \frac{K_E K_I}{\tau p^3 + p^2 + K_I p + K_E K_I}$$

$$\frac{\delta a}{\phi_i} = \left(\frac{\phi_o}{\phi_i} \right) \left(\frac{p}{H(p)} \right)$$



Figure 1

RESPONSE IN BANK FOR STEP INPUT COMMAND

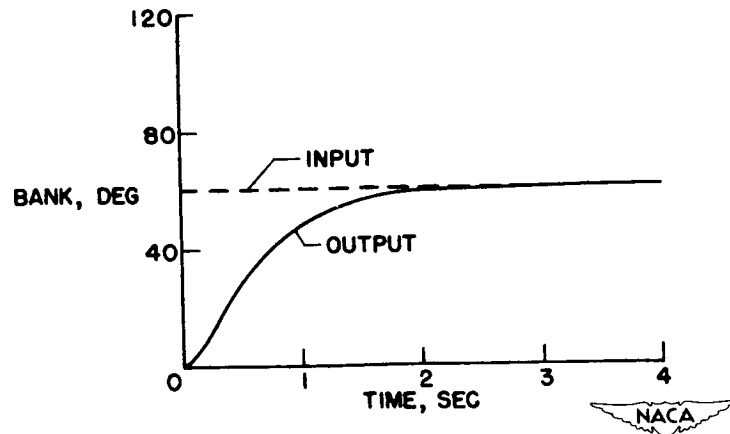


Figure 2



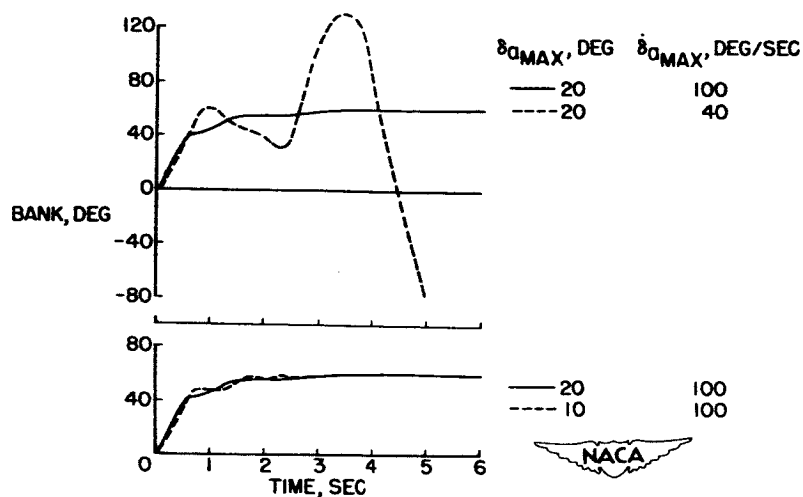
EFFECT OF LIMITING CONTROL DEFLECTION AND
RATE OF CONTROL DEFLECTION

Figure 3

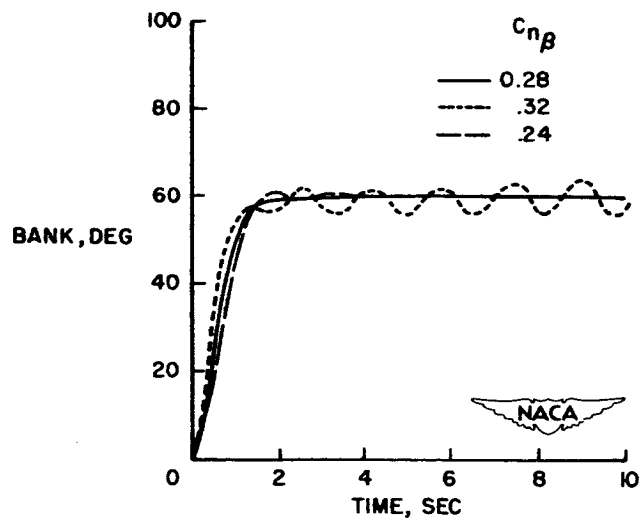
EFFECT OF INACCURACY IN ESTIMATED $C_{n\beta}$ 

Figure 4

GUST RESPONSE OF AIRPLANE WITH COMPENSATING NETWORK

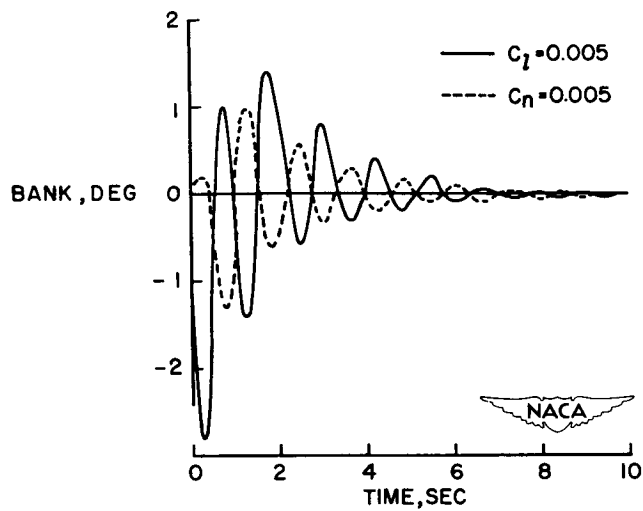
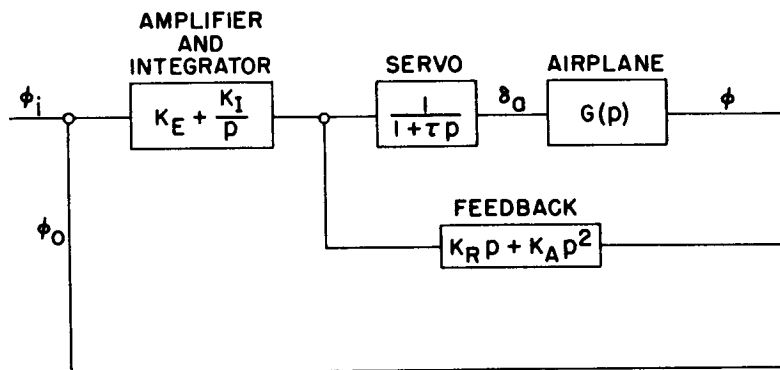


Figure 5

BLOCK DIAGRAM OF AN ATTITUDE CONTROL SYSTEM



$$G(p) = \frac{a_2 p^2 + a_1 p + a_0}{b_4 p^4 + b_3 p^3 + b_2 p^2 + b_1 p + b_0}$$



Figure 6

STABILITY CHARACTERISTICS OF AIRPLANES INCLUDED IN ANALYSIS

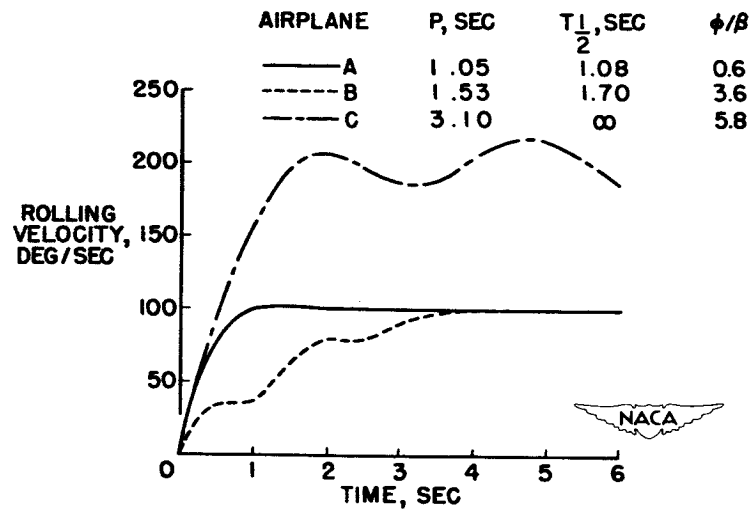


Figure 7

EFFECT OF INTEGRATOR ON REGULATORY RESPONSE

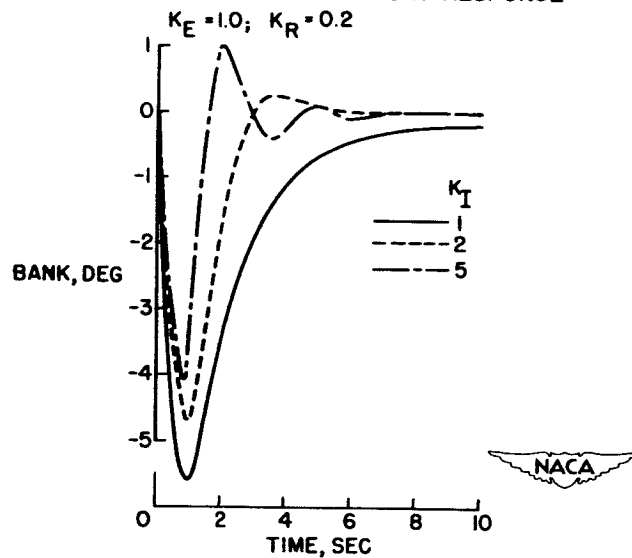


Figure 8

EFFECT OF INTEGRATOR AND RATE FEEDBACK ON COMMAND RESPONSE $K_E = 1.0$

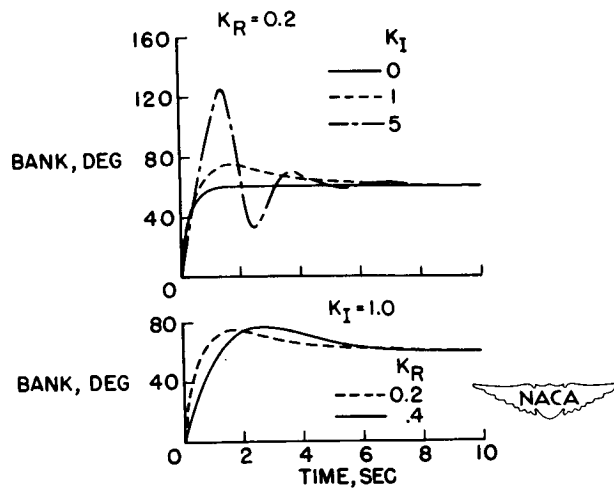


Figure 9

EFFECT OF FORWARD-LOOP GAIN ON COMMAND RESPONSE $K_I = 1.0$

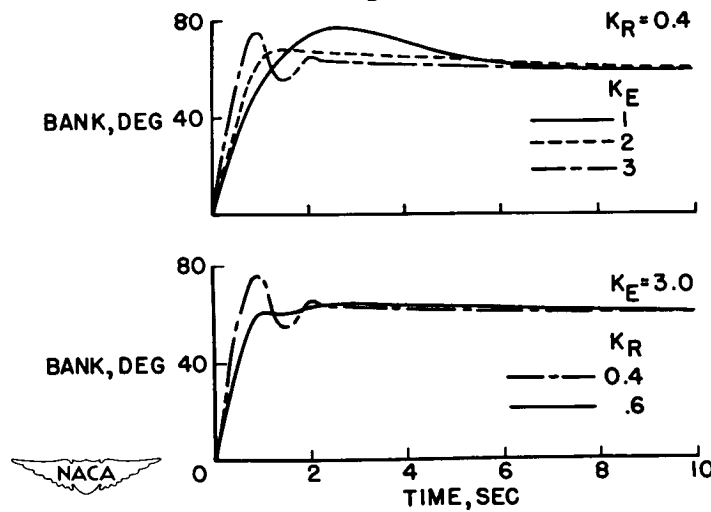


Figure 10

CONFIDENTIAL

EFFECT OF LIMITING CONTROL DEFLECTION AND RATE OF CONTROL DEFLECTION

$$K_E = 3.0; K_I = 1.0$$

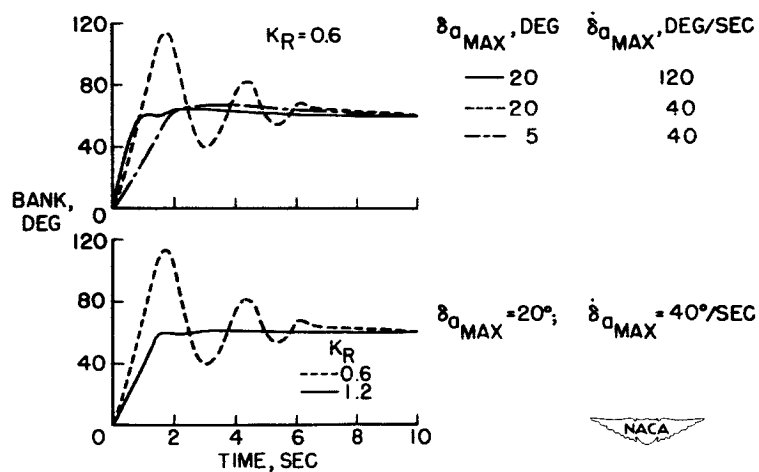


Figure 11

CONFIDENTIAL

APPLICATION OF STATISTICAL THEORY TO THE REDUCTION OF NOISE EFFECTS IN MISSILE GUIDANCE


By Elwood C. Stewart

Ames Aeronautical Laboratory

Noise is a general term often used to describe certain random unwanted effects which tend to reduce missile accuracy in hitting the target. It might be, for instance, atmospheric turbulence, enemy countermeasure devices, or any of a number of extraneous electrical signals. The particular type of noise to be considered in this paper is known as scintillation or glint noise (refs. 1 to 4) and results from the inability of the radar to determine the exact target location due to its variable reflection characteristics.

The manner in which scintillation noise affects the guidance system can be seen from figure 1. For purposes of illustration, typical samples of target motion and noise are shown separately and at different vertical and horizontal scales in order to emphasize the large target motions involved. In the actual case, however, the guidance system can detect only the sum of these two signals indicated in this figure as the apparent target position. The guidance system must then utilize this apparent target information and attempt to make the missile position coincide as closely as possible with the true target position. Thus, the error which represents failure to follow the true target motion should be minimized. This problem is analogous to one previously encountered in the communications field which has led to a statistical theory known as the Wiener filter theory (refs. 5 and 6). This paper deals with the application of this theory, later developments to this theory, and the aerodynamic implications involved in the design of a missile-guidance system.

The time histories of target motion and noise shown in figure 1 are typical of those which might be encountered in an attack against a large bomber. The target motion shown here represents an evasive maneuver consisting of constant-acceleration turns of random duration. Inputs such as these can best be described statistically in terms of spectral density, which is a measure of the energy distribution in the frequency spectrum. Figure 2 illustrates the spectral densities for both target motion and noise. It can be seen that the target-motion energy is concentrated at the lower frequencies, as is typical of all target motions, while there is appreciable noise energy at the higher frequencies. This suggests that the guidance system should be designed to have good low frequency response with minimum response to the higher frequencies. If the target motion and noise spectral-density characteristics are known, the Wiener filter theory prescribes the optimum linear



STEWART

characteristic or transfer function which will minimize the error statistically in terms of root-mean-square, or rms, error. The details of the method are involved and are not described.

For the input characteristics shown in figure 2, the Wiener theory has been applied to different magnitudes of the noise as represented by the low frequency ordinate of the noise spectral-density curve. The results are shown in figure 3. According to the Wiener theory, the dashed curve represents the theoretical lower limit of error corresponding to various noise magnitudes. The value of this result is twofold. First of all, this curve can be used as a standard to compare with the performance of other systems. Secondly, since each point on this curve corresponds to a different transfer function, this transfer function can be used as a guide in designing the guidance system. One question which arises, however, concerns the proper noise magnitude on which to base the design. In practice the guidance system may be forced to operate anywhere within the large operating band shown in figure 3, depending on the particular target. If the system is optimized only at some midrange value of noise, indicated in figure 3 as the design value, the solid curve is obtained. It can be seen that the increase in error above the optimum envelope is insignificant over the range of interest. Thus, it is necessary only to consider systems optimized for the design value of noise.

It is interesting to compare these results with the performance obtained by disregarding noise theory in the design. As an example, the upper curve in figure 3 shows the noise performance of a typical guidance system which was optimized for a target motion with no noise present. The comparison of this curve with the optimum curves shows that significant reduction of error can be achieved by the use of this theory.


In order to apply the Wiener theory to the design of a beam-rider guidance system, consider figure 4 which shows this system in greater detail. It consists of a tracking radar, either ground based or airborne, and a servocontrol system which guides the missile along the radar beam. In general, it is possible to adjust the frequency characteristics of this system in a great variety of ways. For instance, alterations can be made to the response characteristics of the tracking radar, to the control system in the missile, or even to the airframe characteristics. In any case, it is desired to match the frequency characteristic prescribed by the Wiener theory as is indicated in figure 5 in terms of amplitude and phase. This characteristic can be achieved by a linear system either in the tracking radar or in the missile control loop. In general, however, these linear designs demand excessive values of certain quantities such as the amount of control motion, the rate of control motion, and certain voltages in the circuit. In a practical case there are limitations on these quantities. The effect of the nonlinearities

[REDACTED]

just discussed was explored in an analogue study in which these nonlinearities were simulated. The approach used was to design the over-all guidance system to be optimum in the linear range. The results obtained, then, by operating in the nonlinear regions are shown in figure 6 by the upper curve. Essentially this same result is obtained by altering the frequency characteristics in either the missile control loop or the tracking radar. For comparison the previous optimum result corresponding to no limitations is repeated. The difference between these two curves represents the increase in error which is caused by the effects of the nonlinearities. The most serious of the many nonlinearities is due to surface-deflection limiting which is caused by physical stops. This type of limiting is illustrated in figure 7 by the dashed time history. This figure shows that limiting occurs over an appreciable portion of the time.

This limiting of the control motion occurs, of course, because the system was designed according to linear theory which assumes an unlimited amount of surface deflection available. A more realistic approach would be a synthesis procedure which in some manner considers this limitation on surface deflection. The theory for such an approach is available in a recent paper on a modification of the Wiener theory by Newton (ref. 7). With this theory it is possible to synthesize a guidance system so that limiting deflections are seldom called for. This fact is illustrated by the solid curve in figure 7. In this approach, the maximum value of the surface deflection is kept below the limited value by reducing the rms value sufficiently. In this way the probability of the control motion exceeding the limits can be reduced to a low value. The design procedure, then, is to adjust the guidance-system frequency characteristics so that both the rms error is minimized and the rms surface deflection is made small enough so that actual limiting hardly ever occurs. Thus, the guidance system is forced to remain linear.

The effect on the rms error of reducing the surface deflection by this procedure is shown in figure 8. The minimum error according to the Wiener theory is shown as the horizontal line. As discussed previously, this error can be obtained only with prohibitive surface deflections. However, as the maximum surface deflection is reduced from these large values in a manner which results in minimum error, the curve shown in figure 8 is produced. This curve represents the theoretical lower limit of error corresponding to various amounts of maximum surface deflection. Each point of the curve is achieved by a different guidance-system transfer function. It should be pointed out that, since the surface deflection is actually a statistical quantity, the maximum deflections indicated in figure 8 represent values which are exceeded less than 5 percent of the time. The interesting feature of this curve is that, as the surface deflection is reduced from these large values, the minimum error increases extremely slowly. At a realistic surface-deflection value of perhaps 15° , for which limiting hardly ever occurs for this particular missile, the error has



CONFIDENTIAL


increased only 6 feet. This result is surprising inasmuch as the increase in error is very small for such a tremendous reduction in surface deflection. The significance of this result is that the optimum Wiener result can be approached very closely by confining operation of the system to the linear range.

It can be shown that this design is far superior, in many respects, to the previous design in which limiting is allowed to occur. For this purpose the upper point in figure 8 is shown to correspond to the dashed time history of figure 7 which limits a portion of the time. Comparison of the curve in figure 8 with the upper point shows that linear operation of the control motion results in a somewhat smaller error than for the limited case. From an examination of the time histories of figure 7, it can also be shown that the linear case (solid line) consumes about one-third of the servo energy of the limited case, inasmuch as the movement of the control surface is much less. There is a similar advantage in the magnitude of the yawing angle, which is important in drag considerations. There is also a reduction of voltages within the circuit to reasonable and easily obtainable values. Thus, this linear design not only produces a smaller error, but it is accompanied by many desirable effects.

The main assumption that is involved in obtaining the results of figure 8 is the given aerodynamics. Because this is a somewhat arbitrary choice it is desirable to know the effect of this aerodynamic choice on the minimum-error curve. In a study of this problem it has been found that, for other configurations designed for an acceleration of $10g$, the same error curve is obtained. This means that for a wide range of airframe dynamics the guidance system can be designed to produce about the same results. In this manner it is concluded that the minimum attainable error is relatively independent of the dynamics of the airframe.


The dynamics, however, are important in determining the complexity of the electronic shaping circuits. Figure 9 can be used to illustrate this effect. In this figure the previous optimum characteristic is repeated, and, in addition, the aerodynamic response is shown for a typical current missile. The difference between these two curves would ordinarily be supplied electronically by the remainder of the system. However, if an airframe could be designed with frequency characteristics approximating the optimum curve, no frequency shaping would be required from the remainder of the system. It appears that this approach is extreme. For example, one way of achieving the optimum characteristic in a completely aerodynamic way is by the use of a statically unstable missile which may be undesirable from other aspects. Other approaches may be possible, but in the light of present studies this approach appears impractical.

If the aerodynamics are confined more closely to the typical aerodynamics, the complexity of the electronic circuits can still be simplified




by aerodynamic redesign. For example, some simplification can result by eliminating the two peaks in the aerodynamic response. In this case the aerodynamics would be represented by the dashed line in figure 9. This curve could be achieved in two ways. First, it could be achieved on a variable-incidence missile by adjusting the position of the center of gravity and the aerodynamic center so that the rate of change of pitching-moment coefficient with control deflection is zero. In this manner the two peaks in the aerodynamic response would occur at the same frequency, thus canceling each other. This corresponds to a missile which develops all its lift by the movable control surface. A second alternative would be to decrease the magnitude of the two peaks. Both these peaks are due to the small aerodynamic damping term. Thus, a large increase in this term of possibly tenfold to twentyfold would tend to smooth out these peaks so as to approximate more nearly the dashed line. This is a greater change than can be obtained by conventional aerodynamic means, although it appears feasible by the use of a free-floating surface as is discussed in subsequent papers by Howard J. Curfman, Jr., H. Kurt Strass, and Harold L. Crane and by Charles W. Frick, Henry C. Lessing, and Murry Tobak.

In summary, it appears that statistical theory can be a useful tool in the process of guidance-system design. The following observations have been made:

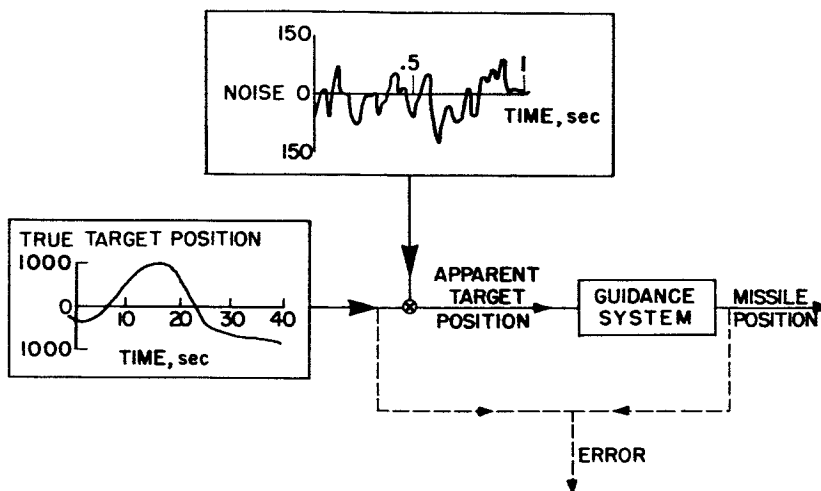
1. The Wiener filter theory establishes a goal and serves as a design guide even in nonlinear cases.
 2. The modified Wiener theory indicates that in a practical case nearly optimum results can be achieved by confining operation of the guidance system to the linear range.
 3. The achievement of the minimum error is relatively independent of the dynamics of the airframe.
 4. In the interests of simplicity of the electronic system, the most desirable airframe characteristics are, first, that prescribed by Wiener theory as indicated by the optimum characteristic in figure 9, and, second, one in which the peaks in the response curve are eliminated as shown by the dashed line in this same figure.
- 

CONFIDENTIAL

REFERENCES

1. James, Hubert M., Nichols, Nathaniel B., and Phillips, Ralph S.: Theory of Servomechanisms. McGraw-Hill Book Co., Inc., 1947.
 2. Lawson, James L., and Uhlenbeck, George E., eds.: Threshold Signals. McGraw-Hill Book Co., Inc., 1950.
 3. Meade, J. E., Hastings, A. E., and Gerwin, H. L.: Noise In Tracking Radars. NRL Rep. 3759, Naval Res. Lab., Nov. 15, 1950.
 4. Brockner, Charles E.: Angular Jitter in Conventional Conical-Scanning, Automatic-Tracking Radar Systems. Proc. I.R.E., vol. 39, no. 1, Jan. 1951, pp. 51-55.
 5. Wiener, Norbert: Extrapolation, Interpolation, and Smoothing of Stationary Time Series With Engineering Applications. The Technology Press, M.I.T., and John Wiley & Sons, Inc., 1949.
 6. Levinson, Norman: A Heuristic Exposition of Wiener's Mathematical Theory of Prediction and Filtering. Appendix C of Extrapolation, Interpolation, and Smoothing of Stationary Time Series With Engineering Applications by Norbert Wiener. The Technology Press, M.I.T., and John Wiley & Sons, Inc., 1949.
 7. Newton, George C., Jr.: Compensation of Feedback-Control Systems Subject to Saturation. Pts. I and II. Jour. Franklin Inst., vol. 254, nos. 4 and 5, Oct. and Nov. 1952, pp. 281-296 and 391-413.
- 

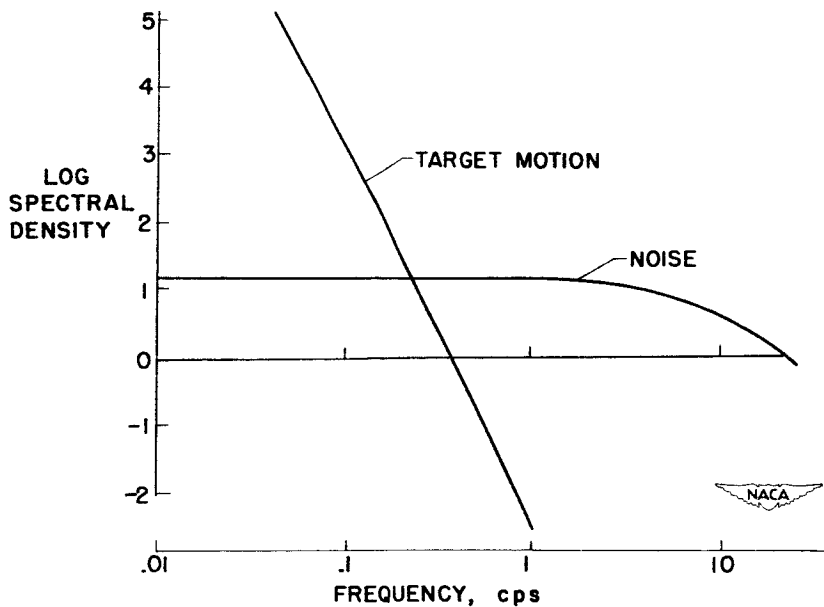
GUIDANCE SYSTEM WITH TYPICAL INPUTS



NACA

Figure 1

SPECTRAL DENSITY OF TARGET MOTION AND NOISE



NACA

Figure 2

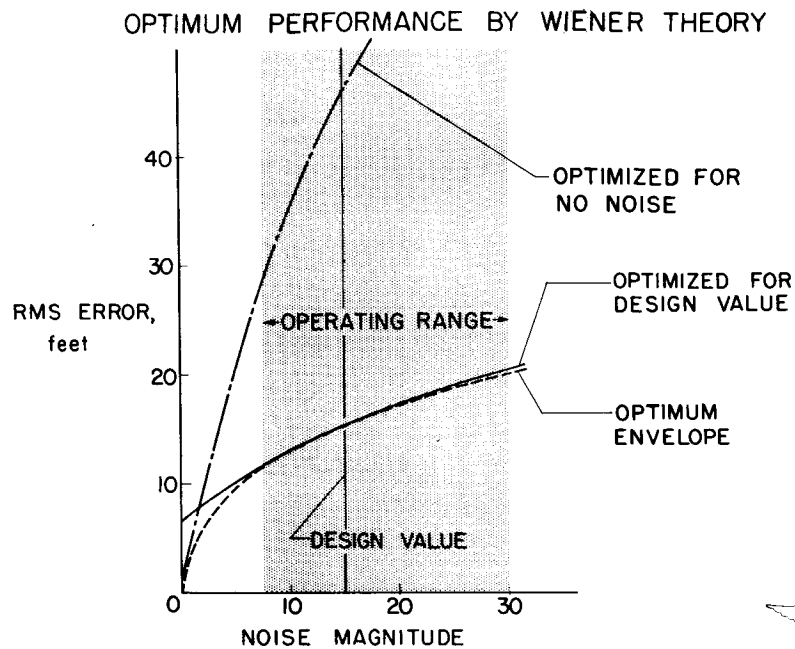


Figure 3

BEAM - RIDER GUIDANCE SYSTEM

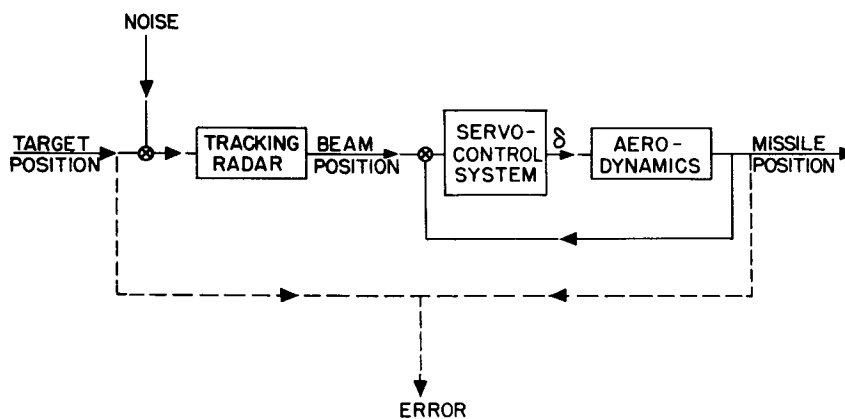


Figure 4

CONFIDENTIAL

DECLASSIFIED

OPTIMUM OPEN-LOOP TRANSFER FUNCTION

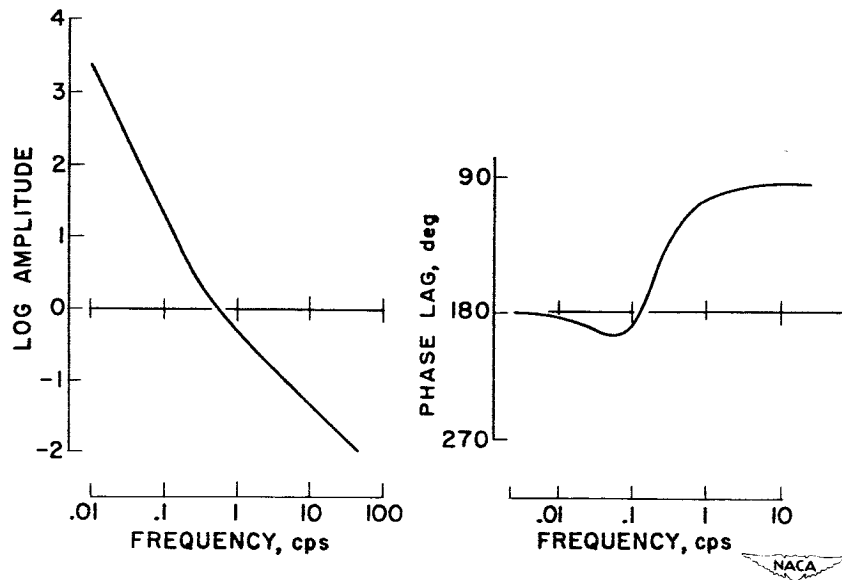


Figure 5

EFFECT OF PRACTICAL LIMITS ON MINIMUM ERROR

(OPTIMIZED FOR DESIGN VALUE)

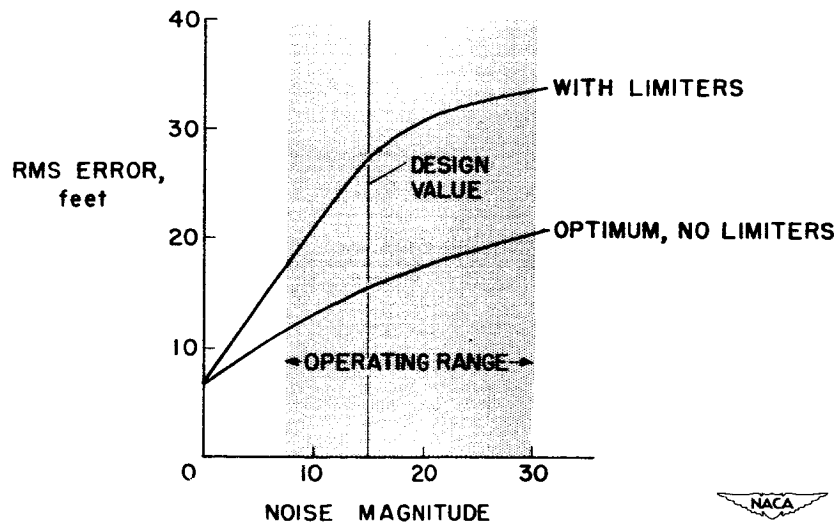


Figure 6

COMPARISON OF SURFACE DEFLECTIONS

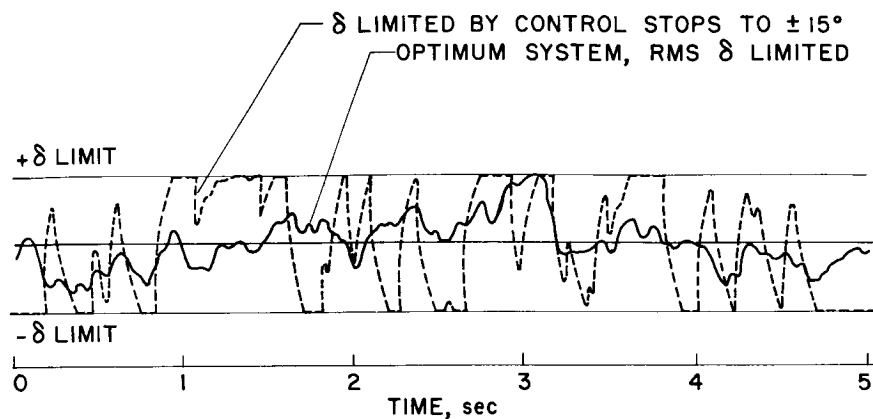


Figure 7

EFFECT OF MAX. SURFACE DEFLECTION ON MIN. ERROR

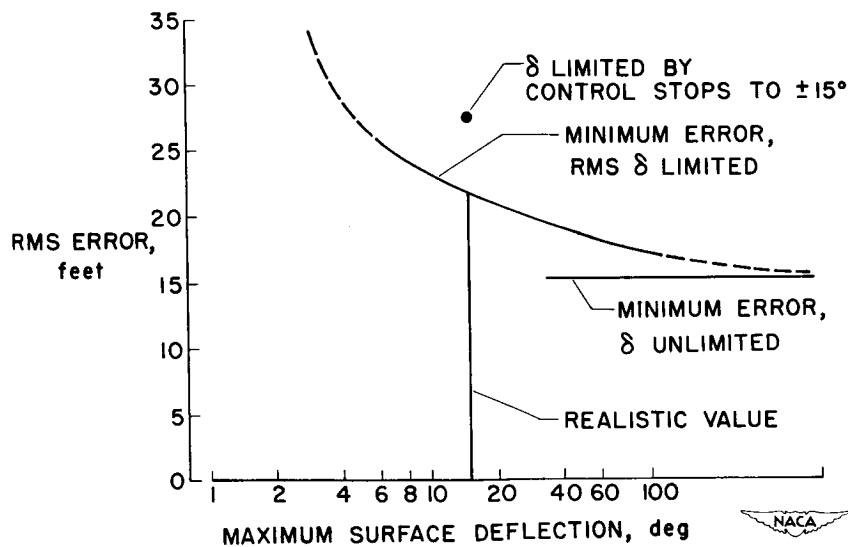


Figure 8

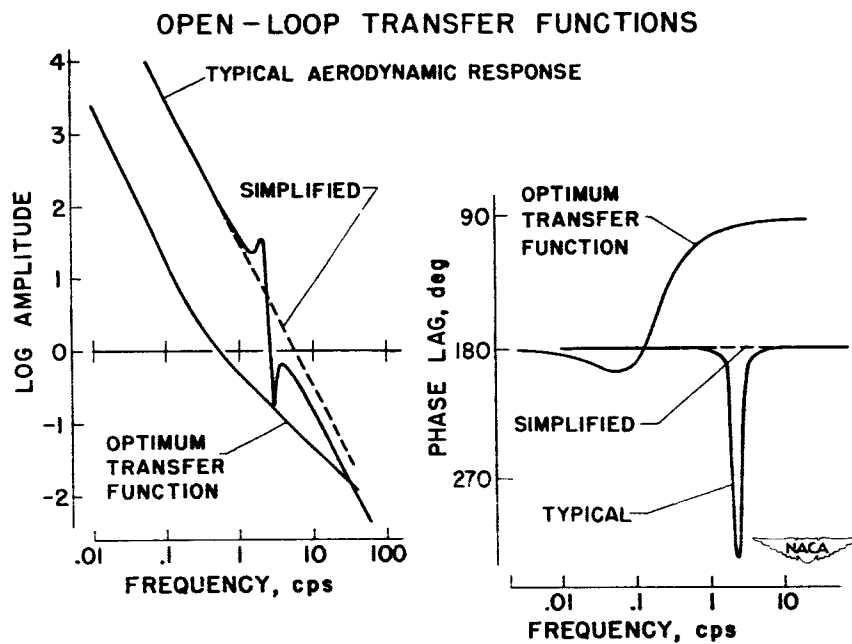


Figure 9

CONFIDENTIAL

DECLASSIFIED

INVESTIGATIONS TOWARD SIMPLIFICATION

OF MISSILE CONTROL SYSTEMS

By Howard J. Curfman, Jr., H. Kurt Strass,
and Harold L. Crane

Langley Aeronautical Laboratory

INTRODUCTION


Simplicity in control-system design is a desire shared by all. The motivation behind this desire is the somewhat elusive factor known as reliability. It is readily recognized, therefore, that the simplification of the control system should lead to improved reliability without sacrificing system performance in the ultimate accomplishment of the desired task.

In general, the approaches to the problem of simplification of control systems must be by new ideas and unique applications or by reevaluations and modifications to current or past ideas. The Sidewinder missile developed by the Naval Ordnance Test Station (ref. 1) and the idea to be presented by Robert A. Gardiner in a subsequent paper are two examples of a basic simplification in missile control systems.

While most of the remarks and ideas presented in this paper seem more readily applicable to missile systems, it is evident that these points or some of their corollaries have direct application to airplane control systems. It is the purpose of this paper to present three ideas that have been investigated. These data will not represent complete systems but rather will represent features and principles that should lead to simplification of control systems.

AUTOROTATING-VANE SPOILER

The first part of this paper deals with an autorotating-vane spoiler. The proposed control method using the autorotating spoiler is the "bang-bang," or flicker, or plus-minus type of control; that is, the spoiler is so arranged as to give either an up or down lift increment at all times. Figure 1 shows a typical installation of an autorotating spoiler. From the cutaway view, it is noted that the spoiler consists of two vanes pivoted on a common shaft which passes through the wing. The vanes are oriented at right angles to each other, as shown; hence, each quarter rotation of the spoiler assembly would cause



CURFMAN, STRASS
H. L. CRANE

CONFIDENTIAL


the vanes to alternately act as spoilers on the top and bottom of the wing. The shape of the spoiler is such as to make the assembly autorotate. Thus, the power that actuates the control is aerodynamic.

To allow control operation to be as desired, an escapement mechanism is used to limit the assembly to intervals of one-quarter revolution. Hence, it is necessary for the intelligence device of the control system to "decide" when the escapement should be released; however, no great amount of power is required to actuate the escapement mechanism. For example, a small solenoid might suffice. Thus, no servomotor is required, and such an arrangement is readily adapted to a thin wing. Such a system might find use with short-range bombs where the simple, flicker control is sufficient and where the additional drag may not be too critical. Since the spoiler effectiveness can be estimated, for example, by the methods suggested previously in the paper presented by John G. Lowry, the first consideration is concerned with how well this spoiler assembly will operate.

Details of the design of the autorotating spoiler tested are shown in figure 2. Only one vane is shown. The inertia given is that of the entire assembly. The design of the vanes is important since the configuration must autorotate.

The results of tests run in a blowdown jet at the Pilotless Aircraft Research Station, Wallops Island, Va. are presented in figure 3 in a plot of the operation time of the autorotating spoiler as a function of sea-level Mach number. This operation time was measured as the time from release of the escapement until 90° of rotation was obtained. This lag time is important since it directly affects the hunting oscillation of the bang-bang system. The control response time averaged about 0.01 second throughout the Mach number range. The aerodynamic lag involved was at most 5 percent of the lag shown. The spoiler response is essentially independent of wing size; therefore, the response was made nondimensional by giving the time required to operate in spoiler lengths. This plot is shown at the bottom of the figure, where the response varied from 40 spoiler lengths at $M = 0.5$ to 85 lengths at $M = 1.6$. As noted, these results were the same for angles of attack of 0° and 7° . Within reasonable limits, increasing spoiler height does not increase the operation time, provided the thickness is unchanged. Increasing spoiler length increases the time to operate in proportion to the square root of the length, also with thickness unchanged. In addition to the blowdown-jet tests, the assembly has also been tested on the transonic bump of the Langley high-speed 7- by 10-foot tunnel and was found to autorotate satisfactorily throughout the transonic region.

Flight-test results of a rocket-powered model equipped with the autorotating-vane spoiler are presented in figure 4. These tests



DECLASSIFIED


showed that the spoiler arrangement having slightly less area than 2 percent of the exposed wing area gave the rolling effectiveness desired in the supersonic region. The use of several small spoilers is, of course, a logical extension of this idea if a greater effectiveness is desired, and the results presented previously in the paper by Lowry can be used to obtain the effectiveness at angles of attack greater than those small values encountered in these tests. Approximately the same drag should be experienced as that attained with a flicker system using conventional flaps.

BELLOWS FLAP

Another scheme that has been investigated is a bellows-actuated flap. This scheme, of course, is not a new idea, having been considered both in this country and abroad in the past. The current study was begun as a reevaluation of this idea with particular emphasis to relieving some space requirements in missiles for control-system power supplies and actuators. Higher speeds have introduced increased dynamic pressures which, of course, offer promise to such a system. Thin surfaces, too, have led to difficult problems concerning torque rods and actuating methods for control surfaces.

A schematic arrangement of the bellows-operated flap is shown in figure 5. It consists of an airtight, flexible chamber installed beneath a split flap and vented through a controlling valve to impact or base pressure. The design of the valves would precisely control the flap deflections. Although the sketch shown has the split flap in a particular chordwise position, the principle allows a very compact arrangement and split flaps at the trailing edge are equally feasible. The bellows-flap arrangement is one which literally supports the control against hinge moments, rather than twisting the control surface.

Results of a free-flight test of a rocket-powered model equipped with the bellows flap are shown in figure 6. The split flap was on the top surface of one semispan wing only and was located as shown. This flap was operated as rapidly as possible within the limitations of the existing air intake and distribution system. This operation was essentially in a square wave manner. The wing section at the flap midspan was 3.7 percent thick, and the bellows was of the simplest design. The maximum control deflection is shown by the solid curve, and the dashed curve shows the rolling effectiveness of the split-flap aileron. The other curve shows that the split-flap effectiveness is essentially the same as that of a conventional trailing-edge aileron of the same chord and spanwise location. Improved bellows design will permit a large increase in maximum flap deflection.



The operation time in seconds required for the flap to move to full deflection is shown as the solid line in the lower part of this figure. The time of operation varied from 0.035 second at $M = 0.7$ to 0.02 second at $M = 1.9$. In nondimensional terms (the dashed curve), the time required for flap operation varied from 280 flap chords traveled at $M = 0.7$ to 400 flap chords at $M = 1.9$. It should be pointed out that the rate of flap deflection could be varied considerably by changing the capacity of the air-distribution system in relation to the bellows volume.

Such a system need not operate as a flicker or bang-bang system as described. Proportional operation of the flap has been obtained by proper valve design. One factor involved, of course, in such an arrangement is the effect of the valve size on the air flow. Also, since the pressure tending to close the flap is usually much less than that for opening it (the base pressure being smaller in magnitude than the impact pressure), the flap will always be somewhat slower in closing, although the design of the system can remove almost completely this feature.

FREE CONTROLS

Another approach toward simplification of control systems would be to improve the aerodynamic response characteristics of the airplane or missile and hence obviate the need for some automatic control equipment. For example, if the original aircraft had better damping characteristics, some automatic control devices might be eliminated, or at least made less complex. It is well known that the floating characteristics of free controls can alter the damping of an aircraft over a wide range. The principle of using free controls to improve the response of aircraft is, of course, not new. The works of Greenberg and Sternfield (refs. 2 and 3) and others offer a sound foundation. It appears, however, that a reevaluation and investigation of this principle, particularly with regard to missiles, would be fruitful. The remainder of this paper will present illustrations of this approach and its effectiveness.

To illustrate this approach, consider as an example the problem of lateral damping of some current airplanes. It is known that if the rudder is freed during a lateral oscillation, the effects of control-surface floating characteristics and friction in the control system have led to snaking or very lightly damped oscillations, that is, oscillations that were reinforced by aerodynamic moments induced by the floating control. The first question that naturally arises is what are the control-surface characteristics required to improve the damping. A conventional stability-boundary plot, a typical one of which is shown in figure 7, can answer this question. This plot is for the lateral case of an airplane at $M = 0.7$ and an altitude of 10,000 feet and is in terms of the rudder hinge-moment derivative $C_{h\delta}$ and the rudder floating tendency $C_{h\downarrow}$.


A positive $C_{h\dot{\psi}}$ is for a rudder that floats against the wind, the negative value for a rudder that floats with the wind. The floating tendency is the action that causes control motion, and it is the response of the control surface, as manifested by $C_{h\delta}$, $C_{h\dot{\delta}}$, inertia, and such factors, that phases the resultant moments so that the aircraft motion is affected. In addition to the usual oscillatory and divergence boundaries are shown lines of constant time to damp to half amplitude. For example, if the time for the airplane to damp to half amplitude $T_{1/2}$ is 2.8 seconds, the line so labeled defines the region that will improve this damping. If twice the damping is required, the line labeled $T_{1/2} = 1.4$ seconds defines this region.

Flight tests were made of an airplane having lightly damped lateral oscillations as shown at the top of figure 8. In these flight results the pilot had disturbed the airplane and had released the rudder when zero time was plotted. The typical motion shown in the lower part of the figure is the result when the rudder characteristics have been modified. In this latter case the aircraft had an auxiliary viscous damper on the rudder, a feature that alone did not offer sufficient improvement to response of the original configuration.

A summary of results of several flights at Mach numbers up to 0.7 at altitudes of 10,000 and 30,000 feet is shown in figure 9. On this conventional plot of $T_{1/2}$ against period, where the hatching represents the unsatisfactory side of the boundary, the circles represent rudder-fixed oscillations, the squares the original rudder free, and the diamonds the modified rudder free. The improvements are such as to make the airplane meet the period-damping specifications at 10,000 feet and to be nearly satisfactory at 30,000 feet.

The use of free controls to augment the longitudinal damping of missiles has been studied for a canard-missile configuration that has been used by the NACA in automatic-control studies. A typical plot of the longitudinal stability boundaries of a missile at supersonic speeds is shown in figure 10. For the condition where the free controls are forward of the center of gravity, the oscillatory and divergence boundaries are reversed; that is, a control that floats against the wind leads to a divergence. The reference line of constant $T_{1/2} = 0.194$ second shown is representative of the missile damping with controls fixed. Thus, to improve on this damping, the region shown represents the values of $C_{h\alpha}$ and $C_{h\delta}$ that must be used.

Figure 11 shows the effects of these free-floating canard controls on the damping of the missile. The configuration is shown in outline form and has 60° delta wings and canard controls. The dashed curve shows the




angle-of-attack response of the missile with controls fixed, while the solid line shows the response with free-floating canard controls. Since the frequency of the oscillations is only slightly changed, the action of the free surfaces has been almost exclusively to give damping. In this case the aircraft damping has been changed from about 10 percent to nearly 50 percent of the critical damping. For comparison, the long-short dashed curve is the result of flight tests of this same missile equipped with a rate-gyro servo arrangement for improving the damping (ref. 4). The solid curve in the figure is a calculated result, while the other curves were obtained from flight data. A recent flight test of a different canard configuration investigating this principle showed essentially the same results. These data were not available for presentation here.

It is emphasized that a separate control for damping is not a necessity, since by effective design the same surfaces can be used for damping as well as for control.

SUMMARY

In summary, three ideas have been discussed that could lead to simplification of control systems. These systems have included the auto-rotating spoiler and a bellows-flap arrangement, which have been discussed as bang-bang or flicker systems, although control-valve design would allow proportional operation of the bellows flap. The use of free controls has also been discussed with regard to improving airplane lateral oscillations as well as the longitudinal damping of a canard missile configuration.



CONFIDENTIAL

DECLASSIFIED 7

REFERENCES

1. Blaise, Robert A.: Report of Flight Tests of Sidewinder Missiles EX-1-2 - Serial No. 1 and Serial No. 2. Test Rep. 30-142, NOTS No. 610, U. S. Naval Ord. Test Station (Inyokern, Calif.), Jan. 20, 1953.
2. Greenberg, Harry, and Sternfield, Leonard: A Theoretical Investigation of the Lateral Oscillations of an Airplane With Free Rudder With Special Reference to the Effect of Friction. NACA Rep. 762, 1943. (Supersedes NACA ARR, Mar. 1943.)
3. Greenberg, Harry, and Sternfield, Leonard: A Theoretical Investigation of Longitudinal Stability of Airplanes With Free Controls Including Effect of Friction in Control System. NACA Rep. 791, 1944. (Supersedes NACA ARR 4B01.)
4. Moul, Martin T.: Flight Investigation of a Supersonic Canard Missile Equipped With an Auxiliary Damping-In-Pitch Control System. NACA RM L52K14b, 1953.

TYPICAL AUTOROTATING-VANE-SPOILER INSTALLATION

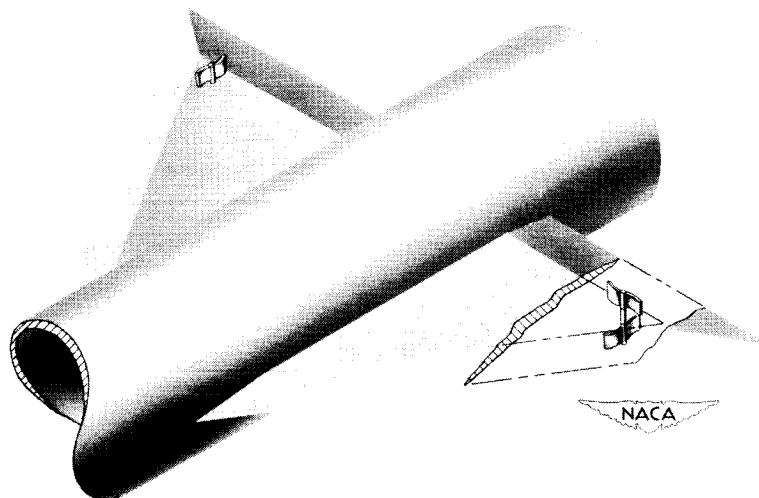


Figure 1

DETAILS OF AUTOROTATING-VANE SPOILER $l = 2$ IN.; $I = 8.125 \times 10^{-6}$ SLUG-FT²

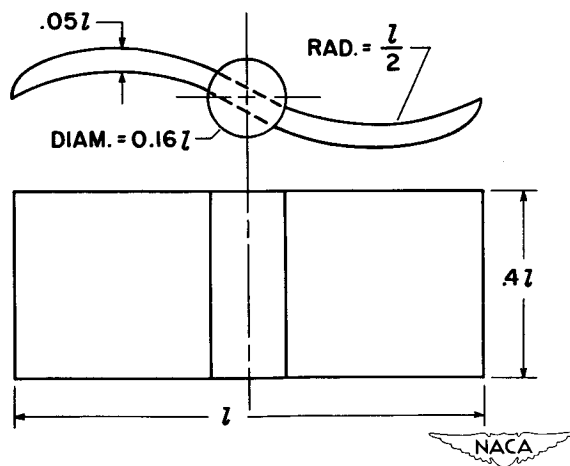


Figure 2

[REDACTED]

[REDACTED]

CONFIDENTIAL

DECLASSIFIED

AUTOROTATING-VANE-SPOILER OPERATION TIME $\alpha = 0^\circ$ AND 7° AT SEA LEVEL

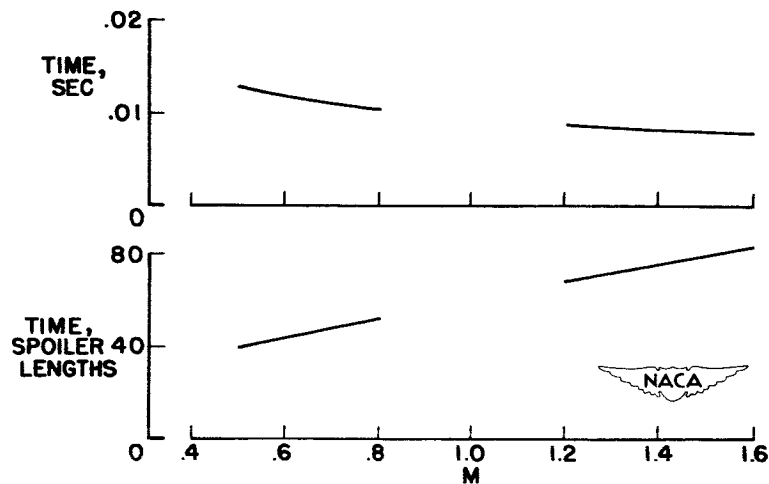


Figure 3

ROLLING EFFECTIVENESS OF AUTOROTATING-VANE SPOILER

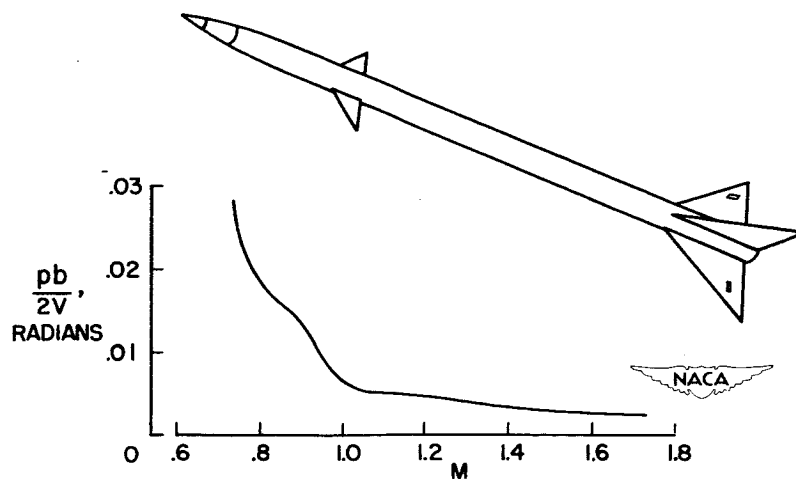


Figure 4

SCHEMATIC OF BELLOWS FLAP

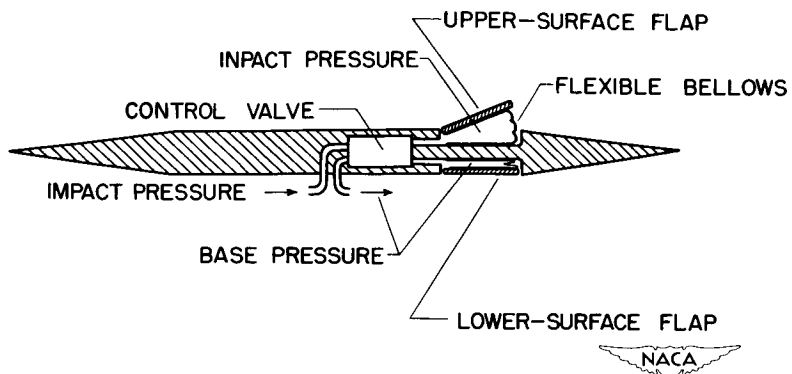


Figure 5

FLIGHT RESULTS OF BELLOWS FLAP

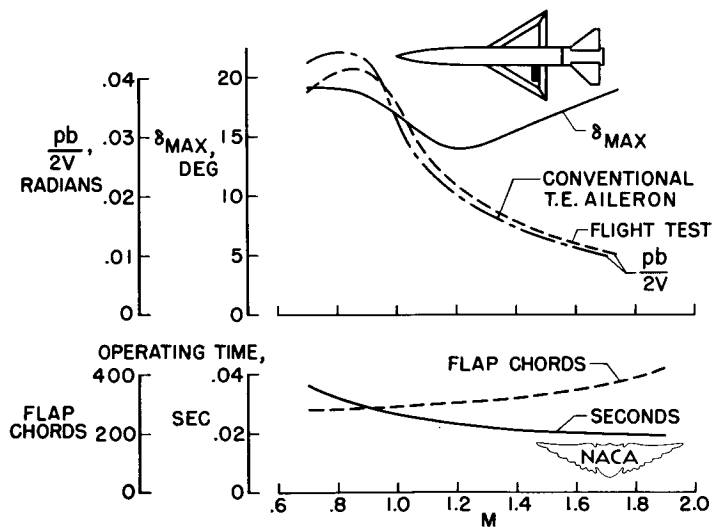


Figure 6

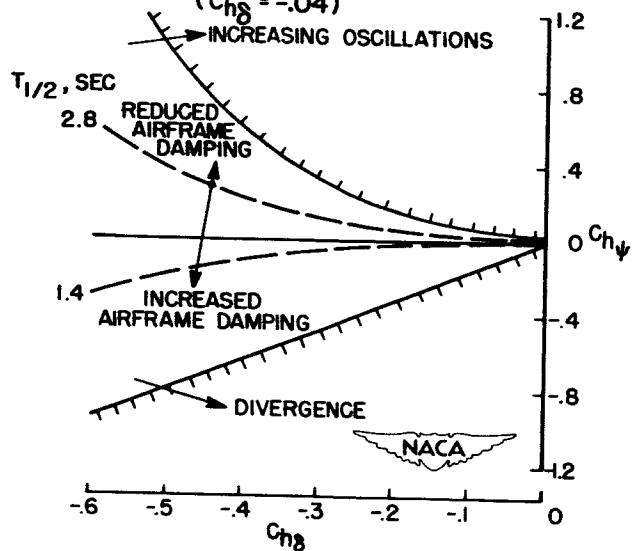
STABILIZATION BOUNDARIES - FREE CONTROLS AFT
($C_{h\delta} = -.04$)

Figure 7

FLIGHT RESULTS WITH RUDDER FREE

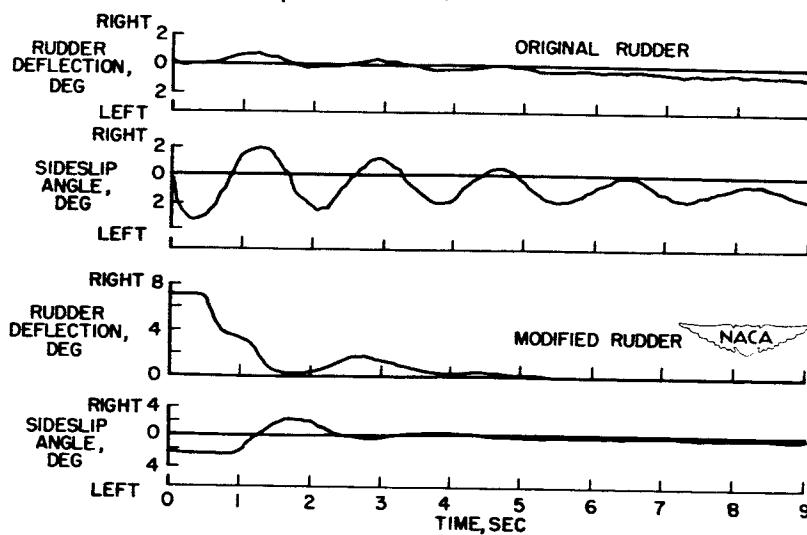
 $h_p = 10,000 \text{ FT}$; $V_i = 300 \text{ KNOTS}$ 

Figure 8

EFFECT OF RUDDER MODIFICATION ON DAMPING

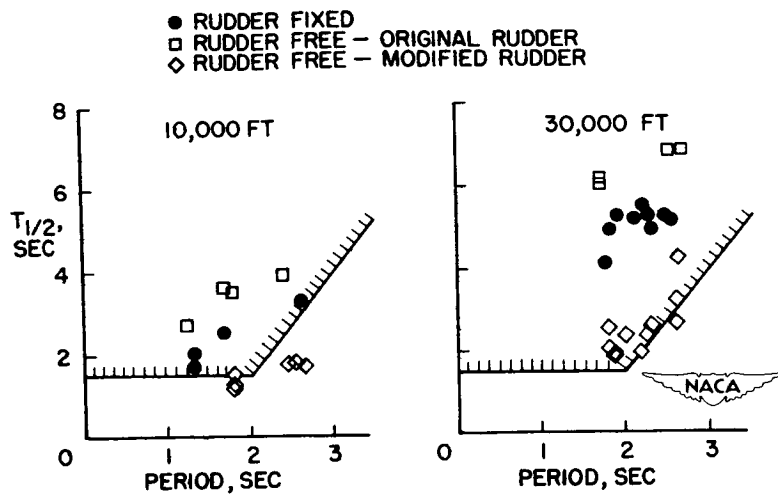


Figure 9

STABILITY BOUNDARIES - FREE CONTROLS FORWARD

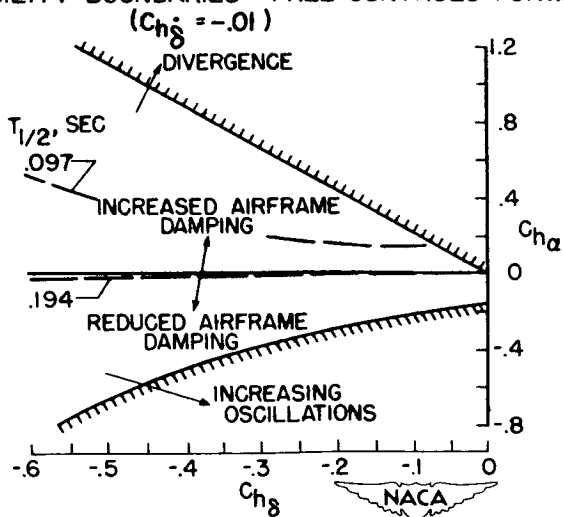


Figure 10

CONFIDENTIAL

DECLASSIFIED

COMPARISON OF TRANSIENT RESPONSES
M=1.81 AT 5000 FT

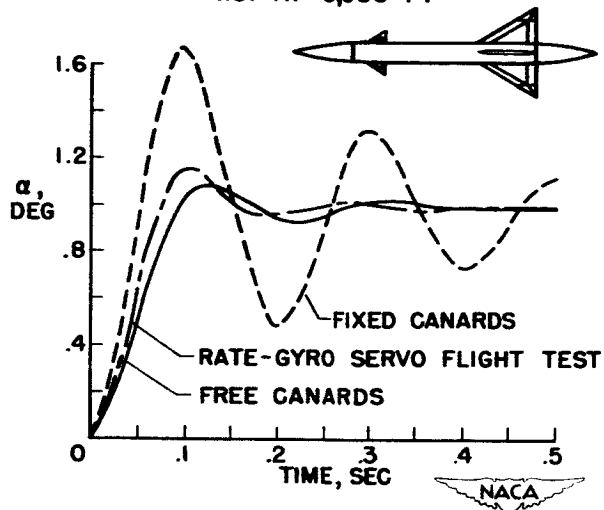


Figure 11

CONFIDENTIAL

SECRET

INFLUENCE OF CONTROL-SURFACE AERODYNAMICS ON MISSILE SIMPLIFICATION

By Charles W. Frick, Henry C. Lessing, and Murray Tobak

Ames Aeronautical Laboratory

In the previous paper, Howard J. Curfman, Jr., H. Kurt Strass, and Harold L. Crane discussed research directed toward simplifying missile components. The present paper explores this field of design further. In the presentation of these ideas, the terminology conforms with that associated with missile design practice, but, insofar as possible, familiar aerodynamic symbols are used in the mathematical definition of these terms.

In figure 1 is shown a block diagram of a guided missile, the various blocks depicting components of the over-all missile system. This particular arrangement of blocks was selected for the purpose of illustrating the ideas of this paper. In the upper half of this figure is the longitudinal dynamic system including the seeker dynamics which translates the missile-target geometry into an error signal, the gain adjuster which accounts for variations in the Mach number and flight altitude, the servomotor which actuates the control surface, and the airframe which responds with a turning rate. One feedback loop is shown incorporating a rate gyro which is required to provide adequate damping of the longitudinal motion, particularly at high altitudes. In the lower half of this figure is shown a roll dynamic system, incorporating a rate gyro as a sensing device, which provides a loose control of the rolling rate of the airframe.

Certain of these blocks represent complicated electronic circuits which probably can be simplified or eliminated by proper design of the airframe, particularly the gain adjuster, the servo itself, and certainly the rate-gyro feedback loop. In addition it appears possible that the electronic circuits represented by the block diagram associated with the roll dynamics can be eliminated.

It is desirable because of the nature of the subject to define certain terms and symbols which are noted in figure 2. Throughout this paper the time rate of change of the angle γ in response to a deflection of the control surface δ is of primary concern since this parameter is a measure of the target-seeking properties of a missile with a perfect seeker. This parameter defines the rate of turn of the missile. The first portion of the discussion is concerned with missile performance criteria best shown by the amplitude curve of the frequency response of the missile, which is a characteristic curve showing the maximum amplitude

FRICK, LESSING
& TOBAK

of the sinusoidal variation of the turning rate for a sinusoidal control motion of unit maximum magnitude. The points of interest on this frequency-response plot are point A, the zero frequency gain, point B, the natural frequency, point C, the infinite frequency gain, and point D, the minimum response frequency. Point E is also of interest since the peak amplitude determines, in large part, the response time of the missile.

The first portion of the discussion is concerned primarily with point A, the zero frequency gain, and to some extent point B, the natural frequency. Points C and D are not discussed; however, they are important in noise studies, such as were discussed by Elwood C. Stewart.

If the missile is equipped with a perfect position servo, the expression derived for the gain or the steady turning rate is shown in figure 3. For this servo system, the movement of the crank ϵ is equal to the deflection of the control surface. Note that in the expression for the gain, the dynamic pressure q and the Mach number appear explicitly. Mach number also enters into the aerodynamic parameters. Because of this dynamic-pressure term, a variation of altitude of from 5,000 feet to 60,000 feet will result in the gain or turning rate varying by a factor of 10. This variation is considered unacceptable since it means that target-seeking maneuvers are optimum for only one altitude, the accuracy becoming impaired as the missile departs from that altitude. This is the reason for what was previously described as the gain adjuster. The natural frequency varies with the square root of 10 or 3.3, which is acceptable.

It has been pointed out previously that it might be possible to utilize the aeroelastic properties of sweptback control surfaces to compensate for the effects of dynamic pressure and to eliminate the gain adjuster from the system. It was found possible, for instance, to reduce the gain variation from 10 to about $2\frac{1}{2}$ through the use of aeroelasticity. Further studies in this respect have now been made.

For instance, the frequency response of a missile equipped with a perfect position servo with a spring inserted in the torque tube driving the control surface has been studied. An examination of the expression for the gain in figure 4 shows that the dynamic pressure still appears in the expression. Its influence may be modified, however, by adjusting the relative magnitude of the two terms in the denominator. The introduction of a spring (k) in the torque tube permits the hinge moments of the control surface to influence the gain, thereby extending the influence of the airframe on the missile response.

The frequency response for two Mach numbers and two altitudes with this spring-position control and with a perfect position servo (no springs)

[REDACTED]

[REDACTED]

DECLASSIFIED


is shown in figure 5. It will be noted that the use of the spring in the torque tube has reduced the gain variation with altitude from 10 to 0 at both Mach numbers but that there still remains some variation in the gain with Mach number. A part of the beneficial effect shown was obtained by shifting the center of gravity rearward. There is a somewhat adverse effect on the variation of the natural frequency with altitude. All in all, however, there seems to be a significant net improvement in the frequency response.

As a further extension of this scheme for modulating the turning rate of the missile, consider what occurs if the spring constant k is permitted to become very small; in this case, the result obtained is shown in figure 6.

The expression shown gives the turning rate $\dot{\gamma}$ in terms of the hinge moment HM about the torque tube corresponding to a servomotor which simply specifies a torque about the control-surface hinge in response to an error signal. It will be noted that, in the expression for the gain of the airframe with a perfect torque servo, the dynamic pressure no longer appears; Mach number still appears explicitly, but the Mach number influence on the aerodynamic terms has been minimized since the aerodynamic terms in the numerator and denominator are affected in the same manner.

The frequency-response curves for Mach numbers of 1.5 and 2.5 for altitudes of 5,000 feet and 60,000 feet for the airframe with a perfect torque servo are shown in figure 7. It will be noted again that the variation in the gain with altitude has been reduced to a very small value. Furthermore, the variation in natural frequency with altitude is less than it was for the position servo with a spring in the torque tube. These results, together with those previously discussed, demonstrate the feasibility of simplifying missile components by eliminating the gain adjuster from the system. The aerodynamic design of the missile airframe is, of course, more complex but this is a favorable exchange for increased reliability.

The foregoing discussion has been concerned primarily with the steady turning rate of the missile with a view toward finding simple ways of achieving the same turning rate for all altitudes and Mach numbers in response to a unit error signal. Another important point involved in missile performance is the length of time required for this steady turning rate to be realized. This time is known as the response time. In order to illustrate the ideas involved in the subsequent discussion, it is best to study what is known as the transient response or, in other words, the history of the missile turning rate over a period of time during and subsequent to a certain control motion.




CONFIDENTIAL

In general, if a perfect position servo is assumed, the control surface responds with a step change in deflection due to a step change in error. The transient response of interest then is the response of the airframe to a step change in control moment. In figure 8 is shown such a transient for a missile flying at a Mach number of 1.5 at an altitude of 60,000 feet. It is evident that, because of the low damping of the oscillatory response, a time for a steady turning rate to be reached is very large. Usually the response time is reduced by providing the rate-gyro feedback loop which was noted on the block diagram. The question that arises is whether the same result can be achieved without this complication.

In order to get at the basic elements of the problem, the idealized missile-airframe turning-rate response to a step change in the error signal is specified as shown by the dashed line. Assume that a reasonable minimum response time possible for a given airframe is the time to reach the first peak of the oscillatory response due to a step change in control moment. With this idealized response, the control-moment input over the time period of the transient turning rate can be calculated. The result is shown by the dashed lines in the control-moment plot on the right. The control-moment transient is seen to vary greatly with the specified turning-rate response. In this case, however, the control input is nearly the same as that usually obtained by a position servo with airframe pitching-rate feedback. In this study, it has been found that the same control input can be provided by using an auxiliary flap as shown in figure 9.

The auxiliary flap is hinged on the rear wing of the missile and is restrained in its motion by a torque spring. The flap is mass overbalanced and is therefore driven by the response of the mass overbalance to the pitching acceleration and the normal acceleration of the airframe. For this airframe, the response to an error signal is initiated by the deflection of the forward control surface which gives the first portion of the moment input given by the dashed line of figure 8. During this time the missile is undergoing a pitching acceleration which causes the auxiliary flap to assume the positive deflection shown (trailing edge down). As the normal acceleration builds up, the flap moves to negative deflections. The transient moment provided by the flap is therefore similar to that required for the idealized response. If a viscous damper is provided, the flap motion can be delayed sufficiently to give the required control-moment input. The transient-response curves of figure 9 show the results of simulator studies of this missile airframe. It will be noted that, as the driving hinge moment of the auxiliary flap is increased by increasing the mass overbalance as measured by the ratio of steady deflection of the rear flap Δ to that of the forward control δ , the idealized response of figure 8 becomes more closely approximated. Effectively, this flap increases the damping of the airframe by a factor of 10.




DECLASSIFIED

This auxiliary flap, of course, is essentially the same as those discussed by Howard J. Curfman, Jr., H. Kurt Strass, and Harold L. Crane. It serves, together with the forward control surface, to give a time history of pitching-moment input that results in a short response time. It is believed that the possibility of achieving short response times with the airframe by programing the control-moment input has special significance in missile simplification. The highly damped transient response, for instance, may permit the use of on-off control motions which allow the substitution of relays for amplifiers. Robert A. Gardiner discusses such a flicker control system in the next paper.

In studying this airframe, it was thought that perhaps the auxiliary flap could be utilized in roll as well as in pitch. The hinge-moment parameter was adjusted by using a horn balance since it was known that the horn balance would be more effective in roll in providing hinge-moment changes than it is in pitch. It was thereby possible to get the flap to lead the roll motion. The response in roll to a step rolling moment is shown in figure 10. The analysis indicates that the flap acts as a fairly satisfactory roll damper. In this case it gives a reduction in rolling rate of some 60 percent. Further studies of such devices may indicate that the use of the roll-rate stabilizing system which was mentioned previously in connection with the block diagram can be eliminated.

The preceding discussion has been concerned with missile types now in planning or undergoing actual firing tests. Generally speaking these missiles are large, carry large warheads, and have large-span wings. Those of the air-to-air type contribute prohibitive drag when mounted externally on supersonic aircraft and gives a not insignificant increase in drag when carried internally. It is felt that something can and should be done about reducing missile sizes significantly without impairing performance. The accomplishment of this objective, of course, will depend in large measure on advancements in electronic design, particularly miniaturization. Concurrently, it will require aerodynamic investigations of missile airframes suitable for internal storage, possibly designed to be fired from tube launchers, similar to those now used for the $2\frac{3}{4}$ -inch folding-fin rockets. As a part of this aerodynamic program one missile airframe, shown in figure 11, has been investigated.


These data are a brief summary of the maximum-normal-force capabilities of an airframe with projecting controls as determined in very recent tests. The control surface of the missile consists simply of a segment of the nose which is pivoted outward; its deflection is measured from the flush position. It is interesting to note that this particular control gives high values of the maximum normal force, particularly at the higher Mach numbers, illustrating the importance of body lift at these Mach numbers. The normal force attainable is higher than that of an equivalent winged missile at Mach numbers greater than 2.4. It should



CONFIDENTIAL

be noted that one reason why higher normal forces are obtained is that the longitudinal stability of the missile with the folding control decreases with increasing Mach number. The control effectiveness $C_{m\delta}$ remains essentially constant with Mach number. For this comparison both missiles have the same frequency at $M = 2$. Controls of this type, which are suitable for tube-launched missiles, need further investigation, but it is believed that the results presented indicate that the maneuverability of tube-launched missiles need not be significantly less than those of more conventional design especially at Mach numbers greater than twice the speed of sound. Incidentally, the angles of attack at which these normal forces are attained are roughly the same for both airframes, about 16° .

In summary, it can be shown, on paper at least, that some simplification of missile components can be achieved by spending a little more ingenuity in airframe design. The practicality of these schemes needs proof through airframe flight tests since there are problems of cross-coupling, nonlinear hinge moments, and so forth. It is my personal belief, however, that a net improvement in missile reliability may come about from these and similar studies.



CONFIDENTIAL

DECLASSIFIED 7

TYPICAL BLOCK DIAGRAM FOR GUIDED MISSILE

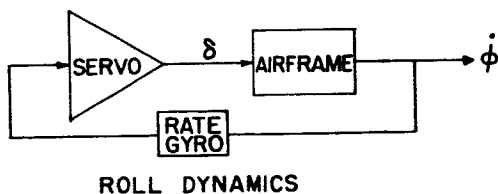
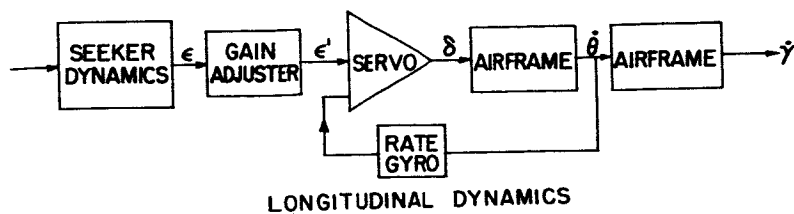
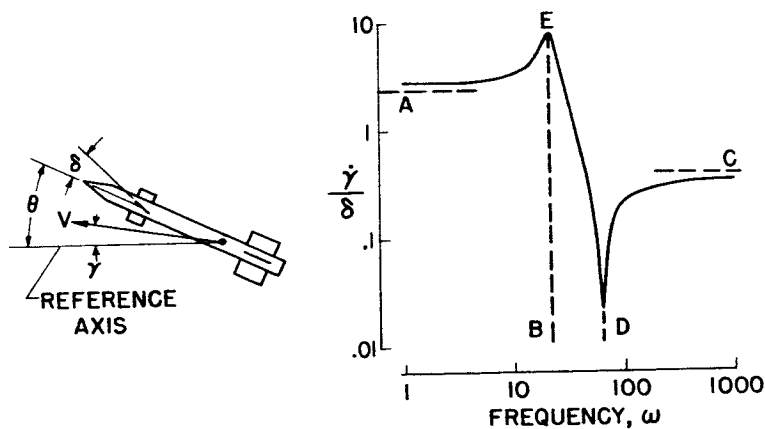


Figure 1

SIGNIFICANT PARAMETERS IN AIRFRAME DYNAMICS

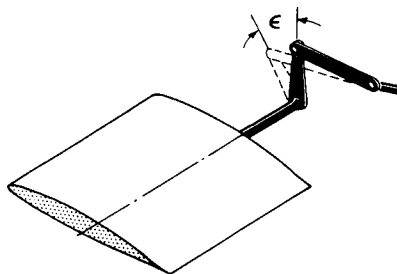


- A- ZERO FREQUENCY GAIN
- B- NATURAL FREQUENCY
- C- INFINITE FREQUENCY GAIN
- D- MINIMUM RESPONSE FREQUENCY
- E- PEAK AMPLITUDE



Figure 2

AIRFRAME DYNAMICS WITH POSITION SERVO



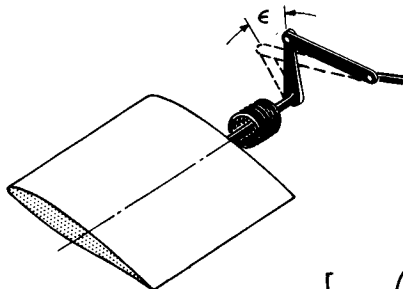
$$\text{GAIN } \omega \rightarrow 0 \quad \frac{\dot{\gamma}}{\epsilon} = -\frac{S}{m\bar{c}a} \left(\frac{q}{M} \right) \left(C_{L\alpha} \frac{C_{m\delta}}{C_{m\alpha}} - C_{L\delta} \right)$$

$$\text{NATURAL FREQUENCY, } \omega_n, \approx \sqrt{q} \sqrt{\left(\frac{S\bar{c}}{I} \right) C_{m\alpha}}$$



Figure 3

DYNAMICS WITH SPRING-POSITION SERVO



$$\text{GAIN } \omega \rightarrow 0 \quad \frac{\dot{\gamma}}{\epsilon} = -\left(\frac{I}{m\bar{c}a} \right) \frac{k}{M} \frac{\left[C_{L\alpha} \left(\frac{C_{m\delta}}{C_{m\alpha}} \right) - C_{L\delta} \right]}{\left\{ \left[C_{h\alpha} \left(\frac{C_{m\delta}}{C_{m\alpha}} \right) - C_{h\delta} \right] + \frac{k}{qS\bar{c}} \right\}}$$

$$\text{NATURAL FREQUENCY } \omega_n = \sqrt{-\frac{C_{m\alpha}}{\sigma} \left[1 - \left(\frac{C_{m\delta}}{C_{m\alpha}} \right) \left(\frac{C_{h\alpha}}{C_{h\delta} - \frac{k}{qS\bar{c}}} \right) \right]}$$

Figure 4

CONFIDENTIAL

DECLASSIFIED

FREQUENCY RESPONSE WITH SPRING-POSITION SERVO

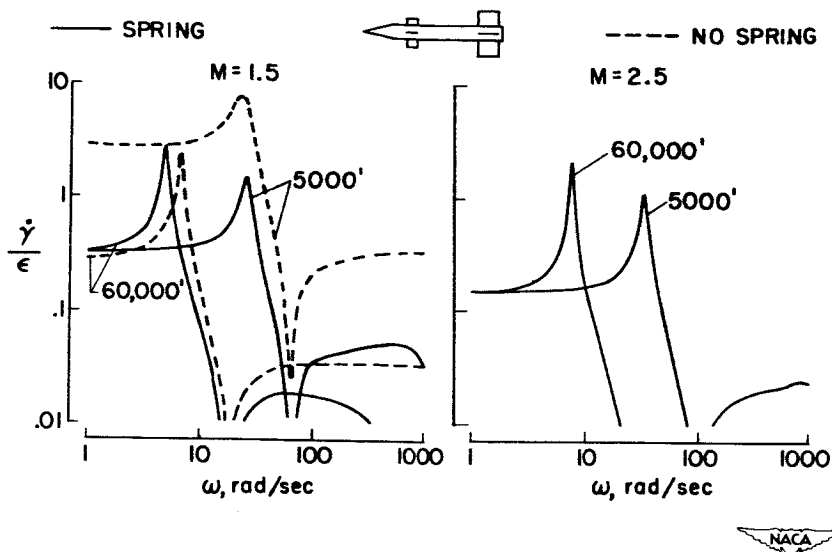


Figure 5

DYNAMICS WITH TORQUE SERVO

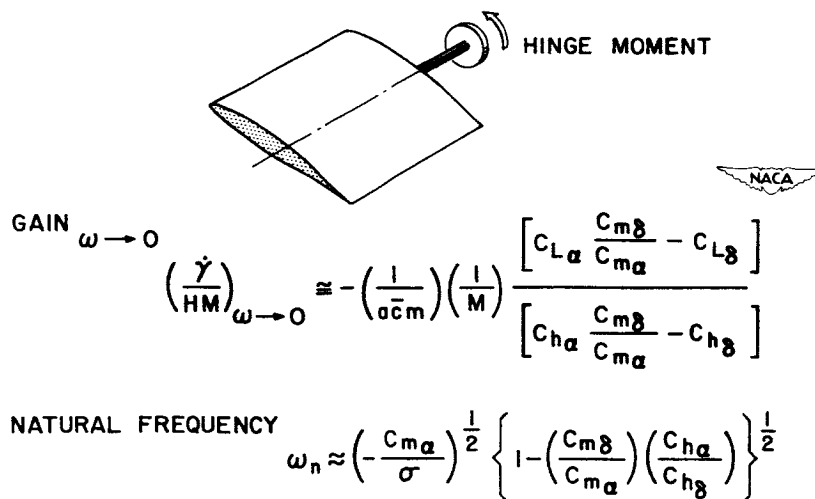


Figure 6

FREQUENCY RESPONSE WITH TORQUE SERVO

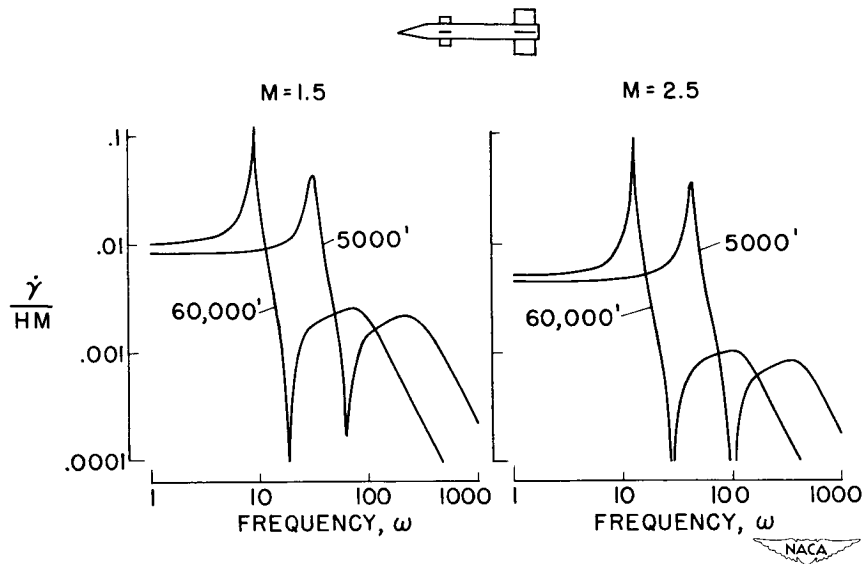


Figure 7

IDEALIZED TRANSIENT RESPONSE

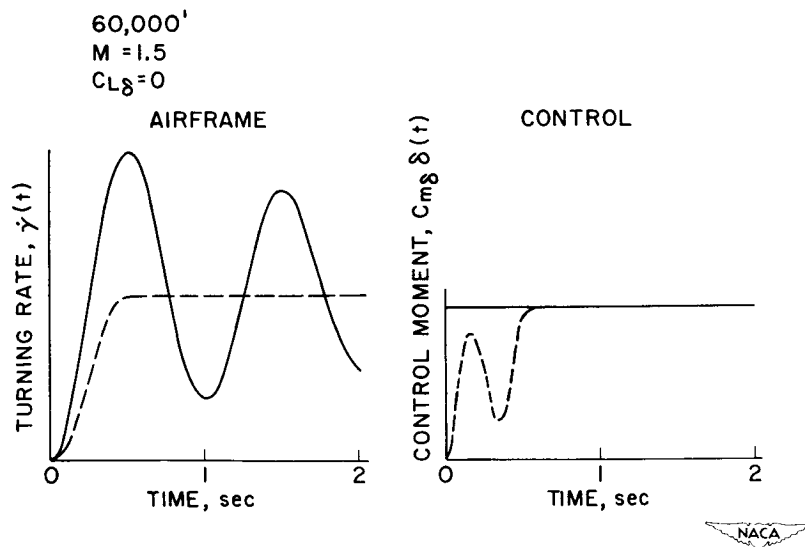


Figure 8

CONFIDENTIAL

DECLASSIFIED 11

TRANSIENT RESPONSE IN PITCH WITH AUXILIARY FLAP

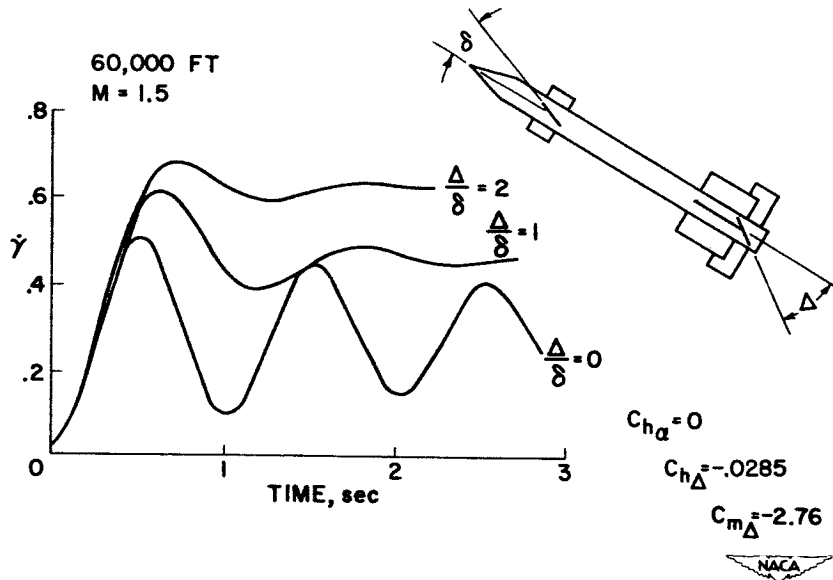


Figure 9

TRANSIENT RESPONSE IN ROLL WITH AUXILIARY FLAP

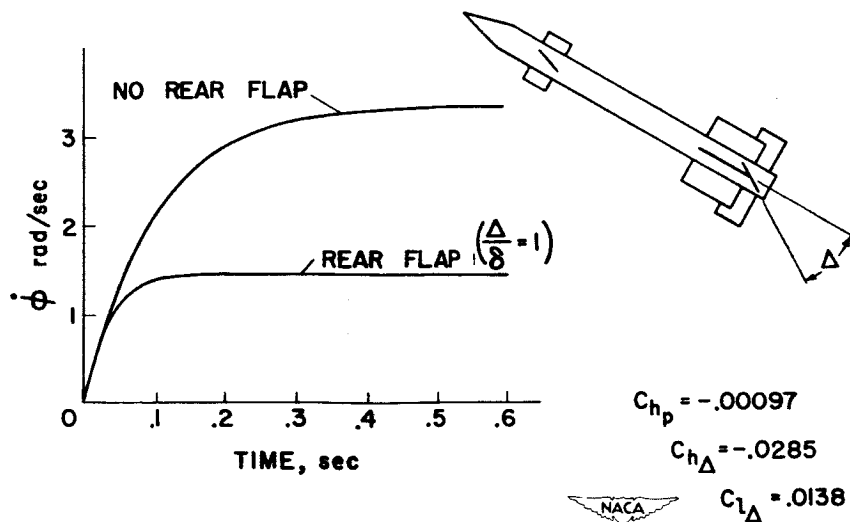


Figure 10

MAX. NORMAL FORCE-WINGED & PROJECTING CONTROL MISSILES

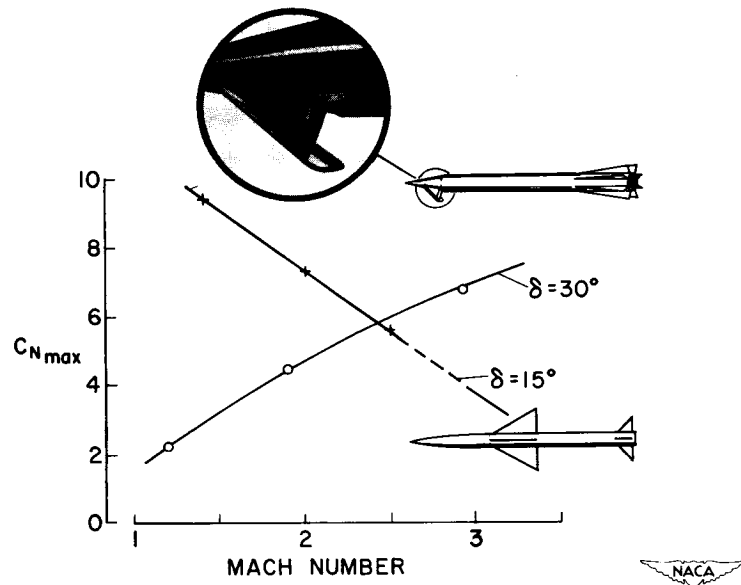


Figure 11

CONFIDENTIAL

GARDINER

A COMBINED AERODYNAMIC AND GUIDANCE APPROACH FOR

A SIMPLE HOMING SYSTEM

By Robert A. Gardiner

Langley Aeronautical Laboratory


This paper deals with the study of a system in which simplicity was achieved by eliminating many components. The basic idea of this system involves the use of aerodynamics to help in reducing homing-system complication and aid in increasing missile reliability. By using flicker controls operating directly from the target position as a primary reference, by using the rolling of the missile to scan the seeker field of view, and by using a rotating lift vector, several control system and guidance functions may be eliminated from an air-to-air missile with a corresponding increase in ruggedness and simplicity.

This subject will be described in the following order: the airframe characteristics, the seeker characteristics, and the combined operation of the airframe and seeker necessary to obtain this simplification.

In order to make a realistic analysis of the system, aerodynamic and guidance hardware has been chosen on the basis of availability and simplicity. The airframe, shown in figure 1, is a canard configuration with the front-end (seeker, control system, and control surfaces) bearing mounted free-to-roll on the aft end. The bearing mounted front end improves the quality of roll control since roll inertia is reduced and aerodynamic-induced rolling moments minimized.

The control end of the airframe is shown by the sketch in figure 1. Two of the canard surfaces are used as ailerons, and the other two are used as elevators. The flicker roll control used requires that the ailerons be deflected fully in one direction or the other, while the elevators are fixed at incidence.

The nose design has been influenced by the choice of guidance. A drag-reducing wind shield is supported by a tripod in front of a flat pyrex plate-glass window. Behind the window, shown dashed, are the mirror and infrared detector. A lead sulfide cell has been chosen principally because of its ruggedness and adaptability for test purposes. This is followed by the electronic element, containing seven vacuum tubes, and power supply. A pneumatic supply and regulator are in the next section which also contains the aileron actuator.



CONFIDENTIAL


The seeker used with this system must be capable of detecting targets within a narrow rectangle about 5° long by 1° wide. The elements of this detecting system are boresighted, as shown in figure 2, with the missile axis in such a manner as to aline one end of the detecting rectangle with the axis around which the missile rolls, while the other end is alined in the direction of lift. No gimbals are necessary since pursuit navigation is used.

In operation the airframe and seeker function together as follows: When the missile rolls, the seeker scans a 12° included angle cone with about a 2° central dead zone. Figure 3 illustrates this operation. If a target is located within the active area of this cone, as the missile rolls the detecting area will cross the target and produce a signal. This signal is used to reverse the ailerons causing roll in the opposite direction. This causes the detecting area to recross the target and again reverse the ailerons. Thus, the missile hunts in roll on the target.

As the missile hunts, the flight path of the missile is curved towards the target, since the detecting area and the lift of the airframe are alined to produce this direction of flight-path correction. As the flight path curves, the relative motion between missile and target causes the target to appear to move towards the center end of the seeker rectangle. When the missile is pointed directly towards the target, the target moves into the central dead spot of the seeker, the roll control is inactive, and the missile rolls continually while moving towards the target on an effective straight flight path.

Another way in which the system operation may be described is by use of the block diagram shown in figure 4. The blocks representing roll response, angle-of-attack response, and flight-path response are airframe responses. The optic block and geometry block are guidance functions and represent the seeker and the geometry. The feedback indicated from angle of attack to the optic input occurs since the seeker is fastened to the airframe without gimbals. The primary feedback of geometry and flight path represents the target motion towards the center of the seeker cone. The roll feedback to the optic input illustrates the roll control system and represents the roll hunting action. An input to angle of attack from roll angle is shown and represents the rotating lift vector and illustrates the point that the direction of lift is dependent on the roll angle.

Two modes of operation of the airframe are used to obtain a pursuit chase of the target. During search or during "on target" operation the missile rolls continually while trimmed in a lifting condition. This results in a small-diameter (about 3 ft) helical motion, shown in figure 5, while the missile pursues an effective straight flight path. When flight-path correction is needed, a flicker roll system functions



to point the airframe lift towards the target path and produce the required corrections. The only moving controls are ailerons which are actuated by the flicker roll control operating directly from target position as the primary reference.

When a symmetrical airframe is subjected to combined pitching, yawing, and rolling motion, as is the case with this system, gyroscopic and other coupling between rolling and the other motions can occur. This has been demonstrated by Phillips (ref. 1) and by Nicolaides (ref. 2). The effect of this coupling is shown by a plot of pitch amplitude ratio against roll frequency (fig. 6). For this system the operating point for constant roll and for roll hunting has been kept low to avoid undesirable resonance effects.

To determine the limitations of the system and to get a quick view of the type of operation which could be expected, a one-to-one time scale simulator was constructed using two moving carts operating on a reduced geometry scale of 30 feet equal to 1 mile. Actual guidance hardware was used on the missile cart shown in figure 7(a). This hardware was mounted on a driving motor chosen to simulate properly the inertia and damping of the airframe in roll. This roll simulator was gimbaled and spring-restrained so that the gimbal inertia, spring, and damping simulated the airframe short-period pitch and yaw oscillation. Two gimbals were used so that both pitch and yaw were represented. The steering gear was directly coupled to the yaw gimbal so that the steering angle was equal to the angle of sideslip.

An automobile headlamp bulb was mounted on the target cart, figure 7(b), to simulate the exhaust of a jet airplane target. The missile cart was accelerated to a speed representing Mach number 1.6 while the target cart ran at a speed representing Mach number 0.8. Various angles of launch, from 0° , directly behind the target, to 45° off the tail of the target, were tried, as well as several launching ranges.

Qualitatively, the nature of the system operation was judged from this simulator and found to be quite satisfactory. However, due to the reduced geometry scale and the physical size of the components, accurate measurements at small ranges could not be made.

In order to provide a more accurate determination a reduced time scale simulation was set up using REAC equipment plus an auxiliary non-linear device to represent the optical system and roll control system.

The REAC was used to represent the airframe and part of the kinematic geometry. The remainder of the geometry, the optical system, and the control system were simulated by a cathode ray oscilloscope (used to present target position), an optical and photoelectric pickup, and an electro-mechanical roll simulator.

[REDACTED]

[REDACTED] L

CONFIDENTIAL

With this equipment, the missile launching range and angle off the tail of the target to assure a successful flight (a hit) could be determined accurately. These coordinates were obtained for all significant positions in the area surrounding the target. This was found to be divided into a firing area where a hit was always obtained and an area from which a hit is impossible as shown in figure 8.

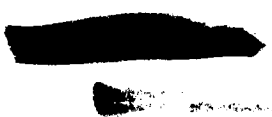
The useful area is fairly large considering the type of navigation used and almost coincides with the infrared signal cone to be expected from jet aircraft.

It should be noted that this confirms previous work which has been done on pursuit navigation (ref. 3); however, it is believed that the useful firing area is larger than it has generally been thought to be.

From this investigation, it may be concluded that a homing system has been devised which attains simplicity by utilizing several aerodynamic properties of the airframe. The possibility that a similar reduction in complication could be made in the case of other systems should be investigated.

Another conclusion is that a missile using pursuit homing has a useful firing area which may well be large enough to be tactically useful.

REFERENCES

1. Phillips, William H.: Effect of Steady Rolling on Longitudinal and Directional Stability. NACA TN 1627, 1948.
 2. Nicolaidis, John D.: On the Free Flight Motion of Missiles Having Slight Configurational Asymmetries. Paper presented at 21st Annual Meeting, I.A.S. (New York), Jan. 26-29, 1953. (Preprint No. 395.)
 3. Watkins, Charles E.: Paths of Target-Seeking Missiles in Two Dimensions. NACA WR L-735, 1946. (Formerly NACA ACR L6B06.)
- 

TEST-VEHICLE AIRFRAME

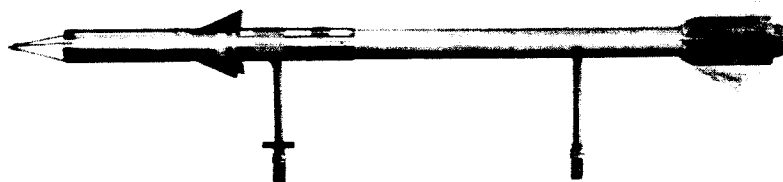
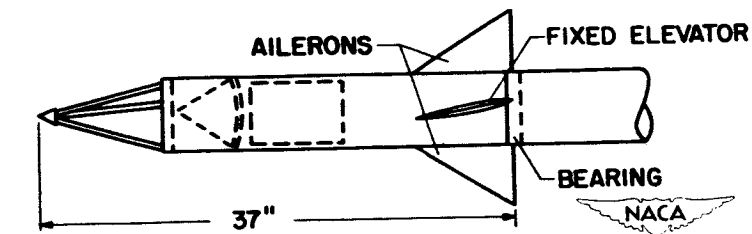


Figure 1

SEEKER BORESIGHTING

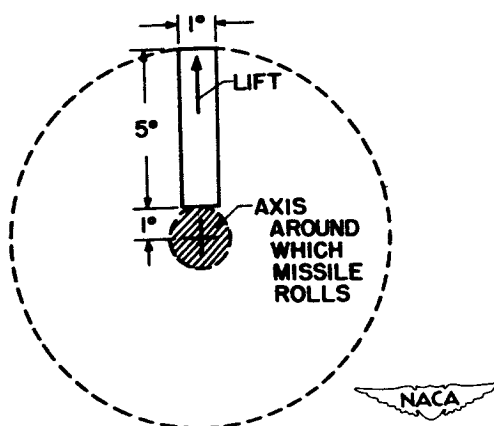


Figure 2

A technical diagram of a rocket engine nozzle. The nozzle is shown in cross-section, with a central throat and a diverging section. The half-angle of the diverging section is labeled as 12° . The nozzle is shown firing, with a plume of gas exiting. A small inset diagram shows a rocket engine with a similar nozzle. The NACA logo is visible in the bottom right corner.

BLOCK DIAGRAM

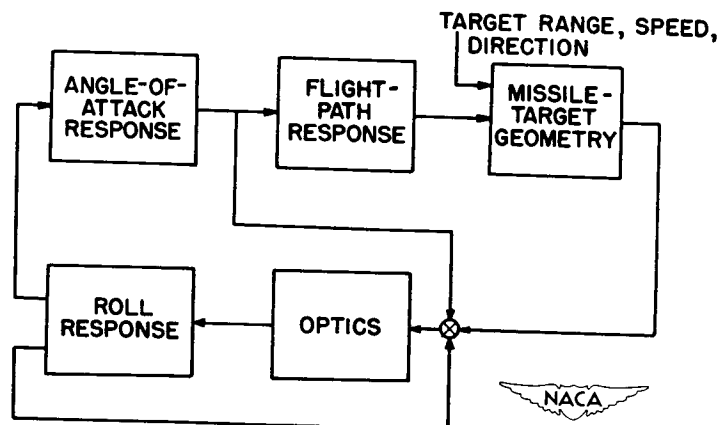


Figure 4

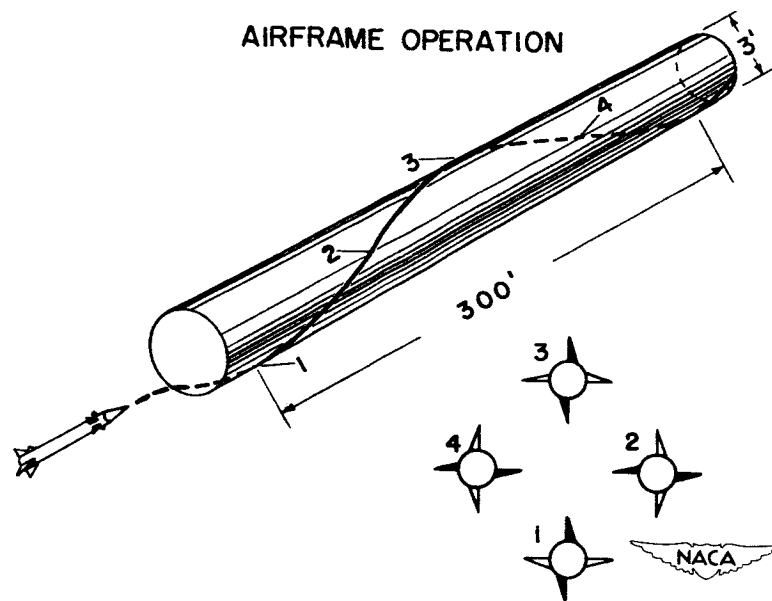


Figure 5

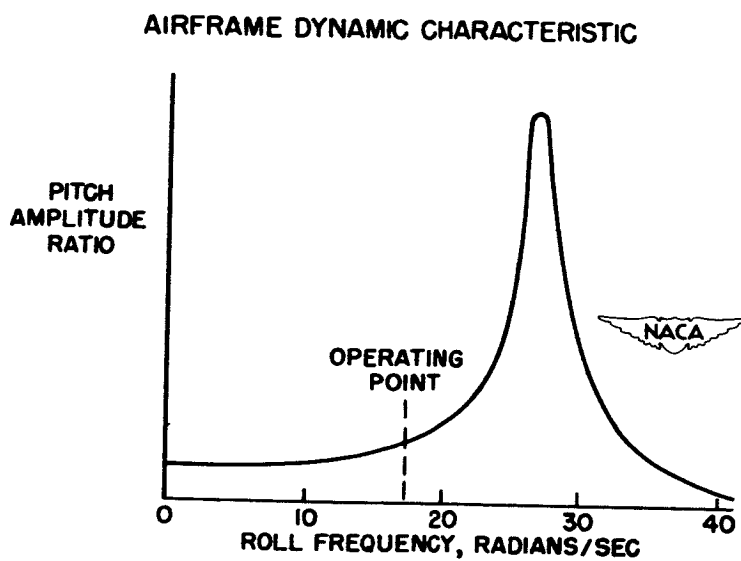


Figure 6

CONFIDENTIAL

MISSILE CART

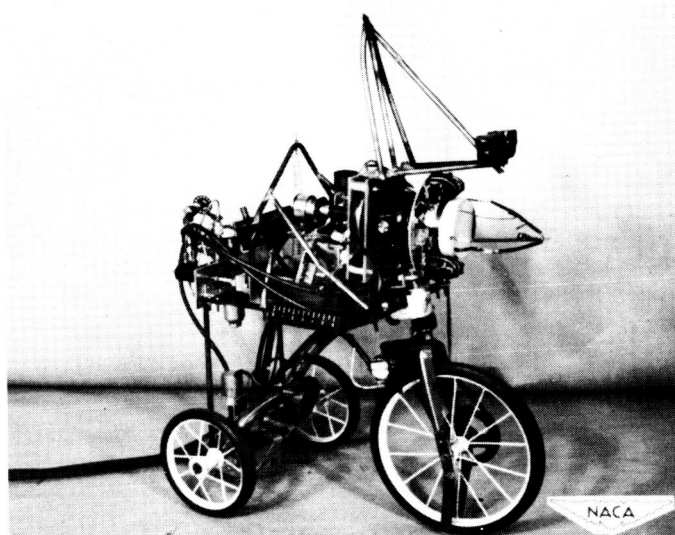


Figure 7(a)

TARGET CART

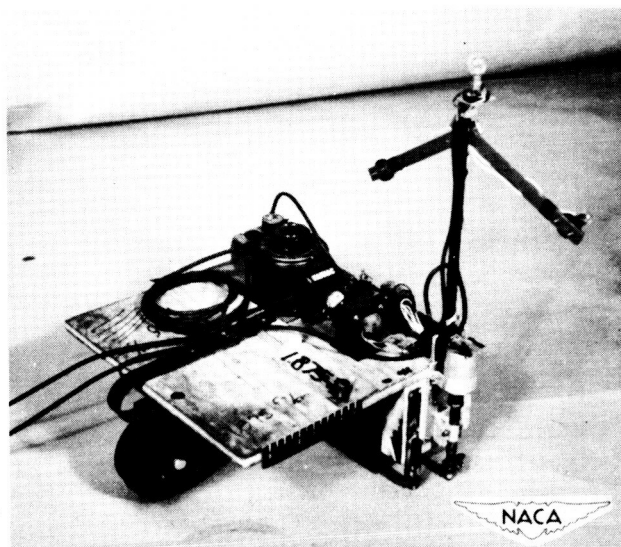


Figure 7(b)



CONFIDENTIAL

USEFUL FIRING AREA

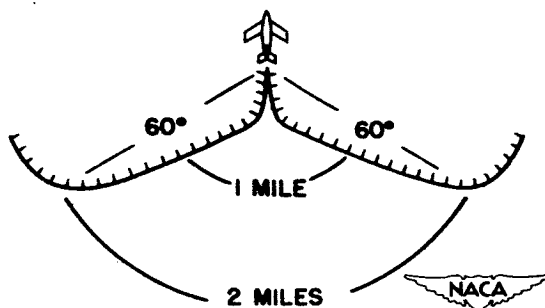
 $V_M/V_T = 2.0$; SEA-LEVEL CONDITIONS

Figure 8

Handwritten signature
~~CONFIDENTIAL~~

E R R A T A

A STUDY OF THE MOTION AND AERODYNAMIC HEATING
OF MISSILES ENTERING THE EARTH'S ATMOSPHERE
AT HIGH SUPERSONIC SPEEDS

By H. Julian Allen

Presented at NACA Conference on Aerodynamics
of High-Speed Aircraft
Ames Aeronautical Laboratory
Moffett Field, Calif.
July 8-10, 1953

It should be noted that there is an error in the total drag coefficient in figures 7 and 9 and an error in the deceleration and speed given in figure 8 of the subject paper. The corrected figures are attached.

Please destroy the original figures 7, 8, and 9 and replace them with these corrected figures.

DECLASSIFIED

FRICTIONAL AND TOTAL DRAG COEFFICIENT FOR
40° CONICAL MISSILE



Figure 7

SPEED AND DECELERATION FOR 10°
CONICAL MISSILE

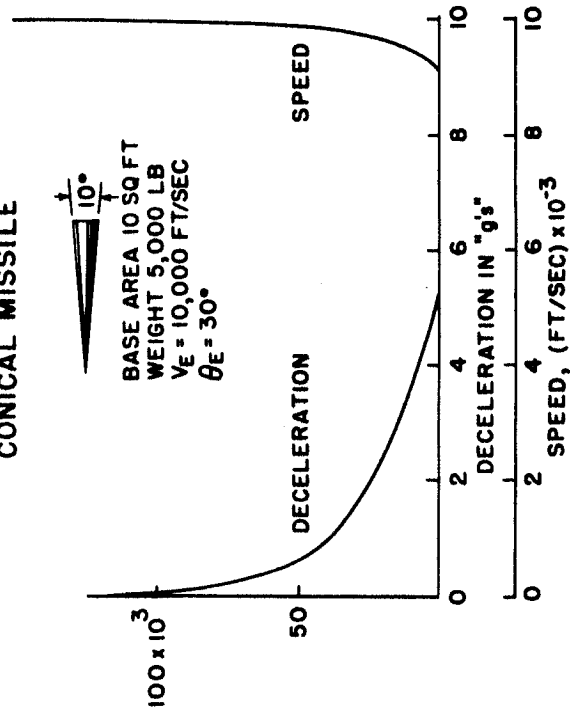


Figure 8

FRICTIONAL AND TOTAL DRAG COEFFICIENT FOR
10° CONICAL MISSILE

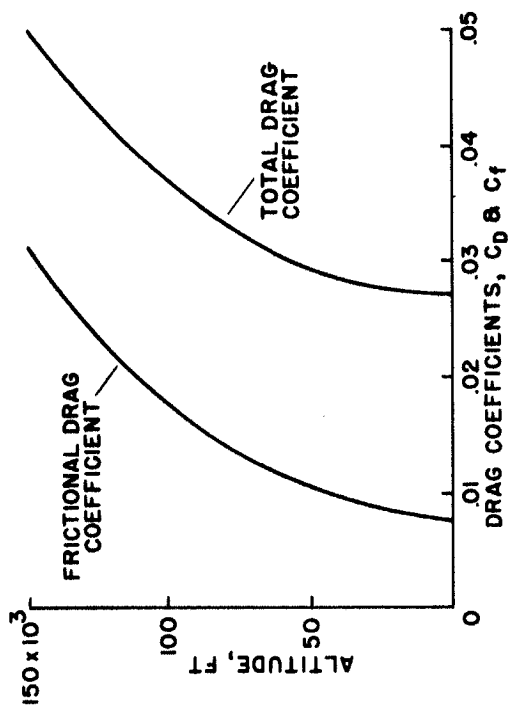


Figure 9

CONFIDENTIAL

CONFIDENTIAL

~~CONFIDENTIAL~~

E R R A T A

A STUDY OF THE MOTION AND AERODYNAMIC HEATING
OF MISSILES ENTERING THE EARTH'S ATMOSPHERE
AT HIGH SUPERSONIC SPEEDS

By H. Julian Allen

Presented at NACA Conference on Aerodynamics
of High-Speed Aircraft
Ames Aeronautical Laboratory
Moffett Field, Calif.
July 8-10, 1953

It should be noted that there is an error in the total drag coefficient in figures 7 and 9 and an error in the deceleration and speed given in figure 8 of the subject paper. The corrected figures are attached.

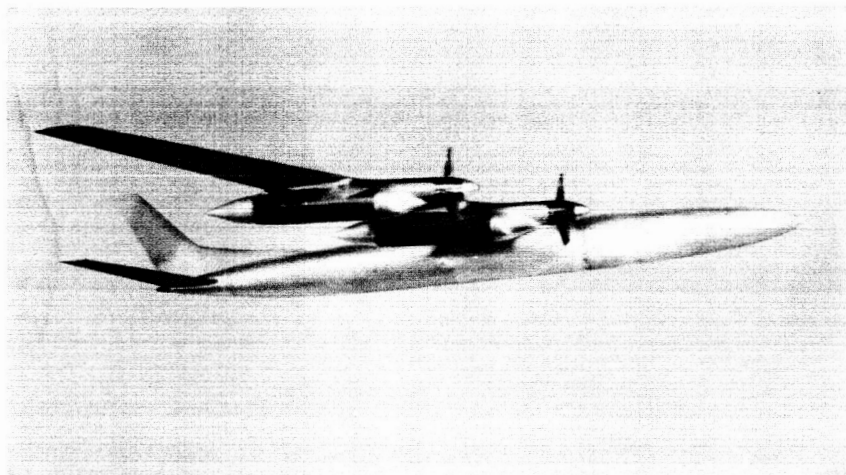
Please destroy the original figures 7, 8, and 9 and replace them with these corrected figures.

CONFIDENTIAL

CONFIDENTIAL

CONFIDENTIAL

POWERED MODEL TESTED IN AMES 12-FOOT TUNNEL



NACA

Figure 1

EFFECT OF PROPELLERS AT HIGH SUBSONIC SPEEDS

40,000 ft, $\frac{W}{S} = 65$ lbs /sq ft

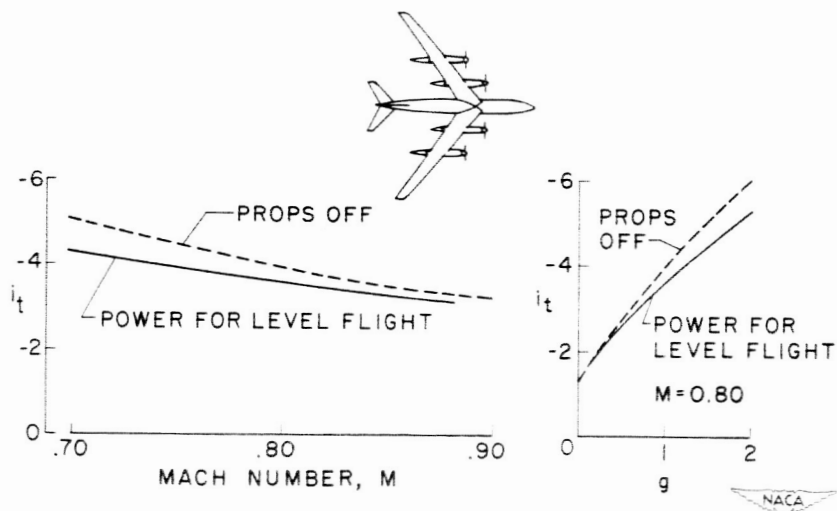
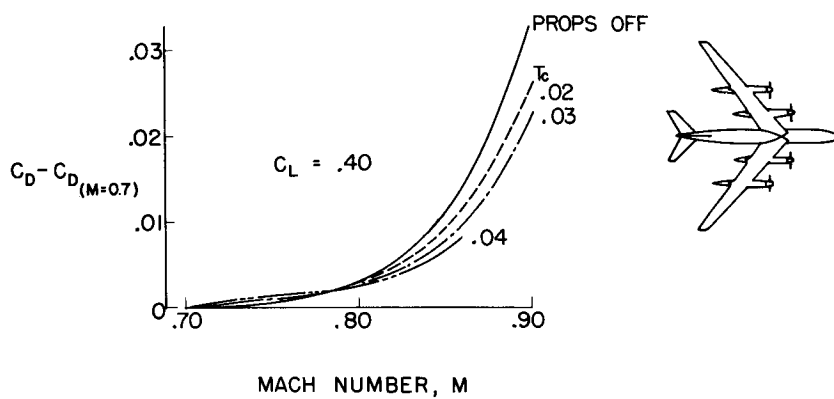


Figure 2

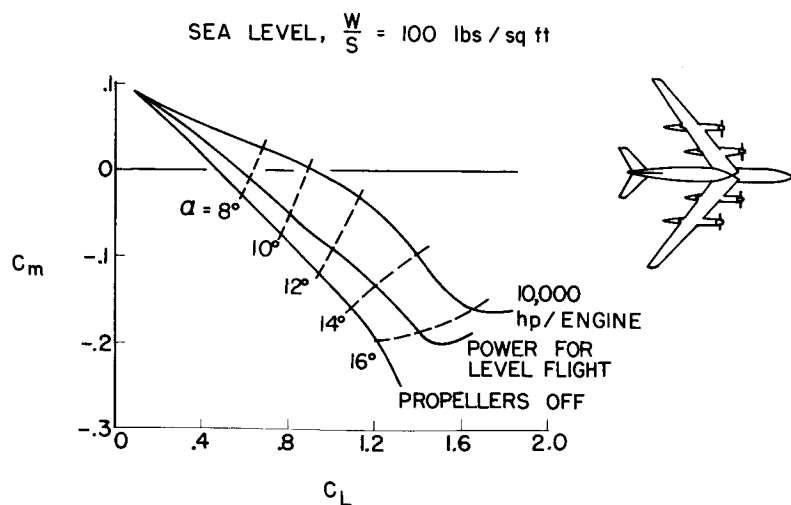
EFFECT OF PROPELLERS ON HIGH SPEED DRAG



NACA

Figure 3

EFFECT OF PROPELLERS ON PITCHING MOMENT



NACA

Figure 4

EFFECT OF MACH NUMBER ON TURBULENT SKIN - FRICTION AT ZERO HEAT TRANSFER

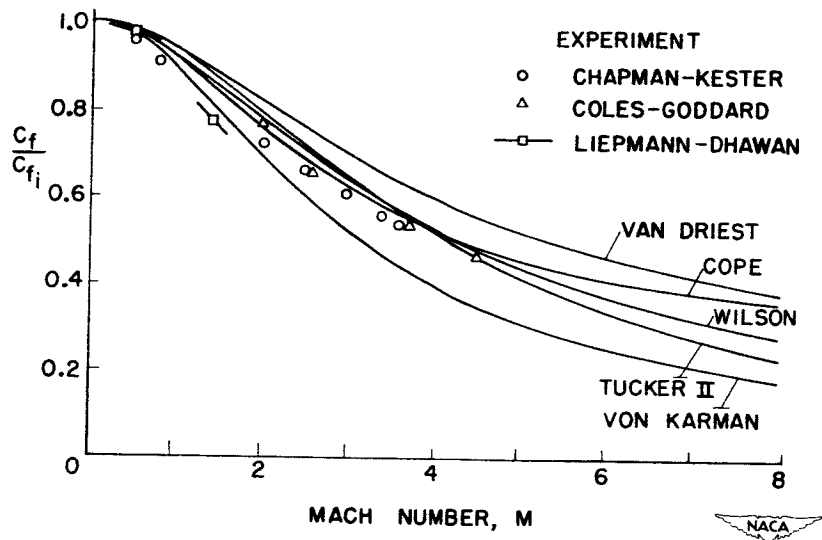


Figure 1

PREDICTED EFFECT OF HEAT TRANSFER ON SKIN FRICTION

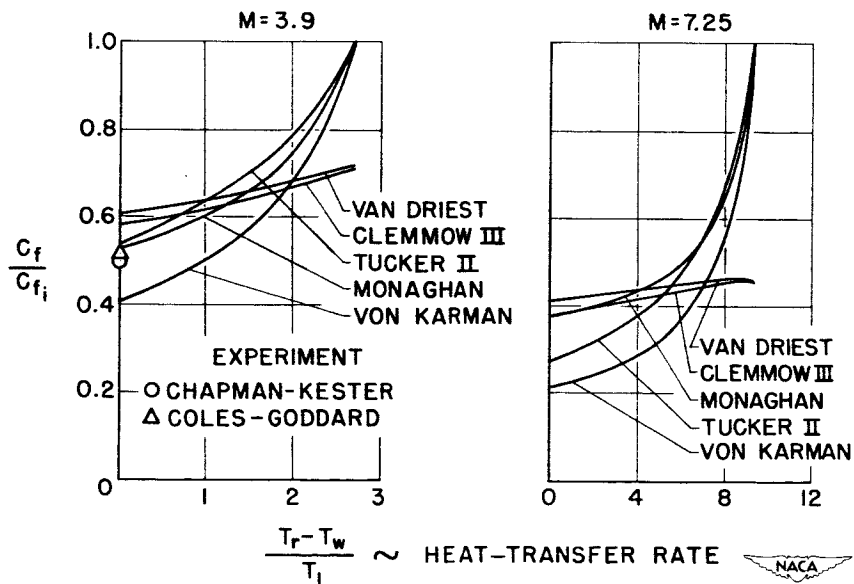


Figure 2

MODELS

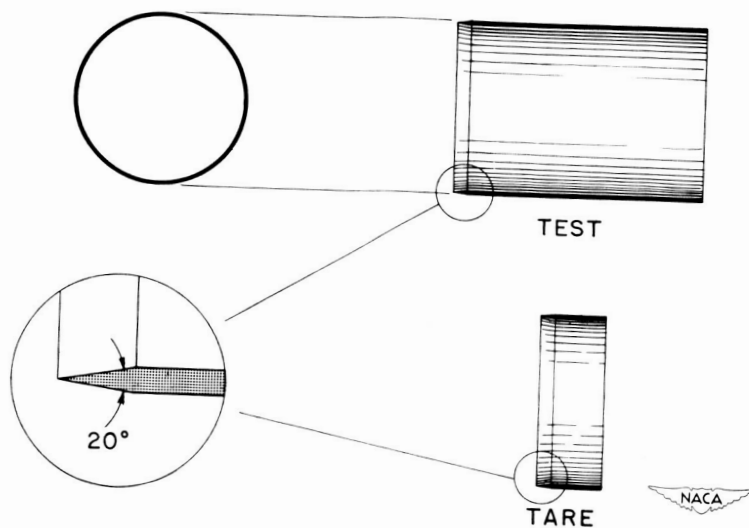


Figure 3

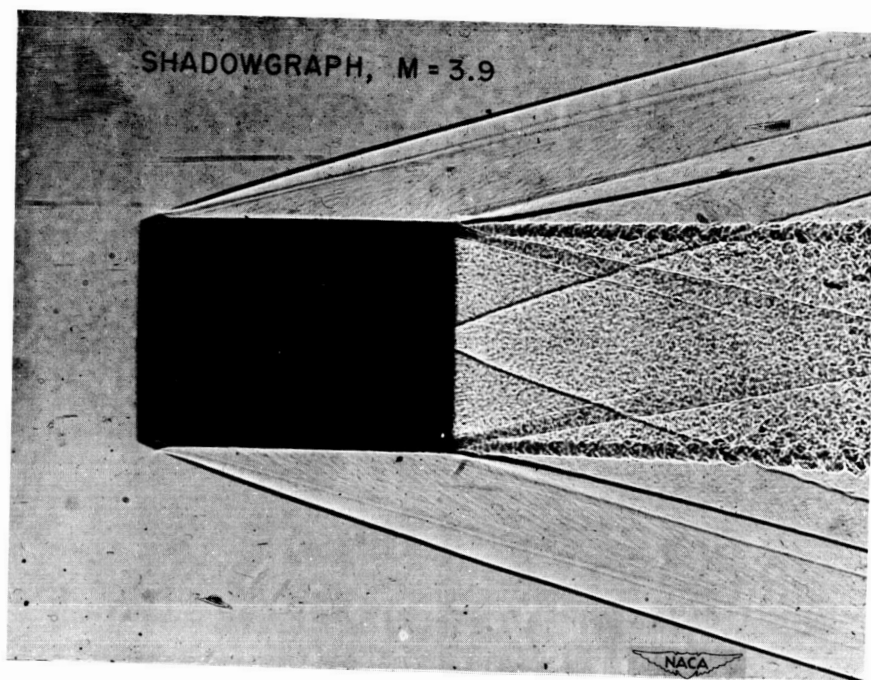


Figure 4

[REDACTED]

PRESENT DATA COMPARED WITH ZERO-HEAT-TRANSFER DATA

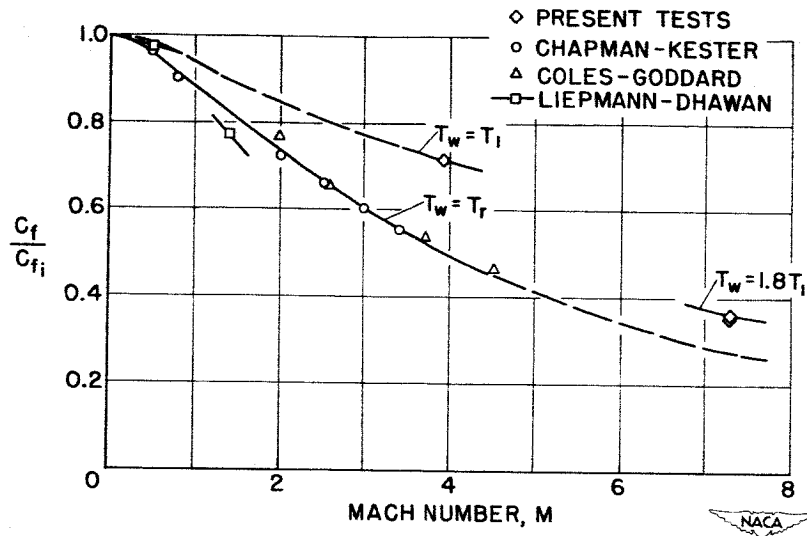


Figure 5

COMPARISON OF DATA WITH THEORETICAL EFFECT OF HEAT TRANSFER

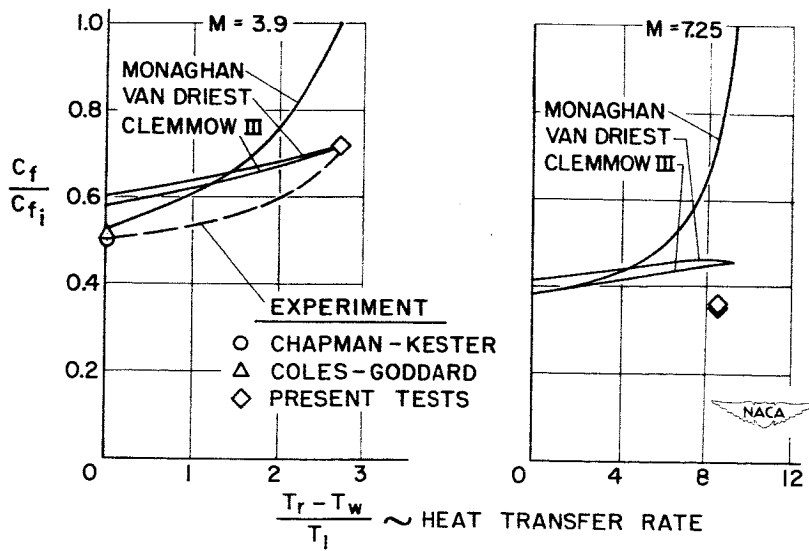


Figure 6

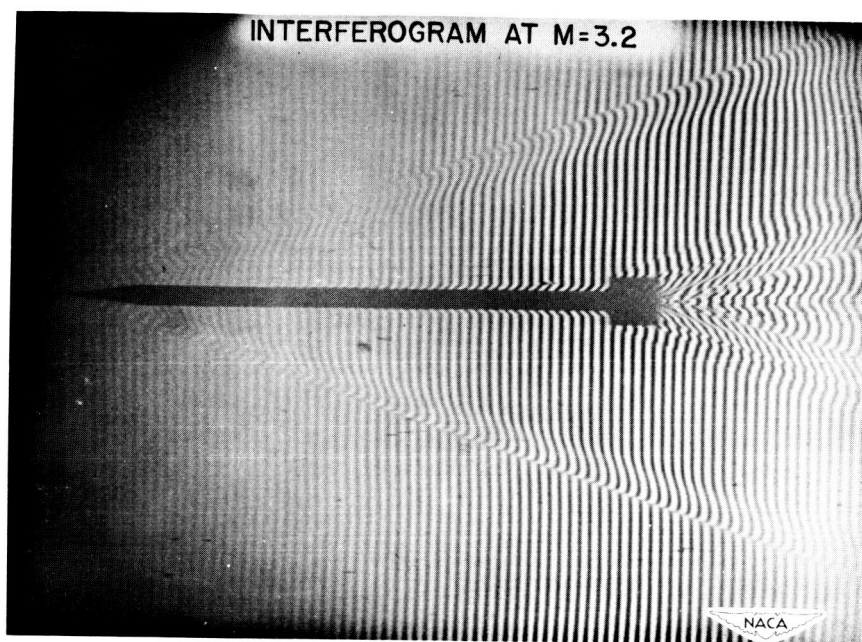


Figure 7

TEMPERATURE PROFILES IN TURBULENT
BOUNDARY LAYER

M = 3.2

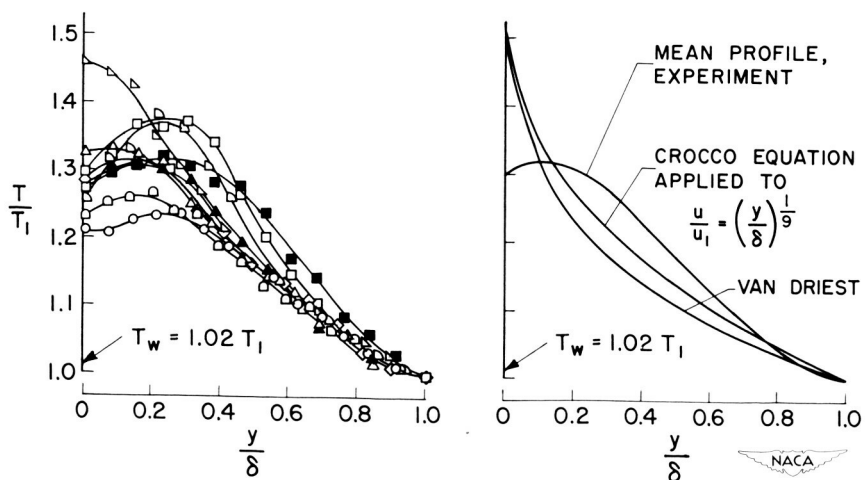


Figure 8

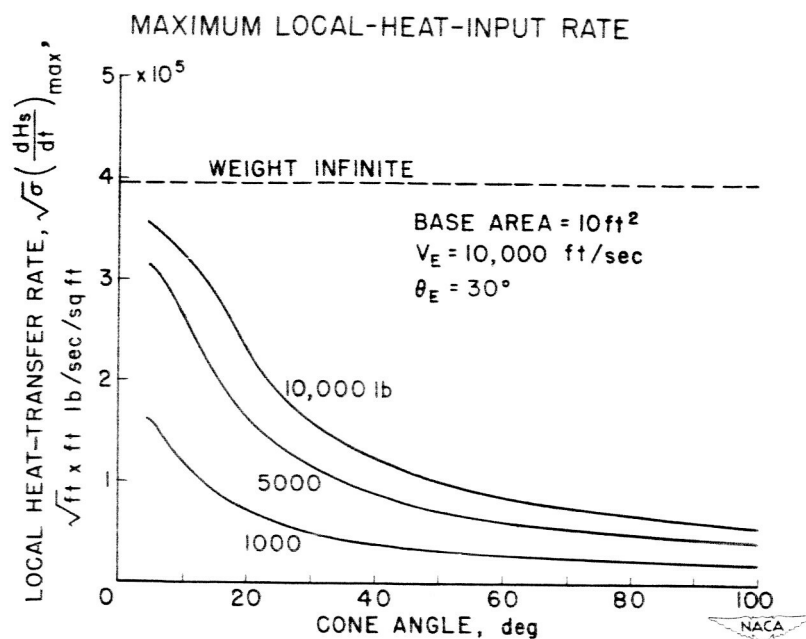


Figure 13

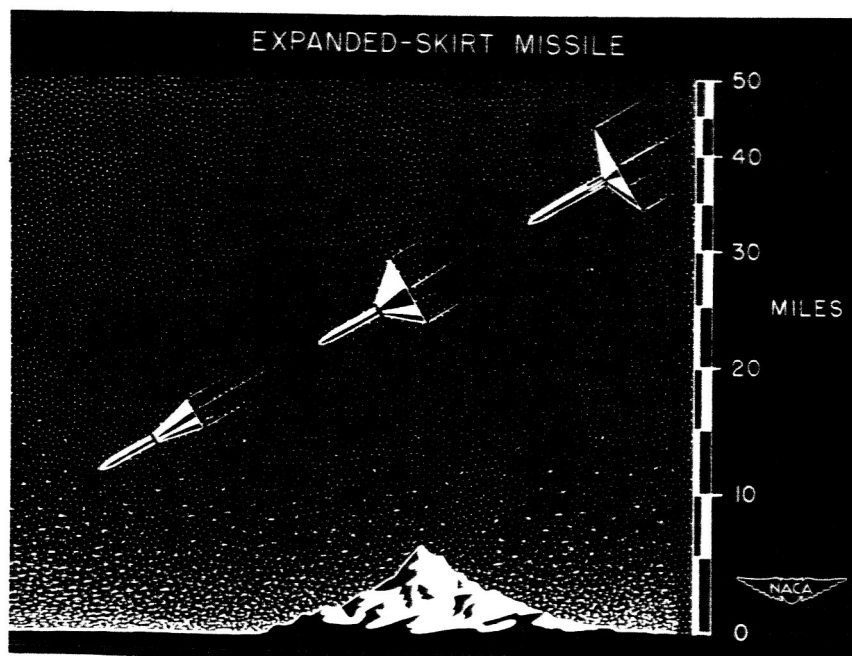


Figure 14

EFFECT OF DISSOCIATION ON HEAT TRANSFER TO STAGNATION POINT OF A SPHERE

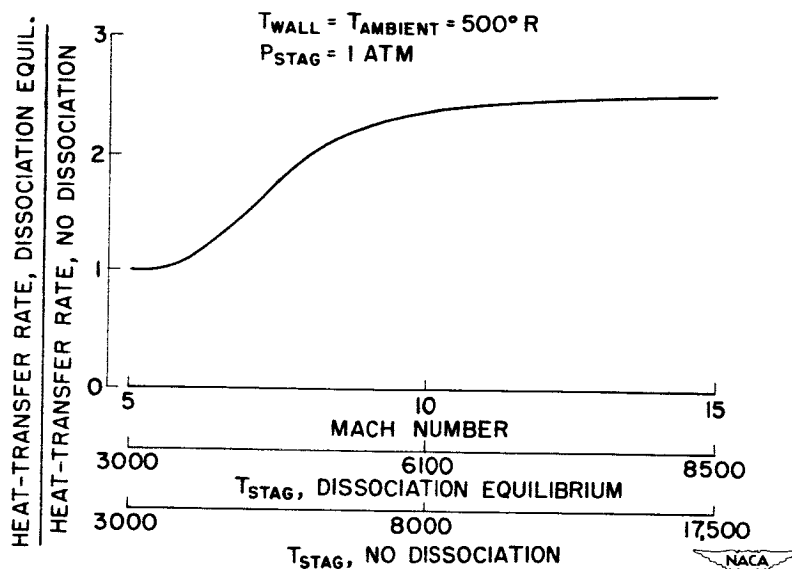


Figure 3

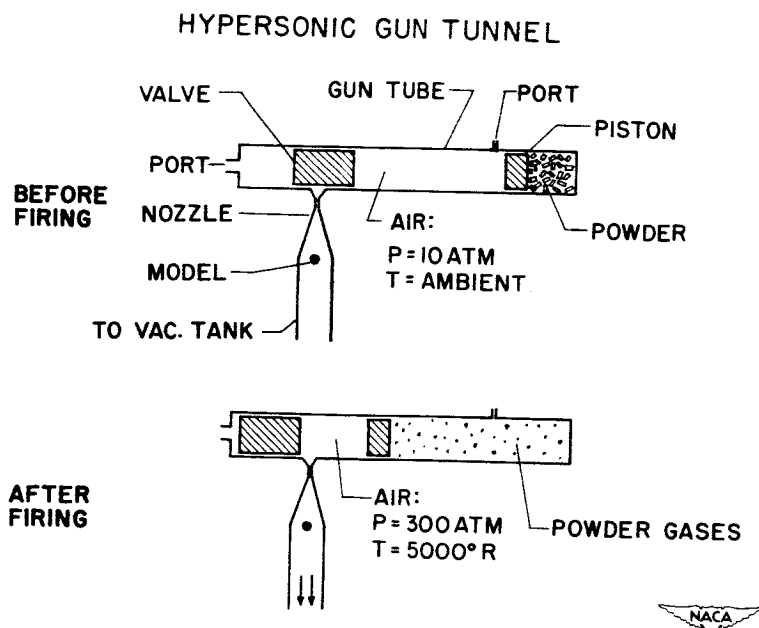


Figure 4

THE 20 MM HYPERSONIC GUN TUNNEL

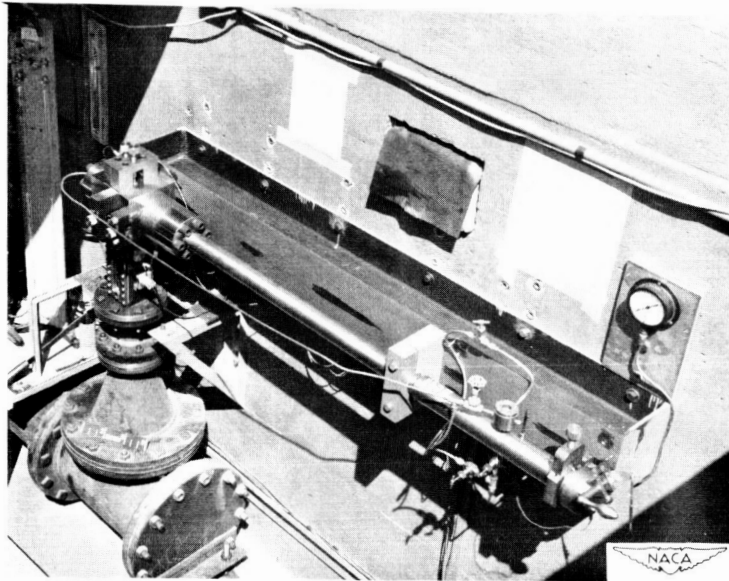


Figure 5

WORKING SECT. OF THE 20 MM HYPERSONIC GUN TUNNEL

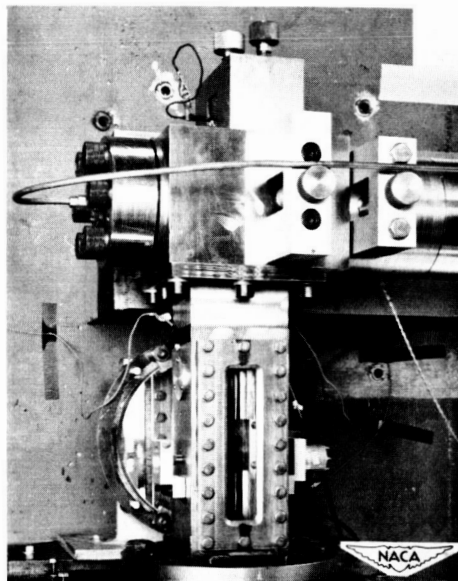


Figure 6

